Natural Products as Kinase Inhibitors: Total Synthesis, *in Vitro* Kinase Activity, *in Vivo* Toxicology in Zebrafish Embryos and *in Silico* Docking

From the Department of Chemistry

at the Technischen Universität Darmstadt

to obtain the degree

Doctor rerum naturalium

(Dr. rer. nat.)

Dissertation

from Annicet Kenfack Sipoho, M.Sc.

First reviewer: Prof. Dr. Boris Schmidt

Second reviewer: Prof. Dr. Katja Schmitz

Darmstadt 2023

Date of submission: 26th September 2023

Day of the oral examination: 13th November 2023

Kenfack Sipoho, Annicet: Natural Products as Kinase Inhibitors: Total Synthesis, *in Vitro* Kinase Activity, *in Vivo* Toxicology in Zebrafish Embryos and *in Silico* Docking

Darmstadt, Technische Universität Darmstadt,

Year thesis published in TUprints: 2023

Date of the viva voce 13.11.2023

>> Life has no limitations except the ones you make. <<

-Les Brown-

I dedicate this work to my family to express my gratitude for their love and support.

This work was conducted between October 2019 and September 2023 under the supervision of Prof. Dr. Boris Schmidt at the Clemens Schoepf Institute for Organic Chemistry and Biochemistry of the Technical University of Darmstadt.

Diese Arbeit wurde zwischen Oktober 2019 und September 2023 unter der Leitung von Prof. Dr. Boris Schmidt am Clemens-Schoepf-Institut für Organische Chemie und Biochemie der Technischen Universität Darmstadt durchgeführt.

Zusammenfassung

Trotz erheblicher Fortschritte bei der Entwicklung niedermolekularer Kinaseinhibitoren fehlt es den meisten menschlichen Kinasen immer noch an hochwertigen selektiven Inhibitoren, die als chemische Sonden zur Untersuchung ihrer biologischen Funktion und Pharmakologie eingesetzt werden könnten. Naturstoffe und ihre synthetischen Derivate könnten einen Weg zur Überwindung dieser häufig auftretenden Herausforderung bieten, da sie nachweislich auf ein breites Spektrum von Kinasen abzielen, einschließlich aller Unterfamilien des bekannten Kinoms. Um diese Naturprodukte aus ihren Quellen zu isolieren, müssen sie jedoch in großem Umfang extrahiert werden, was mit Schwierigkeiten verbunden ist und der Ökologie großen Schaden zufügt. Außerdem gibt es bei der Gewinnung dieser Naturprodukte aus ihren Quellen immer wieder Probleme, für die es nur wenige praktikable Lösungen gibt. In Anbetracht dieser Aspekte wurden die Totalsynthese und die Semisynthese eingesetzt, um die faszinierendsten Verbindungen der lebenden Natur im Labor zu reproduzieren und größere Mengen für ausgedehnte Studien zu erhalten. In der vorliegenden Arbeit wurden die Versuche zur Durchführung der ersten Totalsynthesen und zur Bewertung der biologischen Aktivität von natürlich vorkommenden, potenten Antikrebsverbindungen beschrieben: Depsipeptid PM181110, Eudistomidin C und Fusarithioamid A. Die ersten Totalsynthesen dieser Naturstoffe beruhen auf konvergenten und einheitlichen Ansätzen. Das Depsipeptid PM181110 ist ein bicyclisches Depsipeptid mit vier stereogenen Zentren, dessen erste Totalsynthese durch die Synthese seiner Diastereomere 3*R*,9*R*,14*R*,17*R* und 3*R*,9*S*,14*R*,17*R* versucht wurde. Auch bei Eudistomidin C und Fusaruthioamid A mit bekannter Stereochemie wurden die Syntheseversuche ausgehend von enantiomerenreinen Reagenzien durchgeführt. Die synthetisierten Verbindungen **BSc5484**, **BSc5517** und die Analoga wurden anschließend auf ihre biologische Aktivität hin untersucht. Dementsprechend wurde die kinasehemmende Wirkung untersucht, gefolgt von einem In-vivo-Toxizitätsversuch an Wildtyp- und Goldtyp-Zebrafischembryonen *Danio rerio*. Im Ergebnis zeigten die untersuchten Verbindungen eine mäßige bis gute Hemmung der Kinasen mit einem offensichtlichen Selektivitätsprofil und einer Toxizität in Zebrafischembryonen, die durch die beobachteten Phänotypen veranschaulicht wird. Schließlich ergab ein *In-silico*-Experiment, dass **BSc5484** und **BSc5485** als Typ-IV-Inhibitoren binden könnten, während **BSc5517** im Vergleich zum bekannten β-Carbolin-

Inhibitor Harmine eine bessere Bindungsaffinität zur menschlichen Haspin-Kinase zeigte, und zwar über die gesamte Palette der getesteten Kinasen. Diese Arbeit liefert somit das erste chemische Werkzeug, um mit natürlich gewonnenen Verbindungen, von krankheitsverursachenden Proteinen zu inhibieren, die bei zahlreichen Formen von Krebs und anderen Krankheiten eine Schlüsselrolle spielen. Folglich ist die Etablierung von Depsipeptid und β-Carbolin basierten Verbindungen als therapeutische Leitstrukturen von entscheidender Bedeutung und wird ein leistungsfähiges Werkzeug zur weiteren Aufklärung ihrer biologischen Funktion durch gezielte strukturelle Veränderungen darstellen.

Summary

Despite significant progress in developing small molecule kinase inhibitors, most human kinases still lack high-quality selective inhibitors that might be employed as chemical probes to study their biological function and pharmacology. Natural products (NPs) and their synthetic derivates might give avenues to overcome this frequently encountered challenge as they demonstrated to target a wide range of kinases, including all subfamilies of the known kinome. Nonetheless, isolating these NPs from their sources necessitates massive harvesting, which is fraught with difficulties and triggers enormous harm to the ecology. Moreover, the challenges encountered while extracting these NPs from their sources are constantly present and have few viable solutions. Considering these aspects, total synthesis and semisynthesis have been employed to replicate the most intriguing compounds of living nature in laboratories to obtain larger quantities for extended studies. The present work outlined the attempts to perform the first total syntheses and to evaluate the biological activity of naturally occurring potent anti-cancer compounds: Depsipeptide PM181110, Eudistomidin C, and Fusarithioamide A. Efforts to achieve the first total syntheses of these natural compounds have been based on highly convergent and unified approaches. Depsipeptide PM181110 is a bicyclic depsipeptide featuring four stereogenic centres whose attempts to perform its first total synthesis were undertaken by synthesizing its diastereomers 3*R*,9*R*,14*R*,17*R*, and 3*R*,9*S*,14*R*,17*R*. Similarly, for Eudistomidin C and Fusarithioamide A having known stereochemistry, the attempts to perform their syntheses were made starting from enantiomerically pure reagents. The synthesized compounds **BSc5484**, **BSc5517** and the analogues were subjected to biological activity tests afterwards. Accordingly, a kinase inhibitory activity test was performed, followed by an *in vivo* toxicology assay in wild-type and gold-type zebrafish embryos *Danio rerio*. As a result, the assayed compounds displayed moderate to good inhibition of the kinases with an apparent selectivity profile and toxicity in zebrafish embryos illustrated by the observed phenotypes. Finally, an *in silico* experiment revealed that **BSc5484** and **BSc5485** might bind as type IV inhibitors, while **BSc5517** demonstrated a better binding affinity to human Haspin kinase compared to the known β-carboline inhibitor Harmine across the panel of the tested kinases. This work thus provides the first directed tools about the potential of naturally derived compounds as inhibitors of disease-causing proteins that are key players in numerous forms of cancer and other illnesses. Consequently, establishing depsipeptide and β-carboline-based

compounds as therapeutic leads is crucial and will provide a powerful tool to further elucidate their biological function through targeted structural variations.

Acknowledgements

First, I thank my supervisor, Prof. Dr Boris Schmidt, for the excellent cooperation during my doctorate. In particular, the trust placed in me when I was applying for the scholarship and all the context behind that. I also thank him for the stimulating professional discussions and the constant willingness to address my questions and concerns.

Furthermore, I would like to thank the Deutscher Akademischer Austauschdienst for providing the scholarship. Funding programme/-ID: 57440921; personal reference number: 91732720

I thank Prof. Dr. Katja Schmitz who accepted without any hesitation to Co-supervise this work.

Big thanks go to the active and former members of the Schmidt and Schmitz working groups, especially Robyn, Mirco, Marcel, Farid, Jeffrey, Christian, Johanna, Daniel, Georg, Alexandra, Michele, Steffi and Vicky, for the friendly and pleasant working atmosphere as well as for the good times outside the daily laboratory routine. I would also like to thank all the students who accompanied me during my doctorate. I learned a lot from you, and thank you for your tireless efforts. I want to thank Zehu Men, Egzon Cermjani, Kai Schliessmann, Malin Hohendorf, Maria Wiegand and Laura Rübernacker, whom I was able to supervise and gain valuable experience within the context of research internships and Master's thesis, especially Zehu Men and Kai Schliessmann for their active support in synthesising selected substances. I would also like to thank Alexandra Herbst for her help in performing the cell viability assay.

I thank Barbara Gantt for valuable technical and administrative support at the beginning of my doctoral journey.

Special thanks go to my family, who have supported me in all my decisions throughout my life.

Publications

Poster

- **Total Synthesis of the 3*R*,9*R*,14*R*,17*R* Diastereomer of Depsipeptide PM181110*, in Vitro* Kinase Activity*, in Vivo* Toxicology in Wild-Type Zebrafish Embryos *Danio Rerio* and *in Silico* Docking**
  Annicet Kenfack Sipoho, Boris Schmidt, Frontiers in Medicinal Chemistry, Vienna, Austria, 3-5 April 2023.

Table of Contents

Table of Abbreviations

Å	angstrom
aa	amino acid
AADC	aromatic acid decarboxylase
AChE	acetylcholinesterase
AcOEt	Ethyl acetate
APCI	atmospheric pressure chemical ionization
ARPKD	autosomal-recessive polycystic kidney disease
ASTM	*N*-acetylserotonin *O*-methyltransferase
ATM	ataxia telangiectasia mutated
ATP	adenosine triphosphate
ATR	ataxia telangiectasia mutated and Rad3-related
ATRIP	ataxia telangiectasia mutated and Rad3-related-interacting protein
ATR-IR	attenuated total reflection infrared spectroscopy
BCR/Abl	breakpoint cluster region-Abelson kinase
BCS	biopharmaceutical drug classification system
BD	blind docking
BEI	binding efficiency index
ca.	calculated
CAMK	calmodulin/calcium-regulated kinase
cAMP	cyclic adenosine monophosphate
cAPK	cyclic AMP-dependent protein kinase
CAR	carboxylic acid reductase
$CaCO_3$	Calcium Carbonate
Cbz	Benzyloxycarbonyl
CCl_4	Carbon tetrachloride
$CDCl_3$	Deuterated chloroform
CDK	cyclin-dependent kinase

CDX	ChemDraw
$CHCl_3$	Chloroform (trichloromethane)
CHF	congenital hepatic fibrosis
Chk1	checkpoint kinase 1
Chk2	checkpoint kinase 2
CDX	ChemDraw Exchange
CI	confidence interval
CK	Casein kinase
CK2	Casein Kinase 2
CKD	chronic kidney disease
CLKs	cdc-like kinase (CLKs)
ClogP	calculated n-octanol-water partition coefficient
CML	chronic myeloic leukaemia
CODM	codeine *O*-demethylase
COSY	correlated spectroscopy
COX	cyclooxygenase
CRPC	castration-resistant prostate cancer
Cy	Cyclohexane
DAD	diode-array detector
dba	dibenzylidenacetone
DCE	1,2-dichloroethane
DCM	dichloromethane
DDQ	2,3-Dichloro-5,6-dicyano-1,4-benzoquinone
DIBAL	Diisobutylaluminium hydride
DHJ	double Holliday junction
DIBAL	Diisobutylaluminium hydride
DIPA	diisopropylamine
DMA	Dimethylaniline
DMAP	4-Dimethylaminopyridine

DMF	Dimethylformamide
DMS	dimethyl sulphate
DMSO	Dimethylsulfoxide
DNA	Deoxyribonucleic acid
DNA-PK	DNA-dependent protein kinase
dpf	days post fertilization
dppf	1,1'-Bis(diphenyl-phosphino)ferrocene
DSBR	double-strand break repair
DSBs	DNA double-strand breaks
DSF	differential scanning fluorimetry
dtbpf	1,1′-Bis(di-tert-butylphosphino)ferrocene
DTT	Dithiothreitol
DYRK1A	Dual specificity tyrosine-phosphorylation-regulated kinase 1A
EC50	Half maximal effective concentration
DZIP1L	DAZ-interacting protein 1-like
EA	Ethyl acetate
EC50	Half maximal effective concentration
EDC	1-Ethyl-3-(3-dimethylaminopropyl)carbodiimide
EDTA	ethylenediaminetetraacetic acid
EGTA	Egtazic acid
EGFP	enhanced green fluorescent protein
EGFR	endothelial growth factor receptor
EI	electron ionization
ELKs	Eukaryotic-like protein kinases
EMA	European Medicines Agency
EPKs	eukaryotic protein kinases
ER	endoplasmatic reticulum
ERK	Extracellular Signal-Regulated Kinase
ErbB2	erb-b2 receptor tyrosine kinase 2

ESI	electronspray ionization
ESRD	end-stage renal disease
EtOAc	Ethyl Acetate
EU	European Union
FDA	Food and Drug Administration
FDM	fused deposition modelling
FLK1	fetal liver kinase 1
Fms	Feline McDonough Sarcoma
FTIR	Fourier-transform infrared spectroscopy
GK	Gatekeeper
Glu	Glutamic acid
GPCR	G protein-coupled receptor
GSK-3	Glycogen synthase kinase 3
hr	hour
hrs	hours
HAN	heavy atom number
HAT	Histone acetyltransferase
HCl	Hydrochloric acid
HDAC	Histone deacetylase
His	Histidine
HMBC	heteronuclear multiple bond correlation
HOBt	Hydroxybenzotriazole
Hsp90	Heat shock protein 90
hpf	hours post fertilization
HPLC	High performance liquid chromatography
HR	homologous recombination
HR1	hydrophobic region 1
HR2	hydrophobic region 2
HRMS	High-resolution mass spectrometry

HRR	homology-directed recombination-mediated repair
HSQC	heteronuclear single quantum coherence
IC_{50}	Half maximal inhibitory concentration
ICL	Isocitrate lyase
INNs	international nonproprietary names
IRES	Internal ribosomal entry site
JNK	c-Jun N-terminal kinase
K_2HPO_4	Dipotassium phosphate
Ki	Inhibition constant
KIF3A	kinesin-like protein
KOtBu	potassium tert-butoxide
KP	KinaseProfiler
LE	ligand efficiency
LFU	low frequency ultrasound
$LiAlH_4$	Lithium aluminium hydride
LogP	n-Octanol-water partition coefficient
LSP	Local spatial pattern
mAbs	monoclonal antibodies
MAO-A	Monoamine oxidase A
MAPK	mitogen-activated protein kinase
MCF	methyl chloroformate
mCPBA	meta-chloroperoxybenzoic acid
MDM2	Mouse double minute 2 homolog
MEK	Mitogen-activated protein kinase
$MgSO_4$	Magnesium sulfate
MIC	Minimum inhibitory concentration
mM	Millimolar
MNBA	2-Methyl-6-nitrobenzoic anhydride
MMFF	Merck molecular force field

MNPs	Marine natural products
MOE	Molecular Operating Environment
MOPS	(3-(N-morpholino)propanesulfonic acid)
mRNA	messenger RNA
MS	mass spectrometry
MsCl	mesyl chloride
MTT	3-(4,5-Dimethylthiazol-2-yl)-2,5-diphenyltetrazolium bromide
mTOR	mechanistic target of rapamycin
MW	microwave
MW	molecular weight
NADPH	Nicotinamide adenine dinucleotide phosphate
n.d.	not determined
n.e.	no effect at maximum concentration
NaOtBu	Sodium tert-butoxide
$NaHCO_3$	Sodium bicarbonate
Na_2SO_4	Sodium sulphate
$Na_2S_2O_3$	Sodium thiosulfate
NCEs	new chemical entities
NCS	Norcoclaurine synthase
NF-κB	Nuclear factor kappa-light-chain-enhancer of activated B cells
NHEJ	non-homologous end joining
NIMA	never in mitosis-gene A
nm	nanomolar
NMR	Nuclear magnetic resonance
NPs	natural products
pADPr	poly(adenosine diphosphate-ribose)
PAK1	p21-activated kinase 1
PARP	poly(adenosine diphosphate -ribose)-polymerase
PBS	Phosphate-Buffered Saline

PCT	proximal convoluted tubule
PDB	Protein Database
PDE-5	Phosphodiesterase type 5
PDK1	3-Phosphoinositide-dependent kinase 1
pH	potential Hydrogen
PI3K	Phosphoinositide 3-kinases
PKA	Protein Kinase A
PKC	Protein Kinase C
PKG	Protein Kinase G
PKIS2	Published Kinase Inhibitor Set 2
PKR	Protein kinase R
PLP	Pyridoxal phosphate
PSF	point spread function
PTU	N-Phenylthiourea
RCC1	regulator of chromosome condensation 1
RMSD	root-mean-square deviation
RNA	Ribonucleic acid
RT	Room temperature
SARs	structure-activity relationship
SrtA	Sortase A
SCLC	Small-cell lung carcinoma
SD	standard deviation
SDF	Simulation Description Format
SDSA	synthesis-dependent strand annealing
SIADH	syndrome of inappropriate antidiuretic hormone secretion
SL2	SuperLooper2
SrtA	Sortase A
SR	Sarcoplasmic Reticulum
STE	serine/threonine kinases

SSBs	single-strand DNA breaks
ssDNA	Single-strand DNA
STR	Strictosidine synthase
TAZ	transcriptional coactivator with PDZ-binding motif
TBAF	Tetra-n-butylammonium fluoride
TBAB	tetrabutylammonium bromide
TFA	trifluoroacetic acid
THF	Tetrahydrofuran
TK	tyrosine kinase
TKL	Tyrosine Kinase-Like
TLC	Thin-layer chromatography
Tlk1	tousled-like kinase 1
TLR	Toll-like receptor
TMS	tetramethylsilane
TOF	time-of-flight
TPH	L-tryptophan-5-hydroxylase
t_R	retention time
TR-FRET	time-resolved fluorescence resonance energy transfer
tPSA	topological surface area
TSA	thermal shift assay
Tyr	Tyrosine
U/S	ultrasonic irradiation
UV	ultraviolet
UVA	Ultraviolet A
VEGFA	Vascular Endothelial Growth Factor A
VEGFR2	Vascular endothelial growth factor receptor 2
VDAC1	voltage-dependent anion channel 1
VWD	variable wavelength detector

List of Amino Acid Abbreviations

Alanine	A	Ala
Arginine	R	Arg
Asparagine	N	Asn
Aspartic acid	D	Asp
Cysteine	C	Cys
Glutamic acid	E	Glu
Glutamine	Q	Gln
Glycine	G	Gly
Histidine	H	His
Isoleucine	I	Ile
Leucine	L	Leu
Lysine	K	Lys
Methionine	M	Met
Phenylalanine	F	Phe
Proline	P	Pro
Serine	S	Ser
Threonine	T	Thr
Tryptophan	W	Trp
Tyrosine	Y	Tyr
Valine	V	Val

1 Introduction

1.1 Natural Products as a Source of Pharmacologically Active Compounds

Natural plants have been utilized for ages in both traditional and modern medicine to cure a wide range of diseases thanks to the bioactive natural products they contain. Among the many bioactive products present in plants are terpenes, Phenolic compounds, N-containing compounds, and S-containing compounds. These bioactive compounds, also known as secondary metabolites, have been shown to improve human health by preventing diseases from arising and progressing.

Secondary metabolites are organic substances generated by any living organism, such as bacteria, fungi, animals and plants, but are not directly involved in the organism's natural growth, development, or reproduction. Secondary metabolites also play a role in interactions with other organisms, whether competitors or pathogens. That is why organisms that produce secondary metabolites do so to protect themselves from the harmful effects of the environment in their natural habitat.

Natural product research has advanced several scientific disciplines, including developing novel synthetic techniques, new technology for their isolation and processing, and the knowledge of biosynthetic routes and biological targets. [1] Unsurprisingly, many prescription medications are derived from or inspired by natural products (NPs). Biologically active NPs have been intensively studied as drug candidates for clinical purposes and essential research tools for dissecting biological processes. [2] Furthermore, they are characterized by enormous scaffold diversity and structural complexity illustrated by Rapamycin and Teixobactin, two well-known and frequently used for their property as immunosuppressants and antibiotics, respectively. [3]

In contrast to traditional synthetic compounds, NPs have unique properties that provide advantages and obstacles in drug development. Compared to synthetic compound libraries, they typically have a higher molecular mass and a higher number of sp^3 carbon and oxygen atoms but a lower number of nitrogen and halogen atoms. These distinctions would be useful; for example, the rigidity of NPs might be beneficial in drug development involving protein-protein interactions. [2,4] Nevertheless, NPs and traditional synthetic compounds are, in many aspects, complementary routes to new medicines.

There has been a great interest in finding new chemical pharmacophores in NPs to solve critical unmet medical needs concerning signal transduction pathways and to meet the massive demand for new kinase inhibitors.

As NPs can be isolated or extracted from various natural sources, the subsequent chapters elaborate on some of the most encountered sources of NPs.

1.1.1 Bioactive Natural Products from Endophytic Fungi

It is well known that medicinal plants have been employed to isolate and characterize bioactive compounds directly. However, the discovery of fungal endophytes within these plants capable of manufacturing the same compounds as the plant's host changed the focus of novel medicine sources away from plants and toward fungi (**Figure 1**). Endophytic fungi can mimic plant-associated metabolic pathways (polyketide, shikimate, and mevalonate) to produce a variety of bioactive compounds independent of the growth medium. Endophytes invade living plant tissues without changing the physiology of the host plant via forming a symbiotic relationship with the host and its surrounding environment. De Bary first used the term endophyte to refer to any organism found within living plant tissues that does not cause disease symptoms in the host plant. [5] Plant endophytes have been reported as unique sources of naturally occurring compounds with diverse biological functions, such as cytotoxicity, antibacterial activity, anti-inflammatory activity, anti-cancer activity, herbicides, antileishmanial activity, and antioxidant activity. [6] That is why endophytic fungi remain a principal source of novel bioactive natural compounds with distinct chemical origins among various endophytic organisms. Accordingly, endophytic fungi have attracted considerable interest in the last few decades because of the unexplored pool of novel bioactive compounds they possess. [5, 6]

Following the discovery of the anti-cancer drug paclitaxel or Taxol (**1**) in *Taxomyces andreanae*, an endophytic fungal strain isolated from *Taxus brevifolia*, there has been a surge in interest in bioactive natural compounds generated from endophytic fungi (**Figure 2**). [7] Paclitaxel (**1**) is a natural medication discovered which provides a remarkable therapeutic effect and mode of action for breast and ovarian cancer. Taxol induces mitotic arrest at the G2/M state at high concentrations, while at low concentrations, it initiates programmed cell death at G0 and G1/S through the activation of Raf-1 kinase or p53/p21, contingent on the dosage

administered. Taxol has attracted the curiosity of chemists worldwide because of its structure, particular anti-cancer mechanism, remarkable therapeutic efficacy, and limited resources. Meanwhile, it has frequently advocated discovering and developing natural product-based anti-cancer drugs. [8]

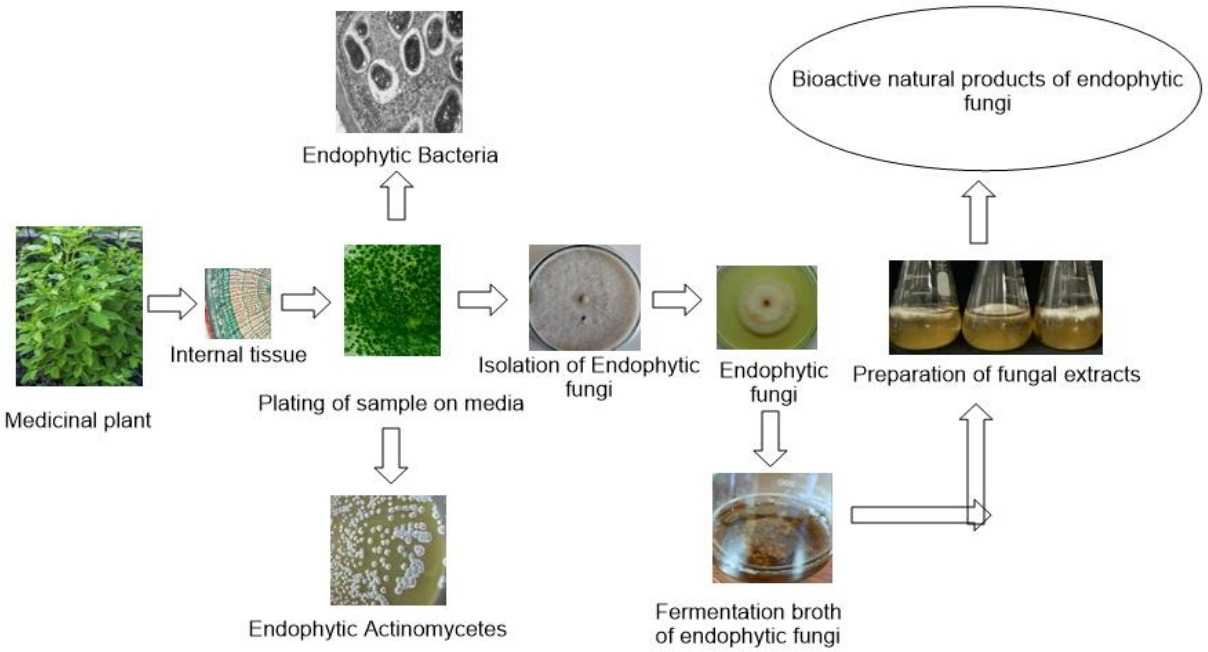

Figure 1: Illustration of the production of bioactive metabolites from endophytic fungi extracted from plants. Figure redrawn and adapted. [9]

Currently, more than 60% of anti-tumour drugs are derived from NPs. [10] The discovery of Vinblastine (**2**), shown in Figure 2a, had an essential impact on the design and synthesis of new highly effective and less toxic anti-cancer drugs. Similarly, this discovery also contributed to research on mitotic tools by utilizing plentiful NPs as lead compounds (**Figure 2a**). [11] Furthermore, Vinblastine's inhibition of mitosis at the metaphase through its interaction with tubulin is believed to be the primary mechanism of its antitumour activity. In this process, Vinblastine connects to mitotic spindle microtubule proteins, causing microtubule crystallisation and mitotic arrest or cell death.

Camptothecin (**3**) is another potent anti-cancer compound attached to topoisomerase I and the DNA complex. They form a ternary complex, stabilising it and inhibiting DNA re-ligation. This results in DNA damage and apoptosis. Camptothecin (**3**) and its derivatives have been

considered the most effective anti-tumour drug classes and have been utilized in emerging cancer treatment owing to the breakthrough and transformation of oncology drug treatment. [12] Besides, Camptothecin research has been fruitful after decades of study, with three camptothecin-derived compounds approved for tumour treatment.

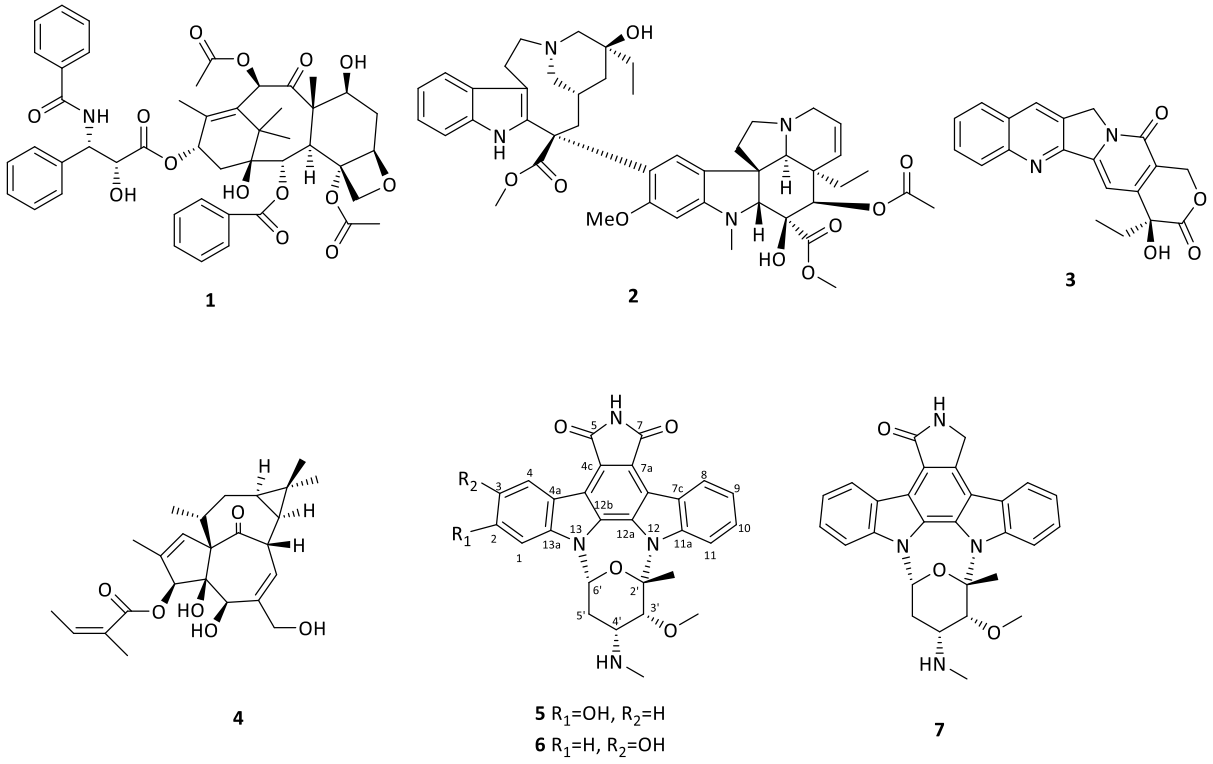

Figure 2a: Chemical structure of isolated natural products from various natural sources: Taxol (**1**), Vinblastine (**2**), Camptothecin (**3**), Ingenol (**4**), 2-hydroxy-7-oxostaurosporine (**5**), 3-hydroxy-7-oxostaurosporine (**6**) and Staurosporine (**7**).

Ingenol (**4**) is a compound discovered in the juice of the plant *big peplus* (milkweed), which is a cell death inducer. [13] In addition, Ingenol operates by a twofold mechanism that includes a fast development of necrosis that mainly targets dysplastic cells. The gel formulation of the drug has been approved by both the EMA and the FDA for the topical treatment of actinic keratosis. Consequently, NPs, with their inherent bioactive diversity and structural variety, will probably continue to be significant sources of novel medications.

1.1.2 Bioactive Natural Products from Marine Sources

Oceans and seas cover almost 70% of the Earth's surface and are home to 80% of all living species. [14] The enormous biodiversity of the marine environment has been indicated to produce an equally rich chemical diversity of marine natural products (MNPs) derived from the many organisms studied. [15] Several marine-derived scaffolds were utilized in clinical drug discovery and development during the golden age of natural product research because of novel ideas and improvements in screening methods. MNPs have been a rich source of novel pharmacologically active compounds, with over 200 isolated each year from marine sponges, corals, tunicates, and other marine invertebrates. [16] Thus, two novel staurosporine derivatives named 2-hydroxy-7-oxostaurosporine (**5**) and 3-hydroxy-7-oxostaurosporine (**6**) (**Figure 2a**) were isolated from the mid-polar fractions of an aqueous methanol extract of *Eudistoma vannamei*. *Eudistoma vannamei* is a tunicate found on Brazil's northeast coast. Using the 3-(4,5-dimethylthiazol-2-yl)-2,5-diphenyltetrazolium bromide assay (MTT assay), the combination of **5** and **6** was roughly 14-fold more cytotoxic than staurosporine (**7**) across a panel of tumour cell lines, with IC_{50} values in the nM range. Furthermore, the combination of compounds **5** and **6** exhibited substantial cytotoxic effects, with IC_{50} values of between 10.33 nM in Jurkat leukaemia cells and 687.08 nM in normal PBMC cells. This was found against seven human tumour cell lines (Molt-4, HL-60, K562, Jurkat, HCT-8, SF-295 and MDA-MB-435) and normal proliferating lymphocytes (PBMC). [17]

There are several natural sources from which NPs can be isolated or extracted, varying from plant entophytes to marine organisms. Depending on the chemical structures, the isolated compounds have indicated distinct to similar biological features. The next chapter reviews some families of isolated NPs and emphasises their biological activity.

1.2 Bioactive Depsipeptides and Fusarithioamides Natural Products

Depsipeptides are non-ribosomal peptides that cyclize through an ester linkage and usually contain non-protein amino acids. When Plattner and Nager discovered two antibiotic compounds called enniatins (**Figure 2b**) from *Fusarium mold* growth media, they sparked interest in this class of compounds. [18] Natural cyclic depsipeptides are an essential source of pharmacologically active compounds. They are peptides with one or more ester bonds in addition to amide bonds and constitute fascinating lead structures for the development of novel synthetically produced drugs. It is well known that cyclic depsipeptides and their derivatives have various biological activities, including insecticidal, antiviral, antimicrobial, antitumor, tumour-promotive, anti-inflammatory, and immunosuppressive activity. Furthermore, cyclic depsipeptides have been identified in multiple natural organisms, including fungi, bacteria, and marine organisms. In addition, they revealed outstanding therapeutic potential as anti-cancer and antibacterial agents. [19]

Besides, benzamide derivatives with diverse and intriguing structures disclosed that they were pharmacologically active in treating several disorders, including cancer. [20] Fusarithioamides are examples of aminobenzamide derivatives featuring a unique carbon skeleton that can be bicyclic. Accordingly, it has been reported the isolation and structural elucidation of Fusarithioamide A (**12**) and Fusarithioamide B (**13**) (**Figure 2b**) from *Fusarium chlamydosporium*, an endophytic fungus isolated from the leaves of *Anvillea garcinii* (Burm.f.) DC. (*Asteraceae*). **12** exhibited selective and potent activity against BT-549 and SKOV-3 cell lines with IC_{50} values of 0.4 and 0.8 μM respectively. **13** on the other hand, revealed potent and selective activity against BT-549, MCF-7, SKOV-3 and HCT-116 cell lines with IC_{50}s of 0.09, 0.21, 1.23 and 0.59 μM, respectively, in comparison to doxorubicin IC_{50}s of 0.046, 0.05, 0.321 and 0.24 μM. [21, 22]

Depsipeptide PM181110 (**9**) is a novel depsipeptide molecule possessing a disulphide bridge (**Figure 2b**). It was isolated from an endophytic fungus named *Phomopsis glabrae* from the leaves of *Pongamia pinnata* (family *Fabaceae*), as reported by Verekar *et al*. PM181110 (**9**) demonstrated cytotoxic efficacy against 40 human cancer cell lines *in vitro*, including a mean IC_{50} value of 89 nM. The compound also exhibited ex vivo efficacy against 24 human tumour xenografts. [23]

Besides, FE399 (**8**), featuring a related structure, was extracted directly from the fermentation broth of the endophytic filamentous fungus *Ascochyta sp*. AJ117309 by researchers from Ajinomoto Co., Inc (**Figure 2b**). FE399 (**8**) indicated selective apoptotic effects against various cancer cell lines with p53 gene alterations and exerted specific antitumor activity in p53 gene-mutant cells.[24] Another cyclic pentapeptide analogue, Malformin A1 (**11**), isolated from *Aspergillus niger*, exhibited several bioactive features, including antibacterial and cytotoxic activity. [24, 25]

The common feature of these bioactive compounds is the disulphide bridge, which supports the remarkable biological activity of strained disulphide-bridged bicyclic NPs. Indeed, disulphide-bridged bicyclic NPs make up an important class of molecules that exhibit a broad range of biological activities and pharmacological properties. Disulphide bridges can give extra stability/rigidity, which is beneficial for biological activities. [26] They also have the potential to be used as cellular redox switches in signal transmission via the thiol-disulphide cascade process and thiol-thiol interaction with cysteine residues. Hence, the significance of cysteine residues has been utilised in the development of covalent-modifier drugs, particularly kinase inhibitors such as Zanubrutinib and Dacomitinib, which have been disclosed as effective cancer chemotherapeutic therapies in recent years. [27]

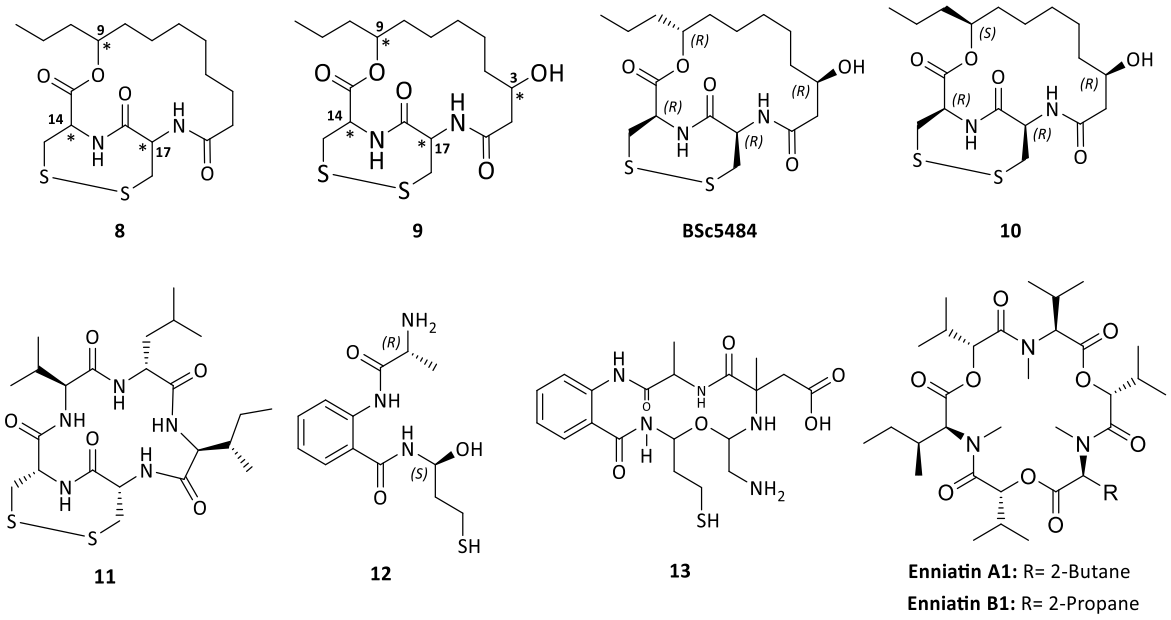

Figure 2b: Chemical structure of natural products isolated from diverse natural sources: depsipeptide FE399 (**8**), depsipeptide PM181110 (**9**), depsipeptide PM181110's diastereomers 3*R*,9*R*,14*R*,17*R* (**BSc5484**) and 3*S*,9*R*,14*R*,17*R* (**10**), Malformin A1 (**11**), Fusarithioamide A (**12)** and Fusarithioamide B (**13**).

Apart from depsipeptides and Fusarithioamides, naturally occurring β-carbolines drew many attractions as they were also revealed to be a source of bioactive compounds. The next chapter reviews some of the most interesting bioactive β-carbolines isolated from various natural sources.

1.3 Bioactive β-Carbolines Natural Products

β-carbolines are a large group of indole-alkaloids with exceptional pharmacological features commonly found in plants and marine organisms. The primary chemical structure of these heterocyclic NPs consists of a tricyclic pyrido-[3,4-β]-indole, where the framework rings are labelled as A, B and C. The distinction of α-, β-, γ- or δ-carbolines is dependent on the position of the N-atom contained in the C-ring (**Figure 3**). Moreover, further differentiations are made according to the degree of saturation between fully saturated, partially saturated and unsaturated carbolines. Furthermore, β-carbolines are widely distributed as secondary metabolites from plants, marine invertebrates, microorganisms, and insects. [29] Numerous β-carbolines exhibit extensive biological activities like cytotoxic, antimicrobial, antiparasitic and antiviral activity, making them desirable drug candidates. [28]

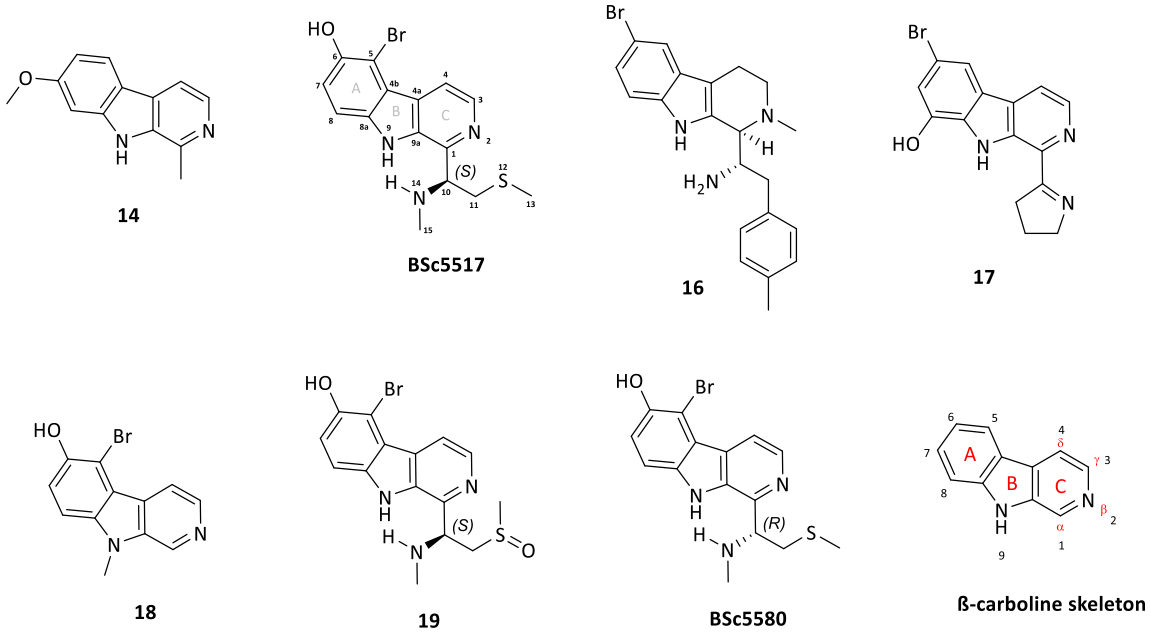

Figure 3: Chemical structure of isolated β-carboline compounds from natural sources: Harmine (**14**), Eudistomidin C (**BSc5517**), Eudistomidin B (**16**), Eudistomidin A (**17**), Eudistomidin D (**18**), Eudistomidin J (**19**)**,** (*R*)-5-bromo-1-(1-(methylamino)-2-(methylthio)ethyl)-9*H*-pyrido[3,4-β]indol-6-ol **(BSc5580)** and **β-carboline skeleton**.

Harmine (**14**) (**Figure 3**) is one of the simplest β-carbolines structurally and well-studied. It was among the first alkaloids isolated in the 19th century from the plant *Peganum harmala*. [30] Furthermore, it indicated various biological activities ranging from anti-inflammatory and antidiabetic to neuroprotective effects. [31-34] Harmine acts as a kinase inhibitor with an excellent specificity for dual-specificity tyrosine-phosphorylation-regulated kinase 1A (DYRK1A). [35] Intellectual developmental disorder, autosomal dominant, and DYRK1A-related intellectual disability syndrome are some diseases associated with DYRK1A. Moreover, **14** revealed inhibition of the monoamine oxidase A (MAO-A), which is a protein found on the outer mitochondrial membrane and is required for the metabolic degradation of monoamine neurotransmitters such as serotonin, melatonin, dopamine, adrenaline, and noradrenaline. [36]

Four pharmacologically active compounds named Eudistomidin C (**BSc5517**), Eudistomidin B (**16**), Eudistomidin A (**17**), and Eudistomidin D (**18**) were isolated from the Okinawan tunicate *Eudistoma glaucus* (**Figure 3**). [37, 38] **BSc5517**, **16**, and **18** revealed potent cytotoxicity against murine leukaemia L1210 (IC_{50} = 0.36, 3.4 and 2.4 µg/mL) and L5178Y (IC_{50} = 0.42, 3.1 and 1.8 µg/mL) cells, respectively. In addition, **16** activated rabbit heart muscle actomyosin ATPase

by 93% at 30 µM concentration, while **BSc5517** exhibited calmodulin antagonistic activity (IC_{50} = 30 µM), given that calmodulin antagonists were revealed in several tumour models to induce apoptosis and prevent tumour cell invasion and metastasis. [39] **16**, on the other hand, evoked Ca^{2+} release from the sarcoplasmic reticulum (SR) ten times stronger than caffeine, a well-known SR Ca^{2+}-inducer. [40] Eudistomidin J (**19**), on the other hand, is another related β-carboline natural compound isolated from the same Okinawan marine tunicate *Eudistoma glaucus*. As **BSc5517**, **19** possesses a *N*-methyl-2-(methylthio)ethan-1-amine moiety at the C-1 position of the β-carboline skeleton, making their structures unique. It is worth mentioning that **19** disclosed approximately potent cytotoxicity against murine leukaemia cells L1210 with an IC_{50} of 0.044 µg/mL. [41]

To sum up, β-carbolines were revealed to be an exciting class of compounds for various clinical applications due to their multiple physiological targets. Moreover, many β-carbolines act as inhibitors for different serine/threonine kinases, as the proliferation of murine leukaemia L1210 is believed to be correlated to the serine/threonine kinase CK2 terms casein kinase 2. Then, CK2 might presumably be a target for this class of compound and improving the yield via a total synthesis is crucial to conducting pharmacological studies and thoroughly investigating the kinase inhibitory activity.

1.4 Protein Kinase Structure and Function

The human kinome encodes around 500 protein kinases, and many more if splice variants must be considered. This equates to roughly 2% of the entire genome, demonstrating the family's importance in regulating biological activities. [42] The Human Genome Project identified about 2,000 human kinase genes, including over 500 protein kinases. [43] Protein kinases have been crucial to dissecting signal transduction pathways since their discovery in the early 1950s. They have been identified as essential players in practically all critical cellular functions, including growth, development, and homeostasis. [44] They carry out their biological processes by transferring gamma phosphate from ATP to tyrosine, threonine, or serine residues in the proteins they bind to. A protein kinase's N-terminus comprises multiple β-sheets, while the C-terminus comprises α-helices; these two sections are connected by a hinge chain (**Figures 4**, **5**). The ATP binding pocket is formed by a cleft between the two termini and the hinge region,

and most ATP-competitive inhibitors are intended for targeting this location (**Figure 4**). [45-47] Protein kinases were indicated to play a vital role in oncogenesis and tumour growth in the early 1980s, making them particularly appealing targets for anti-cancer therapy. [48, 49] Accordingly, subsequent studies facilitated by recently developed tools such as synthetic small molecule inhibitors, genetic modulation, RNAi technology, and bioinformatics disclosed that protein kinases play a role in nearly all human diseases, including cancer, diabetes, cardiovascular diseases, developmental diseases, neurological diseases, and infectious diseases. [43, 50]

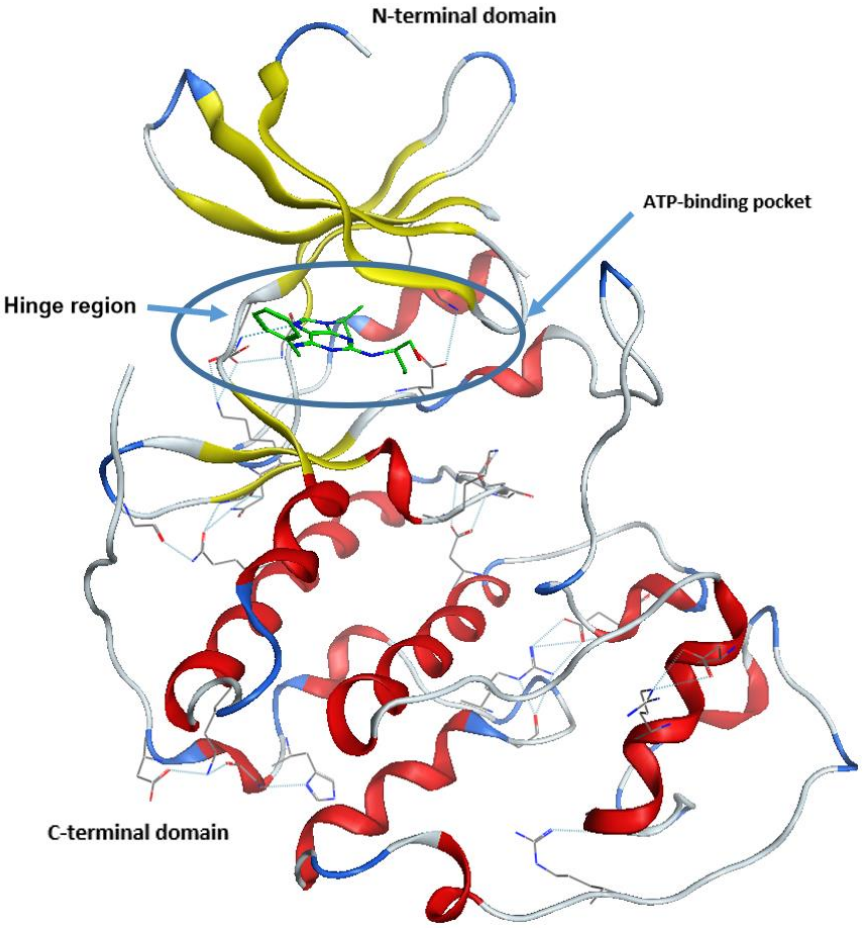

Figure 4: X-ray crystal structures of Human cyclin-dependent kinase 2 (CDK2) in complex with Roscovitine (PDB:2A4L). Image generated using the MOE Database Viewer functions. [51]

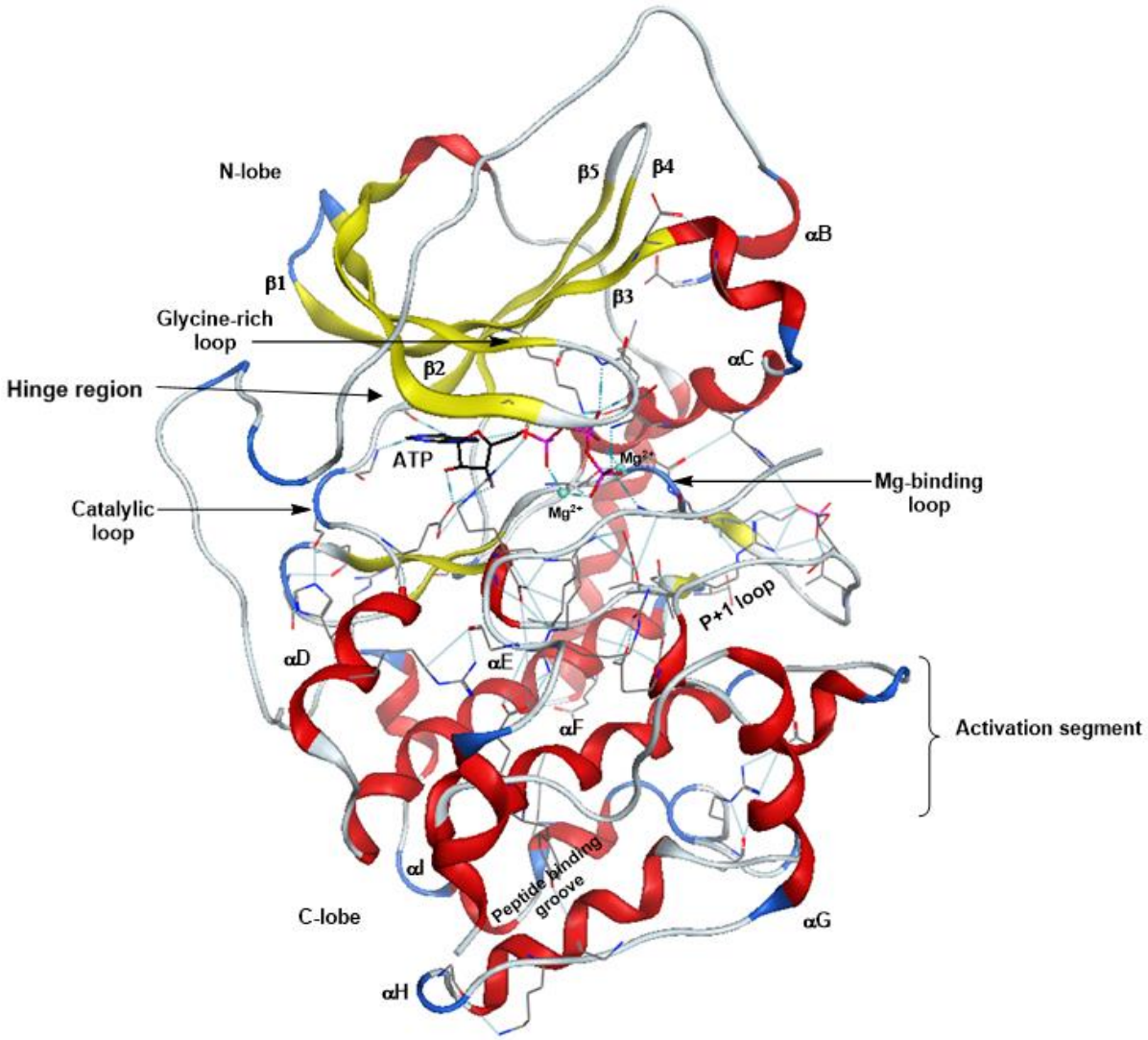

Figure 5: The conserved protein kinase core structure PDB code: 1ATP. Protein kinases have a distinctive bilobal fold. The N-terminal lobe (N-lobe) comprises five β strands (1 through 5) and a universally conserved αC-helix. The C-lobe is mainly helical. A deep cleft between the lobes is filled with an ATP molecule. The major, catalytically significant loops are also shown. The Gly-rich loop coordinates the ATP phosphates. The phosphates are linked to the C-helix by Lys72 from β3. The rigid helical core of the C-lobe is attached to the regulatory and catalytic machinery. The P+1 loop contains the P+1 residue of the peptide substrate docked to the peptide binding groove. Image generated using the MOE Database Viewer functions.

Numerous kinase structures have been identified since kinases are crucial in biology and disease phenotypes. The intrinsic architecture that facilitates the assembly of an active protein kinase was determined by comparing multiple protein kinase structures, especially the spatially conserved residues. It is an architecture that allows conserved hydrophobic components to connect distant regions of the enzyme. Furthermore, this architecture is entirely built in the

kinase's active conformation but disrupted in most inactive kinases. This complex regulatory machinery differentiates Eukaryotic Protein Kinase (EPKs) from Eukaryotic-like protein kinases (ELKs) as well as most metabolic enzymes (**Figure 6**).

EPKs are enzymes from a large family of proteins with a conserved catalytic core, whereas ELKs are a broad set of regulatory, signalling and biosynthetic enzymes previously thought to be exclusively eukaryotic proteins. Allosteric processes and post-translational changes might heavily regulate metabolic enzymes. They are not dynamic switches and are not often connected with the complex regulatory mechanisms that constitute EPKs. On top of that, EPKs have evolved not to efficiently turn over many products but rather to be transiently activated. That is why Local Spatial Pattern alignment (LSP) was created to compare any two structures quickly and find spatially conserved residues. [52, 53] This resulted in the discovery of spatially conserved hydrophobic patterns known as "spines," which explain how a protein kinase is formed into an active enzyme and disclose the internal architecture of the protein kinase core. [54]

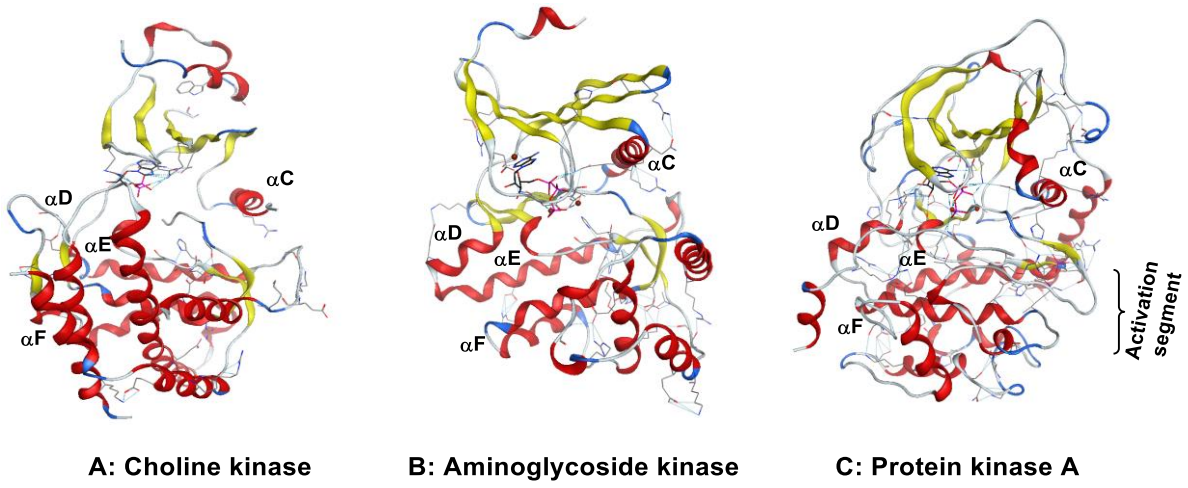

Figure 6: General structural differences between ELKs (Choline kinase and Aminoglycoside kinase; PDB codes 2CKP and 4EJ7, respectively) and EPKs (Protein kinase A; PDB code 4WB5). EPKs are represented by PKA (c) structural components conserved in all kinases (N-lobe and C-lobe shown in cartoon). Non-conserved helical C-terminal regions of the C-lobe are represented as helices. ELKs (a) and (b) possess multiple non-conserved helices that accommodate non-peptide substrates and are unique for each kinase. Another radical difference between EPKs and ELKs is a prolonged activation segment between the F-helix and the DFG motif. The most recent evolutionary feature developed by EPKs permits dynamic regulation of their activity in this segment. Image generated using the MOE Database Viewer functions.

The N-terminal and C-terminal lobe, two subdomains belonging to the preserved protein kinase domain of the EPK superfamily, are often connected by a short polypeptide chain, also known as the hinge region. The structurally significant C-helix is at least one globally conserved α-helical component of the N-terminal lobe, comprising a series of β-strands (**Figure 7**). Consequently, the C-helix, located at the interface of the subdomains, interacts with numerous different molecule components and acts as a dynamic regulatory element in the kinase molecule. [55] The predominantly α-helical C-lobe has a broader range of sizes, topologies, and sequences than its N-terminal counterpart but is typically larger. Furthermore, the diversity of the C-terminal subdomains, which are in charge of substrate binding, enables the accommodation of a wide variety of kinase substrates. [56]

Specific kinases include a C-terminal tail that wraps around the kinase's outside and interacts with hydrophobic regions of the N-lobe. [57] On the other hand, the ATP-binding site is situated in a cleft at the intersection of the two lobes. The backbone of the hinge region and the adenosine moiety of ATP typically form two hydrogen bonds, whereas the core of ATP interacts with the backbone of a glycine-rich phosphate-binding loop (P-loop) that connects the outermost N-terminal β-strands as outlined in **Figure 7**. [56]

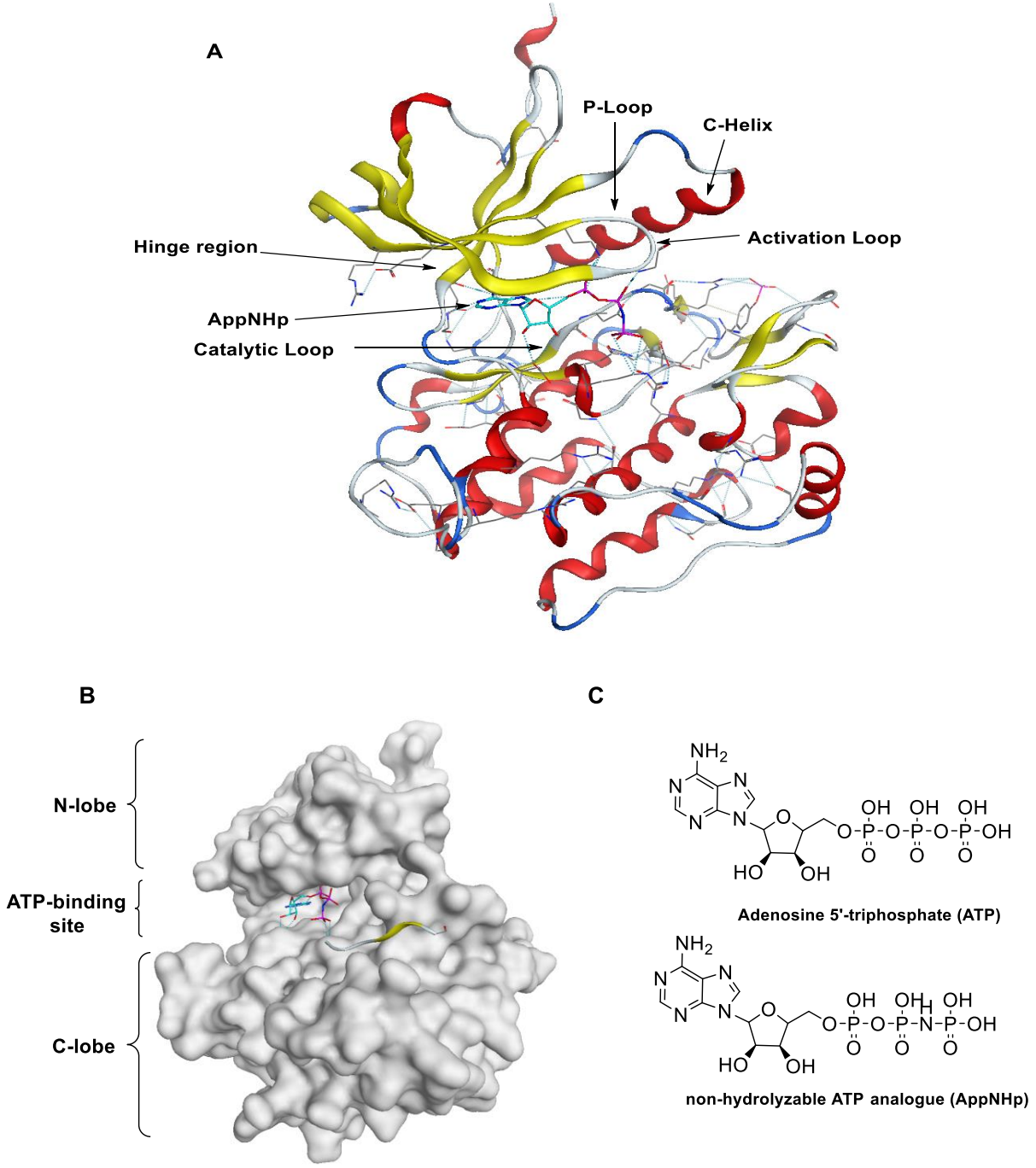

Figure 7: Typical eukaryotic protein kinase domain structure (the insulin receptor kinase domain crystal structure, with the PDB code: 1IR3). (A) Conserved structural elements of EPKs are displayed in the crystal structure of the phosphorylated insulin receptor kinase domain, featuring the C-helix, the P-loop, the hinge region, the activation loop, the catalytic loop and the ATP analogue (AppNHp). (B) Crystal structure-based model protein surface of the activated tyrosine kinase domain of the insulin receptor in complex with the peptide substrate. β, γ non-hydrolyzable ATP analogue (AppNHp), showing the N-terminal lobe, the ATP-binding site and the C-terminal lobe. (C) The chemical structures of ATP and the β, γ non-hydrolyzable AppNHp counterpart. Images generated using MOE software.

An essential amino acid (aa) residue, usually referred to as the gatekeeper (GK), is located immediately at the N-terminus of the hinge region binding sequence (**Figure 8**). This amino acid is essential in designing small-molecule kinase inhibitors as it significantly influences the size of the ATP binding site. The size of the residue varies from kinase to kinase, but it is almost always a bulky residue. [58]

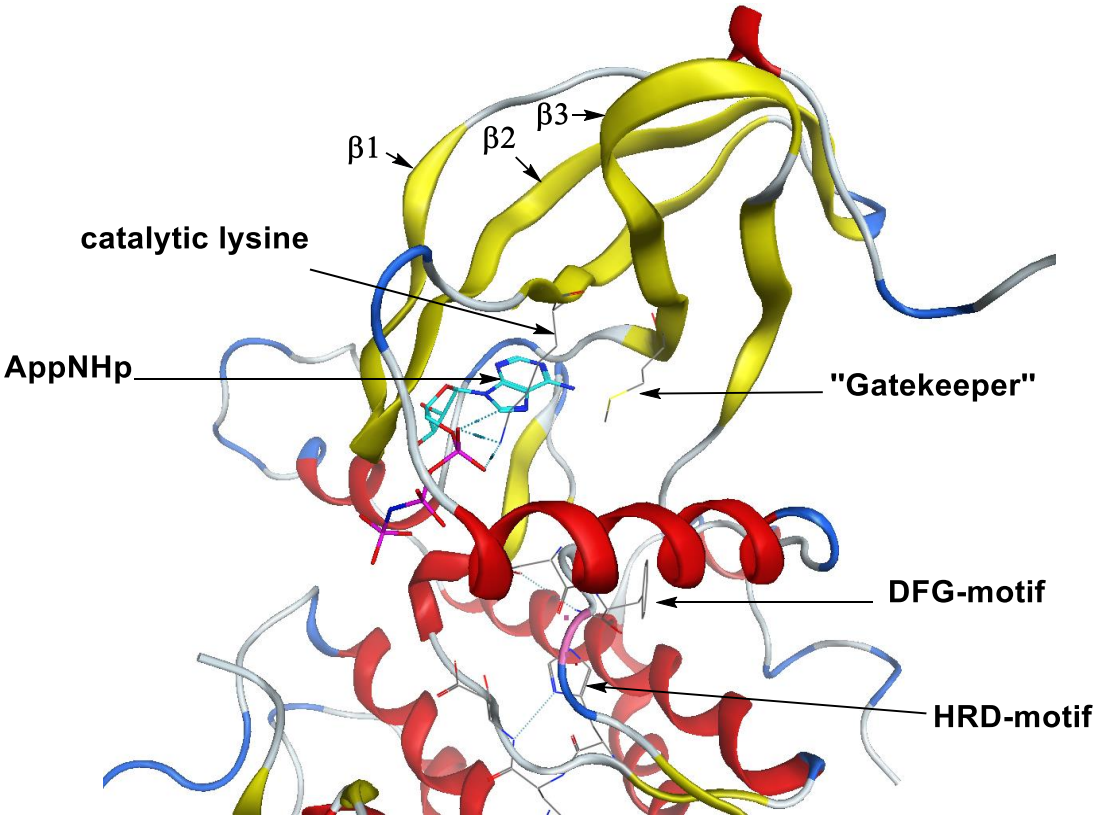

Figure 8: Key amino acid residues and their interactions in the active core domain of the kinase (PDB code: 1IR3). The shape and the size of the ATP-binding site are strongly influenced by the ‘’Gatekeeper’’. In the active conformation, the DFG motif (in red) aspartate coordinates the divalent ATP-bound magnesium. The catalytic aspartate in the HRD motif removes the proton from the substrate's hydroxyl group. The catalytic lysine emanates from the β-strand 3 (β3) and interacts with the α- and β-phosphates belonging to the ATP analogue (AppNHp). Images were generated using MOE software.

Also, the glycine-rich loop, commonly known as the P-loop, directs where the phosphates of ATP are located. It has a typical GxGxxG sequence, with the polypeptide backbone coordinating the γ-phosphate and small glycine side chains, providing additional flexibility. [59] In some kinases, the catalytic lysine that links with the α- and β-phosphates of ATP is located in close C-terminal proximity to the P-loop on β-strand 2. However, for most kinases, the catalytic lysine comes from β-strand 3. [60] The catalytic loop includes the catalytic aspartate, which withdraws the proton from the hydroxyl group that is owned by the substrate amino acid adjacent to the ATP binding site from the C-lobe.

While some protein kinases can use unbound ATP as a phosphoryl donor substrate, most rely on Mg-bound ATP and need at least one other divalent metal (Mg^{2+} or Mn^{2+}) for catalysis. (Because) the high affinity of magnesium ions for ATP means that only a low concentration of non-Mg-bound ATP remains in the cells. [61]

It is worth mentioning that the EPKs have a flexible activation loop close to their catalytic loop, which is relatively static (**Figure 9**). Most of them are activated by site-specific phosphorylation of activation loop residues, which drastically alter the activation loop's conformation by antagonising the arginine's positive charge in the conserved catalytic loop HRD motif. [62] This structural plasticity is critical for regulating kinase and enzymatic activity, and different conformations have been found to reflect other functional states. In addition, two crucial structural features of the active kinase conformation are:

- (a) The orientation of the conserved DFG motif aspartate towards the active site (**Figure 9**).
- (b) A salt bridge between the conserved C-helical glutamate and the catalytic lysine that results from the inward rotation of the C-helix (‘’C-helix in’’) (**Figure 9**).

The total activity of a kinase is determined by the relative stability of its active and inactive conformations, which is susceptible to modification by regulatory proteins, ligands, post-translational modifications, and substrates. [63, 64]

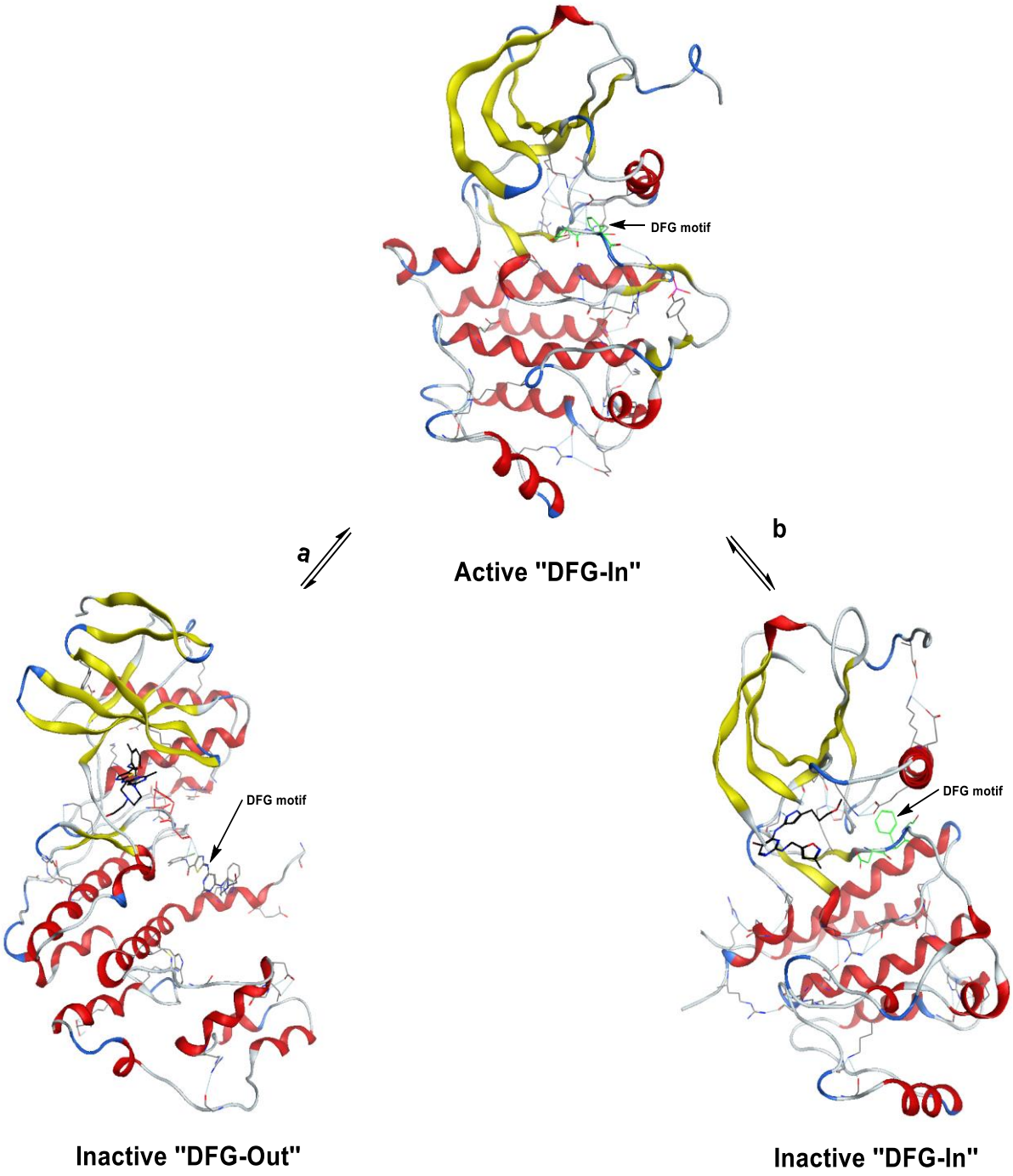

Figure 9: Diagram showing the conformational differences between the Active "DFG-In" (PDB code 3LCK), inactive "DFG-Out" (PDB code 3OHT), and inactive "DFG-In" (PDB code 4F64) of the conformations of EPKs (Eukaryotic protein kinases). (**a**) A 180° rotation of the DFG motif leads to the inactive "DFG-out" conformation, in which the DFG aspartate can no longer co-ordinate the Mg-bound ATP. (**b**) The outward rotation of the C-helix results in the disruption of the salt bridge connecting the conserved glutamate of the C-helix and the catalytic lysine, leading to the inactive "DFG-In" conformation. [63, 64] Image generated using the MOE Database Viewer functions.

Kinases are widely involved in signal transduction and regulation of complex cellular processes, mainly by phosphorylation. Phosphorylation of the kinases can enhance or inhibit their activity, and their ability to interact with other molecules can be modulated. However, dysregulation of this process can lead to diseases and organ dysfunction. This dysregulation has paved the way to study protein kinases as potential drug targets. The following section briefly elaborates on protein kinases as drug targets.

1.4.1 Protein Kinases as Drug Targets

Protein kinases are involved in various illnesses, including immunodeficiencies, cancers and endocrine disorders. Moreover, they are gaining importance in the discovery of new medicines as they are primarily responsible for mediating cellular signal transduction and are critical in regulating most facets of cell life. [65-66]

Approximately one-third of the human proteome is estimated to contain covalently bound phosphate, and dysregulation of the phosphorylation and mutations in protein kinases are known to be central to many human diseases. [67] As a result, kinases are a primary drug target class, with more than 50 approved drugs by the US Food and Drug Administration abbreviated FDA and more than 200 other international non-proprietary names (INNs) in clinical development. [68] Since the 1930s, kinase activity has been altered for medicinal purposes, and tailored kinase inhibitors were not developed through focused medicinal chemistry until the 1980s. [69]

In 1995, Fasudil (**21**) (**Figure 10**), the first small molecule kinase inhibitor, gave the go-ahead for clinical usage. It was subsequently licensed in Japan to treat cerebral vasospasms, and many years later, Sirolimus (**22**), a natural product kinase inhibitor, was developed to target the mechanism of rapamycin (mTOR) to prevent organ transplant rejection. [70, 71] Imatinib (**23**), a first-in-class tyrosine kinase inhibitor, was approved in 2001 for the treatment of chronic myeloic leukaemia (CML) and led to a shift in the development of kinase inhibitors and antineoplastic chemotherapy. This breakthrough drug changed the chemotherapeutic paradigm from highly toxic and non-specific anti-cancer drugs to a targeted therapeutic approach. It selectively inhibited the single oncogenic driver of CML, the breakpoint cluster region-Abelson kinase (BCR/Abl).

The emergence of imatinib, the first approved small molecule inhibitor to elicit a distinct inactive kinase conformation in addition to ATP displacement, has had a lasting and powerful impact on the field. [72] Since then, kinase drugs have redirected their focus from non-receptor tyrosine kinases to other groups of protein kinases, such as receptor tyrosine kinases, serine/threonine kinases, lipid kinases, and carbohydrate kinases.

Whereas most kinase drug development is still focused on cancer, new therapeutic applications are emerging. These include inflammation, autoimmunity, tropical diseases and neurodegenerative diseases. [73]

In light of the coronavirus crisis, protein kinase inhibitors have come to the fore to repurpose approved drugs for their antiviral potential because of their reported activity against key kinases involved in viral entry, metabolism and replication. [74]

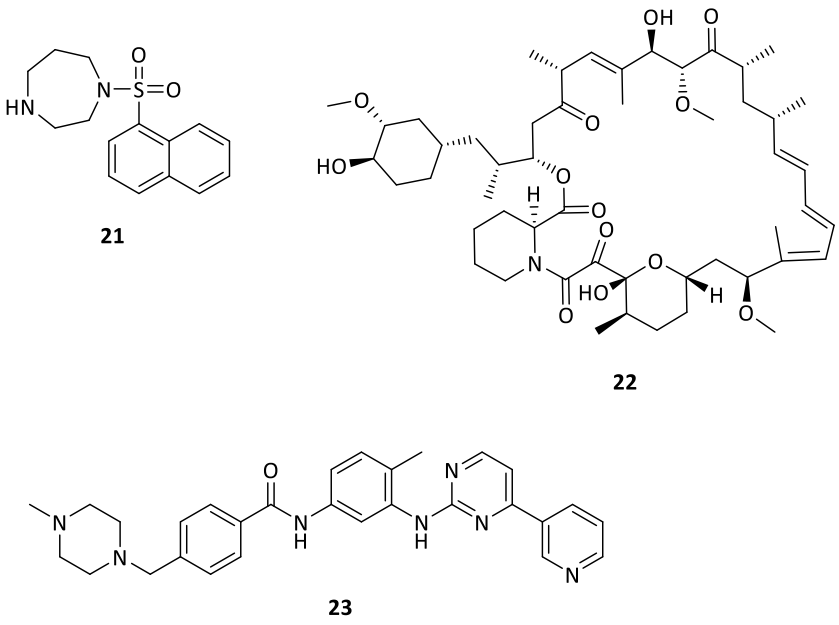

Figure 10: Small molecule kinase inhibitor drugs: Fasudil (**21**), Sirolimus (**22**), Imatinib (**23**).

1.4.2 Strategies for Small Molecule Inhibitors of Protein Kinases

Several strategies for targeting protein kinase activity have been developed over the years. Since the vast majority of kinases are intracellular and cannot be targeted by non-cell-permeable monoclonal antibodies (mAbs), membrane-permeable small molecule inhibitors that closely bind either an allosteric binding site or the active site are commonly utilized to modify protein kinase activity. [75] For small molecules, the enzyme-bound antagonist complex structure is frequently used as a basis for classification. This follows a system first introduced by Dar and Shokat and later extended by others. [76, 77]

Inhibitors which bind to the ATP-binding pocket in any active kinase conformation are categorised as Type I inhibitors (example of the approved drug: Bosutinib). Inhibitors binding to an inactive conformation as Type II inhibitors (example of the approved drug: Imatinib) and allosteric inhibitors not competing with ATP binding as Type III inhibitors (example of the approved drug: Cobimetinib). Current research has resulted in various subtypes that further define the structure of kinase inhibitor drug-enzyme complexes. It is widely accepted that only inhibitors that bind to an active conformation with the DFG-Asp in, the αC helix in and the regulatory spine in its active linear configuration belong to the Type I class. Inhibitors targeting the "DFG in" conformation but reaching into the ATP back cavity resulting from the outward rotation of the C-helix ("αC-helix out") were defined as the Type $I^{1/2}$ (example of the approved drug: Lapatinib) subclass by Zucotto *et al.* (**Figures 11** and **12**). [78]

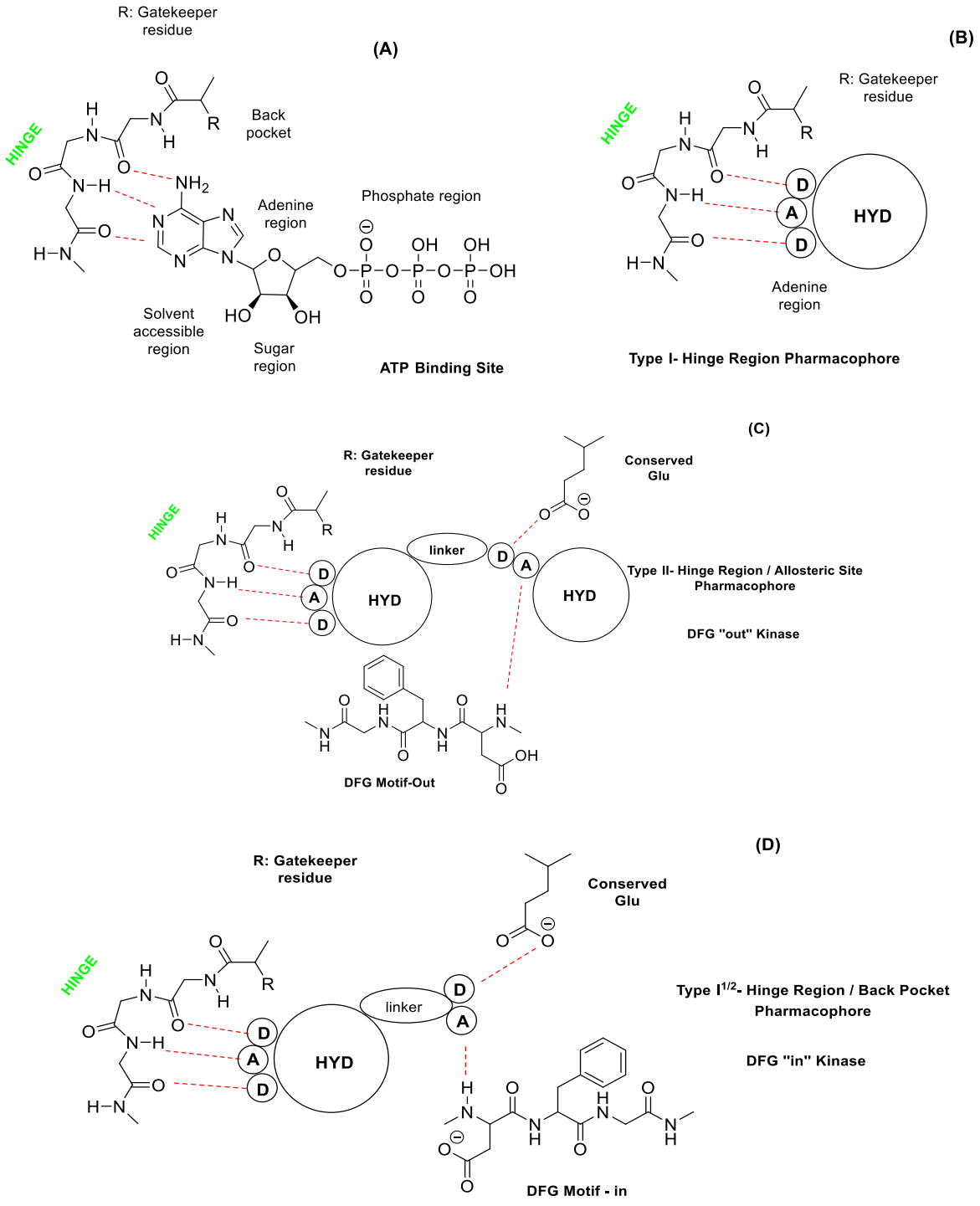

Figure 11: (A) Regions of the ATP-binding site and ATP interacting with the hinge residues. Orange dashed lines represent hydrogen bonds. (B) Pharmacophore of a Type I kinase inhibitor showing the potential hydrogen bonds around the hinge region. (C) Pharmacophore of a type II kinase inhibitor representing the interactions with the hinge region and the allosteric site that is present in the DFG "out" conformation. (D) Type $I^{1/2}$ pharmacophore showing potential interactions at the hinge and in the back cavity. Hydrogen bond donors are indicated by the circles labelled D, and hydrogen bond acceptors by the circles labelled A. The larger circles labelled HYD show the moieties, which are hydrophobic in nature, that bind to the adenine ring region and the allosteric site. [78]

A novel group of inhibitors, known as allosteric protein kinase inhibitors, has been developed in recent years. Allosteric binding sites are their target, with no direct interaction with the ATP-binding pocket hinge region. Type III allosteric kinase inhibitors (example of the approved drug: Cobimetinib) bind to an allosteric binding site directly proximal to the ATP-binding pocket, while Type IV inhibitors (example of the approved drug: Everolimus) bind to a remote allosteric location in the kinase domain (**Figure 12**). In addition, pure allosteric type IV inhibitors are generally characterised by reduced potency compared to active site-directed inhibitors. This is most likely because they attach to much flatter protein-protein interaction areas, which are nonetheless tough to be inhibited upon binding of small molecule inhibitors. [79]

Type V inhibitors are bivalent kinase inhibitors that simultaneously target two sites (**Figure 12**). Type V inhibitors can be generated by linking any combination of the previously described types I-IV through an optimised linker. Theoretically, it would be possible to increase the affinity of type IV compounds while maintaining their selectivity by combining an allosteric inhibitor with a site-directed inhibitor (**Figure 12**). [79]

Covalent kinase inhibitors, commonly known as Type VI inhibitors (Afatinib), have recently witnessed a resurgence in drug research. Small molecules are designed in covalent inhibition to undergo a bond-formation event (**Figure 12**). It happens after being suitably orientated under equilibrium binding conditions via conventional non-covalent molecular interactions. The binding event can result in a covalent bond that is durable enough to be irreversible within the half-life of the target protein. This theoretically allows complete target inactivation that reversible inhibition cannot accomplish. [79]

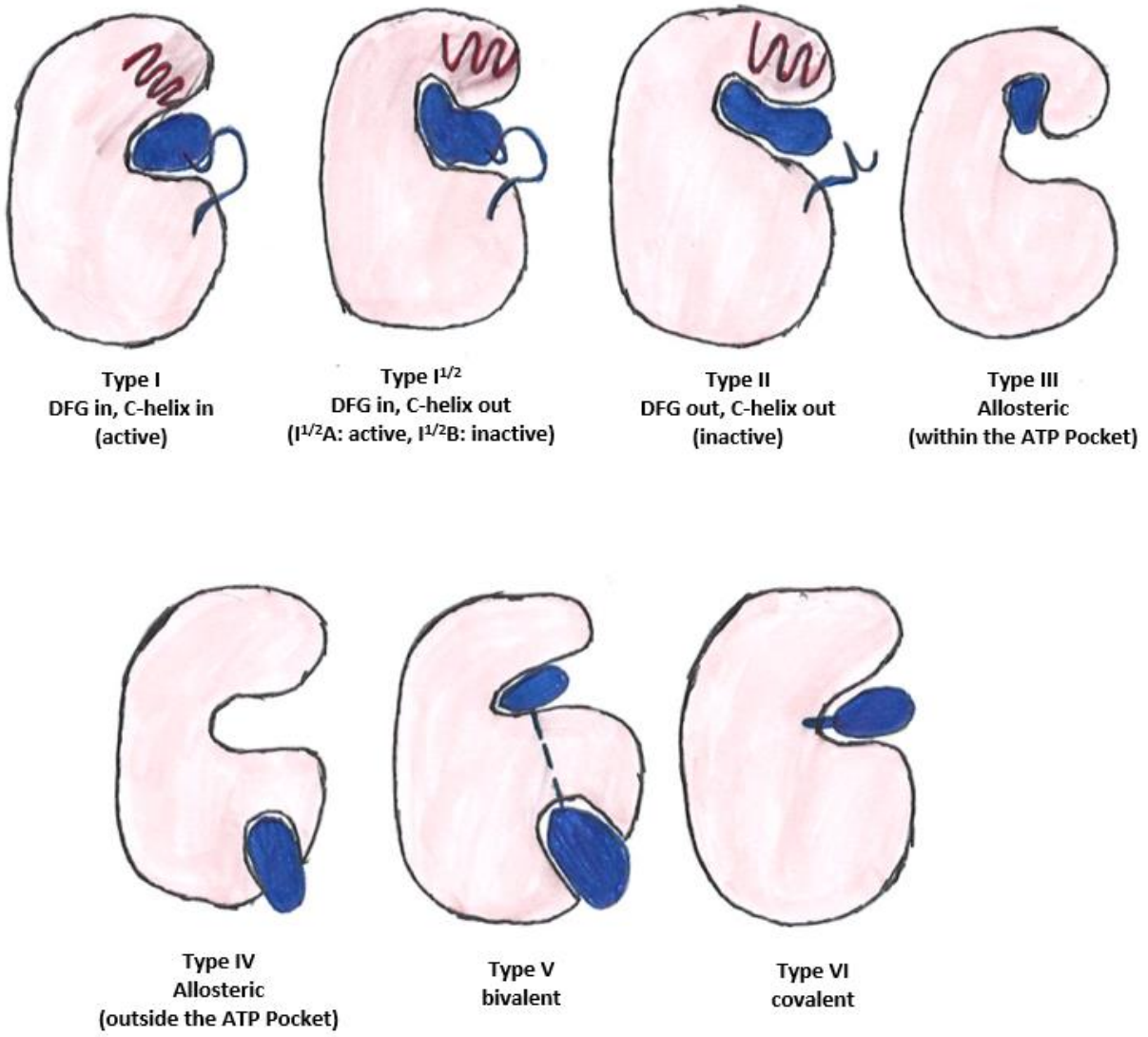

Figure 12: Small molecule protein kinase inhibitor classification. The protein kinase is shown in pink, the inhibitor in blue, and the C-helix in blue. [80]

Given the importance of natural products in drug discovery and development, investigating their potential as kinase inhibitors is of significant interest. The following chapter reviews and examines some naturally occurring compounds used as kinase inhibitors.

1.5 Natural Products as Kinase Inhibitors

NPs were among the first to be discovered as protein kinase inhibitors, and they tremendously aided basic and translational research because they target a diverse set of kinases from all kinome subfamilies. [42, 65] Because small molecule NPs are generated and interact with proteins in their natural environment, some are recognized as signalling molecules in many life forms and have been creatively repurposed for human health benefits. Accordingly, several MNPs have been utilized as lead compounds in pharmaceutical settings, offering a rich resource for discovering next-generation kinase inhibitors. These inhibitors may target allosteric regions away from the ATP-binding sites [81-84] or maintain inactive conformations to prevent specific kinases from functioning. [85-88] This is particularly important for treating cancer and bacterial infections. Small molecule kinase inhibitors such as Fasudil (**21**) have been effective tools for understanding kinase-mediated signal transduction pathways, and more than ten of them have been approved for therapeutic use. [89]

Many natural sources, such as marine sponges, bacteria, fungi and plants, provide NPs with protein kinase inhibitory activity. Furthermore, these NPs target a wide range of protein kinases, including all subfamilies of the known kinome. The subfamilies of the kinome comprise the tyrosine kinase (TK) family, the homologues of the yeast sterile 7, 11 and 20 kinases (STE), the casein kinase 1 family (CK1), the PKA, PKC and PKG kinase families (AGC), the tyrosine kinase-like (TKL) family, the CDK, MAPK, GSK2 and CLK kinase families (CMGC), the calcium/calmodulin-dependent kinase family (CAMK) and other. [46]

NPs usually range from single-digit nanomolar to submillimolar levels of inhibition of kinases. Besides, the binding mechanisms range from ATP-competitive to allosteric, with reversible or irreversible enzymatic kinetics. NPs with suitable core scaffolds may provide excellent medicinal chemistry opportunities, significantly increase kinase inhibitors with structural diversity and provide new clinical candidates for unmet medical needs. As kinase deregulation is essential in many disease states, protein kinases are validated drug targets in several therapeutic areas.

Many protein kinase inhibitors being investigated are small molecules derived from NPs or their derivatives. In the same way, numerous marine-derived natural compounds have been discovered to exhibit significant kinase inhibitory activity or attractive pharmacophores for

further development, including bacteria, cyanobacteria, fungi, mammals, algae, soft corals, sponges, and others. [46]

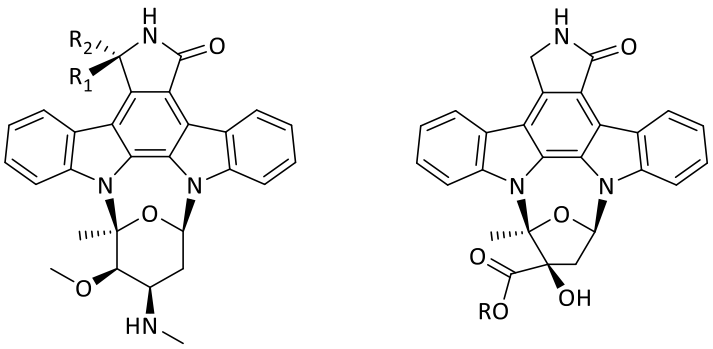

24 $R_1 = R_2 = H$
25: $R_1 = OH$, $R_2 = H$

26: $R = CH_3$
27: R = H

Figure: **13**. Staurosporine (**24**) and analogues UCN-01 (**25**) and K252a/b (**26**).

Staurosporine (**24**), a naturally produced indolocarbazole microbial alkaloid, was extracted in the late 1970s as an anti-fungal reagent from the soil bacterium *Streptomyces staurosporeus* AM-2282^T (**Figure 13**). [90] Over 50 indolocarbazole analogues, including UCN-01 (**25**), K252a (**26**) and K252b (**27**), were later isolated from a range of organisms. Furthermore, **24**, **26** and **27** were revealed to be potent protein kinase C (PKC) inhibitors with an IC_{50} of 2.7 nM, and at that time, much attention was focused on this range of NPs. [91, 92] Subsequent detailed studies indicated that staurosporine and its derivatives are indeed nanomolar IC_{50} pankinome inhibitors (*e.g.*, c-APK and CDK2) to the micromolar IC_{50} range (*e.g.*, CK1/2, CSK and MAPK). [93, 94] Due to its kinome-wide inhibitory activity, Staurosporine is used as a control in many kinase activity assays.

Furthermore, the first crystal structure of Staurosporine with CDK2 kinase solved revealed reversible ATP competitive binding mode (**Figure 14**). The crystal structure of Staurosporine, forming a binary complex with CDK2, a cell-cycle kinase, contributes to the evidence of the inhibitor's binding mechanism. The findings also shed light on the source of selectivity in similar drugs. [95] Additionally, the discovery and development of Staurosporine piqued pharmaceutical companies' interest in screening NPs and synthetic derivatives as selective

protein kinase inhibitors for oncology applications. This further contributed to protein kinases becoming one of the most crucial drug discovery targets in the last 20 years. [96]

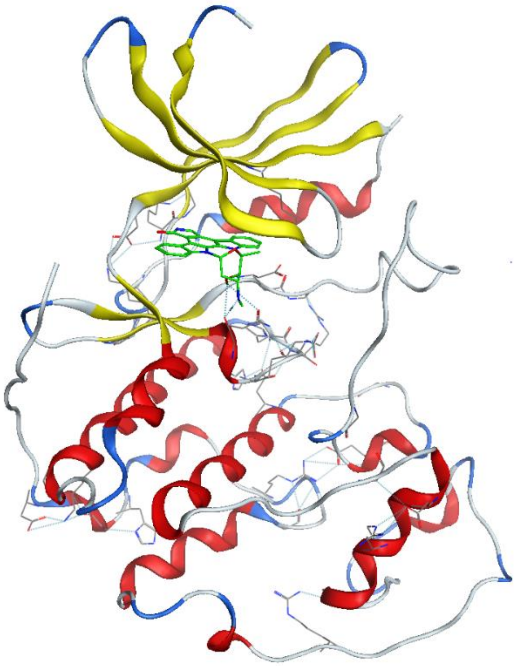

Figure 14: Binding of Staurosporine into CDK2 (PDB: 4ERW). Image generated using UCSF Chimera, production version 1.12 (build 41623). [95]

Most kinase inhibitor medications authorized to date are ATP-competitive inhibitors with a variety of practical off-target risks. In mammalian signalling pathways, four primary groups of kinases occur, which may be roughly divided by substrate specificity: serine/threonine kinases, tyrosine kinases, dual kinases (Ser/Thr and Tyr), and lipid kinases. Protein kinases share a common mechanism, as outlined in **Scheme 1**, in which a phosphate group from ATP is transferred to the free hydroxy of serine, threonine, or tyrosine on the targeted protein. Protein phosphatases, on the other hand, remove a phosphate group from the phosphorylated amino acids, effectively reversing the effect. [97] This mechanism is the same, regardless of the type of inhibitor involved or the origin of the inhibitor.

Regarding kinase research, various marine-derived kinase inhibitors have emerged from multiple sources and targeted a variety of protein kinases (**Figure 15**). [98]

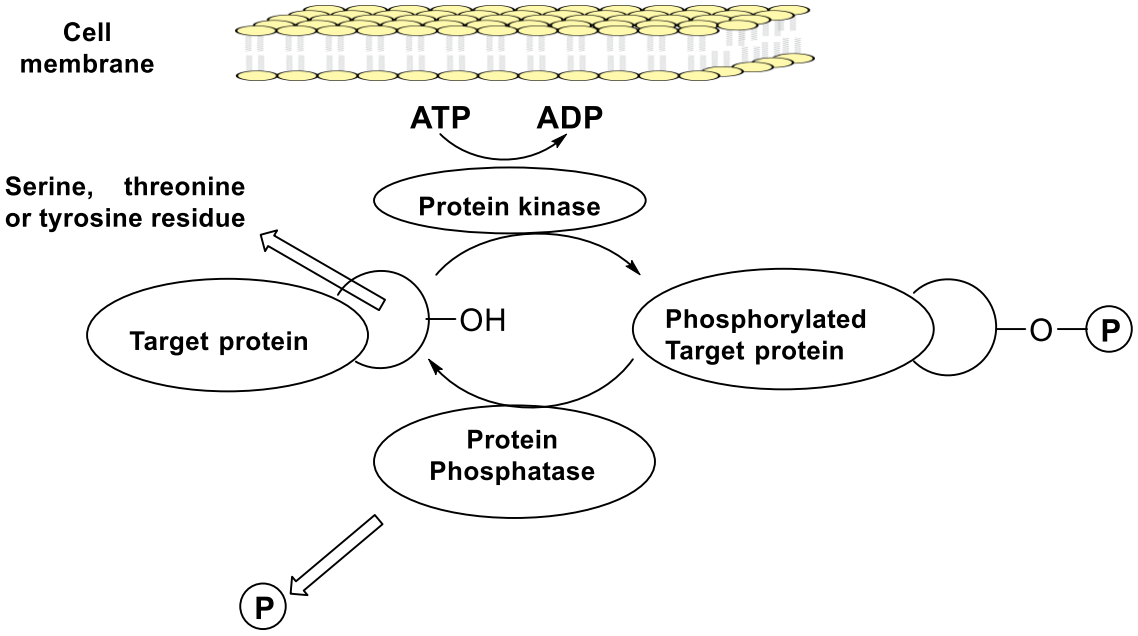

Scheme 1: Catalytic pattern for protein kinase's phosphorylation.

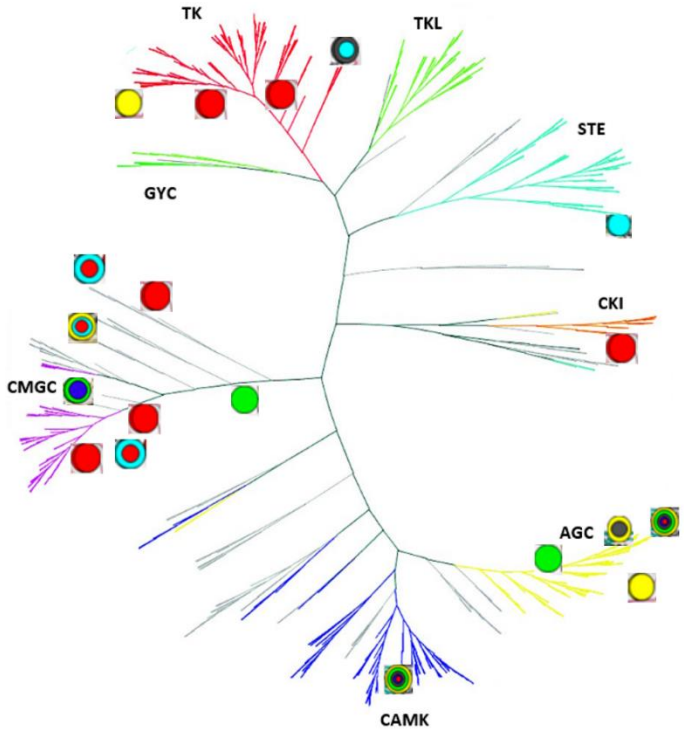

Figure 15: Availability of several marine kinase inhibitors with activity on the human protein kinase family phylogenetic tree. Colour codes indicate the producing or source organisms. Red: Marine sponges, Yellow: Marine bacteria. Green: marine fungi, Dark blue: marine algae and Light blue: marine animals. [98]

1.5.1 Depsipeptides as Kinase Inhibitors

The investigations carried out on depsipeptides as kinase inhibitors revealed high efficacy. [99] As an example, the naturally occurring depsipeptide named Romidepsin FK228 (**28**) is a potent depsipeptide Histone deacetylase (HDAC) inhibitor approved by the US FDA to cure cutaneous and peripheral T-cell lymphoma (**Figure 16**). **28**, and its synthetic analogues FK-A11 (**29**) and FK-A3 (**30**) were previously reported to exert dual HDAC/Phosphoinositide 3-kinase (PI3K) inhibitory activity. Indeed, **29** was identified as the most potent analogue and its biochemical, biological and structural properties as a dual HDAC/PI3K were reported. [99] Furthermore, the findings indicate that **28** can promote growth arrest and apoptosis in a diverse assortment of human cancer cells through mechanisms that cannot be solely attributed to histone acetylation. [99] Incubation of Non-Small Cell Lung Cancer (NSCLC) cells expressing wild-type or mutant p53 with **28** resulted in altered expression of cyclin A, cyclin E, p21, and reduced expression of mutant, but not the wild-type p53. The cells incubated with **28** were also depleted of the ErbB1, ErbB2 and Raf-1 proteins and indicated a lower level of ERK1/2 activity. **28** also revealed inhibition of mutant p53 and Raf-1 binding to Hsp90; this inhibition was associated with Heat shock protein 90 (Hsp90) acetylation. Thus, the ability of **28** to reduce signalling through pathways involving Raf-1 and ERK may contribute to the efficacy and specificity of this novel anti-tumour agent.[100]

In 2015, the depsipeptide Alternaramide (**31**) was isolated from the marine fungus *Alternaria sp.* SF-5016, as reported by Wonmin Ko *et al*. (**Figure 16**). Confirmed by Western blotting, **31** suppressed the development of p-JNK and p-p38 MAPK, implying that it might effectively cure various acute, systemic, and neurological inflammatory illnesses. [101] Furthermore, Serrill *et al*. discovered that Coibamide A (**32**) (originally isolated from the marine cyanobacterium *Leptolyngbya sp*.) reduced VEGFA/VEGFR2 expression in mice and revealed anti-cancer activity against glioblastoma xenografts. [102, 103]

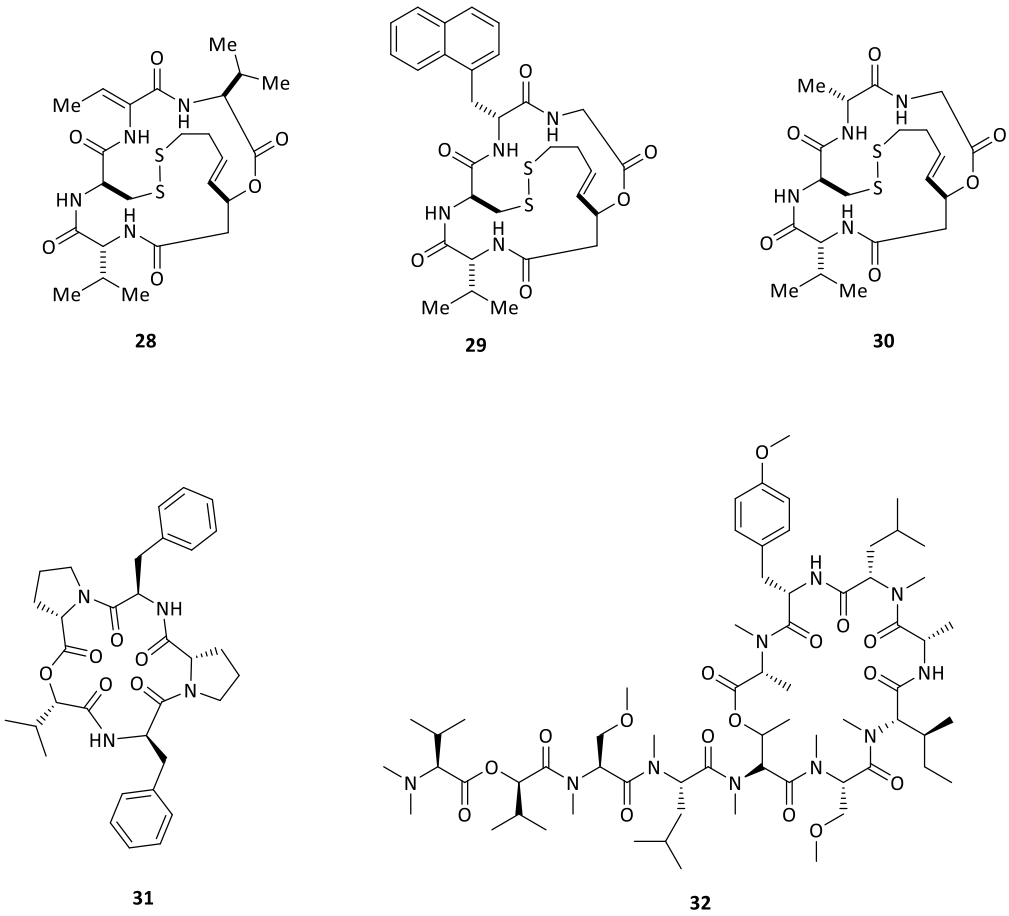

Figure 16: Depsipeptides NPs: Romidepsin FK228 (**28**), Romidepsin analogues FK-A11 (**29**) and FK-A3 (**30**), Alternaramide (**31**) and Coibamide A (**32**).

1.5.2 β-Carboline based Kinase Inhibitors

β-Carbolines have multiple physiological targets, making them an exciting compound class for various clinical applications. [104] Harmine (**14**), found in *Peganum harmala*, is a high-affinity inhibitor of DYRK1A (IC_{50} = 33-80 nM) and one of the structurally simplest active β-carbolines (**Figure 3**). One of its drawbacks, however, is the inhibition of MAO-A at a high potency level with an IC_{50} of 107 nM. [105] **14** indicated to be a potent and selective inhibitor of cyclin-dependent kinases (CDKs), proving that the aromaticity of the tricyclic ring and the position of substituents are essential for inhibitory activity. [106] Using time-resolved fluorescence resonance energy transfer (TR-FRET), Cuny *et al*. demonstrated that **14** is a potent haspin kinase inhibitor (IC_{50} = 0.59 μM). [107] Besides, Harmine derivatives were revealed to be potent inhibitors of GSK-3 (glycogen synthase kinase 3) and DYRK1A (dual-specificity tyrosine phosphorylation-regulated kinase 1A), both implicated in tau pathology. [108] Given that MAO-A inhibition can lead to a longer half-life of psychoactive drugs, **14** is utilized to formulate psychoactive medications. [109]

Different new harmine analogues were designed by Schmidt *et al*. to develop a novel DYRK1A inhibitor without MAO-A inhibitory activity. [105] Apart from this, AnnH31 (**33**) and AnnH75 (**34**) indicated potent inhibition of DYRK1A (IC_{50} = 81 nM and 181 nM), but **33** inhibited MAO-A with an IC50 of 3.2 μM, resulting in a 40-fold selectivity for DYRK1A, while **34** revealed almost no inhibition of MAO-A (IC_{50} > 10.000 nM) (**Figure 17**). [105] Liu *et al*. developed β-carbolines ZDWX-23 (**35**) and ZDWX-25 (**36**), both exhibited potent GSK-3β inhibitory activity (IC_{50} = 6.78 μM and 7.1 nM, respectively). Although **36** indicated lower IC_{50} for GSK-3β, its inhibition of acetylcholinesterase (AChE) (IC_{50} > 20 μM) was significantly higher compared to **35** (IC_{50} = 0.27 μM). [110, 111]

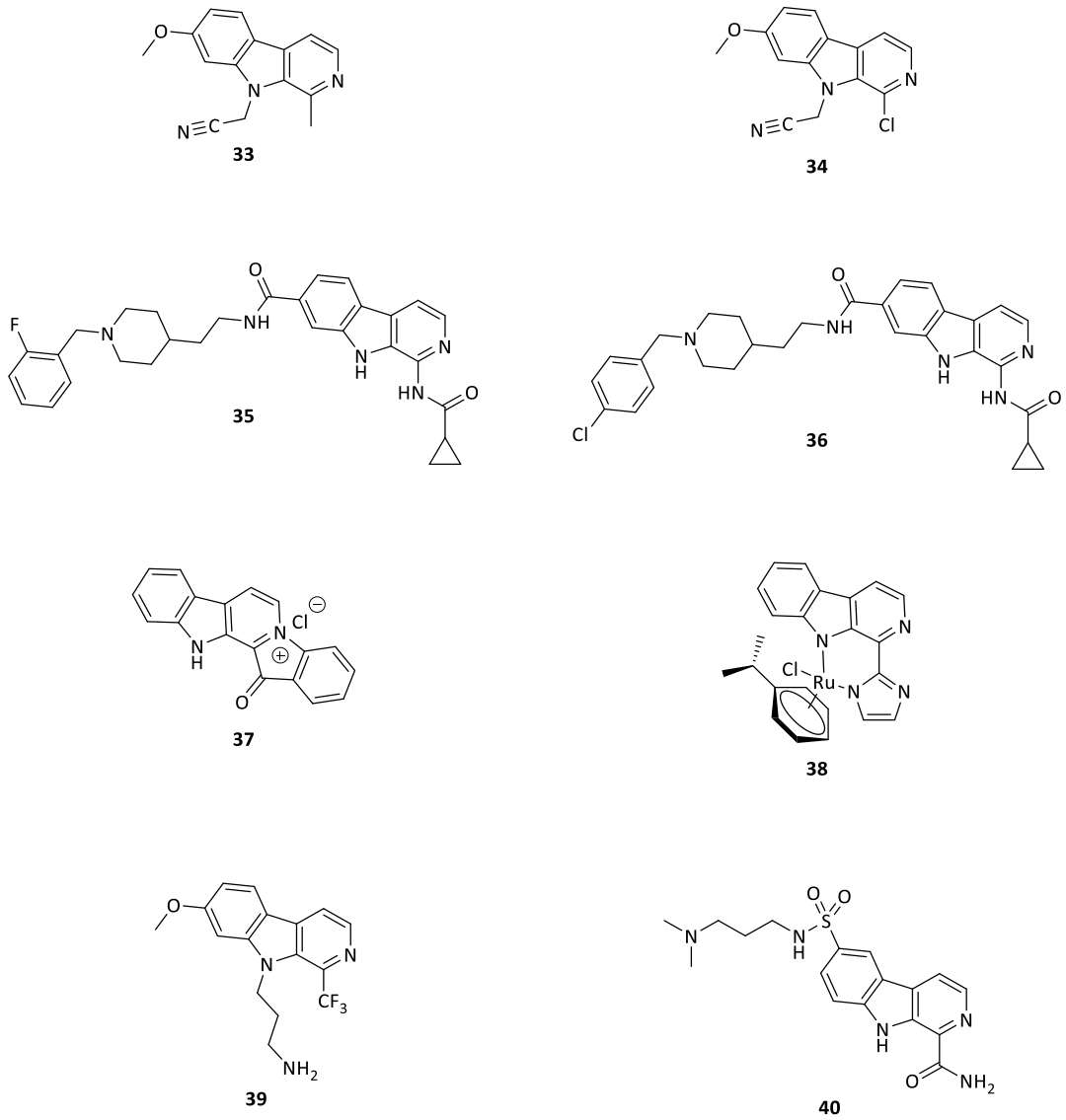

Figure 17: β-carbolines kinases inhibitors: AnnH31 (**33**), AnnH75 (**34**), ZDWX-23 (**35**) and ZDWX-25 (**36**), Fascaplysin (**37**), Ru^{II}-arene-β-carboline complex (**38**), trifluoromethyl-harmine derivative (**39**) and sulfonamide β-carboline (**40**).

Cyclin-dependent kinases (CDKs) are linked to the family of serine/threonine kinases and are important cell cycle regulators through specific interactions with cyclins as regulatory activation partners. Various diseases, including types of cancer, are associated with cell cycle deregulation, leading to uncontrolled cell proliferation. [112, 113] By inhibiting CDKs, it offers avenues of therapeutic targeting. [112] The β-carboline natural product Fascaplysin (**37**),

originally isolated from the sponge *Fascaplynosis bergquist sp*., indicated excellent specific CDK4/cyclin D1 inhibition with an IC_{50} value of 0.55 μM. [113] It is known that the cyclin D-CDK4/6-INK4-RB pathway plays a crucial role in the replication and cell division. [114] It has been disclosed that selective inhibition of CDK4 indicated novel pathways in tumour therapy. [111] Several different Ru^{II}-arene complexes with bidentate β-carboline ligands were studied by He *et al*. and demonstrated CDK1 inhibitory activity, of which Ru^{II}-arene-β-carboline complex (**38**) revealed the highest activity (IC_{50} = 0.90 μM). [96] Gregory *et al*. also reported the inhibitory activity of **14** against Haspin kinase, and using structure-activity relationships, trifluoromethyl-harmine derivative (**39**) exhibited even higher inhibitory activity (IC_{50} = 0.10 μM). [115] Different sulfonamide β-carboline inhibitors were further investigated for the inhibitory activity of β-Raf, and sulfonamide β-carboline (**40**) was the most active (IC_{50} = 1.62 μM). [108]

For this doctoral thesis, the β-carboline targeted for total synthesis has been Eudistomidin C (**BSc5517**). Considering that murine leukaemia L1210 proliferation is hypothetically associated with the serine/threonine kinase casein kinase 2 (CK2), its overexpression results in tumorigenesis, and inhibition induces cell apoptosis. [50], [116]

As several β-carbolines operate as inhibitors of various serine/threonine kinases, CK2 might be a target for **BSc5517** and structurally related β-carbolines. Therefore, increasing the yield of **BSc5517** via semisynthesis or total synthesis is critical to conducting in-depth pharmacological experiments and extensively studying its kinase inhibitory activity.

Several techniques exist for isolating and characterizing NPs from plants, endophytes, and marine organisms. [92] However, extracting these NPs from natural sources necessitates massive

harvesting, which is associated with technical issues and causes enormous damage to the ecosystem. [117] Furthermore, obtaining these compounds has not always been obvious because of the challenges encountered, the risks of infections from microorganisms during their extraction process, and the low isolation yields. The main issue is the quantity of isolated samples. Most of the time, only a microscale quantity of secondary metabolites can be obtained, which is, in most circumstances, insufficient for even spectroscopic characterizations. Furthermore, the cultivation of the extract of these NPs is rarely successful. Therefore, small amounts of isolated compounds and a limited supply pose considerable hurdles to in-depth analysis of biological targets.

Chemical synthesis of complex compounds at even gram-scale quantities has become progressively prevalent, allowing for thorough biological investigation and drug development of NPs formerly isolated in low yields. Given these considerations, developing strategies and methods towards total or semi-synthetic routes is necessary and considered an attractive option to obtain larger quantities of the natural product without straining natural resources.

Furthermore, the large amount of NPs obtained by synthetic approaches not only allows the identification of their mechanisms of action but also favours the optimization of their efficacy through targeted structural variations.

The interest and the goals were focused on the total synthesis of **depsipeptide PM181110**, **Fusarithioamide A**, and **Eudistomidin C** because of their great biological activity and given that they have never been synthesized before.

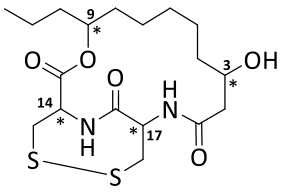

Depsipeptide PM181110 (9)

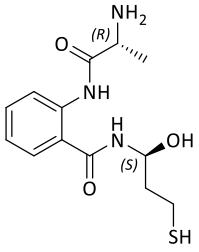

Fusarithioamide A (12)

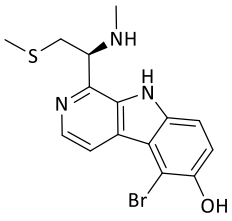

Eudistomidin C (BSc5517)

2 Aims and Objectives

NPs are one of the most prolific sources of compound inspiration for developing new medicines. A significant number of natural product drugs/lead compounds have been produced by marine organisms, endophytic fungi and/or the interactions with the host from whence they were isolated. However, the main issue frequently encountered with the low quantity of isolated samples from their natural sources directs researchers towards semi-synthesis and/or total synthesis. In other words, total synthesis and semi-synthesis are the primary means of replicating the most exciting compounds to obtain large amounts for in-depth biological assays and a better understanding of their pharmacological activity.

Additionally, the total synthesis of NPs has been the hallmark of chemical synthesis for the past century. It has been the primary force behind the discovery of new chemical reactivity, the evaluation of physical-organic theories, the testing of the efficiency of existing synthetic methods, and the development of biology and medicine.

Depsipeptide PM181110, **Fusarithioamide A** and **Eudistomidin C** are naturally occurring compounds that indicate potent anticancer and anti-tumour activity. However, they were isolated from their respective natural sources in tiny amounts. Consequently, the small amounts of the isolated compounds and limited supply create significant challenges for in-depth analysis of biological targets. Therefore, increasing the yield of these compounds via total or semi-synthesis is of great importance.

This thesis aims at developing synthetic strategies for **depsipeptide PM181110**, **Fusarithioamide A** and **Eudistomidin C** in order to perform their first total syntheses, to assess their biological activity *in vitro* and *in vivo* by medicinal chemistry approaches and predict/investigate their complementarity at the molecular level of ligands and protein targets.

Concerning the total synthesis of depsipeptide **PM181110**, based on published data, only its unrefined structure was disclosed after its isolation from natural sources. This means no information regarding its absolute configuration, such as specific rotations, circular dichroism, or the biosynthetic pathway, has been disclosed previously. Therefore, the total synthesis of **depsipeptide PM181110**, was carried out via the syntheses of the selected 3*R*,9*R*,14*R*,17*R*

(**BSc5484**) and 3*R*,9*S*,14*R*,17*R* (**10**) diastereomers. Further explanations regarding the choice of these diastereomers are given in the following pages.

Concerning the syntheses of **Fusarithioamide A** and **Eudistomidin C**, convergent and unified approaches were selected to achieve their syntheses. Besides, enantiomerically pure reagents were utilized. The synthesized compounds' *in vitro* kinase inhibitory activity and their toxicological effects in zebrafish embryos were also investigated.

Due to the scaffold privilege that **depsipeptide PM181110** offers with its strained disulphide bridge, the assessment of the kinase inhibitory activity was performed with selected Cys-DFG-kinases and some kinases harbouring cysteine residues in their active site (control), given that the direction was to induce covalent binding via cysteine targeting covalent inhibition.

Intending to generate highly active and selective compound inhibitors of the Cys-DFG-kinases motif, related derivatives were synthesized and investigated in an iterative process of structure modelling and design.

Aiming at transient pockets, initial derivatives were designed by identifying lipophilic fragments and attaching them to a predicted reactive fragment. This was done to prepare a small, diverse set of analogues. Subsequently, inhibitory activities were determined in various independent *in vitro* kinase activity tests and a focused kinase selectivity panel to gain insight into the links between structure and promiscuity.

The targeted compounds were further profiled for safety, toxicity, and bioavailability using well-established *in vitro* and *in vivo* methodologies. Compounds' buffer stability and bioavailability were assessed *in vitro* by identifying key physicochemical characteristics, while *in vivo* bioavailability, safety, and toxicity were examined in a developmental toxicity screen of wild-type and gold-type zebrafish embryos. Later on, a cell viability assay on human THP-1 cells was also investigated for toxicity assay, followed by an *in silico* experiment to predict the binding mode and the type of interactions between the synthesized compounds and their respective target proteins.

3 Results and Discussion

3.1 Total Synthesis of Fusarithioamide A (2-((*R*)-2-aminopropanamido)-*N*-((*S*)-1-hydroxy-3-mercaptopropyl)benzamide) (12)

This chapter describes the attempt to perform the first total synthesis of **Fusarithioamide A (2-((*R*)-2-aminopropanamido)-*N*-((*S*)-1-hydroxy-3 mercaptopropyl)benzamide) (12)**.

To achieve this synthesis, a retrosynthetic approach was primarily established and discussed.

3.1.1 Retrosynthetic analysis of Fusarithioamide A (2-((*R*)-2-aminopropanamido)-*N*-((*S*)-1-hydroxy-3-mercaptopropyl)benzamide) (12)

In an attempt to achieve the first total synthesis of **Fusarithioamide A (2-((*R*)-2-aminopropanamido)-*N*-((*S*)-1-hydroxy-3-mercaptopropyl)benzamide)** (**12**), a well-elaborated retrosynthetic plan was primarily designed after studying several and realistic retrosynthetic approaches (**Scheme 2**). Following the screening of inexpensive and readily available starting materials, the most comprehensive retrosynthetic plan of **12** was developed. The simplest synthons identified were *D*-alanine on the one hand and a thiol derivate on the other hand. **Scheme 2** describes the retrosynthetic approach and the main chemical reactions involved in the synthesis are nucleophilic additions and substitutions.

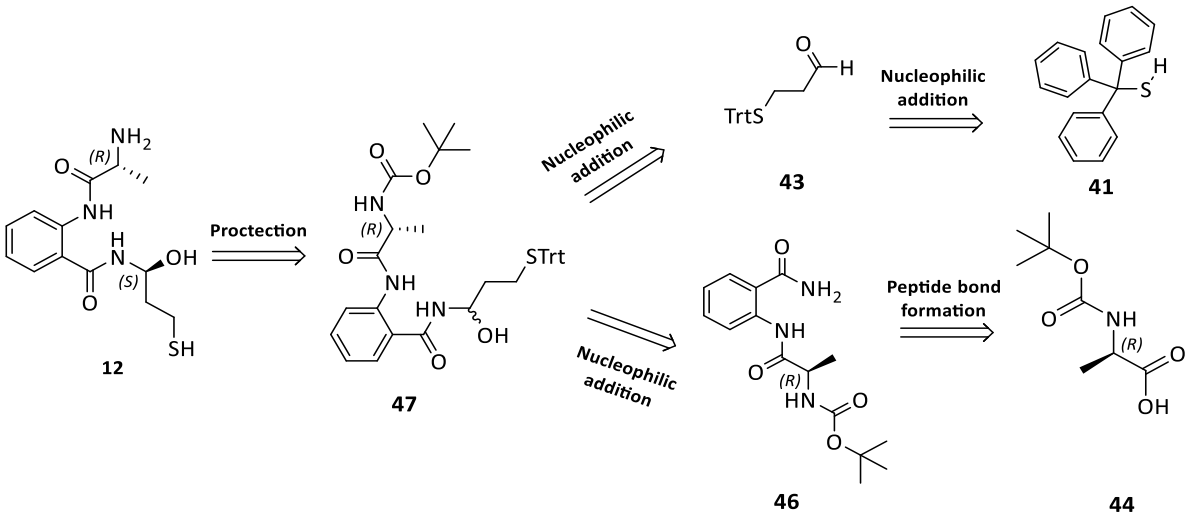

Scheme 2: Retrosynthetic analysis of **Fusarithioamide A** (2-((*R*)-2-aminopropanamido)-*N*-((*S*)-1-hydroxy-3-mercaptopropyl)benzamide) (**12**).

3.1.2 Attempt to Synthesize Fusarithioamide A (2-((*R*)-2-aminopropanamido)-*N*-((*S*)-1-hydroxy-3-mercaptopropyl)benzamide) (12)

The total synthesis **Fusarithioamide A** (2-((*R*)-2-aminopropanamido)-*N*-((*S*)-1-hydroxy-3-mercaptopropyl)benzamide) (**12**) was attempted. Hence, a highly convergent and unified approach was employed to perform the synthesis.

Although the reactive cores **43** and **46** were easily synthesized, there were tremendous reaction inefficiency and stability issues encountered with the key intermediate hemiaminal **47** (**Scheme 3**). As a result, the last steps did not proceed further to provide the desired compound.

The synthetic procedure until obtaining the key hemiaminal (**47**) is depicted in **Scheme 3**.

Description of the synthesis

The synthesis of tritylthio-propanal (**43**) was completed at room temperature in quantitative yield via Michael addition between triphenylmethanethiol (**41**) and acrolein (**42**) under basic conditions (**Scheme 3**). In another step, commercial Boc-protected *D*-alanine (**44**) was reacted

with benzamide (**45**) to furnish tert-butyl (*R*)-(1-((2 carbamoylphenyl)amino)-1-oxopropan-2-yl)carbamate (**46**) in 86% yield. Then, the coupling of the amide (**46**) and the aldehyde (**43**) via nucleophilic addition was attempted under several conditions to secure the desired key hemiaminal (**47**). To this end, five routes were extensively studied and evaluated (**Scheme 3**).

The first route, consisting of a titanium ethoxide-catalyzed nucleophilic addition between **43** and **46**, was tested in order to afford the corresponding hemiaminal (**47**). [118] However, when the reaction was monitored by either TLC or HPLC, no product was formed, and even after several trials, no reaction occurred, albeit with prolonged reaction times. After multiple attempts, other synthetic routes were explored.

For the second synthetic route, **43** and **46** were refluxed in THF. [119] Despite slight changes noticed while monitoring the reaction either with HPLC or TLC, the expected product was still not obtained. A mixture of **43** and **48** was obtained with some by-products that were not characterized.

Then came the third route in which dibenzyl phosphate was assessed to catalyse the nucleophilic addition. [120] After several test reactions, the process always ended up with a mixture of **46** and the trityl-free aldehyde **43**.

Thus, to enhance the reactivity between **43** and **46**, Grignard reagents were tested as bases to catalyse the nucleophilic addition reaction (routes 4 and 5). [121] The readily available isopropylmagnesium bromide (*i*-PrMgBr) and methylmagnesium chloride (MeMgCl) were assessed.

When *i*-PrMgCl was used, no reaction occurred between **43** and **46**. Nevertheless, the needed hemiaminal (**47**) was obtained in trace amounts (confirmed by HRMS analysis of the crude product) when MeMgCl was utilized as the base.

Being obtained in trace amounts, although from a larger reaction scale, **47** indicated being unstable towards contact with water, silica gel and even upon storage.

It was later found out that the stability issue of related hemiaminals had been early reported by Halli and Fernando [121, 122a] in their respective investigations on hemiaminals. Kwiecień and Ciunik also described hemiaminals as highly unstable chemicals that can only be seen under certain conditions. They also added that ‘’hemiaminals are reaction intermediates, formerly called ‘carbinolamines’, which are thermodynamically unstable and highly temperature-

sensitive in both acidic and basic solutions.'' [122b] In their fragmentation pattern, the unstable hemiaminal either decomposes into starting materials, enamines or proceeds to imines with loss of water during formation. For instance, the reaction between primary amines and aldehydes to form imines occurs by forming a hemiaminal intermediate. The catalysis of this process occurs through acids or bases, while the associated proton transfer reactions generate more charged transient intermediates. Iwasawa *et al*. also reported hemiaminals as compounds not typically observed except under exceptional conditions; they are energetically unfavourable due to the high demand of breaking the carbonyl π-bond and the entropic cost associated with bringing the reactants together, which are not offset by the new covalent bonds that have been created.[122c]

Kwiecień *et al*. further comment on hemiaminals as unstable compounds that have generally been obtained and characterised using sophisticated techniques such as polarography in liquid FTIR cells or low-temperature spectroscopy. They also indicated that obtained hemiaminals were typically highly unstable compounds that required additional stabilization through low-temperature isolation from the external environment (via molecular cavitands, metal-organic frameworks, or intramolecular hydrogen bonds). [122d]

Because of the stability issue and the meagre yield, it was difficult to carry out the late deprotection step to the desired Fusarithioamide A (**12**). Consequently, this finding drew attention to the initial chemical structure of the naturally isolated Fusarithioamide A.

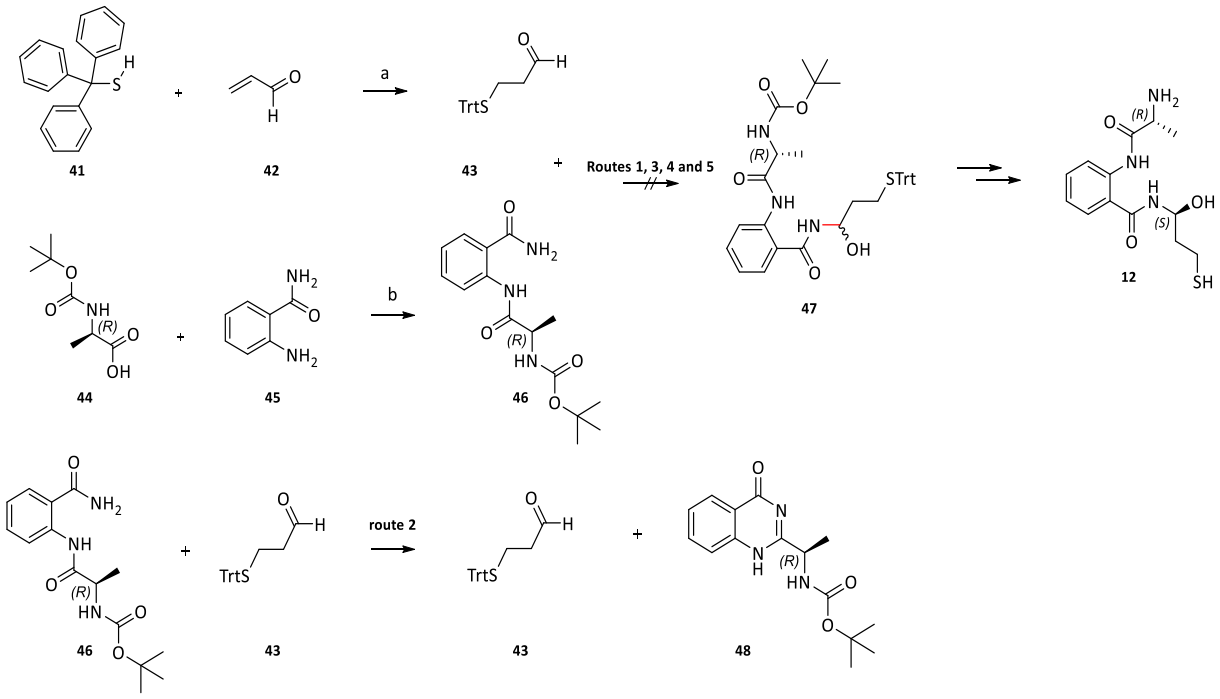

Scheme 3: Attempt to synthesize Fusarithioamide A (2-((*R*)-2-aminopropanamido)-*N*-((*S*)-1-hydroxy-3-mercaptopropyl)benzamide) (**12**). Reagents and conditions: a) Et_3N, CH_2Cl_2, RT, 99%; b) Et_3N, $ClCO_2Et$, THF 0°C to RT. 90%; **route 1**: a) $Ti(OEt)_4$, DCM, RT; b) $Zn(OTf)_2$, MeCN/DCM, 0 °C to RT.; **route 2:** THF, reflux 66 °C; r**oute 3:** $(PhO)_2POOH$, Et_2O, RT; **route 4:** THF, - 40 °C to -50 °C, *i*-PrMgCl; **route 5:** THF, - 40 °C to -50 °C, MeMgCl.

a) The ^{1}H-NMR and ^{13}C-NMR spectra of the isolated Fusarithioamide A (**12**), as reported by Sabrin *et al*. [21]

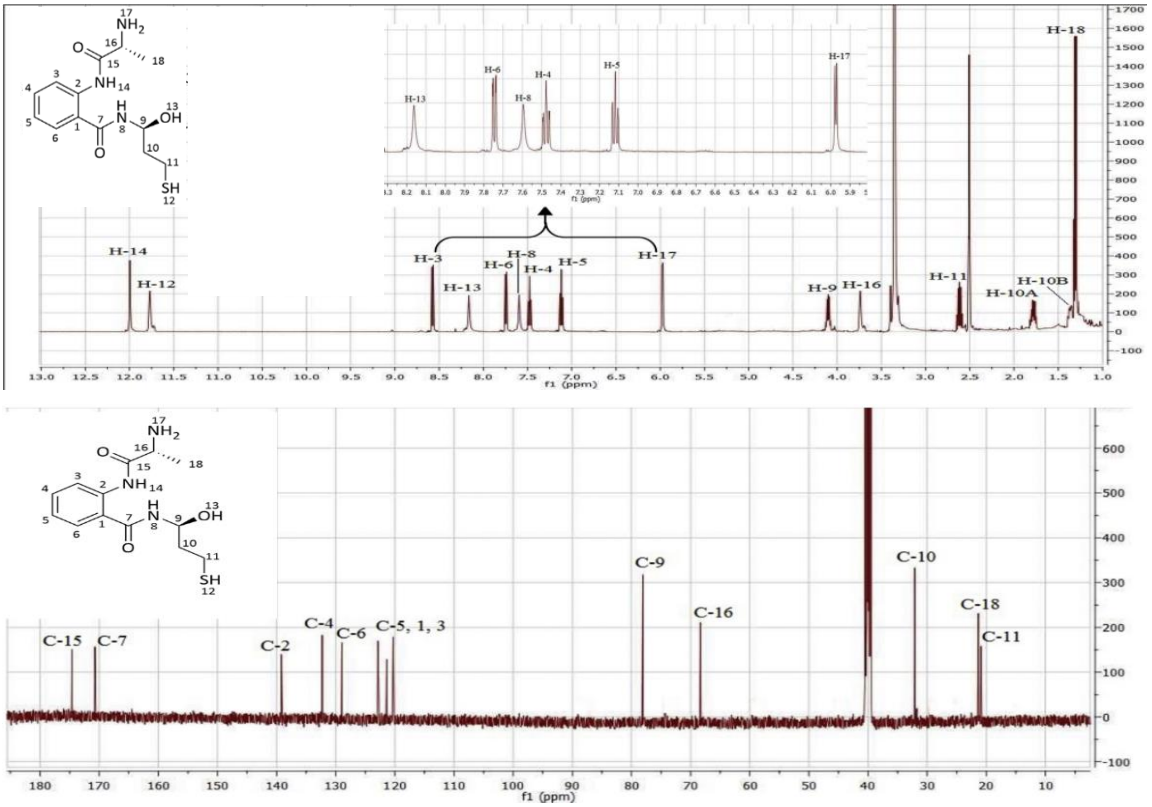

b) The simulated ^{1}H-NMR and ^{13}C-NMR spectra of compound **12** using Chemdraw. [123]

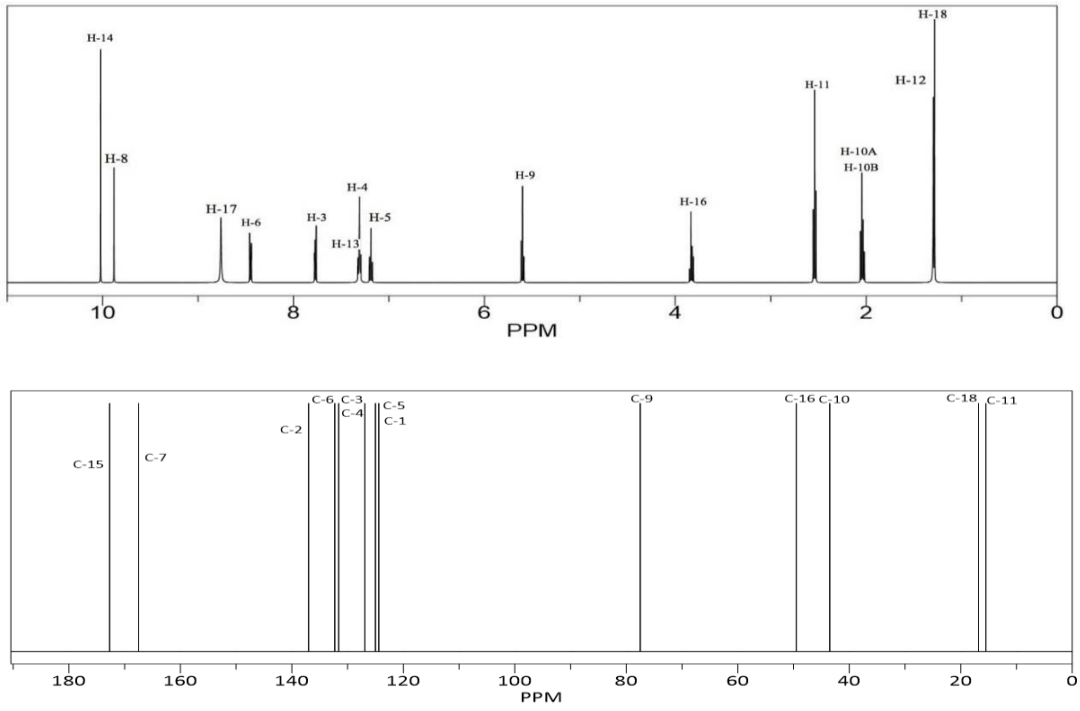

Figure 18: Comparison of the ^{1}H-NMR and ^{13}C-NMR Spectra of the isolated Fusarithioamide A [a](on top) and the simulated (2-((*R*)-2-aminopropanamido)-*N*-((*S*)-1-hydroxy-3-mercaptopropyl)benzamide) (**12**) [b](on the bottom).

The hypothesis of misassignment of **12** upon isolation arose and was strongly supported and investigated. To this end, a direct comparison of the ^{1}H-NMR and ^{13}C-NMR spectra of the isolated Fusarithioamide A (**12**) and the simulated ones using Chemdraw Professional (version 15.0.0.106) was initially investigated. The spectra comparison in **Figure 18** supported the emitted hypothesis as the difference in chemical shift values for the same atoms between the isolated and the simulated compound **12** is significant when comparing the two spectra. The same statement goes for the ^{13}C-NMR spectra. Besides the discordance in chemical shift values, the isolation protocol of 12 did not match the required isolation protocol of hemiaminals. [21] As a result, a revision of the chemical structure of the isolated compound based on the published spectroscopic data has been considered and investigated.

Due to stability issues faced in the attempt to perform the first total synthesis of **Fusarithioamide A (2-((*R*)-2-aminopropanamido)-*N*-((*S*)-1-hydroxy-3-mercaptopropyl)benzamide) (12)**, the synthesis was halted at this stage, and the synthesis of **depsipeptide PM181110** was undertaken.

3.2 Total synthesis of Depsipeptide PM181110

This chapter describes the first total synthesis of the selected diastereomer **BSc5484** and an attempt to perform the total synthesis of compound **10**. To this end, a retrosynthetic approach was primarily established and analysed.

3.2.1 Retrosynthetic analysis of the selected diastereomers of depsipeptide PM181110

The synthesis of depsipeptide **PM181110** (**9**) was attempted via the syntheses of its **3*R*,9*R*,14*R*,17*R*** (**BSc5484**) and **3*R*,9*S*,14*R*,17*R*** (**10**) diastereomers.
Initially, a retrosynthetic plan was established to suggest the most comprehensive synthetic approach (**Scheme 4a**).
Given that the diastereomers to synthesize differed from the stereochemistry of the carbon-9 (C-9), only one retrosynthesis was designed, and the simplest synthons identified were a cysteine derivative and an epoxy chloride.

3.2.2 Total syntheses of Diatereomers 3*R*,9*R*,14R,17*R* (BSc5484) and 3*R*,9*S*,14*R*,17*R* (10)

No information regarding the absolute configuration of depsipeptide **PM181110** (**9**), such as specific rotations, circular dichroism, or the biosynthetic pathway, has been disclosed yet. Thus, the absolute stereochemistry of depsipeptide **PM181110** (**9**) will be determined by comparing the spectroscopic data of the two selected diastereomers against the reported data.

Depsipeptide **PM181110** (**9**) is a structurally distinct depsipeptide with four chiral centres rather than three and six, as featured by the respective analogues **FE399** (**8**) and **Malformin A1** (**11**). Depsipeptide **PM181110** is a 16-membered bicyclic depsipeptide with an ω-hydroxy fatty acid moiety and two cysteines connected by an 8-membered cyclic disulphide. [124] However, neither

the relative and absolute configurations at the chiral centres C-3, C-9, C-14, and C-17 nor the specific optical rotation are revealed. As far as it is known, only the unrefined structure was disclosed after isolation from natural sources.

Based on the data retrieved in the literature, only the total syntheses of **FE399** (**8**) and **Malformin A1** (**11**) were performed, and their stereochemistries were determined to be 9*R*,14*R*,17*R* and 1*R*,4*S*,7*R*,10*S*,13*S* respectively. [124 - 126]

In an attempt to identify the principal natural diastereomer of **9** whose NMR data will agree with the original isolation report, the focus was on the relative and absolute structures. Four diastereomers are theoretically conceivable, with two chiral centres excluding the two cysteines. Because of the abundance of natural *L*-amino acids in comparison to *D*-amino acids, and since the stereochemistry of the close analogue **FE399** (**8**) was determined to be 9*R*,14*R*,17*R*, the syntheses of the selected diastereomers of **9** were attempted: **BSc5484** and **10**, as they are readily available from inexpensive materials. [124, 125]

However, only **BSc5484** was successfully synthesized as the late macrolactonization step leading to either **BSc5484** or compound **10** turned out to be a dead-end for the synthesis of compound **10**, likely owing to the unfavourable spatial orientation adopted by the functional groups involved in that step (**Scheme 5b**). This hypothesis was further confirmed even after switching from the frequently employed MNBA reagent to the Yamaguchi reagent, Shiina reagent and Corey-Nicolaou macrolactonization reagent; the macrolactonization still did not happen. [127- 129]

Description of the synthesis of depsipeptide PM181110: Diastereomer 3*R*,9*R*,14*R*,17*R* (BSc5484)

A convergent and unified approach was employed to complete the synthesis of **BSc5484**. The critical steps of this synthesis involve the formation of a dithiazocane peptide bond with a ω-hydroxy fatty acid derivative and the subsequent sixteen-membered macrolactonization. Since the eight-membered cyclodithiazocane is already strained, they should be synthesized without any additional constraints caused by the closure of the bridge and without epimerization of the C14 and C17 stereogenic centres. [125] Thus, commercial **49** was transformed into aminoester **50** and the N-Boc derivative **51** in 99% and 90% yields respectively (**Scheme 4b**). Utilizing EDC/HOBt, the obtained compounds were reacted to produce the protected dicysteine **52** in 70% yield. [130] Subsequent iodine treatment of **52** at 0.5 mM substrate concentration in MeOH/CH_2Cl_2 resulted in a sequential detritylation and disulphide bond formation, providing dithiazocane **BSc5483**. It is worth mentioning that with a 9/1 ratio solvent mixture of MeOH/CH_2Cl_2, the formation of oligomeric disulphides was avoided. [131]

Next, the key silyl-protected hydroxydodecanoic acid (**69**) was synthesized (**Scheme 5a**). To achieve this, (*R*)-1-chloropentan-2-ol (**57**) was first readily obtained in a 93% yield from a nucleophilic addition between commercially available epoxide (**56**) and the *in-situ* generated Grignard reagent (**55**) (**Scheme 4b**). The obtained hydroxyl-chloride (**57**) was subsequently subjected to stereoselective epoxidation using NaOH, affording **58** with 94% yield. A subsequent nucleophilic addition via epoxide ring opening with the corresponding *in-situ* generated Grignard reagent of **59**, in the presence of a catalytic amount of CuCN, afforded the desired secondary alkenol (**60**) in a one-pot operation. [132, 133]

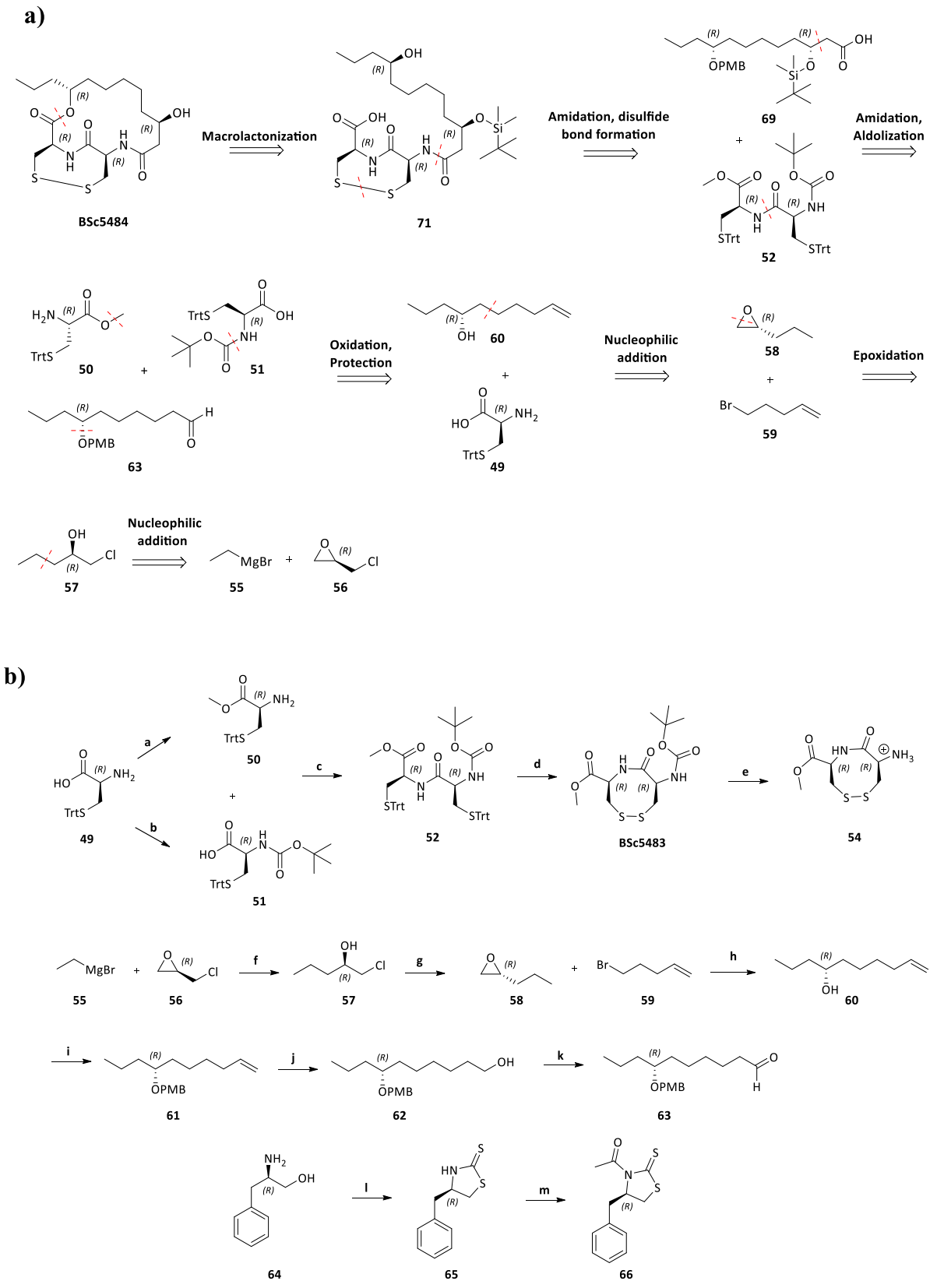

Scheme 4: [a]Retrosynthesis analysis of **BSc5484**; [b]Reagents and conditions: a) MeOH; b) NaOH, Boc_2O, 90%; c) DCM, HOBt, EDC.HCl 70%; d) DCM/MeOH, I_2, 76%; e) DCM/TFA; f) THF, 93%; g) Et_2O, NaOH, 94%; h) THF, Mg, 69%; i) THF, PMBCl, 87%; j) THF, 9-BBN, 64.3%; k) DMSO, IBX, 93%; l) KOH, CS_2; m) DCM, AcCl, 97%.

Next, the PMB protection of **60** into **61** was followed by subsequent hydroboration mediated by 9-BBN furnishing **62**. **62** was later oxidized to provide the hydroxy-protected aldehyde **63** in 56% yield (2 steps). [134, 135]

Afterwards, the required *N*-acetyl-4-benzyl-thiazolidinethione (**66**) was prepared in two steps starting from **64**, which was consistently refluxed in the presence of carbon disulphide, providing the needed auxiliary **65**. The obtained auxiliary was further acylated using triethylamine, 4-dimethylaminopyridine and acetic chloride to secure **66**. [136] Subsequently, **66** underwent a titanium tetrachloride-mediated enantioselective aldol reaction with aldehyde **63** (**Scheme 5a**), providing the PMB-protected alcohol **67** (70% yield). [137] The protection of the resulting alcohol as its TBS ether **68**, followed by a hydrolytic cleavage of the chiral auxiliary, furnished the desired ω-hydroxy fatty acid **69** in 92% yield. [138, 139]

It is worth mentioning that the commonly utilized for TBS protection, 2,6-lutidine or imidazole as bases, always led to the decomposition of **67**.

After the removal of the Boc-protecting group of **BSc5483** into **54** (**Scheme 4**) with excess trifluoroacetic acid in dichloromethane, [140] the corresponding TFA salt was smoothly acylated with **69** under EDC/HOBt conditions early mentioned to secure amide **70** (**Scheme 6**). [125] Afterwards, the PMB deprotection of **70** using DDQ in a 10/1 DCM-H_2O solvent mixture afforded the desired alcohol-ester **71** in 85% yield. [141, 142]

Next, the initial attempt for methyl ester hydrolysis of **71** under basic saponification conditions involving aqueous LiOH always led to the opening of the disulphide moiety. However, the hydrolysis using trimethyltin hydroxide resulted in the formation of the needed hydroxy acid **72** in moderate yield. [143] Following that, **72** was cyclized at 0.5 mM substrate concentration in the presence of MNBA, 4-dimethylaminopyridine and triethyl amine via a MNBA-mediated dehydration cyclization reaction of the corresponding precursor. This led to the formation of the 16-membered TBS-protected depsipeptide core **73** in moderate yield. [125] Finally, the late TBS deprotection step under TBAF in a THF potassium phosphate buffer secured the desired diastereomer **BSc5484**.

Contrary to what was reported for the synthesise **depsipeptide FE399**, the ^{1}H-NMR spectrum of the synthetic material **BSc5484** in DMSO-d_6 does not reveal a mixture of conformers. Using preparative thin-layer chromatography (TLC) and chiral reversed-phase flash chromatography, **BSc5484** was isolated, and the ^{13}C-NMR chemical shifts were assigned to the predominant isomer. [144]

a)

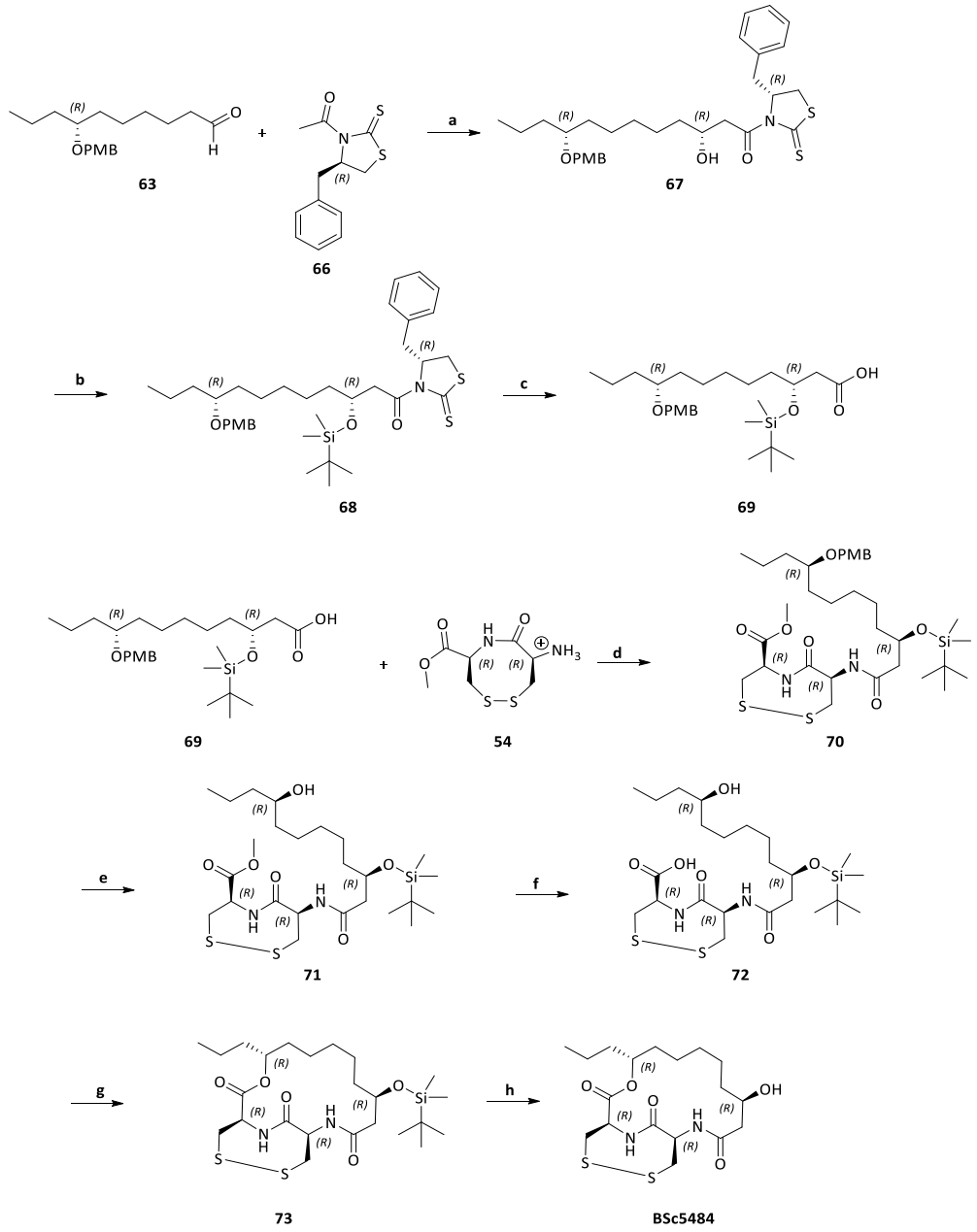

b) Attempted synthesis of the diastereoisomer **3*R*,9*S*,14*R*,17*R*** (**10**)

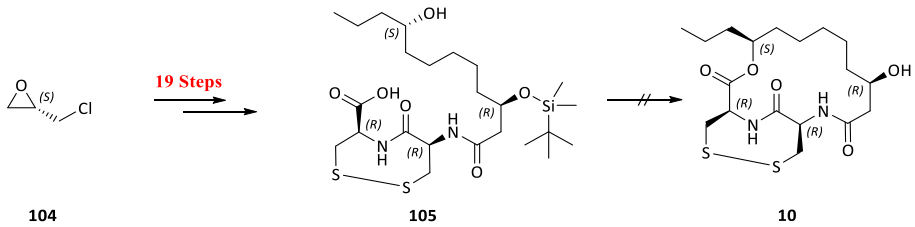

Scheme 5: [a]Synthesis of the diastereomer 3*R*,9*R*,14*R*,17*R* (**BSc5484**). Reagents and conditions: a) DCM, $TiCl_4$, 0 °C to -78 °C, 70%; b) DCM, TBSOTf, 0 °C, 87%; c) THF/H_2O, H_2O_2, LiOH, 0 °C, 92%; d) DMF, EDC, HOBt, Et_3N, rt, 70%; e) DDQ, rt, 85%; f) 1,2-DCE, $(CH_3)_3SnOH$, 60 °C, 85%; g) THF, MNBA, DMAP, Et_3N, rt, 60%; h) THF-buffer, TBAF, 85%. [b]Attempt to synthesize the diasteromer 3*S*,9*R*,14*R*,17*R* (**10**).

Table 1: Comparison of the ^{13}C-NMR chemical shifts (δ, *ppm*) in DMSO-d_6 of natural depsipeptide **PM181110** and its synthetic diastereomer **BSc5484**.

Position	Natural	Synthetic	Position	Natural	Synthetic
1	173.9	174.9	**10**	36.2	34.1
2	35.5	31.7	**11**	18.3	14.4
3	70.3	70.2	**12**	13.7	13.9
4	34.3	31.1	**13**	169.4	167.0
5	27.9	29.1	**14**	52.0	53.4
6	26.7	24.9	**15**	42.7	40.4
7	22.0	22.5	**16**	174.1	176.8
8	32.9	29.4	**17**	51.2	52.2
9	74.5	72.8	**18**	43.2	40.2

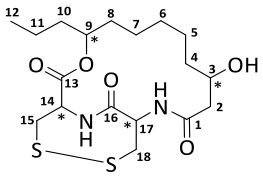

Far from the expectations, the ^{13}C-NMR chemical shifts of the synthesized **BSc5484** did not correlate with published literature values of **depsipeptide PM181110**.
Despite this result, the synthesized **BSc5484** was still considered and further profiled for biological experiments *in vitro*, *in vivo* and *in silico* (see section **3.4**).

The following section describes the first total synthesis of Eudistomidin C ((*S*)-5-bromo-1-(1-(methylamino)-2-(methylthio)ethyl)-9*H*-pyrido[3,4-β]indol-6-ol) (**BSc5517**) via a highly convergent approach.

3.3 Total synthesis of Eudistomidin C ((*S*)-5-bromo-1-(1-(methylamino)-2-(methylthio)ethyl)-9*H*-pyrido[3,4-β]indol-6-ol) (BSc5517)

Like depsipeptides, β-carbolines have been extensively studied and utilized. This allowed further investigation for the sake of this doctoral thesis. Thus, to better understand the formation of **BSc5517**, it was essential to first focus on how nature produced it. To this end, the investigation of the compound's probable biosynthesis was undertaken and discussed in detail in the following pages.

3.3.1 Proposed biosynthesis of Eudistomidin C ((*S*)-5-bromo-1-(1-(methylamino)-2-(methylthio)ethyl)-9*H*-pyrido[3,4-β]indol-6-ol) (BSc5517)

To have a clear and concise synthetic route of **Eudistomidin C** ((*S*)-5-bromo-1-(1-(methylamino)-2-(methylthio)ethyl)-9*H*-pyrido[3,4-β]indol-6-ol) (**BSc5517**), it was exciting and instructive to understand its biosynthetic pathway. Consequently, a biosynthetic approach of **BSc5517** was developed and proposed.

Based on the work proposed by Wu *et al.* [145] in the biosynthesis of aromatised β-carbolines, it is believed that the biosynthesis of **BSc5517** involves the coupling of **81** with **86** deriving from **74** and **82** respectively, via a tandem enzymatic reaction (**Scheme 6**). [145 - 148] A schematic representation of the proposed biosynthesis is outlined in **Scheme 6**.

In the first step, **74** was converted into **75**, and then, an aldehyde oxidoreductase, also known as a carboxylic acid reductase (CAR), which requires ATP, Mg^{2+}, and NADPH as cofactors, was needed for the reaction to take place. The reduction was a sequential process that begins with binding both ATP and carboxylic acid to the enzyme, resulting in mixed 5′-adenylic acid-carbonyl anhydride intermediates **78** and **79**. They were subsequently reduced by hydride delivery from NADPH to form **81** and regenerate CAR. [147] In another step, the biosynthetic pathway for **84** initially involved the conversion of **82** to its short-lived analogue **83** by the enzyme L-tryptophan-5-hydroxylase (TPH). The subsequent metabolic action required the

expressed cytosolic enzyme aromatic acid decarboxylase (AADC), catalysing the decarboxylation of 5-TPH (**83**) into **84**. Conversely, **84** was methoxylated by *N*-acetylserotonin *O*-methyltransferase (ASMT) to form **85**. [149] In the following step, the β-carboline backbone was assembled by an enzyme catalysing a Pictet-Spengler cyclisation between **81** and serotonin **85**. [145] After cyclization, the obtained tetrahydro-β-Carboline **86** was oxidized through an oxidase, resulting in the formation of the β-Carboline **BSc5515**. In the final steps, **BSc5515** underwent bromination and demethylation utilizing brominase enzymes and codeine *O*-demethylase (CODM) to yield **BSc5517**. [150]

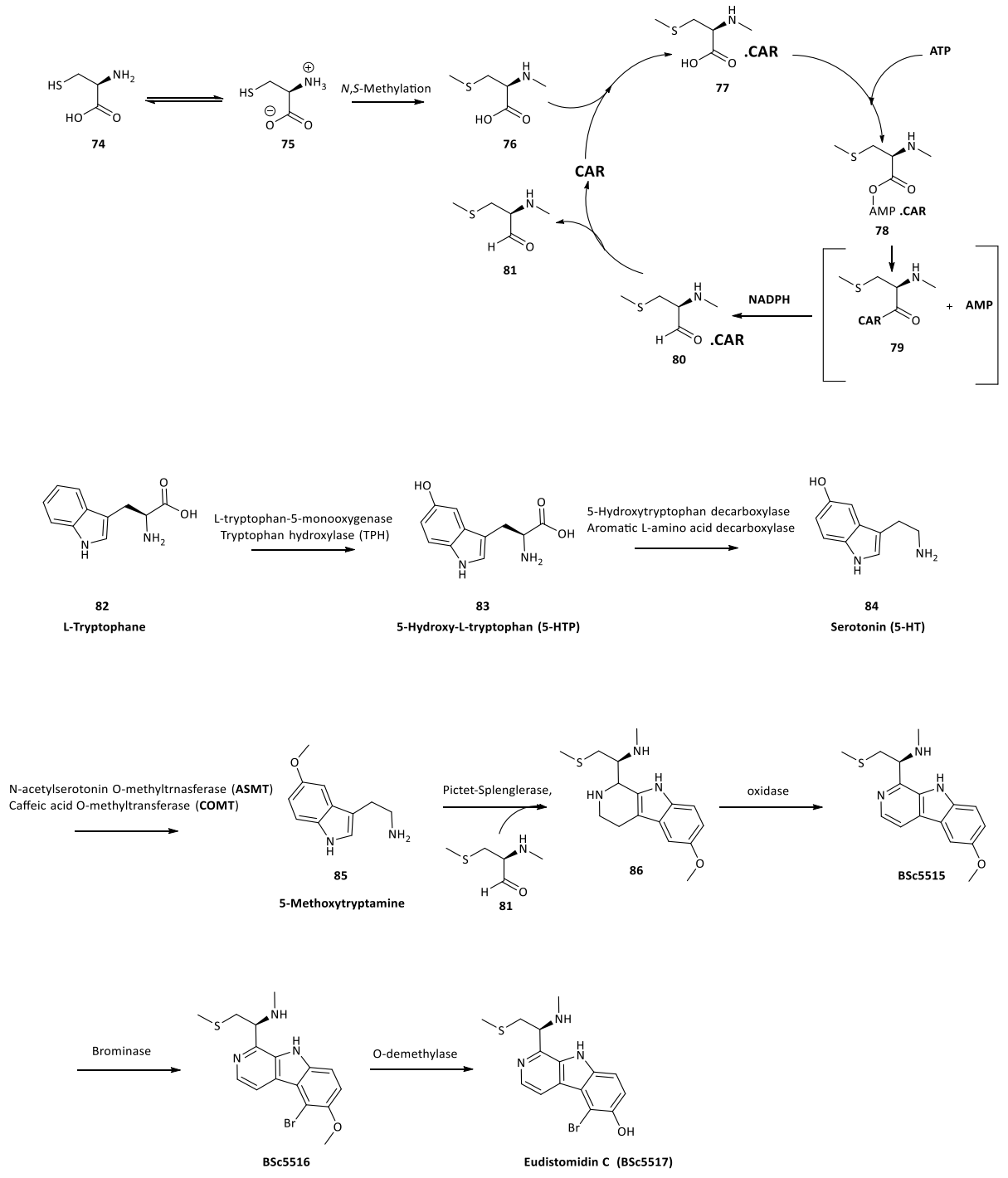

Scheme 6: Proposed biosynthesis of **Eudistomidin C** ((*S*)-5-bromo-1-(1-(methylamino)-2-(methylthio)ethyl)-9*H*-pyrido[3,4-β]indol-6-ol) (**BSc5517**).

3.3.2 Retrosynthetic analysis of Eudistomidin C ((*S*)-5-bromo-1-(1-(methylamino)-2-(methylthio)ethyl)-9*H*-pyrido[3,4-β]indol-6-ol) (BSc5517)

Inspired by the proposed biosynthetic pathway of **BSc5517**, it was much easier to establish a comprehensive and robust retrosynthetic analysis, which might lead to a clear and concise synthetic route of **BSc5517**. Thus, a schematic representation of the retrosynthetic approach of **BSc5517** is presented in **Scheme 7**.

There are several avenues for the preparation of β-carbolines. To this end, a Pictet-Spengler cyclization reaction was chosen to assemble the β-carboline skeleton. Moreover, several reactions were screened to predict the most realistic disconnections, including the Vilsmeier-Haack and Ullmann condensation.

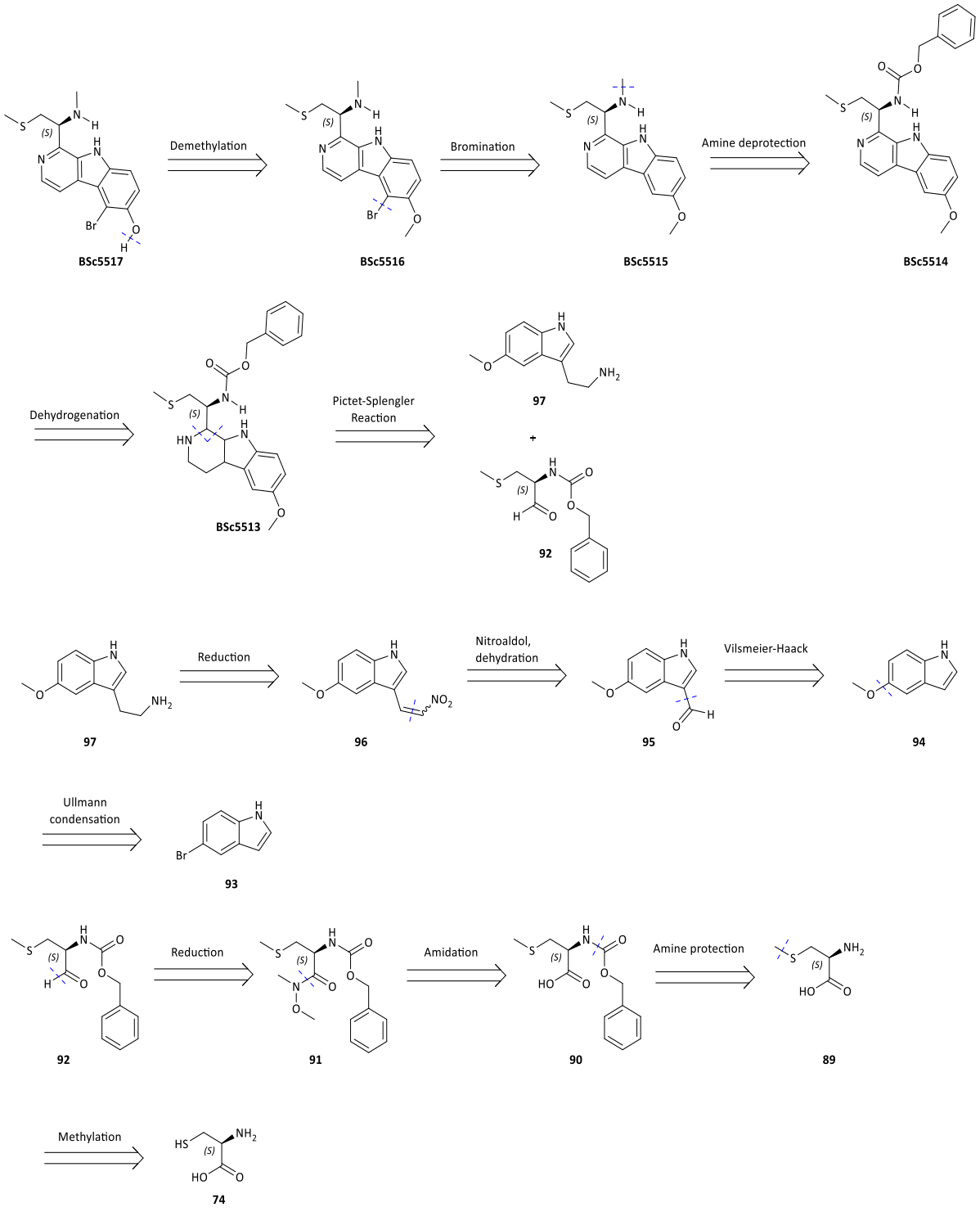

Scheme 7: Retrosynthetic analysis of Eudistomidin C ((*S*)-5-bromo-1-(1-(methylamino)-2-(methylthio)ethyl)-9*H*-pyrido[3,4-β]indol-6-ol) (**BSc5517**).

3.3.3 Total synthesis of Eudistomidin C ((*S*)-5-bromo-1-(1-(methylamino)-2-(methylthio)ethyl)-9*H*-pyrido[3,4-β]indol-6-ol) (BSc5517)

The total synthesis of **BSc5517** was initiated after proposing the most convenient and realistic retrosynthetic approach. As for the synthesis of **BSc5484**, the synthesis of (**(*S*)-5-bromo-1-(1-(methylamino)-2-(methylthio)ethyl)-9*H*-pyrido[3,4-β]indol-6-ol**) (**BSc5517**) was undertaken based on a highly convergent and unified approach. The synthesis features the formation of tetrahydro-β-carboline **BSc5513** via a TFA-catalysing Pictet-Spengler cyclization between **92** and **97** as the critical step (**Scheme 8**).

The thiol group of commercial (*D*)-cysteine (**74**) was methylated into **89** in 88% yield. Then, the subsequent incorporation of the benzyloxycarboxyl group was achieved via a base-catalysed nucleophilic addition of **89** and benzyl chloroformate in 2N aqueous NaOH as a solvent to secure **90** with 84% yield. Next, the synthesized **90** underwent an esterification reaction under EDC and *N*, *O*-dimethylhydroxylamine hydrochloride condition to secure the needed Weinreb amide **91** in 86% yield. Then, aldehyde **92** was obtained after DIBAL-H reduction of the corresponding Weinreb amide **91** in an excellent yield (95%).

In another step, commercial **93** was converted into **94** via a copper (I)-promoted Ullmann condensation in 80% yield. Next, the desired C-3 position of the indole was smoothly formylated using phosphorous oxychloride as the catalyst in DMF via a Vilsmeier-Haack reaction and afforded **95** in 97% yield. Subsequently, **95** was converted into **96** (in 90% yield) via nitroaldol condensation and subsequent dehydration. In the last step, **96** was reduced using $LiAlH_4$ to secure **97** in a 38% yield.

Following that, the β-carboline backbone was assembled via an acid-catalysed Pictet-Spengler reaction. Based on the model of biosynthesis shown earlier (**Scheme 6**). The reaction was performed in DCM using TFA as the catalyst at 0 °C with 4 Å powdered molecular sieves. This process secured **BSc5513** with a 75 % yield. After successful cyclization, **BSc5513** was converted into a fully aromatic β-carboline by oxidative dehydrogenation by refluxing the starting material and DDQ in THF at 40 °C. The reaction then afforded **BSc5514** in 60% yield. Next, $LiAlH_4$ (1 M solution in THF) was utilized to cleave the *CBZ*-protecting group of **BSc5514** and secured **BSc5515**. Then, the regioselective bromination of **BSc5515** was performed using bromine in acetic acid to afford **BSc5516** in 80% yield. The last demethylation

step of **BSc5516** was achieved at -78 °C using BBr_3 in anhydrous DCM to secure **BSc5517** in a 76% yield.

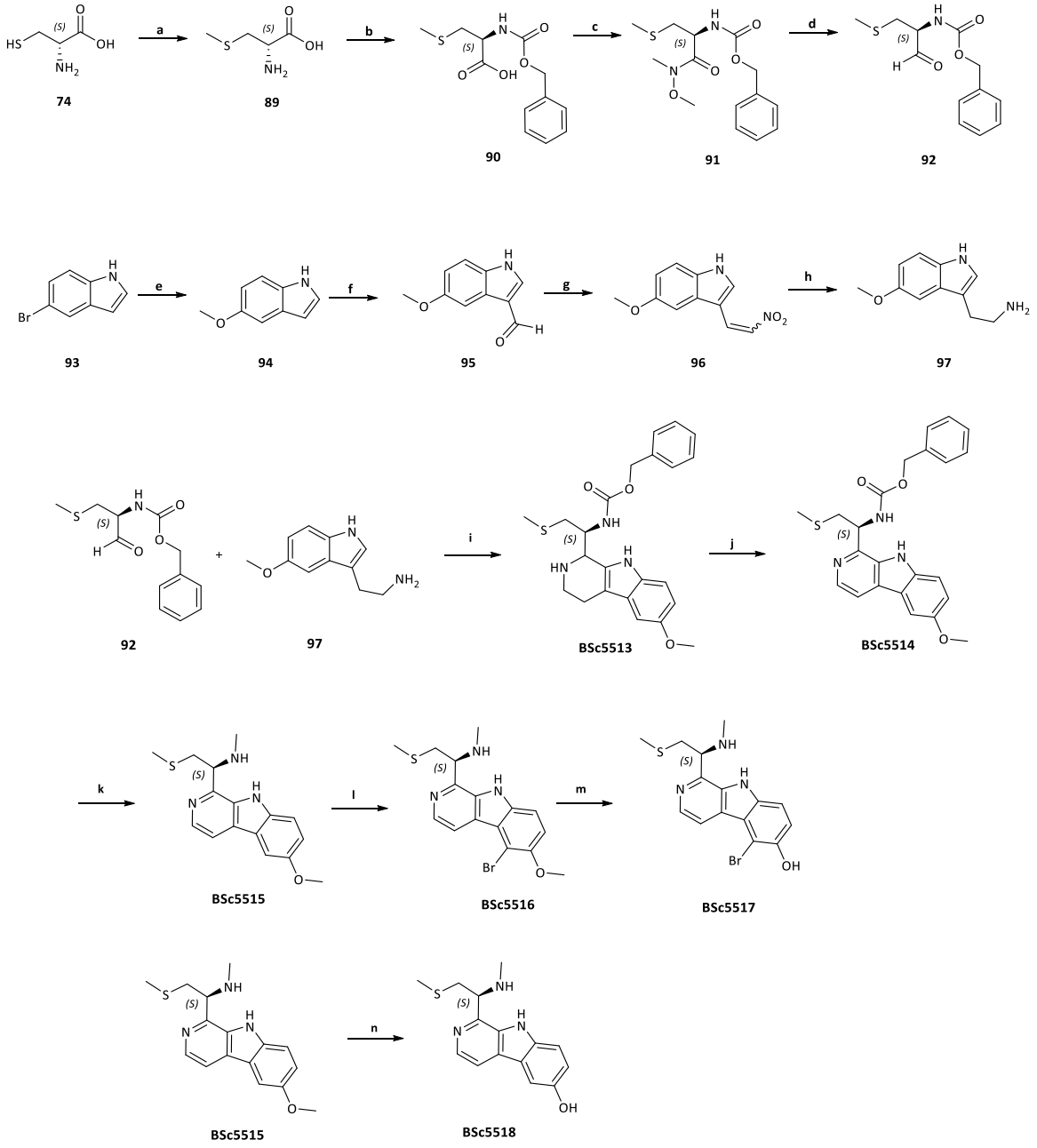

Scheme 8: Synthesis of **Eudistomidin C** ((*S*)-5-bromo-1-(1-(methylamino)-2-(methylthio)ethyl)-9*H*-pyrido[3,4-β]indol-6-ol) (**BSc5517**) and some analogues. Reagents and conditions: (a) EtOH, Na, MeI, 0 °C to rt, 89%; (b) Aqueous 2 N NaOH, CBZCl, 0 °C to rt, 84%; (c) DCM, Et_3N, EDC.HCl, $NH(OCH_3)CH_3$.HCl, 0 °C to rt, 86%; (d) Toluene, DIBAL-H, -78 °C, 95%. (e) MeOH, Na, CuI, DMF, reflux, 80%; (f) DMF, $POCl_3$, 0 °C to rt, 97%; (g) CH_3NO_2, $AcONH_4$, reflux, 90%; (h) THF, $LiAlH_4$, 0 °C to rt, 38%. (i) DCM, TFA, 0 °C to rt, 75%; (j) THF, DDQ, reflux, 60%; (k) THF, $LiAlH_4$, reflux, 70%; (l) AcOH, Br_2, 80 %; (m) DCM, BBr_3, -78 °C, 76 %; (n) DCM, BBr_3, -78 °C, 90%.

For the sake of structure-activity-relationship study, **BSc5518** was synthesized starting from **BSc5515** in 90% yield (**Scheme 8**). The reaction was carried out following the same procedure utilized in the last step of the synthesis of **BSc5517**.

After achieving the total synthesis, The NMR data of the synthesized ((*S*)-5-bromo-1-(1-(methylamino)-2-(methylthio)ethyl)-9***H***-pyrido[3,4-β]indol-6-ol) (**BSc5517**) and the naturally isolated **Eudistomidin C** were not in total agreement.

A comparison of the ^{13}C-NMR spectra was made between the synthesized Eudistomidin C (**BSc5517**) and the naturally isolated compound (**Figure 19**). As shown in **Figure 19**, the ^{13}C-NMR spectrum of the isolated compound from the natural source (on the top) is not ''clean'' and obviously contains some impurities compared to the spectrum of synthesized **BSc5517** (on the bottom). Besides that, the following remarks were noticed: Firstly, the assignment of the chemical shifts, as reported by Kobayashi *et al.,* did not match the spectra depicted in the supplementary data of their paper. [151] In their article, C-1 has been assigned to a chemical shift of 140.06 *pp*m. However, there is no signal at that chemical shift range in their ^{13}C-NMR spectrum (**Figure 19**). [144] In addition, the spectrum of their ^{13}C-NMR displays a well-resolved signal at approximately 142.50 *ppm,* which was not assigned to any carbon atom. [151] Furthermore, in their ^{13}C-NMR spectrum, one can obviously observe the signal of CCl_4, meaning that CCl_4 might have been used to remove residual solvents, and the remaining could have impacted the chemical shift values. Thus, it is believed that the presence of CCl_4 and the impurities in their sample might have significantly affected the chemical shifts of the atoms. Hence, the origin of specific signals that are incompatible.

To further support the emitted hypothesis and eliminate doubts, **BSc5580** (**Figure 3**) which is the enantiomer of **BSc5517**, was synthesized starting from **(*L*)-Cysteine** using the same synthetic procedure. After achieving the total synthesis of **BSc5580**, its NMR data (see Appendix Section A2) were similar to synthesized Eudistomidin **C** (**BSc5517**), confirming the initial hypothesis.

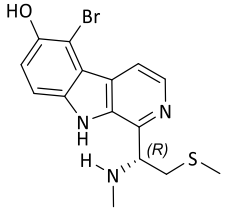

BSc5580

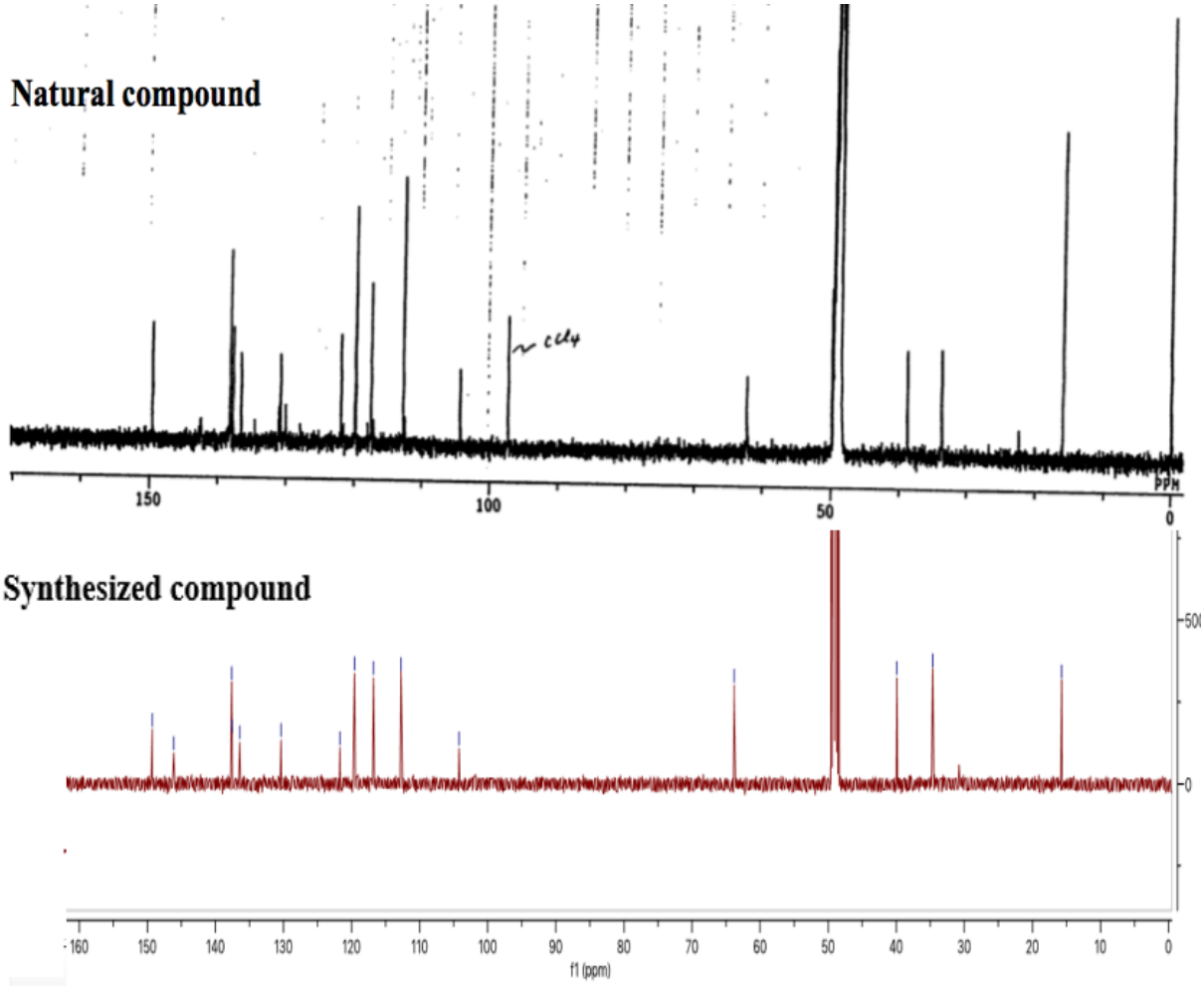

Figure 19: Comparison of the ^{13}C-NMR chemical shifts (δ, ppm) in MeOH-d_4 of the natural (isolated) and the synthesized Eudistomidin C ((*S*)-5-bromo-1-(1-(methylamino)-2-(methylthio)ethyl)-9*H*-pyrido[3,4-β]indol-6-ol) (**BSc5517**).

Having achieved the total synthesis of **BSc5484** and **BSc5517**, the new direction was to study their biological activity *in vivo* and *in vitro*. Similarly, the investigation of the complementarity at the molecular level of ligands and protein targets was also studied.

3.4 Synthesis of a diverse set of analogues of BSc5484

The following chapters describe the study undertaken to understand better the biological activity of the synthesised compounds **BSc5484**, **BSc5517** and their analogues.

3.4.1 Synthesis of a diverse set of analogues of BSc5484

A diverse set of analogues of **BSc5484** was synthesized, and the biological activity was studied. Given the interest in the chemical structure of **BSc5484**, especially with its strained disulphide-bridged moiety, it was relevant to assess its potential as a cysteine-targeting compound to induce protein refolding and thereby modulate kinase activity. At that time, the approach was the identification of ligands for a hidden transient pocket of kinases.
Aiming at transient pockets, frequently identified lipophilic fragments were selected and attached to the assumed reactive core **54**. Then, a small diverse set of analogues was prepared.
As a result, the diverse sets of analogues were synthesized on the one hand from the Boc-deprotected dithiazocane **54** undergoing peptide coupling reactions, while the others were prepared from the very cysteine **49**.

- Series I synthesized from peptide coupling involving the Boc-deprotected dithiazocane (**54**).

The first series of analogues was synthesized mainly via peptide coupling reactions.
Starting from compound **54**, a series of peptide coupling reactions were completed mostly in moderate yield under EDC/HOBt conditions. [125] As a result, **BSc5488**, **BSc5487** and **BSc5486** were synthesized using 1*H*-benzimidazole-5-carboxylic acid, 5-bromo-3-pyridine-acetic acid and *trans*-4-methoxycinnamic acid respectively as coupling partners (**Scheme 9**).

- Series II synthesized from **49** and **BSc5483.**

The second series of analogues was prepared following two different approaches (**Scheme 9**). In the first approach, **BSc5485** was ready in 61% yield from **BSc5489** via hydrolysis of

BSc5483 under mild conditions using the trimethyl tin hydroxide procedure reported earlier.[143] Afterwards, with sufficient **BSc5489** in hand, it was further formylated with the commercial *L*-tryptophan methyl ester using EDC/HOBt to secure **BSc5485**. The second approach involved an aminoester (**102**), which was prepared in a 50% yield via an esterification reaction between absolute *iso*-butyl alcohol and **49** at low pressure using thionyl chloride in catalytic amounts (**Scheme 9**). [152] The resulting aminoester was also coupled under EDC/HOBt conditions with the *N*-Boc-protected cysteine **51** to first secure the peptide **103** in 78% yield. [125] Then, simultaneous detritylation and disulphide bond formation were all proceeded by treatment of **103** with iodine at 0.5 mM substrate concentration to afford **BSc5482** in 79% yield (**Scheme 9**).

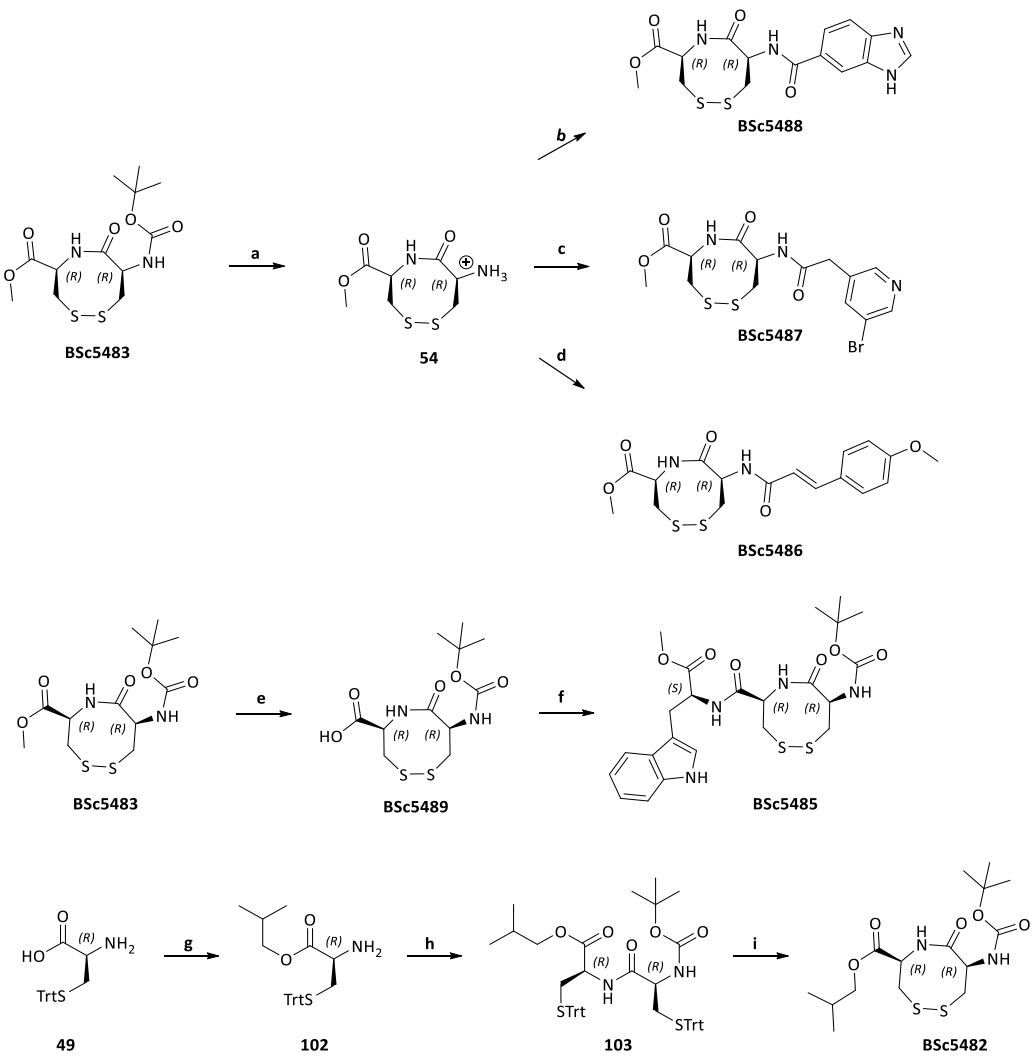

Scheme 9: Synthesis of a diverse set of analogues. Reagents a) DCM/TFA; b) DMF, 1H-benzo[d]imidazole-6-carboxylic, EDC, HOBt, 68%; c) DMF, 2-(5-bromopyridin-3-yl)acetic, EDC, HOBt, rt, 62%; d) DMF, (E)-3-(4-methoxyphenyl)acrylic, EDC.HCl, HOBt, 70%; e) DCE, $(CH_3)_3SnOH$, 98%; f) DMF, EDC, HOBt, 61%; g) *i*-Bu-OH, $SOCl_2$, 50%; h) DCM, N-(tert-butoxycarbonyl)-S-trityl-L-cysteine, EDC, HOBt, 78%; i) DCM/MeOH, I_2, 79%.

Having synthesized the main targets **BSc5484** and **BSc5517** with their analogues, they were further profiled regarding their solubility, kinase activity, cell permeability, *in vivo* efficacy, and toxicity. The upcoming chapters elaborate on the studies conducted with the synthesized compounds.

3.5 Biological Assays

3.5.1 *In vitro* assay

This chapter describes the *in vitro* kinase assay performed with the synthesized compounds **BSc5484**, **BSc5517** and their analogues.

3.5.1.1 *In vitro* kinase assay of BSc5484 and its diverse set of analogues

The *in vitro* kinase assay of **BSc5484** and its diverse analogues was carried out to evaluate their inhibitory activity against selected kinases. The assay was carried out based on a dose-response manner with the following kinases: ErbB2(h), Flt1(h), Fms(h), GSK-3β(h), PAK1(h), PDK1(h).

Since the aim was for cysteine targeting compounds to induce protein refolding or modulate kinase activity, the choice of kinases was based on the CysDFG-Kinases motif (Flt1(h), GSK-3β(h), and PAK1(h)) on the one hand, and for kinases harbouring cysteine residues either at the front region (ErbB2(h) and PDK1(h)) or at the hinge region (Fms(h)) (utilized as controls) on the other hand.

The residual kinase inhibition was determined with the commercial Eurofins Discovery KinaseProfiler service (KinaseProfiler Items 14-923KP, 14-551KP, 14-306KP, 14-939KP, 14-927KP, 14-452KP see experimental section **5.4.1** for detailed assay results).

Assay conditions

Residual kinase inhibition was determined with the commercial Eurofins Discovery Kinase Profiler service at three different concentrations of the compounds (2 μM, 20 μM and 100 μM). The ATP concentrations were 10 μM for PDK1(h) and ErbB2(h), 200 μM for Flt1(h) and Fms(h), 15 μM for GSK-3β(h) and 45 μM for PAK1(h) of the apparent Km for ATP. The human kinases were assessed in an enzymatic biochemical type utilizing a radiometric detection

technique, and the responses were evaluated using scintillation. Additional information about the testing procedure for each kinase is discussed in the following pages.

General procedure: The reaction commenced with the addition of the Mg/ATP mixture. After being incubated at room temperature for 40 minutes, the process was terminated by the addition of 0.5% phosphoric acid. Ten microlitres of the reaction were then transferred onto a P30 filter mat and subsequently washed four times for four minutes in 0.425% phosphoric acid and once in methanol. The filter mat was then dried, and scintillation counting was performed. The values obtained were averaged from two independent experiments.

In the case of Flt1(h) (Kinase Profiler ITEM 14-923KP), recombinant human Flt1 (783-end) was incubated with 0.2 mM EDTA, 8 mM MOPS pH 7.0, 250 uM KKKSPGEYVNIEFG, 10 mM MgAcetate and [g- 33P]-ATP (If needed, precise activity and concentration). The addition of the Mg/ATP mixture started the process. The reaction was stopped by the addition of 0,5 % phosphoric acid after 40 minutes of incubation at room temperature. After that, a reaction sample was taken, filtered, rinsed four times for four minutes in 0.425% phosphoric acid and one time in methanol, dried and counted by scintillation. The reference compound for inhibition, Staurosporine, had an IC_{50} of 2.2 nM.

In the case of Fms(h) (Kinase Profiler ITEM 14-551KP), recombinant human Fms (538-end) was incubated with 0.2 mM EDTA, 8 mM MOPS pH 7.0, 250 uM KKKSPGEYVNIEFG, 10 mM MgAcetate and [g- 33P]-ATP (If needed, precise activity and concentration). The addition of the Mg/ATP mixture started the process. The reaction was halted by the addition of 0.5% phosphoric acid after 40 minutes of incubation at room temperature. Before drying and scintillation counting, a reaction sample was transferred to a filter and washed four times for four minutes in 0.425% phosphoric acid and one time in methanol. The reference compound for inhibition, Staurosporine, had an IC_{50} of 5.39 nM.

In the case of GSK-3β(h) (Kinase Profiler ITEM 14-306KP), recombinant human GSK-3 (2-end; H350L) was incubated with 0.2 mM EDTA, 8 mM MOPS pH 7.0, 20 uM YRRAAVPPSPSLSRHSSPHQS(p) EDEEE (phospho GS2 peptide), 10 mM MgAcetate and [gamma-33P]-ATP (If needed, precise activity and concentration). Adding the Mg/ATP mixture started the process and was stopped after 40 minutes of incubation at room temperature by adding 0.5% phosphoric acid. A sample of the reaction was taken, filtered, rinsed four times

during four minutes in 0.425% phosphoric acid and one time in methanol, dried and counted by scintillation. The reference compound for inhibition, Staurosporine, had an IC_{50} of 9.3 nM.

In the case of ErbB2(h) (Kinase Profiler ITEM 14-939KP), recombinant human ErbB2 (676-end; G778D) was incubated with 0.2 mM EDTA, 8 mM MOPS pH 7.0, 0.1 mg/mL poly(Glu-Tyr), 5 mM MnCl2, 10 mM MgAcetate and [gamma-33P]-ATP (Specific activity and concentration on demand). The addition of the Mg/ATP mixture started the process and was stopped after 40 minutes of incubation at room temperature by the addition of 0.5% phosphoric acid. A sample of the reaction was then filtered and washed four times for four minutes in 0.425% phosphoric acid and one time in methanol before being dried and counted by scintillation. The reference compound for inhibition, Staurosporine, had an IC_{50} of 346.1 nM.

In the case of PAK1(h) (Kinase Profiler, ITEM 14-927KP), recombinant human PAK1 (150-end) was incubated with 0.2 mM EDTA, 8 mM MOPS pH 7.0, 200 uM RRRLSFAEPG, 10 mM MgAcetate and [gamma-33P]- ATP (If needed, precise activity and concentration). Adding the Mg/ATP mixture started the process and was stopped after 40 minutes of incubation at room temperature by adding 0.5% phosphoric acid. A reaction sample was subsequently taken, filtered, and rinsed four times for four minutes in 0.425% phosphoric acid and one time in methanol after being dried and counted by scintillation. The reference compound for inhibition, Staurosporine, had an IC_{50} of 0.68 nM.

In the case of PDK1(h)) (Kinase Profiler, ITEM 14-452KP), recombinant human PDK1 (52 end) was incubated with 100 uM KTFCGTPEYLAPEVRREPRILSEEEQEMFRDFDYIADWC (PDKtide), 50 mM Tris pH 7.5, 0.1% 6-mercaptoethanol, 10 mM MgAcetate and [gamma-33P]-ATP (If needed, precise activity and concentration). Adding the Mg/ATP mixture started the process and was stopped after 40 minutes of incubation at room temperature by adding 0.5% phosphoric acid. A reaction sample was later filtered and washed four times for four minutes in 0.425% phosphoric acid and once in methanol before being dried and counted by scintillation. The reference compound for inhibition, Staurosporine, had an IC_{50} of 3.83 nM.

TEST SAMPLE REQUIREMENTS

Minimum amounts for 1) Screening 60 µL 50X stock based on the highest concentration to be tested -OR- 100 µL 10 mM stock -OR- 1.5 mg (pre-weighed). 2) Dose-response: 100 µL 10 mM stock -OR- 1.5 mg (preweighed). 80 µL of 50X stock relative to the peak concentration to be tested.

As a result of the kinase assay, **BSc5484** revealed strong inhibition of human GSK-3β in a dose-dependent manner with apparent selectivity over the other tested kinases. Although almost all the kinases incubated with **BSc5484** were inhibited to a certain extent, Flt1(h), in contrast, indicated an increase in activity as the concentration of **BSc5484** diminished. Indeed, Flt1(h) activity increased gradually from 100 μM to 2 μM (concentration of **BSc5484**). However, **BSc5488** and **BSc5487** disclosed inhibition of human Flt1 at 100 μM compound concentration in a good to potent manner respectively (**Figure 20a**).

In the same way, **BSc5488** revealed strong inhibition of Flt1(h) in a dose-dependent manner, and **BSc5487** fully inhibited the activity of Flt1(h) at 100 μM compound's concentration.

It is worth mentioning that Flt1 kinase, also identified as vascular endothelial growth factor receptor-1 (VEGFR-1), has been connected with various pathological conditions, especially in angiogenesis and blood vessel formation. Disruption of Flt1 signalling has been suggested to have a role in diseases like cancer, diabetic retinopathy, and preeclampsia. It serves as a receptor for vascular endothelial growth factor (VEGF), which is important in stimulating blood vessel growth. In some instances, over activity of Flt1 may contribute to disease development by promoting excessive angiogenesis. Therefore, the remarkable inhibition of Flt1(h) by **BSc5487** might open paths for designing potent and selective Flt1(h) inhibitors via QSAR study in order to improve the compound's potency via targeted structural variations.

A moderate to strong inhibition of Human Fms by compounds **BSc5486**, **BSc5483**, **BSc5485** and **BSc5489** was also revealed in a dose-dependent manner.

Indeed, **BSc5485** revealed strong inhibition of human Fms and PDK1 in a dose-dependent manner, indicating that the indol ring was essential for inhibiting these kinases when comparing its activity to **BSc5483**.

The IC_{50}s of the compounds that disclosed either an apparent selectivity through specific kinase inhibition or which disclosed a moderate to strong inhibition (as highlighted with blue circles on their respective diagrams) were determined in **Figure 20b**. A relative IC_{50} value was provided.

Further details about the testing procedure can be found in the experimental section **5.4.1**.

As a side note, the increase of kinase activity, as noticed in some assay results, might be explained by the fact that:

- The incubated compound might be an activator of the kinase. This suggests that the compound binds to the kinase and induces a conformational change that enhances its activity.
- Alternatively, the compound may stabilise the kinase by maintaining the kinase in an active conformation.
- Finally, it is also conceivable that the compound might work as an inhibitor of a negative kinase regulator, leading to an increase in kinase activity.

a)

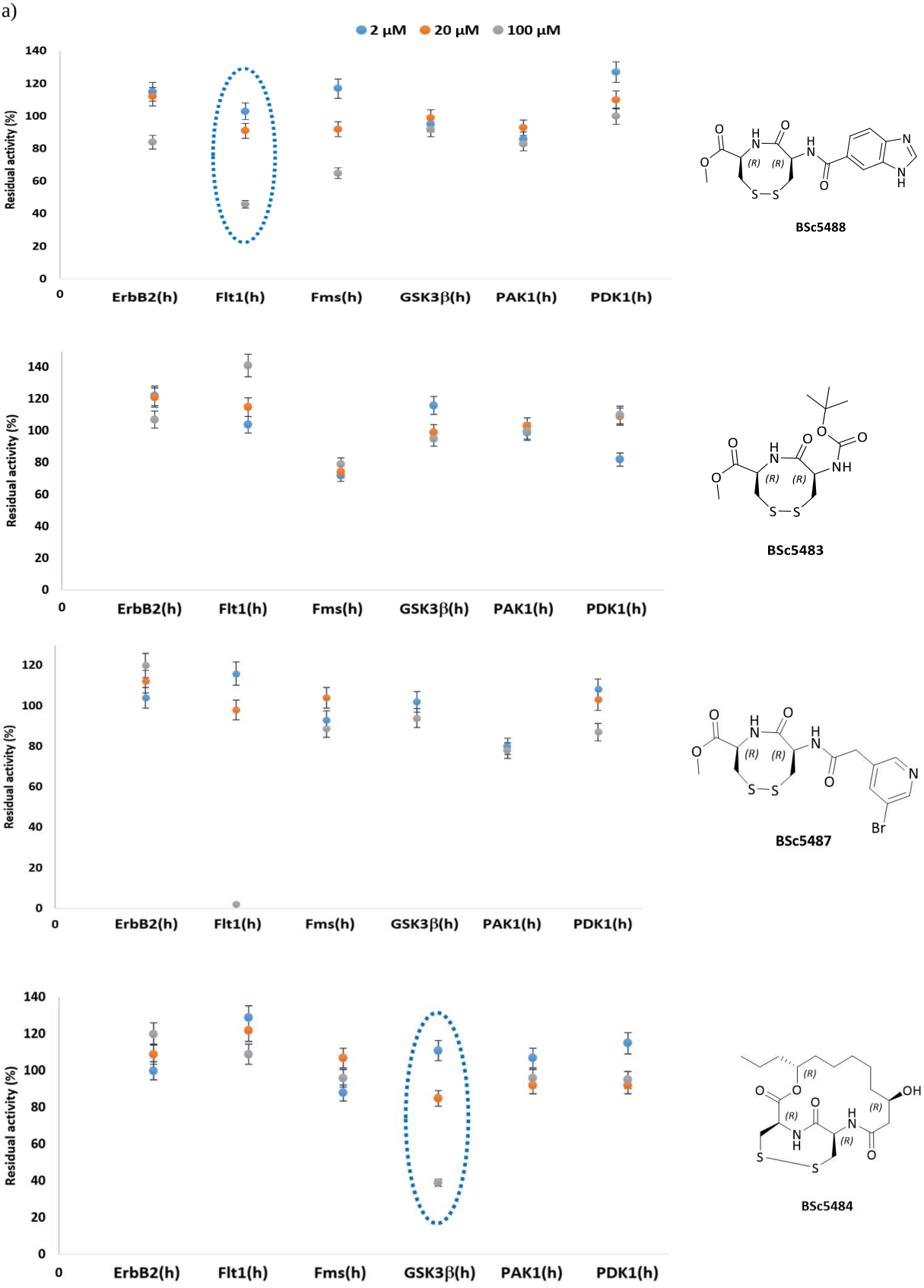

Figure 20: [a]Kinase inhibitory activity and [b]IC_{50} determination. [a]Eurofins Discovery KinaseProfiler service at ATP concentrations of 200 µM for Flt1(h), 15 µM for GSK-3β(h), 10 µM for PDK1(h) and ErbB2(h), 200 µM for Fms and 45 µM for PAK1(h).

a)

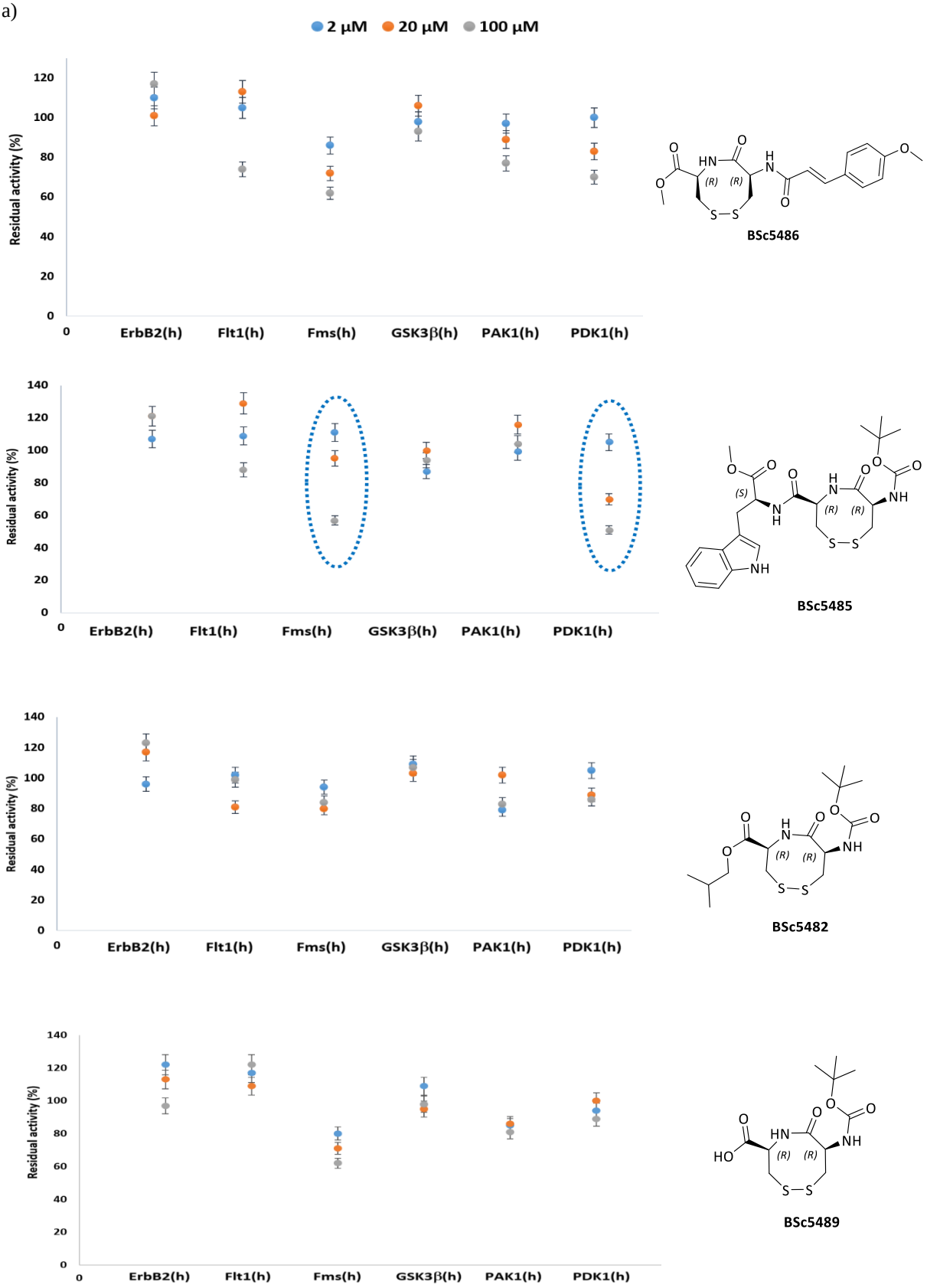

Figure 20: [a]Kinase inhibitory activity and [b]IC_{50} determination. [a]Eurofins Discovery KinaseProfiler service at ATP concentrations of 200 µM for Flt1(h), 15 µM for GSK-3β(h), 10 µM for PDK1(h) and ErbB2(h), 200 µM for Fms and 45 µM for PAK1(h).

b)

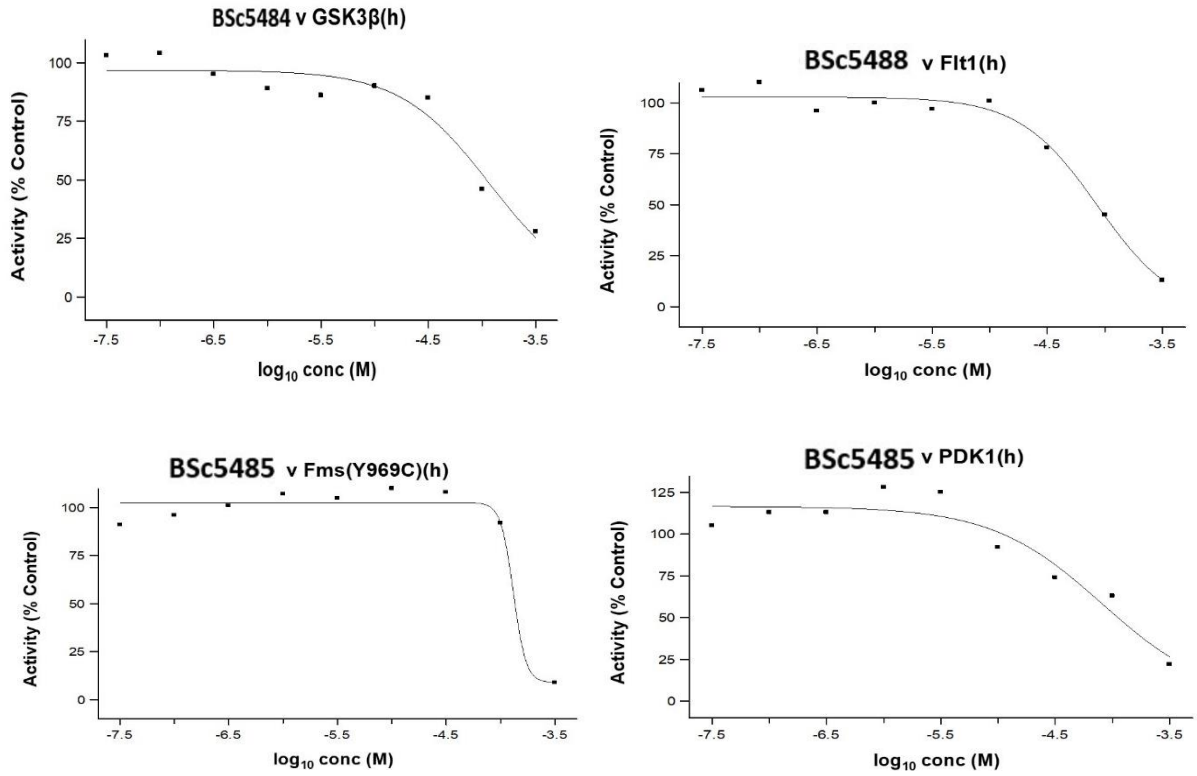

	IC50 / µM							
Cpds.	GSK-3β(h)	95% CI	Fms(Y969C)(h)	95% CI	Flt1(h)	95% CI	PDK1(h)	95% CI
BSc5484	116.9	112.3 - 121.15	n.d.		n.d.		n.d.	
BSc5488	n.d.		n.d.		86.5	84.5 – 88.5	n.d.	
BSc5485	n.d.		131.1	125.1 - 137.1			111.6	109.6 – 113.6

Figure 20: [a]Kinase inhibitory activity and [b]IC_{50} determination. [b]Eurofins Discovery IC_{50}Profiler service at Km, ATP. CI, confidence interval; n.d., not determined.

As a conclusion of this kinase assay conducted, most of the tested compounds revealed moderate inhibition of the kinases in a dose-dependent manner. **BSc5487** and **BSc5485** were the more active and **BSc5485** indicated remarkable inhibition of Fms(h) and PDK1(h). **BSc5487** indicated almost complete inhibition of Flt1(h) at 100 µM concentration.

A crystallographic experiment to confirm the binding mode of **BSc5484**, **BSc5485** and **BSc5488** into their respective target proteins might be important for structural optimization. Alternatively, a mass-spectroscopy experiment to identify any covalent adduct to the kinase might also provide the first clues about the binding mode.

3.5.1.2 *In Vitro* Kinase assay of synthesized (*S*)-5-bromo-1-(1-(methylamino)-2-(methylthio)ethyl)-9*H*-pyrido[3,4-β]indol-6-ol (BSc5517) and its diverse set of analogues

The *in vitro* kinase assay of **BSc5517** and its synthesized analogues (**BSc5515**, **BSc5516** and **BSc5518)** was performed to evaluate the inhibitory activity against preselected kinases. The assay was carried out based on a dose-response manner with the following kinases: β-Raf(h), CDK1/cyclinB(h), CDK4/cyclinD3(h), CK2α1(h), DYRK1A(h), GSK-3α(h), GSK-3β(h), Haspin(h) and MEK1(h).

These kinases were selected for the following reasons:

- To have clues of the therapeutic potential of these compounds against diseases associated with the dysregulation of these kinases.
- After carefully screening kinases whose activity was strongly influenced upon incubation with related β-carbolines. [153-158a]
- To have an idea of the possible mechanism of action of these compounds and how they interact with these kinases

Description of the assay condition

The residual kinase inhibition was determined with the commercial Eurofins Discovery KinaseProfiler service (KinaseProfiler Items 14-530KP, 14-450KP, 14-957KP, 14-445KP, 14-951KP, 14-492KP, 14-306KP, 14-744KP, 14-429KP see experimental section **5.4.1.1** for detailed about the procedure).

Residual kinase inhibition was determined with the commercial Eurofins Discovery Kinase Profiler service at three different concentrations of the compounds (2, 20 and 100 μM) and ATP concentrations of 120 μM for B-Raf(h); 45 μM for CDK1/cyclinB(h); 200 μM for CDK4/cyclinD3(h); 10 μM for CK2α1(h), MEK1(h) and GSK-3α(h); 45 μM for DYRK1A(h); 15 μM for GSK-3β(h); 70 μM for Haspin(h) of the apparent Km for ATP. Human kinases were assessed in an enzymatic biochemical type utilizing a radiometric detection technique, and the

responses were evaluated using scintillation. Additional information about the testing procedure for each kinase is described below.

General procedure: The reaction was initiated by the addition of the Mg/ATP mix. The reaction was halted by the addition of 0.5% phosphoric acid after 40 minutes of incubation at room temperature. Ten microlitres of the reaction were briefly spotted onto a P30 filter mat and rinsed four times for four minutes in 0.425% phosphoric acid and once in methanol before the samples were dried and counted by scintillation.

TEST SAMPLE REQUIREMENTS: Minimum for 1) Screen: 60 µL of 50X stock solution relative to the highest concentration to be assayed -OR- 100 µL of 10 mM stock solution -OR- 1.5 mg (pre-weighed). 2) Dose-response: 80 µL of 50X stock solution based on the peak concentration to be determined -OR- 100 µL of 10 mM stock solution -OR- 1.5 mg (pre-weighed).

In the case of B-Raf(h) (Kinase Profiler ITEM 14-530KP), recombinant human B-Raf (416-end) was incubated with 25 mM Tris/HCl pH 7.5, 0.2 mM EGTA, 10 mM DTT, 0.01% Triton X-100, 0.5 mM sodium orthovanadate, 0. 5 mM 6-glycerophosphate, 1% glycerol, 34 nM inactive MEK1, 69 nM inactive MAPK2, 0.5 mg/mL myelin basic protein and 10 mM MgAcetate and [gamma-33P]-ATP (specific activity and concentration as needed). The reaction was activated by the introduction of the Mg/ATP combination and stopped by adding phosphoric acid to a concentration of 0.5% after incubation for 40 minutes at room temperature. A reaction sample was taken, filtered, rinsed four times during four minutes in 0.425% phosphoric acid and one time in methanol, dried and counted by scintillation. The reference compound for inhibition, Staurosporine, had an IC_{50} of 61.02 nM.

In the case of CDK1/cyclinB(h) (Kinase Profiler ITEM 14-450KP), 8 mM MOPS pH 7.0, 0.2 mM EDTA, 0.1 mg/mL histone H1, 10 mM MgAcetate, and [gamma-33P]-ATP (specific activity and concentration as necessary) were incubated with full length recombinant human CDK1/cyclinB. The addition of the Mg/ATP mixture started the process, and after 40 minutes of incubation at room temperature, the stage was terminated by the addition of 0.5% phosphoric acid. Prior to drying and scintillation counting, an aliquot of the reaction was spotted on a filter and washed four times for four minutes in 0.425 % phosphoric acid and one time in methanol. The reference compound for inhibition, Staurosporine, had an IC_{50} of 1.59 nM.

In the case of CDK4/cyclinD3(h) (Kinase Profiler ITEM 14-957KP), Full length recombinant human CDK4/cyclinD3 was incubated with 8 mM MOPS pH 7.0, 0.2 mM EDTA, 0.03% BSA, 0.03% Tween 20, 0.2 mg/ml Rb fragment and 20 mM DTT, 10 mM MgAcetate and [gamma-

33P-ATP] (specific activity and concentration as needed). The addition of the Mg/ATP mixture started the process. After an incubation period of 40 minutes at room temperature, the process was stopped by the addition of 0.5 % phosphoric acid. A sample of the reaction was then applied to a filter and washed four times for 4 minutes in 0.425% phosphoric acid and one time in methanol before being dried and counted by scintillation. The reference compound for inhibition, Staurosporine, had an IC_{50} of 89.01 nM.

Full-length recombinant human CK2α1 (h) (Kinase Profiler ITEM 14-445KP) was incubated with 20 mM HEPES pH 7.4, 0.15M NaCl, 0.1mM EDTA, 5mM DTT, 0.1% Triton X-100, 165 uM RRRDDDSDDD, 10 mM MgAcetate, and [gamma-33P-ATP] (As needed, specific activity and concentration). The addition of the Mg/ATP mixture started the process and stopped by incubating it with 0.5% phosphoric acid after incubation for 40 minutes at room temperature. Prior to being dried and scintillation counted, an aliquot of the reaction was spotted on a filter and washed four times for four minutes in 0.425 % phosphoric acid and one time in methanol. The reference compound for inhibition PKR Inhibitor had an IC_{50} of 741.88 nM.

In the case of DYRK1A(h) (Kinase Profiler ITEM 14-951KP), full length recombinant human DYRK1A was incubated with 0.2 mM EDTA, 8 mM MOPS pH 7.0, 50 uM RRRFRPASPLRGPPK, 10 mM MgAcetate and [gamma-33P]-ATP (As needed, specific activity and concentration). The addition of the Mg/ATP mixture started the process and stopped by administrating it with 0.5% phosphoric acid after incubation for 40 minutes at room temperature. Prior to being dried and scintillation counted, an aliquot of the reaction was spotted on a filter and washed four times for four minutes in 0.425 % phosphoric acid and one time in methanol. The reference compound for inhibition, Staurosporine, had an IC_{50} of 6.71 nM.

In the case of GSK-3α(h) (Kinase Profiler ITEM 14-492KP), recombinant human GSK-3α (2-end; S449A) was incubated with 0.2 mM EDTA, 8 mM MOPS pH 7.0, 20 uM YRRAAVPPSPSLSRHSSPHQS(p) EDEEE (phospho GS2 peptide), 10 mM MgAcetate and [gamma-33P]-ATP (specific activity and concentration as required). The addition of the Mg/ATP mixture started the process and stopped by administrating it with 0.5% phosphoric acid after incubation for 40 minutes at room temperature. Prior to being dried and scintillation counted, an aliquot of the reaction was spotted on a filter and washed four times for four minutes in 0.425 % phosphoric acid and one time in methanol. The reference compound for inhibition, Staurosporine, had an IC_{50} of 4.93 nM.

In the case of GSK-3β(h) (Kinase Profiler ITEM 14-306KP), recombinant human GSK-3α (2-end; H350L) was incubated with 0.2 mM EDTA, 8 mM MOPS pH 7.0, 20 uM YRRAAVPPSPSLSRHSSPHQS(p) EDEEE (phospho GS2 peptide), 10 mM MgAcetate and [gamma-33P]-ATP (specific activity and concentration as required). The addition of the Mg/ATP mixture started the process and stopped by administrating it with 0.5% phosphoric acid after incubation for 40 minutes at room temperature. Prior to being dried and scintillation counted, an aliquot of the reaction was spotted on a filter and washed four times for four minutes in 0.425 % phosphoric acid and one time in methanol. The reference compound for inhibition, Staurosporine, had an IC_{50} of 9.3 nM.

In the case of Haspin(h) (Kinase Profiler ITEM 14-744KP), recombinant human Haspin (471-end) was incubated with 0.2 mM EDTA, 8 mM MOPS pH 7.0, 500 uM RARTLSFAEPG, 10 mM MgAcetate and [g- 33P]-ATP (specific activity and concentration as required). The addition of the Mg/ATP mixture started the process. The reaction was halted by adding 0.5% phosphoric acid after incubating for 40 minutes at room temperature. Prior to being dried and scintillation counted, an aliquot of the reaction was spotted on a filter and washed four times during four minutes in 0.425 % phosphoric acid and one time in methanol. The reference compound for inhibition, Staurosporine, had an IC_{50} of 2.41 nM.

In the case of MEK1(h) (Kinase Profiler ITEM 14-429KP), full-length recombinant human MEK1 was incubated with 0.2 mM EGTA, 50 mM Tris pH 7.5, 0.1% 6-mercaptoethanol, 0.01% Brij-35, 1 uM unactive MAPK2 (m), 10 mM MgAcetate and cold ATP (Specific activity and concentration according to the requirements). The addition of Mg/ATP initiated the process. After incubation for 40 minutes at ambient temperature, 5 uL of this incubation mixture was used to initiate a MAPK2 (m) assay. The reference compound for inhibition, Staurosporine, had an IC_{50} of 6.76 nM.

According to the kinase assay, it was constantly remarked that DYRK1A(h) and Haspin(h) were drastically inhibited by all the compounds in a dose-dependent manner (**Figure 21**). Furthermore, **BSc5515** and **BSc5516** particularly inhibited CDK1/cyclinB(h), DYRK1A(h) and Haspin(h). Indeed, **BSc5515** revealed strong inhibition of DYRK1A (h) and potent inhibition of Haspin(h) in a dose-dependent mode. **BSc5516**, on the other hand, indicated strong inhibition of CDK1/cyclinB(h) and Haspin(h) while potently inhibiting Haspin(h) also in a dose-dependent fashion. **BSc5517** was the most potent compound with remarkable inhibition of all the tested kinase dose-dependently. **BSc5518**, on the other hand, was the second most potent compound, although it indicated only moderate inhibition of CDK4/cyclinD3(h).

To summarise, **BSc5517** and **BSc5518** revealed moderated to potent inhibition of all the kinases in a dose-dependent manner. Despite **BSc5517** happened to be the most potent compound, **BSc5515** and **BSc5516** indicated selective inhibition of specific kinases.

This experiment's results followed previous works reported on the same kinases with related β-carboline-based compounds. [153, 157]

Haspin(h) was revealed to be the most inhibited kinase in this series and the Eudistomidin C's scaffold indicated to be a viable structure for obtaining potent lead compounds upon further structural refinement for disease associated with Haspin kinase dysregulation.

Melms et al. disclosed that inhibition of haspin kinase promotes both cell-intrinsic and extrinsic anti-tumour activity. This includes reduced proliferation, recruitment of cGAS, frequent micronuclei formation, and activation of the cyclic GMP-AMP synthase (cGAS)-stimulator of interferon genes (STING) route. [158b]

Moreover, Cuny *et al*. reported Harmine (**14**) as a potent Haspin inhibitor. Although Harmine might provide a valuable scaffold for the design of optimised drug candidates, its adverse effects on the central nervous system limit interest in its use as therapeutic. [157] The main problem to be solved is the co-inhibition of MAO-A-Harmine, which generates severe side effects upon treatment. [159] Therefore, the identification of related β-carboline with potent inhibitory activity against Haspin and weak inhibition of MAO-A might be a promising compound for disease-causing Haspin dysregulation, such as cancer and neurodegenerative diseases.

3.5.1.3 Structure-activity relationship study of the synthesized (*S*)-5-bromo-1-(1-(methylamino)-2-(methylthio)ethyl)-9*H*-pyrido[3,4-β]indol-6-ol (BSc5517) and its analogues

The structural similarity between **BSc5517**, **BSc5515**, **BSc5516** and **BSc5518** was utilized to comment on how their chemical structure influences the kinase activity. From a direct comparison of the kinase assay results of **BSc5518** and **BSc5515**, one might firmly hypothesise that having the free hydroxyl as a substituent at the C-6 position of the β-carboline skeleton is essential for inhibitory activity. This was confirmed by the kinase inhibitory activity result of **BSc5518** and **BSc5515**, respectively, disclosing that more kinases were inhibited when incubated with **BSc5518** rather than when incubated with **BSc5515** (**Figure 21**). The kinase assay results of **BSc5517** and **BSc5516** further confirmed this remark.

Although **BSc5516** and **BSc5517** harbour a bromine atom at the C-5 position, **BSc5517** was the most potent, likely due to the possible interactions established by the free hydroxyl group at the C-6 position acting as a hydrogen bond donor/acceptor. Thus, the free hydroxyl group might interact with amino acid residues of the kinases, drastically influencing the inhibitory activity. Furthermore, having the bromine and the free hydroxyl group at the C-5 and C-6 positions was beneficial for inhibitory activity, as confirmed by the kinase activity diagrams of **BSc5517** and **BSc5518** compared to **BSc5515** and **BSc5516**. This is likely because the bromine atom might be involved in halogen bond interactions influencing the kinase activity. Furthermore, **BSc5516** displayed a better inhibition of CDK1 than **BSc5515**, likely due to an additional bromine atom at the C-5 position of **BSc5516**, which is believed to be involved in a halogen bond interaction.

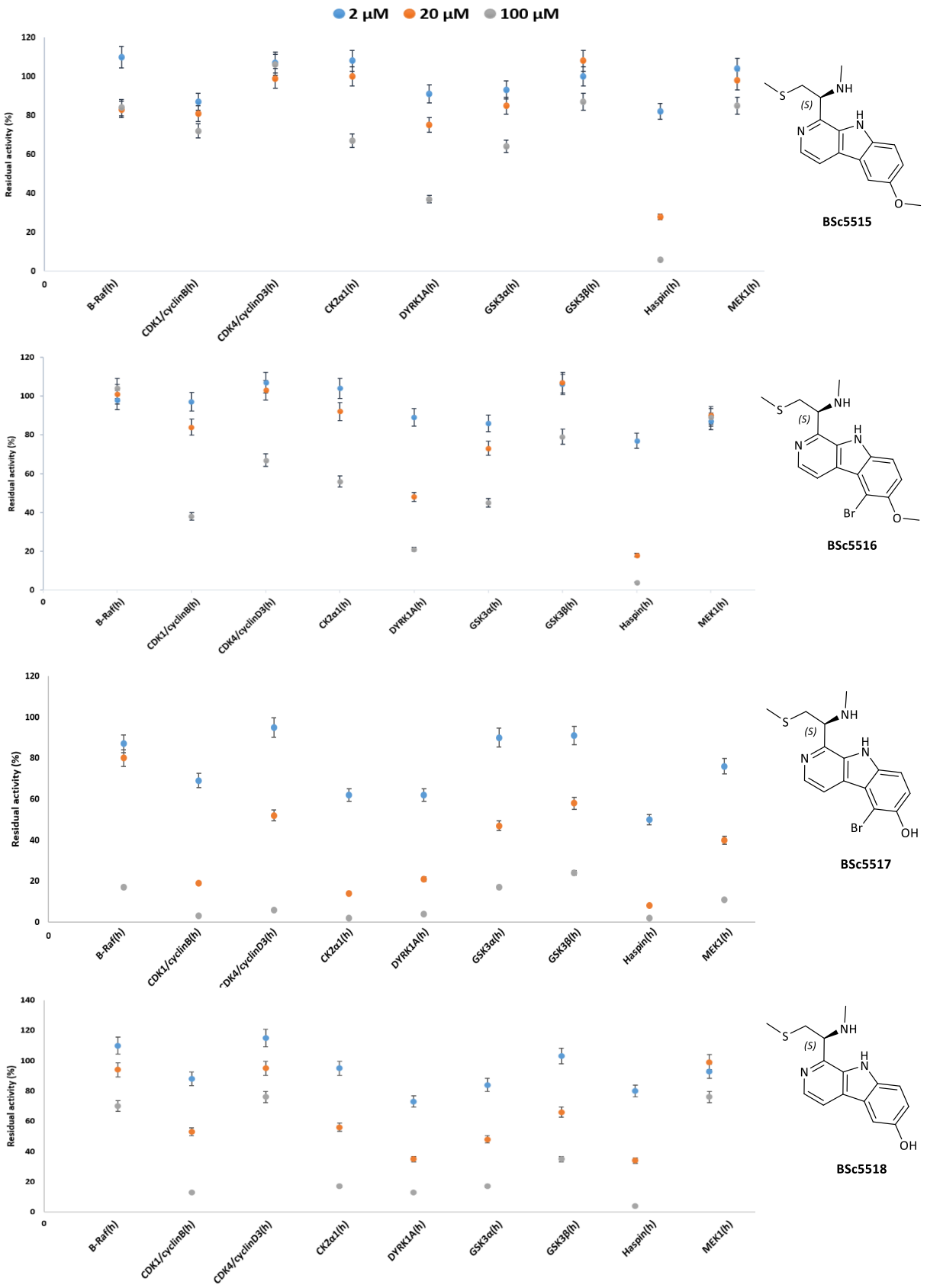

Figure 21: Kinase inhibitory activity of **BSc5517**, **BSc5515**, **BSc5516** and **BSc5518**. Eurofins Discovery KinaseProfiler service at ATP concentrations of 120 µM for β-Raf(h), 45 µM for CDK1 and DYRK1A(h), 200 µM for CDK4, 10 µM for CK2α1, MEK1(h) and GSK-3α(h), 15 µM for GSK-3β(h) and 70 µM for Haspin(h). Error bars, which are smaller compared to the size of the symbol, are not displayed. See the experimental section **5.4.1.1** for more details.

3.5.2 Cell viability assay of Eudistomidin C ((*S*)-5-bromo-1-(1-(methylamino)-2-(methylthio)ethyl)-9H-pyrido[3,4-β]indol-6-ol) (Bsc5517)

Recent work indicated that the naturally isolated Eudistomidin C (**BSc5517**) revealed single-digit micromolar inhibition of murine leukaemia cells. [39] To have an idea of the effect of the synthesized **BSc5517** in human cells, **BSc5517** was profiled *in vitro* for cell viability on THP-1 cells.

THP-1 is a monocytic human leukaemia cell line frequently used in studies on monocyte/macrophage activities, processes, drug transport, signalling pathways and nutrients. Besides, this cell line has become a popular model for estimating monocyte and macrophage activity regulation. THP-1 cell lines can be utilized to study immune system disorders, immunology, and toxicology. It should be noted that these are suspension cells, and floating cells are viable.

To evaluate whether **BSc5517** is toxic for human cells, THP-1 cells were incubated with 0.1 µM, 1 µM and 10 µM of **BSc5517** for 24 hrs, 2 hrs, 1 h, 30 minutes and 10 minutes. The assay was carried out in triplicates, and non-incubated cells were utilized as control (0 µM). The viability of THP-1 cells after incubating with **BSc5517** is shown in **Figure 22** (See experimental section **5.4.1.4**. for details on the testing procedure).

As a result of the assay, the cells incubated with 0.1 µM, 1 µM and 10 µM of **BSc5517** slightly affected the viability of THP-1 cells, especially 10 min and 24 hrs after incubation. The result indicated that **BSc5517** was not toxic for THP-1 cells at concentrations below or equal to 10 µM and revealed no measurable influence on cell viability.

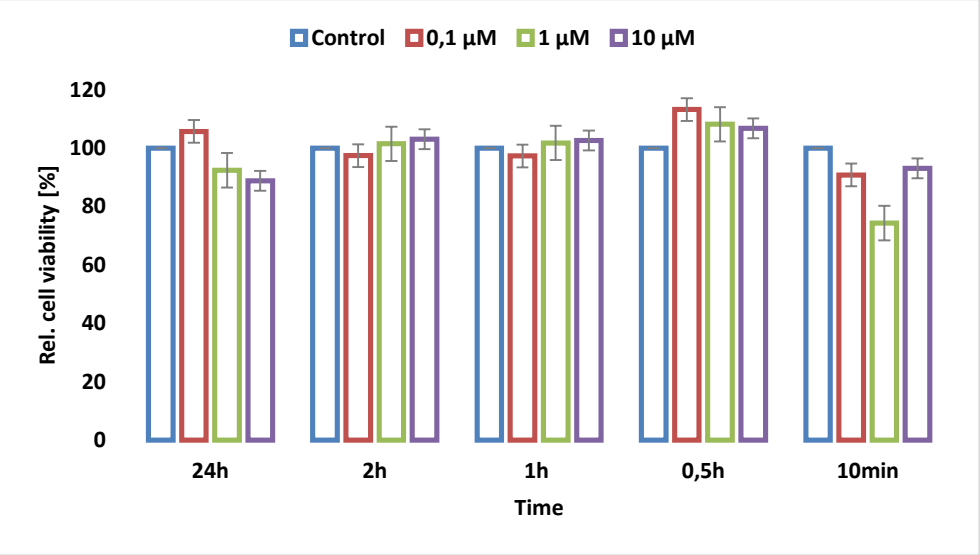

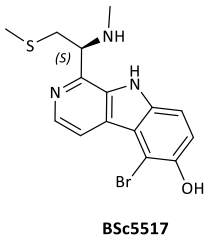

BSc5517

Standard deviations				
	Control	**0,1µM**	**1 µM**	**10 µM**
24 hrs	0.94675	6.67342	15.07825	6.99932
2 hrs	0.88978	5.68817	14.67248	7.11478
1 hr	0.90395	5.61987	15.09098	6.42876
0.5 hr	0.61179	5.41664	14.62948	6.3381
10 min	0.88612	5.56156	14.82096	7.37146

Figure 22: Cell viability of THP-1 cells incubated with various concentrations of **BSc5517** at different incubation times. The cells were seeded with a density of 1x105 cells per well on poly-L-Lysine coated black 96 well-plates with a clear bottom and incubated with 0 µM (control), 0.1 µM, 1 µM and 10 µM of **BSc5517** for 24 hrs, 2 hrs, 1 h, 30 minutes or 10 minutes at 37 °C and 5% CO_2. PBS was used to wash the cells (pH 7.4) and incubated with 0,01 mg/mL Resazurin in PBS (pH 7.4) for 3 hours. The assay was performed in triplicates and measured at λ_{ex} 535 nm and λ_{em} 585 nm. The gain was adjusted to the positive control (Gain 95). The mean and the standard deviation were calculated and normalized to the positive control of the same timepoint (100%) and shown as the relative cell viability in %. The error bars, which are smaller than the symbol's size, are not displayed. The error bars specify the standard deviation (SD) of 3 experiments.

3.5.3 *In vivo* assay

3.5.3.1 Shake-Flask Solubility assay

With the promising activity of the synthesized compounds *in vitro*, their study *in vivo* was undertaken. A bioavailability profile and stability evaluation under buffer conditions were investigated as a primary step.

In drug discovery and development, the aqueous solubility of pharmaceutically active compounds and their accurate determination play a central role. Approximately 90% of molecules in the discovery pipeline and almost 40% of New Chemical Entities (NCEs) are believed to have low water solubility, resulting in poor oral bioavailability and suboptimal drug delivery. [160, 161] Poor solubility is a primary reason for the failure of drug candidates and tops the list of undesirable compound properties. A compound must first reach the desired site of action and bind to the target protein to succeed as an active ingredient. The physicochemical properties of a chemical, such as solubility, lipophilicity and acidity or basicity, are the main determinants of its bioavailability.

The most critical physicochemical parameter for sufficient compound bioavailability is its solubility in water. This is because most of the dissolved substances can be distributed in the body easily via the bloodstream and thus reach the site of action. Therefore, high water solubility is essential for a compound to be effective in the body.

The shake-flask method was utilised to evaluate the solubility properties of the synthesised compounds, and their ClogP values were calculated. [162]

As water solubility also serves as selection criteria for candidate compounds for further evaluation of derivatives in cellular and *in vivo* assays, the solubility of **BSc5484**, **BSc5485**, **BSc5486**, **BSc5487**, **BSc5488**, **BSc5482**, **BSc5517**, **BSc5483**, **BSc5515**, **BSc5516** and **Bsc5518** was measured.

The shake-flask method used in this case is described in detail in the experiment section **5.4.1.3**. According to the *in vivo* assay conditions, the measurements were performed in deionised water with 2 vol% DMSO.

Table 2: Aqueous solubility determination of the synthesized compounds. The solubility was revealed using the shake-flask method [162] followed by HPLC measurements. According to the *in vivo* assay conditions, all samples were dissolved in deionized water with 2-vol% DMSO content.

Compounds	*ClogP[a]*	*Solubility [µg/mL]*	*Solubility [µM]*
BSc5484	2.62	28.04	67.0
BSc5485	2.92	8.3	15.9
BSc5486	2.28	10.3	26.0
BSc5487	1.05	30.02	69.1
BSc5488	1.48	25.4	66.8
BSc5482	3.15	7.03	18.7
BSc5517	2.81	10.6	29.0
BSc5483	1.70	24.9	74.0
BSc5515	2.57	9.6	32.0
BSc5516	3.21	8.9	26.5
BSc5518	2.07	11.04	38.4

[a] Computed with ChemDraw Professional (version 15.0.0.106). [123]

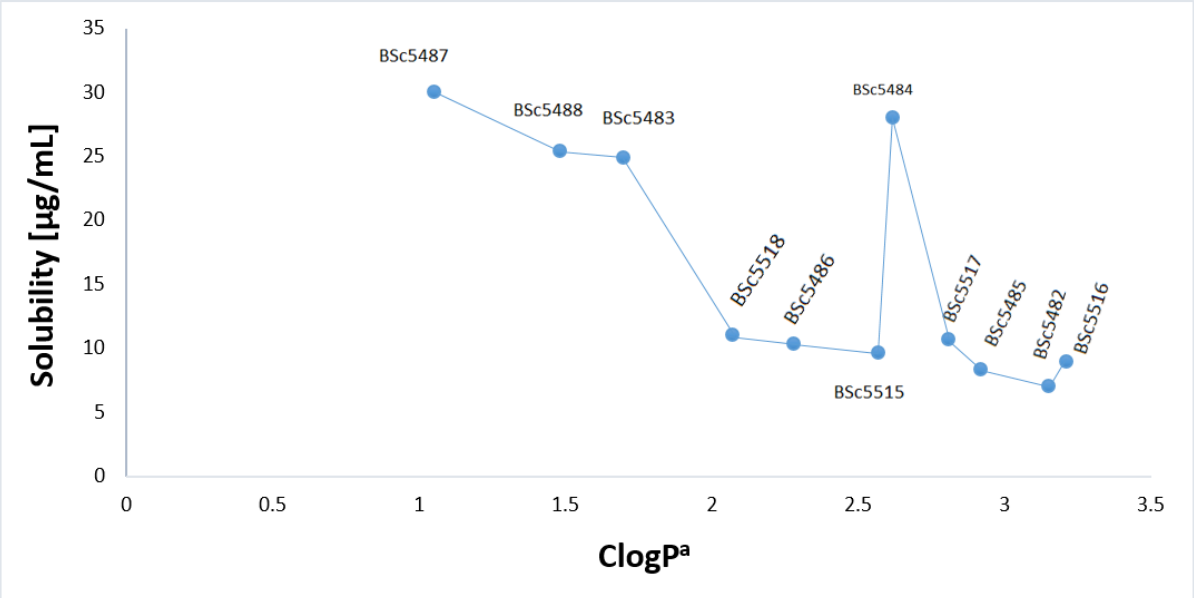

Plot of solubility curve versus ClogP

The calculated ClogP values correlated with the measured aqueous solubility values. However, **BSc5482** and **BSc5516**, with ClogP values of 3.15 and 3.2 respectively, were hardly water-soluble (**Table 2**). An unexpectedly poor solubility of **BSc5486** and **BSc5485**, with calculated

ClogP values of 2.28 and 2.92 respectively, was also registered. Moreover, the newly developed dithiazocane derivatives **BSc5487**, **BSc5488** and **BSc5483** indicated they were more soluble in water than **BSc5484** and might give avenues for further *in vivo* testing. **BSc5487** revealed the highest solubility compared to **BSc5482**, which might be explained by the relatively high polarity and the electronegativity of the atoms linked to the lipophilic fragment of **BSc5487**.
On the other hand, the high aqueous solubility revealed by **BSc5517** compared to **BSc5515** and **BSc5516** is more likely due to the free hydroxy on ring A of its β-carboline skeleton, which is methyl-protected on ring A of **BSc5515** and **BSc5516**, respectively. Moreover, it is believed that the higher polarity disclosed by **BSc5518** compared to **BSc5517** is likely owed to the absence of the bromine atom on ring A of **BSc5518**.

3.5.3.2 Buffer-stability assay

The stability of the synthesized compounds under buffer conditions was assessed by employing an HPLC-based assay. The experiment was carried out over 144 hours (6 days), and the buffers were made of potassium phosphate at pHs 6.8, 7.4 and 8.0, as indicated in the diagrams (**Figure 23**). Further details can be found in the experimental section **5.4.1.5**.

According to the assay performed, all the tested compounds displayed stability under the different buffer conditions for up to 96 hours (4 days). At pH 7.4, **BSc5485**, **BSc5487**, **BSc5488**, **BSc5515** and **BSc5517** displayed a minor degradation from day 6 onwards and under very slightly acidic conditions (pH 6.8), **BSc5483** and **BSc5482** revealed degradation from day 4 onwards. This degradation is likely due to the cleavage of the Boc-Protecting group, which is usually easily cleaved under acidic conditions. At pH 8.0, all the tested compounds revealed stability until at least day 5 (after 120 hours in the buffer). From day 6 onwards, the first signs of degradation were observed for **BSc5485**, **BSc5487**, **BSc5488**, **BSc5515** and **BSc5517**.
F**igure 22** on the following pages highlights the diagrams of each compound utilized for the buffer stability test.

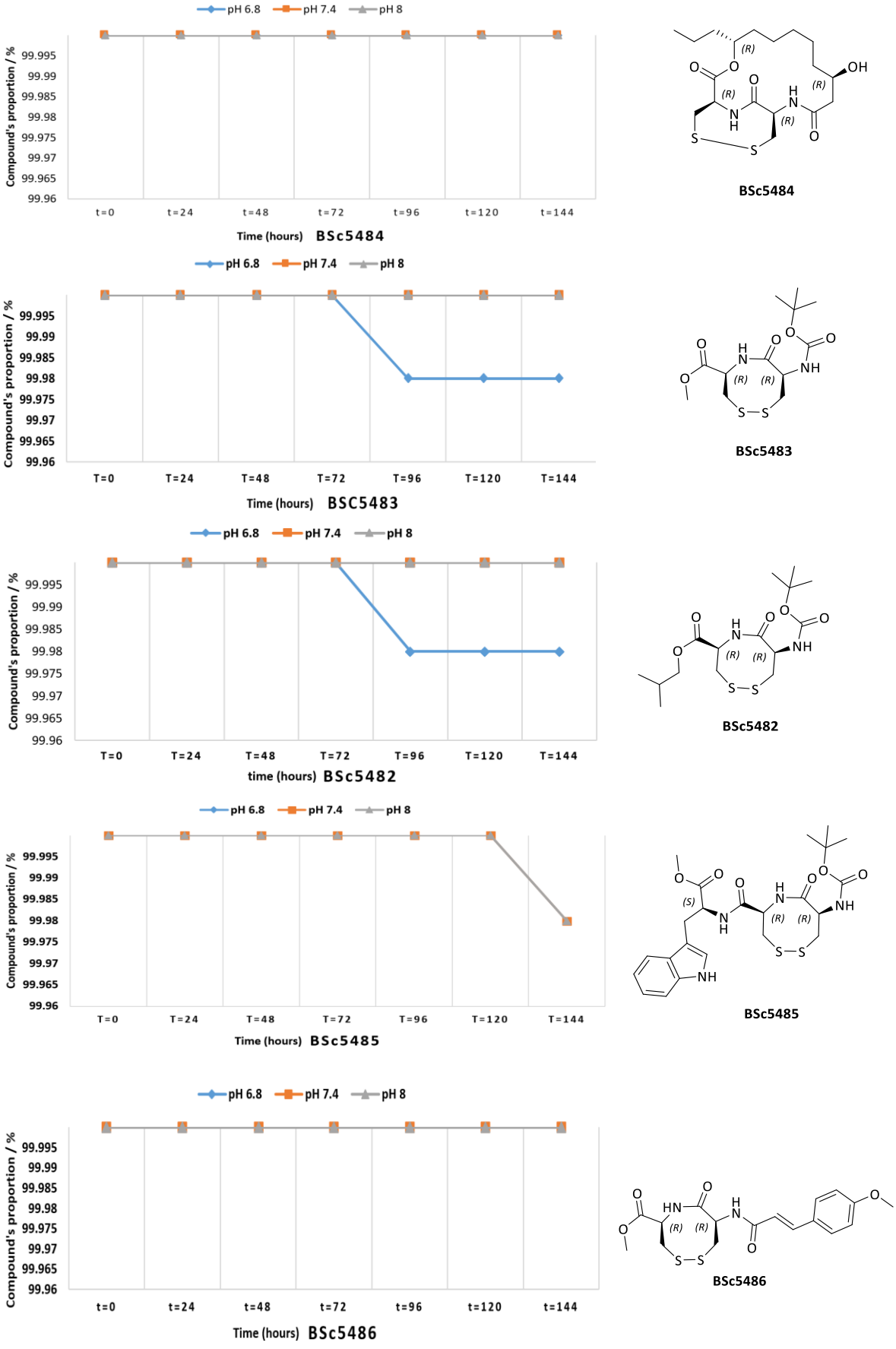

Figure 23: Stability assay of the compounds under Potassium phosphate buffer conditions (pHs 6.8, 7.4 and 8.0).

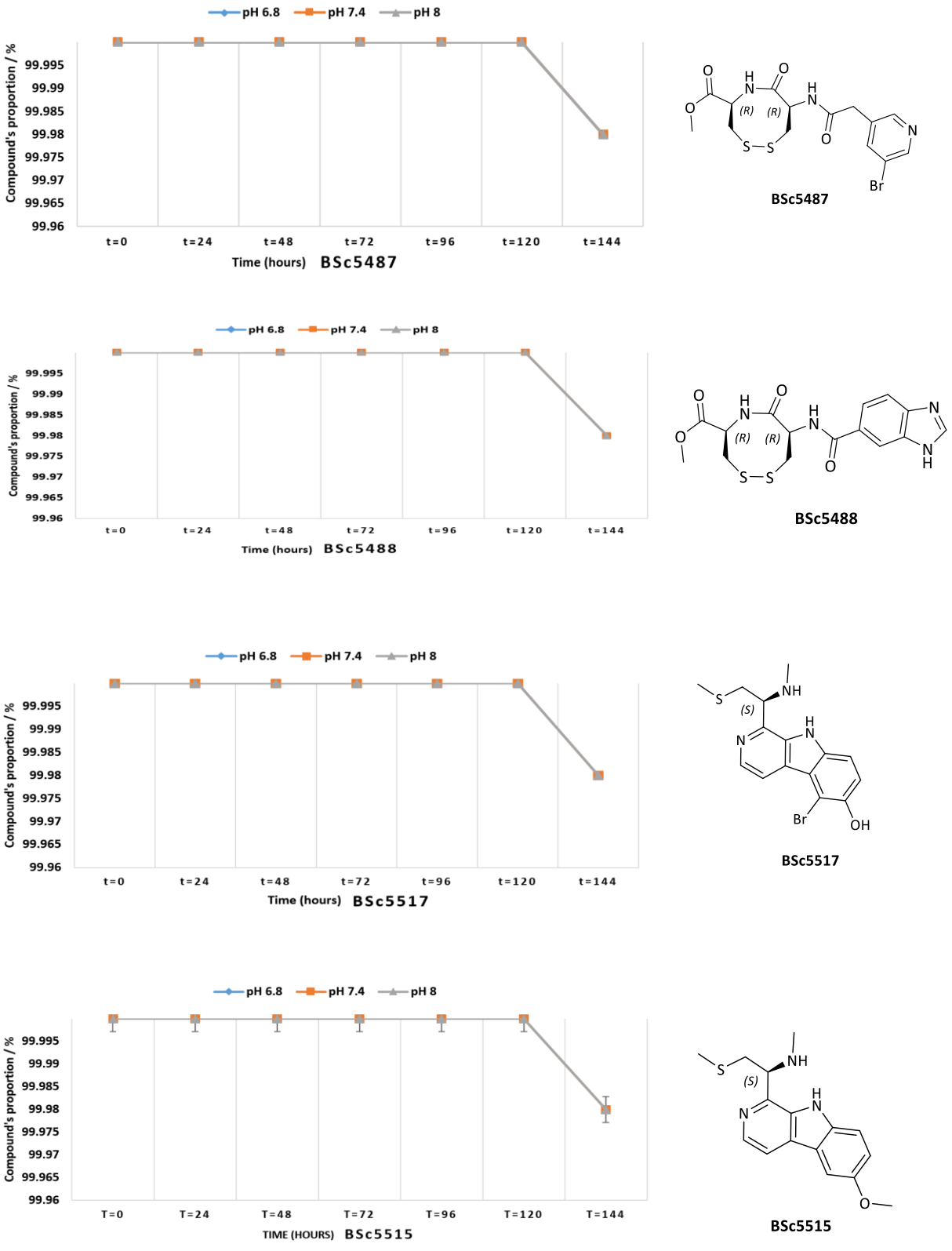

Figure 23: Stability assay of the compounds under Potassium phosphate buffer conditions (pHs 6.8, 7.4 and 8.0).

The following chapter describes the *in vivo* toxicology assay performed in zebrafish embryos.

3.5.3.3 *In Vivo* Profiling of the compounds in Wild-Type and Gold-type Zebrafish embryos *Danio rerio*

With the promising *in vitro* kinase assay of some of the synthesized compounds, a study of their *in vivo* efficacy in zebrafish embryos *Danio rerio* was undertaken. The investigation was performed with wild-type and gold-type zebrafish embryos according to the guidelines released by M. Haldi *et al*. in the article entitled ‘’Zebrafish: Methods for Assessing Drug Safety and Toxicity’’ (see experimental section **5.4.2.1** for further details of the experiments). [163]

The zebrafish (*Danio rerio*) has become a practical aquatic vertebrate model for studying developmental processes and determining the toxicological effects of chemicals and drugs in recent decades. It is an internationally standardized model. [164] The zebrafish of *Danio rerio* type is a freshwater fish which inhabits tropical regions. It originates from Pakistan and India, having a small size. [165, 166] Naturally, distinct lines appear with characteristic pigmentation. Zebrafish have a high fertility rate (60-200 eggs per spawning), a short embryo development period (5 days) and a small size. The embryo is generally transparent and develops outside the mother’s body. [167, 168] The zebrafish has become a helpful model in toxicological and pharmacological research because of these characteristics.

Phenotypic changes can occur when zebrafish are incubated with test drugs or chemicals. This allows conclusions to be drawn about the safety and permeability of the substances in question.

The synthesized compounds were tested in *Danio rerio* wild-type and gold-type for toxicity in order to provide first indications about the toxicological and teratological effects of the synthesised compounds and to relate these to the structural variations. [169a]

Given that the tested compounds indicated inhibition of the kinases *in vitro,* toxicity, death, phenotype change, and retarded development could be determined *in vivo* using the embryos.

The embryos were monitored daily at 26 °C to see their evolution, and their heartbeats were recorded. E-3 medium is the accepted standard medium for working with growing zebrafish embryos as it contains many salts that provide the embryos with minerals such as calcium and magnesium, which are needed for growth. Methylene blue is utilized as an anti-fungal agent. [170] The Cold Spring Harbor protocol was used to prepare the E3 medium for zebrafish embryos. [171]

The aqueous medium surrounding the embryos in the experiments contains the dissolved compounds (inhibitors) to be evaluated. Hence, for the inhibitor efficacy, permeability is required through the chorion 3 days post-fertilisation (dpf) and through the skin or gills (>3 dpf). Further details about the experimental procedure are in the experimental section **5**.**4**.**2**.**1**.

3.5.3.4 *In vivo* efficacy of BSc5484 and its diverse analogues in wild-type zebrafish embryos

Four (4) hours post fertilization (hpf), embryos with intact chorionic membranes were selected according to the referenced guidelines and grouped in E3-medium. The stock solutions of the compounds to be analysed were made in an E3 medium with 2% vol DMSO content as a solvent mediator for solubility.

The prepared solutions were subsequently added to the isolated eggs in E3 medium so that the concentrations in each well were 100 µM, 50 µM, 40 µM, 20 µM, 10 µM and 1 µM. Also, 2% vol DMSO in E3-medium was utilized as a control.

50 µM and 100 µM compound concentrations were prepared despite being above the maximum solubility of some tested compounds. This was carried out because the aim was to perform the *in vivo* experiment with the maximum concentrations of the compounds set to 100 µM and to compare this experiment to the one realized by Griffin *et al*. [169b] On the other hand, observing the development of the embryos in a saturated medium to see how they develop and act was another motif that boosted the choice this approach.

Therefore, saturated solutions of 50 µM and 100 µM concentrations were included and prepared using a sonicator and a shaker. Although slight turbidities were perceived in the prepared solutions, there was no deposition until at least 24 h (see **Scheme 10** for the physical aspect of the designed solutions from 2 minutes to 24 hours).

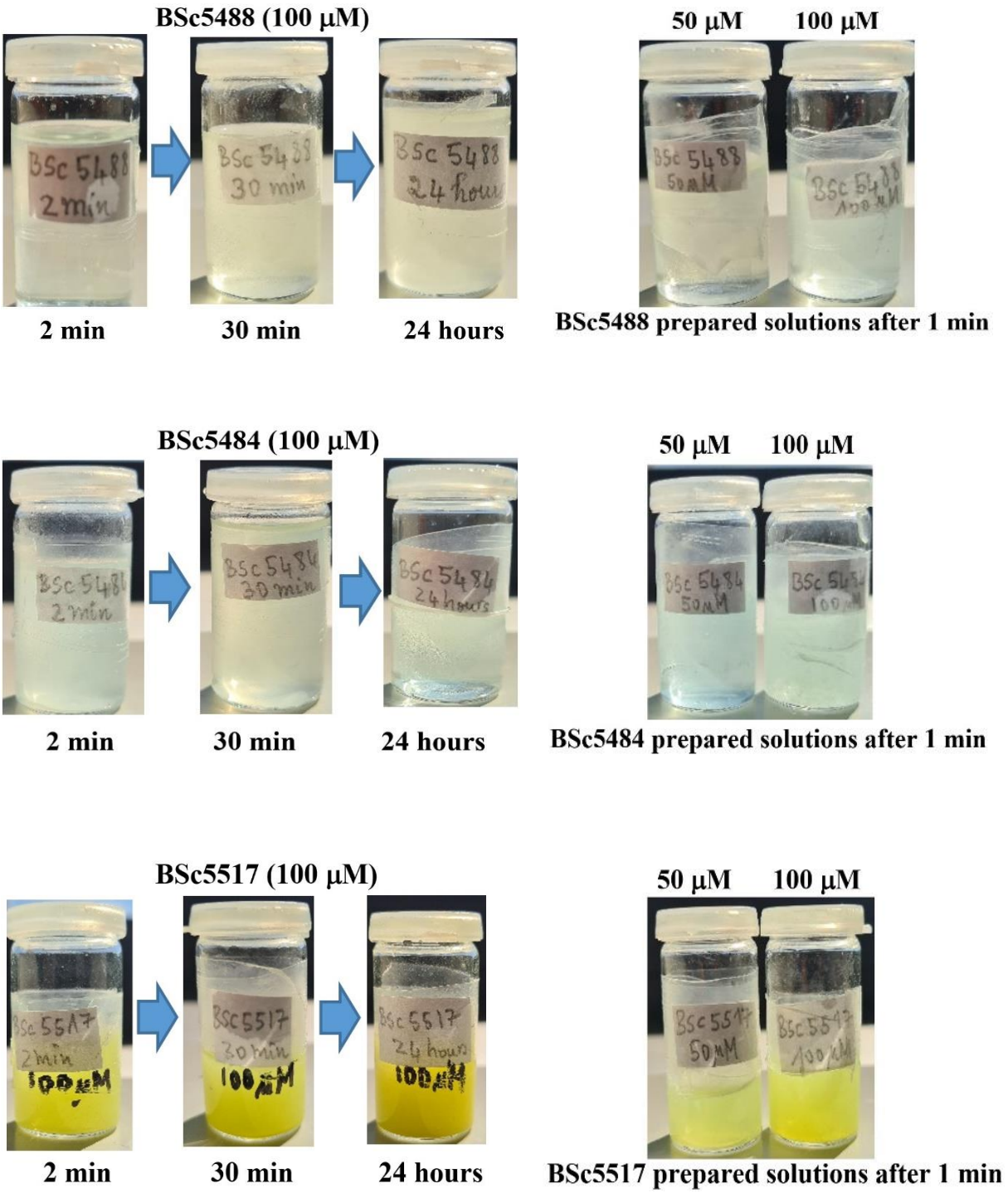

Scheme 10. Physical aspects over time of some of the solutions prepared above their maximum solubility for the *in vivo* toxicology assay in Zebrafish embryos.

24-well plates were utilized for the experiment, with the total volume per well set to 1 mL. The development of the embryos at 26 °C was subsequently monitored every day, and their heartbeat was recorded. All survival rates were determined at least three times, with the controls and the survival rate at 50 µM and 100 µM determined for some compounds in five replicates. The experiment was carried out with 10 eggs per well, and the observed phenotypes were photographed and monitored.

- **BSc5484** phenotype study in the embryos

Embryos incubated with **BSc5484** revealed a delayed development compared to the control (**Figure 24**). The delayed effect was more pronounced as the concentration of **BSc5484** increased. This was discovered from day 1 until day 3. During the first days that followed the incubation, the first phenotypes were observed, such as short bent bodies, small eyes, pericardial oedema, brain ventricle oedema, enlarged yolk sac, absence of body and eye pigmentation and stunted and crooked tails. The phenotypes were more pronounced as **BSc5484**'s concentration increased.

Over the course of the experiment, a strong lack of body and eye pigmentation of the embryos was noticed from day 3 onward, and inconspicuous heartbeats were also recorded. The lethality increased with the concentration of **BSc5484**, and the highest lethality was detected at 100 µM (**Figure 26**).

As a result, the phenotype identified was directly linked to a probable GSK-3 inhibition, given that GSK-3 activity is crucial for the alignment of the cortical microtubules, the dorsoventral axis determination, and the body/eye pigmentations of the embryos. Furthermore, embryonic body curvature is primarily owing to the activation of β-catenin within the Wnt signalling pathway. However, GSK-3β is believed to be mainly responsible for β-catenin activation. [172, 173] Meaning that the observed phenotypes are probably linked to disruption of β-catenin signalling.

Note: No pictures were recorded at 100 µM because embryos incubated at that concentration were all dead at 48 hpf.

- Phenotype study on the embryos incubated with **BSc5483**

Embryos incubated with **BSc5483** also displayed a delayed development compared to the control (**Figure 24**). However, the phenotypes detected were less severe than those on the embryos incubated with **BSc5484**.

BSc5483, in contrast, was somehow well tolerated in embryos up to a test dose of 1 μM. The first apparent phenotypes were perceived at 10 μM with persistent crooked tail embryos, and further phenotypes such as enlarged yolk sac were also perceived. The abnormal phenotypes on the embryos got severe as the concentration of **BSc5483** increased. In contrast, the treated embryos exhibited normal eye development but an inconspicuous heartbeat.

In addition, embryos incubated with **BSc5483** were less agile compared to the control. The phenotypes noticed could not be related to GSK-3 inhibition, given that **BSc5483** revealed almost no inhibition against GSK-3β *in vitro*. Also, embryos incubated with **BSc5483** disclosed weak lethality compared to those incubated with **BSc5484**, and the survival rate was 30 % for the embryos incubated at the highest concentration of **BSc5483** (**Figure 26**).

- **BSc5486** phenotype study on the embryos

Embryos incubated with **BSc5486** indicated severe toxicity and high lethality (**Figure 24**). As an illustration, hatched embryos at **BSc5486**'s concentration equal to or greater than 40 μM were all dead from day 3 onwards. At the highest concentration (100 μM), the treated embryos were all dead just a few hours after incubation (**Figure 26**). The main phenotypes discerned were enlarged yolk sacs with crooked and stunted tails. Additionally, the survival embryos seemed knocked out with inconspicuous heartbeats.

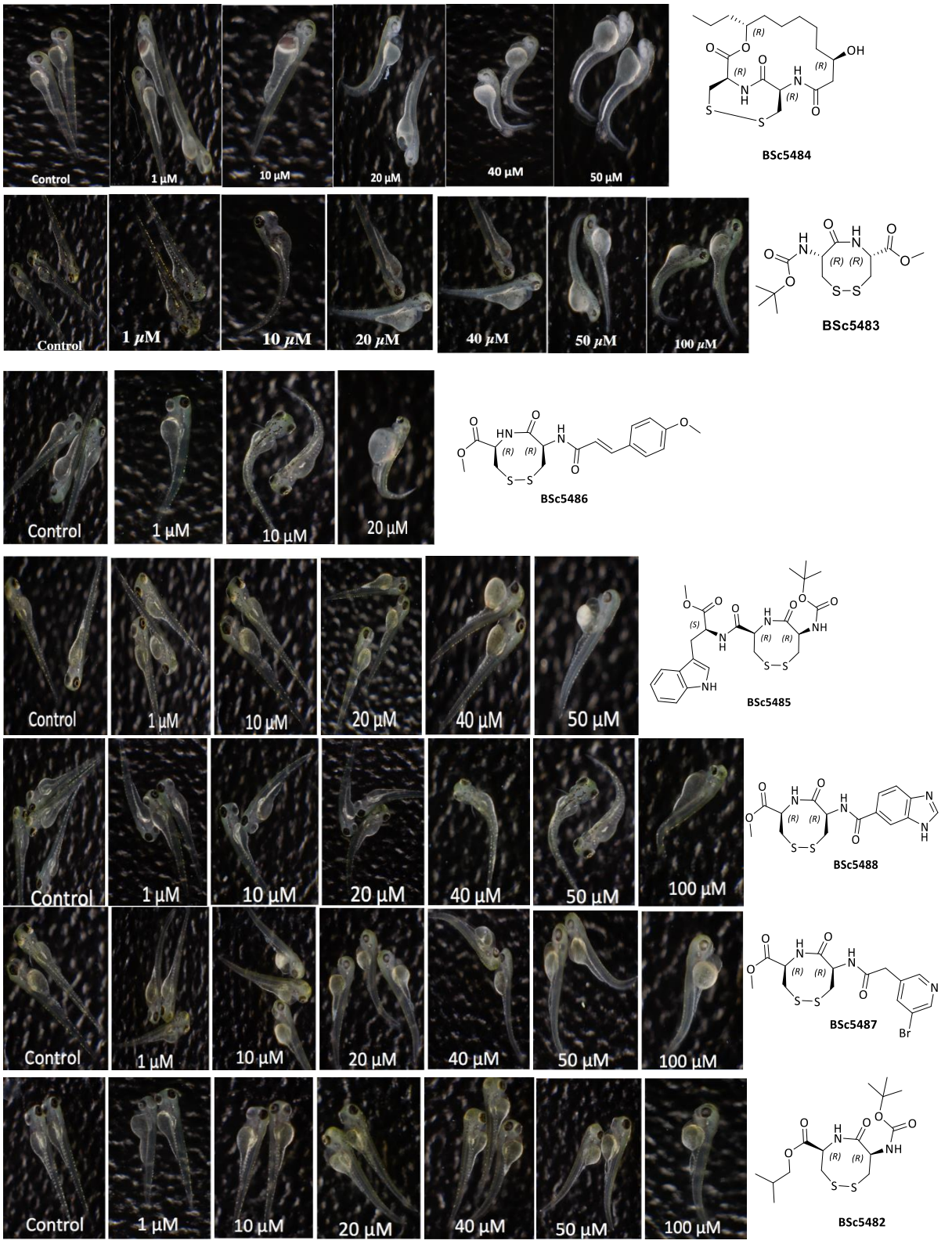

Figure 24: Recorded phenotypes at day 5 on the wild-type embryos *Danio rerio* when treated with **BSc5484**, **BSc5483**, **BSc5486**, **BSc5485**, **BSc5488**, **BSc5487** and **BSc5482** at various concentrations.

- **BSc5485** phenotype study on the embryos

Embryos incubated with **BSc5485** revealed moderate toxicity and lethality compared to those incubated with **BSc5486** (**Figure 24**). A full lethality was only noticed from day 4 onwards for embryos incubated at 100 µM concentration, and the prominent phenotype noted on the survival embryos was the enlarged yolk sacs.

- **BSc5488** phenotype study on the embryos

Embryos incubated with **BSc5488** indicated moderate toxicity and lethality (**Figures 24** and **26**). As a result, no complete lethality was remarked, although the striking toxicity of **BSc5488**. The main phenotypes spotted were enlarged yolk sacs (especially for embryos incubated at 100 µM) with crooked and stunted tails.

- **BSc5487** phenotype study on the embryos

Embryos incubated with **BSc5487** indicated a delayed development compared to the control (**Figure 24**). From day 5 onward, the incubated embryos were less agile and looked knout out. The phenotypes detected were slightly crooked tails, enlarged heart chambers, yolk sacs and lack of eye pigmentation. However, no full lethality was recorded (**Figure 26**). Although **BSc5487** revealed potent inhibition of Flt1 (h) at 100 µM concentration, none of the observed phenotypes differed from the frequently encountered ones. This was because zebrafish's Flt1 gene encodes a vascular endothelial growth factor receptor, contributing to blood vessel development. The phenotype of this gene in zebrafish embryos may be related to irregularities in blood vessel formation that could lead to potential flaws in the circulatory system. It can adversely affect the overall development and survival of the embryo without any striking observable phenotype.

- **BSc5482** phenotype study on the embryos

Embryos incubated with **BSc5482** also exhibited moderate lethality and toxicity (**Figures 24** and **26**). The incubated embryos revealed normal development, and the phenotypes perceived were very minor. The most striking phenotype distinguished was crooked tails embryos. Additionally, the hatched embryos disposed of regular heartbeat rates and were fully agile.

To sum up, the noticed phenotypes demonstrated, on the one hand, the permeability of the compounds through the chorion and the skin and, on the other hand, the disruption of embryonic development. As a result of the permeability, it was presumed that **BSc5484** and its analogues were taken up by the embryos.

During the observation period, there was no lethality for the control across the whole concentration range. This suggests that there was no coagulation (decomposition of the embryo within the egg), no absence of heartbeat, and no altered spontaneous movement.

3.5.3.5 *In vivo* efficacy of Eudistomidin C ((*S*)-5-bromo-1-(1-(methylamino)-2-(methylthio)ethyl)-9*H*-pyrido[3,4-β]indol-6-ol) (BSc5517) and the analogue BSc5515 in gold-type zebrafish embryos

Gold-type zebrafish embryos were incubated with solutions of **BSc5517** and **BSc5515** in E3-medium using the same procedure employed for the wild-type zebrafish embryos, and the phenotypic changes were monitored. Surprisingly, none of the incubated groups indicated either abnormal phenotypes or lethality. Even at 120 hpf, the incubated embryos were still alive with a normal phenotype/heartbeat rate as in the control. This result was unexpected given that **BSc5517** and **BSc5515** revealed good to potent kinase inhibitory activity respectively, including the inhibition of GSK-3α and GSK-3β. Therefore, it was concluded that **BSc5517** and **BSc5515** might have weak permeability through the chorion of the embryos.

Alternatively, dechorionated gold-type embryos were incubated with **BSc5517** and **BSc5515**. The protocol for dechorionation is detailed in the experimental section **5.4.2.2**.

From a **BSc5517** stock solution in E3-medium containing 2% vol DMSO, 20 µM and 60 µM of **BSc5517** were prepared still in E3-medium as solvent. The prepared solutions were subsequently incubated to the dechorionated embryos in the wells.

From a **BSc5515** stock solution in E3-medium containing 2% vol DMSO, were prepared: 100 µM, 50 µM, 40 µM, 20 µM, 10 µM and 1 µM of **BSc5515** still in E3-medium as solvent. Similarly, the prepared solutions were incubated to the dechorionated embryos in the wells. The experiment was conducted in a 24-well microtitre plate with the volume per well set to 1 mL. The embryos' development at 26 °C was then monitored daily, and their heartbeats were recorded.

a)

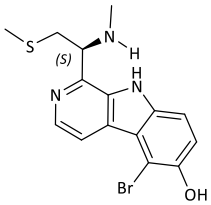

BSc5517

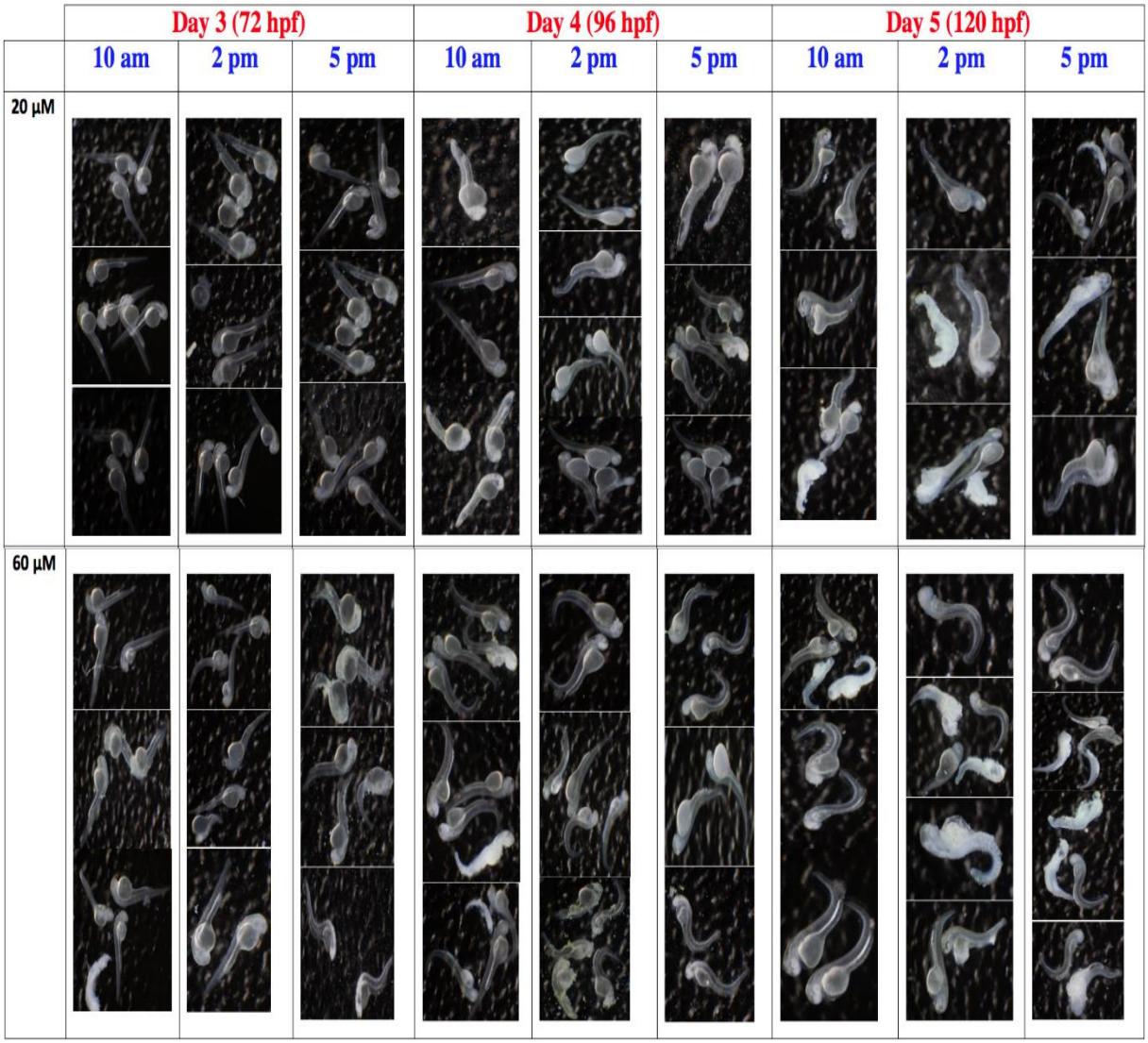

b)

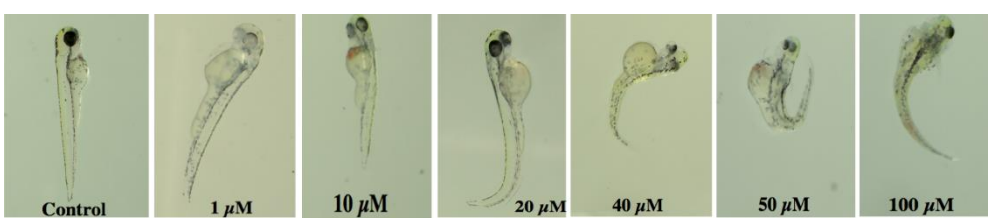

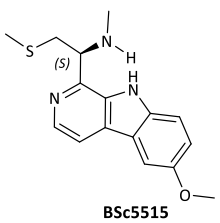

BSc5515

Figure 25: Observed phenotypes on the embryos gold-type *Danio rerio* at day 5 when treated with **BSc5517** and **BSc5515** at various concentrations.

- Dechorionated embryos incubated with **BSc5517**.

The study of the phenotype of the dechorionated embryos incubated with **BSc5517** revealed a persistent lack of body/eye pigmentation, eyeless phenotype and a strong and constant body curvature. This was noticed mainly for the embryos incubated at 60 µM (**Figure 25**).

As a result, the phenotypes detected were directly linked to probable GSK-3 inhibition, given that GSK-3 activity is crucial for orienting cortical microtubules, the dorsoventral axis determination, and the body/eye pigmentations of the embryos. The incubated dechorionated embryos also demonstrated an inconspicuous heartbeat and looked knocked out. Their lethality rate also increased with concentrations of **BSc5517** (**Figure 26**).

- Dechorionated embryos incubated with **BSc5515**.

The study of the phenotype of dechorionated embryos incubated with **BSc5515** indicated slow development compared to the control from day 3 onwards (**Figure 25**). The lethality rate increased with the concentration, so the highest lethality was perceived at the maximum concentration (100 µM) (**Figure 26**). Concerning the phenotype, the mains were inconspicuous heartbeats, the enlargement of the yolk sac, pericardial oedema and crooked and stunted tails. The most intriguing phenotype was one-eye embryos (observed on embryos incubated at 100 µM). The crooked and stunted tails phenotype was detected from 20 µM, and the tails got more crooked as the concentration of **BSc5515** increased.

The discovered phenotypes were attributed to a possible GSK-3 and MEK1 inhibition, knowing that embryos treated with MEK1 inhibitor usually display pericardial oedema, enlarged heart chambers and vessel collapse.

During the observation period, there was no lethality for the control across the whole concentration range. This suggests no coagulation (decomposition of the embryos), no absence of heartbeat, and altered spontaneous movement.

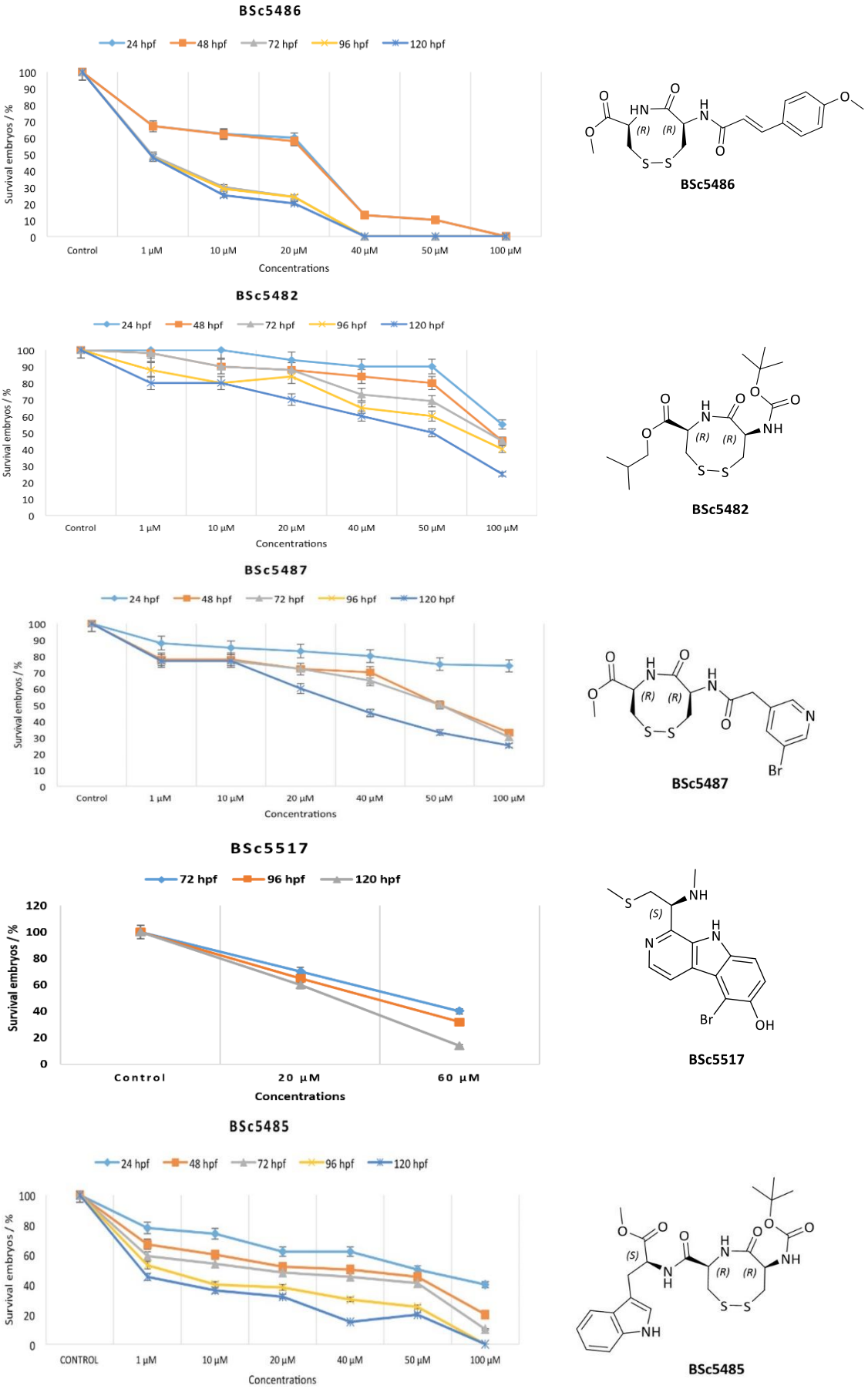

Figure 26: Evolution of the survival rate of the embryos from day 1 to day 5 at different concentrations.

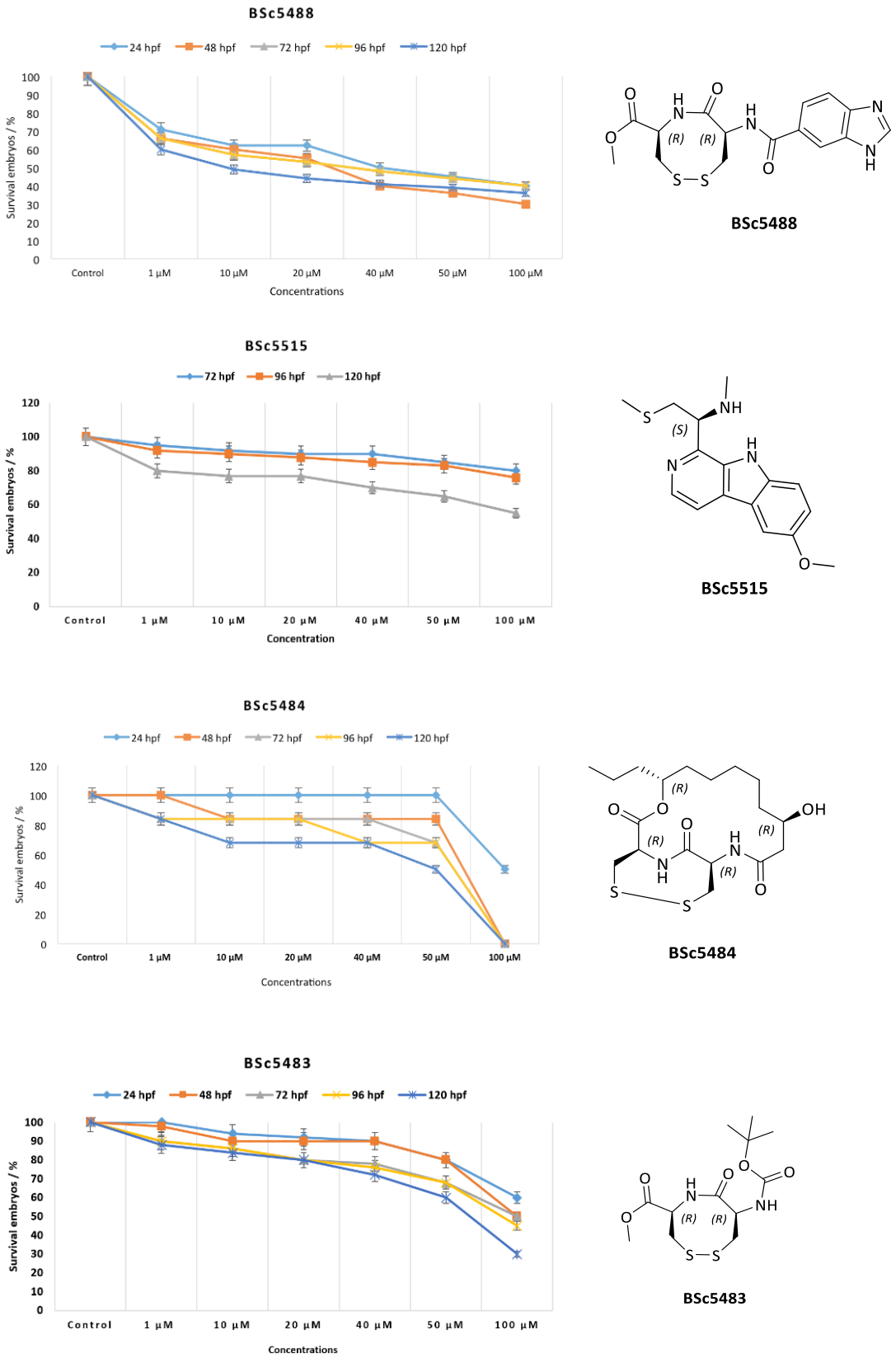

Figure 26: Evolution of the survival rate of the embryos from day 1 to day 5 at different concentrations.

The activation of β-catenin within the Wnt signalling pathway is primarily responsible for embryo skeleton curvature. The Wnt signalling pathway is responsible for many processes in zebrafish embryonic development, including body axis formation. [174] Besides, this signalling pathway is mainly influenced by GSK-3. [175] If inhibition of GSK-3 occurs during zebrafish embryonic development, the embryos develop abnormally. [174, 176]

The specific phenotype with body curvature is formed so the *in vivo* effectiveness of the inhibitor can be demonstrated. In addition, GSK-3α and GSK-3β are functionally redundant within the Wnt signalling pathway, and GSK-3β is thought to be predominantly responsible for β-catenin activation. [177 - 180]

Given that **BSc5484** and **BSc5517** have indicated good to potent *in vitro* kinase inhibitory against GSK-3β (**BSc5484** and **BSc5517**) and GSK-3α (**BSc5517**), the concentrations used in the zebrafish embryos assay could be relatively consistent with achieving isoform-specific selectivity. Thus, the zebrafish embryos assay conducted is too imprecise to detect any isoform selectivity.

3.6 *In silico* docking

This chapter describes the *in silico* experiments performed to predict and investigate the complementarity at the molecular level of synthesized compounds (ligands) and their respective kinases (target proteins).

3.6.1 Blind docking experiment

Since **BSc5484**, **BSc5488**, and **BSc5485** revealed good to strong inhibition of some kinases *in vitro*, a study of their probable binding mode/interaction with their corresponding target proteins was relevant. Since no information regarding the binding sphere of the dithiazocane-derived compounds within the kinases is known, a blind docking experiment was employed to predict the most probable binding sphere.

The blind docking (BD) experiment is a technique that has been utilized to give insight into the potential binding interactions between ligands and their corresponding targeted proteins. The

experiment can also provide predictions of the binding affinities. Blind Docking (BD) is considered objective since it examines the complete structure of the protein to discover the potential ligand's binding site. [181 - 183] The more significant the exhaustiveness, the more vigorously the ligand will scan the protein for the best binding space.

AutodockVina (Vina) is a non-covalent docking software used for the experiment. Vina is a widely employed technique when no information about the binding site is available, ensuring a successful docking procedure.

Thus, the blind docking experiment was performed as follows**:** **BSc5485** was docked into Human Fms (CSFR) (CSF1R) (Y969C) (PDB ID = 7MFC) and human PDK1 (PDPK1) (PDB ID = 1OKY). [184, 185] **BSc5488** was docked into human Flt-1 (VEGFR1) (FLT1) (PDB ID = 3HNG) and **BSc5484** was docked into Human GSK-3β (PDB ID = 5HLN). [186] The docking images are depicted in **Figure 27**. See the experimental section **5.3.1** for details about the procedure.

The blind docking results demonstrated that the different docking poses for each ligand partially overlapped for various hits, occupying the same cavity, which probably correlates to the protein's active site. Nevertheless, the results generated from the best-docked poses with the lowest energy conformation at the exhaustiveness 12 revealed that **BSc5484** and **BSc5485** bind in a non-ATP-competitive mode while **BSc5488** might bind in an ATP-competitive mode or as a type III inhibitor.
Indeed, **BSc5485** was found embedded into a pocket distinct from the ATP binding site of Fms and PDK1 as a type IV inhibitor, establishing hydrogen bonds with the residues Tyr665, Asn214 and Gln220. In addition, **BSc5484** was also found in an allosteric pocket of GSK-3β as a type IV inhibitor, establishing hydrogen bonds with the residue Ser236. Similarly, **BSc5488** was confirmed found in the allosteric pocket of Flt-1 (as a type III inhibitor), interacting via hydrogen bonds with residues Asp1040 and Leu1043.

a)

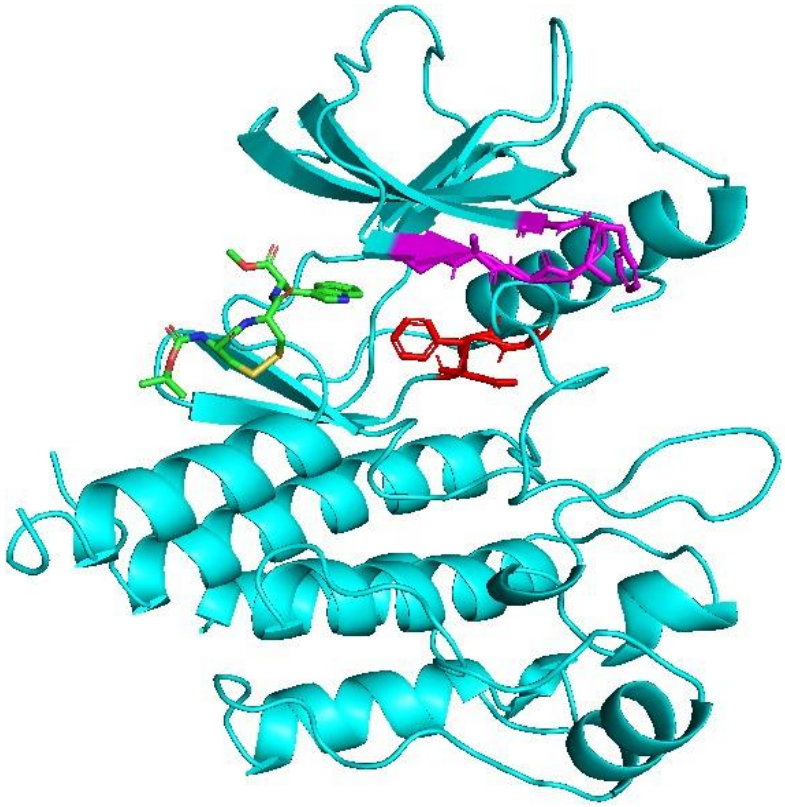

b)

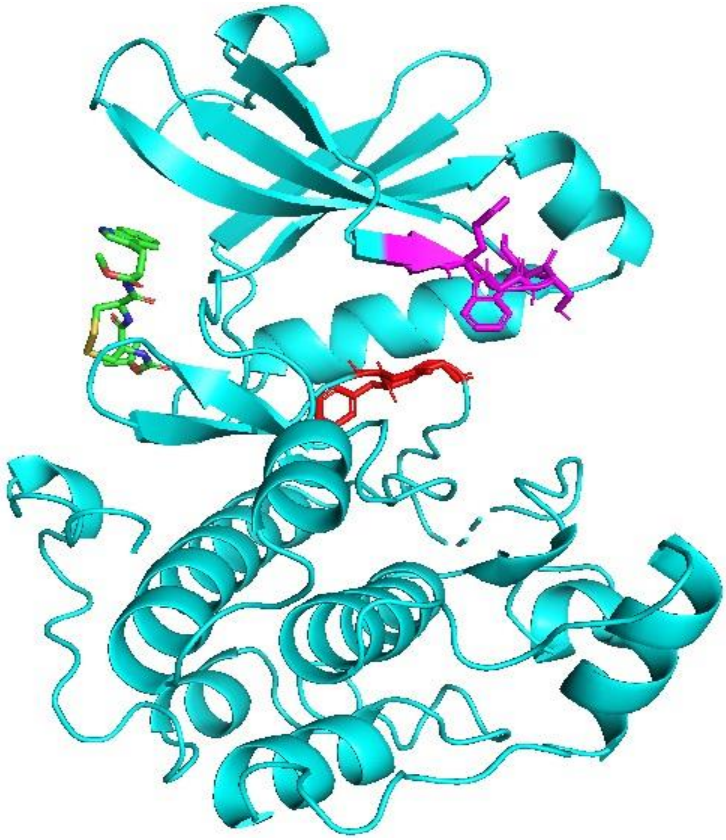

Figure 27: Best poses binding affinity of **BSc5485** with corresponding proteins as viewed using Pymol (sticks and cartoon representations). a) **BSc5485** (green) bound to 7MFC (cyan) with a binding affinity of -7.117 Kcal/mol. b) **BSc5485** (green) bound to 1OKY (cyan) with a binding affinity of -7.192 Kcal/mol; DFG motif (red) and the Gly-rich loop (magenta).

c)

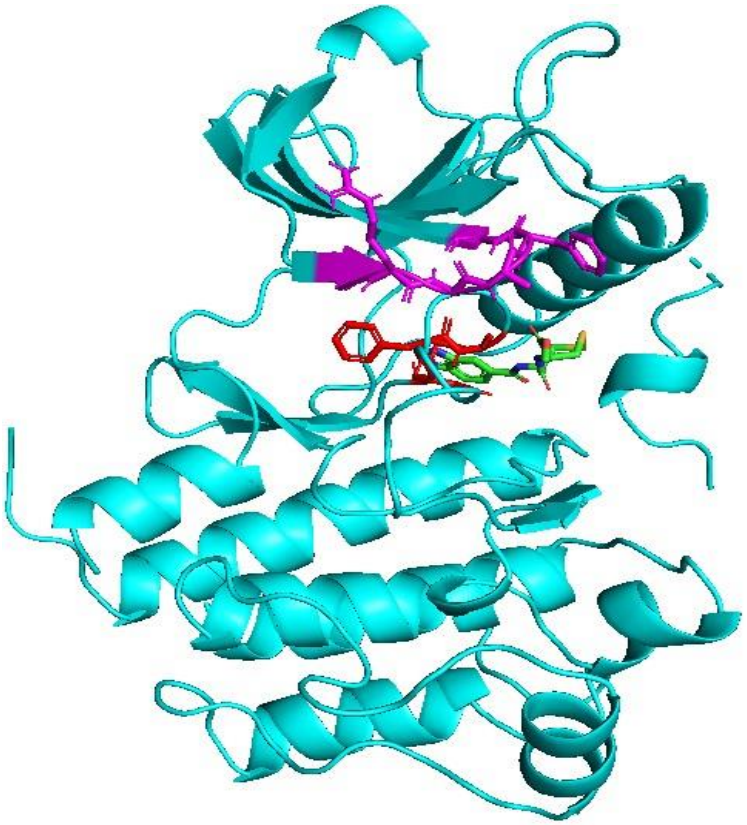

d)

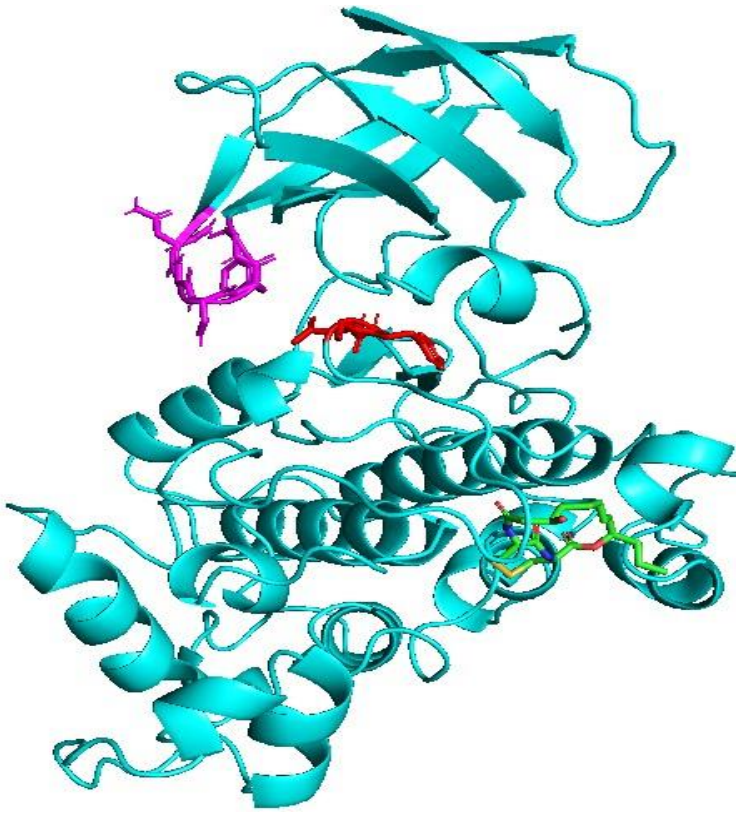

Figure 27: Best poses binding affinity of **BSc5488** and **BSc5484** with their corresponding target proteins as viewed using Pymol: c) **BSc5488** (green) bound to 3HNG (cyan) with a binding affinity of -7.807 Kcal/mol. d) **BSc5484** (green) bound to 5HLN (cyan) with a binding affinity of -6.405 Kcal/mol. DFG motif (red) and the Gly-rich loop (magenta).

Table 3. Interacting residues determined using PyMOL

Ligands	PDB proteins codes	Residues forming hydrogen bond Exhaustiveness = 12
BSc5485	7MFC	Tyr 665 = 1
	1OKY	Asn 214 = 1, Gln 220 =1
BSc5488	3HNG	Asp 1040 = 1, Leu 1043 = 1
BSc5484	5HLN	Ser 236 = 2

3.6.2 Docking experiment of Eudistomidin C ((*S*)-5-bromo-1-(1-(methylamino)-2-(methylthio)ethyl)-9*H*-pyrido[3,4-β]indol-6-ol) (BSc5517)

The investigation of published *in silico* docking experiments with related β-carbolines revealed that the compounds frequently compete with ATP for binding to the highly conserved ATP-binding site (Type I, $I^{1/2}$ and II inhibitors). Therefore, the prediction of the binding sphere of **BSc5517** was more specific.

Molecular Operating Environment (MOE) software was utilized for protein/ligand docking to gain insights into the binding interactions of **BSc5517** into the ATP-binding sphere of the targeted proteins. Consequently, **BSc5517** was docked into the ATP binding sphere of CDK1, CK2α1, DYRK1A, GSK-3β and Haspin. These kinases were selected based on their inhibition ratio *in vitro* by **BSc5517** (from the *in vitro* kinase assay early performed).
The X-ray crystal structure of the kinases (5HQ0 for CDK1, 1J91 for CK2α1, 3ANR for DYRK1A, 7B6F for GSK-3β and 3DLZ for Haspin) were retrieved from the Protein Data bank. [40], [187-190] See the experimental section **5.3.2** for details.

Concerning the docking of **BSc5517** into CDK1, it was identified next to the protein hinge region that the amine function of Gln132 hydrogen bonds with the hydrogen linked to the nitrogen atom of the side chain of **BSc5517** assuming an ATP-mimetic orientation (**Figure 28**).
Concerning the docking of **BSc5517** into CK2*α*1, an Arene–H interaction was perceived between the side chain of Val45 and ring A.
As for the interaction with DYRK1A, **BSc5517** was found encased into the catalytic site between several hydrophobic and hydrophilic residues, such as Met240, Phe238, Leu241, Val173, Glu203, Lys188, and Asp307. Furthermore, they establish an arene-H hydrogen bond anchors with the main chain of Phe238. Additional hydrogen bonds identified with the side chain amine function of Glu203 and Lys188 were similar to the crystalized ligand data. [153] Consequently, **BSc5517** was found to share similar binding interactions and space with the known DYRK1A inhibitor Harmine (**14**).

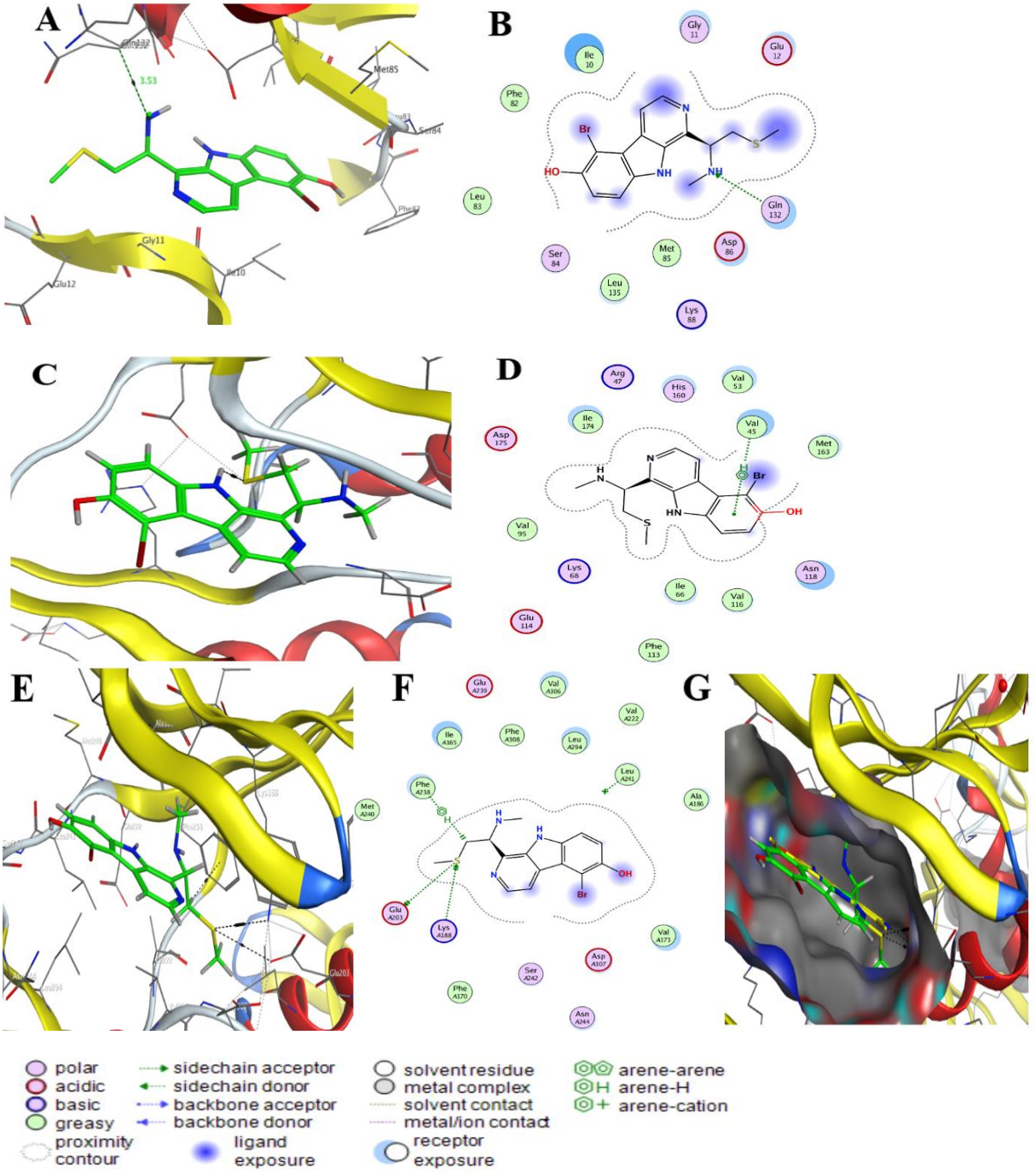

Figure 28: (A) Predicted binding mode of **BSc5517** in the ATP binding pocket of CDK1, S-score values of -6.9503. Hydrogen bonds are depicted as green dots. (B) Interactions of **BSc5517** in the ATP binding pocket of CDK1. (C) Predicted binding mode of **BSc5517** in the ATP binding pocket of CK2α1 S-score values of - 6.7247. The hydrogen bonds are depicted as blue dots. (D) Interactions of **BSc5517** in the CK2α1 binding pocket; Green-dashed lines indicate hydrogen-bond interactions. (E) Predicted binding mode **BSc5517** (green) in the ATP binding pocket of DYRK1A S-score values of -7.1623. Hydrogen bonds are depicted as black dots. (F) Interactions of **BSc5517** in the DYRK1A binding pocket. Hydrogen bonds are represented as green dots. (G) Comparison of **BSc5517** (green) versus the known inhibitor **Harmine** (yellow) in the DYRK1A binding space. Green-dashed lines indicate hydrogen-bond interactions.

Moreover, **Harmine** was docked into DYRK1A using the same parameter as the docking performed with **BSc5517**. The docking of **BSc5517** into DYRK1A provided a S-score value of -7.1623, while the docking of **Harmine** provided a S-score of -6.4663, which allows to conclude that **BSc5517** might have a better binding affinity with DYRK1A compared to the known inhibitor **Harmine** (**Figure 28**).

Concerning the docking of **BSc5517** into GSK-3β, there is an apparent binding mode between the β-carboline scaffold and GSK-3β according to the formation of the classic acceptor–donor-acceptor motif between the β-carboline fragment and the kinase hinge region (**Figure 29**). Interestingly, the ring A of **BSc5517** was found interacting with Cys199 in the active site of GSK-3β via an arene-H interlinkage. The 4-position of the β-carboline structure was found pointing toward the solvent front region, which mainly contains residues Val70, Leu188, Gln185, Tyr134, cys199 and Arg141. The side chain of **BSc5517** was pointing toward the DFG region, which includes residues Glu137, Val135, Leu62 and Lys85.

As for the docking of **BSc5517** into Haspin, analysis of the results revealed an essential halogen bond between the bromine atom on ring A and the protein backbone atoms of residue Glu606 (**Figure 29**). Furthermore, the docking calculations with **BSc5517** disclosed that it was well accommodated within the binding site and satisfied the hydrogen bonding constraint on Glu606. Moreover, **BSc5517** was also exposed via its methyl group at its side chain next to Lys511, which likely disrupted a critical salt bridge between this residue and Glu535 required for the ATP-binding cleft to close, allowing kinase activity.

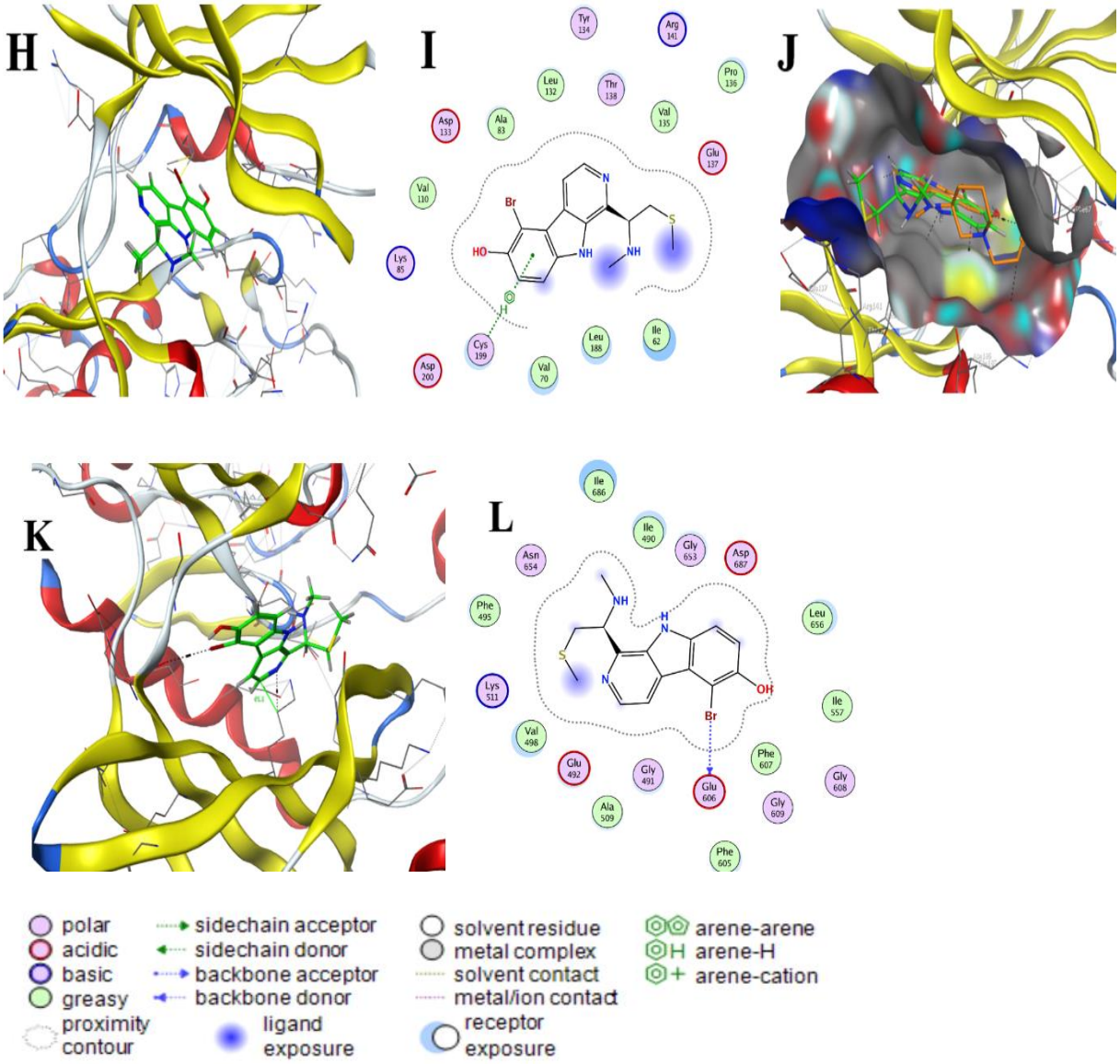

Figure 29: (**H**) Predicted binding mode **BSc5517** (green) in the ATP binding site of GSK-3β; S-score values of -6.9639. Hydrogen bonds are depicted as blue dots. (**I**) Interactions of **BSc5517** in the GSK-3β binding pocket. Hydrogen bonds are represented as green dots. (**J**) Comparison of **BSc5517** (green) vs the known inhibitor (S)-3-(3-((7-Chloro-9H-pyrimido[4,5-β]indol-4-yl)(methyl)-amino)piperidin-1-yl)propanenitrile [189] (orange) in the GSK-3β ATP binding space. Green-dashed lines indicate hydrogen-bond interactions. (**K**) Predicted binding mode of **BSc5517** in the ATP binding site of Haspin; S-score values of – 5.7648. Hydrogen bonds are depicted as black dots. (**L**) Interactions of **BSc5517** in Haspin binding pocket.

Given that Harmine (**14**) is a potent MAO-A inhibitor void of psychoactive properties, which imposes a safety alert and limits its uses in animals, **BSc5517** was docked into MAO-A wild type. The protein structure and the detailed binding mode of **14** in the active site of MAO-A were published by Tsukihara *et al*. in 2008 (PDB-ID: 2Z5X). [191] The docking of **BSc5517** into MAO-A was performed and revealed that **BSc5517** was located in the active site, interacting with residues Tyr69, Asn181, Phe352, Val210, Gln215, Cys323, Ile180, Ile335, Leu337, Phe208, Tyr407, Cys323, Thr336, Met350, Thr336 and Tyr444 (**Figure 30**). A reported hydrogen bond interaction between Asn181 and the sulfur atom of **BSc5517** was mentioned, as well as another hydrogen bond interaction between the hydroxyl of **BSc5517** and Cys323, which seem to be essential components of the interaction pattern. Using the docking software, a comparison of the complexes **14**/MAO-A and **BSc5517**/MAO-A revealed that **BSc5517** has a weaker binding affinity with MAO-A compared to **14**, with the S-score values of -5.6825 and -7.6333 respectively. Considering that weaker binding affinity correlates with weaker inhibition, this result becomes relevant given that **14** poses a safety concern and severely limits its use because of its potent inhibition of MAO-A.

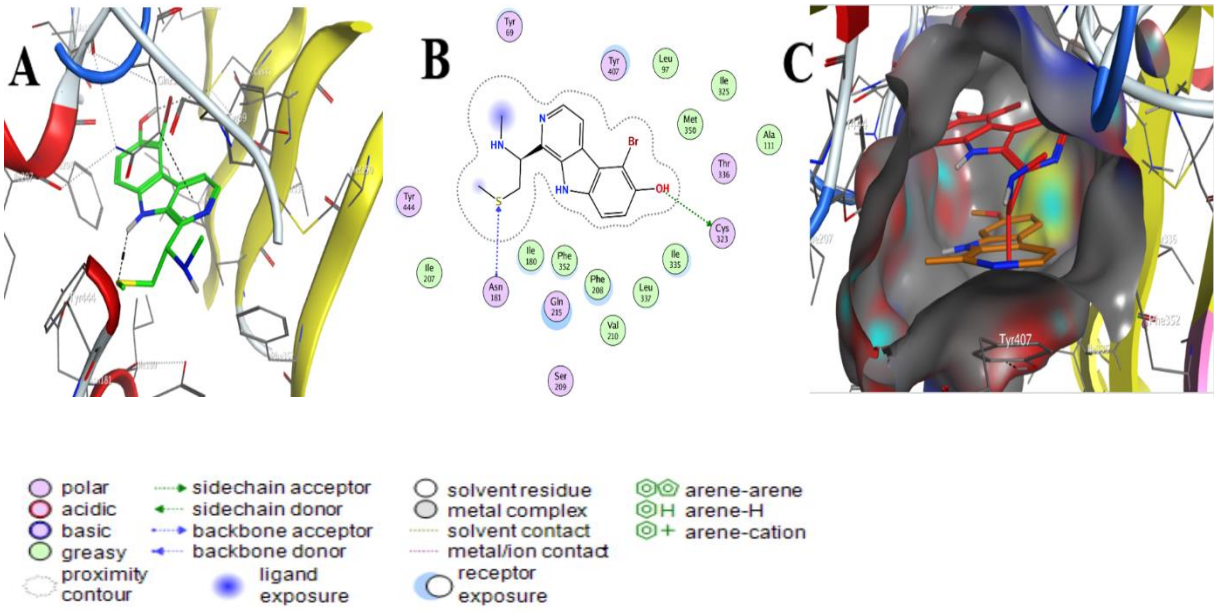

Figure 30: (A) Predicted binding mode **BSc5517** in the active site of MAO-A (PDB code 2Z5X) with hydrogen bonds depicted as black dots; S-score values of – 5.6825. (B) Interactions of **1** in MAO-A binding pocket with hydrogen bonds are shown as green and blue dots. (C) Comparison of the binding conformation of **BSc5517** (red) vs **Harmine** (orange) in the MAO-A active site. [189]

4 Summary and Outlook

Despite significant progress in the development of small molecule kinase inhibitors over the last 25 years, the majority of human kinases currently lack high-quality selective inhibitors that may be employed as chemical probes to study their biological function and pharmacology. NPs and their synthetic derivates might give avenues to overcome this frequently encountered challenge. Owing to their diverse structures and rigidity, NPs have been revealed to target a wide range of protein kinases, including all subfamilies of the known kinome. They have served as drug lead compounds, which provided an abundant resource for the discovery of next-generation kinase inhibitors that can target, if possible, allosteric regions away from the ATP binding sites in the prospect of gaining a more selectivity profile.

Nonetheless, isolating these NPs from their natural sources necessitates massive harvesting, which is fraught with technical difficulties and triggers enormous harm to the ecology. The challenges and limitations encountered while isolating these NPs from their sources are constantly present and have few viable solutions.

Considering these aspects, researchers have employed total synthesis and semisynthesis to replicate the most intriguing compounds of living nature in laboratories. This will serve to obtain significant quantities of the compounds which will serve to identify the mechanism of action of these NPs and optimize their effectiveness via targeted structural variations.

Depsipeptide PM181110, **Fusarithioamide A** and **Eudistomidin C** are examples of NPs isolated from natural sources disclosing highly potent pharmacological activities, especially against Cancer. Still, neither directed medicinal chemistry efforts toward studying their kinase inhibitory activity, their *in vivo* profiling in Zebrafish embryos, their *in silico* study, nor their first total synthesis have been made publicly available before this work. To address these challenges, this doctoral thesis discloses the development of total synthetic pathways of **BSc5484**, compounds **10** and **12**, and **BSc5517**. Furthermore, the structure-guided design and synthesis of their corresponding derivatives/analogues were also addressed to evaluate their kinase inhibitory activity, to conduct their *in vivo* profiling in zebrafish embryos and to investigate their complementary at the molecular level of ligands and protein targets.

After establishing comprehensive retrosynthetic plans and proposing biosynthetic approaches, **BSc5484** and **BSc5517** were successfully synthesized. The attempt to synthesise compounds **10** and **12** was unsuccessful due to the failure of the critical macrolactonization step related to

the synthesis of **10**, on the one hand, and the stability issue encountered with the key intermediate **47** related to the synthesis of **12** on the other hand.
Consequently, the hypothesis of probable misassignment of **12** after its isolation from the natural source was emitted. Subsequently, a revision of its chemical structure based on the published data was considered and is currently being investigated.

The total syntheses of the targets **BSc5484** and **BSc5517** were performed based on highly convergent and unified approaches. Since these target compounds were never synthesized before, retrosynthetic and biosynthetic processes were first established, allowing the design of the most realistic synthetic routes.
The synthesis of the depsipeptide scaffold was based after being inspired by the synthesis of the versatile analogues **FE399** (**8**) and **Malformin A1** (**11**) on the one hand, and the synthesis of the β-carboline scaffold was based on the analogue Harmine (**14**) on the other hand.
Starting from affordable commercial materials, both routes delivered key synthetic intermediates poised for modular diversification by a range of synthetic methods. After initial studies on the site-selective modification of the synthetic analogues of **BSc5484** by conserving the probable reactive scaffold **49**, some peptide coupling reactions were successfully achieved. Nonetheless, additional compounds require synthesis and evaluation to investigate, for instance, the effect of the indole moiety on the kinase activity, as noticed with the good kinase inhibitory activity of synthesized analogues **BSc5488** and **BSc5485**.

In addition, **BSc5484** possesses a strained disulphide bridge, which might be targeted by free cysteines such as the CysDFG-Kinase motif, thereby inducing protein refolding or modulating kinase activity. The viability of this hypothesis might contribute to a higher selectivity profile and specificity of the inhibitor, as one of the significant drawbacks in kinase inhibitor drug discovery is selectivity.
In this context, this proposal was challenged by the series of synthesized analogues. The initial focus for designing and synthesising the analogues was set on conserving predicted reactive fragment **49**. As a result, one of the most potent analogues, **BSc5488**, displayed a middle micromolar range IC_{50} value against human Flt1(h). **BSc5484**, on the other hand, revealed strong inhibition of human GSK-3β *in vitro*, with an IC_{50} value also in the micromolar range. **BSc5487** and **BSc5488** similarly indicated apparent selectivity by inhibiting human Flt-1 in a moderate to good manner dose-dependently. Likewise, **BSc5485** inhibited human Fms and PDK1 in a good way as well.

In the same way, **BSc5517**, **BSc5515**, **BSc5516**, and **BSc5518** revealed promising inhibition of various kinases *in vitro*, including CDK1/cyclinB(h), CK2α1(h), DYRK1A(h) and Haspin(h). Although a large panel of kinases were inhibited, **BSc5517** and its analogues were revealed to be particularly good to potent inhibitors of human Haspin and DYRK1A kinases, giving evidence that this β-carboline scaffold might be a good starting point for arising a potent human Haspin and DYRK1A kinase inhibitors.

Additionally, ample bioavailability and dose-dependent *in vivo* efficacy were shown for **BSc5484**, **BSc5517,** and their respective analogues in wild-type and gold-type zebrafish embryos. Also, in the last part of this doctoral thesis, *in silico* docking experiments were performed to predict probable binding affinities/modes of the synthesis compounds into their corresponding target proteins.

Thus, synthesized compounds were profiled *in vitro* and *in vivo* for their bioavailability, safety, and efficacy. The bioavailability of the compounds was estimated *in vitro* by the determination of the aqueous solubility in a shake-flask solubility assay. Accordingly, some tested compounds displayed sufficient aqueous solubility to be considered research tool compounds for the planned *in vivo* efficacy studies. Next, a stability assay under buffer conditions at various pH was performed. Consequently, all the assayed compounds indicated *in vitro* buffer stability for at least 96 hours. Nevertheless, the metabolic stability *in vivo* of **BSc5484** and **BSc5517** should be investigated in future studies to have an overall idea of their stability.

With ample *in vitro* bioavailability data in hand, the safety and toxicity of the compounds were investigated in wild-type and gold-type zebrafish embryos.

Treatment of wild-type embryos with **BSc5484** was not tolerated, as complete lethality was detected for the embryos incubated at 100 μM. Furthermore, severe morphological changes were discerned, and the noticed phenotypes were characteristic of GSK-3 inhibition. Also, severe lethality and high toxicity were distinguished on embryos incubated with **BSc5486**.

In addition, treatment of dechorionated gold-type embryos with **BSc5517** was not tolerated. The spotted phenotypes were more severe than those perceived on embryos incubated with **BSc5484**. The morphology of the incubated embryos was attributed to probable GSK-3 and MEK1 inhibition.

Next, **BSc5517** was further assessed on THP-1 cells for toxicity assay, and the result revealed that at a concentration equal to or below 10 μM, **BSc5517** did not show significant toxicity on THP-1 cells. In contrast, Harmine was able to decrease the number of THP-1 cells adhering to Human umbilical vein endothelial cells induced by oscillatory shear stress, as reported by Yang *et al*. [192]

Despite the successful advances toward NP kinase inhibitors, the publication of a highly selective impactful NP kinase inhibitors cross-screening study at the beginning of this work shifted attention to studying their interactions and binding mode into their corresponding target proteins. Therefore, molecular docking experiments were performed to have predictions of the binding mode/affinities of the compounds into their related target proteins. The blind docking experiment conducted with the target **BSc5484** and its analogues **BSc5485** and **BSc5488** revealed that **BSc5484** and **BSc5485** might bind into their respective target proteins in a non-ATP-competitive mode, likely as type IV inhibitors while **BSc5488** might bind as type III inhibitor. To assess the viability of the early emitted hypothesis and to verify any covalent interaction with cysteine residues of the Cys-DFG kinase motif, the identification of possible covalent adducts to the kinase by mass spectroscopy should first be evaluated. The information obtained from the mass spectrometry analysis might then be confirmed via a crystallographic experiment. Besides, the docking of **BSc5517** into the ATP binding pocket of CK2α indicated better binding affinity than the known inhibitor **Harmine**. Additional docking experiments performed also revealed that **BSc5517** might have a better binding affinity to DYRK1A than **Harmine**. This finding might open up paths in the perspective of further optimization of **BSc5517**, which might result in a potent DYRK1A inhibitor lead compound, especially for Down syndrome therapy as the overexpression of DYRK1A in the Down syndrome brain causes neurofibrillary degeneration *via* hyperphosphorylated tau. **BSc5517** also indicated a weaker binding affinity to MAO-A than **Harmine**, as **Harmine** is a potent MAO-A inhibitor void of psychoactive properties, imposing a safety alert and limiting its uses in animals.

To sum up, the results of the present work are of broad interest among the biomedical research community, as they provide high-quality NP-derived inhibitors against impactful kinases, providing members of the research community with much-needed tools. Furthermore, the methods utilized give a blueprint for the fast and resource-efficient development of NP-derived kinase inhibitors from the available library of NPs.

This work thus provides the first directed instrument about the potential of synthesized naturally derived compounds as inhibitors of disease-causing proteins that have been indicated to be key players in numerous forms of diseases like cancer. It is crucial to establish depsipeptide and β-carboline-based compounds as therapeutic leads and provide a powerful tool to further elucidate their biological function through targeted structural variations.

5 Experimental section

5.1 General Information

Unless otherwise stated, the starting materials and reagents were provided by *Acros Organics, Activate Scientific, Alfa Aesar, Merck, Fluka, Carl Roth, Sigma-Aldrich, TCI, Carbolution Chemicals and VWR* and used without purification. Anhydrous conditions were employed for all reactions, which were carried out in dried glassware with dry solvents under an argon atmosphere (5.0 quality) unless otherwise specified. Degassed solvents were used for cross-coupling reactions.

5.1.1 Thin-layer and Column Chromatography

Thin-layer chromatography was performed on pre-coated 0.2 mm silica gel 60 F254 aluminium sheets supplied by the company Merck KGaA, Darmstadt, Germany. The detection was performed using UV light (254 and 365nm) or potassium permanganate staining. The first use of technical terms has been explained, and British English spelling and grammar have been used throughout. Column chromatography was performed using isocratic elution on a 40-63 μm NORMASIL 60 silica gel (VWR International, Radnor, USA) with solvent systems specified for each experiment. Automated flash column chromatography was performed using Reversed-Phase C18(EC) cartridges (Kinesis GmbH, Langenfeld, Germany) or TELOS Flash-Silica of a specified size on a Combiflash Rf 4x system (Teledyne ISCO Inc., California, USA). Manual elution solvent gradients (Solvent A: Solvent B: The technical term abbreviations were explained when they were first used. The language was kept objective and value-neutral, with proper grammar, spelling, and punctuation. Acetonitrile with 0.1% trifluoroacetic acid and water with 0.1% trifluoroacetic acid) were set for each experiment. All cartridges underwent conditioning with the initial solvent composition before sample loading. Technical term abbreviations were explained upon their first use. Detection of compounds occurred through utilization of the UV-Vis absorption module at 254 nm and 280 nm for normal-phase or 214 nm and 254 nm for reversed-phase chromatography.

5.1.2 Infrared spectroscopy

IR spectra were registered with a Spectrum Two (PerkinElmer Inc., Waltham, USA) attenuated total reflection (ATR) Fourier-transform infrared (FTIR) spectrometer. KBr pellets were used for preparing and measuring all solid samples. Wavenumbers (cm^{-1}) were reported for absorption peaks. Vibrational modes were designated as asymmetric stretching (*vas*), symmetric stretching (*vs*), deformation vibrations (*d*) and latitudinal scissoring (δ).

5.1.3 Nuclear Magnetic Resonance Spectroscopy

An Avance II was used to perform NMR spectra (*Bruker Corporation*, Billerica, Massachusetts, USA) at 300 MHz for ^{13}C-NMR and for ^{1}H and 75 MHz. Also, an *Avance III* (*Bruker Corporation*, Billerica, USA) spectrometer at 75 MHz for ^{13}C-NMR and 300 MHz for ^{1}H-NMR or a *DRX500* (*Bruker Corporation*, Billerica, USA) spectrometer at 500 MHz for ^{1}H and 126 MHz for ^{13}C-NMR. The measuring frequency and solvent were specified for each experiment. The chemical shifts were given in *ppm* according to the frequency downfield of tetramethylsilane.

As internal standards, the following residual solvent signals were used:

$\delta^{1}H$ ($CDCl_3$) = 7.26 ppm

$\delta^{13}C$ ($CDCl_3$) = 77.16 ppm

$\delta^{1}H$ (DMSO-d_6) = 2.50 ppm

$\delta^{13}C$ (DMSO-d_6) = 39.52 ppm

$\delta^{1}H$ (D_2O) = 4.79 ppm

$\delta^{1}H$ (CD_3OD) = 3.31 ppm

$\delta^{13}C$ (CD_3OD) = 49.00 ppm

Coupling constants were reported in Hertz (Hz). Signal multiplicities were denominated as singlet (s), doublet (d), triplet (t), quartet (q) multiplet (m) or a combination. Processing and

analysis of the acquired spectra were carried out by the mean of *MestReNova 14.0.0-23239* software (2019 *Mestrelab Research S.L*., Santiago de Compostela, A Coruña, Spain).

5.1.4 Mass Spectrometry

Mass spectrometry was performed on an *Impact II* quadrupole-TOF spectrometer (*Bruker Corporation*, Massachusetts, USA) used for atmospheric pressure chemical ionization (APCI) and for the ESI experiments. As for EI experiments, they were carried out on either a *MAT95* (*Thermo Finnigan LLC*, of the city San José, California, USA) sector field or an *MD 800* (*Fisons plc*, Ipswich, United Kingdom) quadrupole spectrometer.

5.1.5 High-Performance Liquid Chromatography

The High-performance liquid chromatography (HPLC) was carried out on an *Agilent 1100* system from *Agilent Technologies Inc.,* Santa Clara, California, USA, utilizing a *Synergi Polar-RP* (*Phenomenex Inc.*, Torrance, from the state of California, USA) reversed-phase column (with the specifications: 4 μm particle size, pore size 80 Å, 150×3.0 mm) connected to device name variable wavelength detector (VWD) or even a *Synergi Hydro-RP* (*Phenomenex Inc.*, Torrance, California, USA) reversed-phase column (with the specifications: 4 μm particle size, pore size 80 Å, 150×3.0 mm) connected to a diode array detector (DAD). The solvent gradient was 30% A for ca. 1 min, and linear gradient to 10% A for ca. 10 min, 10% A for ca. 1 min; the solvent A = 0.1% trifluoroacetic acid (TFA) in water; the solvent B = acetonitrile with a flow rate of 1.0 mL/min. All the compounds used in biological or biochemical assays had a ca. 95% purity as determined using the HPLC method described above, if not explicitly stated otherwise.

5.1.6 Sonochemical synthesis

All sonochemical reactions were performed using low-frequency ultrasound (LFU) at 35 kHz and deionised water as the transmission medium in a Bandelin Sonorex Digitec DT 52 ultrasonic bath (BANDELIN electronic GmbH & Co. KG, Berlin, Germany).

5.1.7 Lyophilization

Lyophilisation was performed in combination with an ILMVAC Chemvac combination pump type 109030 (ILMVAC GmbH, Ilmenau, Germany) in an Alpha 2-4 LD plus freeze dryer from the manufacturer Martin Christ Gefriertrocknungsanlagen GmbH, Osterode am Harz, Germany.

5.2 Synthetic Procedures

5.2.1 Attempt to synthesize 2-((*R*)-2-aminopropanamido)-*N*-((*S*)-1-hydroxy-3-mercaptopropyl)benzamide (12) (Fusarithioamide A)

5.2.1.1 Synthesis of 3-(tritylthio)propanal (43)

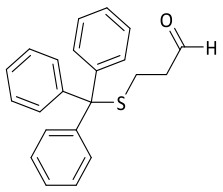

$C_{22}H_{20}OS$: 332.12 g/mol

To a solution of triphenylmethanethiol (1 g, 3.6 mmol, 1 equivalent) in dichloromethane (20 mL) were added acrolein (0.28 g, 5.07 mmol, 1.4 equivalent) and triethylamine (0.5 g, 5 mmol, 1.4 equivalent). The reaction mixture was later allowed to stir at room temperature for a period of 60 minutes and then concentrated under reduced pressure conditions to give aldehyde as an off-white amorphous solid 1.2 g (97% yield).

Rf = 0.57 (cyclohexane / AcOEt = 2:1)

HPLC (254 nm, VWD): t_R = 7.923 min

ESI-MS: *m/z* 355.11 ($[M+Na]^+$)

For the ^{1}H NMR (500 MHz, $CDCl_3$) δ 9.59 (s, 1H), 7.52 – 7.08 (m, 15H), 2.50 (dd, *J* = 7.7, 6.8 Hz, 3H), 2.43 – 2.31 (m, 3H).

^{13}C NMR (126 MHz, $CDCl_3$) δ 200.28, 144.90, 144.55, 129.69, 129.63, 129.57, 127.99, 127.93, 127.85, 126.78, 126.58, 67.02, 42.69, 24.44.

Melting point: 81-82 °C

The spectral data obtained were consistent with published literature. [193]

5.2.1.2 Synthesis of Tert-butyl (*R*)-(1-((2-carbamoylphenyl)amino)-1-oxopropan-2-yl)carbamate (46)

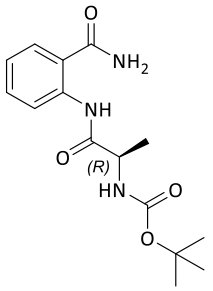

$C_{15}H_{21}N_3O_4$: 307.35 g/mol

To a solution of N-Boc-amino acid (977.7 µMol) in THF (1.54 mL) at 0 °C were added triethylamine (977.7 µMol) and ethyl chloroformate (977.7 µMol) over a period of ca. 10 min and stirred for 30 min. After the addition of the 2-aminobenzamide (1.5 mmol), The mixture was then stirred for a further 1 h at 0 °C. The reaction mixture was, in due course, allowed to warm and reach the ambient temperature and stirred overnight. After the solvent evaporated under reduced pressure, the residue was directly dissolved in EtOAc (2.31 mL) and washed with 3 M HCl (2 times 1.5 mL) and brine (1.5 mL). The organic layer was later dried using Na_2SO_4, and the solvent was, in due course, evaporated under reduced pressure (20 mbar, 20 °C). Crystallization of crude mixture gave the corresponding colourless amide 258 mg, 86% yield.

Rf = 0.25 (cyclohexane / AcOEt = 1:5)
HPLC (254 nm, VWD): t_R = 2.377 min

^{1}H NMR (400 MHz, DMSO-d_6, ppm) d 12.00 (br s, 1H), 8.52 (d, J = 8.4 Hz, 1H), 8.19 (br s, 1H), 7.76 (d, J = 7.9 Hz, 1H), 7.58 (br s, 1H), 7.53–7.39 (m, 2H), 7.18–7.02 (m, 1H), 3.95–3.91 (m, 1H), 1.39 (s, 9H), 1.27 (d, J = 7.3 Hz, 3H);

^{13}C NMR (100 MHz, DMSOd_6, ppm) d 172.7, 171.0, 156.0, 140.1, 132.7, 129.2, 122.9, 120.6, 120.5, 79.0, 52.3, 28.9, 18.0.

Melting point: 107–109 °C

The spectral data obtained were consistent with published literature. [194]

5.2.2 Synthesis of (1*R*,5*R*,11*R*,14*R*)-5-hydroxy-11-propyl-12-oxa-16,17-dithia-2,20-diazabicyclo[12.4.2]icosane-3,13,19-trione (BSc5484)

5.2.2.1 Synthesis of (*R*)-1-chloropentan-2-ol (57)

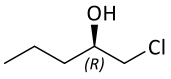

Ethylmagnesium bromide 3M in Et_2O (5.3 mL, 40.5 mmol) was added in a dropwise way to a solution of (*R*)-epichlorohydrin 1.1 mL (13.5 mmol) and CuCN 121 mg (1.4 mmol) in dry THF (15 mL) at -78 °C. The mixture was allowed to warm to -20 °C over 3 hours, poured into 18 mL of saturated NH_4Cl solution, and stirred for a few hours while open to the atmosphere. The two layers were separated, and following that, the aqueous layer was, in due course, extracted with Et_2O (3 x 20 mL). Following that, the combined organic phases were washed with saturated aqueous NH_4Cl (2 x 17 mL) and with brine (20 mL) and later on, as usual, dried with Na_2SO_4, filtered and concentrated in a vacuum to afford (*R*)-1-chloro-pentan-2-ol 1.54 g 93% yield as a yellow oil.

R_f = 0.66 (cyclohexane / AcOEt = 3:1)

HPLC (254 nm, VWD): t_R = 7.311 min

^{1}H NMR (500 MHz, $CDCl_3$) δ = 3.83 (tdd, *J* = 7.5, 4.7, 3.2 Hz, 1H), 3.65 (dd, *J* = 11.1, 3.3 Hz, 1H), 3.49 (dd, *J* = 11.1, 7.1 Hz, 1H), 2.26 (s, 1H), 1.74 – 1.34 (m, 4H), 0.96 (t, *J* = 7.2 Hz, 2H).
^{13}C NMR (126 MHz, $CDCl_3$) δ = 71.19, 50.58, 36.31, 18.76, 13.94.

MS (70 eV): *m/z* (%)122 (5) $[M]^+$

The spectral data obtained were consistent with published literature. [195]

5.2.2.2 Synthesis of (*R*)-2-propyloxirane (58)

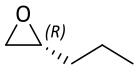

To a solution of (*R*)-1-Chloro-pentan-2-ol 1.6 g (13.5 mmol) in Et_2O (25 mL) was added finely powdered NaOH 3.06 g (76.5 mmol) with a mortar and pestle. The mixture was stirred constantly and vigorously for 24 hours and gently poured into 15 mL water. After the separation of the two layers (organic and aqueous). Then, the aqueous layer was extracted in due course with Et_2O (3 x 13 mL), and the combined organic layers were later on dried over $MgSO_4$. Removal of the solvent by distillation over a 10 cm vigorous column afforded the product a yellowish oil 1.1 g 94% yield, which was used without further purification.

R_f = 0.72 (cyclohexane / AcOEt = 4:1)

HPLC (254 nm, VWD): t_R = 6.467 min

^{1}H NMR (300 MHz, $CDCl_3$) δ = 3.80 – 3.68 (Brs, 1H), 2.90 (ddd, *J* = 7.8, 3.9, 2.0 Hz, 1H), 2.73 (dd, *J* = 5.1, 4.0 Hz, 1H), 2.45 (dd, *J* = 5.1, 2.7 Hz, 1H), 1.60 – 1.38 (m, 4H), 0.96 (t, *J* = 7.2 Hz, 3H).

^{13}C NMR (75 MHz, $CDCl_3$) δ = 52.15, 47.01, 34.50, 19.26, 13.89.

APCI-MS: *m/z* calculated for $C_5H_{10}O+H^+$: *m/z* = 87.08 $[M+H]^+$ Found: 87.09

The spectral data obtained were consistent with published literature. [196]

5.2.2.3 Synthesis of (*R*)-dec-9-en-4-ol (60)

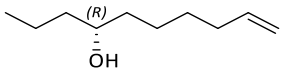

With a two-necked flask equipped with a reflux condenser, was charged magnesium turnings 2 g (82.3 mmol) and was subsequently flame-dried under vacuum, flushed with positive steam of argon. The process was repeated three times. Succeeding cooling to room temperature, a small crystal of iodine was added and treated with the heat gun until the iodine vapours were evenly distributed inside the flask. A solution of 4- bromopent-1-ene 2.38 mL (3 g, 20.1 mmol) in dry THF (12 mL) was added first portion-wise until the formation of a grey slurry and then drop-wise through a dropping funnel during a calculated period of 30 min, so that the reaction mixture was continuously boiling. The dark (Murky Brown) reaction mixture was cooled down to room temperature. In the following phase, the substance was utilized without additional purification. In other cases, external heating with a heat gun was required to speed up the beginning. The resulting solution of pentene magnesium bromide was added in a dropwise way over 15 min to a solution of (*R*)-2-propyloxirane 1.41 mL (1.2 g, 13.6 mmol) and CuCN (0.2 g, 2.3 mmol) in an initially dried THF (15 mL) at - 78 °C under argon atmosphere. After adding, the reaction was stirred at - 45 °C for 2 hours. The mixture was subsequently allowed to warm up to 0 °C before being quenched with a ca. 20 mL saturated NH_4Cl solution and stirred for a few hours open to the atmosphere. The layers were later separated, the aqueous layer was later extracted with DCM (3 x 25 mL), and then, the combined ethereal extracts were washed with brine (18 mL) and dried (Na_2SO_4). The evaporation of the solvent via reduced pressure and purification by silica gel flash chromatography (cyclohexanes/EtOAc = 60:4) gave the product a slightly yellow oil 1.5 g 69% yield.

R_f = 0.516 (cyclohexane / AcOEt = 3:1)

HPLC (254 nm, VWD): t_R = 2.453 min

^{1}H NMR (500 MHz, $CDCl_3$) δ = 5.82 (ddt, *J* = 16.9, 10.2, 6.7 Hz, 1H), 5.05 – 4.89 (m, 2H), 3.61 (tq, *J* = 6.8, 3.8 Hz, 1H), 2.12 – 2.01 (m, 2H), 1.67 – 1.20 (m, 10H), 0.96 (t, *J* = 7.2 Hz, 3H).

^{13}C NMR (126 MHz, $CDCl_3$) δ = 137.91, 113.33, 70.66, 38.68, 36.32, 32.73, 27.96, 24.12, 17.81, 13.09.

ESI-MS: *m/z* calculated for $C_{10}H_{20}O+H^+$:157.160 $[M+H]^+$; found: 157.159

5.2.2.4 Synthesis of (*R*)-1-((dec-9-en-4-yloxy)methyl)-4-methoxybenzene (61)

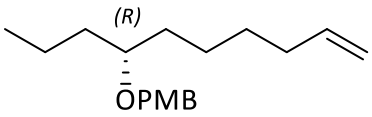

Under an argon atmosphere, to a solution of (*R*)-dec-9-en-4-ol 460 mg (2.9 mmol) in THF 15 mL was added potassium terbutoxyde 397 mg (3.5 mmol) followed by 4-Methoxybenzyl chloride 476.9 mmL (3.5 mmol) at 0 °C degree. The reaction was subsequently allowed to reach room temperature before being stirred overnight. After adding H_2O, the mixture was extracted using CH_2Cl_2. The organic layers were then combined in due course, dried (Na_2SO_4), and the volatiles were removed under reduced pressure. The evaporation of the solvent under reduced pressure and purification by silica gel flash chromatography (cyclohexanes/EtOAc = 97:3) gave the product as a yellow oil 708 mg 87% yield.

R_f = 0.68 (cyclohexane / AcOEt = 3:1)

HPLC (254 nm, VWD): t_R = 8.284 min

^{1}H NMR (300 MHz, $CDCl_3$) δ = 7.19 (d, J = 6.4 Hz, 2H), 6.84 – 6.74 (m, 2H), 5.73 (ddt, J = 17.0, 10.1, 6.6 Hz, 1H), 4.89 (dd, J = 17.2, 13.7 Hz, 2H), 4.35 (s, 2H), 3.71 (d, J = 6.2 Hz, 3H), 3.28 (p, J = 5.4 Hz, 1H), 1.96 (t, J = 6.6 Hz, 2H), 1.59 – 1.06 (m, 10H), 0.83 (t, J = 6.9 Hz, 3H).
^{13}C NMR (75 MHz, $CDCl_3$) δ = 159.05, 139.04, 131.33, 129.29, 114.26, 113.73, 78.45, 70.42, 55.30, 36.23, 33.80, 33.75, 29.14, 24.87, 18.68, 14.31.
MS (70 eV): *m/z* (%): 276 (5) ([M]$^+$).

5.2.2.5 Synthesis of (*R*)-7-((4-methoxybenzyl)oxy)decan-1-ol (62)

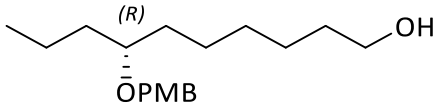

9-BBN (0.5 M in THF, 17 mL, 8.5 mmol) was then added dropwise to a solution of (*R*)-1-((dec-9-en-4-yloxy)methyl)-4-methoxybenzene (693 mg, 2.5 mmol) in anhydrous THF (15 mL) at 0 °C, and the solution was later on stirred at room temperature for at least 13 hours. The mixture was directly allowed to cool to 0 °C, and water (3.3 mL), aqueous NaOH (2 M, 18 mL, 36 mmol), and H_2O_2 (35% w/w, 6 mL) were all added dropwise. The biphasic mixture was subsequently stirred at room temperature for 6 h, diluted with brine, extracted with a small EtOAc three times, dried over anhydrous Na_2SO_4, and evaporated via reduced pressure. Afterwards, the crude product was then purified by using flash column chromatography (20% EtOAc in cyclohexane), giving a colourless oil (474.6 mg; 64.3% yield).

R_f = 0.45 (cyclohexane / AcOEt = 3:1)

HPLC (254 nm, VWD): t_R = 6.471 min

^{1}H NMR (300 MHz, $CDCl_3$) δ = 7.27 (d, J = 8.5 Hz, 1H), 6.88 (d, J = 8.6 Hz, 0H), 4.44 (s, 2H), 3.81 (s, 3H), 3.64 (t, J = 6.6 Hz, 2H), 3.36 (m, 1H), 1.75 – 1.18 (m, 14H), 0.91 (t, J = 6.9 Hz, 3H).

^{13}C NMR (75 MHz, $CDCl_3$) δ = 159.05, 131.34, 129.30, 113.74, 78.47, 70.42, 63.04, 55.30, 36.22, 33.85, 32.78, 29.63, 25.75, 25.33, 18.66, 14.31.

ESI-MS: *m/z* calculated for $C_{18}H_{30}O_3+H^+$; 295.22 $[M+H]^+$; found: 295.23

5.2.2.6 Synthesis of (*R*)-7-((4-methoxybenzyl)oxy)decanal (63)

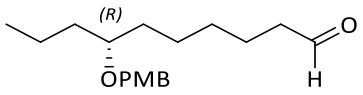

To a solution of alcohol (287 mg, 0.9 mmol) in DMSO (10 mL) at 10 °C was added freshly prepared 2-Iodoxybenzoic acid (IBX) (545.9 mg, 1.9 mmol). The resulting solution was later allowed to settle to ambient temperature before being agitated overnight. The reaction was subsequently quenched with 30 mL of EtOAc, washed 3 times with water, 3 times with $NaHCO_3$, one time with brine and dried Na_2SO_4, filtered, and was concentrated under reduced pressure (not below 240 Mbar at 40 °C) to give the product as a colourless oil 265.1 mg 93% yield used for the next step without further purification.

HPLC (254 nm, VWD): t_R = 2.672 min

^{1}H NMR (300 MHz, $CDCl_3$) δ = 9.69 (s, 1H), 7.27 – 7.21 (d, J = 8.6 Hz, 2H), 6.87 – 6.78 (d, J = 8.6 Hz, 2H), 4.43 (s, 2H), 3.81 (s, 3H), 3.36 (dq, J = 11.2, 5.4 Hz, 1H), 2.42 (td, J = 7.3, 1.9 Hz, 2H), 1.65 – 1.10 (m, 12H), 0.92 (t, J = 7.0 Hz, 3H).
^{13}C NMR (75 MHz, $CDCl_3$) δ = 202.80, 159.07, 131.24, 129.29, 113.73, 78.32, 70.44, 55.29, 43.86, 36.18, 33.70, 29.35, 25.11, 22.09, 18.64, 14.30.
ESI-MS: *m/z* calculated for $C_{18}H_{28}O_3$+Na^+: 315.20 ($[M+Na]^+$ found: 315.19

The spectral data obtained were consistent with published literature. [197]

5.2.2.7 Synthesis of (*R*)-1-(4-benzyl-2-thioxothiazolidin-3-yl)ethan-1-one (66)

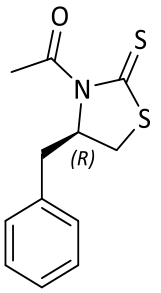

To a suspension of (*R*)-phenylalaninol (2 g, 13.2 mmol) in 3M aqueous KOH (30 mL) at 23 ºC was added under an argon atmosphere, CS_2 (4 mL, 66.1 mmol). After 10 min, an orange solution appeared, which was refluxed for 22 h. The resulting tan solution was cooled to 23 ºC and extracted with CH_2Cl_2 (3 x 25 mL). The combined organic layers were later washed with a saturated aqueous solution of NaCl (brine) (25 mL calculated volume), dried using Na_2SO_4, and, in due course, filtered and concentrated via reduced pressure, affording the needed colourless solid (auxiliary), which was utilized for the next step without further purification.

Auxiliary HPLC (254 nm, VWD): t_R = 4.645 min.

The auxiliary (1.25 g, 6 mmol), 4-dimethylaminopyridine (0.073 g, 0.6 mmol), and triethylamine (1.25 mL, 9 mmol) were dissolved in molecular sieved dried CH_2Cl_2 (20 mL) and cooled to 0 °C. Acetyl chloride (0.64 mL, 9 mmol) was added in a dropwise way, and the reaction was slowly allowed to reach the ambient temperature and stirred overnight. Following, the reaction was quenched with saturated NH_4Cl (15 mL), diluted with Et_2O (15 mL), and the organic phase was washed with saturated $CuSO_4$ as follows, 3 x 25 mL, and later with 20 mL of dist. water, and then brine (20 mL), later on, dried ($MgSO_4$), was filtered and concentrated to give the crude compound as a yellow solid. Recrystallization from EtOH afforded (*R*)-1-(4-benzyl-2-thioxothiazolidin-3-yl)ethan-1-one (1.4 g, 97%) as yellow crystalline needles.
HPLC (254 nm, VWD): t_R = 6.767 min.

^{1}H NMR (300 MHz, $CDCl_3$) δ = 7.45 – 7.22 (m, 5H), 5.48 – 5.35 (m, 1H), 3.41 (ddd, *J* = 11.6, 7.2, 1.1 Hz, 1H), 3.25 (dd, *J* = 13.2, 3.9 Hz, 1H), 3.09 (dd, *J* = 13.2, 10.6 Hz, 1H), 2.88 (dd, *J*= 11.5, 0.7 Hz, 1H), 2.82 (s, 3H).

^{13}C NMR (75 MHz, $CDCl_3$) δ = 201.57, 170.72, 136.54, 129.47, 128.92, 127.24, 68.23, 36.73, 31.85, 27.07.

ESI-MS: *m/z* calculated for $C_{12}H_{13}NOS_2$+Na^+; 274.05 ($[M+Na]^+$) found: 274.03

Melting point: 88-90 °C.

The spectral data obtained were consistent with published literature. [198]

5.2.2.8 Synthesis of (3*R*,9*R*)-1-((*R*)-4-benzyl-2-thioxothiazolidin-3-yl)-3-hydroxy-9-((4-methoxybenzyl)oxy)dodecan-1-one (67)

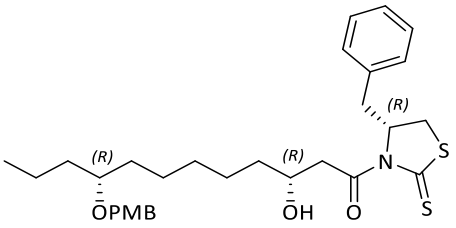

To a solution of (*R*)-1-(4-benzyl-2-thioxothiazolidin-3-yl)ethan-1-one 104 mg (0.4 mmol) in dry dichloromethane (3.5 mL) at 0 °C was added dropwise 49.5 µL of $TiCl_4$ (1M in CH_2Cl_2 0.5 mL). After stirring the reaction mixture for a period of 10 minutes, *i*Pr_2NEt 0.09 mL (0.6 mmol) was added dropwise to the viscous orange solution. The resulting blood-red titanium enolate solution was stirred at 0 °C for a period of 45 minutes and then cooled to -78 °C. A solution of (*R*)-7-((4-methoxybenzyl)oxy)decanal 110 mg (0.4 mmol) in dichloromethane (2 mL) was added in a dropwise way, and the obtained reaction mixture was stirred for a period of 1 hour. Following completion (monitored by TLC), the reaction was quenched by the addition of a half-saturated aqueous NH_4Cl solution, the organic layer was later separated, and then, the aqueous layer was subsequently extracted with CH_2Cl_2 (3 × 10 mL). The mixed organic layers were brine-washed, dried over Na_2SO_4, later filtered, and concentrated in a vacuum. Purification of the residue by column chromatography (cyclohexane–EtOAc, 80:20 to 70:30) gave the desired major aldol adduct as a yellowish oil 143.2 mg (70% yield).

R_f = 0.61 (cyclohexane / AcOEt = 2:1)

HPLC (254 nm, VWD): t_R = 4.510 min

^{1}H NMR (300 MHz, $CDCl_3$) δ = 7.44 – 7.31 (m, 5H), 7.30 (d, *J* = 5.6 Hz, 2H), 6.90 (d, *J* = 8.3 Hz, 2H), 5.43 (d, *J* = 3.7 Hz, 1H), 4.46 (s, 2H), 4.24 – 4.03 (m, 1H), 3.83 (s, 3H), 3.73 – 3.61 (m, 1H), 3.50 – 3.32 (m, 2H), 3.26 (dd, *J* = 13.2, 3.9 Hz, 1H), 3.13 (dt, *J* = 20.1, 9.5 Hz, 1H), 3.03 (d, *J* = 7.1 Hz, 1H), 2.93 (d, *J* = 11.5 Hz, 1H), 1.64 – 1.24 (m, 14H), 0.94 (t, *J* = 7.0 Hz, 3H).

^{13}C NMR (75 MHz, $CDCl_3$) δ = 201.49, 173.34, 159.04, 136.41, 131.33, 129.44, 129.29, 128.95, 127.30, 113.74, 78.46, 70.41, 68.33, 67.86, 55.31, 45.90, 36.86, 36.36, 36.22, 33.84, 32.06, 29.75, 25.56, 25.29, 18.67, 14.31.

ESI-MS: *m/z* calculated for $C_{30}H_{41}NO_4S_2+H^+$; 544.23 ($[M+H]^+$); found: 544.25

5.2.2.9 Synthesis of (3*R*,9*R*)-1-((*R*)-4-benzyl-2-thioxothiazolidin-3-yl)-3-((tert-butyldimethylsilyl)oxy)-9-((4-methoxybenzyl)oxy)dodecan-1-one (68)

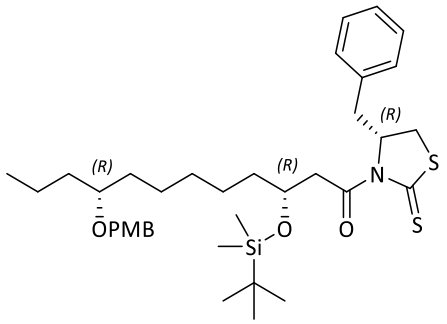

To a stirred solution of (3*R*,9*R*)-1-((*R*)-4-benzyl-2-thioxothiazolidin-3-yl)-3-hydroxy-9-((4-methoxybenzyl)oxy)dodecan-1-one 112 mg (0.2 mmol) in anhydrous 5 mL CH_2Cl_2 at 0ºC under argon was added *N*,*N*-diisopropylethyl amine 53.81 μL (0.3 mmol), and after 10 min TBSOTf 61.6 μL (0.3 mmol) was added dropwise sequentially. After 1 h at 0 °C degrees and upon completion monitored by TLC or HPLC, the reaction was, in due course, quenched by the addition of 8 mL aqueous saturated $NaHCO_3$. The two layers were then separated. The aqueous layer was later extracted with CH_2Cl_2 (3 x 50 mL). The combined organics were washed with brine (8 mL), dried over Na_2SO_4 and later concentrated under reduced pressure. The crude product was, after some time, purified by silica gel column chromatography (Cyclohexane-Ethyl acetate 95:5) to provide the product as bright yellow oil 118 mg (87%).

R_f = 0.53 (cyclohexane / AcOEt = 3:1)

HPLC (254 nm, VWD): t_R = 11.644 min

^{1}H NMR (300 MHz, $CDCl_3$) δ = 7.32 (dd, *J* = 14.2, 6.7 Hz, 5H), 7.26 (d, *J* = 3.3 Hz, 2H), 6.88 (d, *J* = 8.3 Hz, 2H), 5.40 – 5.20 (m, 1H), 4.44 (s, 2H), 4.32 (dq, *J* = 16.4, 5.6, 4.8 Hz, 1H), 3.81 (s, 3H), 3.58 (dd, *J* = 16.7, 8.3 Hz, 1H), 3.41 – 3.31 (m, 2H), 3.27 (dd, *J* = 13.3, 3.6 Hz, 1H), 3.17 (dd, *J* = 16.9, 3.9 Hz, 1H), 3.05 (dd, *J* = 13.0, 10.7 Hz, 1H), 2.88 (dd, *J* = 11.5, 4.8 Hz, 1H), 1.67 – 1.19 (m, 14H), 0.90 (t, *J* = 7 Hz, 3H), 0.87 (s, 9H), 0.10 (s, 3H), 0.06 (s, 3H).

^{13}C NMR (75 MHz, $CDCl_3$) δ = 201.15, 172.49, 159.04, 136.64, 131.33, 129.46, 129.27, 128.93, 127.21, 113.73, 78.48, 70.40, 69.31, 68.72, 55.30, 45.84, 37.77, 36.56, 36.22, 33.84, 32.20, 29.97, 25.87, 25.36, 25.00, 18.68, 18.05, 14.31, -4.36, -4.60 *ppm*.

ESI-MS: *m/z* calculated for $C_{36}H_{55}NO_4SSi+H^+$; 658.31 ($[M+H]^+$) found: 658.34.

5.2.2.10 Synthesis of (3*R*,9*R*)-3-((tert-butyldimethylsilyl)oxy)-9-((4-methoxybenzyl)oxy)dodecanoic acid (69)

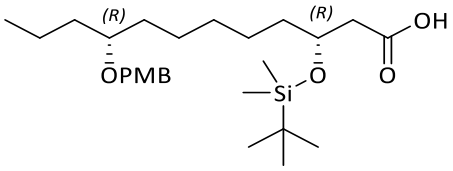

To a stirred solution of the (3*R*,9*R*)-1-((*R*)-4-benzyl-2-thioxothiazolidin-3-yl)-3-((tert-butyldimethylsilyl)oxy)-9-((4-methoxybenzyl)oxy)dodecan-1-one (43.3 mg, 0.06 mmol) in tetrahydrofuran-water (4:1, 1.6 mL) was added 30% aqueous hydrogen peroxide (43 µL, 0.88 mmol) and 0.8 M aqueous lithium hydroxide (0.4 mL) at 0 °C. After 5 hours of stirring, the reaction was terminated by adding aqueous Na_2SO_3 (1.3 M solution, 3.0 mL, 4.0 mmol) and aqueous saturated NH_4Cl (10 mL). The resulting mixture was therefore extracted with ether (3 × 10 mL). The organic layer was subsequently dried ($MgSO_4$) and, in due course, concentrated via a rotary evaporator. The purification of the residue through flash chromatography (using Ethyl acetate in cyclohexane 35%) afforded the desired carboxylic acid 28.3 mg (92%). The final product was obtained in the form of a colourless oil.

R_f = 0.714 (cyclohexane / AcOEt = 1:1)

HPLC (254 nm, VWD): t_R = 8.815 min

^{1}H NMR (500 MHz, $CDCl_3$) δ = 7.27 (d, *J* = 8.1 Hz, 2H), 6.88 (d, *J* = 8.0 Hz, 2H), 4.44 (s, 2H), 4.15 – 4.06 (m, 1H), 3.81 (s, 3H), 3.36 (m, 1H), 2.51 (d, *J* = 7.7 Hz, 2H), 1.69 – 1.15 (m, 14H), 0.92 (s, 9H), 0.89 (t, *J* = 7 Hz 3H), 0.10 (s, 3H), 0.09 (s, 3H).
^{13}C NMR (126 MHz, $CDCl_3$) δ = 176.00, 159.04, 131.27, 129.29, 113.73, 78.45, 70.40, 69.44, 55.29, 41.96, 37.28, 36.18, 33.79, 29.82, 25.76, 25.28, 18.65, 17.97, 14.29, -4.52, -4.84 *ppm*.
ESI-MS: *m/z* calculated for $C_{26}H_{46}O_5Si+H^+$; 489.32 ($[M+Na]^+$) found: 489.30.

5.2.2.11 Synthesis of methyl *S*-trityl-*L*-cysteinate (50)

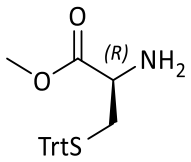

S-Trityl-*L*-cysteine (0.25 g, 687.8 μmoles) was dissolved in 12.5 mL of anhydrous MeOH and was cooled to 0 °C. After 20 minutes, thionyl chloride (375 μL, 5.2 μmol) was slowly added, and the resulting solution was permitted to stir at 0 °C for 1 h. The solution was warmed and reached the ambient temperature for 2 hours and was subsequently heated to reflux for 18 hours. The reaction was afterwards allowed to cool to room temperature, and THF (30 mL) was added and evaporated. The residue was dried in a high vacuum, giving a colourless, finely crystalline solid of 0.26 g (99 % yield).

HPLC (254 nm, VWD): t_R = 5.392 min

^{1}H NMR (500 MHz, $CDCl_3$) δ = 7.34 (m, 6H), 7.17 (m, 11H), 3.58 (s, 3H), 3.14 (m, 2H), 2.53 (d, J = 11.8 Hz, 1H), 2.42 (d, J = 11.3 Hz, 1H).
^{13}C NMR (126 MHz, $CDCl_3$) δ = 173.96, 144.51, 129.59, 127.97, 126.80, 66.92, 53.73, 52.24, 36.77 *ppm*.
ESI-MS: *m/z* calculated for $C_{23}H_{24}NO_2S+H^+$, 378.13 ($[M+H]^+$) found: 378.15.

Melting point: 76 °C.

The spectral data obtained were consistent with published literature. [199]

5.2.2.12 Synthesis of *N*-(tert-butoxycarbonyl)-*S*-trityl-*L*-cysteine (51)

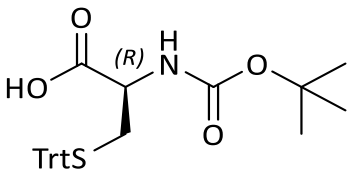

To a solution of *S*-Trityl-*L*-cysteine, (500 mg, 1.4 mmol) in NaOH 2N (10 mL) was added Boc_2O (600 mg, 2.8 mmol) and stirred for 24 hours at room temperature. The aqueous solution was later on acidified with HCl concentrated until pH 2 and extracted with CH_2Cl_2 (2 time10 mL); the combined organic phases were in due course washed first with brine, dried over Na_2SO_4 and concentrated via reduced pressure to give without any further purification N-Boc protected compound (574 mg, 90% yield) as a colourless foam.

HPLC (254 nm, VWD): t_R = 7.528 min

^{1}H NMR (300 MHz, DMSO) δ = 7.43 – 7.21 (m, 15H), 3.81 (td, *J* = 9.1, 4.7 Hz, 1H), 2.61 – 2.53 (m, 1H), 2.37 (dd, *J* = 12.2, 4.8 Hz, 1H), 1.39 (s, 9H).
^{13}C NMR (75 MHz, DMSO) δ = 172.56, 155.66, 144.76, 129.55, 128.52, 127.25, 78.69, 66.62, 53.48, 33.43, 28.64.
ESI-MS: *m/z* calculated for $C_{27}H_{29}NO_4S+Na^+$; 486.19 ($[M+Na]^+$); found: 486.17

Melting point: 76 - 77 °C
The spectral data obtained agree with the data published in the literature. [200]

5.2.2.13 Synthesis of methyl *N*-(*N*-(tert-butoxycarbonyl)-*S*-trityl-*L*-cysteinyl)-*S*-trityl-*D*-cysteinate (52)

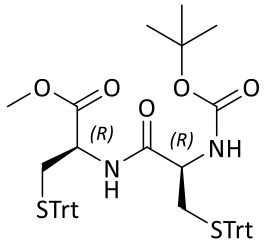

To DCM (16 mL) in a 50 mL round bottom flask was added *N*-(tert-butoxycarbonyl)-*S*-trityl-*L*-cysteine (198.94 mg, 0.4 mmol), followed by EDC (98.7 mg, 0.5 mmol), and HOBt (78.9 mg, 0.5 mmol) were then added, stirred at RT for 20 min. In a separate 50 mL flask H-SCystri-OMe (162 mg, 0.4 mmol) was dissolved in DCM (13 mL), and DIPEA was added (187 µL, 1.1 mmol). The solution of activated ester was cooled to 0 °C, and the solution of H-S-Trityl-Cyst-OMe was added dropwise via syringe. When the solution became clear, it was directly stirred at 0 °C for a calculated 30 min and then warmed to room temperature. Following this, it was again stirred for 2 hrs. After that, the solution was mixed into cold water (100 mL). The aqueous layer was later extracted with DCM (2 x 50 mL). The organics were cleaned with a saturated solution of $NaHCO_3$, water, brine, dried (Na_2SO_4), filtered and concentrated in a vacuum. Flash column chromatographic purification (15 % EtOAc in cyclohexane as the eluent) of the resultant residue gave the product a colourless amorphous solid (247.2 mg, 70% yield).

R_f = 0.692 (cyclohexane / AcOEt = 4:1)

HPLC (254 nm, VWD): t_R = 10.136 min

^{1}H NMR (300 MHz, DMSO) δ = 8.14 (d, J = 7.6 Hz, 1H), 7.47 – 7.11 (m, 30H), 6.94 (d, J = 8.6 Hz, 1H), 4.09 – 3.88 (m, 2H), 3.49 (s, 3H), 2.47 – 2.28 (m, 4H), 1.38 (s, 9H).
^{13}C NMR (75 MHz, DMSO) δ = 174.79, 170.56, 155.29, 144.71, 129.49, 128.46, 127.20, 79.01, 66.69, 66.35, 55.29, 52.52, 51.81, 30.87, 28.54, 18.92.
ESI-MS: *m/z* calculated for $C_{50}H_{50}N_2O_5S_2$+Na^+; 845.34 ([M+Na]$^+$) found: 845.31.

Melting point: 216 - 227 °C

The spectral data obtained are in agreement with the data published in the literature. [201]

5.2.2.14 Synthesis of Methyl (4*R*,7*R*)-7-((tert-butoxycarbonyl)amino)-6-oxo-1,2,5-dithiazocane-4-carboxylate (BSc5483)

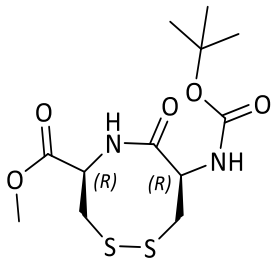

A solution of methyl *N*-(*N*-(tert-butoxycarbonyl)-*S*-trityl-*L*-cysteinyl)-*S*-trityl-*L*-cysteinate (1.1 g, 1.4 mmol) in CH_2Cl_2/MeOH (9:1; 360 mL) was added dropwise to a vigorously stirred solution of I_2 (3.4 g, 13.6 mmol) in CH_2Cl_2/MeOH (9:1; 2.9 L, 0.5 mM concentration) over 10 min at room temperature. After 25 min of stirring at the same temperature, the reaction was, in due course, quenched with 10% aq $Na_2S_2O_3$ (372 mL) at r.t. The resulting mixture was next diluted with CH_2Cl_2 (500 mL), and the organic layer was cleaned with sat. aq $NaHCO_3$ (2 × 372 mL) and brine (2 × 372 mL), and then dried over $MgSO_4$. Removal of the solvent in a vacuum afforded a colourless residue, which was purified by column chromatography (silica gel, $CHCl_3$), giving a colourless amorphous solid (348 mg, 76% yield).

R_f = 0.66 (CCl_3 / MeOH = 5:0.5)

HPLC (205 nm, VWD): t_R = 3.986 min

^{1}H NMR (500 MHz, DMSO) δ = 7.30 (Brs, 1H, NH), 6.57 (Brs, 1H, NH), 4.92 (m, 2H), 3.97 (dd, *J* = 15.4, 12.7 Hz, 1H), 3.72 (s, 3H), 3.22 (dd, *J* = 15.1, 12.2 Hz, 1H), 2.80 (m, 2H), 1.38 (s, 9H).

^{13}C NMR (75 MHz, DMSO) δ = 172.65, 170.83, 155.14, 79.07, 53.22, 52.99, 52.73, 52.38, 41.41, 28.59.

ESI-MS: *m/z* calculated for $C_{12}H_{20}N_2O_5S_2$+Na^+; 359.09 ($[M+Na]^+$); found: 359.07.

Melting point: 161 – 164 °C.

5.2.2.15 Synthesis of methyl (4*R*,7*R*)-7-((3*R*,9*R*)-3-((tert-butyldimethylsilyl)oxy)-9-((4-methoxybenzyl)oxy)dodecanamido)-6-oxo-1,2,5-dithiazocane-4-carboxylate (70)

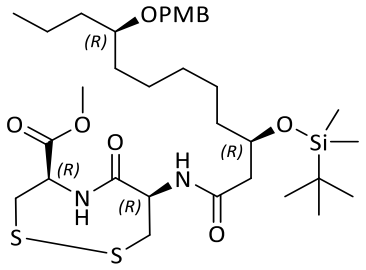

Methyl (4*R*,7*R*)-7-((tert-butoxycarbonyl)amino)-6-oxo-1,2,5-dithiazocane-4-carboxylate (85 mg, 0.3 mmol) was introduced in a round bottom flask and washed with 3 mL DCM/TFA/1:1: at 0 °C and then left for 90 minutes with constant mixing until the reaction shows complete conversion of the starting material. The reaction mixture was directly diluted with toluene and concentrated in a vacuum to give the crude TFA salt, which was used for the next step without further purification. To a DMF (5 mL) in a 25 mL round bottom flask was added (3*R*,9*R*)-3-((tert-butyldimethylsilyl)oxy)-9-((4-methoxybenzyl)oxy)dodecanoic acid (55 mg, 0.1 mmol) followed by EDC (27.1 mg, 0.1 mmol), and 30 min later, HOBt (19.1 mg, 0.1 mmol) was added, stirred at room temperature for 20 min. In a separate flask, the crude TFA salt previously synthesized (55.4 mg, 0.2 mmol) was dissolved in DMF (3 mL) and Et_3N (41 µL, 0.3 mmol) was added. To the solution of activated ester, was added H-Cys-Cys-OMe dropwise via syringe and stirred for 21 hours at room temperature. The solution was then poured onto ice-cold water. It was extracted with 20 mL of EtOAc, and the combined organic layer was later cleaned with distilled water, then a solution of brine, and dried over anhydrous Na_2SO_4. The residue was chromatographed over silica gel after being concentrated in a vacuum. Elusion with MeOH in DCM (6%) produced the product as a yellowish sticky solid (56.5 mg, 70% yield).

R_f = 0.66 (Dichloromethane / Methanol = 3:1)

HPLC (205 nm, VWD): t_R = 8.977 min

^{1}H NMR (300 MHz, $CDCl_3$) δ = 7.26 (d, *J* = 6.9 Hz, 2H), 6.87 (d, *J* = 8.1 Hz, 2H), 4.88 (t, *J* = 7.6 Hz, 1H), 4.74 (t, *J* = 7.1 Hz, 1H), 4.42 (s, 2H), 4.05 (q, *J* = 5.6, 5.2 Hz, 1H), 3.82 (s, 3H), 3.80 (s, 3H), 3.45 (dd, *J* = 10.3, 6.5 Hz, 1H), 3.35 (q, *J* = 5.5 Hz, 1H), 3.01 (dd, *J* = 7.4, 8 Hz,

1H), 2.95 (dd, *J* = 7.12, 8,1 Hz, 1H), 2.52 (dd, *J* = 8.01, 7.45 Hz, 1H), 2.40 (dd, *J* = 10.3, 6.7 Hz, 1H), 2.33 (dd, *J* = 10.3, 6.7 Hz, 1H), 1.73 – 1.04 (m, 14H), 0.91 (s, 9H), 0.88 (t, *J* = 7 Hz, 3H), 0.09 (s, 3H), 0.07 (s, 3H).

^{13}C NMR (75 MHz, $CDCl_3$) δ = 172.03, 170.41, 168.05, 159.03, 131.32, 129.26, 113.73, 78.48, 70.39, 69.58, 55.30, 52.98, 52.15, 43.75, 42.61, 36.86, 36.20, 33.81, 29.86, 29.70, 26.03, 25.84, 25.34, 22.69, 18.66, 18.03, 14.31, -4.49, -4.67.

ESI-MS: *m/z* calculated for $C_{33}H_{56}N_2O_7S_2Si+H^+$; 685.37 ($[M+H]^+$); found: 685.34.

Melting point: 240 – 249 °C

5.2.2.16 Synthesis of methyl (4*R*,7*R*)-7-((3*R*,9*R*)-3-((tert-butyldimethylsilyl)oxy)-9-hydroxydodecanamido)-6-oxo-1,2,5-dithiazocane-4-carboxylate (71)

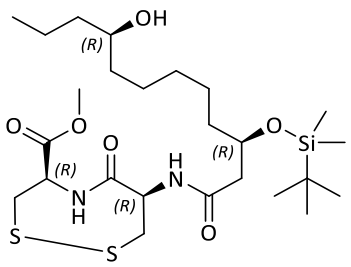

To a solution of methyl (4*R*,7*R*)-7-((3*R*,9*R*)-3-((tert-butyldimethylsilyl)oxy)-9-((4-methoxybenzyl)oxy)dodecanamido)-6-oxo-1,2,5-dithiazocane-4-carboxylate (53 mg, 0.1 mmol) in CH_2Cl_2 (5.3 mL) at 0 °C were added water (0.35 mL) and 22.8 mg, 0.1 mmol 2,3-dichloro-5,6-dicyano-1,4-benzoquinone (DDQ). After being stirred for 60 minutes at the ambient temperature, the mixture was later diluted with a saturated solution of aqueous $NaHCO_3$ (4 mL) and stirred for 15 min. Ethyl acetate (10 mL) was introduced, and the organic phase was cleaned with saturated aqueous $NaHCO_3$ (7.5 mL) and brine (9.5 mL), dried ($MgSO_4$), and evaporated. The crude product was finally purified using flash chromatography MeOH in Chloroform 6% to give a yellowish amorphous solid (37.2 mg, 85% yield).

R_f = 0.66 (Chloroform / Methanol = 4:1).

HPLC (205 nm, VWD): t_R = 2.281 min

^{1}H NMR (300 MHz, $CDCl_3$) δ = 5.18 – 5.15 (m, 1H), 5.16 – 5.14 (m, 1H), 4.04 (q, *J* = 6.4, 6.0 Hz, 1H), 3.82 (s, 3H), 3.62 (dd, *J* = 11.5, 6.4 Hz, 1H), 3.42 (q, *J* = 6.0, 6.3 Hz, 1H), 3.02 (dd, *J* = 11.3, 6.4 Hz, 1H), 2.93 (dd, *J* = 11.4, 6.2 Hz, 1H), 2.62 (dd, *J* = 11.3, 6.3 Hz, 1H), 2.42 (d, *J* = 4.2 Hz, 1H), 2.35 (d, *J* = 4.2 Hz 1H), 1.27 (m, 14H), 0.90 (s, 9H), 0.88 (t, *J* = 7.1, 3H), 0.07 (s, 3H), 0.06 (s, 3H).

^{13}C NMR (75 MHz, $CDCl_3$) δ = 172.30, 172.19, 170.45, 71.64, 69.58, 52.09, 45.37, 43.70, 39.69, 37.31, 32.78, 31.92, 30.04, 29.70, 29.35, 27.38, 25.82, 22.69, 18.84, 18.01, 14.12, -4.54.

ESI-MS: *m/z* calculated for $C_{25}H_{48}N_2O_6S_2Si+H^+$; 568.30 ($[M+H]^+$); found: 565.28.

Melting point: 255 – 262 °C

5.2.2.17 Synthesis of (4*R*,7*R*)-7-((3*R*,9*R*)-3-((tert-butyldimethylsilyl)oxy)-9-hydroxydodecanamido)-6-oxo-1,2,5-dithiazocane-4-carboxylic acid (72)

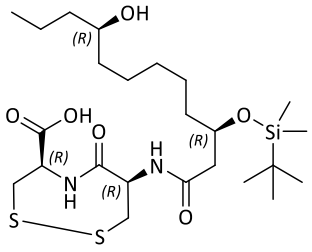

Methyl (4*R*,7*R*)-7-((3*R*,9*R*)-3-((tert-butyldimethylsilyl)oxy)-9-hydroxydodecanamido)-6-oxo-1,2,5-dithiazocane-4-carboxylate (42 mg, 0.1 mmol) was dissolved in 1,2-dichloroethane 6 mL and after addition of trimethyltin hydroxide (87.4 mg, 0.5 mmol), the mixture was later on allowed to heat at 60 °C until TLC analysis indicated a complete reaction. After the reaction was completed, the mixture was, in due course, concentrated in a vacuum, and the residue was collected in ethyl acetate (= 13 mL). The organic layer was washed with aqueous $KHSO_4$ (0.01N) (3 times 15 mL). The organic layer was then rinsed with brine (15 mL) and dried over sodium sulfate. Removal of the solvent in a vacuum afforded the carboxylic acid as an amorphous solid (34.8 mg, 85% yield).

R_f = 0.733 (Chloroform / Methanol = 4:1)

HPLC (205 nm, VWD): t_R = 1.112 min

^{1}H NMR (300 MHz, $CDCl_3$) δ = 5.44 – 5.27 (t, *J* = 8.2 Hz, 1H), 5.03 (t, *J* = 8.0 Hz, 1H), 4.04 (q, *J* = 6.1, 5.7 Hz, 1H), 3.83 – 3.57 (m, 2H), 3.56 (q, *J* = 6.0, 6.3 Hz, 1H), 3.55 – 3.36 (dd, *J* = 11.1, 6.3 Hz, 1H), 3.14 – 2.88 (dd, *J* = 11.5, 6.4 Hz, 1H), 2.36 (d, *J* = 7.0 Hz, 1H), 2.04 (d, *J* = 7.1 Hz, 1H), 1.39 – 1.14 (m, 14H), 0.92 (s, 9H), 0.90 (t, *J* = 7.1 Hz, 3H), 0.09 (s, 3H).
^{13}C NMR (75 MHz, $CDCl_3$) δ = 177.79, 171.19, 170.48, 70.61, 69.60, 60.41, 45.37, 42.92, 39.57, 37.10, 31.92, 30.04, 29.70, 29.36, 27.72, 25.82, 22.69, 21.49, 18.88, 14.11, -4.60, -4.73.
APCI-MS: *m/z* calculated for $C_{24}H_{46}N_2O_6S_2Si+H^+$; 551.28 ($[M+H]^+$); found: 551.26

Melting point: 257 – 262 °C

5.2.2.18 Synthesis of (1*R*,5*R*,11*R*,14*R*)-5-((tert-butyldimethylsilyl)oxy)-11-propyl-12-oxa-16,17-dithia-2,20-diazabicyclo[12.4.2]icosane-3,13,19-trione (73)

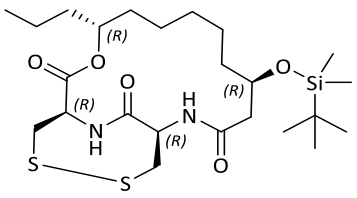

A solution of crude acid alcohol (4*R*,7*R*)-7-((3*R*,9*R*)-3-((tert-butyldimethylsilyl)oxy)-9-hydroxydodecanamido)-6-oxo-1,2,5-dithiazocane-4-carboxylic acid (33.2 mg, 0.1 mmol) in anhydrous THF 56 mL) was slowly added to a 16.7 mL solution of 2-methyl-6-nitrobenzoic anhydride (26.7 mg, 0.1 mmol), 4-DMAP (1.47 mg, 0.01 mmol) and triethylamine (17 µL, 0.1 mmol) during 12 hours at ambient temperature. The mixture was kept stirring for an additional 12 hours at the same temperature and poured into an ice-cold saturated $NaHCO_3$ solution. It was extracted with EtOAc, dried over anhydrous Na_2SO_4 and concentrated in a vacuum. After concentration in a vacuum, the residue was chromatographed over silica gel flash chromatography MeOH in $CHCl_3$ 4%, affording the desired pure product 19.3 mg (60% yield as a colourless amorphous solid).

R_f = 0.75 (Chloroform / Methanol = 4:1)

HPLC (205 nm, VWD): t_R = 2.925 min

^{1}H NMR (500 MHz, $CDCl_3$) δ = 5.36 (t, *J* = 8.2 Hz, 1H), 4.12 (t, *J* = 8.0 Hz, 1H), 4.08 (q, *J* = 6.1, 5.7 Hz, 1H), 3.66 (m, 1H), 3.01 – 2.5 (m, 4H), 2.30 (m, 1H), 1.99 (m, 1H), 1.76 – 0.99 (m, 14H), 0.90, (s, 9H), 0.87 (t, *J* = 7.6 Hz, 3H), 0.074 (s, 6H) .

^{13}C NMR (126 MHz, $CDCl_3$) δ = 170.47, 168.83, 164.68, 75.96, 75.56, 52.18, 43.79, 31.93, 30.94, 29.71, 29.67, 29.37, 29.25, 29.08, 24.75, 22.70, 14.13, 13.58, -0.22.

APCI-MS: *m/z* calculated for $C_{24}H_{44}N_2O_5S_2Si+H^+$; 533.29 ($[M+H]^+$); found: 533.25

Melting point: 286 – 290 °C

5.2.2.19 Synthesis of (1*R*,5*R*,11*R*,14*R*)-5-hydroxy-11-propyl-12-oxa-16,17-dithia-2,20-diazabicyclo[12.4.2]icosane-3,13,19-trione (BSc5484)

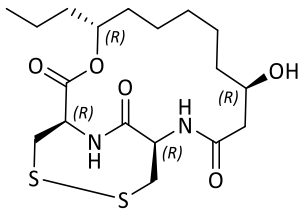

Buffered tetrabutylammonium fluoride solution (10 µL from a 3.3 M solution, 0.01 mmol fluoride, 0.5 equiv) was added to a 4 mL THF solution of (1*R*,5*R*,11*R*,14*R*)-5-((tert-butyldimethylsilyl)oxy)-11-propyl-12-oxa-16,17-dithia-2,20-diazabicyclo[12.4.2]icosane-3,13,19-trione (31 mg, 0.1 mmol), the cap was affixed to a polypropylene tube, and the reaction mixture kept stirring at 23 °C. The reaction was complete after 24 hours, at which point the crude material was purified directly using silica gel flash chromatography MeOH in $CHCl_3$ 6% to give the product a colourless amorphous solid 20.7 mg, 85% yield.

Making a 3.3 M buffered TBAF solution: The trihydrate of tetrabutylammonium fluoride (0.3 g, 0.9 mmol) was dissolved in dry tetrahydrofuran. For 10 minutes, the resultant solution was sonicated. Aqueous dibasic potassium phosphate (K_2HPO_4) (0.1 M, pH 7.1) was introduced to the TBAF solution and sonicated for another 3 minutes. There were no steps taken to keep air out. The colourless crude residue and anhydrous tetrahydrofuran (0.25 mL) were added to a 1.7 mL polypropylene microcentrifuge tube charged with a magnetic stirrer.

R_f = 0.68 (Chloroform / Methanol = 4:1)

HPLC (205 nm, VWD): t_R = 3.120 min

^{1}H NMR (500 MHz, DMSO) δ = 8.33 (Brs, 1H), 7.26 (Brs, 1H), 5.34 (t, *J* = 8.2 Hz, 1H), 4.88 (t, *J* = 8.0 Hz, 1H), 4.62 (q, *J* = 6.1, 5.7 Hz, 1H), 4.24 (dd, *J* = 11.4, 6.0 Hz 1H), 4.11 – 3.94 (dd, *J* = 11.0 , 6.5 Hz, 1H), 3.70 (dd, *J* = 11.6 , 6.8 Hz, 1H), 3.52 (m, 2H), 3.47 (dd, *J* = 11.1 , 6.3 Hz, 1H), 3.08 – 2.94 (dd, *J* = 11.5, 6.4 Hz, 1H), 2.20 (dd, *J* = 7.6 , 7.1 Hz, 1H), 1.99 (dd, *J* = 7.5 , 7.0 Hz, 1H), 1.71 – 0.99 (m, 14H), 0.85 (t, *J* = 7.6 Hz, 3H).

^{13}C NMR (126 MHz, DMSO) δ = 176.88, 174.95, 167.04, 72.80, 70.25, 53.45, 52.27, 40.41, 40.24, 34.12, 31.76, 31.16, 29.48, 29.17, 24.96, 22.56, 14.42, 13.99

APCI-MS: *m/z* calculated for $C_{18}H_{30}N_2O_5S_2+H^+$; 419.23 ($[M+H]^+$); found: 419.17

Melting point: 260 – 273 °C

5.2.3 Synthesis of the diverse set of analogues

5.2.3.1 Synthesis of isobutyl *S*-trityl-*L*-cysteinate (102)

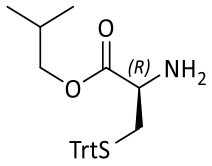

S-Trityl-*L*-cysteine (0.2 g, 550.2 μmols) was dissolved in 25 mL of anhydrous isobutyl alcohol and was cooled to 0 °C. After 20 minutes, thionyl chloride (160 μL, 2.2 μmol) was slowly added, and the resulting solution was kept stirred at 0 °C for 10 min. The solution was, in due course, warmed to room temperature for 2 h and was then heated to reflux for 18 hours at 9 mmHg. The reaction was later cooled to room temperature and evaporated in a vacuum. The residue was dried at 30 °C in a high vacuum. The product was further purified with flash chromatography silica gel Dichloromethane / Methanol = 5:1, giving a colourless, finely crystalline solid of 104 mg (50% yield).

R_f = 0.61 (Dichloromethane / Methanol = 5:1)

HPLC (254 nm, VWD): t_R = 6.321 min

^{1}H NMR (500 MHz, $CDCl_3$) δ = 7.34 (m, J = 6.3 Hz, 6H), 7.16 (m, 9H), 3.75 (d, J = 7.6 Hz, 2H), 3.11 (m, 1H), 2.53 – 2.45 (m, 1H), 2.42 (m, 1H), 1.96 – 1.76 (m, 1H), 0.80 (d, J = 6.4 Hz, 6H).

^{13}C NMR (126 MHz, $CDCl_3$) δ = 173.74, 144.56, 129.58, 127.96, 126.77, 71.20, 66.87, 53.88, 37.06, 27.63, 19.03.

ESI-MS: *m/z* calculated for $C_{26}H_{29}NO_2S+H^+$; 420.24 ($[M+H]^+$); found: 420.20

Melting point: 54 – 59 °C

5.2.3.2 Synthesis of isobutyl *N*-(*N*-(tert-butoxycarbonyl)-*S*-trityl-*L*-cysteinyl)-*S*-trityl-*D*-cysteinate (103)

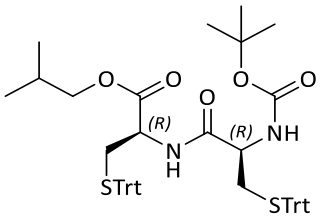

To DCM (5 mL) in a 25 mL round bottom flask was added Boc-Cys-tri-OH (91.9 mg, 198.3 μmols) followed by EDC (0.04 g, 0.2 mmol), and 20 min later, HOBt (0.02 g, 0.2 mmol) was added, stirred at room temperature for 20 min. In a separate 25 mL flask *H*-Cys-tri-O-*isobutyl*·HCl (0.1 g, 0.2 mmol) was solubilised in DCM 5 mL, and DIPEA was added (66.4 mmL, 0.4 mmol). The solution of activated ester was cooled to 0 °C, and the solution of Boc-Cys-tri-OH was added dropwise via syringe. The solution became clear and was kept stirred at 0 °C for 0.5 hour, heated to room temperature, and subsequently kept stirring for 2 hrs. The solution was then poured into cold water (10 mL). The aqueous layer was isolated with DCM (3 x 10 mL). The organics were, therefore, cleaned with saturated solutions of $NaHCO_3$, water, and brine and dried using Na_2SO_4, filtered and concentrated under a vacuum. Flash column chromatographic purification with silica gel 15% Ethyl acetate in cyclohexane of the resultant residue gave the product a colourless amorphous solid 103 mg (78% yield).

R_f = 0.73 (cyclohexane / AcOEt = 3:1)

HPLC (254 nm, VWD): t_R = 10.632 min

^{1}H NMR (500 MHz, $CDCl_3$) δ = 7.34 - 7.21 (m, 30H), 4.68 (m, 1H), 4.37 (m, 1H), 3.70 (d, J = 5.8 Hz, 2H), 2.71– 1.66 (m, 4H), 1.32 (s, 9H), 0.78 (d, J = 5.8 Hz, 6H).
^{13}C NMR (126 MHz, $CDCl_3$) δ = 170.04, 169.88, 146.87, 144.42, 129.48, 127.93, 126.87, 82.03, 71.72, 67.22, 66.65, 53.38, 51.30, 33.86, 29.72, 28.28, 27.58, 19.03.
ESI-MS: *m/z* calculated for $C_{53}H_{56}N_2O_5S_2+H^+$; 887.39 ($[M+Na]^+$); found: 887.35

Melting point: 184 – 189 °C

5.2.3.3 Synthesis of isobutyl (4*R*,7*R*)-7-((tert-butoxycarbonyl)amino)-6-oxo-1,2,5-dithiazocane-4-carboxylate (BSc5482)

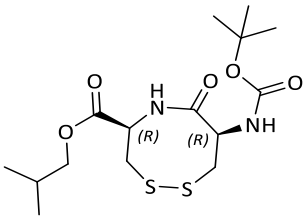

A solution of isobutyl *N*-(*N*-(tert-butoxycarbonyl)-*S*-trityl-*L*-cysteinyl)-*S*-trityl-*D*-cysteinate (121 mg) in CH_2Cl_2/MeOH (9:1; 37.3 mL) was added dropwise to a vigorously stirred solution of I_2 (355 mg, 502 mmol) in CH_2Cl_2/MeOH (9:1; 297 mL, 0.5 mM concentration) over 10 min at room temperature. After a quarter hour, the reaction was quenched with 10% aq $Na_2S_2O_3$ (70 mL) at the same temperature. Later on, the resulting mixture was weakened with 50 mL of CH_2Cl_2. Afterwards, the organic layer was cleaned with saturated aqueous solution of $NaHCO_3$ ca. 2 × 20 mL and brine ca. 2 × 20 mL and then dried over $MgSO_4$. The solvent concentration in a vacuum afforded a residue, which was cleaned by column chromatography (silica gel, $CHCl_3$) to give the product (41.8 mg 79% yield) as a yellowish crystal.

R_f = 0.66 (Chloroform / Methanol = 5:0.5)

HPLC (254 nm, VWD): t_R = 3.294 min

^{1}H NMR (500 MHz, $CDCl_3$) δ = 6.32 (Brs, 1H, NH), 5.80 (Brs, 1H, NH), 4.87 (t, *J* = 9.2 Hz, 1H), 4.56 (t, *J* = 9.0 Hz, 1H), 3.92 (d, *J* = 6.6 Hz, 2H), 3.41 – 3.26 (dd, *J* = 27.1, 14.4 Hz, 1H), 3.02 (dd, *J* = 27.2, 14.5 Hz, 1H), 2.94 – 2.76 (dd, *J* = 27.6, 14.3 Hz, 1H), 2.54 (dd, *J* = 27.2, 14.1 Hz, 1H), 2.01 – 1.82 (m, 2H), 1.36 (s, 9H), 0.89 (d, *J* = 6.7 Hz, 6H).
^{13}C NMR (126 MHz, $CDCl_3$) δ = 172.34, 169.98, 154.67, 80.26, 72.46, 53.53, 52.19, 42.78, 29.70, 28.33, 27.62, 18.99.
ESI-MS: *m/z* calculated for $C_{15}H_{26}N_2O_5S_2$+Na^+; 401.14 ($[M+Na]^+$); found: 401.12.

Melting point: 166 – 170 °C

5.2.3.4 Synthesis of (4*R*,7*R*)-7-((tert-butoxycarbonyl)amino)-6-oxo-1,2,5-dithiazocane-4-carboxylic acid (BSc5489)

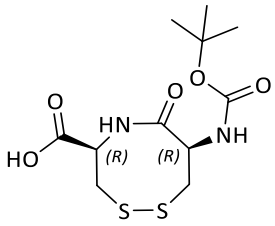

Methyl (4*R*,7*R*)-7-((tert-butoxycarbonyl)amino)-6-oxo-1,2,5-dithiazocane-4-carboxylate (60 mg) was dissolved in 1,2-dichloroethane 6 mL, and after addition of trimethyltin hydroxide (161.3 mg, 0.9 mmol), the mixture was consequently refluxed at 60 °C until TLC analysis indicated a complete reaction. After the reaction was totally completed, the mixture was concentrated with a rotary evaporator in a vacuum, and the obtained residue was later dissolved in ethyl acetate (10 mL). The organic layer was washed with aqueous $KHSO_4$ (0.01N) or HCl (5%) (3 times 5–15 mL). The organic layer was then rinsed with brine (15 mL) and dried over Na_2SO_4. Removal of the solvent in a vacuum afforded the carboxylic acid as a colourless amorphous solid: 56.4 mg in 98% yield.

HPLC (254 nm, VWD): t_R = 3.374 min

^{1}H NMR (500 MHz, DMSO) δ = 7.74 (d, J = 10.1 Hz, 1H, NH), 7.36 – 7.26 (Brs, 1H, NH), 4.78 (t, J = 9.1 Hz, 1H), 4.61 (s, t, J = 9.4 Hz, 1H) 3.09 (dd, J = 14.4, 6.6 Hz, 1H), 2.95 (dd, J = 7.1, 12.6 Hz, 1H), 2.84 (dd, J = 7.2, 12.2 Hz, 1H), 2.77 (dd, J = 7.0, 12.3 Hz, 1H), 1.39 (s, 9H).

^{13}C NMR (75 MHz, DMSO) δ = 172.50, 171.68, 155.16, 79.04, 70.27, 55.37, 51.76, 41.80, 28.60.

ESI-MS: *m/z* calculated for $C_{11}H_{18}N_2O_5S_2+H^+$; 345.09 ($[M+Na]^+$); found: 345.05.

Melting point: 150 – 154 °C

5.2.3.5 Synthesis of (4*R*,7*R*)-4-(methoxycarbonyl)-6-oxo-1,2,5-dithiazocan-7-aminium 2,2,2-trifluoroacetate (54)

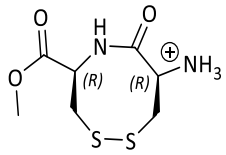

Manual removal of the N-terminal Boc-group was accomplished by placing the amino acid (37 mg, 0.1 mmol) in a round bottom flask and washing it with 3 mL DCM/TFA/1:1: at 0 °C and then leaving it stirring at the same temperature for 90 minutes with constant mixing until the reaction shows complete consumption of the starting material. The reaction medium was diluted with toluene and concentrated in a vacuum to give the crude TFA salt as an off-white solid (26 mg) in quantitative yield.

ESI-MS: m/z 237.04 ($[M+H]^+$).

Melting point: 159 – 165 °C

5.2.3.6 Synthesis of methyl ((4*R*,7*R*)-7-((tert-butoxycarbonyl)amino)-6-oxo-1,2,5-dithiazocane-4-carbonyl)-*L*-tryptophanate (BSc5485)

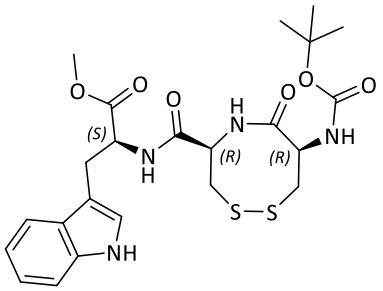

To a 3 mL DMF in a 25 mL round bottom flask was added (4R,7R)-7-((tert-butoxycarbonyl)amino)-6-oxo-1,2,5-dithiazocane-4-carboxylic acid (67.4 mg, 0.2 mmol), followed by EDC (52.1 mg, 0.3 mmol), and 30 min later, HOBt (36.7 mg, 0.3 mmol) was added, stirred at room temperature for 20 min. In a separate flask, the methyl L-tryptophanate (63.9 mg, 0.3 mmol) was solubilised in 5 mL of DMF and Et_3N (0.5 mmol) was added. The solution of methyl L-tryptophanate was added to the solution of activated ester dropwise via syringe at 0°C and permitted to stir for 18 hours at room temperature. The mixture was later poured into ice-cold water. It was extracted with EtOAc 12 mL, and the combined organic layer was cleaned with water (6 mL) and a solution of brine (6 mL) and dried over anhydrous Na_2SO_4. The residue was chromatographed over silica gel after being concentrated in a vacuum. The peptide was obtained as a colourless amorphous solid (66.6 mg, 61% yield) after elution with DCM/MeOH (7%).

R_f = 0.53 (Dichloromethane / Methanol = 5:0.5)

HPLC (254 nm, VWD): t_R = 5.238 min

^{1}H NMR (500 MHz, DMSO) δ = 10.88 (d, J = 10.5 Hz, 1H, NH), 8.88 (d, J = 7.3 Hz, 1H, NH), 8.40 (Brs, 1H, NH), 7.53 (Brs, 1H, NH), 7.50 (dd, J = 12.7, 7.8 Hz, 1H), 7.35 (dd, J = 8.0, 2.7 Hz, 1H), 7.17 (dd, J = 11.6, 2.5 Hz, 1H), 7.08 (dd, J = 8.1, 2.6 Hz, 1H), 7.00 (d, J = 6.9 Hz, 1H), 4.83 (dd, J = 17.1, 8.3 Hz, 1H), 4.80 (dd, J = 17.1, 8.3 Hz, 1H), 4.56 (m, 1H), 3.57 (s, 3H), 3.47 – 3.41 (m, 1H), 3.29 – 3.20 (m, 1H), 3.20 – 3.10 (m, 2H), 3.09 – 3.03 (m, 1H), 2.85 – 2.67 (m, 1H), 1.40 (s, 9H).

^{13}C NMR (126 MHz, DMSO) δ = 171.76, 171.71, 169.19, 162.77, 136.09, 127.00, 123.64, 120.96, 118.44, 118.02, 111.41, 108.98, 78.62, 66.05, 53.64, 53.17, 51.85, 28.97, 28.14, 27.00. ESI-MS: *m/z* calculated for $C_{23}H_{30}N_4O_6S_2+H^+$; 523.20 ($[M+H]^+$); found 523.17

Melting point: 272 – 274 °C

5.2.3.7 Synthesis of methyl (4*R*,7*R*)-7-((*E*)-3-(4-methoxyphenyl)acrylamido)-6-oxo-1,2,5-dithiazocane-4-carboxylate (BSc5486)

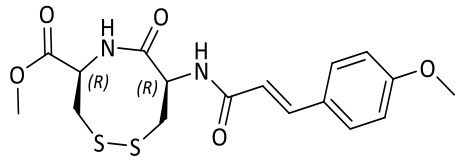

To DMF (3 mL) in a 25 mL round bottom flask was added (*E*)-3-(4-methoxyphenyl)acrylic acid (21.6 mg, 0.1 mmol), followed by EDC (25.3 mg, 0.1 mmol), and 30 min later, HOBt (17.8 mg, 0.1 mmol) was added, stirred at room temperature for 20 min. In a separate flask, the crude TFA salt (26 mg, 0.1 mmol) was solubilised in DMF (5 mL), and Et_3N was added (38.3 µL, 0.3 mmol). The solution of activated ester was added to the solution of crude TFA salt dropwise via syringe and stirred for 18 hours at room temperature. The solution was then poured onto ice-cold water. It was extracted with 15 mL EtOAc, and the combined organic layer was washed with 8 mL water and 8 mL brine and dried over anhydrous Na_2SO_4. The residue was chromatographed over silica gel after being concentrated in a vacuum. Elusion in DCM with 7% vol MeOH yields the product (30.5 mg, 70%) as colourless crystals.

R_f = 0.724 (Dichloromethane / Methanol = 5:1).

HPLC (205 nm, VWD): t_R = 2.341 min.

^{1}H NMR (500 MHz, DMSO) δ = 8.16 – 8.10 (Brs, 1H, NH), 7.49 (d, *J* = 6.6 Hz, 2H), 7.35 d, *J* = 15.6 Hz, 1H), 6.96 (d, *J* = 7.5 Hz, 2H), 6.76 (d, *J* = 15.8 Hz, 1H), 6.65 – 6.56 (Brs, 1H, NH), 5.04 – 4.94 (m, 1H), 4.91 – 4.84 (m, 1H), 3.77 (s, 3H), 3.68 (s, 3H), 3.50 (m, 1H), 3.15 – 2.93 (m, 1H), 2.79 (m, 1H), 2.70 (m, 1H).

^{13}C NMR (126 MHz, DMSO) δ = 170.33, 164.92, 160.40, 138.94, 129.89, 129.14, 127.38, 119.29, 114.36, 55.24, 52.64, 51.88, 50.08, 40.95, 28.97.

APCI-MS: *m/z* calculated for $C_{17}H_{20}N_2O_5S_2+H^+$; 397.12 ($[M+H]^+$); found: 397.09.

Melting point: 266 – 269 °C

5.2.3.8 Synthesis of methyl (4*R*,7*R*)-7-(2-(5-bromopyridin-3-yl)acetamido)-6-oxo-1,2,5-dithiazocane-4-carboxylate (BSc5487)

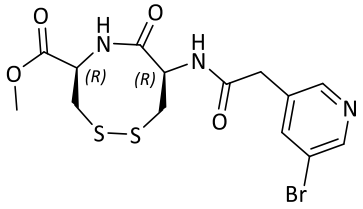

To DMF (3 mL) in a 25 mL round bottom flask was added the 2-(5-bromopyridin-3-yl)acetic acid (23.8 mg, 0.1 mmol), followed by EDC (25.3 mg, 0.1 mmol), and 30 min later, HOBt (17.8 mg, 0.1 mmol) was added, stirred at room temperature for 20 min. In a separate flask, the crude TFA salt (26 mg, 0.1 mmol) was solubilised in DMF (3 mL), and Et_3N was added (38.3 µL, 0.3 mmol). To the solution of activated ester, the solution of crude amide dropwise via syringe was added and stirred for 18 hours at room temperature. The solution was then poured onto ice-cold water. It was extracted with 15 mL EtOAc, and the combined organic layer was washed with 8 mL water and 8 mL of brine and dried over anhydrous Na_2SO_4. The residue was chromatographed over silica gel after being concentrated in a vacuum. Elusion in DCM with 8 % vol MeOH yields the product (29.6 mg, 62%) as colourless crystals.

R_f = 0.333 (Dichloromethane / Methanol = 5:1).

HPLC (205 nm, VWD): t_R = 1.977 min.

^{1}H NMR (500 MHz, DMSO) δ = 8.85 (Brs, 1H, NH), 8.57 (d, *J* = 7.1 Hz, 1H), 8.44 (s, 1H), 7.95 (d, *J* = 6.8 Hz, 1H), 4.93 (t, *J* = 13.9, 8.2 Hz, 1H), 4.78 (t, *J* = 6.4 Hz, 1H), 3.96 (dt, *J* =

11.5, 6.0 Hz, 1H), 3.90 (dt, *J* = 11.7, 6.1 Hz, 1H), 3.69 (s, 3H), 3.64 (s, 2H), 3.62 – 3.58 (m, 1H), 2.99 – 2.65 (m, 1H).

^{13}C NMR (126 MHz, DMSO) δ = 172.28, 170.80, 169.42, 149.14, 148.76, 139.68, 134.60, 120.22, 53.10, 52.40, 50.62, 41.43, 38.47, 29.46.

APCI-MS: *m/z* calculated for $C_{14}H_{15}N_3O_4S_2Br+H^+$; 433.99 ($[M+H]^+$); found: 433.98

Melting point: 272 – 276 °C

5.2.3.9 Synthesis of methyl (4*R*,7*R*)-7-(1*H*-benzo[d]imidazole-6-carboxamido)-6-oxo-1,2,5-dithiazocane-4-carboxylate (BSc5488)

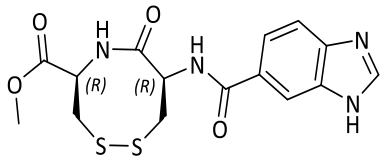

To DMF (4 mL) in a 25 mL round bottom flask was added 1*H*-benzo[d]imidazole-6-carboxylic acid (19.6 mg, 0.1 mmol), followed by EDC (25.3 mg, 0.1 mmol), and 30 min later, HOBt (17.8 mg, 0.1 mmol) was added, stirred at room temperature for 20 min. In a separate flask, the crude TFA salt previously prepared (26 mg, 0.1 mmol) was dissolved in DMF (4 mL), and Et_3N was added (38.3 μL, 0.3 mmol). To the solution of activated ester, the solution of crude amide dropwise via syringe was added and stirred for 18 hours at room temperature. The solution was then poured onto ice-cold water. It was extracted with 15 mL EtOAc, and the combined organic layer was washed with 8 mL water and 8 mL of brine and dried over anhydrous Na_2SO_4. The residue was chromatographed over silica gel after being concentrated in a vacuum. Elution with DCM containing 7% vol MeOH yields a yellow amorphous solid (28.5 mg, 68% yield).

R_f = 0.344 (Dichloromethane / Methanol = 5:1).

HPLC (205 nm, VWD): t_R = 1.404 min.

^{1}H NMR (500 MHz, DMSO) δ = 12.75 (Brs, 1H, NH) 8.37 (s, 1H), 8.18 (Brs, 1H, NH), 7.88 – 7.68 (d, *J* = 7.6 Hz, 1H), 7.69 – 7.48 (d, *J* = 7.75 Hz, 1H), 5.21 (t, *J* = 9.6 Hz, 1H) – 4.92 (t, *J*

= 9.2 Hz, 1H), 3.70 (dd, *J* = 13.0, 4.5 Hz, 1H), 3.61 (dd, *J* = 13.0, 4.5 Hz, 1H), 3.48 (s, 3H), 3.23 – 2.64 (m, 2H).

^{13}C NMR (126 MHz, DMSO) δ = 172.25, 170.45, 166.41, 143.67, 142.47, 135.45, 132.83, 122.22, 118.52, 111.20, 53.71, 51.90, 47.43, 40.97, 28.95.

ESI-MS: *m/z* calculated for $C_{15}H_{16}N_4O_4S_2+H^+$; 381.09 ($[M+H]^+$); found: 381.07.

Melting point: 268 – 273 °C

5.2.4 Synthesis of Eudistomidin C (BSc5517)

5.2.4.1 Synthesis of 5-methoxy-1*H*-indole (94)

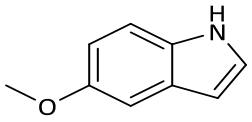

To a solution of 5-bromoindole **93** (2.73 g, 14 mmol, 1.0 eq) in dry methanol (40 mL) Sodium metal (3.2 g, 139.3 mmol, 10.0 eq) was added and dissolved. Then copper-(I) iodide (5.29 g, 28 mmol, 2.0 eq) and dry DMF (40 mL) were added. The reaction mixture was subsequently refluxed for ca. 3 h. After the addition of EtOAc (300 mL), the mixture was filtered in due course through a celite pad and washed with brine (3x 125 mL). The combined organic layers were assembled and concentrated in a vacuum. After purification by column chromatography (1:1 EtOAc/Cyclohexane), 5-Methoxyindole **94** (1.6 g, 80%) was obtained as a colourless amorphous solid.

R_f = 0.43. (Cy/AcOEt = 3:1)

HPLC (254 nm, VWD): t_R = 3.446 min.

^{1}H-NMR ($CDCl_3$, 300 MHz): δ = 8.08 (s, 1 H), 7.30 (d, 1 H, ^3J = 8.8 Hz) 7.20 (d, 2 H, ^3J = 4.6 Hz), 6.95 (dd, 1 H, ^3J = 8.8, 2.0 Hz), 6.55 (s, 1 H), 3.92 (s, 3 H, H-6) *ppm*.

^{13}C-NMR ($CDCl_3$, 75 MHz, 300 K): δ = 154.2, 131.0, 128.3, 125.0, 112.4, 111.8, 102.4, 102.3, 55.9 *ppm*.

ESI-MS: *m/z* calculated for $C_9H_9NO+H^+$; 148.04 ($[M+H]^+$); found: 148.08.

Melting point: 56-58 °C

The spectral data obtained agree with the data published in the literature. [202]

5.2.4.2 Synthesis of 5-methoxy-1*H*-indole-3-carbaldehyde (95)

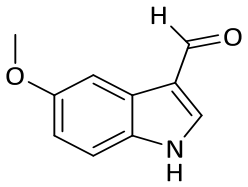

Dry DMF (10 mL) was added to an oven-dried flask under an argon atmosphere and cooled to 0 °C. Then $POCl_3$ (1.5 mL, 16.3 mmol, 2.4 eq) was added dropwise over 10 min. The solution was stirred at this temperature for 15 min, and 5-methoxyindole **94** (1 g, 6.8 mmol, 1.0 eq) dissolved in dry DMF (10 mL) was added dropwise. The reaction mixture was consequently allowed to warm to RT and stirred for 2 h. After completion, aqueous 1N NaOH (15 mL) was added in a slow way, and the mixture was extracted with EtOAc (3x 40 mL). The combined organic layers were, in due course, washed with ca. 3x 50 mL of water and brine (2x 50 mL) and dried over $MgSO_4$. The solvent was removed in vacuo, and 3-Formyl-5-methoxyindole **95** (1.2 g, 97%) was obtained without further purification as a pale yellow solid.

R_f = 0.65 (Cy/AcOEt = 1:5)

HPLC (254 nm, VWD): t_R = 2.057 min.

^{1}H-NMR ($CDCl_3$, 300 MHz): δ = 12.03 (s, 1 H), 9.92 (s, 1 H), 8.20 (s, 1 H), 7.62 (s, 1H), 7.42 (d, 1 H, ^3J = 8.8 Hz), 6.90 (dd, 1 H, H-3, ^3J = 8.8, 2.5 Hz), 3.80 (s, 3 H) *ppm*.

^{13}C-NMR ($CDCl_3$, 75 MHz): δ = 185.2, 156.1, 138.8, 132.3, 125.4, 118.5, 113.8, 113.7, 103.0, 55.7 *ppm.*

ESI-MS: *m/z* calculated for $C_{10}H_9NO_2$+H^+: 176.04 ([M+H^+]); found: 176.07

Melting point: 178 °C

The spectral data obtained agree with the data published in the literature. [203]

5.2.4.3 Synthesis of (*Z*)-5-methoxy-3-(2-nitrovinyl)-1*H*-indole (96)

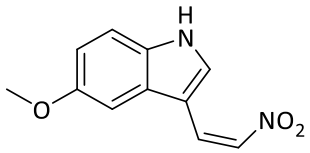

To a solution of 3-Formyl-5-methoxyindole **95** (1.2 g, 6.6 mmol, 1.0 eq) in nitromethane (20 mL), ammonium acetate (1.5 g, 20 mmol, 3 eq) was added. Then, the reaction mixture was consistently refluxed for 2 h and concentrated in a vacuum. The obtained solid was dissolved in EtOAc (75 mL) and washed with ca. 2x 50 mL of water and then with brine (50 mL), dried over $MgSO_4$ and concentrated *in vacuo*. After purification by column chromatography (1:1 EtOAc/Cyclohexane) 5-Methoxy-3-(2-nitrovinyl)-indole **96** (1.3 g, 90%) was obtained as a yellow chrystalline solid.

R_f = 0.78 (Cy/AcOEt = 3:1)

HPLC (254 nm, VWD): t_R= 4.563 min.

^{1}H-NMR (DMSO-d_6, 300 MHz): δ = 12.14 (*s*, 1 H), 8.41 (*d*, 1 H, ^3J = 13.4 Hz), 8.19 (*s*, 1 H, H-10), 8.04 (*d*, 1 H, H-12, *3J* = 13.4 Hz), 7.42 (*d*, 1 H, H-3, 3J = 8.8 Hz), 7.39 (*d*, 1 H, H-7, *4J* = 2.4 Hz), 6.90 (*dd*, 1 H, H-4, *3J* = 8.8, 2.4 Hz), 3.86 (*s*, 3 H, H-6) *ppm*.

^{13}C-NMR (DMSO-d_6, 300 MHz, 300 K): δ = 156.0, 136.6, 135.3, 132.8, 131.2, 126.0, 114.0, 113.6, 108.7, 103.1, 56.2 *ppm*.

ESI-MS: *m/z* calculated for $C_{11}H_{10}N_2O_3$+H^+: 219.1 ([M+H]$^+$); found: 219.08.

Melting point: 159-160 °C

The spectral data obtained are in agreement with the data published in the literature. [204]

5.2.4.4 Synthesis of 2-(5-methoxy-1*H*-indol-3-yl)ethan-1-amine (97)

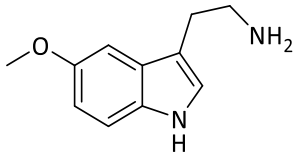

In an oven-dried flask, dry THF (75 mL) and LiAlH4 (730 mg, 19.3 mmol, 6.0 eq) were added and cooled to 0 °C. 5-Methoxy-3-(2-nitrovinyl)-indole **96** (700 mg, 3.2 mmol, 1.0 eq) was dissolved in molecular sieves, dried THF 100 mL and added over 20 min. The reaction mixture was heated to reach ambient temperature and stirred for 40 hours. Following, the mixture was cooled to 0 °C, and water (20 mL) was added slowly until the cessation of bubbles. It was diluted with Et_2O (100 ml), saturated sodium potassium tartrate solution (125 mL), and stirred for 24 h. The layers were divided, and the aqueous layer was isolated with Et_2O (100 ml). The combined organic layers were cleaned with a calculated volume of 2N HCl (3x 50 mL), and the aqueous layer was cooled to a temperature of 0 °C and later basified with 3M KOH to pH = 10. After extraction with Et_2O (3x 100 mL), drying over MgSO4, and concentration *in vacuo* 5-methoxytryptamine **97** (232 mg, 38%) was obtained without further purification as a brown oil.

R_f = 0.62. (*n*-Bu/CH_3COOH/H_2O = 4:1:1):

HPLC (254 nm, VWD): t_R = 1.162 min.

^{1}H-NMR (DMSO-d_6, 300 MHz, 300 K): δ = 10.68 (s, 1 H), 7.24 (d, 1H, ^3J = 8.7 Hz), 7.10 (s, 1H), 7.01(d, 1H, ^4J = 2.5 Hz), 6.72 (dd, 1H, ^3J = 8.7 Hz, ^3J = 2.5 Hz), 3.77 (s, 3H), 2.83 (t, 2H, ^3J = 7.0 Hz), 2.74 (t, 2H, ^3J = 7.0 Hz), 2.11 (*s*, 2H) *ppm*.

^{13}C-NMR (DMSO-d_6, 300 MHz, 300 K): δ = 153.4, 131.9, 128.1, 123.8, 122.7, 112.4, 111.4, 107.6, 55.8, 43.0, 29.9 *ppm*.

ESI-MS: *m/z* calculated for $C_{11}H_{14}N_2O+H^+$: 191.15 ($[M+H]^+$); found: 191.12.

Melting point: 121.5 °C

The spectral data obtained are in agreement with the data published in the literature. [204]

5.2.4.5 Synthesis of *S*-methyl-*D*-cysteine (89)

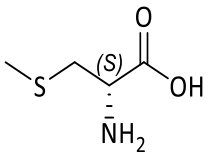

To a cooled suspension of *D*-Cysteine **74** (2 g, 16.5 mmol, 1.0 eq) in absolute ethanol (50 mL), sodium metal (1.5 g, 66 mmol, 4.0 eq) was added. The mixture was stirred until the sodium was dissolved, and then methyl iodide (258 mL, 18.2 mmol, 1.1 eq) was added. The reaction mixture was heated to an ambient temperature and was stirred for 1 h. Then water was added until the precipitate was dissolved, and the solution was acidified to pH = 5 with concentrated HCl and Et_2O (50 mL) added. The mixture was left in the refrigerator overnight. After filtration and washing with Et_2O (3x 30 mL), *S*-Methyl-*D*-cysteine **89** (1.9 g, 89%) was obtained as a white solid.

R_f = 0.23 (*n*-Bu/CH_3COOH/H_2O = 4:1:1)

HPLC (254 nm, VWD): t_R= 0.797 min

^{1}H NMR (300 MHz, DMSO) δ = 3.66 (dd, *J* = 7.8, 4.2 Hz, 1H), 2.92 (dd, *J* = 14.5, 4.2 Hz, 1H), 2.81 (dd, *J* = 14.7, 7.8 Hz, 1H), 2.00 (s, 3H) *ppm*.

^{13}C NMR (75 MHz, DMSO) δ 171.58, 52.86, 34.43, 15.09 *ppm*.
ESI-MS: *m/z* calculated for $C_4H_9NO_2S+Na^+$; 158.07 ($[M+Na]^+$); found: 158.02.

Melting point: 248 °C (decomposition)

The spectral data obtained are in agreement with the data published in the literature. [205]

5.2.4.6 Synthesis of *N*-((benzyloxy)carbonyl)-*S*-methyl-*D*-cysteine (90)

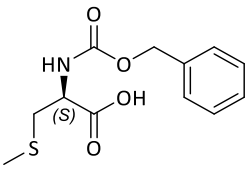

To a solution of *S*-methyl-*D*-cysteine **89** (2.2 g, 16.3 mmol, 1.0 eq) in 2N aqueous NaOH (10 mL) was added benzyl chloroformate (3.80 g, 21.2 mmol, 1.3 eq) at 0 °C. After stirring for 60 minutes at 0 °C, the reaction medium was consequently warmed to room temperature and stirred overnight. The mixture was washed with Et_2O (3x 30 mL). Then, the aqueous solution was acidified to a calculated pH = 2 with 2N HCl and extracted with Et_2O (3x 30 mL). The combined organic layers were directly dried over $MgSO_4$ and concentrated *in vacuo* to yield *N*-((Benzyloxy)carbonyl)-*S*-methyl-*D*-cysteine **90** as a colourless oil (3.7 g, 84%). The compound was used without further purification in the next step.

R_f = 0.49 (Cy/EA = 3:1)

HPLC (254 nm, VWD): t_R = 3.305 min.

^{1}H-NMR ($CDCl_3$, 300 MHz, 300 K): δ = 9.74 (*s*, 1 H), 7.38 (*m*, 5 H), 5.74 (*d*, 1 H), 5.16 (*s*, 2 H), 4.67 (*m*, 1 H), 3.03 (*m*, 2 H,), 2.12 (*s*, 3 H) *ppm*.

^{13}C-NMR ($CDCl_3$, 300 MHz, 300 K): δ = 177.5, 156.0, 136.0, 128.6, 128.3, 128.1, 67.3, 53.3, 36.4, 16.2 *ppm.*

ESI-MS: *m/z* calculated for $C_{12}H_{15}NO_4S+Na^+$; 292.08 ($[M+Na]^+$); found: 292.08.

The spectral data obtained are in agreement with the data published in the literature. [206]

5.2.4.7 Synthesis of benzyl (*S*)-(1-(methoxy(methyl)amino)-3-(methylthio)-1-oxopropan-2-yl)carbamate (91)

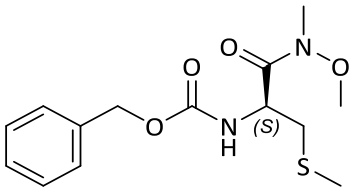

N,*O*-dimethylhydroxylamine hydrochloride (0.50 g, 5.1 mmol, 1.1 eq) and triethylamine (0.7 mL, 5.1 mmol, 1.1 eq) were added to a solution of N-((Benzyloxy)carbonyl)-*S*-methyl-*D*-cysteine **90** (1.3 g, 4.6 mmol, 1.0 eq) in DCM (60 mL) at 0 °C. *N*-(3-Dimethylaminopropyl)-*N*'-ethylcarbodiimide hydrochloride (1 g, 5.1 mmol, 1.1 eq) was added slowly over 30 min. Then the reaction mixture was kept stirring at RT for 60 minutes. After completion of the reaction, the mixture was later poured into ice/2N HCl (80 mL) and the layers were separated. Afterwards, the aqueous layer was extracted with DCM ca. 3x 50 mL, and the combined organic layers were as usual, dried over $MgSO_4$ and concentrated *in vacuo*. After purification by column chromatography (1:9 Et_2O/DCM), (*S*)-Benzyl-(1-methoxy(methyl)amino)-3-(methylthio)- 1-oxopropan-2-yl)carbamate **91** (1.3 g, 86 %) was obtained as a colourless oil.

R_f = 0.57 (DCM/Et_2O = 9:1)

HPLC (254 nm, VWD): t_R = 4.326 min.

^{1}H-NMR ($CDCl_3$, 300 MHz, 300 K): δ = 7.37 (d, 4 H), 7.33 (*m*, 1 H), 5.71 (d, 1 H), 5.12 (*m*, 2 H), 4.97 (q, 1 H, ^3J= 7.3 Hz), 3.80 (*s*, 3 H), 3.23 (s, 3 H), 2.93-2.75 (dd, 2 H, ^2J= 13.8 Hz, ^3J = 5.5 Hz), 2.14 (s, 3 H) *ppm*.

^{13}C-NMR ($CDCl_3$, 300 MHz, 300 K): δ = 171.1, 156.0, 136.3, 128.5, 128.1, 128.0, 67.0, 61.7, 50.1, 36.7, 32.2, 16.1 *ppm*.

ESI-MS: *m/z* calculated for $C_{14}H_{20}N_2O_4S+Na^+$; 335.14 ([M+Na]$^+$); found: 305.10.

The spectral data obtained are in agreement with the data published in the literature. [207]

5.2.4.8 Synthesis of benzyl (*S*)-(1-(methylthio)-3-oxopropan-2-yl)carbamate (92)

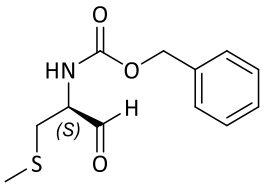

To a solution of (*S*)-Benzyl-(1-methoxy(methyl)amino)-3-(methylthio)-1-oxopropan-2-yl)carbamate **91** (1.4 g, 4.5 mmol, 1.0 eq) in dry toluene (50 mL), a solution of DIBAL (1.0 M in hexane, 6.7 mL, 6.7 mmol, 1.5 eq) was added dropwise over half an hour at -78 °C. The reaction mixture was kept stirred for 120 minutes at -78 °C. After completion, 6 mL EtOAc was added in a dropwise way, and the mixture was kept stirring for 15 min. Then EtOAc (50 mL) and saturated sodium potassium tartrate solution (50 mL) were added, and the mixture was warmed to RT. The organic phase was rinsed with saturated sodium potassium tartrate solution (3x 50 mL) and brine (75 mL). After drying over $MgSO_4$ and concentration using a rotary evaporator, the product (*S*-Benzyl-(1-(methylthio)-3-oxopropan-2-yl)carbamate **92** (1.1 g, 95%) was obtained as a colourless oil.

R_f = 0.31 (Cy/EA = 3:1)

HPLC (254 nm, VWD): t_R = 4.513 min.

^{1}H-NMR ($CDCl_3$, 300 MHz, 300 K): δ = 9.67 (*s*, 1 H), 7.40-7.31 (*m*, 5 H,), 5.80 (*s*, 1 H), 5.71 (d, 1 H), 5.15 (d, 2 H), 4.45 (q, 1 H, ^3J = 6.2 Hz), 2.98 (d, 2 H, ^3J= 6.2 Hz), 2.15 (s, 3 H) *ppm*.

^{13}C-NMR ($CDCl_3$, 300 MHz, 300 K): δ = 198.5, 188.3, 156.0, 128.6, 128.3, 128.2, 67.3, 59.3, 33.6, 16.5 *ppm*.

ESI-MS: *m/z* calculated for $C_{12}H_{15}NO_3S+H^+$; 254.08 ($[M+Na]^+$); found: 254.08.

The spectral data obtained are in agreement with the data published in the literature. [207]

5.2.4.9 Synthesis of benzyl ((1*S*)-1-(6-methoxy-2,3,4,9-tetrahydro-1*H*-pyrido[3,4-β]indol-1-yl)-2-(methylthio)ethyl)carbamate (BSc5513)

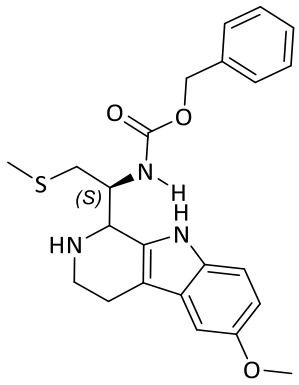

Powdered molecular sieve 4 Å (1370 mg) and (*S*-Benzyl-(1-(methylthio)-3-oxopropan-2-yl) carbamate **92** (626 mg, 2.5 mmol, 1 eq) were added to a solution of 5-Methoxytryptamine **97** (470 mg, 2.5 mmol, 1 eq) in DCM (30 mL). The mixture was frozen to 0 °C, and TFA (495 µL, 6.4 mmol, 2.6 eq) in DCM (20 mL) was added slowly. The reaction mixture was kept stirring for 120 minutes at 0 °C. After completion, the mixture was, as usual, filtered and washed with DCM (20 mL). The organic phase was rinsed with a calculated 100 mL saturated aqueous $NaHCO_3$ solution, and the aqueous layer was extracted with a calculated volume of 3x 40 mL DCM. The combined organic layer was rinsed with a calculated 50 mL of brine, dried over $MgSO_4$ and concentrated *in vacuo*. After purification by column chromatography (40:1 DCM/MeOH) benzyl ((1*S*)-1-(6-methoxy-2,3,4,9-tetrahydro-1*H*-pyrido[3,4-β]indol-1-yl)-2 (methylthio)ethyl)carbamate **BSc5513** (788 mg, 75 %) was obtained as a yellow sticky oil. R_f = 0.27 (DCM/MeOH = 40:1).

HPLC (254 nm, VWD): t_R = 4.199 min.

^{1}H NMR (500 MHz, $CDCl_3$) δ 8.23 (s, 1H), 7.45 – 7.06 (m, 7H), 6.95 (d, *J* = 2.7 Hz, 1H), 6.83 (d, *J* = 8.7 Hz, 1H), 4.99 (s, 2H), 4.52 (m, 1H), 4.44 – 4.23 (m, 1H), 3.88 (s, 3H), 3.37 – 3.29 (m, 1H), 3.06 (td, *J* = 11.0, 4.1 Hz, 1H), 2.81 (m, 3H), 2.69 (d, *J* = 14.3 Hz, 1H), 2.22 (s, 3H), 1.27 (s, 1H).

^{13}C NMR (126 MHz, $CDCl_3$) δ = 156.59, 154.02, 136.24, 133.31, 131.32, 128.51, 128.44, 128.03, 127.99, 127.75, 127.68, 111.85, 111.49, 100.30, 66.76, 56.01, 54.01, 43.19, 36.73, 35.99, 22.10, 16.07 *ppm*.

ESI-MS: *m/z* calculated for $C_{23}H_{27}N_3O_3S+H^+$; 426.184 ($[M+H]^+$); found: 426.185.

The spectral data obtained are in agreement with the data published in the literature. [208]

5.2.4.10 Synthesis of benzyl (*S*)-(1-(6-methoxy-9*H*-pyrido[3,4-β]indol-1-yl)-2-(methylthio)ethyl)carbamate (BSc5514)

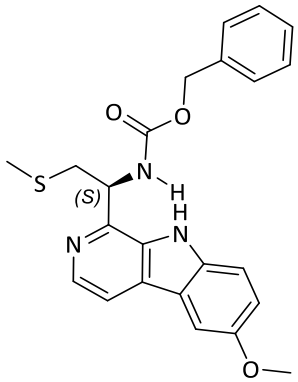

DDQ (1.21 g, 5.4 mmol, 4 eq) was added to a solution of tetrahydro-*β*-carboline **BSc5513** (569 mg, 1.3 mmol, 1.0 eq) in dry THF (60 mL). Then, the mixture was heated to a temperature of 40 °C and stirred for ca. 5 h. The reaction mixture was later filtered, and the residue was rinsed with THF (3x 25 mL). The combined filtrate was allowed to evaporate *in vacuo*, and after purification over a silica gel column (40:1 DCM/MeOH) benzyl (*S*)-(1-(6-methoxy-9*H*-pyrido[3,4-β]indol-1-yl)-2-(methylthio)ethyl)carbamate **BSc5514** (338.2 mg, 60 %) was obtained as a yellow-green amorphous solid.

R_f = 0.43 (DCM/MeOH = 40:1)

HPLC (254 nm, VWD): t_R = 4.890 min.

^{1}H-NMR ($CDCl_3$, 300 MHz, 300 K):

^{1}H NMR (300 MHz, $CDCl_3$) δ = 9.55 (s, 1H), 8.34 (d, *J* = 5.3 Hz, 1H), 7.86 (d, *J* = 5.4 Hz, 1H), 7.53 (d, *J* = 2.5 Hz, 1H), 7.40 – 7.26 (m, 15H), 7.21 (dd, *J* = 8.9, 2.5 Hz, 1H), 6.21 (s, 1H), 5.56 (d, *J* = 9.2 Hz, 1H), 5.14 (s, 3H), 3.95 (s, 3H), 3.31 (t, *J* = 6.0 Hz, 2H), 2.07 (s, 3H), 1.28 (s, 3H) *ppm*.

^{13}C-NMR ($CDCl_3$, 300 MHz,): ^{13}C NMR (126 MHz, $CDCl_3$) δ = 156.92, 154.14, 142.93, 137.49, 136.19, 135.61, 129.06, 128.52, 128.13, 127.86, 125.33, 121.88, 118.59, 114.30, 112.86, 103.28, 66.97, 56.01, 51.91, 38.28, 16.29 *ppm*.

Melting point: 130 - 131 °C

The spectral data obtained are in agreement with the data published in the literature. [208]

5.2.4.11 Synthesis of (*S*)-1-(6-methoxy-9*H*-pyrido[3,4-β]indol-1-yl)-*N*-methyl-2-(methylthio)ethan-1-amine (BSc5515)

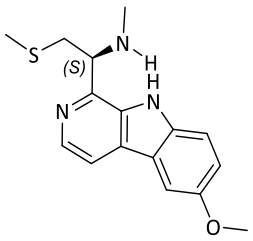

To a stirred suspension of the aminomethyl Cbz protected (*S*)-(1-(6-methoxy-9*H*-pyrido[3,4-*β*]indol-1-yl)-2-(methylthio)ethyl)carbamate **BSc5514** (201 mg, 0.5 mmol) in anhydrous THF (60 mL), 1M THF solution of $LiAlH_4$ (8 eq.) was added slowly at 0 ^oC under argon atmosphere. After the completion of the addition in the medium, the reaction mixture was heated to reach ambient temperature and then heated to reflux for ca. 4 h. The evolution of the reaction was followed by TLC. After reaching completion of the reaction, the mixture was cooled to a specified temperature of 0°C and carefully quenched with the incorporation of saturated Na_2SO_4 aqueous solution. The reaction mixture was then kept stirring for ca. 4 h at ambient temperature and filtered off. The residue was washed well with THF. The filtrate and washings were mixed, and the volatilities were later stripped off under vacuum to furnish the crude product, which was directly purified using flash column chromatography (DCM/MeOH: 97:3) to obtain the pure product (*S*)-1-(6-methoxy-9*H*-pyrido[3,4-*β*]indol-1-yl)-*N*-methyl-2-(methylthio)ethan-1-amine **BSc5515** (100.6 mg, 70 % yield).

R_f = 0.19 (DCM/MeOH = 97:3)

HPLC (254 nm, VWD): t_R = 2.329 min.

^{1}H NMR (500 MHz, $CDCl_3$) δ = 10.19 (s, 1H), 8.34 (d, *J* = 5.3 Hz, 1H), 7.84 (d, *J* = 5.2 Hz, 1H), 7.58 (d, *J* = 2.4 Hz, 1H), 7.46 (d, *J* = 8.8 Hz, 1H), 7.23 (dt, *J* = 9.0, 1.8 Hz, 1H), 4.21 (dd, *J* = 11.1, 3.4 Hz, 1H), 3.95 (s, 4H), 3.07 (dd, *J* = 13.9, 3.4 Hz, 1H), 2.88 (dd, *J* = 13.9, 11.1 Hz, 1H), 2.48 (s, 3H), 2.20 (s, 3H), 1.27 (s, 3H) *ppm*.

^{13}C NMR (126 MHz, $CDCl_3$) δ = 153.94, 145.23, 137.82, 134.97, 134.51, 129.19, 121.57, 118.46, 113.65, 112.57, 103.42, 65.14, 56.07, 39.53, 35.25, 14.93 *ppm*.

ESI-MS: *m/z* calculated for $C_{16}H_{19}N_3O_1S+H^+$; 302.13 ($[M+H]^+$); found: 302.13.

Melting point: 50 - 53 °C

The spectral data obtained are in agreement with the data published in the literature. [208]

5.2.4.12 Synthesis of (*S*)-1-(5-bromo-6-methoxy-9*H*-pyrido[3,4-β]indol-1-yl)-*N*-methyl-2-(methylthio)ethan-1-amine (BSc5516)

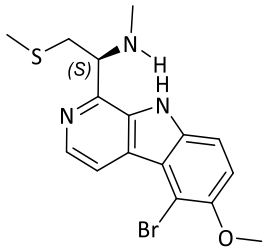

Bromine (8.5 mg, 0.05 mmol) in acetic acid (0.03 mL) was added to 6-methoxy-3-carboline **BSc5515** (16 mg, 0.05 mmol) in 5 mL of acetic acid. The mixture was left stirring overnight at ambient temperature, and following this, the solvent was dried and removed using a rotary evaporator, and the crude product was extracted from aqueous sodium bicarbonate with chloroform, washed with brine, and dried over Na_2SO_4. The solvent was evaporated, and following this, the crude product was cleaned in a solvent mixture DCM/MeOH (97:3), giving the desired (*S*)-1-(5-bromo-6-methoxy-9*H*-pyrido[3,4-*β*]indol-1-yl)-*N*-methyl-2-(methylthio)ethan-1-amine **BSc5516** (16.2 mg 80 % yield) as a yellow amorphous solid.

R_f = 0.27 (DCM/MeOH = 20:1):

HPLC (254 nm, VWD): t_R = 2.225 min.

^{1}H-NMR ($CDCl_3$, 300 MHz, 300 K): δ = 10.47 (*s*, 1 H, H-1), 8.57 (*d*, 1 H, H-12, *3J* = 5.4 Hz), 8.41 (*d*, 1 H , H-11, *3J* = 5.4 *Hz*), 7.48 (*d*, 1 H, H-3, *3J* = 8.8 Hz), 7.29 (*d*, 1 H, H-4, *3J* = 8.8

Hz), 4.27 (*d*, 1 H, H-14), 4.01 (*s*, 3 H, H-6), 3.95 (*m*, 1 H, H-17), 2.96 (*m*, 2 H, H-15), 2.49 (*s*, 3 H, H-18), 2.21 (3 H, H-16) *ppm*.

^{13}C NMR (126 MHz, $CDCl_3$) δ = 150.90, 137.94, 136.88, 136.16, 131.30, 128.54, 127.88, 121.30, 115.28, 111.11, 107.13, 57.91, 31.93, 25.91, 22.69, 14.12 *ppm*.

ESI-MS: *m/z* calculated for $C_{14}H_{11}BrN_2O_2S+H^+$; 319.00 ($[M+H]^+$); found: 319.01
Melting point: 125 - 130 °C

The spectral data obtained agree with the data published in the literature. [208]

5.2.4.13 Synthesis of (*S*)-5-bromo-1-(1-(methylamino)-2-(methylthio)ethyl)-9*H*-pyrido[3,4-β]indol-6-ol (BSc5517)

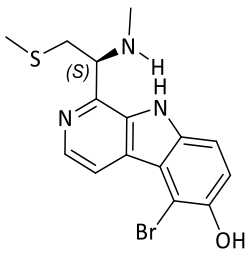

A solution of 6-*O*-methyleudistomidinderivative **BSc5516** (15 mg, 39.4 µMol, 1.0 eq) in dry DCM (12 mL) was cooled to -78 °C. Then BBr_3 (1.0 M in DCM, 236.7 µL, 236.7 µMol, 6.0 eq) was added dropwise under vigorous stirring. The mixture was slowly allowed to reach ambient temperature overnight. After completion, the reaction was quenched with a dropwise addition of MeOH (6 mL). The solvent was evaporated as required using a rotary evaporator, and the residue was purified in due course by column chromatography (20:1 DCM/MeOH). (*S*)-5-bromo-1-(1-(methylamino)-2-(methylthio)ethyl)-9*H*-pyrido[3,4-*β*]indol-6-ol (**BSc5517**)**,** 11 mg, 76% was obtained as a yellow amorphous solid.

R_f = 0.38 (DCM/MeOH = 10:1)

HPLC (254 nm, VWD): t_R = 1.916 min.

^{1}H NMR (300 MHz, MeOD) δ 8.57 (d, *J* = 5.5 Hz, 1H), 8.30 (d, *J* = 5.5 Hz, 1H), 7.50 (d, *J* = 8.7 Hz, 1H), 7.25 (d, *J* = 8.7 Hz, 1H), 4.35 (t, *J* = 7.0 Hz, 1H), 3.05 (d, *J* = 7.0 Hz, 2H), 2.36 (s, 3H), 2.00 (s, 3H), 1.30 (s, 1H; NH).

^{13}C NMR (126 MHz, MeOD) δ 149.29, 146.13, 137.62, 137.55, 136.44, 130.36, 121.71, 119.58, 116.81, 112.75, 104.21, 63.78, 39.92, 34.65, 15.70.

ESI-MS: *m/z* calculated for $C_{15}H_{17}BrN_3OS+H^+$; 366.02 ($[M+H]^+$); found: 366.02.

Melting point: 120 – 122 °C

5.2.4.14 Synthesis of (*S*)-1-(1-(methylamino)-2-(methylthio)ethyl)-9*H*-pyrido[3,4-β]indol-6-ol (BSc5518)

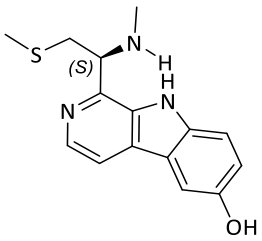

A solution of N-methylated *β*-carboline **BSc5515** (18 mg, 0.06 mmol) in dry DCM (20 mL) was cooled to -78 °C. Then BBr_3 (1.0 M in DCM, 358.3 µL, 358.3 µMol, 6.0 eq) was added dropwise under vigorous stirring. The reaction mixture was warmed to ambient temperature overnight. After completion, the reaction was quenched with a dropwise addition of MeOH (5 mL). The solvent was removed using a vacuum, and the residue was cleaned by column chromatography (DCM/MeOH: 15/1) affording (*S*)-1-(1-(methylamino)-2-(methylthio)ethyl)-9H-pyrido[3,4-β]indol-6-ol **BSc5518** (15.44 mg, 90%) as a yellow amorphous solid.

R_f = 0.34 (DCM/MeOH = 10:1)

HPLC (254 nm, VWD): t_R = 1.467 min.

^{1}H NMR (500 MHz, MeOD) δ 8.23 (d, *J* = 5.3 Hz, 1H), 7.91 (d, *J* = 5.2 Hz, 1H), 7.52 (s, 1H), 7.47 (d, *J* = 8.8 Hz, 1H), 7.13 (dd, *J* = 8.9, 2.4 Hz, 1H), 4.33 (t, *J* = 7.0 Hz, 1H), 3.03 (d, *J* = 7.0 Hz, 2H), 2.35 (s, 3H), 2.00 (s, 3H), 1.29 (s, 3H) *ppm*.

^{13}C NMR (126 MHz, MeOD) δ 152.33, 145.86, 137.68, 136.96, 136.60, 130.59, 122.94, 119.77, 115.12, 113.64, 106.62, 63.72, 39.93, 34.66, 15.70 *ppm*.

ESI-MS: *m/z* calculated for $C_{15}H_{17}N_3OS+H^+$; 288.12 ($[M+H]^+$); found: 288.12.

Melting point: 105 – 112 °C

5.2.4.15 Synthesis of (*R*)-5-bromo-1-(1-(methylamino)-2-(methylthio)ethyl)-9*H*-pyrido[3,4-β]indol-6-ol (BSc5580)

This Product was obtained as a yellow-green amorphous solid.

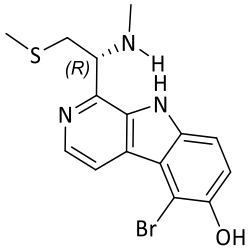

Obtained as a yellow-green amorphous solid

R_f = 0.37 (DCM/MeOH 10:1)
HPLC (254 nm, VWD): t_R = 1.913 min

^{1}H NMR (500 MHz, MeOD) δ = 8.59 (d, *J* = 5.5 Hz, 1H), 8.32 (d, *J* = 5.5 Hz, 1H), 7.51 (d, *J* = 8.7 Hz, 1H), 7.26 (d, *J* = 8.7 Hz, 1H), 4.40 (t, *J* = 6.9 Hz, 1H), 3.07 (d, *J* = 7.0 Hz, 2H), 2.39 (s, 3H), 2.00 (s, 3H), 1.31 (s, 1H, NH).
Melting point: 118 – 123 °C.

5.3 *In silico* docking

5.3.1 Blind docking experiment with AutodockVina (Vina)

AutoDock Vina 1.1.2. was used for the blind docking (BD) experiment, and every compound was docked three times to test the protocol's repeatability regarding protein interacting residues and binding affinity. Three independent docking runs on grid boxes centred on the macromolecule at exhaustiveness 12 were employed.

Protein structure, data acquisition and preparation:

The crystallographic structure files (PDB = 7MFC) for human Fms (CSFR) (CSF1R) (Y969C), (PDB ID = 1OKY) for Human PDK1 (PDPK1), (PDB ID = 3HNG) for human Flt-1 (VEGFR1) (FLT1) and (PDB ID = 5HLN) on Human GSK-3beta (GSK-3β) were obtained from the RCSB Protein Data Bank (PDB). Prior to BD, the bound ligand and all crystallographic water molecules were deleted from protein 3D structures and the energy of protein structure was minimized. MarvinSketch software was used to produce SDF files of the compounds' 3D structures from their original CDX files. PyMOL software was used to convert the SDF files into PDB format before docking.

The proteins were maintained rigid during the docking, while the ligands were kept flexible. Each compound was docked three times with the target proteins at exhaustiveness 12 to determine the relative binding affinity of a ligand at various hits and to check the protocol's repeatability. For ligand PDB files, polar hydrogens were added, Kollman charges were attributed to all atoms, and Gasteiger charges for the protein were determined. All the compounds' ligand PDB data were likewise processed using Vina. Vina's Autodocks tool was used to specify the rigid root and the number of rotatable bonds.

Concerning **BSc5485**, the BD was performed with affinity grid maps of (31.338) x (-12.469) x (-8.91) points and (80.422) x (20.656) x (3.747) points for docking into 7MFC and 1OKY respectively and the grid points spacing used were 0.532 Å for 7MFC and 0.481 Å for 1OKY respectively.

As for **BSc5488**, its BD was performed with affinity grid maps of (100) x (90) x (126) points for docking into 3HNG, and the grid point spacing used was 0.547 Å. Concerning **BSc5484**, its BD was performed with affinity grid maps of (126) x (98) x (126) points for docking into 5HLN, and the grid point spacing used was 0.547 Å. Using Vina, the auto grid tools were centred around the whole protein structure. The docking process was realized using the specified command prompts, and the minimal energy conformation state of ligands with binding affinities was considered in kcal/mol. PyMOL was also utilized to examine the protein-ligand interaction for the hits by retaining the protein as a rigid molecule and overlaying each ligand at all thirty poses acquired after docking over it. The best-docked pose with the lowest energy conformation of each ligand was chosen from the set of hits. Using PyMOL, the best pose image of ligand and protein-bound complexes was generated, and the result contained the position of the hydrogen bond established.

5.3.2 Docking experiment using MOE software

Molecular Operating Environment, version 2016.0802 of Chemical Computing Group in Montreal, Canada, was utilized for protein/ligand docking in order to gain insights into the possible binding mode. For the experiment, hydrogens were added, water molecules were removed, and the London dG scoring function was set to 1000 poses and minimized using MMFF94x within a rigid receptor, while the GBVI/WSA dG scoring function was set to 500 poses. The X-ray crystal structure of the kinases (5HQ0 for CDK1, 1J91 for CK2α1, 3ANR for DYRK1A, 7B6F for GSK-3β and 3DLZ for Haspin), 2Z5X for MAO-A were retrieved from the Protein Data bank. The receptors were prepared using the 'QuickPrep' function without 'automated structure preparation'. Using the MOE Database Viewer functions, all ligands were ''cleaned'' before partial charges were determined, and the structures underwent energy minimization. The docking poses were adjusted thanks to the Triangle Matcher procedure and scored by a 'London dG' function. The poses' refinements were performed utilizing the Rigid Receptor method. Then, they were finally scored using a 'GBVI/WSA dG' function. Based on the cocrystallized ligand, a hinge-binding pharmacophore was defined to dock the compounds into the apo structure.

For all docking experiments, residual water molecules in or out of the ATP-binding pocket were

removed, and the receptors were made ready by the mean of the ‘QuickPrep’ function without the automated structure preparation but with the assigned functions of the ‘MOE Viewer.’ All the ligands were cleaned before partial charges were fully determined, and later on, the structures underwent energy minimization. The binding sites were attributed from the cocrystallized ligands (PDB code: 5HQ0 for CDK1/cyclinB(h), 1J91 for CK2α1(h), 3ANR **for** DYRK1A(h), 7B6F for GSK-3β(h) and 3DLZ for Haspin(h)), which was placed in the binding site and for some protein by superposition in case of the apo structure and the homology model. The software provided the S-score values at the end of every docking, and the ligand efficiency was calculated based on the value of the quotient of the best S-score and the number of non-hydrogen atoms (a_heavy).

5.4 Biological assays

5.4.1 *In Vitro* Kinase Assays

5.4.1.1 General procedure and data analysis

- *In vitro* kinase activity determination of **BSc5484** and its diverse set of analogues

Table 4: ErbB2(h) assay results

Workorder: FR095-0027393

Customer: TECHNICAL UNIVERSITY DARMSTADT

Kinase: ErbB2(h)

Batch Reference: D13NP005NB

Plate Ref: W32-21-P13

ATP Concentration: 10 µM

Sample	Counts	Mean (Counts - Blanks)	Activity (% Control)		Mean	SD*
BSc5486 @ 2 µM	6515	5956	110		/	/
BSc5486 @ 20 µM	6028	5469	101		/	/
BSc5486 @ 100 µM	6890	6331	117		/	/
BSc5484 @ 2 µM	5964	5405	100		/	/
BSc5484 @ 20 µM	6455	5896	109		/	/
BSc5484 @ 100 µM	7074	6515	120		/	/
BSc5482 @ 2 µM	5760	5201	96		/	/
BSc5482 @ 20 µM	6910	6351	117		/	/
BSc5482 @ 100 µM	7245	6686	123		/	/
BSc5488 @ 2 µM	6810	6251	115		/	/
BSc5488 @ 20 µM	6652	6093	112		/	/
BSc5488 @ 100 µM	5088	4529	84		/	/
BSc5485 @ 2 µM	6356	5797	107		/	/
BSc5485 @ 20 µM	7103	6544	121		/	/
BSc5485 @ 100 µM	7116	6557	121		/	/
BSc5489 @ 2 µM	7176	6617	122		/	/

BSc5489 @ 20 µM	6711	6152	113		/	/
BSc5489 @ 100 µM	5833	5274	97		/	/
BSc5487 @ 2 µM	6196	5637	104		/	/
BSc5487 @ 20 µM	6638	6079	112		/	/
BSc5487 @ 100 µM	7047	6488	120		/	/
BSc5483 @ 2 µM	7147	6588	122		/	/
BSc5483 @ 20 µM	7145	6586	121		/	/
BSc5483 @ 100 µM	6352	5793	107		/	/
CONTROL	6289	5422	106		100	9
	5736		95			
	6448		109			
	5451		90			
BLANK	584	/	/		/	/
	534		/			

* NB. Where n = 2, the reported value here is range / √ 2

Table 5: Flt1(h) assay results

Workorder: FR095-0027393

Customer: TECHNICAL UNIVERSITY DARMSTADT

Kinase: Flt1(h)

Batch Reference: 208744

Plate Ref: W32-21-P385

ATP Concentration: 200 µM

Sample	Counts	Mean (Counts - Blanks)	Activity (% Control)	Mean	SD*
BSc5486 @ 2 µM	10440	9879	105	/	/
BSc5484 @ 2 µM	12720	12159	129	/	/
BSc5484 @ 20 µM	12059	11498	122	/	/
BSc5484 @ 100 µM	10838	10277	109	/	/
BSc5482 @ 2 µM	10235	9674	102	/	/
BSc5482 @ 20 µM	8234	7673	81	/	/
BSc5482 @ 100 µM	9863	9302	99	/	/
BSc5488 @ 2 µM	10318	9757	103	/	/
BSc5488 @ 20 µM	9157	8596	91	/	/
BSc5488 @ 100 µM	4916	4355	46	/	/
BSc5485 @ 2 µM	10891	10330	109	/	/
BSc5485 @ 20 µM	12700	12139	129	/	/

BSc5485 @ 100 µM	8912	8351	88	/	/
BSc5489 @ 2 µM	11584	11023	117	/	/
BSc5489 @ 20 µM	10855	10294	109	/	/
BSc5489 @ 100 µM	12083	11522	122	/	/
BSc5487 @ 2 µM	11499	10938	116	/	/
BSc5487 @ 20 µM	9815	9254	98	/	/
BSc5487 @ 100 µM	777	216	2	/	/
BSc5483 @ 2 µM	10402	9841	104	/	/
BSc5483 @ 20 µM	11458	10897	115	/	/
BSc5483 @ 100 µM	13844	13283	141	/	/
CONTROL	10259	9442	103	100	5
	10121		101		
	9334		93		
	10297		103		
BLANK	593	/	/	/	/
	529		/		

Plate Ref: W32-21-P380

ATP Concentration: 200 µM

Sample	**Counts**	**Mean (Counts - Blanks)**	**Activity (% Control)**	**Mean**	**SD***
BSc5486 @ 20 µM	11770	11520	113	/	/
BSc5486 @ 100 µM	7819	7569	74	/	/
CONTROL	10723	10180	103	100	3
	10611		102		
	9992		96		
	10394		100		
BLANK	272	/	/	/	/
	228		/		

* NB. Where n = 2, the reported value here is actually range / √ 2

Table 6: Fms(h)assay results

Workorder: FR095-0027393

Customer: TECHNICAL UNIVERSITY DARMSTADT

Kinase: Fms(h)

Batch Reference: 1625861

Plate Ref: W32-21-P392

ATP Concentration: 200 µM

Sample	Counts	Mean (Counts - Blanks)	Activity (% Control)	Mean	SD*
BSc5486 @ 2 µM	11033	10654	86	/	/
BSc5486 @ 20 µM	9230	8851	72	/	/
BSc5486 @ 100 µM	8068	7689	62	/	/
BSc5484 @ 2 µM	11294	10915	88	/	/
BSc5484 @ 20 µM	13592	13213	107	/	/
BSc5484 @ 100 µM	12238	11859	96	/	/
BSc5488 @ 2 µM	14828	14449	117	/	/
BSc5488 @ 20 µM	11705	11326	92	/	/
BSc5488 @ 100 µM	8355	7976	65	/	/
BSc5489 @ 2 µM	10223	9844	80	/	/
BSc5489 @ 20 µM	9091	8712	71	/	/
BSc5489 @ 100 µM	8052	7673	62	/	/
BSc5487 @ 2 µM	11925	11546	93	/	/
BSc5487 @ 20 µM	13238	12859	104	/	/
BSc5487 @ 100 µM	11373	10994	89	/	/
BSc5483 @ 2 µM	9245	8866	72	/	/
BSc5483 @ 20 µM	9521	9142	74	/	/
BSc5483 @ 100 µM	10156	9777	79	/	/
CONTROL	12790	12357	100	100	12
	14719		116		
	12027		94		
	11407		89		
BLANK	324	/	/	/	/
	434		/		

Plate Ref: W32-21-P534

ATP Concentration: 200 µM

Sample	Counts	Mean (Counts - Blanks)	Activity (% Control)	Mean	SD*
BSc5482 @ 2 µM	20665	19770	94	/	/
BSc5482 @ 20 µM	17623	16728	80	/	/
BSc5482 @ 100 µM	18557	17662	84	/	/
BSc5485 @ 2 µM	24088	23193	111	/	/
BSc5485 @ 20 µM	20861	19966	95	/	/
BSc5485 @ 100 µM	12913	12018	57	/	/
CONTROL	20869	20956	95	100	7
	22404		103		
	23641		109		
	20488		93		
BLANK	1029	/	/	/	/
	761		/		

* NB. Where n = 2, the reported value here is actually range / √ 2

Table 7: GSK-3β(h) assay results

Workorder: FR095-0027393
Customer: TECHNICAL UNIVERSITY DARMSTADT
Kinase: GSK-3β(h)
Batch Reference: WAA0024

Plate Ref: W32-21-P118

ATP Concentration: 15 µM

Sample	Counts	Mean (Counts - Blanks)	Activity (% Control)	Mean	SD*
BSc5486 @ 2 µM	8350	7933	98	/	/
BSc5486 @ 20 µM	9006	8589	106	/	/
BSc5486 @ 100 µM	7940	7523	93	/	/
BSc5484 @ 2 µM	9413	8996	111	/	/
BSc5484 @ 20 µM	7342	6925	85	/	/
BSc5484 @ 100 µM	3609	3192	39	/	/
BSc5482 @ 2 µM	9279	8862	109	/	/
BSc5482 @ 20 µM	8793	8376	103	/	/
BSc5482 @ 100 µM	9076	8659	107	/	/
BSc5488 @ 2 µM	8151	7734	95	/	/
BSc5488 @ 20 µM	8437	8020	99	/	/
BSc5488 @ 100 µM	7882	7465	92	/	/
BSc5485 @ 2 µM	7511	7094	87	/	/
BSc5485 @ 20 µM	8542	8125	100	/	/
BSc5485 @ 100 µM	8032	7615	94	/	/
BSc5489 @ 2 µM	9277	8860	109	/	/
BSc5489 @ 20 µM	8133	7716	95	/	/
BSc5489 @ 100 µM	8338	7921	98	/	/
BSc5487 @ 2 µM	8678	8261	102	/	/
BSc5487 @ 20 µM	8029	7612	94	/	/
BSc5487 @ 100 µM	8011	7594	94	/	/
BSc5483 @ 2 µM	9818	9401	116	/	/
BSc5483 @ 20 µM	8447	8030	99	/	/
BSc5483 @ 100 µM	8160	7743	95	/	/
CONTROL	7528	8113	88	100	15
	7462		87		
	9722		115		
	9408		111		
BLANK	404	/	/	/	/
	431		/		

* NB. Where n = 2, the reported value here is actually range / √ 2

Table 8: PAK1(h) assay results

Workorder: FR095-0027393

Customer: TECHNICAL UNIVERSITY DARMSTADT

Kinase: PAK1(h)

Batch Reference: D12PP001NB

Plate Ref: W32-21-P220

ATP Concentration: 45 µM

Sample	Counts	Mean (Counts - Blanks)	Activity (% Control)	Mean	SD*
BSc5486 @ 2 µM	9147	8749	97	/	/
BSc5486 @ 20 µM	8376	7978	89	/	/
BSc5486 @ 100 µM	7343	6945	77	/	/
BSc5484 @ 2 µM	10011	9613	107	/	/
BSc5484 @ 20 µM	8669	8271	92	/	/
BSc5484 @ 100 µM	9050	8652	96	/	/
BSc5482 @ 2 µM	7453	7055	79	/	/
BSc5482 @ 20 µM	9547	9149	102	/	/
BSc5482 @ 100 µM	7854	7456	83	/	/
BSc5488 @ 2 µM	8095	7697	86	/	/
BSc5488 @ 20 µM	8717	8319	93	/	/
BSc5488 @ 100 µM	7882	7484	83	/	/
BSc5485 @ 2 µM	9262	8864	99	/	/
BSc5485 @ 20 µM	10820	10422	116	/	/
BSc5485 @ 100 µM	9779	9381	104	/	/
BSc5489 @ 2 µM	8053	7655	85	/	/
BSc5489 @ 20 µM	8095	7697	86	/	/
BSc5489 @ 100 µM	7701	7303	81	/	/
BSc5487 @ 2 µM	7607	7209	80	/	/
BSc5487 @ 20 µM	7382	6984	78	/	/
BSc5487 @ 100 µM	7402	7004	78	/	/
BSc5483 @ 2 µM	9259	8861	99	/	/
BSc5483 @ 20 µM	9620	9222	103	/	/
BSc5483 @ 100 µM	9398	9000	100	/	/
CONTROL	9759	8985	104	100	4
	9312		99		
	9605		102		
	8854		94		
BLANK	508	/	/	/	/

	288		/		

* NB. Where n = 2, the reported value here is actually range / √ 2

Table 9: PDK1(h) assay results

Workorder: FR095-0027393

Customer: TECHNICAL UNIVERSITY DARMSTADT

Kinase: PDK1(h)

Batch Reference: D9AN019U

Plate Ref: W32-21-P66

ATP Concentration: 10 µM

Sample	Counts	Mean (Counts - Blanks)	Activity (% Control)	Mean	SD*
BSc5486 @ 2 µM	4971	4633	100	/	/
BSc5486 @ 20 µM	4167	3829	83	/	/
BSc5486 @ 100 µM	3564	3226	70	/	/
BSc5484 @ 2 µM	5639	5301	115	/	/
BSc5484 @ 20 µM	4605	4267	92	/	/
BSc5484 @ 100 µM	4742	4404	95	/	/
BSc5482 @ 2 µM	5167	4829	105	/	/
BSc5482 @ 20 µM	4455	4117	89	/	/
BSc5482 @ 100 µM	4299	3961	86	/	/
BSc5488 @ 2 µM	6224	5886	127	/	/
BSc5488 @ 20 µM	5410	5072	110	/	/
BSc5488 @ 100 µM	4965	4627	100	/	/
BSc5485 @ 2 µM	5190	4852	105	/	/
BSc5485 @ 20 µM	3591	3253	70	/	/
BSc5485 @ 100 µM	2678	2340	51	/	/

BSc5489 @ 2 µM	4687	4349	94	/	/
BSc5489 @ 20 µM	4939	4601	100	/	/
BSc5489 @ 100 µM	4430	4092	89	/	/
BSc5487 @ 2 µM	5340	5002	108	/	/
BSc5487 @ 20 µM	5099	4761	103	/	/
BSc5487 @ 100 µM	4372	4034	87	/	/
BSc5483 @ 2 µM	4109	3771	82	/	/
BSc5483 @ 20 µM	5360	5022	109	/	/
BSc5483 @ 100 µM	5431	5093	110	/	/
CONTROL	4375	4620	87	100	10
	4820		97		
	5277		107		
	5362		109		
BLANK	260	/	/	/	/
	417		/		

* NB. Where n = 2, the reported value here is actually range / √ 2

Determination of the IC_{50} values

Table 10: GSK-3β(h) assay results

Workorder: FR095-0028927

Customer: TECHNICAL UNIVERSITY DARMSTADT

Kinase: GSK-3β(h)

Batch Reference: WAA0024

Plate Ref: W46-21-P305

ATP concentration: 15 µM

Sample	Counts	Mean (Counts - Blanks)	Activity (% Control)	Mean	SD*
BSc5484 @ 0.03 µM	10287	9860	103	/	/
BSc5484 @ 0.095 µM	10440	10013	104	/	/
BSc5484 @ 0.3 µM	9527	9100	95	/	/
BSc5484 @ 0.95 µM	8992	8565	89	/	/
BSc5484 @ 3 µM	8689	8262	86	/	/
BSc5484 @ 9.5 µM	9065	8638	90	/	/
BSc5484 @ 30 µM	8571	8144	85	/	/
BSc5484 @ 95 µM	4875	4448	46	/	/
BSc5484 @ 300 µM	3086	2659	28	/	/
CONTROL	10233	9605	102	100	7
	10783		108		
	9862		98		
	9253		92		
BLANK	391	/	/	/	/
	464		/		

* NB. Where n = 2, the reported value here is actually range / √ 2

Table 11: Fms(Y969C)(h) assay results

Workorder: FR095-0028927

Customer: TECHNICAL UNIVERSITY DARMSTADT

Kinase: Fms(Y969C)(h)

Batch Reference: D8DN074N

Plate Ref: W46-21-P260

ATP concentration: 200 µM

Sample	**Counts**	**Mean (Counts - Blanks)**	**Activity (% Control)**	**Mean**	**SD***
BSc5485 @ 0.03 µM	5684	5015	91	/	/
BSc5485 @ 0.095 µM	5960	5291	96	/	/
BSc5485 @ 0.3 µM	6210	5541	101	/	/
BSc5485 @ 0.95 µM	6562	5893	107	/	/
BSc5485 @ 3 µM	6466	5797	105	/	/
BSc5485 @ 9.5 µM	6749	6080	110	/	/
BSc5485 @ 30 µM	6641	5972	108	/	/
BSc5485 @ 95 µM	5721	5052	92	/	/
BSc5485 @ 300 µM	1142	473	9	/	/
CONTROL	6554	5510	107	100	9
	5728		92		
	6617		108		
	5819		93		
BLANK	674	/	/	/	/
	665		/		

* NB. Where n = 2, the reported value here is actually range / √ 2

Table 12: PDK1(h) assay results

Workorder:	FR095-0028927
Customer:	TECHNICAL UNIVERSITY DARMSTADT
Kinase:	PDK1(h)
Batch Reference:	D9AN019U

Plate Ref: W46-21-P78

ATP concentration: 10 µM

Sample	Counts	Mean (Counts - Blanks)	Activity (% Control)	Mean	SD*
BSc5485 @ 0.03 µM	5431	5099	105	/	/
BSc5485 @ 0.095 µM	5806	5474	113	/	/
BSc5485 @ 0.3 µM	5804	5472	113	/	/
BSc5485 @ 0.95 µM	6581	6249	128	/	/
BSc5485 @ 3 µM	6421	6089	125	/	/
BSc5485 @ 9.5 µM	4787	4455	92	/	/
BSc5485 @ 30 µM	3937	3605	74	/	/
BSc5485 @ 95 µM	3417	3085	63	/	/
BSc5485 @ 300 µM	1419	1087	22	/	/
CONTROL	5068	4864	97	100	3
	5076		98		
	5306		102		
	5335		103		
BLANK	343	/	/	/	/
	321		/		

* NB. Where n = 2, the reported value here is actually range / √ 2

Table 13: Flt1(h) assay results

Workorder: FR095-0028927

Customer: TECHNICAL UNIVERSITY DARMSTADT

Kinase: Flt1(h)

Batch Reference: 208744

Plate Ref: W46-21-P258

ATP concentration: 200 µM

Sample	Counts	Mean (Counts - Blanks)	Activity (% Control)	Mean	SD*
BSc5488 @ 0.03 µM	10086	9276	106	/	/
BSc5488 @ 0.095 µM	10459	9649	110	/	/
BSc5488 @ 0.3 µM	9247	8437	96	/	/
BSc5488 @ 0.95 µM	9566	8756	100	/	/
BSc5488 @ 3 µM	9329	8519	97	/	/
BSc5488 @ 9.5 µM	9653	8843	101	/	/
BSc5488 @ 30 µM	7661	6851	78	/	/
BSc5488 @ 95 µM	4784	3974	45	/	/
BSc5488 @ 300 µM	1993	1183	13	/	/
CONTROL	9768	8780	102	100	3
	9192		95		
	9699		101		
	9703		101		
BLANK	757	/	/	/	/
	864		/		

* NB. Where n = 2, the reported value here is actually range / √ 2

- ***In vitro* IC_{50} estimation**

Estimated IC_{50} values are as follows:

Compounds	Kinase	IC_{50} (nM)
BSc5484	GSK-3β(h)	116855
BSc5485	Fms(Y969C)(h)	131067
BSc5485	PDK1(h)	111603
BSc5488	Flt1(h)	86465

PDK1 (h) was incubated with 100 uM KTFCGTPEYLAPEVRREPRILSEEEQEMFRDFDYIADWC (PDKtide), 50 mM Tris pH 7.5, 0.1% 6-mercaptoethanol, 10 mM MgAcetate and [gamma-33P]-ATP (If needed, precise activity and concentration). The addition of the Mg/ATP mixture started the process, and after about 40 minutes of incubation at ambient temperature, the reaction was halted by adding 0.5 % phosphoric acid. A sample of the reaction was then taken, filtered, rinsed four times for four minutes in 0.425% phosphoric acid and one time in methanol, dried and counted by scintillation. The reference compound data Staurosporine had an IC_{50} of 3.83 nM

Fms (Y969C) (h) was incubated with 8 mM MOPS pH 7.0, 0.2 mM EDTA, 100 uM EEEEYEEEEEEYYIIEEEEEEYEEEEEEYYEEEEEEKKKK, 10 mM MgAcetate and [gamma-33P]-ATP (If needed, precise activity and concentration). The addition of the Mg/ATP mixture started the process. After about 40 minutes of incubation at room temperature, the reaction was halted by adding 0.5 % phosphoric acid. A sample of the reaction was then taken, filtered, rinsed four times for four minutes in 0.425% phosphoric acid and one time in methanol, dried and counted by scintillation.

Recombinant human Flt1 (783-end) was incubated with 0.2 mM EDTA, 8 mM MOPS pH 7.0, 250 uM KKKSPGEYVNIEFG, 10 mM MgAcetate and [g- 33P]-ATP (If needed, precise activity and concentration). The addition of the Mg/ATP mixture started the process. After about 40 minutes of incubation at room temperature, the reaction was halted by adding 0.5 % phosphoric acid. Next, a sample of the reaction was filtered and washed four times for four

minutes in 0.425% phosphoric acid and one time in methanol before being dried and counted by scintillation. Reference compound data Staurosporine had an IC_{50} of 2.2 nM.

GSK-3β(h) was assayed with 8mM MOPS pH 7.0, 0.2mM EDTA, 20uM YRRAAVPPSPSLSRHSSPHQS(p) EDEEE (phospho-GS2 peptide), 10mM MgAcetate and [gamma-33P]-ATP (exact activity and concentration if required). The addition of the Mg/ATP mixture started the process. After about 40 minutes of incubation at room temperature, the reaction was halted by adding 0.5 % phosphoric acid and a sample of the reaction was taken, filtered, rinsed four times for four minutes in 0.425% phosphoric acid and one time in methanol, dried and counted by scintillation. Reference compound data Staurosporine had an IC_{50} of 9.3 nM.

- ***In vitro* residual kinase activity determination of the synthesized β-Carbolines**

Table 14: B-Raf(h) assay results

Workorder: FR095-0034856
Customer: TECHNICAL UNIVERSITY DARMSTADT
Kinase: B-Raf(h)
Batch Reference: WAD0132-D

Plate Ref: W32-22-P383
ATP Concentration: 120 µM

Sample	Counts	Mean (Counts - Blanks)	Activity (% Control)	Mean	SD*
BSc5518 @ 2 µM	11206	10777	110	/	/
CONTROL	11049	9803	108	100	9
	9786		95		
	10865		106		
	9230		90		
BLANK	463	/	/	/	/
	396		/		

Plate Ref: W32-22-P382
ATP Concentration: 120 µM

Sample	Counts	Mean (Counts - Blanks)	Activity (% Control)	Mean	SD*
BSc5515 @ 2 µM	15940	15241	110	/	/
BSc5515 @ 20 µM	12183	11484	83	/	/
BSc5515 @ 100 µM	12306	11607	84	/	/
BSc5516 @ 2 µM	14184	13485	98	/	/
BSc5516 @ 20 µM	14623	13924	101	/	/
BSc5516 @ 100 µM	15062	14363	104	/	/
BSc5517 @ 2 µM	12687	11988	87	/	/
BSc5517 @ 20 µM	11794	11095	80	/	/
BSc5517 @ 100 µM	2984	2285	17	/	/
BSc5518 @ 20 µM	13656	12957	94	/	/
BSc5518 @ 100 µM	10436	9737	70	/	/
CONTROL	15785	13814	109	100	7
	14879		103		
	13924		96		
	13464		92		
BLANK	610	/	/	/	/
	788		/		

* NB. Where n = 2, the reported value here is actually range / √ 2

Table 15: CDK1/cyclinB(h) assay results

Workorder: FR095-0034856
Customer: TECHNICAL UNIVERSITY DARMSTADT
Kinase: CDK1/cyclinB(h)
Batch Reference: 25729U

Plate Ref: W32-22-P238
ATP Concentration: 45 µM

Sample	Counts	Mean (Counts - Blanks)	Activity (% Control)	Mean	SD*
BSc5515 @ 2 µM	10033	9808	87	/	/
BSc5515 @ 20 µM	9377	9152	81	/	/
BSc5515 @ 100 µM	8391	8166	72	/	/
BSc5516 @ 2 µM	11217	10992	97	/	/
BSc5516 @ 20 µM	9700	9475	84	/	/
BSc5516 @ 100 µM	4468	4243	38	/	/
BSc5517 @ 2 µM	8048	7823	69	/	/
BSc5517 @ 20 µM	2331	2106	19	/	/
BSc5517 @ 100 µM	600	375	3	/	/
BSc5518 @ 2 µM	10193	9968	88	/	/
BSc5518 @ 20 µM	6201	5976	53	/	/
BSc5518 @ 100 µM	1709	1484	13	/	/
CONTROL	11676	11291	101	100	5
	11261		98		
	10857		94		
	12273		107		
BLANK	220	/	/	/	/
	231		/		

* NB. Where n = 2, the reported value here is actually range / √ 2

Table 16: CDK4/cyclinD3(h) assay results

Workorder: FR095-0034856
Customer: TECHNICAL UNIVERSITY DARMSTADT
Kinase: CDK4/cyclinD3(h)
Batch Reference: 208483

Plate Ref: W32-22-P438
ATP Concentration: 200 µM

Sample	Counts	Mean (Counts - Blanks)	Activity (% Control)	Mean		SD*
BSc5515 @ 2 µM	11099	9720	107	/		/
BSc5515 @ 20 µM	10388	9009	99	/		/
BSc5515 @ 100 µM	11039	9660	106	/		/
BSc5516 @ 2 µM	11106	9727	107	/		/
BSc5516 @ 20 µM	10781	9402	103	/		/
BSc5516 @ 100 µM	7490	6111	67	/		/
BSc5517 @ 2 µM	10054	8675	95	/		/
BSc5517 @ 20 µM	6113	4734	52	/		/
BSc5517 @ 100 µM	1911	532	6	/		/
BSc5518 @ 2 µM	11855	10476	115	/		/
BSc5518 @ 20 µM	10064	8685	95	/		/
BSc5518 @ 100 µM	8343	6964	76	/		/
CONTROL	10393	9113	99	100		2
	10379		99			
	10771		103			
	10426		99			
BLANK	1058	/	/	/		/
	1701		/			

* NB. Where n = 2, the reported value here is actually range / √ 2

Table 17: CK2α1(h) assay results

Workorder: FR095-0034856
Customer: TECHNICAL UNIVERSITY DARMSTADT
Kinase: CK2α1(h)
Batch Reference: 2363220

Plate Ref: W32-22-P54
ATP Concentration: 10 µM

Sample	Counts	Mean (Counts - Blanks)	Activity (% Control)	Mean	SD*
BSc5515 @ 2 µM	8920	8329	108	/	/
BSc5515 @ 20 µM	8335	7744	100	/	/
BSc5515 @ 100 µM	5782	5191	67	/	/
BSc5516 @ 2 µM	8634	8043	104	/	/
BSc5516 @ 20 µM	7678	7087	92	/	/
BSc5516 @ 100 µM	4947	4356	56	/	/
BSc5517 @ 2 µM	5391	4800	62	/	/
BSc5517 @ 20 µM	1705	1114	14	/	/
BSc5517 @ 100 µM	750	159	2	/	/
BSc5518 @ 2 µM	7939	7348	95	/	/
BSc5518 @ 20 µM	4931	4340	56	/	/
BSc5518 @ 100 µM	1946	1355	17	/	/
CONTROL	8398	7741	101	100	1
	8274		99		
	8372		101		
	8284		99		
BLANK	539	/	/	/	/
	644		/		

* NB. Where n = 2, the reported value here is actually range / √ 2

Table 18: DYRK1A(h) assay results

Workorder: FR095-0034856
Customer: TECHNICAL UNIVERSITY DARMSTADT
Kinase: DYRK1A(h)
Batch Reference: D14JP002N

Plate Ref: W32-22-P249
ATP Concentration: 45 µM

Sample	Counts	Mean (Counts - Blanks)	Activity (% Control)	Mean	SD*
BSc5515 @ 2 µM	14735	14367	91	/	/
BSc5515 @ 20 µM	12080	11712	75	/	/
BSc5515 @ 100 µM	6157	5789	37	/	/
BSc5516 @ 2 µM	14278	13910	89	/	/
BSc5516 @ 20 µM	7976	7608	48	/	/
BSc5516 @ 100 µM	3724	3356	21	/	/
BSc5517 @ 2 µM	10125	9757	62	/	/
BSc5517 @ 20 µM	3679	3311	21	/	/
BSc5517 @ 100 µM	992	624	4	/	/
BSc5518 @ 2 µM	11766	11398	73	/	/
BSc5518 @ 20 µM	5792	5424	35	/	/
BSc5518 @ 100 µM	2353	1985	13	/	/
CONTROL	16046	15711	100	100	4
	16083		100		
	16933		105		
	15257		95		
BLANK	305	/	/	/	/
	432		/		

* NB. Where n = 2, the reported value here is actually range / √ 2

Table 19: GSK-3α(h) assay results

Workorder: FR095-0034856
Customer: TECHNICAL UNIVERSITY DARMSTADT
Kinase: GSK-3α(h)
Batch Reference: D8SN021U

Plate Ref: W32-22-P67
ATP Concentration: 10 µM

Sample	Counts	Mean (Counts - Blanks)	Activity (% Control)	Mean	SD*
BSc5515 @ 2 µM	20131	19399	93	/	/
BSc5515 @ 20 µM	18479	17747	85	/	/
BSc5515 @ 100 µM	14110	13378	64	/	/
BSc5516 @ 2 µM	18738	18006	86	/	/
BSc5516 @ 20 µM	15897	15165	73	/	/
BSc5516 @ 100 µM	10034	9302	45	/	/
BSc5517 @ 2 µM	19443	18711	90	/	/
BSc5517 @ 20 µM	10541	9809	47	/	/
BSc5517 @ 100 µM	4230	3498	17	/	/
BSc5518 @ 2 µM	18195	17463	84	/	/
BSc5518 @ 20 µM	10814	10082	48	/	/
BSc5518 @ 100 µM	4378	3646	17	/	/
CONTROL	22209	20853	103	100	3
	22001		102		
	21256		98		
	20875		97		
BLANK	690	/	/	/	/
	774		/		

* NB. Where n = 2, the reported value here is actually range / √ 2

Table 20: GSK-3β(h) assay results

Workorder: FR095-0034856
Customer: TECHNICAL UNIVERSITY DARMSTADT
Kinase: GSK-3β(h)
Batch Reference: 215518

Plate Ref: W32-22-P168
ATP Concentration: 15 µM

Sample	Counts	Mean (Counts - Blanks)	Activity (% Control)	Mean	SD*
BSc5515 @ 2 µM	9697	9394	100	/	/
BSc5515 @ 20 µM	10402	10099	108	/	/
BSc5515 @ 100 µM	8494	8191	87	/	/
BSc5516 @ 2 µM	10239	9936	106	/	/
BSc5516 @ 20 µM	10315	10012	107	/	/
BSc5516 @ 100 µM	7676	7373	79	/	/
BSc5517 @ 2 µM	8865	8562	91	/	/
BSc5517 @ 20 µM	5757	5454	58	/	/
BSc5517 @ 100 µM	2530	2227	24	/	/
BSc5518 @ 2 µM	9937	9634	103	/	/
BSc5518 @ 20 µM	6469	6166	66	/	/
BSc5518 @ 100 µM	3554	3251	35	/	/
CONTROL	10515	9387	109	100	7
	8999		93		
	9709		100		
	9538		98		
BLANK	348	/	/	/	/
	259		/		

* NB. Where n = 2, the reported value here is actually range / √ 2

Table 21: Haspin(h) assay results

Workorder: FR095-0034856
Customer: TECHNICAL UNIVERSITY DARMSTADT
Kinase: Haspin(h)
Batch Reference: D9AN003U

Plate Ref: W32-22-P2
ATP Concentration: 70 µM

Sample	Counts	Mean (Counts - Blanks)	Activity (% Control)	Mean	SD*
BSc5515 @ 2 µM	10670	10320	82	/	/
BSc5515 @ 20 µM	3823	3473	28	/	/
BSc5515 @ 100 µM	1103	753	6	/	/
BSc5516 @ 2 µM	10024	9674	77	/	/
BSc5516 @ 20 µM	2668	2318	18	/	/
BSc5516 @ 100 µM	799	449	4	/	/
BSc5517 @ 2 µM	6691	6341	50	/	/
BSc5517 @ 20 µM	1354	1004	8	/	/
BSc5517 @ 100 µM	555	205	2	/	/
BSc5518 @ 2 µM	10475	10125	80	/	/
BSc5518 @ 20 µM	4588	4238	34	/	/
BSc5518 @ 100 µM	899	549	4	/	/
CONTROL	13302	12608	103	100	6
	13676		106		
	12782		99		
	12072		93		
BLANK	437	/	/	/	/
	263		/		

* NB. Where n = 2, the reported value here is actually range / √ 2

Table 22: MEK1(h) assay results

Workorder: FR095-0034856
Customer: TECHNICAL UNIVERSITY DARMSTADT
Kinase: MEK1(h)
Batch Reference: 2055150-C

Plate Ref: W32-22-P4
ATP Concentration: 10 µM

Sample	Counts	Mean (Counts - Blanks)	Activity (% Control)	Mean	SD*
BSc5515 @ 2 µM	17263	17026	104	/	/
BSc5515 @ 20 µM	16211	15974	98	/	/
BSc5515 @ 100 µM	14161	13924	85	/	/
BSc5516 @ 2 µM	14382	14145	87	/	/
BSc5516 @ 20 µM	14928	14691	90	/	/
BSc5516 @ 100 µM	14751	14514	89	/	/
BSc5517 @ 2 µM	12568	12331	76	/	/
BSc5517 @ 20 µM	6755	6518	40	/	/
BSc5517 @ 100 µM	1972	1735	11	/	/
BSc5518 @ 2 µM	15394	15157	93	/	/
BSc5518 @ 20 µM	16303	16066	99	/	/
BSc5518 @ 100 µM	12628	12391	76	/	/
CONTROL	17672	16301	107	100	5
	16593		100		
	15963		96		
	15924		96		
BLANK	267	/	/	/	/
	207		/		

* NB. Where n = 2, the reported value here is actually range / √ 2

5.4.1.2 HPLC purity determination of the tested compounds

Compounds	t_R / min	Purity / %	λ / nm
BSc5483	3.98	99.93	205
BSc5485	5.23	95.93	254
BSc5486	2.34	97.18	205
BSc5487	1.97	97.58	205
BSc5488	1.40	100.00	205
BSc5489	3.37	95.40	254
BSc5484	3.12	97.68	205
BSc5482	3.29	95.16	254
BSc5515	2.33	97.79	254
BSc5516	2.22	97.63	254
BSc5517	1.91	98.98	254
BSc5518	1.46	98.71	254

5.4.1.3 Shake-Flask Solubility Assay

The aqueous solubility was determined in a shake-flask HPLC solubility assay. The HPLC system was connected to a variable wavelength detector (VWD). All measurements were performed in triplicate at the equilibrium, and the absorbance was registered at 254 nm.

Saturated solutions of the compounds were prepared in E3-medium with 2 % vol DMSO by shaking for 24 hrs at 25 °C. Then, for each compound, a calibration curve (peak area [mAu*s] against the concentration in µM was designed by dilution of a 10 mM compounds stock solution in DMSO to 1 µM, 5 µM, 10 µM, 50 µM, and then 100 µM solutions in acetonitrile. The aqueous solubility was estimated by interpolation utilising *GraphPad Prism version 8.4.3 (471) for OS X*, originating from *GraphPad Software*, San Diego, California, USA, www.graphpad.com.

5.4.1.4 Cell viability assay

Experimental procedure

A flat black 96 well plate (Tecan Microplates, black, clear flat bottom, with lid, sterile) was coated with 50 µL poly-L-lysine for 5 min at 380 rpm. The plate was washed twice with 50 µL sterile water for 5 min at 380 rpm and dried on air for 1 hour. THP-1 cells were cultivated at 37 °C and 5 % CO_2 in RPMI-1640 media (10 % FCS, 2 mM L-glutamine, 100 µg/mL streptomycin, 100 µg/mL penicillin), counted and seeded with a number of 100.000 cells per well. The cells were later incubated for 1 hour at 37 °C and 5 % CO_2. 1.28 mg of **BSc5517** was solved in 1 mL DMSO and diluted in RPMI-1640 media. Different concentrations of **BSc5517** (0 µM, 0.1 µM, 1 µM, and 10 µM) were incubated in the cells. After different incubation times (24 hrs, 2 hrs, 1 hr, 0.5 hr and 10 min), the cells were centrifuged for 1 min at 300 x g. Then, the cells were subsequently washed with 100 µL PBS (10 mM disodium hydrogen phosphate, 137 mM sodium chloride, 2 mM dipotassium hydrogen phosphate, 2.7 mM potassium chloride, pH 7.4). The supernatant was totally removed, and 100 µL of a fresh 0.01 mg/mL resazurin in PBS solution (pH 7.4) was carefully added to the cells after a calculated 3 hours of incubation

at 37 °C with 5 % CO_2. Also, the fluorescence intensity was measured with a TECAN M1000 at λ_{ex} 535 nm and λ_{em} 585 nm with the optimal gain for the control (gain 95). The samples were measured in triplicates. The mean and the standard deviation were calculated and normalized to the non-incubated control (0 µM) of the same incubation time.

Table 24: BSc5517 Cells viability assay results

		Concentrations of BSc5517/ cell survival rate (%)		
Time	**Control**	0,1 µM	1 µM	10 µM
10 min	100	90.7	74.3	93.1
1 h	100	97.3	101.8	102.6
2 hrs	100	97.4	101.5	103.1
24 hrs	100	105.7	92.4	88.8

5.4.1.5 Buffer stability assay

The determination of the buffer stability of the inhibitors was performed with a HPLC-based assay. The buffers were incubated for 30 min in an ultrasonic bath, and then argon was passed through the solution for 6 hours. The inhibitors were then incubated with buffers (pHs 6.8, 7.4, 8.0). 5 µL of 1 mM of inhibitor stock solution in DMSO was added to an HPLC vial (1.5 mL) with 45 µL acetonitrile, 50 µL of E3-medium in 100 mM of potassium phosphate buffer and 400 µL of 100 mM potassium phosphate buffer under an argon atmosphere. The first injection (20 µL) into the HPLC started immediately after combining (t=0). The pH of the buffer (potassium phosphate) was adjusted to pH 6.8, 7.4 and 8.0, as indicated in the diagrams of the respective assay. Samples were injected and measured at t = 0, t = 24 hours, t = 48 hours, t = 72 hours, t = 96 hours, t = 120 hours and t = 144 hours. Based on a run time of 17 min per

sample. The area of the signal associated with the inhibitor was determined (mAU – s), and the area relative to the measurement at 0 min was plotted against the time of injection for each time point.

5.4.2 *In vivo* assay in zebrafish embryos

5.4.2.1 Zebrafish Developmental Toxicity Assay

Zebrafish embryos were collected and deposited in 24-well plates, ten embryos per well, and kept at 26 °C in E3-medium. The phenotypes were compared using Euromex's StereoBlue Bino Zoom microscope system and a Lumix camera. The images were captured using a EUROMEX Edublue series stereo microscope and a Lumix camera.

Raising of animals: All animal studies were carried out and documented following federal and local regulations.

5.4.2.2 Protocol for dechorionation of the embryos

The protocol for dechorionation of the embryos was as follows: 9 mL of embryonic medium (E3-medium) containing 0.003% PTU was added to 15 mL falcon tubes containing 1 mL of Pronase stock solution to obtain a 10 mL working solution at 1 mg/mL. The working solution was then placed in a Petri dish, and the embryos, still in their chorion, were transferred to the solution. The embryos were then stirred until the chorion softened. The embryos, without delay, were immediately moved to a Petri dish containing fresh embryonic medium before freeing them from their chorion. The dechorionated embryos were washed three times in a new embryonic medium before being used for the experiments.

5.5 Zebrafish Origin, Maintenance and Husbandry

The protocols for the care and husbandry of the fish were documented and approved by the Darmstadt administrative authority. All animals were treated humanely according to German Animal Welfare Standards and EU Directive 2010/63/EU of the European Parliament and Council.

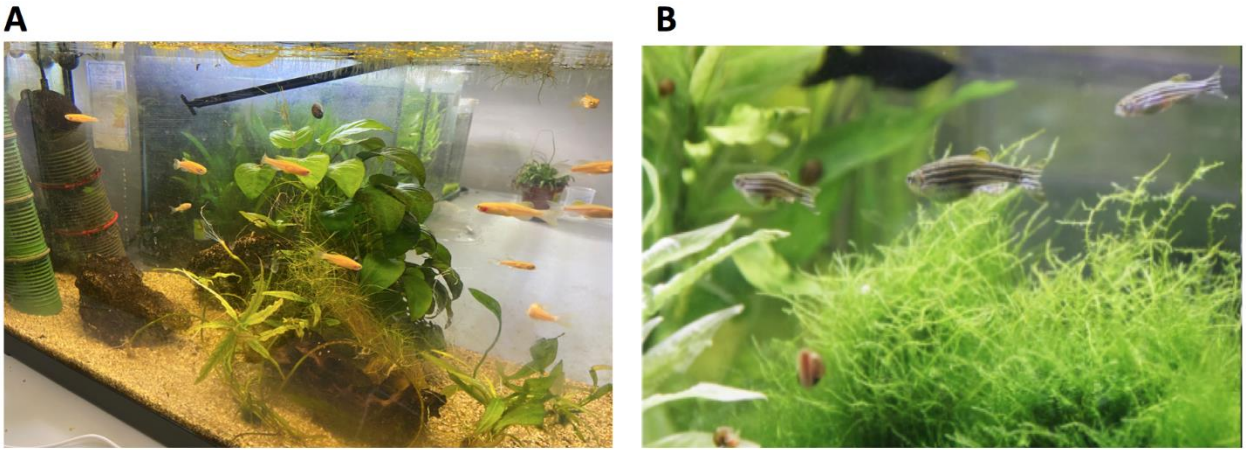

Figure 31: Different species of zebrafish. (A) *Danio rerio* gold-type with yellow-gold stripes. (B) *Danio rerio* wild-type with blue-black stripes. The aquaria are equipped with two filter pumps, aquarium plants and automated lighting.

- **Origin of Zebrafish**

The zebrafish (**Figure 31**) belongs to the family Cyprinidae, and their genome contains 1.7 billion base pairs, which have been completely sequenced. Thus, the genome of the zebrafish is only half the size of the human genome. However, about 70% of human protein-coding gene sequences have homologous sequences in zebrafish. [211]

Zebrafish are a very popular model organism because of their small size, inexpensive and easy to keep, genetic manipulability, and accessible embryology. Zebrafish have been used to develop new drugs and have become an established *in vivo* model for drug discovery. The zebrafish embryo assay constitutes an early-stage test of potential compounds for their efficacy,

permeability and toxicity *in vivo*. This involves observing embryos developing in aqueous concentrations of active compounds and interpreting the phenotypes identified. [209, 210]

- **Maintenance and Husbandry**

A ventilated and heated room with a constant temperature of 26 °C was used to house the adult fish. A timer-controlled skylight provides a 12 hours/12 hours day/night cycle as the room had no windows. A standard aquarium contained a layer of gravel, approximately 3 cm thick, as a substrate and a variety of aquarium plants. An additional light source, timed to match the ceiling light, was required per aquarium because of the natural plants growing inside. Aquaria were filled with a 1/2 mixture of Darmstadt tap water (total hardness: 17.7-20.0 °dH) and deionised water. There was no use of antibiotics or other additives. To maintain water quality, two aquarium filters were used per aquarium (e.g. Eheim Biopower 160). In addition, water changes and cleaning of the aquaria were carried out on a regular basis, and the changing water frequency depended on the fish and plants stocked. The fish population was not higher than 0.2 animals/litre. In addition to the zebrafish, at least 2 algae-eating fish were kept in the aquaria. These include *Garra rufa* or Endler guppies to control the abundant algae growth. The animals were fed daily, except on weekends, with one portion of dry flake food (TetraMin from Tetra) and one piece of frozen food (Cyclops, red or white mosquito larvae from Hornbach). The approximate food ratio per adult animal was dried flake food: 40 mg/week, pellet food: 40 mg/week and frozen food: 400 mg/week.
Feeding, changing the water and checking the water temperature and quality on a regular basis were documented.

A healthy adult female was able to lay up to 200 eggs per week, which were fertilized outside the mother and could be taken simply from the spawning aquarium. On a 12 hours/12 hours light cycle, spawning happened within the first 2 hours after the light was turned on. 0 hour/day post fertilisation (hpf/dpf) was defined as the time of spawning and fertilisation. Embryonic development was swift and monitored under a microscope, thanks to the transparency of the chorions and the embryos. Rapid growth meant that independent organs and tissues were rapidly formed, with physiological functions similar to their human counterparts. For example, the brain, heart, liver, eyes and many other organs were identified as early as 2 dpf. [209, 210]

Embryos began to hatch between 2-3 dpf. At 5 dpf, embryos were capable of feeding on their own. This was indicated because the embryo had freed itself from the protective chorion, no longer feeds on the yolk sac, and the jaws had developed to take in food. [209, 210]

Following the directive 2010/63/EU, the European Parliament set defined standards for the handling of animals for scientific research purposes. The directive became valid once the embryo could locate and ingest food in its immediate environment independently. [212] According to this, experiments on zebrafish that went beyond the fifth day of embryonic development were animal experiments that required a licence.

5.5.1 Maintenance of parental fish for the experiments performed

Sexually mature zebrafish (*Danio rerio*) were maintained at the Animal Physiological Ecology Section and were kept in 25-L aquaria with the following control settings: temperature (26.5 °C), conductivity (350 µS/cm), hardness (379 mg/L $CaCO_3$ 1⁄4 21.31dH), pH (7.570.25), dissolved oxygen (10.570.5 mg/L O; 95% saturation), and 12 hours light/12 hours dark photoperiod.

5.5.2 Spawning procedure

The zebrafish might spawn between the ages of 6 months and 24 months. [210] As the adult zebrafish would have eaten the spawn and the fry, a spawning aquarium with a spawning grate from Aquatic Habitats was used (**Figure 32**). The spawning grate was a special perforated insert to protect the spawn from predators.

A pair of adult fish were placed in a breeding aquarium filled with aquarium water and covered with plastic plants or moss the afternoon before spawning. The spawning aquarium was then well covered. Spawning occurred naturally the following day. After spawning, the adults were returned to their original aquarium around midday, and the eggs were collected after removing the spawning grid. For that purpose, the water was stirred for a short time. The dirt was still floating when the eggs were back on the bottom. After that, the rest of the water and the eggs were later placed in a petri dish.

The water was changed 5 dpf after three washes with E3 medium, and simultaneously, sterile eggs and dirt were sorted out under the light microscope. The embryos were transferred either to Petri dishes or to a 24-well microtitre plates, depending on their future use.

a) 

b) 

Figure 32: Zebrafish *Danio rerio* mating aquaria. (A) Sieve-bottomed mating aquaria for 6-8 animals, with oxygenators, filter pumps, and plastic plants. (B) Sieve-bottomed mating container for approximately 2-3 animals, equipped with plastic and aquatic plants.

5.5.3 Preparation of E3-medium

E3 medium was prepared according to the Cold Spring Harbor protocol for zebrafish embryo E3 medium. [213]

- 34.8 g NaCl
- 1.6 g KCl
- 5.8 g $CaCl_2 \cdot 2H_2O$
- 9.78 g $MgCl_2 \cdot 6H_2O$

To prepare a 60 times E3-medium stock, the ingredients were dissolved in deionized water to a final volume of 2 Liters. After adjustment to pH 7.2 with diluted NaOH, the solution was autoclaved. The 1 x E3 medium was obtained after making up 160 mL of the 60 x stock solution

to 10 L with deionised water. The 1 x E3 medium was obtained after making up to 160 mL of the 60 x stock solution to 10 L with demineralised water. 30 mL of a 0.01% methylene blue solution was added as a fungicide.

5.5.4 Breeding

Juveniles were fed with dusty food (TetraMinBaby from Tetra), coarser dusty food (Granocolor mini from JBL) from about 14 dpf and regular dry food (TetraMin from Tetra) from 40 dpf. Three times a week, they were also fed with Cyclops frozen food (Hornbach).
After approximately 1 month of age, the juveniles were transferred to a smaller aquarium with normal fish water. Only youths and no adults remained in the aquaria as they were large enough to be added to the larger aquaria with the other adult fish after about 3 months.

References

[1] Shultz, M.D., Two decades under the influence of the rule of five and the changing properties of approved oral drugs: miniperspective. *Journal of Medicinal Chemistry* **2018**, *62* (4), 1701-1714.

[2] Atanasov, A.G.; Zotchev, S.B.; Dirsch, V.M. *et al.* Natural products in drug discovery: advances and opportunities. *Nature Reviews Drug Discovery* **2021**, *20*, 200–216.

[3] Feher, M. and Schmidt, J. M., Property distributions: differences between drugs, natural products, and molecules from combinatorial chemistry. *Journal of chemical information and computer sciences* **2003**, *43*, 218–227.

[4] Lawson, A. D. G.; MacCoss, M.; Heer, J. P., Importance of rigidity in designing small molecule drugs to tackle protein–protein interactions (PPIs) through stabilization of desired conformers. *Journal of Medicinal Chemistry* **2018**, *61*, 4283–4289.

[5] Paramanantham, P.; Subhaswaraj P.; and Busi Siddhardha, Natural products from endophytic fungi: synthesis and applications. *Advances in Endophytic Fungal Research: Present Status and Future Challenges* **2019**, 83-103.

[6] Suryanarayanan TS., Endophyte research: going beyond isolation and metabolite documentation. *Fungal Ecology* **2013**, *6*, 561–568.

[7] Ye, K.; Ai, HL.; Liu, JK, Identification and Bioactivities of Secondary Metabolites Derived from Endophytic Fungi Isolated from Ethnomedicinal Plants of Tujia in Hubei Province. *A Review Natural Products and Bioprospecting* **2021**, *11*, 185–205.

[8] Brito, D.A.; Yang, Z.; Rieder C.L., Microtubules do not promote mitotic slippage when the spindle assembly checkpoint cannot be satisfied. *Journal of Cell Biology* **2008**, *182*, 623-629.

[9] Sharma, N.; Vishal S.; Vidushi, A.; Anil, P.; Sundeep, J., An update on bioactive natural products from endophytic fungi of medicinal plants. *Pharmaceuticals from Microbes: Impact on Drug Discovery* **2019**, 121-153.

[10] Newman, D; Cragg, M.; Snader, M., Natural products as sources of new drugs over the period 1981-2002. *Journal of Natural Products* **2003**, *66*, 1022 - 1037.

[11] Yang, H.; Ganguly, A.; Cabral, F., Inhibition of cell migration and cell division correlates with distinct effects of microtubule inhibiting drugs. *Journal of Biological Chemistry* **2010**, *285*, 32242 - 32250.

[12] Adams, J.; Wahl, L.; Flowers, L.; Sen, M.; Colvin, W.; Dewhirst, G.; Manikumar, M., Camptothecin analogs with enhanced activity against human breast cancer cells. II. Impact of the tumor pH gradient. *Cancer Chemotherapy and* Pharmacology **2006**, *57*, 145 - 154.

[13] Ingenol mebutate (Picato) for actinic keratosis. *The Medical letter on drugs and therapeutics* **2012**, *54*, 35 - 36.

[14] Shang, J.; Hu, B.; Wang, J.; Zhu, F.; Kang, Y.; Li, D.; Sun, H.; Kong, D.X.; Hou, T. A cheminformatic insight into the differences between terrestrial and marine originated natural products. *Journal of Chemical Information and Modeling* **2018**, *58*, 1182–1193.

[15] Pye, R.; Bertin, J.; Lokey, S.; Gerwick, H.; Linington, G., Retrospective analysis of natural products provides insights for future discovery trends. *Proceedings of the National Academy of Sciences of the United States of America* **2017**, *114*, 5601–5606.

[16] Mehbub, F.; Lei, J.; Franco, C.; Zhang, W., Marine sponge derived natural products between 2001 and 2010: trends and opportunities for discovery of bioactives. *Marine drugs* **2014**, *12* (8), 4539 - 4577.

[17] Jimenez, C.; Wilke, D.; Ferreira, G.; Takeara, R.; De Moraes, M,; Silveira, E.; Da Cruz Lotufo, T.; Lopes, N.; Costa-Lotufo, L.; Structure Elucidation and Anticancer Activity of 7-Oxostaurosporine Derivatives from the Brazilian Endemic Tunicate Eudistoma vannamei *Marine Drugs* **2012**, *10* (5), 1092 - 1102.

[18] Wieland, Theodor, The history of peptide chemistry. In *Peptides: Synthesis, Structures and Applications* **1995**, Academic Press, 1-38.

[19] Stawikowski, M.; Cudic, P., Depsipeptide Synthesis. In: Fields, G.B. (eds) Peptide Characterization and Application Protocols. *Methods in Molecular Biology*™ **2007**, 386. Humana Press.

[20] Ibrahim, M.; Elkhayat, S.; Mohamed, A.; Fat'hi, M.; Ross, A., Fusarithioamide A, a new antimicrobial and cytotoxic benzamide derivative from the endophytic fungus Fusarium chlamydosporium. *Biochemical and Biophysical Research Communications* **2016**, *479*, 211–216.

[21] Sabrin, I.; Ehab, E.; Gamal, M.; Shaukat, F.; Samir, A., Fusarithioamide A, a new antimicrobial and cytotoxic benzamide derivative from the endophytic fungus Fusarium chlamydosporium, *Biochemical and Biophysical Research Communications* **2016**, *479*, (2), 211-216.

[22] Sabrin, M.; Ibrahim, A.; Mohamed, A.; Al Haidari, F.; Zayed, A.; El-Kholy, S.; Elkhayat, R., Fusarithioamide B, a new benzamide derivative from the endophytic fungus Fusarium chlamydosporium with potent cytotoxic and antimicrobial activities. *Bioorganic & Medicinal Chemistry* **2018**, *26*, (3), 786-790.

[23] Verekar, S.; Mishra, P.; Sreekumar, E. *et al*., Anticancer activity of new depsipeptide compound isolated from an endophytic fungus. *The Journal of Antibiotics* **2014**, *67***,** 697–70.

[24] Katsuta, R.; Masada, N.; Kimura, K.; Yajima, A.; Ishigami, K.; Nukada, T., Synthesis and stereochemistry of (−)-FE399. *Tetrahedron Letters* **2020**, *61*, 151783.

[25] Park, S.; Oh, H.; Park, Y.; Yu, H.; Myung, D.; Cho, S.; Lee, W.; Park, D.; Joo, Y., Malformin A1 treatment alters invasive and oncogenic phenotypes of human colorectal cancer cells through stimulation of the p38 signalling pathway. *International Journal of Oncology* **2017**, *51*, 959-966.

[26] Li, Y.; Ducasse, R. *et al*.; Characterization of sviceucin from Streptomyces provides insights into enzyme exchangeability and disulfide bond formation in lasso peptides. *Chemical Biology,* **2015**, *10*, 2641-9

[27] Ernest Awoonor-Williams; **2020**, Modelling Covalent Modification of Cysteine Residues in Proteins (Doctoral dissertation, Memorial University, St. John's, Newfoundland and Labrador, Canada)

[28] Szabó, T.; Volk, B.; Milen, M., Recent advances in the synthesis of β-carboline alkaloids. *Molecules* **2021**, *26* (3), 663.

[29] Stachel, J.; Stockwell, S.; Van Vranken, L., The fluorescence of scorpions and cataractogenesis. *Chemistry & biology* **1999**, *6* (8), 531-539.

[30] *Justus Liebigs Annalen der Chemie* **1848**, *64*, 360.

[31] Xin, L.; Mingxia, L.; Si, T.; Changhong, W.; Shengjie, F.; Cheng, H., Harmine is an inflammatory inhibitor through the suppression of NF-κB signaling. *Biochemical and Biophysical Research Communications* **2017**, *489*, 332.

[32] Waki, H.; Won Park, K.; Mitro, N.; Pei, L.; Damoiseaux, R.; Wilpitz, D.; Reue, K.; Saez, E.; Tontonoz, P., The small molecule harmine is an antidiabetic cell-type-specific regulator of PPAR γ expression. *Cell Metabolism* **2007**, *5*, 357.

[33] Dos Santos. G.; Hallak, J., Effects of the natural β-carboline alkaloid harmine, a main constituent of ayahuasca, in memory and in the hippocampus: A systematic literature review of preclinical studies. *Journal of Psychoactive Drugs* **2017**, *49*, 1.

[34] Kamlah, Alexandra (**2018**): Entwicklung neuer Synthesewege zu β-Carbolinen. Dissertation, LMU München: Faculty of Chemistry and Pharmacy.

[35] Becker, W.; Sippl, W., Activation, regulation, and inhibition of DYRK1A. *The FEBS journal* **2011**, *278* (2), 246 - 256.

[36] Gaweska, H.; Fitzpatrick, F., Structures and mechanism of the monoamine oxidase family **2011,** 365-377.

[37] Atanasov, G.; Waltenberger, B.; Pferschy-Wenzig, E.; Linder, T.; Wawrosch, C.; Uhrin, P.; Temml, V.; Wang, L.; Schwaiger, S.; Heiss, E.; Rollinger, J. Discovery and resupply of pharmacologically active plant-derived natural products: A review. *Biotechnology advances* **2015**, *33* (8), 1582-1614.

[38] Newman, D.; Cragg, G.; Natural products as sources of new drugs from 1981 to 2014. *Journal of natural products* **2016**, *79* (3), 629-661.

[39] Bailly, C., Ready for a comeback of natural products in oncology. *Biochemical pharmacology* **2009**, *77*(9), 1447-1457.

[40] Battistutta, R., De Moliner, E., Sarno, S., Zanotti, G. and Pinna, L.A. Structural features underlying selective inhibition of protein kinase CK2 by ATP site-directed tetrabromo-2-benzotriazole. *Protein Science* **2001**, *10*, 2200 - 2206.

[41] Sefton, M.; Hunter, T.; Beemon, K.; Eckhart, W.; Evidence that the phosphorylation of tyrosine is essential for cellular transformation by Rous sarcoma virus. *Cell* **1980**, *20* (3), 807-816.

[42] Manning, G., Plowman, G.D., Hunter, T. and Sudarsanam, S., Evolution of protein kinase signaling from yeast to man. *Trends in biochemical sciences* **2002**, *27*(10), 514-520.

[43] Manning, G., Whyte, B., Martinez, R., Hunter, T.; Sudarsanam, S., The protein kinase complement of the human genome. *Science* **2002**, *298* (5600), 1912-1934.

[44] Burnett, G.; Kennedy, E.; The enzymatic phosphorylation of proteins. *Journal of Biological Chemistry* **1954**, *211*(2), 969-980.

[45] Adams, A., Kinetic and catalytic mechanisms of protein kinases. *Chemical reviews* **2001**, *101* (8), 2271-2290.

[46] Liu, J.; Hu, Y.; Waller, L.; Wang, J.; Liu, Q., Natural products as kinase inhibitors. *Natural Product Reports* **2012**, *29*(3), 392 - 403.

[47] Bridges, J., Chemical inhibitors of protein kinases. *Chemical reviews* **2001**, *101* (8), 2541-2572.

[48] Hunter, T.; Sefton, B., Transforming gene product of Rous sarcoma virus phosphorylates tyrosine. *Proceedings of the National Academy of Sciences* **1980**, *77*(3), 1311-1315.

[49] Gani, O.A. and Engh, R.A., Protein kinase inhibition of clinically important staurosporine analogues. *Natural product reports* **2010**, *27* (4), 489-498.

[50] Hu, Y.; Tong, Y., A Trojan horse for Parkinson's disease. *Science Signaling* **2010**, *3* (116), 13.

[51] De Azevedo, F.; Leclerc, S.; Meijer, L.; Havlicek, L.; Strnad, M.; Kim, S., Inhibition of Cyclin-Dependent Kinases by Purine Analogues. European Journal of Biochemistry **1997**, *243*, 518-526.

[52] Kornev, A.; Haste, M.; Taylor, S.; Eyck, F.; Surface comparison of active and inactive protein kinases identifies a conserved activation mechanism. *Proceedings of the National Academy of Sciences* **2006**, *103*(47), 17783-17788.

[53] Kornev, P.; Taylor, S.; Ten Eyck, F., A helix scaffold for the assembly of active protein kinases. *Proceedings of the National Academy of Sciences* **2008**, *105*(38), 14377-14382.

[54] Wang, Z., Cole, A., Catalytic mechanisms and regulation of protein kinases. *Methods Enzymol* **2014**, *548*, 1-21.

[55] Taylor, S.; Kornev, A., Protein kinases: evolution of dynamic regulatory proteins. *Trends in Biochemical Sciences* **2011**, *36* (2), 65-77.

[56] Johnson, N.; Lowe, D.; Noble, M.; Owen, J., The structural basis for substrate recognition and control by protein kinases. *FEBS Letters* **1998**, *430* (1), 1-11.

[57] McClendon, L.; Kornev, P.; Gilson, K.; Taylor, S., Dynamic architecture of a protein kinase. *Proceedings of the National Academy of Sciences* **2014**, *111* (43), E4623 - E4631.

[58] Keyloun, R.; Reid, C.; Choi, R.; Song, Y.; Fox, W.; Hillesland, K.; Zhang, Z.; Vidadala, R.; Merritt, E.; Lau, T.; Maly, J.; Fan, E.; Barrett, K.; Van Voorhis, C.; Ojo, K., The gatekeeper residue and beyond: homologous calcium-dependent protein kinases as drug development targets for veterinarian Apicomplexa parasites. *Parasitology* **2014**, *141* (11), 1499-1509.

[59] Grant, D.; Hemmer, W.; Tsigelny, I.; Adams, A.; Taylor, S., Kinetic Analyses of Mutations in the Glycine-Rich Loop of cAMP-Dependent Protein Kinase. *Biochemistry* **1998**, 37 (21), 7708-7715.

[60] Knight, R.; Qian, B.; Baker, D.; Kothary, R.; Conservation, variability and the modeling of active protein kinases. *PloS one* **2007**, *2* (10), 982 - 982.

[61] Wang, Z.; Cole, A., Chapter One - Catalytic Mechanisms and Regulation of Protein Kinases. In Methods in Enzymology, Shokat, K. M., Ed. Academic Press: Vol. 548, **2014**, 1-21.

[62] Scheeff, D.; Eswaran, J.; Bunkoczi, G.; Knapp, S.; Manning, G., Structure of the Pseudokinase VRK3 Reveals a Degraded Catalytic Site, a Highly Conserved Kinase Fold, and a Putative Regulatory Binding Site. *Structure* **2009**, *17* (1), 128-138.

[63] Tong, M.; Seeliger, M. A., Targeting Conformational Plasticity of Protein Kinases. *Chemical Biology* **2015**, *10* (1), 190-200.

[64] Treiber, K.; Shah, P.; Ins and Outs of Kinase DFG Motifs. *Chemistry & Biology* **2013**, *20* (6), 745-746.

[65] Baier A.; Szyszka R., Compounds from Natural Sources as Protein Kinase Inhibitors. *Biomolecules* **2020**, 10, 1546.

[66] Cori, F.; Schmidt, G.; Cori, T., The Synthesis of a Polysaccharide from Glucose-1 phosphate in Muscle Extract. *Science* **1939**, *89* (2316), 464.

[67] Cohen, P., The origins of protein phosphorylation. *Nature cell biology* **2002**, *4* (5), E127-E130.

[68] Roskoski, R., Properties of FDA-approved small molecule protein kinase inhibitors: A 2020 update. *Pharmacological Research* **2020**, 152, 104609.

[69] Lightfoot, H. L.; Goldberg, F. W.; Sedelmeier, J., Evolution of Small Molecule Kinase Drugs. *Medicinal Chemistry Letters* **2019**, *10* (2), 153-160.

[70] Augustine, J.; Bodziak, A.; Hricik, E., Use of Sirolimus in Solid Organ Transplantation. *Drugs* **2007**, 67 (3), 369-391.

[71] Nahta, R.; Esteva, F. J., Trastuzumab: triumphs and tribulations. *Oncogene* **2007**, *26* (25), 3637-3643.

[72] Iqbal, N.; Iqbal, N., Imatinib: a breakthrough of targeted therapy in cancer. *Chemotherapy Research and Practice* **2014**, 357027-357027.

[73] Laufer, S.; Briner, K.; Bajorath, J.; Georg, I.; Wang, S., New Horizons in Drug Discovery - Understanding and Advancing Kinase Inhibitors. *Journal of Medicinal Chemistry* **2020**, *63* (15), 7921-7922.

[74] Weisberg, E.; Parent, A.; Yang, L.; Sattler, M.; Liu, Q.; Liu, Q.; Wang, J.; Meng, C.; Buhrlage J.; Gray, N.; Griffin, D., Repurposing of Kinase Inhibitors for Treatment of COVID-19. *Pharmaceutical Research* **2020**, *37* (9), 167.

[75] Gharwan, H.; Groninger, H., Kinase inhibitors and monoclonal antibodies in oncology: clinical implications. *Nature Reviews Clinical Oncology* **2016**, *13* (4), 209-227.

[76] Roskoski, R., Classification of small molecule protein kinase inhibitors based upon the structures of their drug-enzyme complexes. *Pharmacological Research* **2016**, *103*, 26-48.

[77] Dar, A. C.; Shokat, K. M., The Evolution of Protein Kinase Inhibitors from Antagonists to Agonists of Cellular Signaling. *Annual Review of Biochemistry* **2011**, *80* (1), 769-795.

[78] Zuccotto, F.; Ardini, E.; Casale, E.; Angiolini, M., Through the "Gatekeeper Door": Exploiting the Active Kinase Conformation. *Journal of Medicinal Chemistry* **2010**, *53* (7), 2681-2694.

[79] Baumann, G. Development and Characterization of new Inhibitors for Protein Kinase Nek1. TU Darmstadt, 2021, [Ph.D. Thesis].

[80] Martinez, R.; Defnet, A; Shapiro, P; Avoiding or Co-Opting ATP Inhibition: Overview of Type III, IV, V, and VI Kinase Inhibitors. *Next Generation Kinase Inhibitors* **2020**, 29–59.

[81] Hassan, Q.; Sharma, V.; Markus, W., Allosteric inhibition of BCR-ABL. *Cell Cycle 9* **2010**, 3734–3738.

[82] Hardy, A.; Wells, A., Searching for new allosteric sites in enzymes. *Current Opinion in Structural Biology* **2004**, *14*, 706–715.

[83] Lamba, V.; Ghosh, I., New directions in targeting protein kinases: Focusing upon true allosteric and bivalent inhibitors. *Current Pharmaceutical Design* **2012**, *18*, 706–715.

[84] Schenone, S.; Brullo, C.; Musumeci, F.; Radi, M.; Botta, M., ATP-competitive inhibitors of mTOR: An update. *Current Medicinal Chemistry* **2011**, *18*, 2995–3014.

[85] Bonnet, P.; Mucs, D.; Bryce, R.; Targeting the inactive conformation of protein kinases: Computational screening based on ligand conformation. *Medicinal Chemistry Communications* **2012**, *3*, 434 – 440.

[86] Dar, C.; Shokat, M., The Evolution of Protein Kinase Inhibitors from Antagonists to Agonists of Cellular Signaling. *Annual Review of Biochemistry* **2011**, *80*, 769–795.

[87] Liu, Y.; Gray, N., Rational design of inhibitors that bind to inactive kinase conformations. *Nature Chemical Biology* **2006**, *2*, 358–364.

[88] Simard, R.; Pawar, V.; Aust, B.; Wolf, A.; Rabiller, M.; Wulfert, S.; Robubi, A.; Klüter, S.; Ottmann, C.; Rauh, D., High-Throughput Screening To Identify Inhibitors Which Stabilize Inactive Kinase Conformations in p38α. *Journal of the American Chemical Society* **2009**, *51*, 18478–18488.

[89] Rask-Andersen, M.; Almén, M.; Schiöth, B., Trends in the exploitation of novel drug targets. *Nature reviews Drug discovery* **2011**, *10* (8), 579-590.

[90] Omura, S.; Iwai, Y.; Hirano, A.; Nakagawa, A.; Awaya, J.; Tsuchiya, H.; Takahashi, Y.; Asuma, R., A new alkaloid AM-2282 of Streptomyces origin taxonomy, fermentation, isolation and preliminary characterization. *The Journal of antibiotics* **1977**, *30* (4), 275-282.

[91] Tamaoki, T.; Nomoto, H.; Takahashi, I.; Kato, Y.; Morimoto, M.; Tomita, F., Staurosporine, a potent inhibitor of phospholipidCa++ dependent protein kinase. *Biochemical and biophysical research communications* **1986**, *135* (2), 397-402.

[92] Kase, H.; Iwahashi, K.; Matsuda, Y., K-252a, a potent inhibitor of protein kinase C from microbial origin. *The Journal of antibiotics* **1986**, *39* (8), 1059-1065.

[93] Lamers, B.; Antson, A.; Hubbard, E.; Scott, R.; Williams, H., Structure of the protein tyrosine kinase domain of C-terminal Src kinase (CSK) in complex with staurosporine. *Journal of molecular biology* **1999**, *285* (2), 713-725.

[94] Carna Biosciences Inc., Kinase Profiling Book, http://www.carnabio.com/output/pdf/ProfilingProfilingBook_ja.pdf (accessed 8/19/2011).

[95] Toledo, M.; Lydon, B., Structures of staurosporine bound to CDK2 and cAPK–new tools for structure-based design of protein kinase inhibitors. *Structure* **1997**, *5* (12), 1551-1556.

[96] He, L.; Liao, Y.; Tan, P.; Ye, R.; Xu, W.; Zhao, M.; Ji, L.; Mao, Z., Ruthenium–Arene–β-Carboline Complexes as Potent Inhibitors of Cyclin-Dependent Kinase 1: Synthesis, Characterization and Anticancer Mechanism Studies. *Chemistry–A European Journal* **2013**, *19* (36), 12152-12160.

[97] Patterson, H.; Nibbs, R.; Mcinnes, I.; Siebert, S., Protein kinase inhibitors in the treatment of inflammatory and autoimmune diseases. *Clinical and Experimental Immunology* **2014**, *176*, 1–10.

[98] Li, T.; Wang, N.; Zhang, T.; Zhang, B.; Sajeevan, P.; Valsamma, J.; Armstrong, L.; He, S.; Naman, C., A Systematic Review of Recently Reported Marine Derived Natural Product Kinase Inhibitors. *Marine Drugs* **2019**, *17*, 493.

[99] Saijo, K.; Imai, H.; Chikamatsu, S.; Narita, K.; Katoh, T.; Ishioka, C.; Antitumor activity and pharmacologic characterization of the depsipeptide analog as a novel histone deacetylase/phosphatidylinositol 3-kinase dual inhibitor. *Cancer Science* **2017**, *108* (7), 1469-1475.

[100] Yu, X.; Guo, Z.; Marcu, M.; Neckers, L.; Nguyen, D.; Chen, G.; Schrump, D.; Modulation of p53, ErbB1, ErbB2, and Raf-1 expression in lung cancer cells by depsipeptide FR901228. *Journal of the National Cancer Institute* **2002**, *94* (7), 504-513.

[101] Ko, W.; Sohn, H.; Jang, H.; Ahn, S.; Kang, G.; Lee, S.; Kim, S.; Kim, C.; Oh, H., Inhibitory effects of alternaramide on inflammatory mediator expression through TLR4-MyD88-mediated inhibition of NF-κB and MAPK pathway signaling in lipopolysaccharide-stimulated RAW264.7 and BV2 cells. *Chemico-Biological Interactions* **2016**, *244*, 16–26.

[102] Serrill, D.; Wan, X.; Hau, M.; Jang, S.; Coleman, J.; Indra, K.; Alani, G.; Mcphail, L.; Ishmael, E., Coibamide A, a natural lariat depsipeptide, inhibits VEGFA/VEGFR2 expression and suppresses tumor growth in glioblastoma xenografts. *Investigational New Drugs* **2016**, 34, 24–40.

[103] Medina, A.; Goeger, E.; Hills, P.; Mooberry, L.; Huang, N.; Romero, I.; Ortega-Barri, E.; Gerwick, H.; McPhail, K., Coibamide A, a Potent Antiproliferative Cyclic Depsipeptide from

the Panamanian Marine Cyanobacterium Leptolyngbya sp. *Journal of the American Chemical Society* **2008**, *130*, 6324–6325.

[104] Ahmad, I.; Fakhri, S.; Khan, H.; Jeandet, P.; Aschner, M.; Yu, L., Targeting cell cycle by β-carboline alkaloids *in vitro*: Novel therapeutic prospects for the treatment of cancer. *Chemico-biological interactions* **2020**, *330*, 109229.

[105] Drung, B.; Scholz, C.; Barbosa, A.; Nazari, A.; Sarragiotto, H.; Schmidt, B.; Computational & experimental evaluation of the structure/activity relationship of β-carbolines as DYRK1A inhibitors, *Bioorganic & Medicinal Chemistry Letters* **2014**, *24*, 4854-4860.

[106] Rinehart, K.; Kobayashi, J.; Harbour, G.; Gilmore, J.; Mascal, M.; Holt, T.; Shield, L.; Lafargue, F.; Eudistomins A-Q, beta.-carbolines from the antiviral Caribbean tunicate Eudistoma olivaceum. *Journal of the American Chemical Society* **1987**, *109* (11), 3378-3387.

[107] Newman, J., Natural products as leads to potential drugs: an old process or the new hope for drug discovery? *Journal of medicinal chemistry* **2008**, *51* (9), 2589-2599.

[108] Xin B.; Tang, W.; Wang, Y.; Lin, G.; Liu, H.; Yu Jiao, Zhu, Y.; Yuan, H.; Chen, Y.; Lu, T.; Design, synthesis and biological evaluation of β-carboline derivatives as novel inhibitors targeting B-Raf kinase, *Bioorganic & Medicinal Chemistry Letters* **2012**, *22*, 4783.

[109] Roskoski Jr, R., Orally effective FDA-approved protein kinase targeted covalent inhibitors (TCIs). *Pharmacological Research* **2021**, *165*, 105422.

[110] Liu, W.; Liu, X.; Liu, W.; Gao, Y.; Wu, L.; Huang, Y.; Chen, H.; Li, D.; Zhou, L.; Wang N.; Xu, Z.; Discovery of novel β-carboline derivatives as selective AChE inhibitors with GSK-3β inhibitory property for the treatment of Alzheimer's disease. *European Journal of Medicinal Chemistry* **2022**, *229*, 114095.

[111] Talesa, N., Acetylcholinesterase in Alzheimer's disease. *Mechanisms of ageing and development* **2001**, *122* (16), 1961-1969.

[112] García, D.; Wilson, J.; Emmerson, D.; Jenkins, R.; Mahale, S.; Chaudhuri, B.; Synthesis, crystal structure and biological activity of β-carboline based selective CDK4-cyclin D1 inhibitors. *Organic & biomolecular chemistry* **2006**, *4* (24), 4478-4484.

[113] Liang, Y.; Quan, H.; Bu, T.; Li, X.; Liu, X.; Wang, S.; He, D.; Jia, Q.; Zhang, Y.; Comparison of the Inhibitory Binding Modes Between the Planar Fascaplysin and Its Nonplanar Tetrahydro-β-carboline Analogs in CDK4. *Frontiers in chemistry* **2021**, *9*, 614154.

[114] Spring, L.; Bardia, A.; Modi, S.; Targeting the cyclin D–cyclin-dependent kinase (CDK) 4/6–retinoblastoma pathway with selective CDK 4/6 inhibitors in hormone receptor-positive breast cancer: rationale, current status, and future directions. *Discovery medicine* **2016**, *21* (113), 65.

[115] Cuny, D.; Ulyanova, N.; Patnaik, D.; Liu, J.; Lin, X.; Auerbach, K.; Ray, S.; Xian, J.; Glicksman, A.; Stein, R.; Higgins, J., Structure–activity relationship study of beta-carboline derivatives as haspin kinase inhibitors. *Bioorganic & medicinal chemistry letters* **2012**, *22* (5), 2015-2019.

[116] Cell Signaling Technology Inc. http://www.cellsignal.com/reference/kinase_disease.html (accessed 8/19/2011).

[117] Ramesh, C.; Tulasi, R.; Raju, M.; Thakur, N.; Dufossé, L., Marine natural products from tunicates and their associated microbes. *Marine Drugs*, *19* (6), **2021**, 308.

[118] Li, M.; Luo, B.; Liu, Q.; Hu, Y.; Ganesan, A.; Huang, P.; Wen, S.; Synthesis of N-acyl-N, O-acetals mediated by titanium ethoxide. *Organic letters* **2014**, *16* (1), 10-13.

[119] Zhang, J.; Polishchuk, A.; Chen, J.; Ciufolini, A.; Development of an oxazole conjunctive reagent and application to the total synthesis of siphonazoles. *The Journal of Organic Chemistry* **2009**, *74* (23), 9140-9151.

[120] Zhang, Y.; Dai, Y.; Li, G.; Cheng, X., The Catalytic Synthesis of Carboniolamide: The Role of sp3 Hybridized Oxygen. *Synlett* **2014**, *25* (18), 2644-2648.

[121] Halli, J.; Hofman, K.; Beisel, T.; Manolikakes, G., Synthesis of N-Acyl-N, O-acetals from Aldehydes, Amides and Alcohols. *European Journal of Organic Chemistry* **2015**, *21*, 4624-4627.

[122] a) Fernando, E.; Nakano, Y.; Zhang, C.; Lupton, W., Enantioselective N-Heterocyclic Carbene Catalysis that Exploits Imine Umpolung. *Angewandte Chemie* **2019**, *131* (12), 4047-4051. b) Kwiecień, A.; Ciunik, Z.; Stable Hemiaminals: 2-Aminopyrimidine Derivatives. *Molecules* **2015**, *20* (8), 14365-14376. c) Iwasawa, T.; Hooley, R.; Rebek Jr, J., Stabilisation of labile carbonyl addition intermediates by a synthetic receptor. *Science* **2007**, *317* (5837), 493-496. d) Kwiecień, A.; Barys, M.; Ciunik, Z., Stable Hemiaminals with a Cyano Group and a Triazole Ring. *Molecules* **2014**, *19* (8), 11160-11177.

[123] ChemDraw Professional, version 15.0.0.106, Home 96457737, 1985-2015 PerkinElmer Informatics, Inc. All rights reserved.

[124] Tonoi, T.; Inohana, T.; Kawahara, R.; Sato, T.; Ikeda, M.; Akutsu, M.; Murata, T.; Isamu, S., 4-(Dimethylamino)pyridine N -Oxide-Catalyzed Macrolactamization Using 2-Methyl-6-nitrobenzoic Anhydride in the Synthesis of the Depsipeptidic Analogue of FE399, *ACS Omega*, **2021**, *6*, 3571-3577.

[125] Katsuta, R.; Masada, N.; Kimura, K.; Yajima, A.; Ishigami, K.; Nukada, T.; Synthesis and stereochemistry of (−)-FE399, *Tetrahedron Letters* **2020**, *61*, 151783.

[126] Bodanszky, M.; Stahl, L., Structure and synthesis of malformin A1. *Bioorganic Chemistry* **1975**, *4* (1), 93-105.

[127] Majhi, S., Applications of Yamaguchi method to esterification and macrolactonization in total synthesis of bioactive natural products. *ChemistrySelect* **2021**, *6* (17), 4178-4206.

[128] Shiina, I.; Mukaiyama, T., "A Novel Method for the Preparation of Macrolides from ω-Hydroxycarboxylic Acids." *Chemistry Letters* **1994**, *23* (4) 677 – 680.

[129] Corey, E.; Nicolaou, C.; Melvin Jr, L., Synthesis of novel macrocyclic lactones in the prostaglandin and polyether antibiotic series. *Journal of the American Chemical Society* **1975**, *97* (3), 653-654.

[130] König, W.; Geiger, R., Eine neue Methode zur Synthese von Peptiden: Aktivierung der Carboxylgruppe mit Dicyclohexylcarbodiimid unter Zusatz von 1-Hydroxy-benzotriazolen. *Chemische Berichte* **1970**, *103*, 788-798.

[131] Kamber, B.; Hartmann, A.; Eisler, K.; Riniker, B.; Rink, H.; Sieber, P.; and Rittel, W.; The Synthesis of Cystine Peptides by Iodine Oxidation of *S*-Trityl-cysteine and *S*-Acetamidomethyl-cysteine Peptides. *HCA* **1980**, *63*, 899-915.

[132] Aubry, S.; Aubert, G.; Cresteil, T.; Crich, D., Synthesis and biological investigation of the β-thiolactone and β-lactam analogs of tetrahydrolipstatin. *Organic & Biomolecular Chemistry* **2012**, *10* (13), 2629-2632.

[133] Richers, J.M., **2017**. *Studies toward the Synthesis and Biological Activity of Illicium Sesquiterpenoids via C–H Functionalization* (Doctoral dissertation, Technische Universität München).

[134] Aird, J.; Hulme, A.; White, J., An Evans− Tishchenko− Ring-Closing Metathesis Approach to Medium-Ring Lactones. *Organic Letters* **2007**, *9* (4), 631-634.

[135] Josa-Culleré, L.; Pretsch, A.; Pretsch, D.; Moloney, G., Antibacterial Mimics of Natural Products by Side-Chain Functionalization of Bicyclic Tetramic Acids. *The Journal of Organic Chemistry* **2018**, *83* (17), 10303-10317.

[136] Sun, S.; Oliveira, L.; Jiménez-Osés, G.; Bernardes, J.; Radical-Mediated Thiol-Ene Strategy: Photoactivation of Thiol-Containing Drugs in Cancer Cells. *Angewandte Chemie International Edition* **2018**, *57* (48), 15832-15835.

[137] Yan, J.; Cheng, Y.; Chen, J.; Ratnayake, R.; Dang, L.; Luesch, H.; Guo, Y.; Ye, T., Total Synthesis of Asperphenins A and B. *Organic letters* **2018**, *20* (19), 6170 - 6173.

[138] Yadav, J.; Raju, A.; Ravindar, K.; Subba Reddy, B., A formal stereoselective synthesis of (−)-brevisamide, *Tetrahedron Letters* **2013**, 54, 3227-3229.

[139] Xuan, R., Hong-Se, O.; Lee, Y.; Han-Young, K.; Total synthesis of 10-deoxymethynolide and narbonolide. *The Journal of Organic Chemistry* **2008**, 73, 1456-1461.

[140] Zhang, G; Parkin, K.; S-Alk(en)ylmercaptocysteine: Chemical Synthesis, Biological Activities, and Redox-Related Mechanism. *Journal of Agricultural and Food Chemistry*, **2013**, *61*, 1896-1903.

[141] Williams, D.; Jass, P.; Allan, T.; Gaston, D., Total synthesis of (+)-breynolide. *Journal of the American Chemical Society* **1990**, *112*, 4552 - 4554.

[142] Fang, L.; Yang, J.; Yang, F.; Enantioselective synthesis of a diastereomer of iriomoteolide-1a. What is the correct structure of the natural product? *Organic Letters* **2010**, *12* (14), 3124 - 3127.

[143] Nicolaou, C.; Estrada, A.; Zak, M.; Lee, H.; Safina, S., A Mild and Selective Method for the Hydrolysis of Esters with Trimethyltin Hydroxide. *Angewandte Chemie International Edition* **2005**, *44*, 1378-1382.

[144] Ando, T.; Sato, S.; Oobayashi, Y.; Yoshimura, T.; Murata, M.; Suga, Y.; Fudo, M.; *Symposium papers, 42nd Symposium on the chemistry of natural products, Okinawa, Japan, Nov 6-8,* **2000**, 337-342.

[145] Wang, X.; Xiang, C.; Cheng, Y.; Ma, T.; Wu, Y.; Wu, A., Direct biomimetic synthesis of β-carboline alkaloids from two amino acids. *The Journal of Organic Chemistry* **2018**, *83* (19), 12247-12254.

[146] Nelson, M.; Reisberg, S.; Shunatona, H.; Patel, J.; Toste, F., Chiral anion phase transfer of aryldiazonium cations: an enantioselective synthesis of C3-diazenated pyrroloindolines. *Angewandte Chemie International Edition* **2014**, *53* (22), 5600-5603.

[147] Aimin, H.; Tao, L.; Lacy, D.; Ian, F.; Rosazza, N., "Nocardia sp. carboxylic acid reductase: cloning, expression, and characterization of a new aldehyde oxidoreductase family." *Applied and Environmental Microbiology* **2004**, *70*, (3) 1874-1881.

[148] Fanciulli, G.; Ruggeri, R.; Grossrubatscher, E.; Calzo, F.; Wood, T.; Faggiano, A.; Isidori, A.; Colao, A.; NIKE, Serotonin pathway in carcinoid syndrome: Clinical, diagnostic, prognostic and therapeutic implications. *Reviews in Endocrine and Metabolic Disorders* **2020**, *21*, 599 - 612.

[149] Tan, D.; Reiter, R., An evolutionary view of melatonin synthesis and metabolism related to its biological functions in plants. *Journal of Experimental Botany* **2020**, *71* (16), 4677-4689.

[150] Hagel, J.; Facchini, P.; Biochemistry and Occurrence of O-Demethylation in Plant Metabolism. *Frontiers in physiology* **2010**. *1*, 14.

[151] Kobayashi, J.; Nakamura, H.; Ohizumi, Y.; Hirata, Y., The tunicate was identified by Dr. T. Nishikawa, Biological Laboratory, College of General Education, Nagoya University, Japan. *Tetrahedron Letters* **1986**, *27*,1191.

[152] National Center for Biotechnology Information **2022**, PubChem Patent Summary for WO-0246197-A1. Retrieved February 21, 2022, from https://pubchem.ncbi.nlm.nih.gov/patent/WO-0246197-A1.

[153] Drung, B.; Scholz, C.; Barbosa, V.; Nazari, A.; Sarragiotto, M.; Schmidt, B., Computational & experimental evaluation of the structure/activity relationship of β-carbolines as DYRK1A inhibitors. *Bioorganic & medicinal chemistry letters* **2014**, *24* (20), 4854 - 4860.

[154] Xin, B.; Tang, W.; Wang, Y.; Lin, G.; Liu, H.; Jiao, Y.; Zhu, Y.; Yuan, H.; Chen, Y.; Lu, T., Design, synthesis and biological evaluation of β-carboline derivatives as novel inhibitors targeting B-Raf kinase. *Bioorganic & medicinal chemistry letters* **2012**, *22* (14), 4783-4786.

[155] Karan, D.; Dubey, S.; Pirisi, L.; Nagel, A.; Pina, I.; Choo, Y.; Hamann, M.; The marine natural product manzamine A inhibits cervical cancer by targeting the SIX1 protein. *Journal of natural products* **2020**, *83* (2), 286-295.

[156] Chen, H.; Yu, C.; Liu, W.; Zhu, C.; Jiang, X.; Xu, C.; Liu, W.; Huang, Y.; Xu, Z.; Zhao, Q., Discovery of novel α-carboline derivatives as glycogen synthase kinase-3β inhibitors for the treatment of Alzheimer's disease. *Archiv der Pharmazie* **2022**, *355* (10), 2200156.

[157] Cuny, D.; Ulyanova, P.; Patnaik, D.; Liu, F.; Lin, X.; Auerbach, K.; Ray, S.; Xian, J.; Glicksman, A.; Stein, L.; Higgins, M., Structure–activity relationship study of beta-carboline derivatives as haspin kinase inhibitors. *Bioorganic & medicinal chemistry letters* **2012**, 22 (5), 2015-2019.

[158] a) Liang, J.; Wang, M.; Li, X.; He, X.; Cao, C.; Meng, F.; Determination of Structural Requirements of N-Substituted Tetrahydro-*β*-Carboline Imidazolium Salt Derivatives Using *in Silico* Approaches for Designing MEK-1 Inhibitors. *Molecules* **2017**, *22* (6), 1020. b) Melms, C.; Vallabhaneni, S.; Mills, E.; Yapp, C.; Chen, J.; Morelli, E.; Waszyk, P.; Kumar, S.; Deming, D.; Moret, N.; Rodriguez, S., Inhibition of haspin kinase promotes cell-intrinsic and extrinsic antitumor activity. *Cancer research* **2020**, *80* (4), 798-810.

[159] Gaweska, H.; Fitzpatrick, F., Structures and mechanism of the monoamine oxidase family **2011**.

[160] Savjani, T.; Gajjar, K.; Savjani, K.; Drug solubility: importance and enhancement techniques. *ISRN Pharmaceutics* **2012**, 195727-195727.

[161] Kalepu, S.; Nekkanti, V., Insoluble drug delivery strategies: review of recent advances and business prospects. *Acta Pharmaceutica Sinica B* **2015**, *5* (5), 442-453.

[162] *Test Guideline 107*, OECD, Paris, **1981**.

[163] Haldi, M.; Harden, M.; D'Amico, L.; DeLise, A.; Seng, L., Developmental Toxicity Assessment in Zebrafish. *In Zebrafish: Methods for Assessing Drug Safety and Toxicity, P. McGrath, Ed*. John Wiley & Sons, Inc.: Hoboken, New Jersey, **2012**, p Ch. 2, 15 - 17.

[164] a) Giannaccini, M.; Cuschieri, A.; Dente, L.; Raffa, V., Non-mammalian vertebrate embryos as models in nanomedicine. *Nanomedicine: Nanotechnology, Biology and Medicine* **2014**, 10 (4), 703 - 719. b) Lammer, E.; Carr, G.; Wendler, K.; Rawlings, J.; Belanger, S.; Braunbeck, T., Is the fish embryo toxicity test (FET) with the zebrafish (Danio rerio) a potential alternative for the fish acute toxicity test?. Comparative Biochemistry and Physiology Part C: *Toxicology & Pharmacology* **2009**, *149* (2), 196 - 209.

[165] Mannhold, R.; Kubinyi, H.; Folkers, G.;. *In vivo* models for drug discovery. **2014** (Vol. 62). John Wiley & Sons.

[166] Arunachalam, M.; Raja, M.; Vijayakumar, C.; Malaiammal, P.; Mayden, R., Natural history of zebrafish (*Danio rerio*) in India. *Zebrafish* **2013**, *10* (1), 1-14.

[167] Vitale, G.; Gaudenzi, G.; Dicitore, A.; Cotelli, F.; Ferone, D.; Persani, L., Zebrafish as an innovative model for neuroendocrine tumors. *Endocrine-Related Cancer* **2014**, *21* (1), R67-R83.

[168] a) Deeti, S.; O'Farrell, S.; Kennedy, N., Early safety assessment of human oculotoxic drugs using the zebrafish visualmotor response. *Journal of pharmacological and toxicological methods* **2014**, *69* (1), 1-8. b) Lee, J.; Freeman, L., Zebrafish as a model for investigating developmental lead (Pb) neurotoxicity as a risk factor in adult neurodegenerative disease: a mini-review. *Neurotoxicology* **2014**, *43*, 57-64.

[169] a) Strähle, U.; Scholz, S.; Geisler, R.; Greiner, P.; Hollert, H.; Rastegar, S.; Schumacher, A.; Selderslaghs, I.; Weiss, C.; Witters, H.; Braunbeck, T., Zebrafish embryos as an alternative to animal experiments a commentary on the definition of the onset of protected life stages in animal welfare regulations. *Reproductive Toxicology* **2012**, *33* (2), 128-132. b) Griffin, A.; Anvar, M.; Hamling, K.; Baraban, C., Phenotype-based screening of synthetic cannabinoids in a dravet syndrome zebrafish model. *Frontiers in Pharmacology* **2020**, *11*, 464.

[170] Meyers, R.; Zebrafish: Development of a Vertebrate Model Organism. *Current Protocols Essential Laboratory Techniques* **2018**, *16* (1), 19.

[171] Cold Spring Harbor Protocols, **2011**. E3 medium (for zebrafish embryos). doi:10.1101/pdb.rec066449. (Accessed 2021 March 12).

[172] Neumann, T.; Benajiba, L.; Göring, S.; Stegmaier, K; Schmidt, B., Evaluation of improved glycogen synthase kinase-3α inhibitors in models of acute myeloid leukemia. *Journal of medicinal chemistry* **2015**, *58* (22), 8907-8919.

[173] Paquet, D.; Bhat, R.; Sydow, A.; Mandelkow, M.; Berg, S.; Hellberg, S.; Fälting, J.; Distel, M.; Köster, W.; Schmid, B.; Haass, C., A zebrafish model of tauopathy allows *in vivo* imaging of neuronal cell death and drug evaluation. *The Journal of clinical investigation* **2009**, *119* (5), 1382-1395.

[174] Nishiya, N.; Oku, Y.; Kumagai, Y.; Sato, Y.; Yamaguchi, E.; Sasaki, A.; Shoji, M.; Ohnishi, Y.; Okamoto, H.; Uehara, Y., A zebrafish chemical suppressor screening identifies

small molecule inhibitors of the Wnt/beta-catenin pathway. *Chemical Biology* **2014**, *21*, 530-540.

[175] Huang, J.; Guo, X.; Li, W.; Zhang, H., Activation of Wnt/β-catenin signalling via GSK3 inhibitors direct differentiation of human adipose stem cells into functional hepatocytes. *Scientific Reports* **2017**, *7* (1), 1-12.

[176] Paquet, D.; Bhat, R.; Sydow, A.; Mandelkow, M.; Berg, S.; Hellberg, S.; Fälting, J.; Distel, M.; Köster, R.; Schmid, B.; Haass, C., A zebrafish model of tauopathy allows *in vivo* imaging of neuronal cell death and drug evaluation. *The Journal of clinical investigation* **2009**, *119* (5), 1382-1395.

[177] Takahashi-Yanaga, F., Activator or inhibitor? GSK-3 as a new drug target. *Biochemical pharmacology* **2013**, *86* (2), 191-199.

[178] Doble, W.; Patel, S.; Wood, A.; Kockeritz, L.; Woodgett, R., Functional redundancy of GSK-3α and GSK-3β in Wnt/β-catenin signaling shown by using an allelic series of embryonic stem cell lines. *Developmental cell* **2007**, *12* (6), 957 - 971.

[179] Selland, L. (2018), *Roles for Transcription Factors and Signaling Pathways in Hindbrain Segmentation and Ventricle Morphogenesis*, A thesis submitted in partial fulfillment of the requirements for the degree of Doctor of Philosophy, Department of Biological Sciences University of Alberta.

[180] McCubrey, J.; Steelman, L.; Bertrand, F.; Davis, N.; Abrams, S.; Montalto, A.; Libra, M.; Nicoletti, F.; Maestro, R.; Basecke, J.; Cocco, L.; Cervello, M.; Martelli, A., Multifaceted roles of GSK-3 and Wnt/β-catenin in hematopoiesis and leukemogenesis: Opportunities for therapeutic intervention. *Leukemia* **2013**, *28* (1), 15-33.

[181] Sharmar, S.; Garg, I.; Kumar, B.; Ashraf, Z., Comparative analysis of blind docking reproducibility. *Research Journal of Life Sciences, Bioinformatics, Pharmaceutical and Chemical Sciences* **2018**, *4* (3), 211-222.

[182] Eberhardt, J.; Santos-Martins, D.; Tillack, A.; Forli, S., AutoDock Vina 1.2. 0: New docking methods, expanded force field, and python bindings. *Journal of chemical information and modeling* **2021**, *61* (8), 3891-3898.

[183] Trott, O.; Olson, J., AutoDock Vina: improving the speed and accuracy of docking with a new scoring function, efficient optimization, and multithreading. *Journal of computational chemistry* **2010**, *31* (2), 455-461.

[184] Smith, D.; Kaufman, D.; Wise, C.; Ahn, M.; Caldwell, M.; Leary, B.; Lu, W.; Tan, G.; Vogeti, L.; Vogeti, S.; Wilky, B., Vimseltinib: a precision CSF1R therapy for tenosynovial giant cell tumors and diseases promoted by macrophages. *Molecular cancer therapeutics* **2021**, *20* (11), 2098 - 2109.

[185] Komander, D.; Kular, S.; Bain, J.; Elliott, M.; Alessi, D.; Van Aalten, M.; 2003. Structural basis for UCN-01 (7-hydroxystaurosporine) specificity and PDK1 (3-phosphoinositide-dependent protein kinase-1) inhibition. *Biochemical Journal* **2003**, *375* (2), 255-262.

[186] Wagner, F.; Bishop, A.; Gale, P.; Shi, X.; Walk, M.; Ketterman, J.; Patnaik, D.; Barker, D.; Walpita, D.; Campbell, A.; Nguyen, S., Inhibitors of glycogen synthase kinase 3 with exquisite kinome-wide selectivity and their functional effects. *ACS Chemical Biology* **2016**, *11* (7), 1952 - 1963.

[187] Brown, R.; Korolchuk, S.; Martin, M.; Stanley, W.; Moukhametzianov, R.; Noble, E.; Endicott, A., CDK1 structures reveal conserved and unique features of the essential cell cycle CDK. *Nature communications* **2015**, *6* (1), 6769.

[188] Ogawa, Y.; Nonaka, Y.; Goto, T.; Ohnishi, E.; Hiramatsu, T.; Kii, I.; Yoshida, M.; Ikura, T.; Onogi, H.; Shibuya, H.; Hosoya, T., Development of a novel selective inhibitor of the Down syndrome-related kinase Dyrk1A. *Nature communications* **2010**, *1* (1), 86.

[189] Andreev, S.; Pantsar, T.; Tesch, R.; Kahlke, N.; El-Gokha, A.; Ansideri, F.; Grätz, L.; Romasco, J.; Sita, G.; Geibel, C.; Lämmerhofer, M., Addressing a Trapped High-Energy Water: Design and Synthesis of Highly Potent Pyrimidoindole-Based Glycogen Synthase Kinase-3β Inhibitors. *Journal of Medicinal Chemistry* **2021**, *65* (2), 1283-1301.

[190] Eswaran, J.; Patnaik, D.; Filippakopoulos, P.; Wang, F.; Stein, R.; Murray, J.; Higgins, J.; Knapp, S., Structure and functional characterization of the atypical human kinase haspin. *Proceedings of the National Academy of Sciences* **2009**, *106* (48), 20198-20203.

[191] Son, Y.; Ma, J.; Kondou, Y.; Yoshimura, M.; Yamashita, E.; Tsukihara, T., Structure of human monoamine oxidase A at 2.2-Å resolution: the control of opening the entry for substrates/inhibitors. *Proceedings of the National Academy of Sciences* **2008**, *105* (15), 5739-5744.

[192] Yang, Y.; Ma, Q.; Li, Z.; Wang, H.; Zhang, C.; Liu, Y.; Li, B.; Wang, Y.; Cui, Q.; Xue, F.; Ai, D., Harmine alleviates atherogenesis by inhibiting disturbed flow-mediated endothelial

activation via protein tyrosine phosphatase PTPN14 and YAP. *British Journal of Pharmacology* **2021**, *178* (7), 1524-1540.

[193] Almaliti, J.; Al-Hamashi, A.; Negmeldin, T.; Hanigan, L.; Perera, L.; Pflum, H.; Casero Jr, A.; Tillekeratne, L., Largazole analogues embodying radical changes in the depsipeptide ring: Development of a more selective and highly potent analogue. *Journal of Medicinal Chemistry* **2016** *59* (23), 10642-10660.

[194] Cakici, M.; Catir, M.; Karabuga, S.; Ulukanli, S.; Kilic, H., Synthesis and asymmetric catalytic activity of (1S, 1′ S)-4, 4′-biquinazoline-based primary amines. *Tetrahedron: Asymmetry* **2011**, *22* (3), 300-308.

[195] Bates, R.; Lu, Y., A formal synthesis of porantheridine and an epimer. *The Journal of Organic Chemistry* **2009**, *74* (24), 9460-9465.

[196] Holub, N.; Neidhöfer, J.; Blechert, S., Total Synthesis of (+)-trans-195A. *Organic Letters* **2005**, *7* (7), 1227-1229.

[197] Kobayashi, Y.; Hayashi, N.; Kishi, Y.; Toward the creation of NMR databases in chiral solvents: bidentate chiral NMR solvents for assignment of the absolute configuration of acyclic secondary alcohols. *Organic Letters* **2002**, *4* (3), 411-414.

[198] Kitir, B.; Baldry, M.; Ingmer, H.; Olsen, A., Total synthesis and structural validation of cyclodepsipeptides solonamide A and B. *Tetrahedron* **2014**, *70* (42), 7721-7732.

[199] Swarbrick, D.; Ung, P.; Chhabra, S.; Graham, B., An Iminodiacetic Acid Based Lanthanide Binding Tag for Paramagnetic Exchange NMR Spectroscopy. *Angewandte Chemie International Edition* **2011**, *50* (19), 4403-4406.

[200] Silvia, V.; Baldisserotto, A.; Scalambra, E.; Malisardi, G.; Durini, E.; Manfredini, S., Novel molecular combination deriving from natural aminoacids and polyphenols: Design, synthesis and free-radical scavenging activities. *European Journal of Medicinal Chemistry* **2012**, *50*, 383-392.

[201] Weber, U.; Hartter, P., Synthese und Stabilität von cyclischen Disulfiden des Typs. *Biological Chemistry* **1974**, *355* (1), 189-199.

[202] Xu, H.; Fan, L., Antifungal agents. Part 4: synthesis and antifungal activities of novel indole [1, 2-c]-1, 2, 4-benzotriazine derivatives against phytopathogenic fungi *in vitro*. *European journal of medicinal chemistry* **2011**, *46* (1), 364-369.

[203] Ghashghaei, O.; Pedrola, M.; Seghetti, F.; Martin, V.; Zavarce, R.; Babiak, M.; Novacek, J.; Hartung, F.; Rolfes, M.; Haarmann-Stemmann, T.; Lavilla, R., Extended multicomponent reactions with indole aldehydes: access to unprecedented polyheterocyclic scaffolds, ligands of the aryl hydrocarbon receptor. *Angewandte Chemie* **2021**, *133* (5), 2635-2640.

[204] Nelson, M.; Reisberg, H.; Shunatona, H.; Patel, J.; Toste, D., Chiral Anion Phase Transfer of Aryldiazonium Cations: An Enantioselective Synthesis of C3-Diazenated Pyrroloindolines. *Angewandte Chemie International Edition* **2014**, *53* (22), 5600-5603.

[205] Kolodiazhna, O.; Skliarov, I.; Slastennikova, A.; Kolodiazhnyi, O., Asymmetric synthesis of (S, R)-and (R, R)-methiin stereoisomers. *Phosphorus, Sulfur, and Silicon and the Related Elements* **2020**, *195* (9), 713-717.

[206] Hwang, R.; Helquist, P.; Shekhani, S., Total synthesis of (+)-sparsomycin. Approaches using cysteine and serine inversion. *The Journal of Organic Chemistry* **1985**, *50* (8), 1264-1271.

[207] Hooper, F.; Seo, S.; Truscott, R.; Neuhaus, J.; Willis, C., α-Amino aldehydes as readily available chiral aldehydes for Rh-catalyzed alkyne hydroacylation. *Journal of the American Chemical Society* **2016**, *138* (5), 1630-1634.

[208] Kobayashi, J.; Cheng, F.; Ohta, T.; Nozoe, S.; Ohizumi, Y.; Sasaki, T., Eudistomidins B, C, and D: novel antileukemic alkaloids from the Okinawan marine tunicate Eudistoma glaucus. The Journal of Organic Chemistry **1990**, *55* (11), 3666-3670.

[209] Mannhold, R.; Kubinyi, H.; Folkers, G., In vivo models for drug discovery (Vol. 62). *John Wiley & Sons* **2014**.

[210] C. Nusslein-Volhard, R. Dahm, Zebrafish, Oxford University Press, 2002.

[211] Howe, K.; Clark, D.; Torroja, F.; Torrance, J.; Berthelot, C.; Muffato, M.; Collins, E.; Humphray, S.; McLaren, K.; Matthews, L.; McLaren, S., The zebrafish reference genome sequence and its relationship to the human genome. *Nature* **2013**, *496* (7446), 498-503.

[212]http://eurlex.europa.eu/LexUriServ/LexUriServ.do?uri=OJ:L:2010:276:0033:0079:de:PDF, Zugriff: 02.03.2016

[213] Cold Spring Harbor Protocols (2011). E3 medium (for zebrafish embryos). doi:10.1101/pdb.rec066449. (Accessed 2021 March 12).

Appendix

A. NMR spectra of all the synthesized compounds

1. 2-((R)-2-aminopropanamido)-N-((S)-1-hydroxy-3-mercaptopropyl)benzamide (12) (Fusarithioamide A)

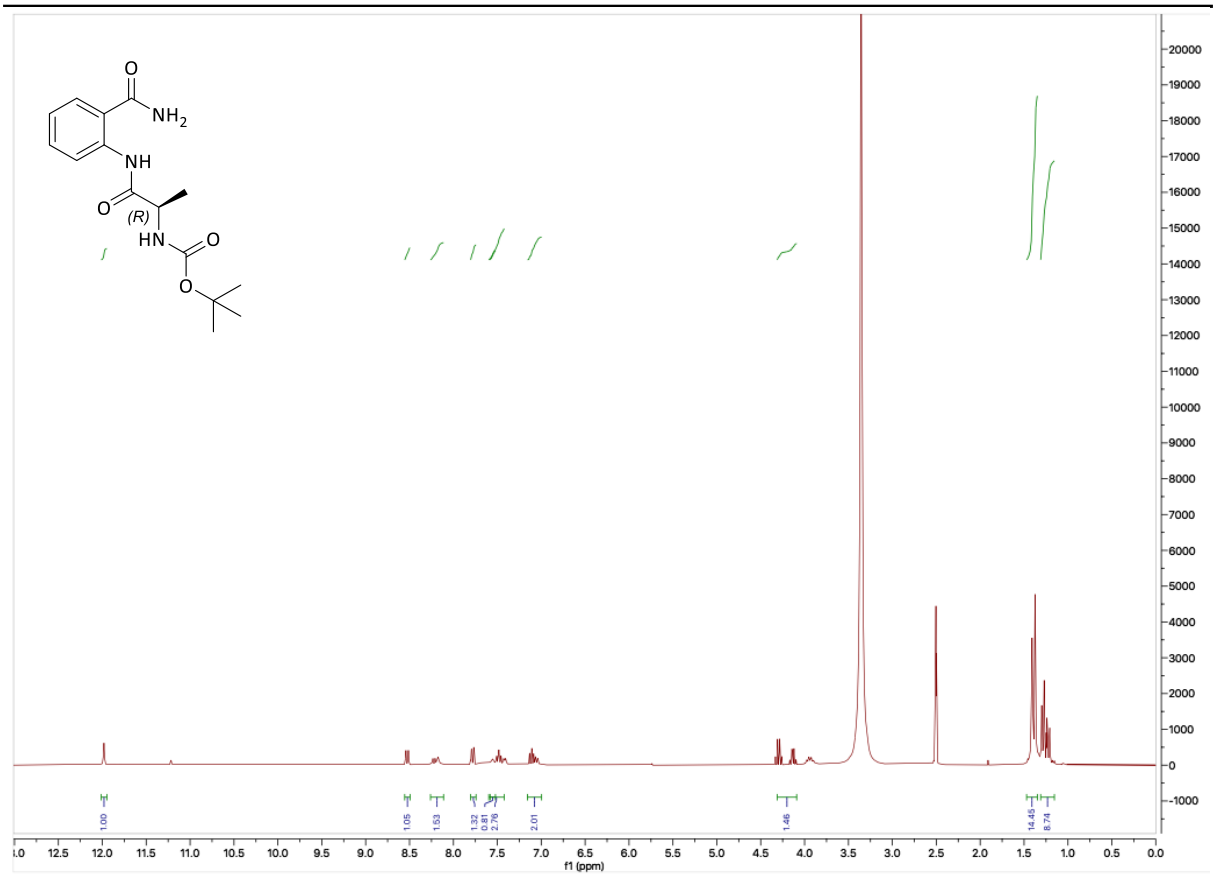
O
NH2
NH
O
(R)
HN
O
O
1.00
1.05
1.53
1.32
0.81
2.78
2.01
1.46
14.45
6.74
f1 (ppm)

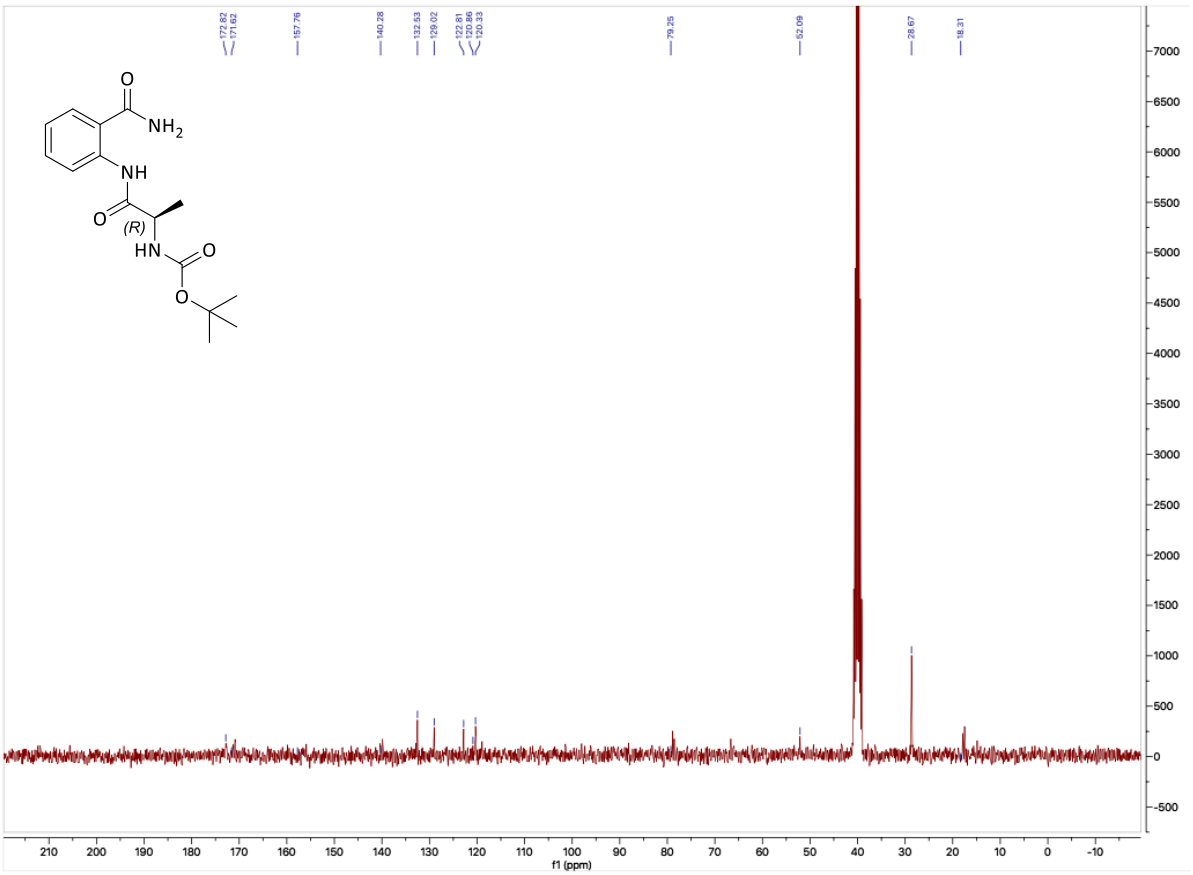
O
NH2
NH
O
(R)
HN
O
O
172.82
171.62
157.76
140.28
132.53
129.02
122.81
120.86
120.33
79.25
52.09
28.67
18.31
f1 (ppm)

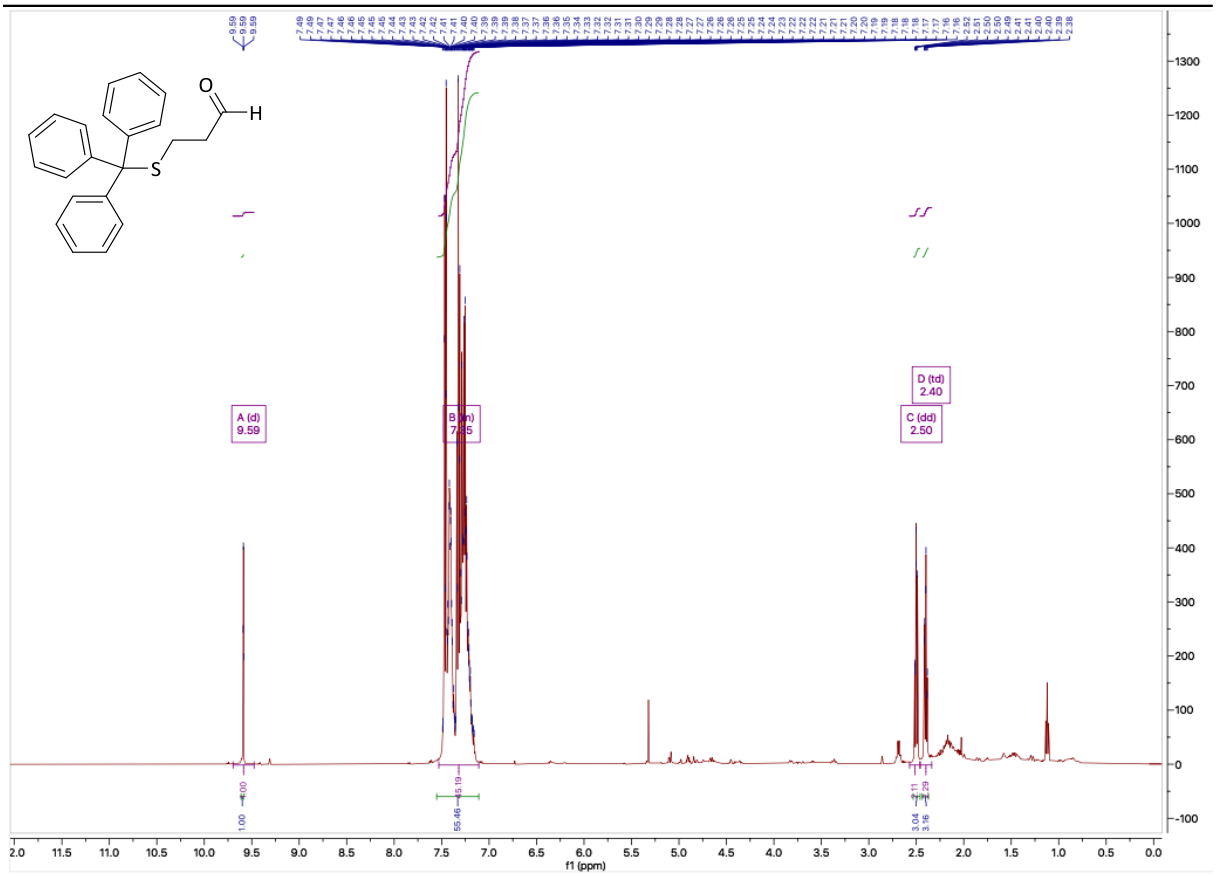
O
H
S
A (d)
9.59
D (td)
2.40
C (dd)
2.50
f1 (ppm)

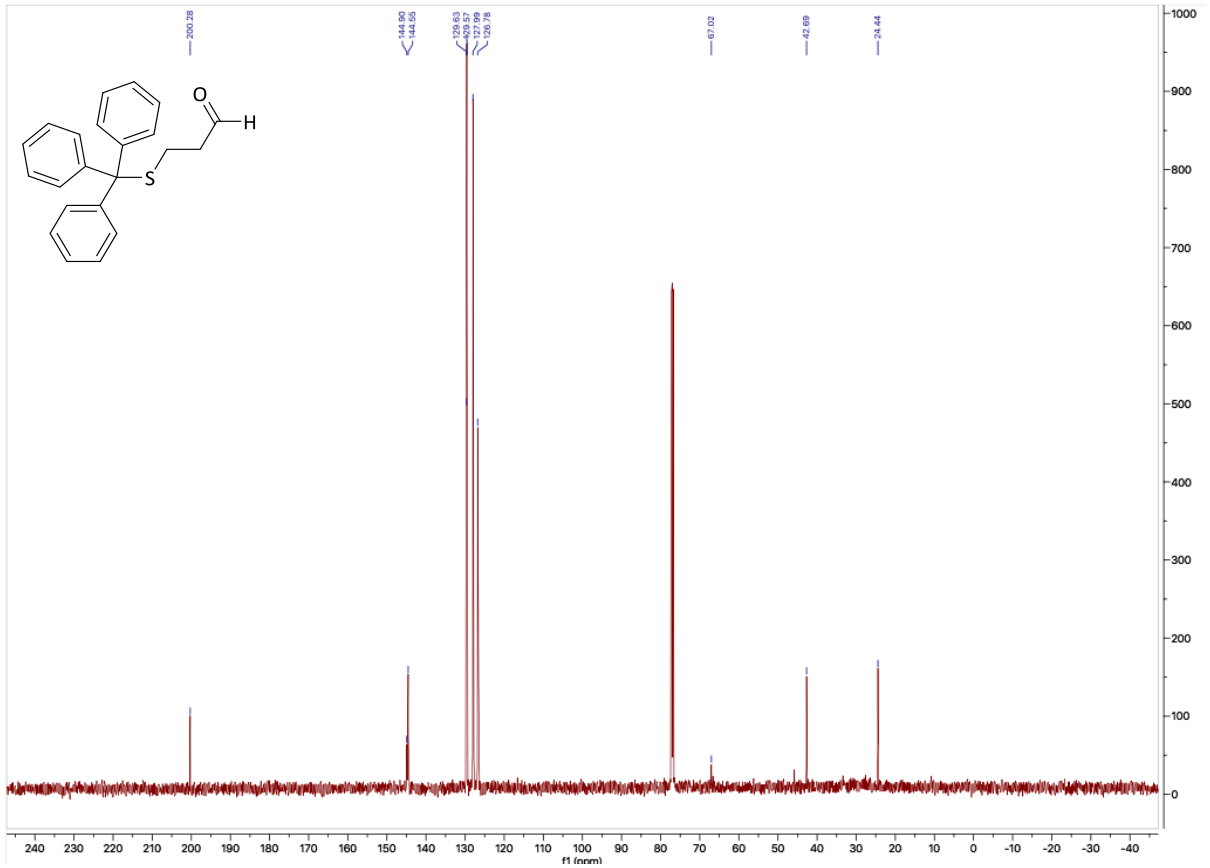
O
H
S
200.28
144.90
144.05
129.63
129.57
127.99
126.78
67.02
42.69
24.44
f1 (ppm)

2. Syntheses of **BSc5484** and the diverse set of analogues

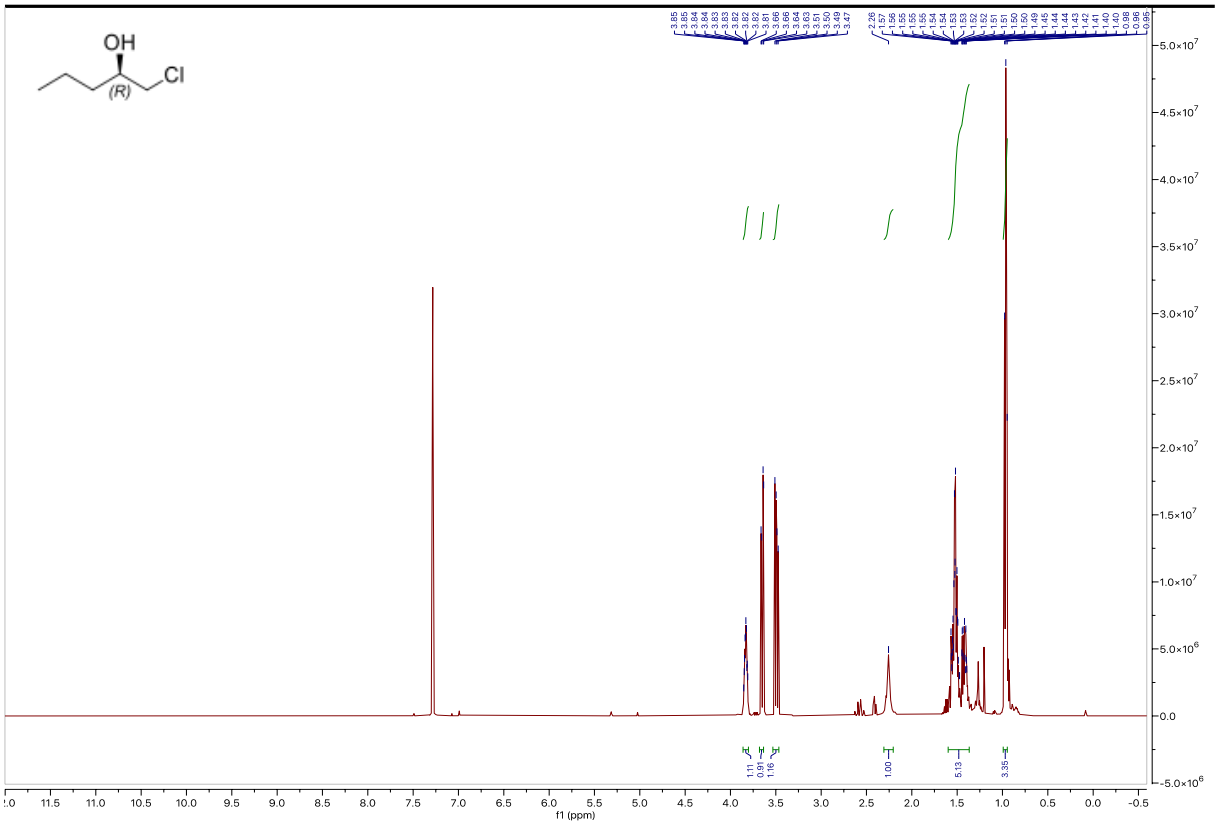
OH
Cl
(R)
f1 (ppm)

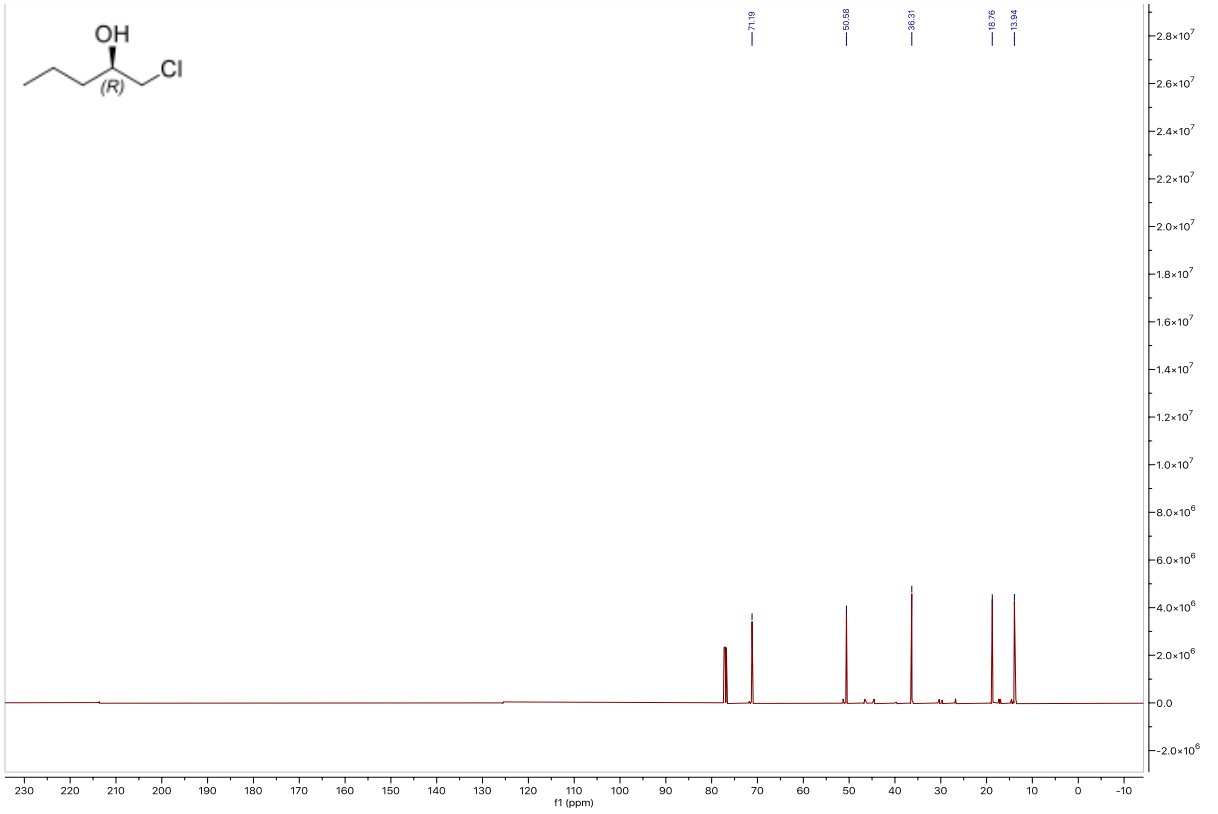
OH
Cl
(R)
71.19
50.58
36.31
18.76
13.94
f1 (ppm)

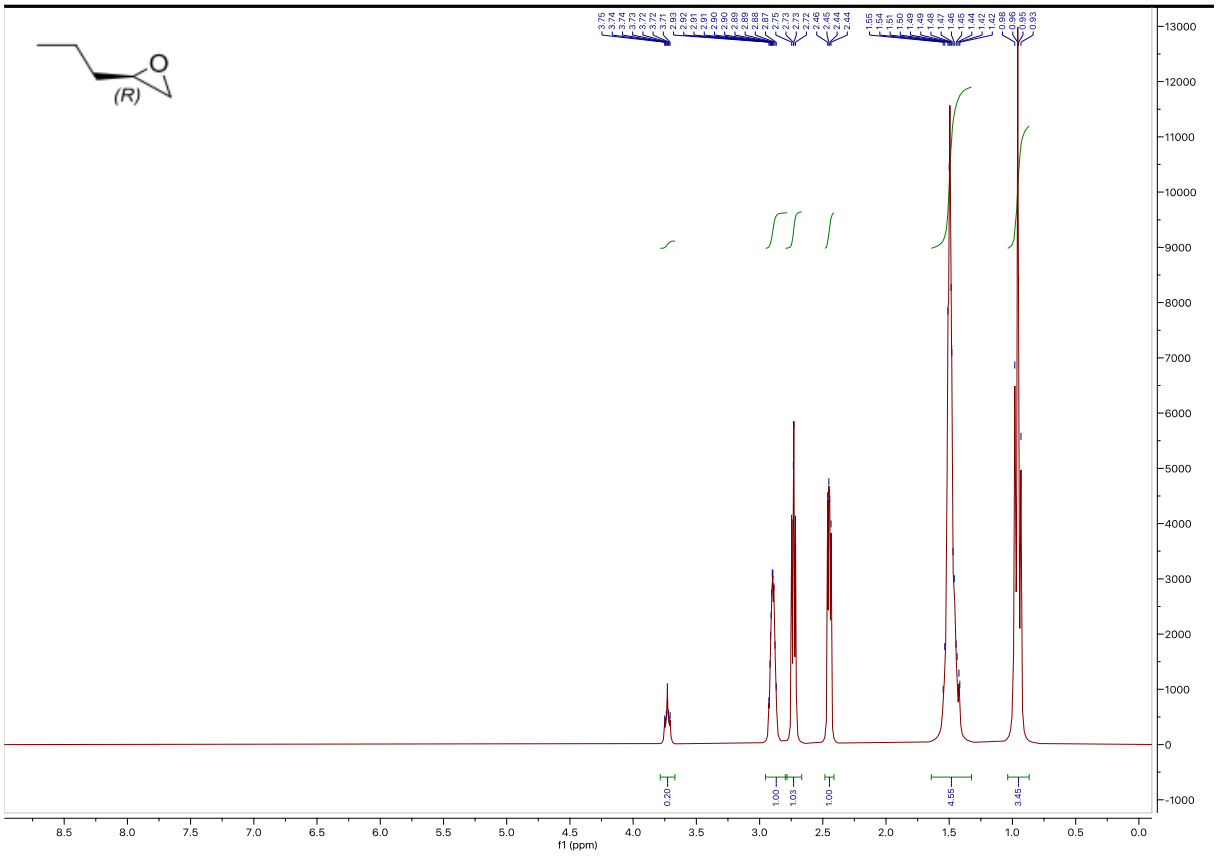
(R)
f1 (ppm)

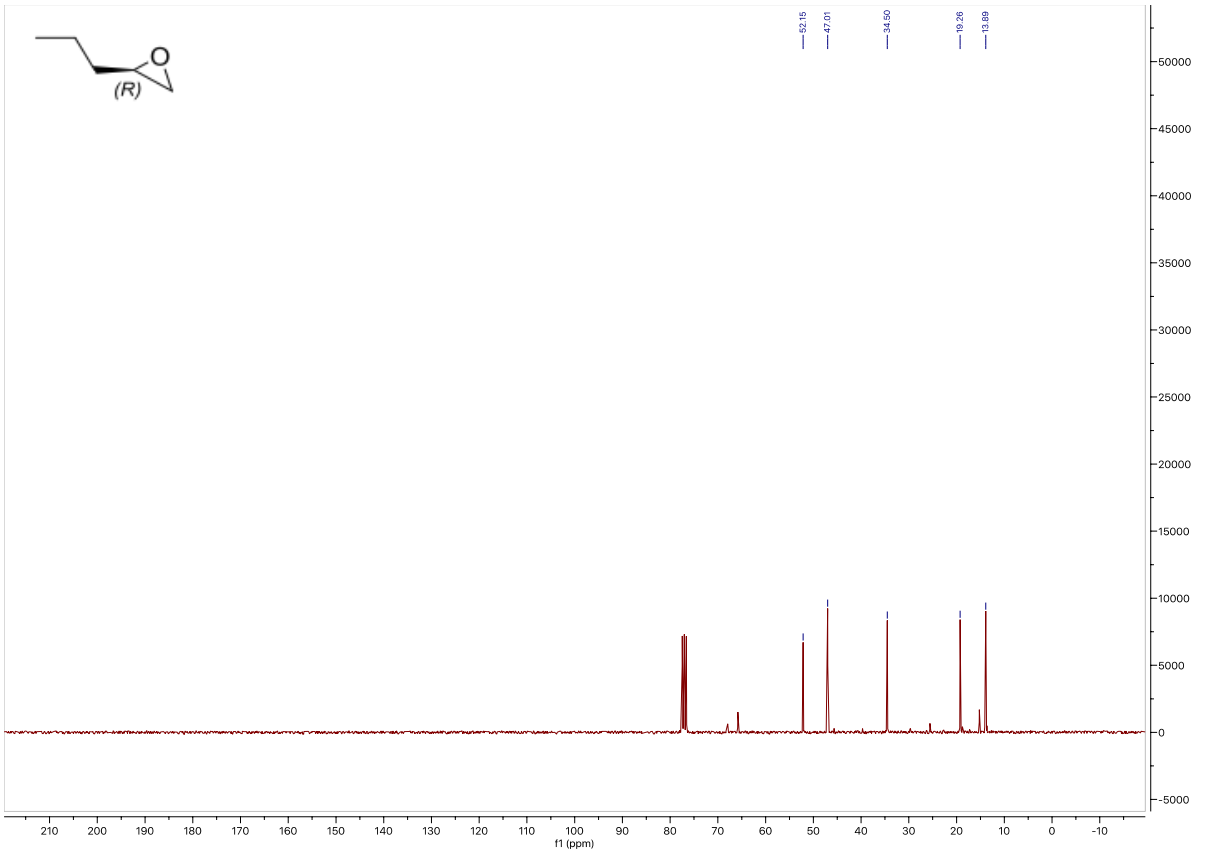
(R)
52.15
47.01
34.50
19.26
13.89
f1 (ppm)

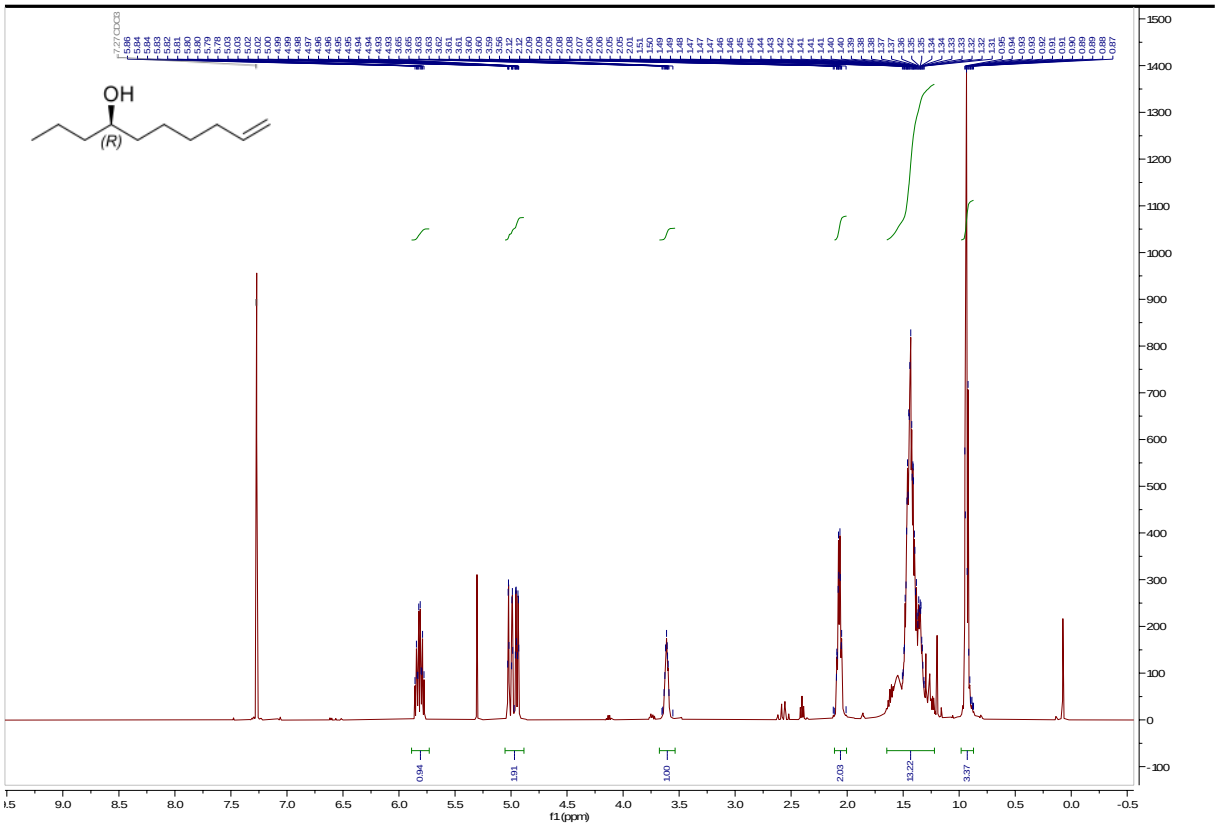
OH
(R)
f1 (ppm)

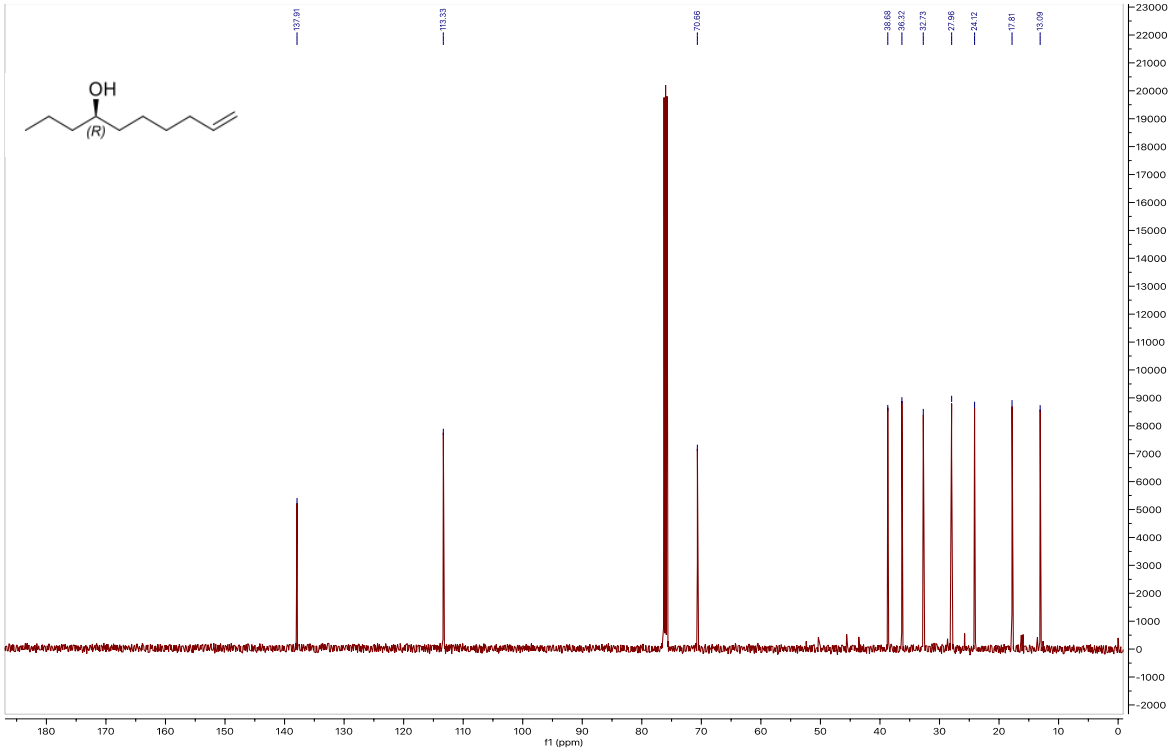
OH
(R)
137.91
113.33
70.66
38.68
38.32
32.73
27.96
24.12
17.81
13.09
f1 (ppm)

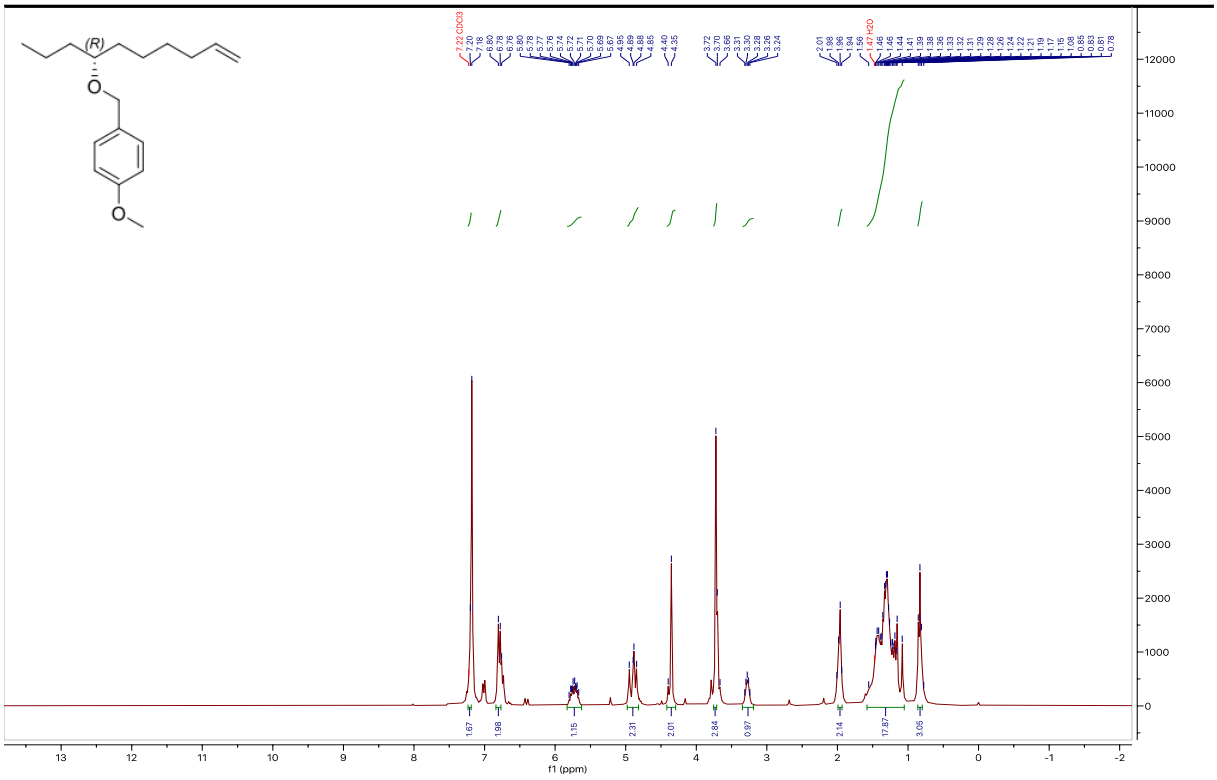
(R)
O
O
f1 (ppm)

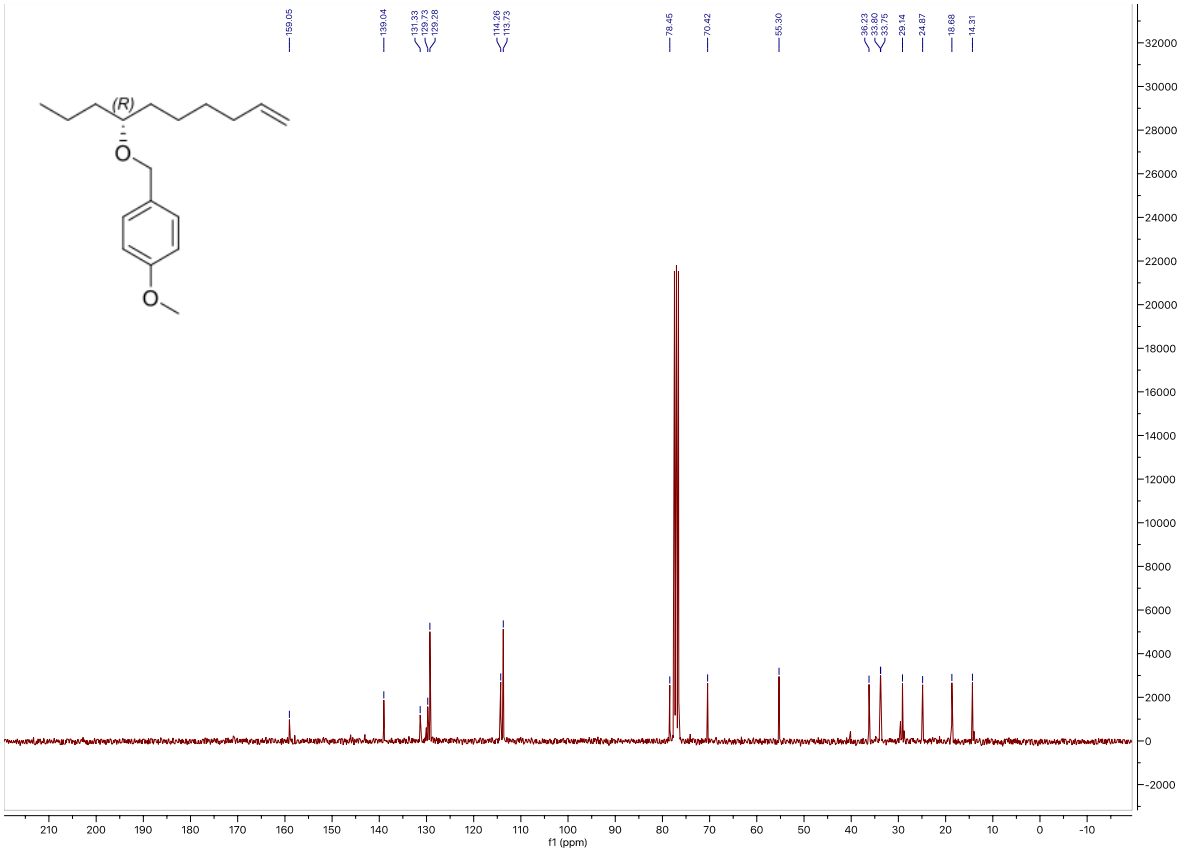
159.05
139.04
131.53
129.33
129.28
114.26
113.73
78.45
70.42
55.30
36.23
29.80
29.40
33.75
29.14
24.87
18.68
14.31
(R)
O
O
f1 (ppm)

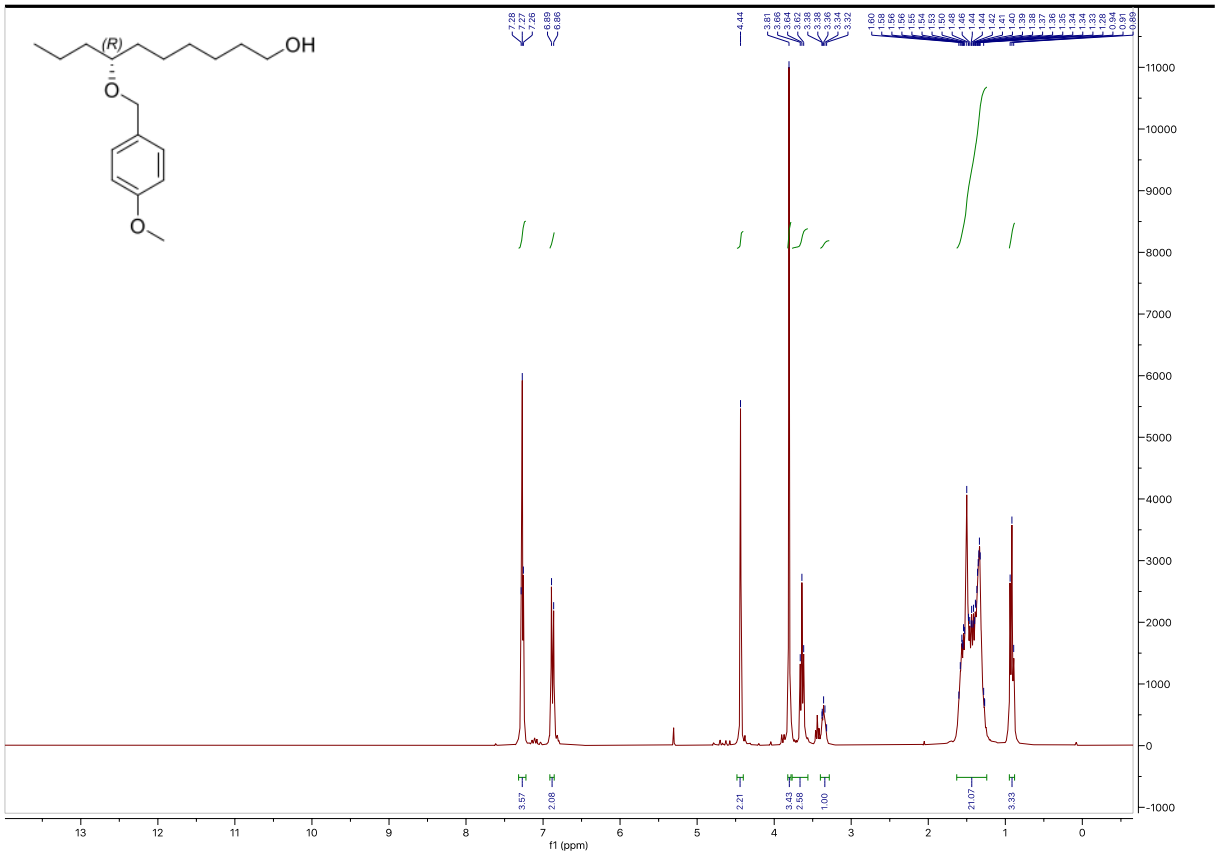
(R)
OH
O
O
f1 (ppm)

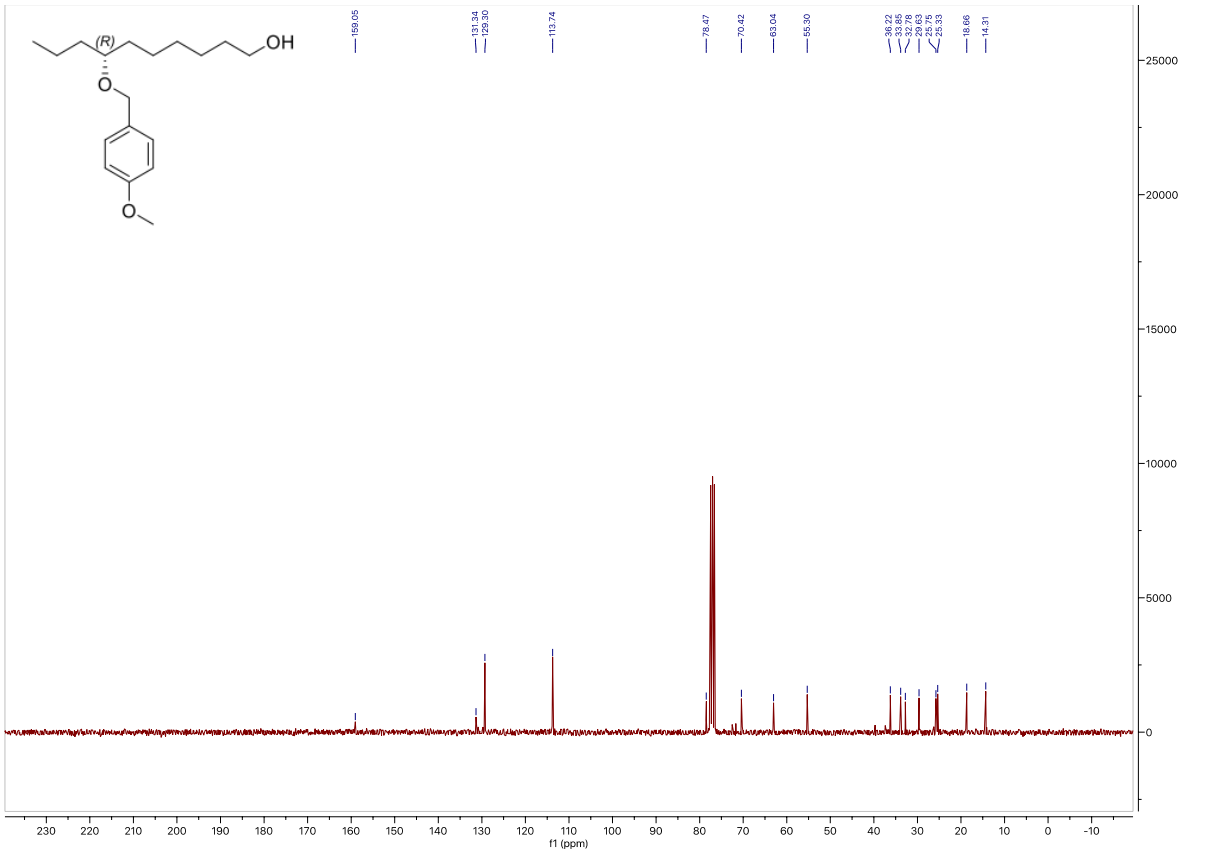
(R)
OH
O
O
f1 (ppm)

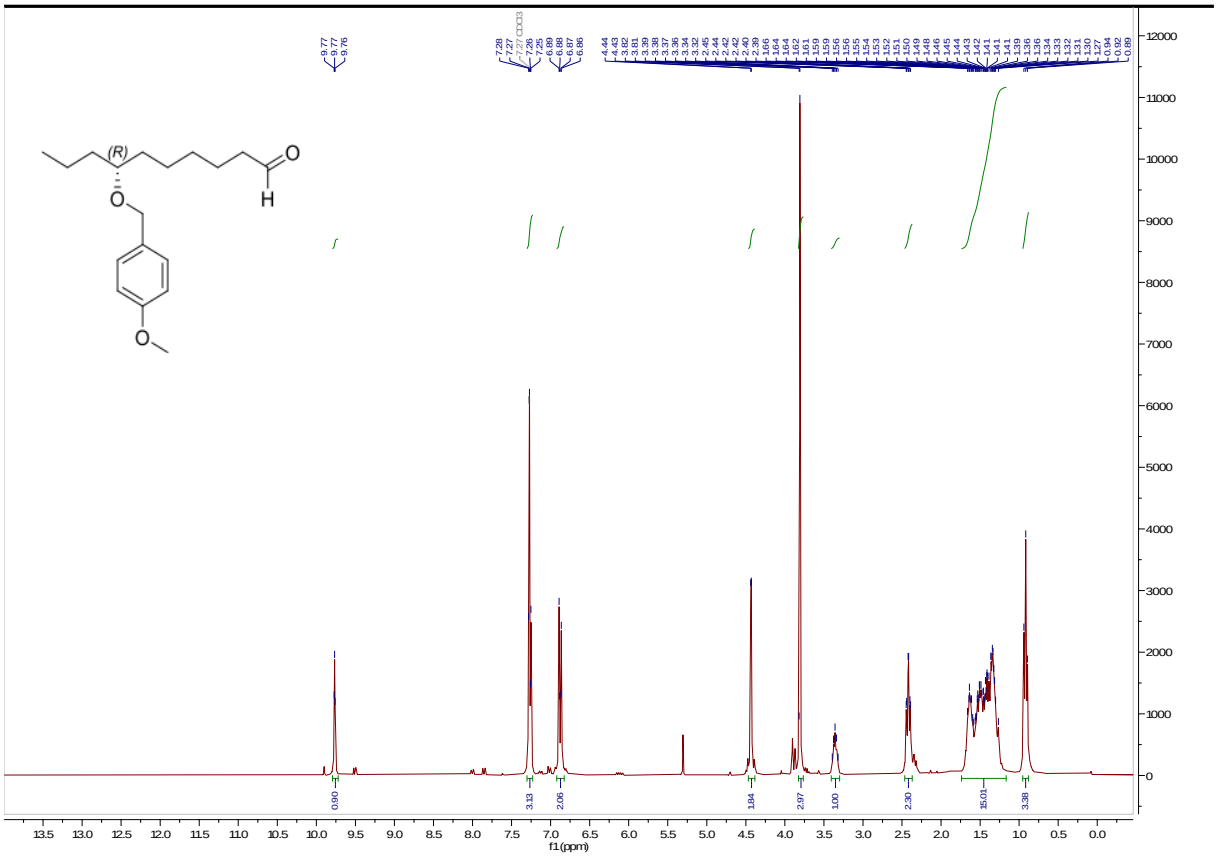
(R)
O
H
O
O
f1 (ppm)

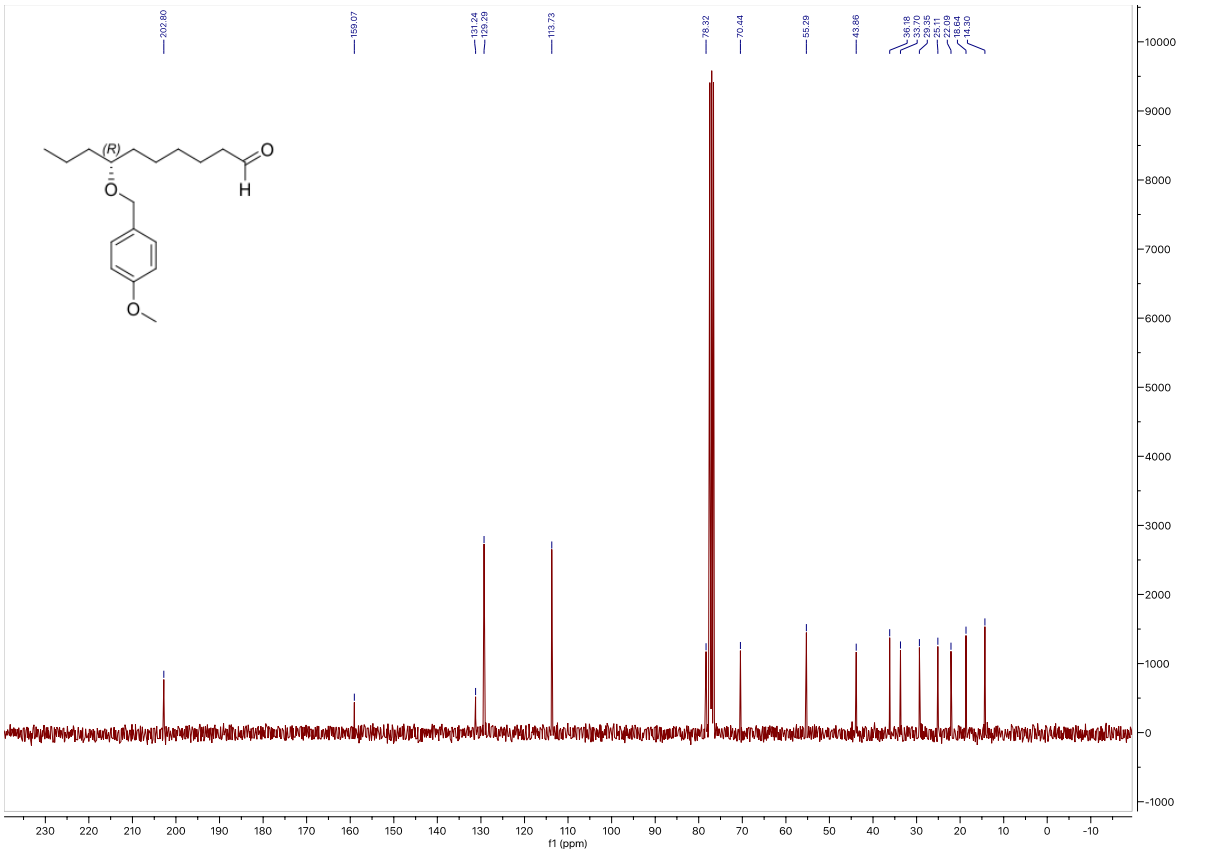
(R)
O
H
O
O
f1 (ppm)

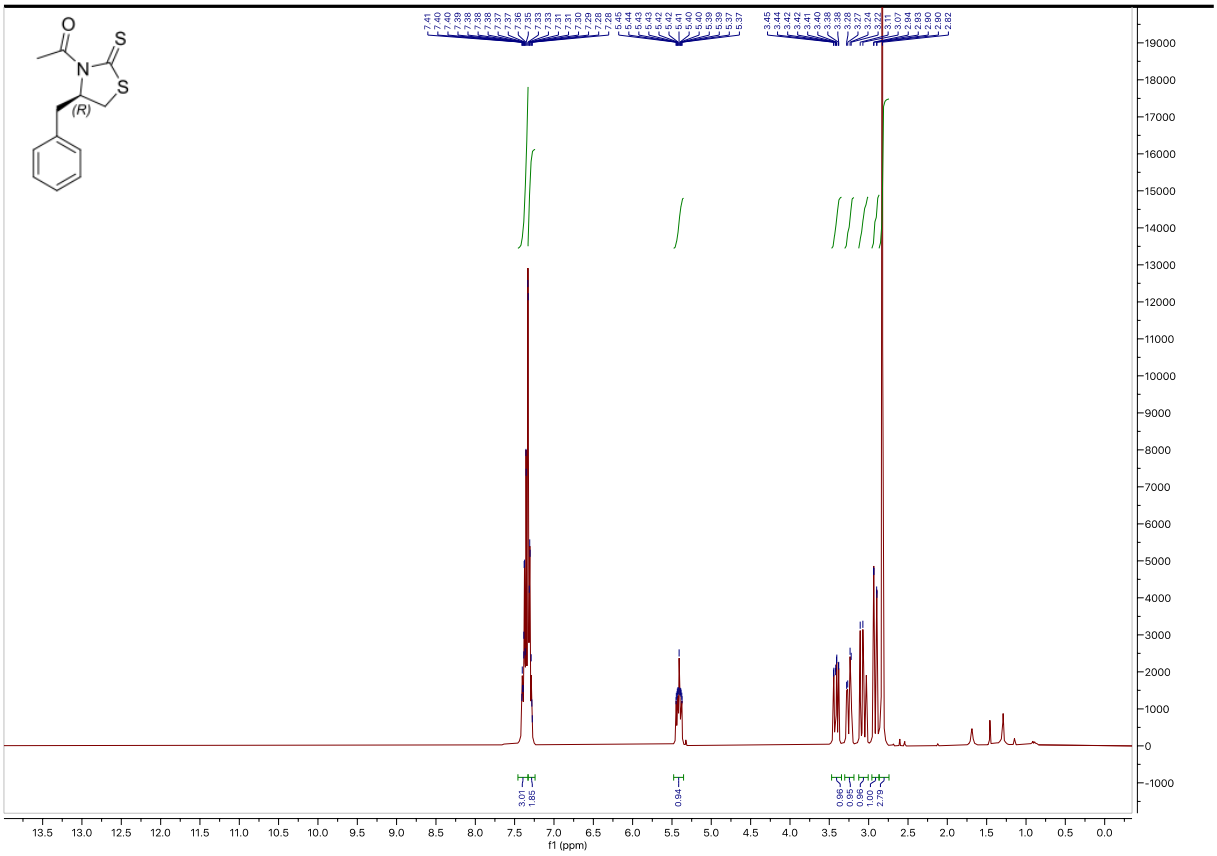
O
S
N
S
(R)
f1 (ppm)

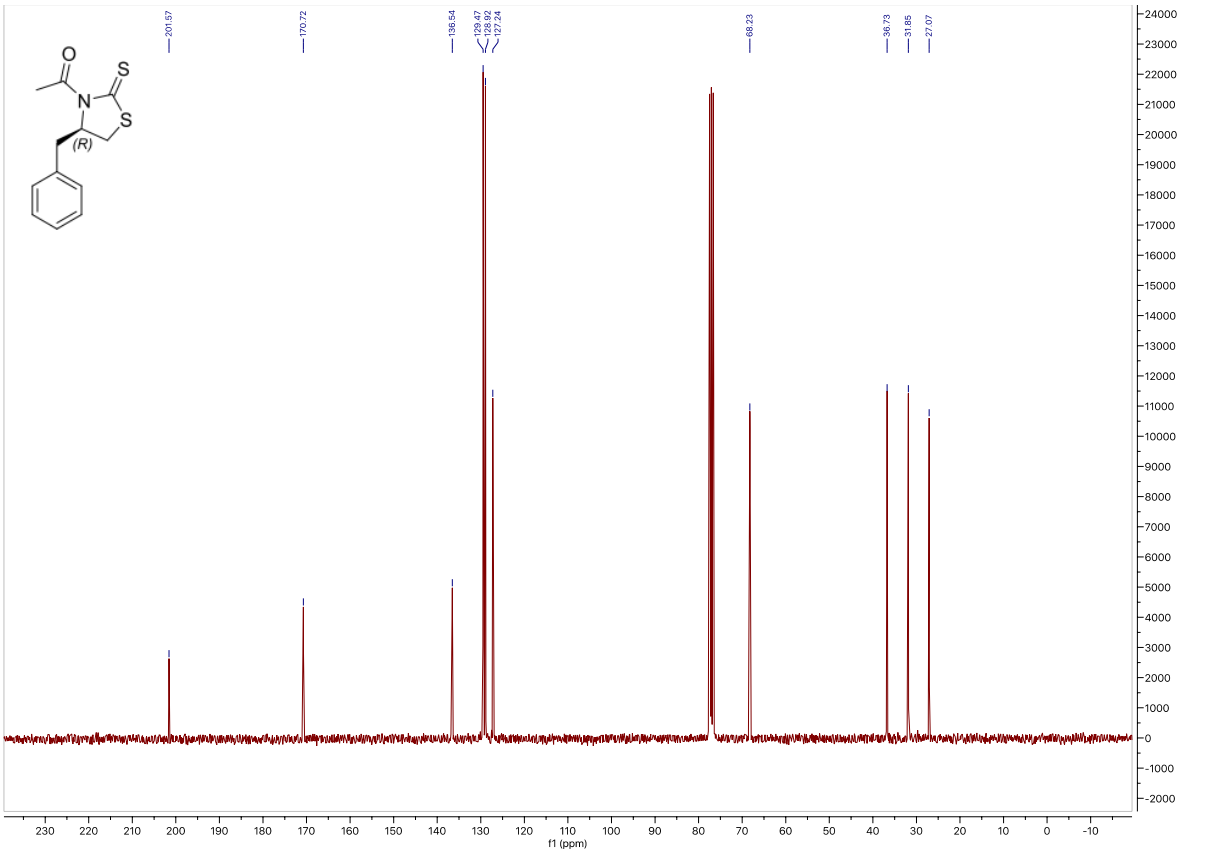
201.67
170.72
138.54
129.47
128.92
127.24
68.23
36.73
31.85
27.07
O
S
N
S
(R)
f1 (ppm)

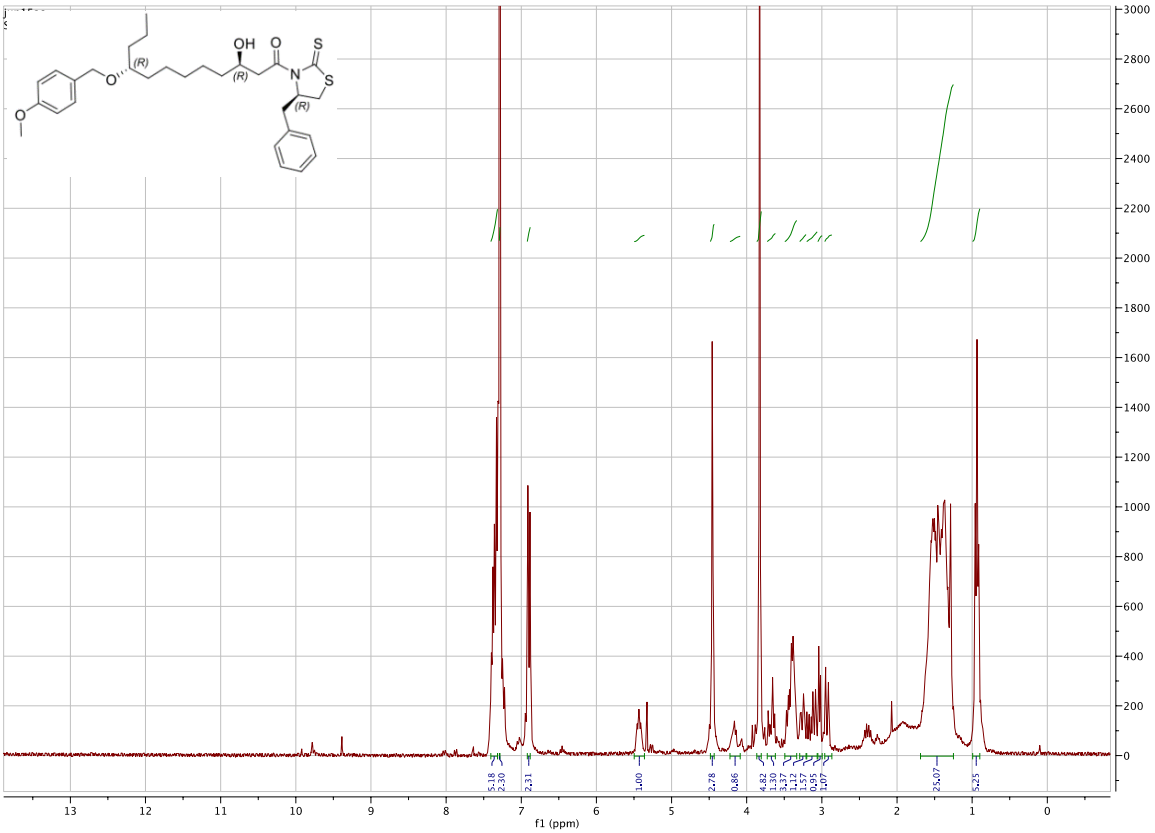
OH
O
S
N
S
(R)
(R)
(R)
O
f1 (ppm)

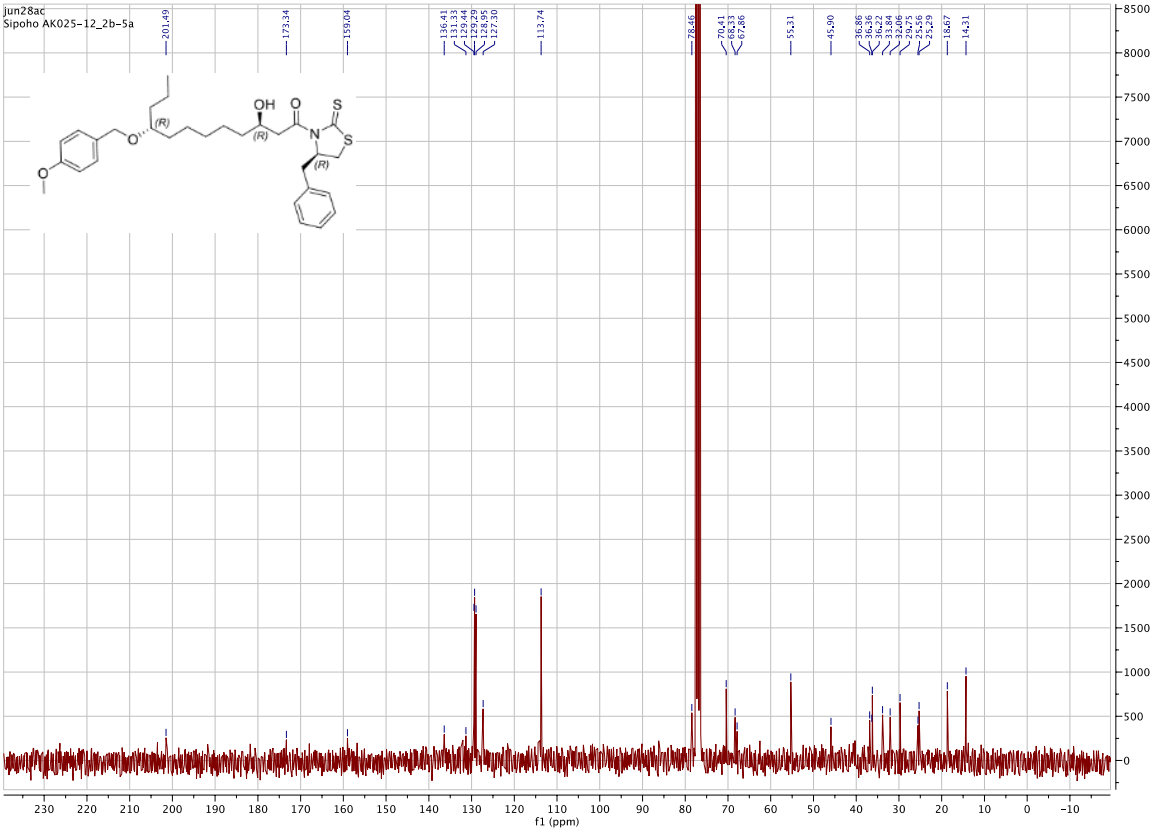
jun28ac
Sipoho AK025-12_2b-5a
OH
O
S
N
S
(R)
(R)
(R)
O
f1 (ppm)

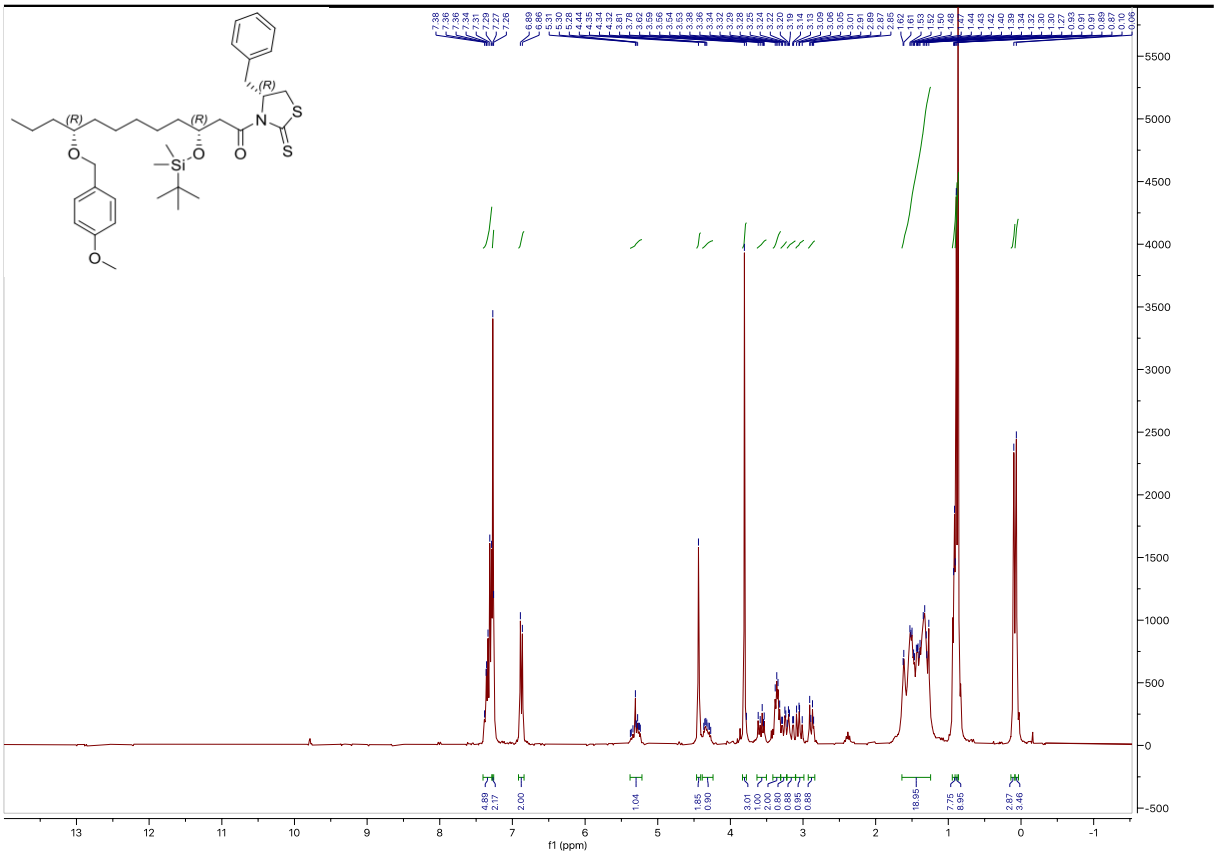
f1 (ppm)

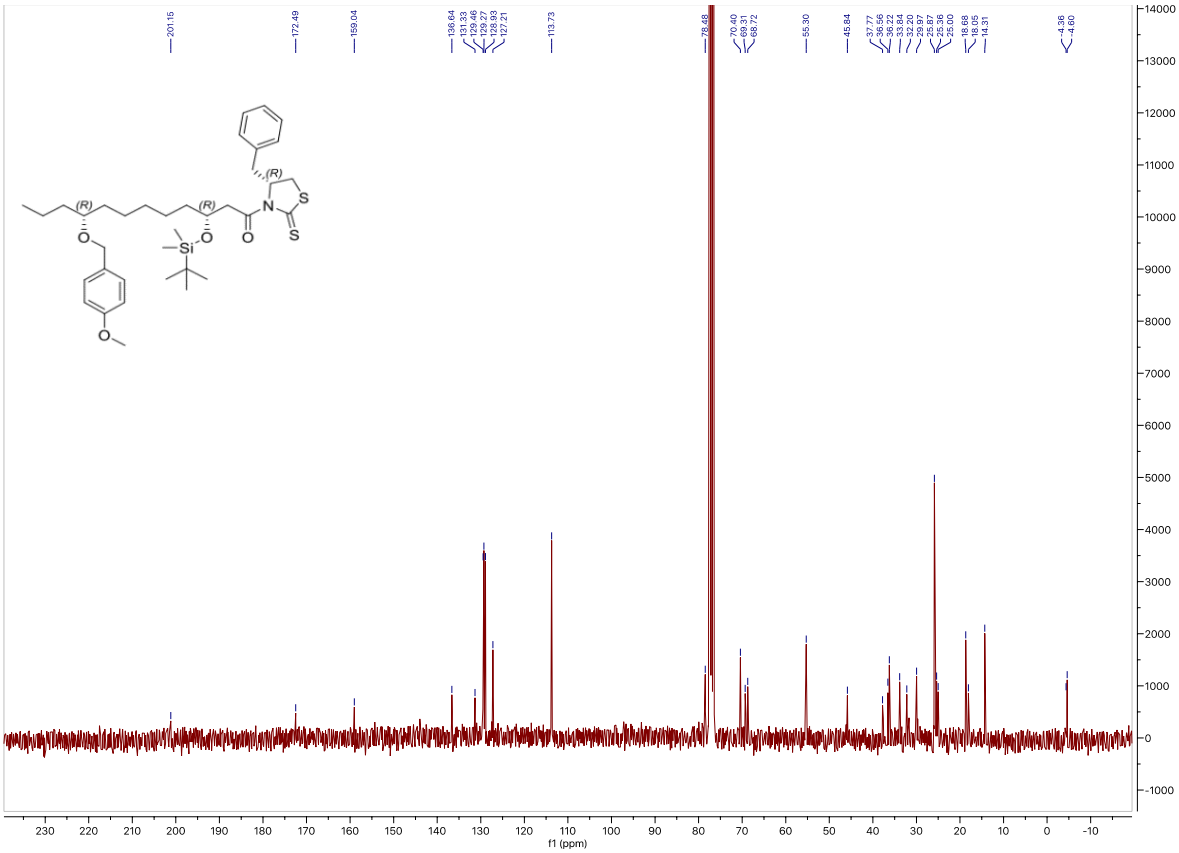
f1 (ppm)

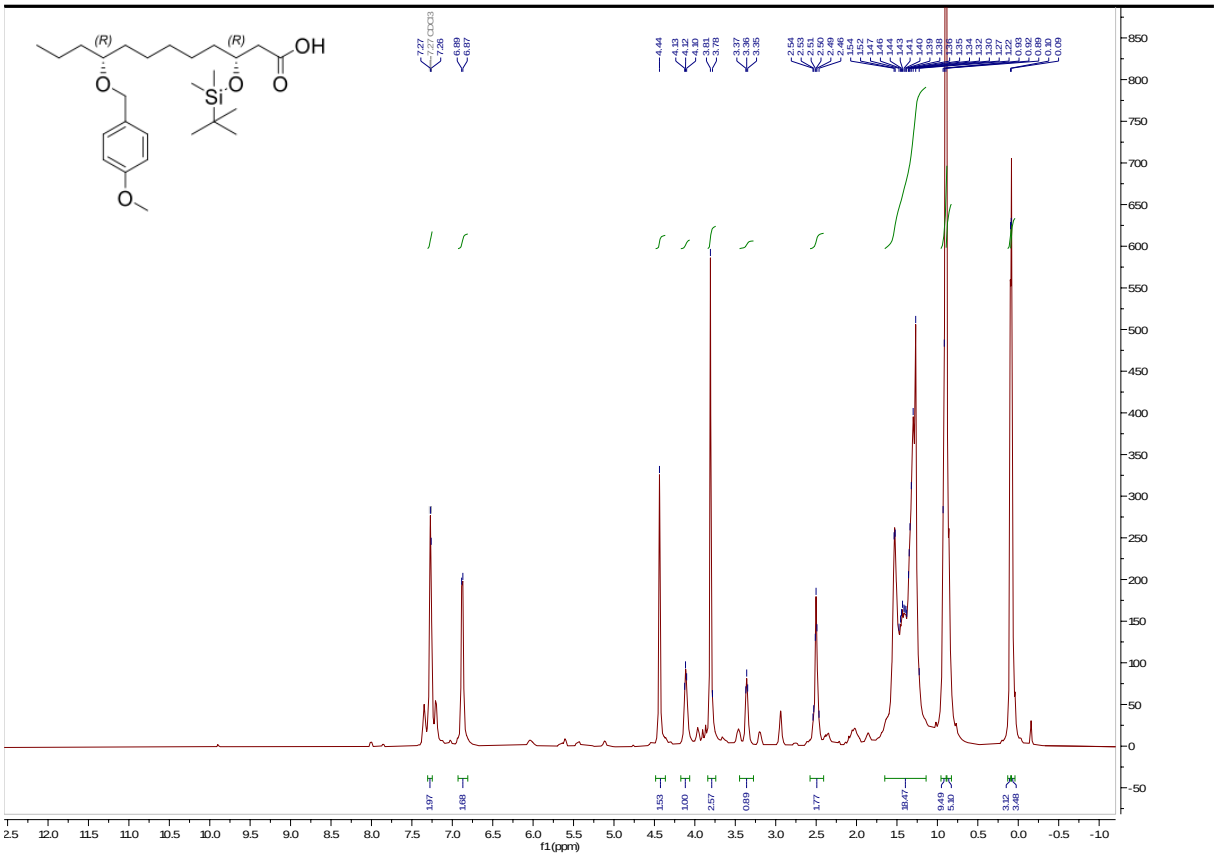
(R)
(R)
OH
O
Si
O
O
O
7.27
7.26
6.89
6.87
4.44
4.13
4.12
4.10
3.81
3.78
3.37
3.36
3.35
2.54
2.53
2.51
2.50
2.49
2.46
1.97
1.68
1.53
1.00
2.57
0.89
1.77
10.47
9.49
5.30
3.12
3.48
f1 (ppm)

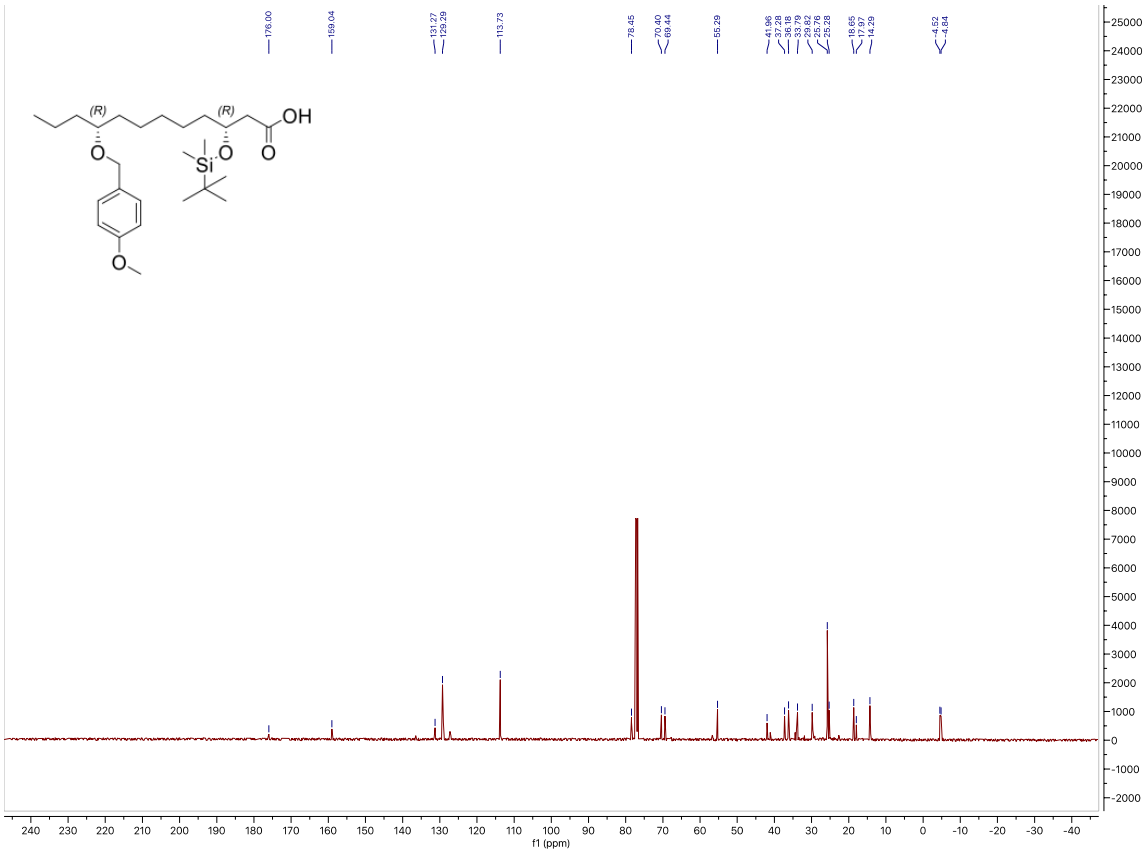
(R)
(R)
OH
O
Si
O
O
O
176.00
169.04
131.27
129.29
113.73
78.45
70.40
69.44
55.29
41.96
37.78
36.18
33.79
29.82
27.76
25.28
18.65
18.07
14.29
4.62
4.84
f1 (ppm)

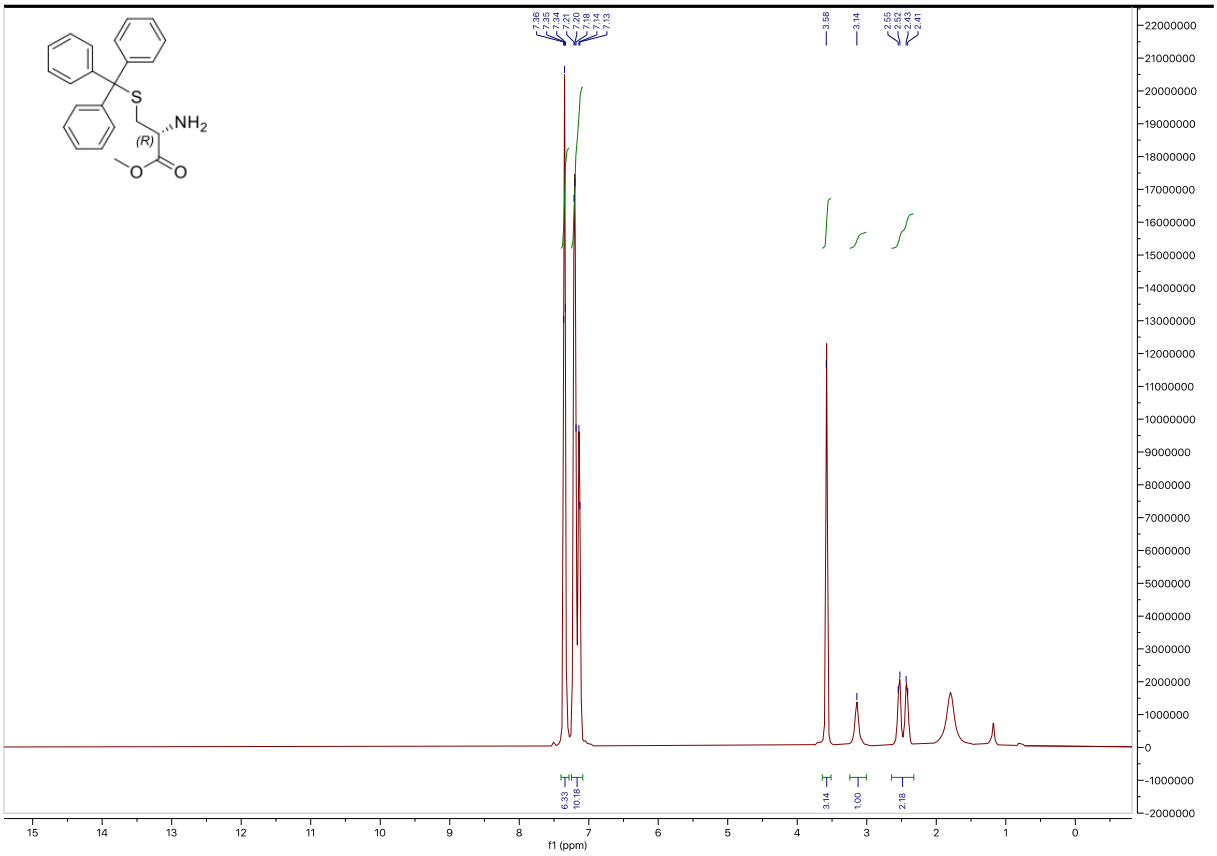
7.36
7.35
7.34
7.21
7.20
7.19
7.14
7.13
3.58
3.14
2.55
2.53
2.43
2.41
NH2
(R)
O
O
S
6.33
10.18
3.14
1.00
2.18
f1 (ppm)

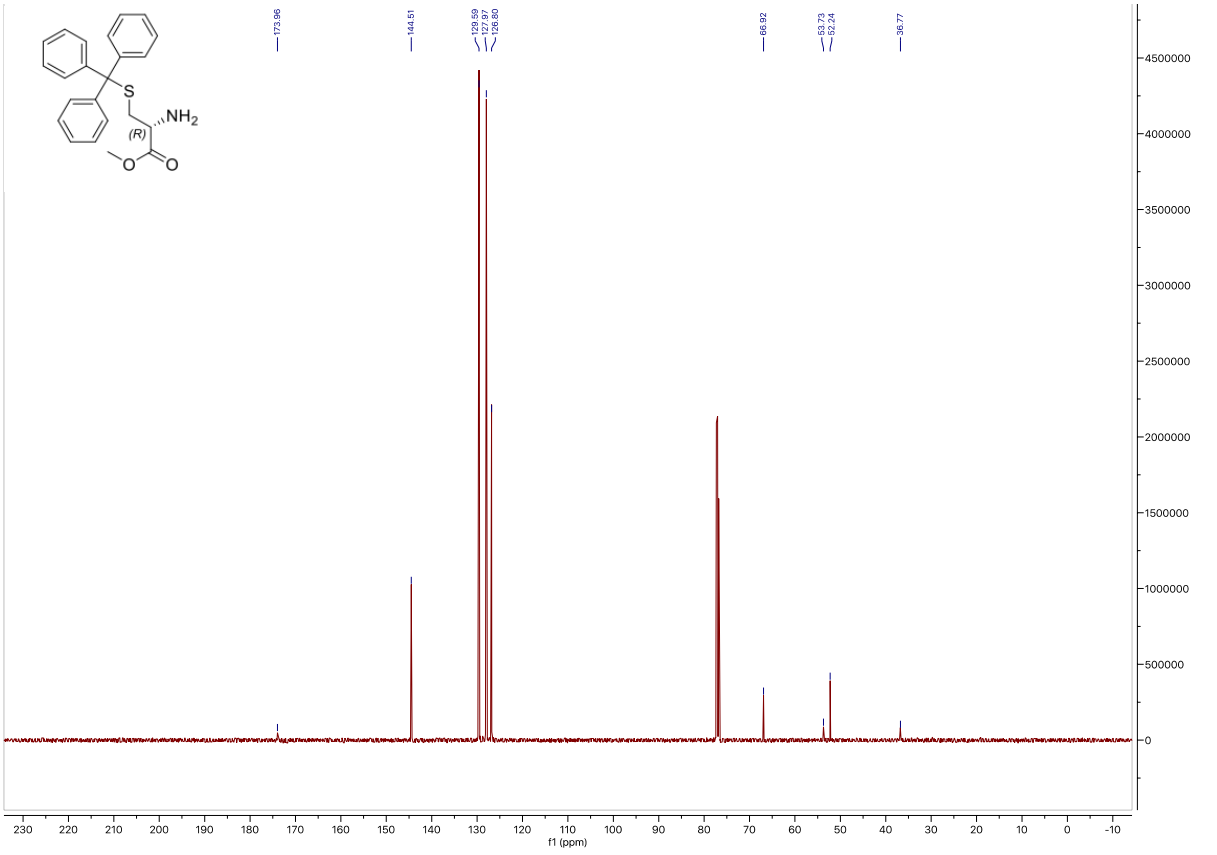
173.96
144.51
129.59
127.97
126.80
66.92
53.73
52.24
35.77
NH2
(R)
O
O
S
f1 (ppm)

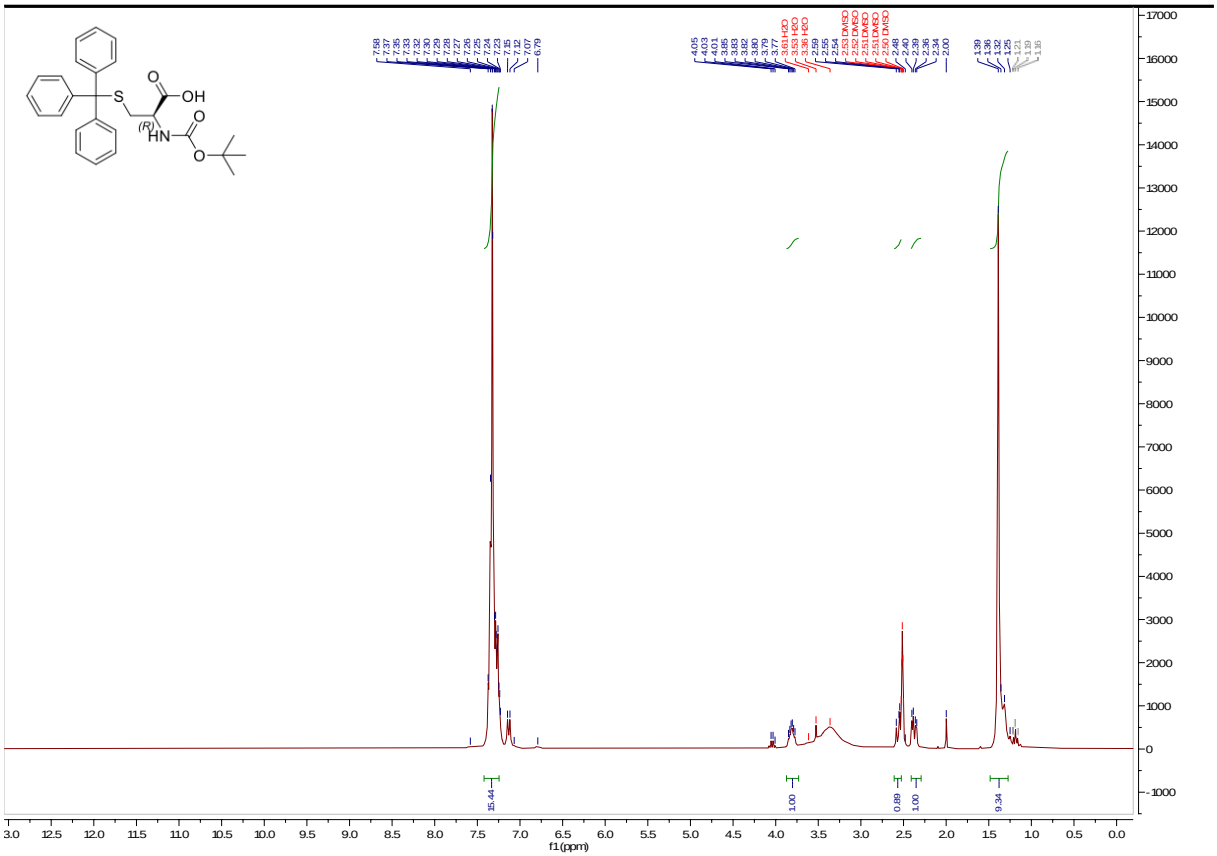
7.58
7.37
7.35
7.33
7.32
7.30
7.29
7.28
7.27
7.26
7.25
7.24
7.23
7.15
7.12
7.07
6.79
4.05
4.03
4.01
3.85
3.83
3.82
3.80
3.79
3.77
3.61 HDO
3.53 HDO
3.36 HDO
2.59
2.55
2.54
2.53 DMSO
2.52 DMSO
2.51 DMSO
2.50 DMSO
2.48
2.40
2.38
2.36
2.34
2.00
1.39
1.36
1.35
1.25
1.21
1.19
1.16
15.44
1.00
0.89
1.00
9.34
f1 (ppm)

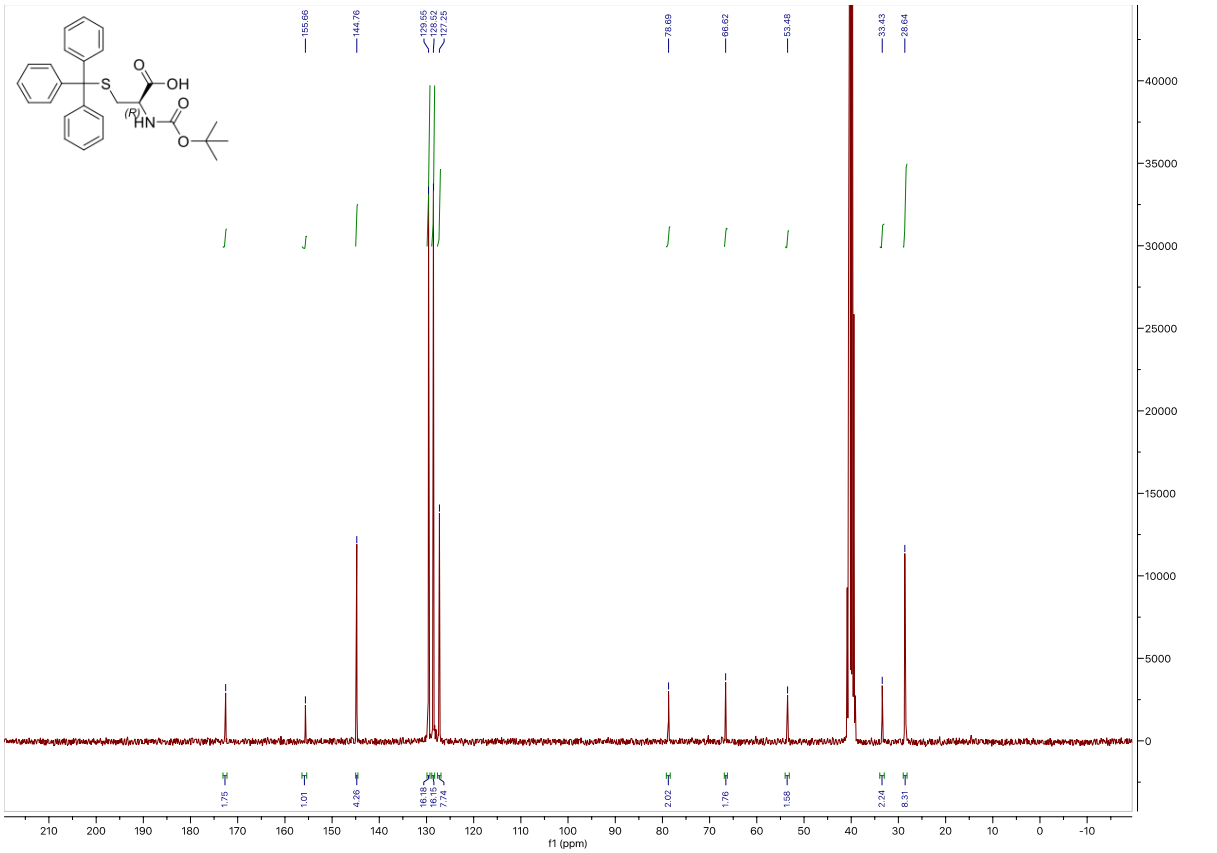
155.66
144.76
129.55
128.52
127.25
78.69
66.62
53.48
33.43
28.64
1.75
1.01
4.26
16.18
16.15
7.74
2.02
1.76
1.58
2.24
8.31
f1 (ppm)

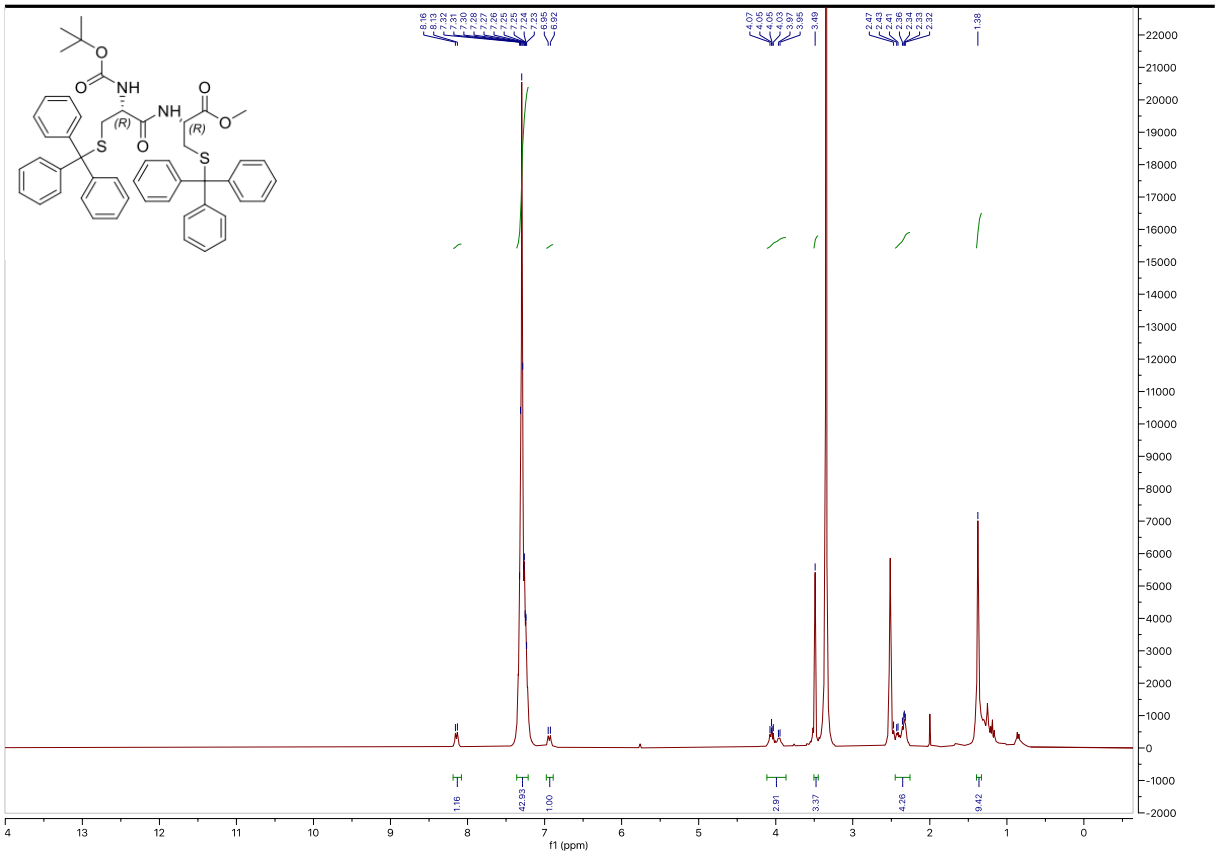
8.16
8.13
7.32
7.31
7.30
7.28
7.27
7.26
7.25
7.24
7.23
6.95
6.92
4.07
4.05
4.04
4.03
3.97
3.95
3.49
2.47
2.43
2.41
2.36
2.34
2.33
2.32
1.38
1.16
42.93
1.00
2.91
3.37
4.26
9.42
f1 (ppm)

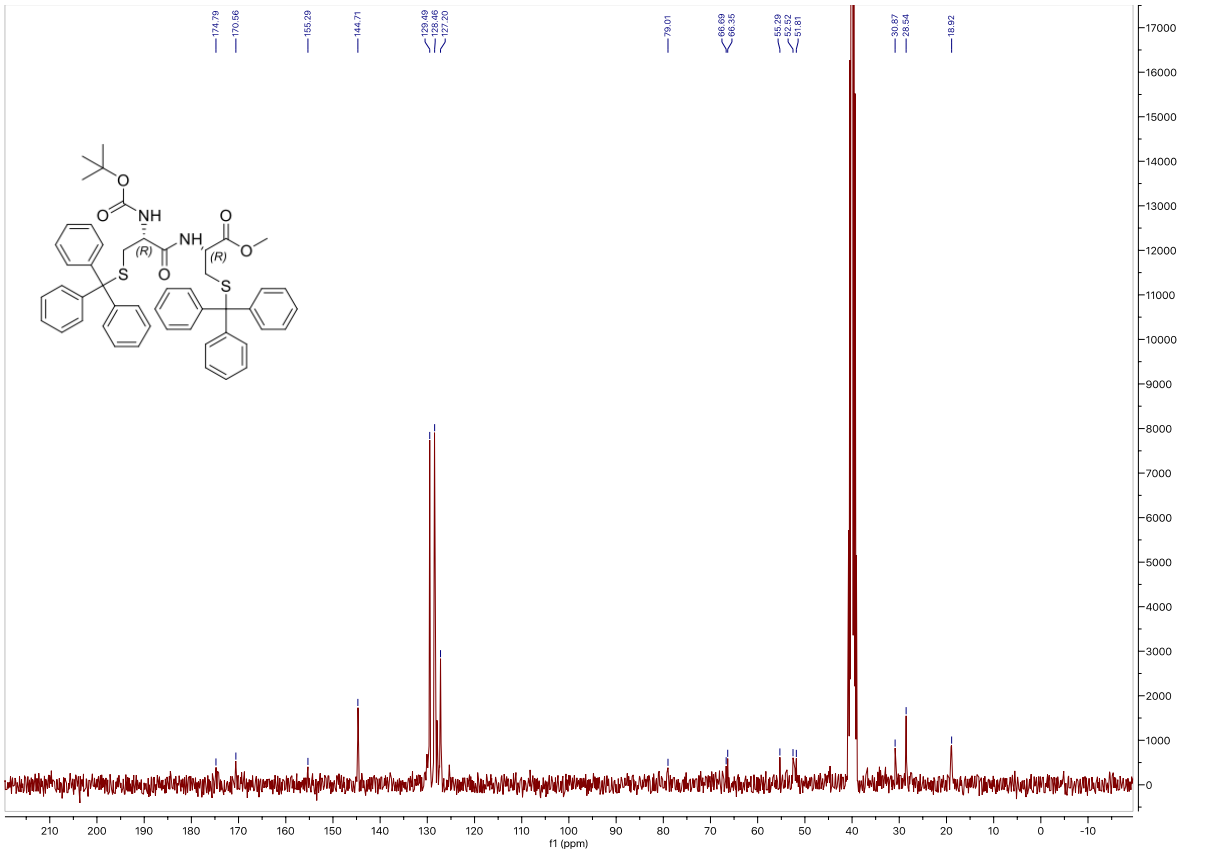
174.79
170.66
155.29
144.71
129.49
129.46
127.20
79.01
66.69
66.35
55.29
52.52
51.81
30.87
28.54
18.92
f1 (ppm)

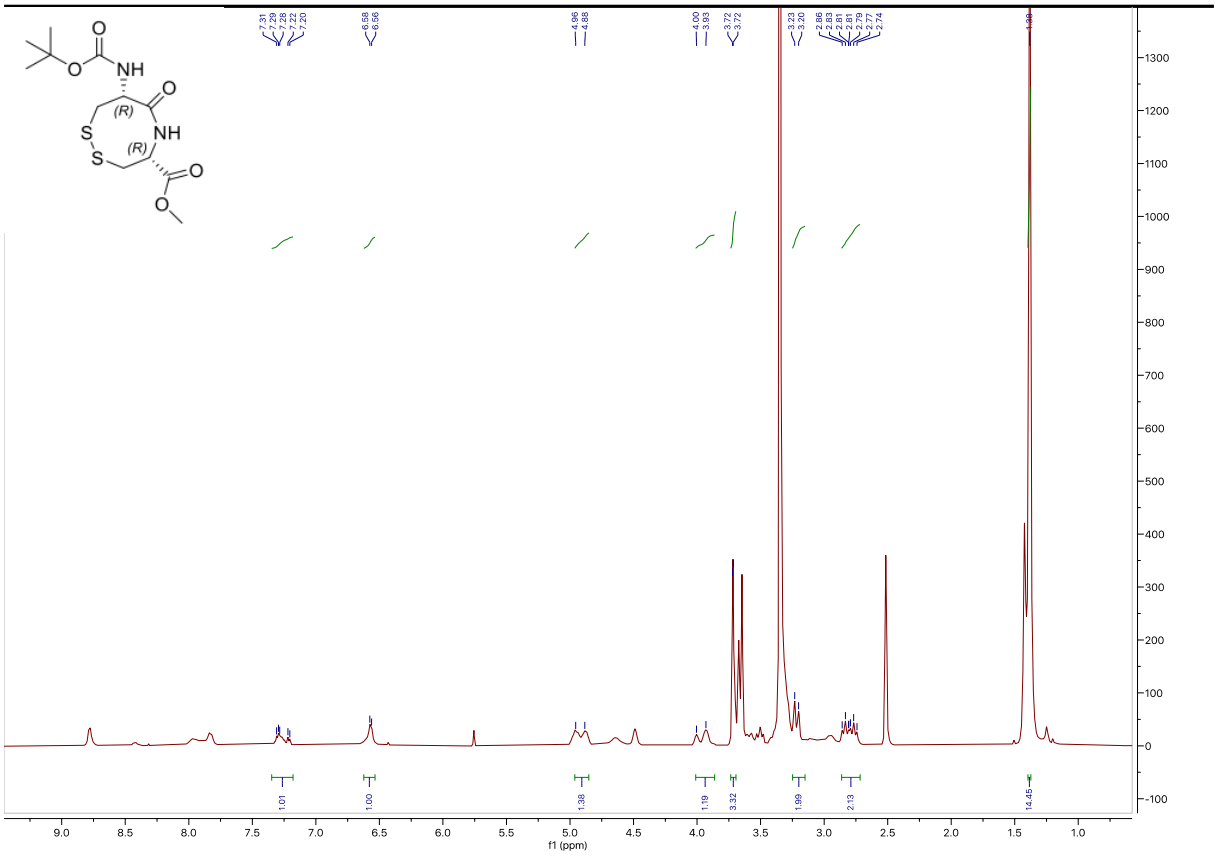
7.31
7.29
7.28
7.22
7.20
6.58
6.56
4.95
4.88
4.00
3.89
3.72
3.72
3.23
3.20
2.86
2.83
2.81
2.79
2.77
2.74
1.66
1.01
1.00
1.38
1.19
3.32
1.99
2.13
14.45
f1 (ppm)

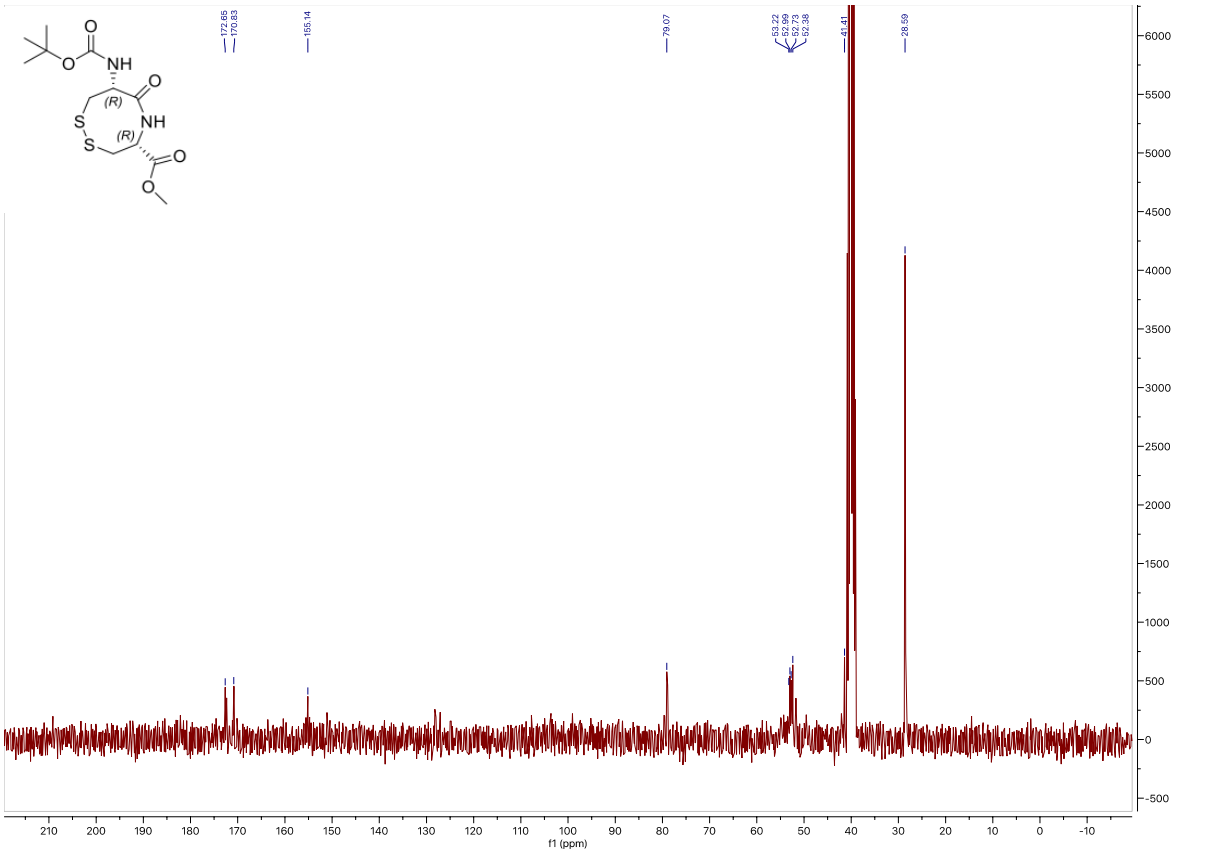
172.65
170.83
155.14
79.07
63.22
62.99
62.73
62.38
41.41
28.59
f1 (ppm)

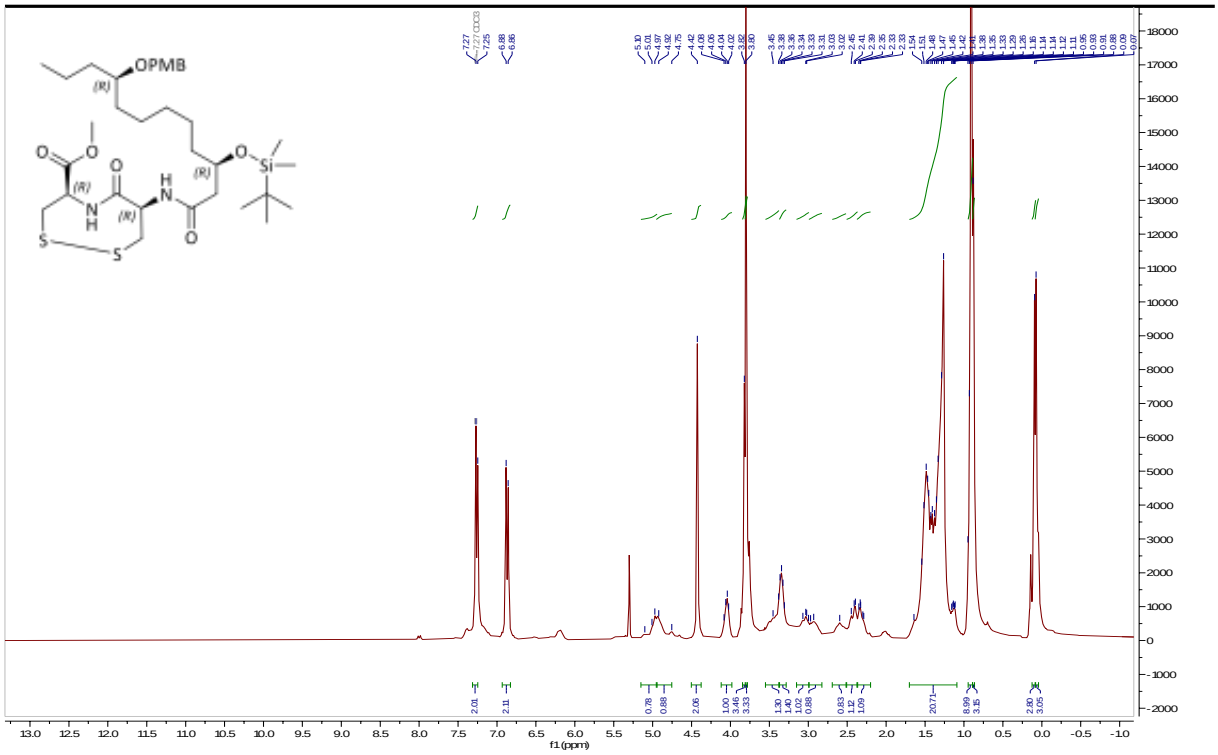
OPMB
f1 (ppm)

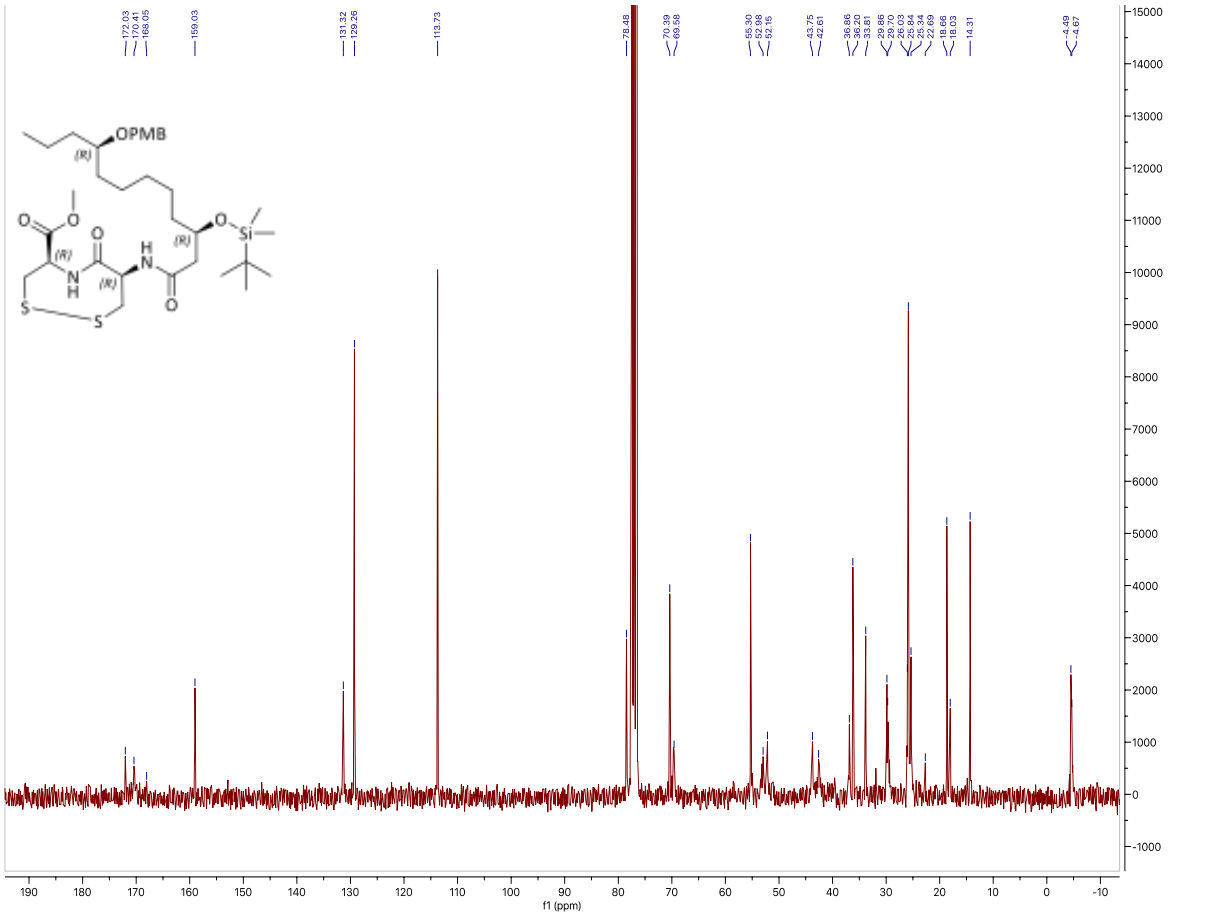
OPMB
f1 (ppm)

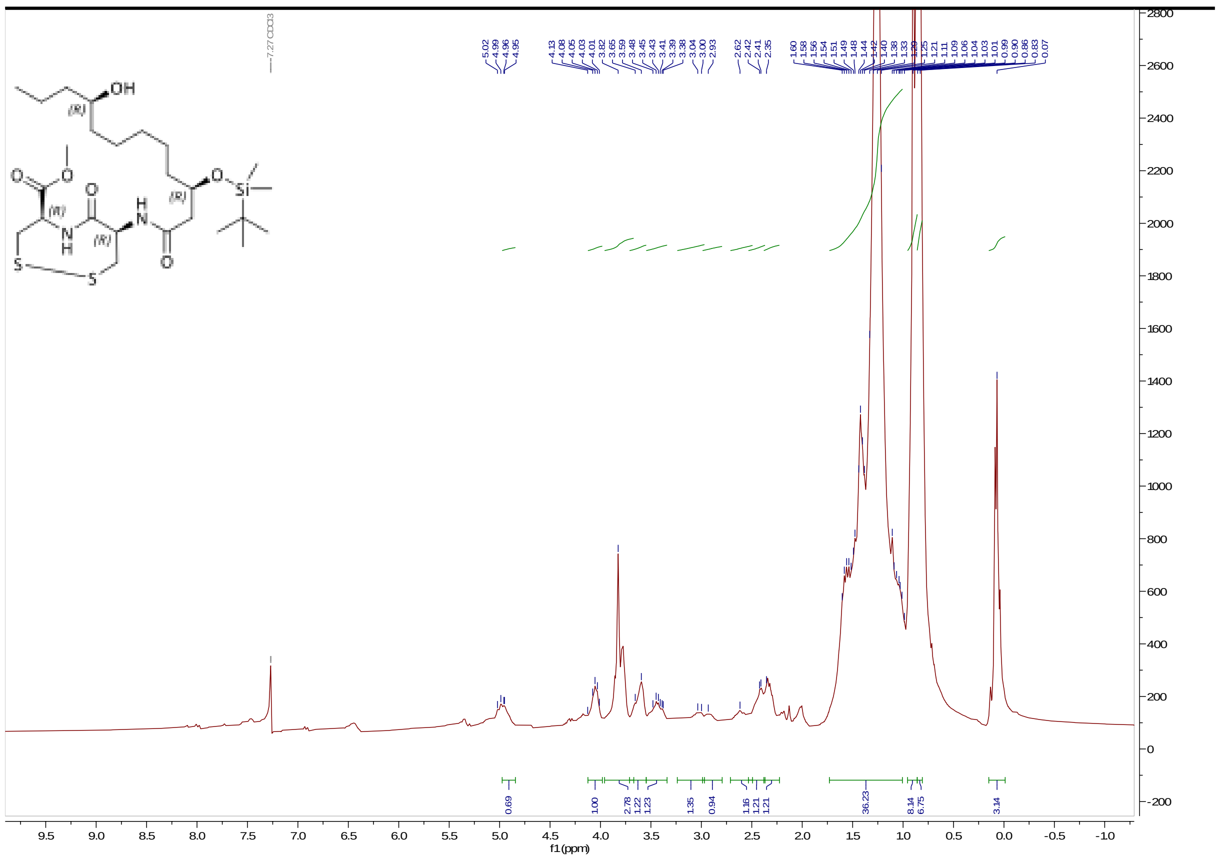

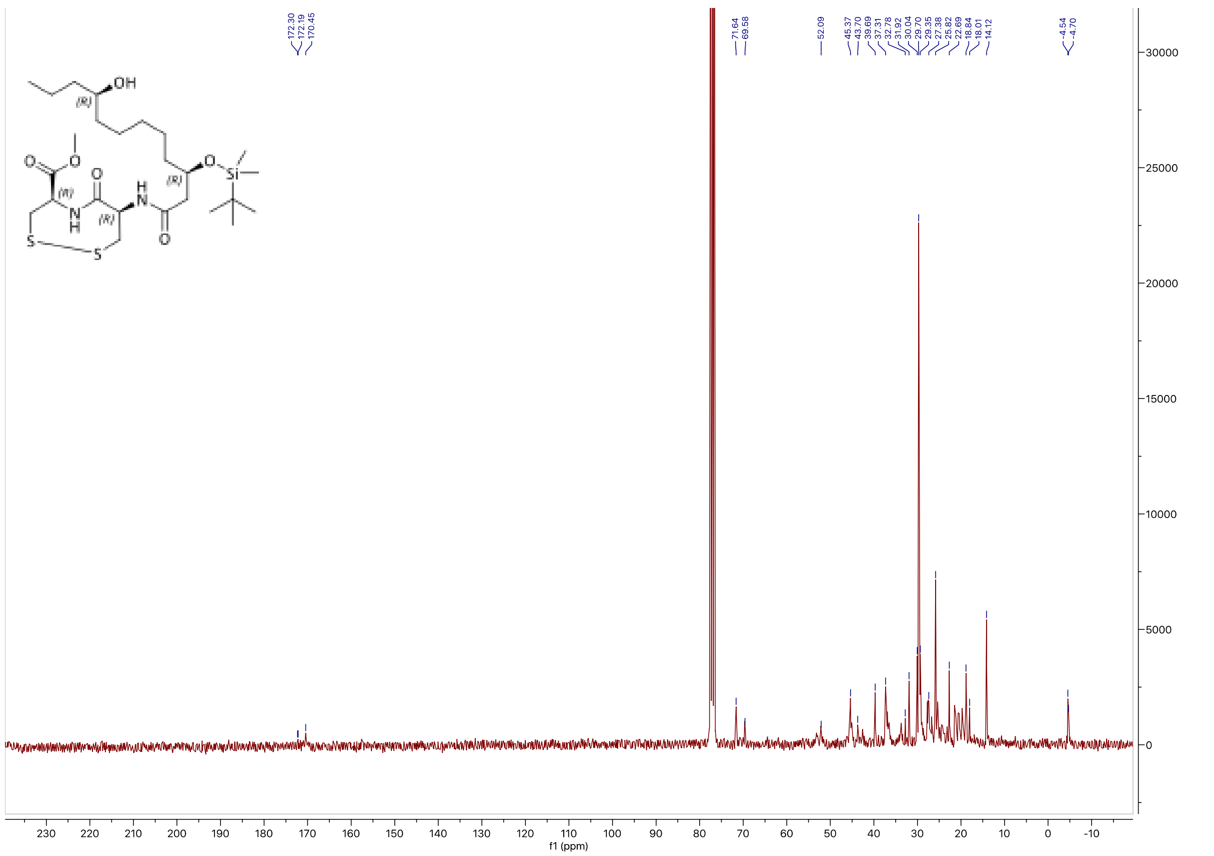

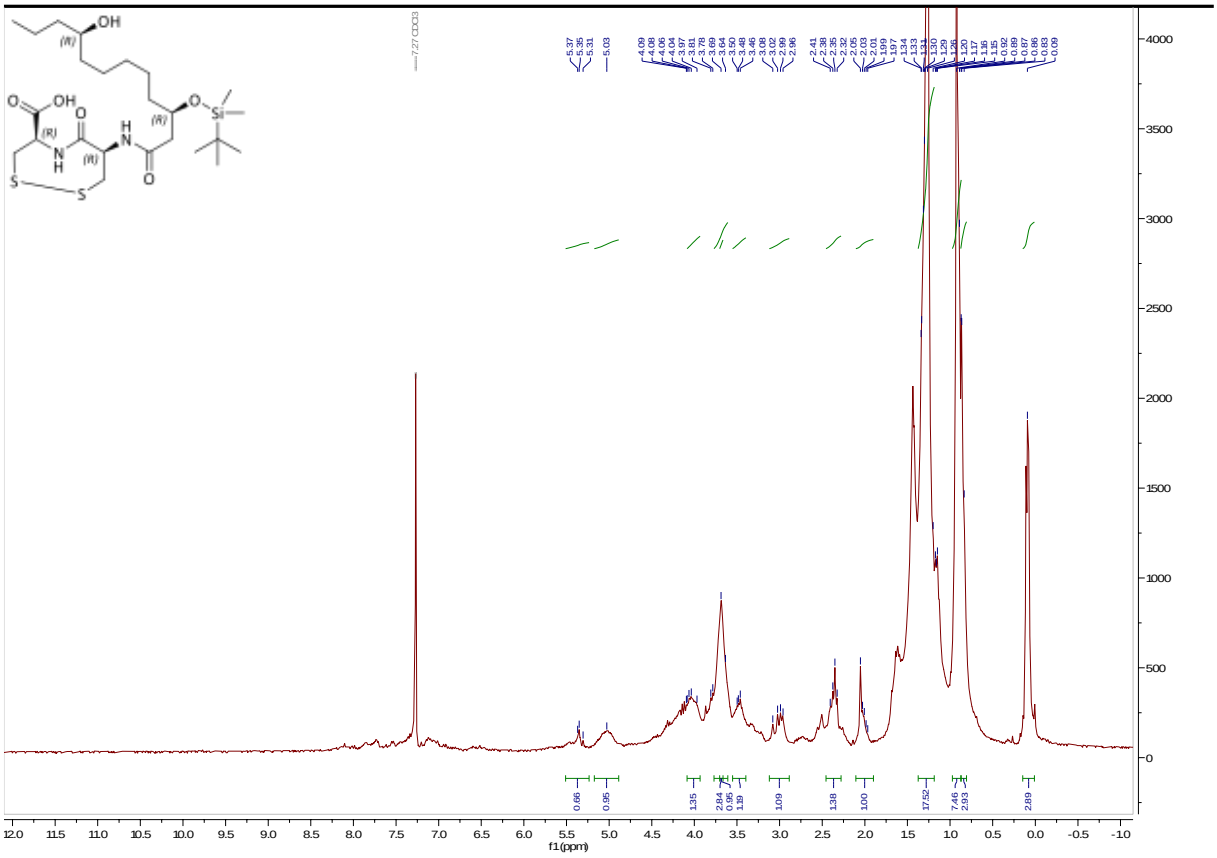
OH
(R)
OH
O
(R)
N
H
(R)
H
N
(R)
O
O
Si
S
S
O
7.27 CDCl3
5.37
5.35
5.31
5.03
4.09
4.08
4.06
4.04
3.97
3.81
3.79
3.69
3.64
3.50
3.48
3.46
3.08
3.02
2.98
2.96
2.41
2.38
2.35
2.32
2.25
2.03
2.01
1.99
1.97
1.34
1.33
1.31
1.30
1.29
1.28
1.20
1.17
1.16
1.15
1.05
0.92
0.89
0.87
0.86
0.83
0.09
0.66
0.95
1.35
2.84
0.95
1.39
1.09
1.38
1.00
17.52
7.46
2.93
2.89
f1 (ppm)

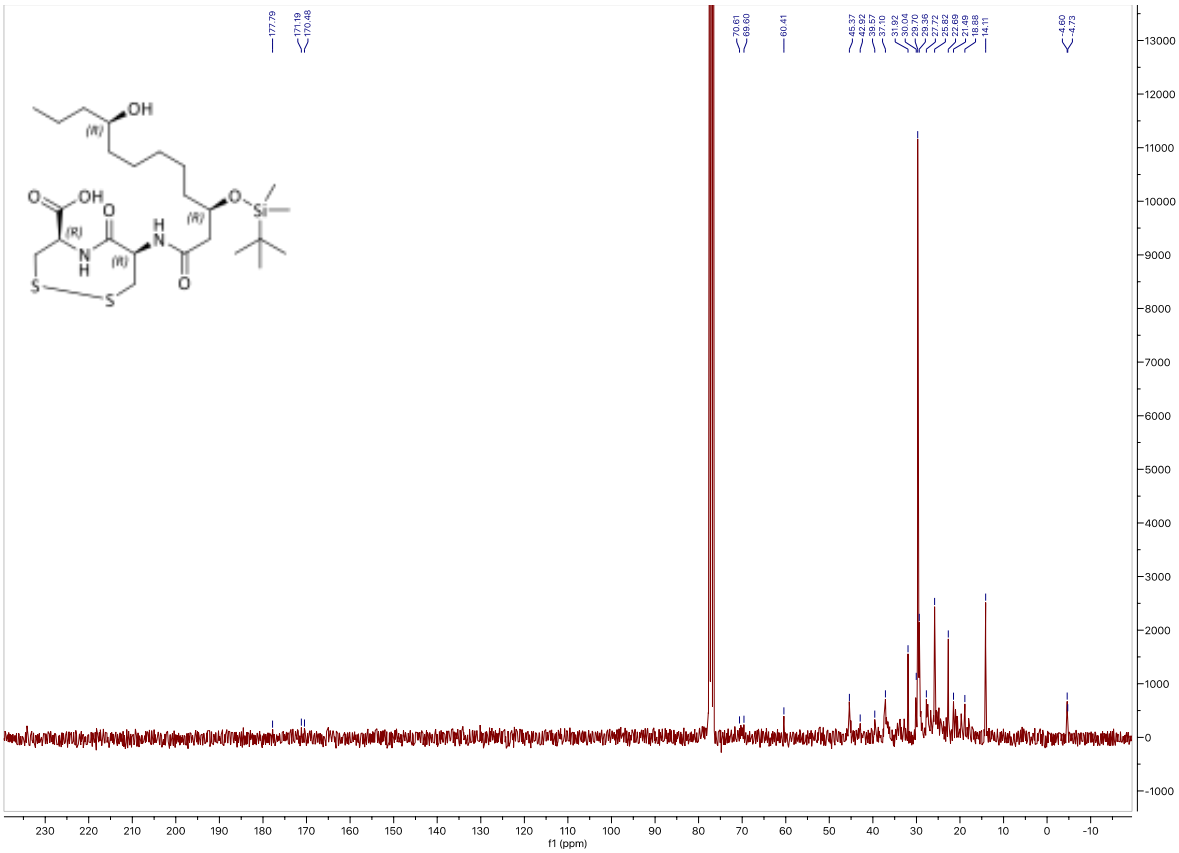
OH
(R)
OH
O
(R)
N
H
(R)
H
N
(R)
O
O
Si
S
S
O
177.79
171.19
170.48
70.61
69.60
60.41
45.37
42.92
39.57
37.70
31.92
30.04
29.70
29.35
27.72
25.82
22.69
21.49
18.88
14.11
-4.60
-4.73
f1 (ppm)

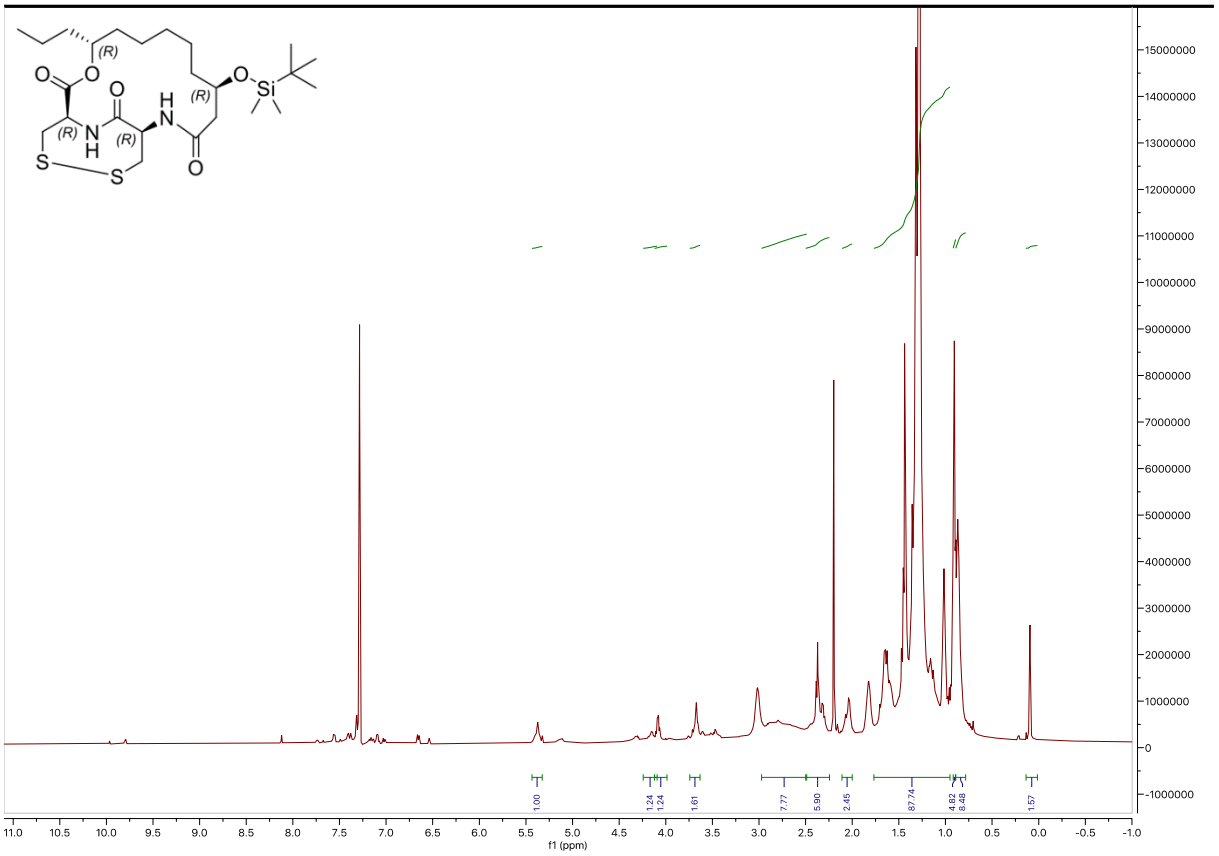
f1 (ppm)

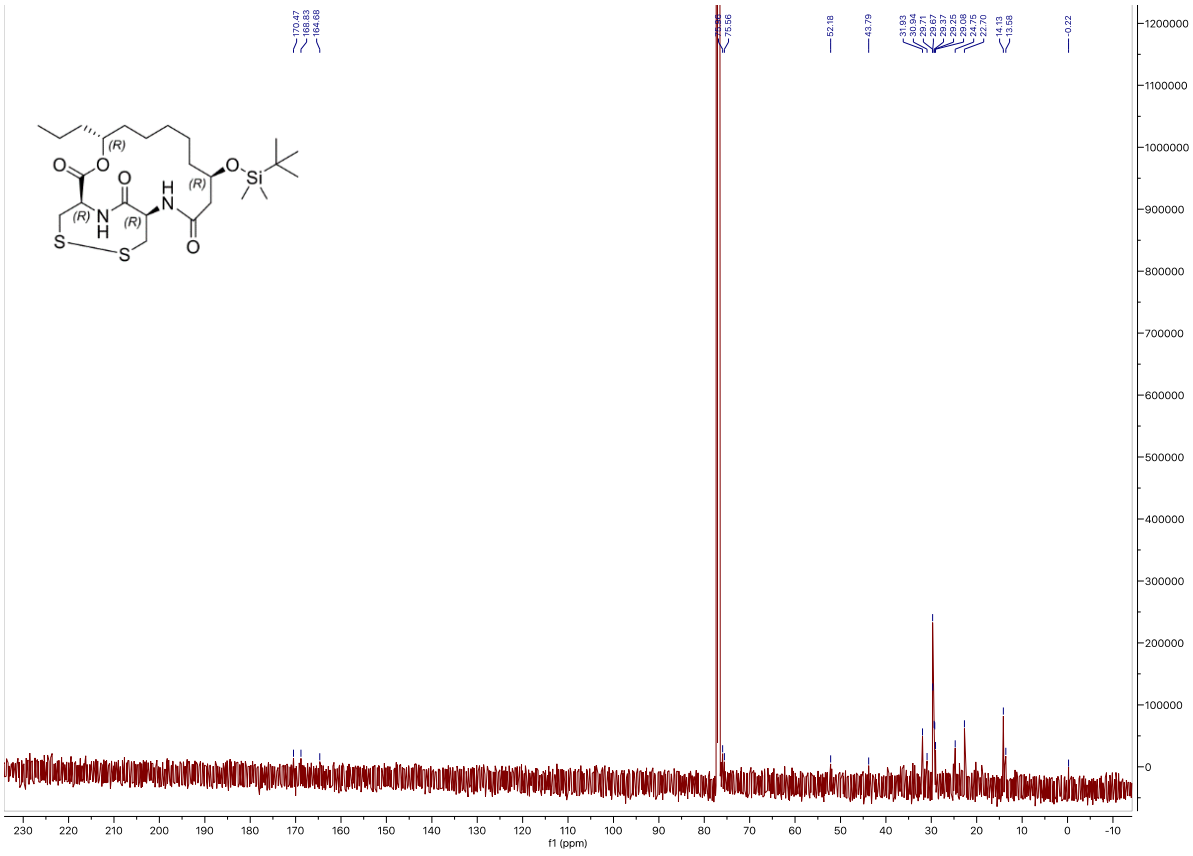
170.47
168.83
164.68
77.58
75.56
52.18
43.79
31.93
30.94
29.71
29.67
29.37
29.25
29.08
25.75
22.70
14.13
13.68
-0.22
f1 (ppm)

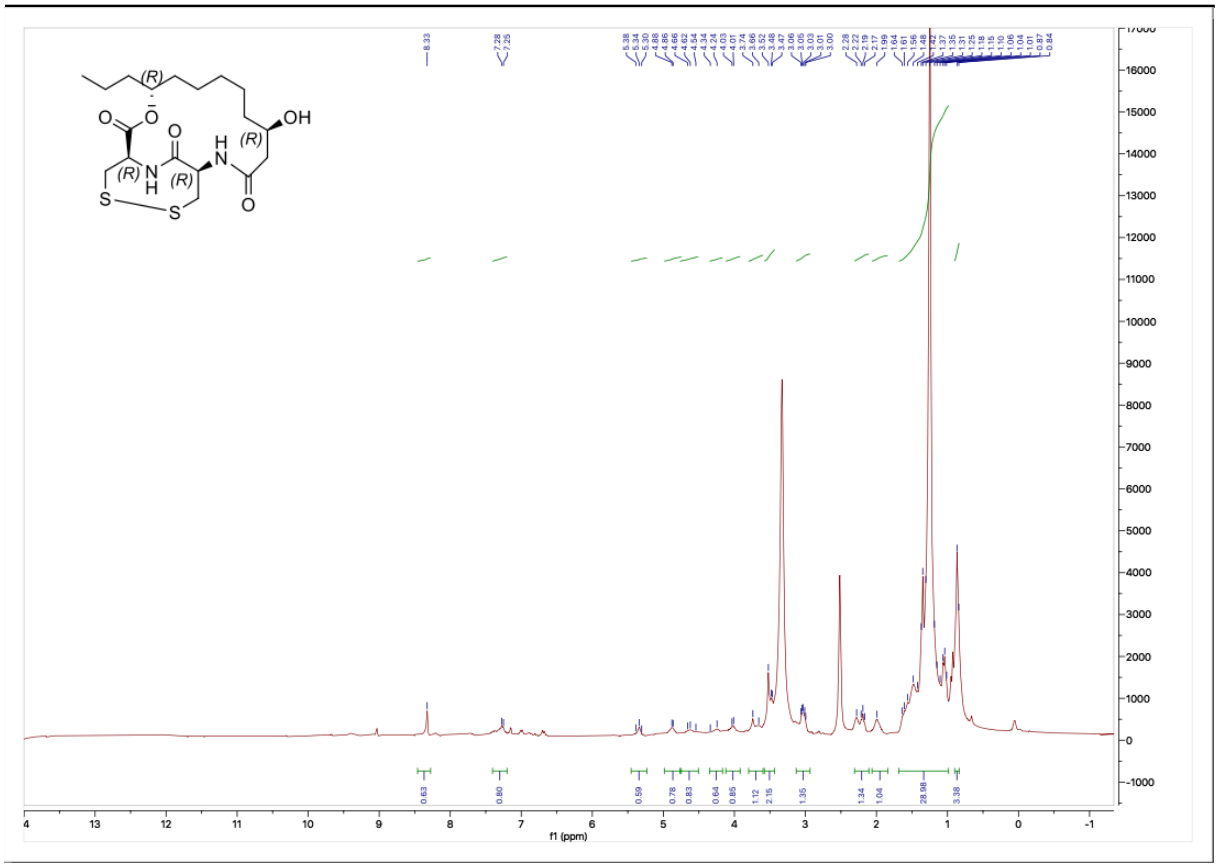
f1 (ppm)

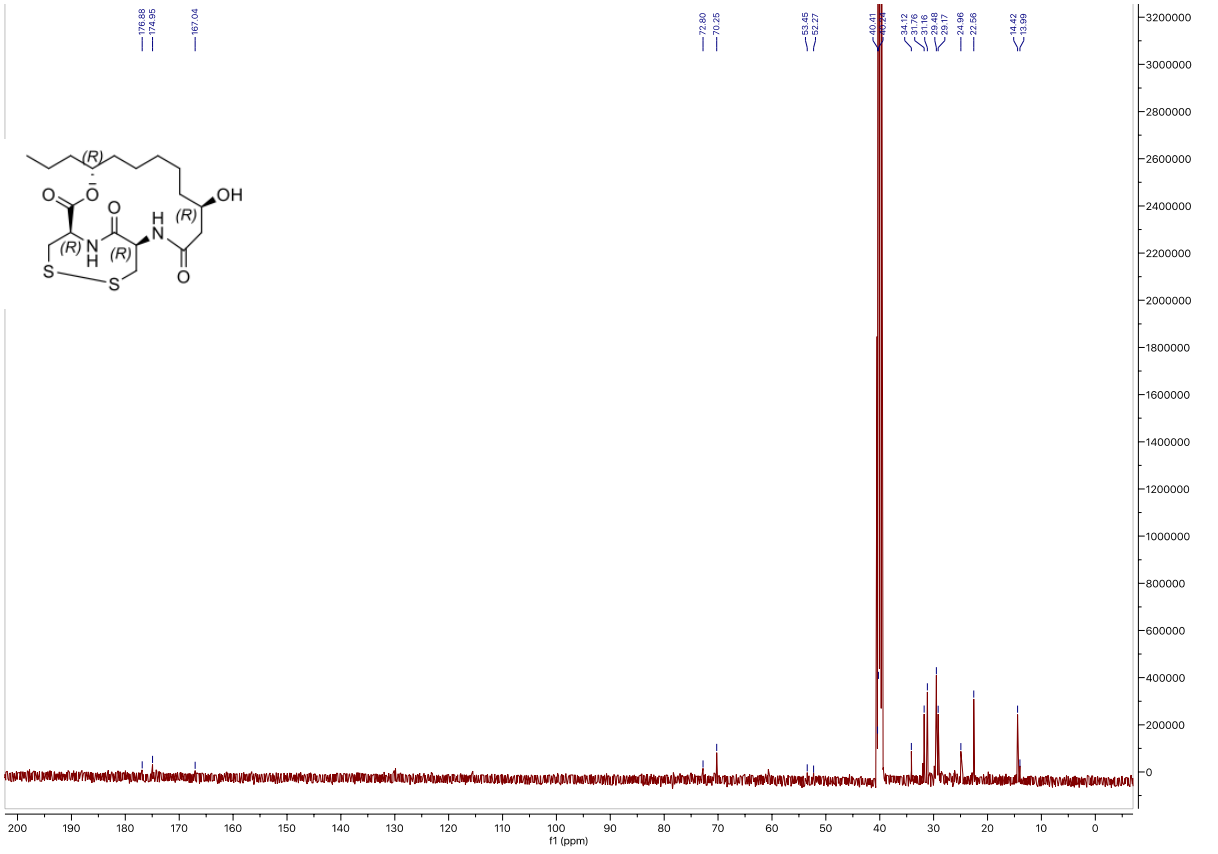
f1 (ppm)

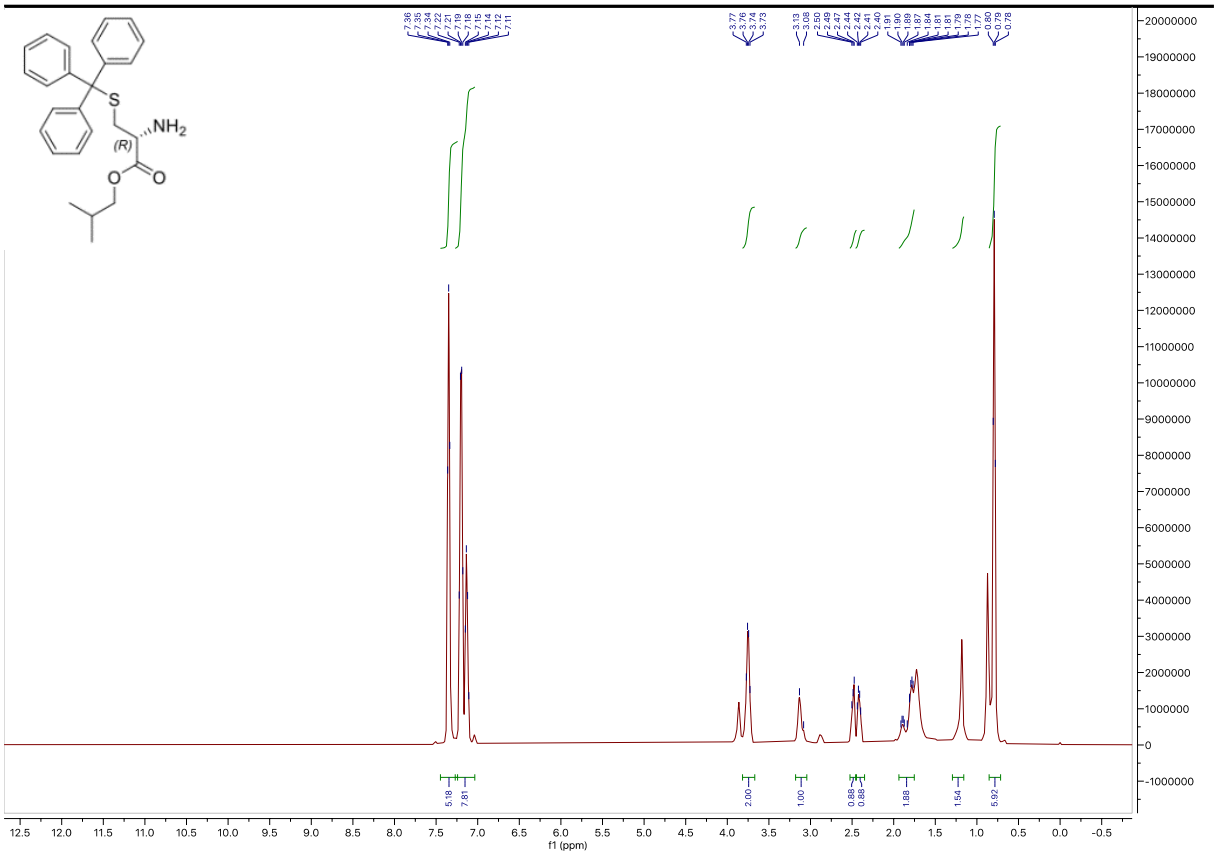
7.36
7.35
7.34
7.22
7.21
7.19
7.18
7.15
7.14
7.12
7.11
3.77
3.76
3.74
3.73
3.13
3.08
2.50
2.49
2.47
2.44
2.42
2.41
2.40
1.90
1.89
1.87
1.84
1.81
1.81
1.79
1.78
1.77
0.89
0.79
0.78
5.18
7.81
2.00
1.00
0.88
0.88
1.88
1.54
5.92
f1 (ppm)

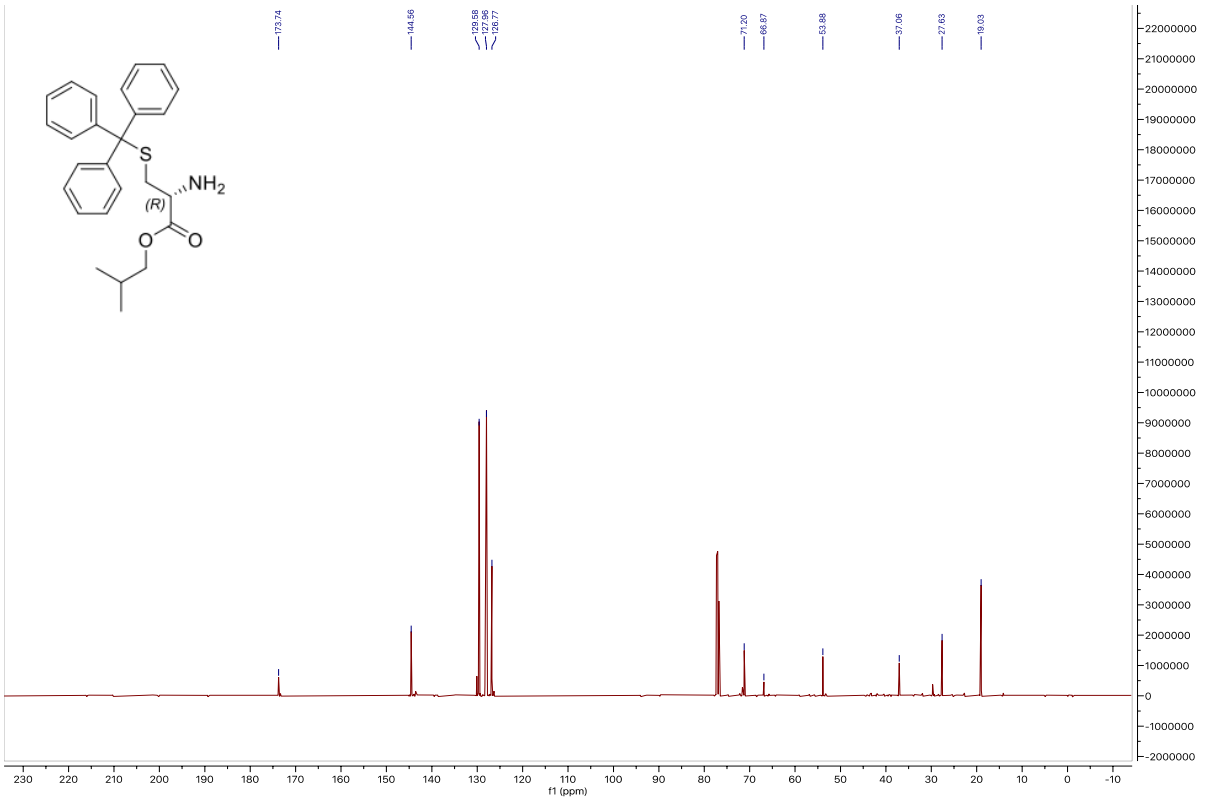
173.74
144.56
129.58
127.96
127.25
126.77
71.20
66.67
53.88
37.06
27.63
19.03
f1 (ppm)

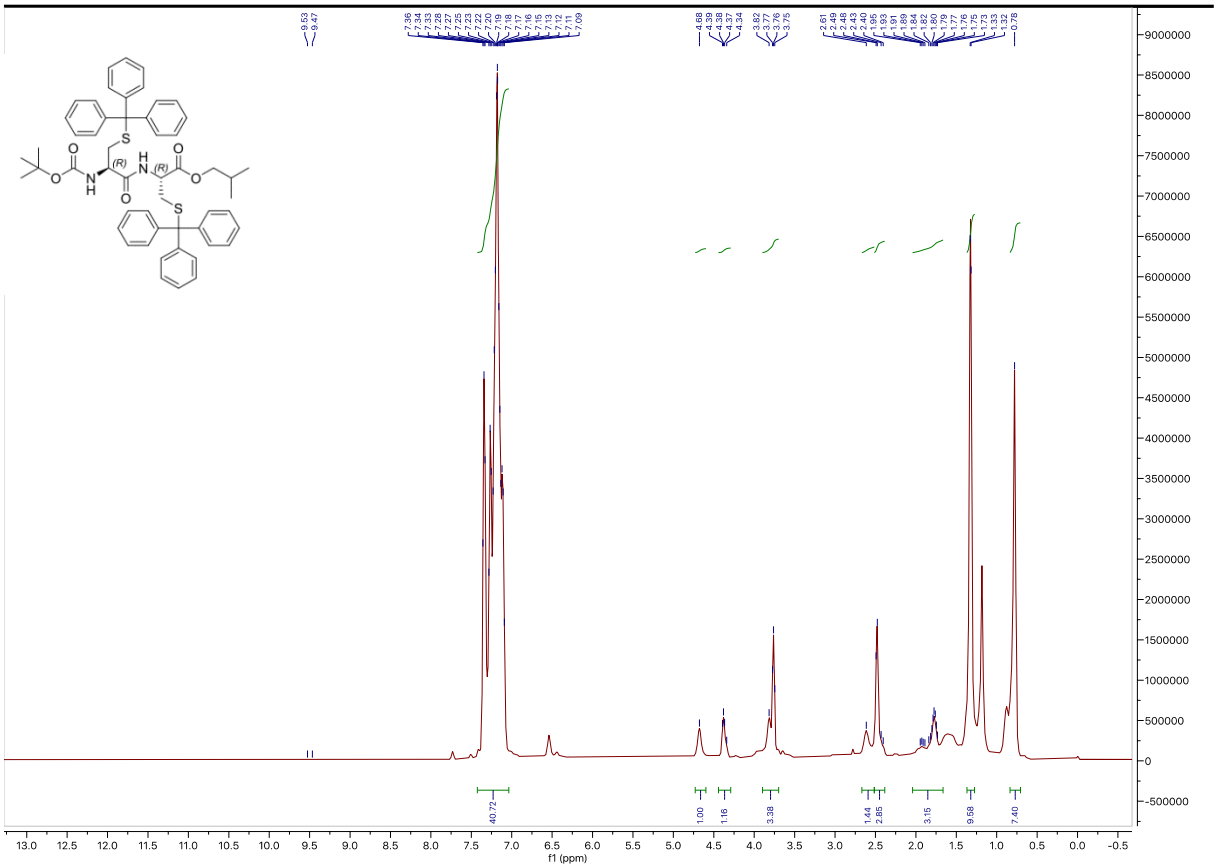
9.53
9.47
7.36
7.34
7.33
7.28
7.27
7.25
7.23
7.22
7.20
7.19
7.18
7.17
7.16
7.15
7.13
7.12
7.11
7.09
4.68
4.39
4.38
4.37
4.34
3.92
3.77
3.76
3.75
2.61
2.49
2.48
2.43
2.40
1.95
1.93
1.91
1.89
1.84
1.82
1.80
1.79
1.77
1.76
1.75
1.73
1.33
1.32
0.78
40.72
1.00
1.16
3.38
1.44
2.85
3.15
9.58
7.40
f1 (ppm)

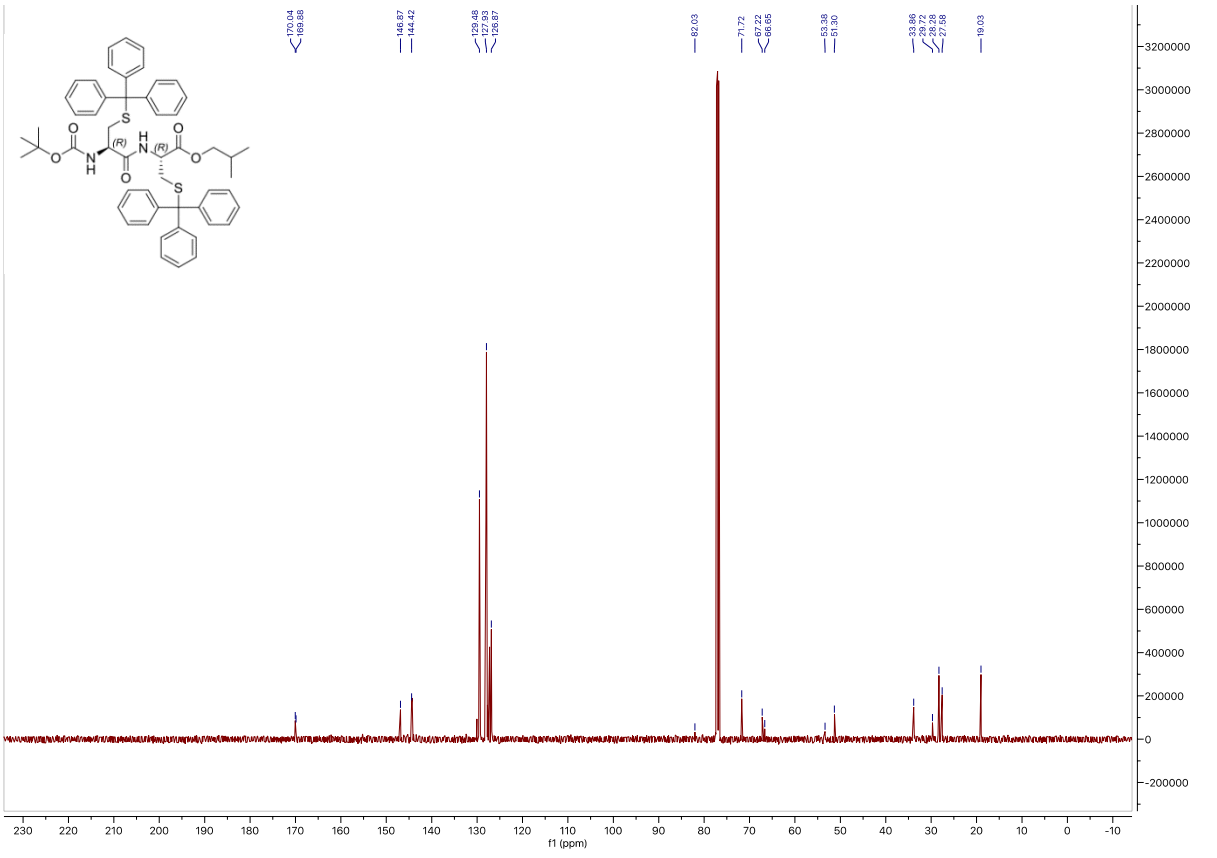
170.04
169.88
146.87
144.42
129.48
127.93
126.87
82.03
71.72
67.22
66.65
53.38
51.30
33.86
29.37
28.28
27.58
19.03
f1 (ppm)

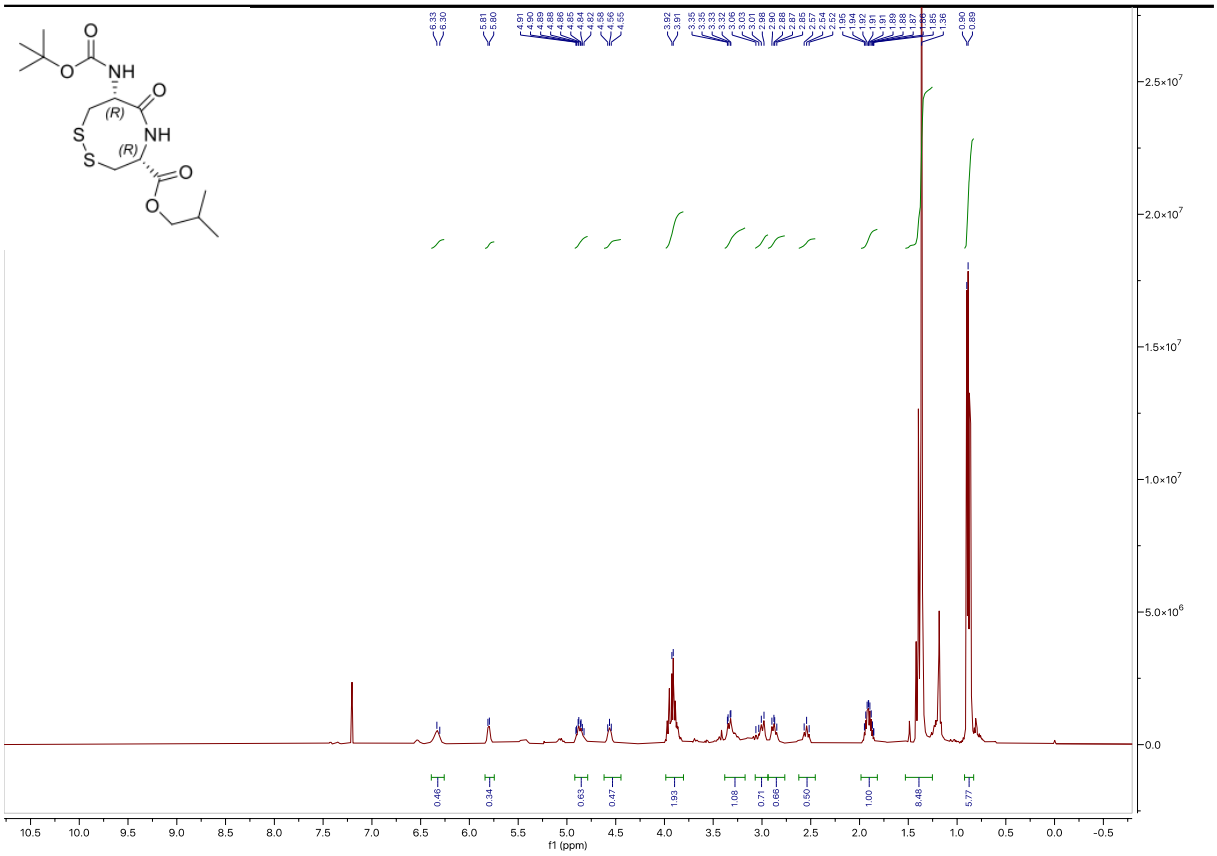
f1 (ppm)

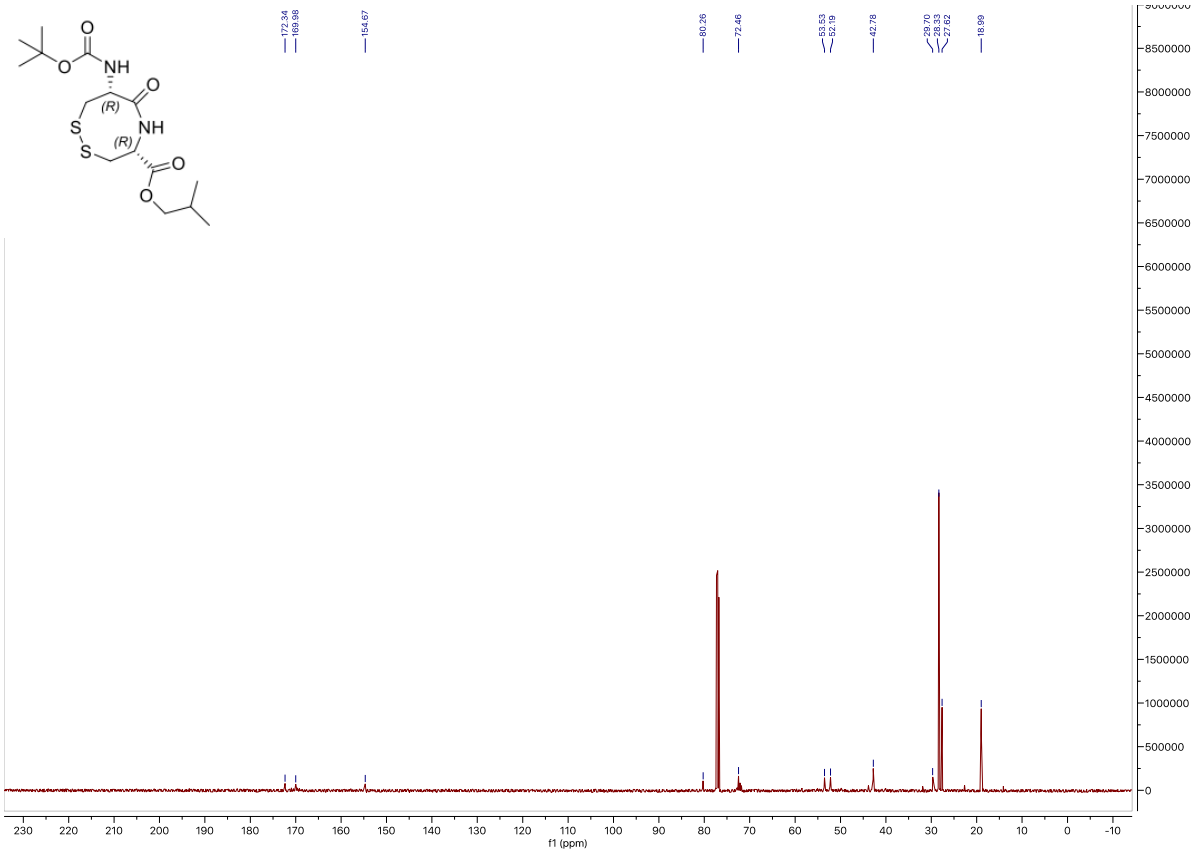
f1 (ppm)

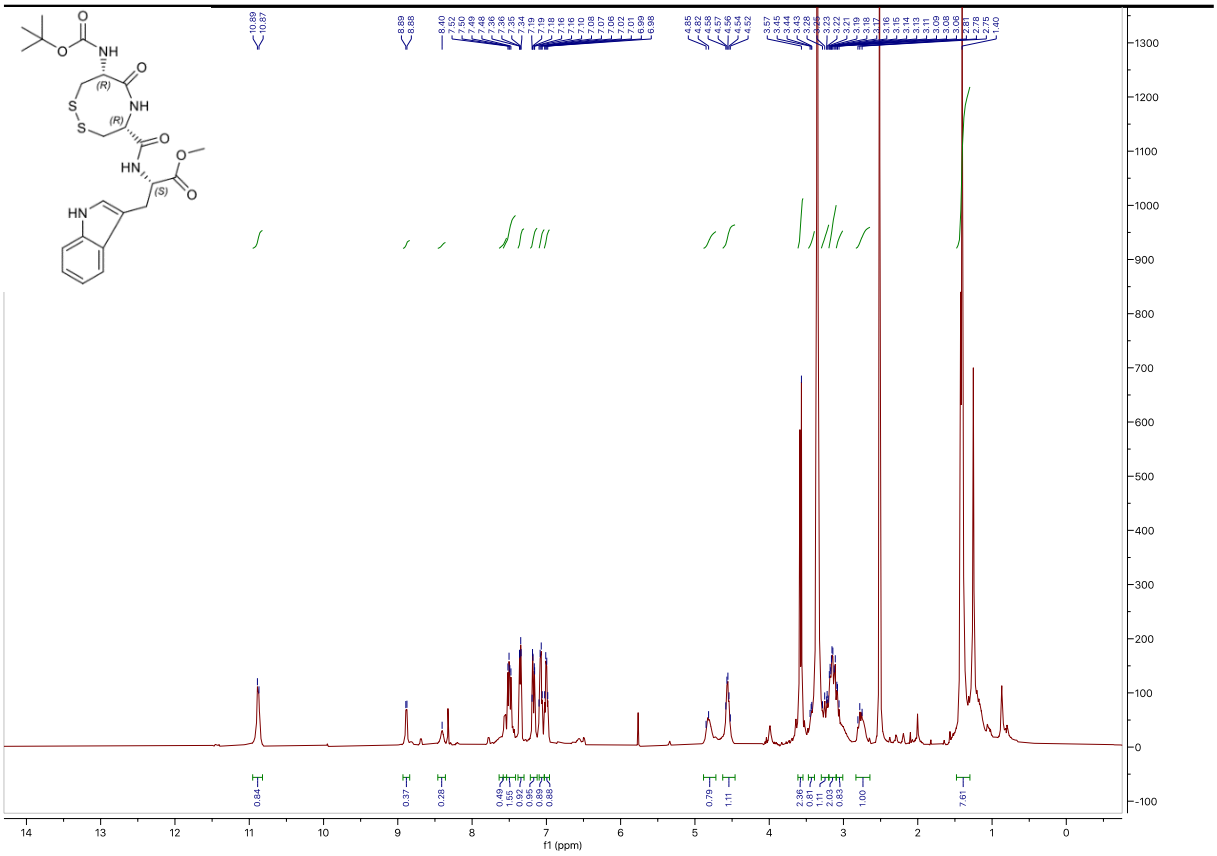
f1 (ppm)

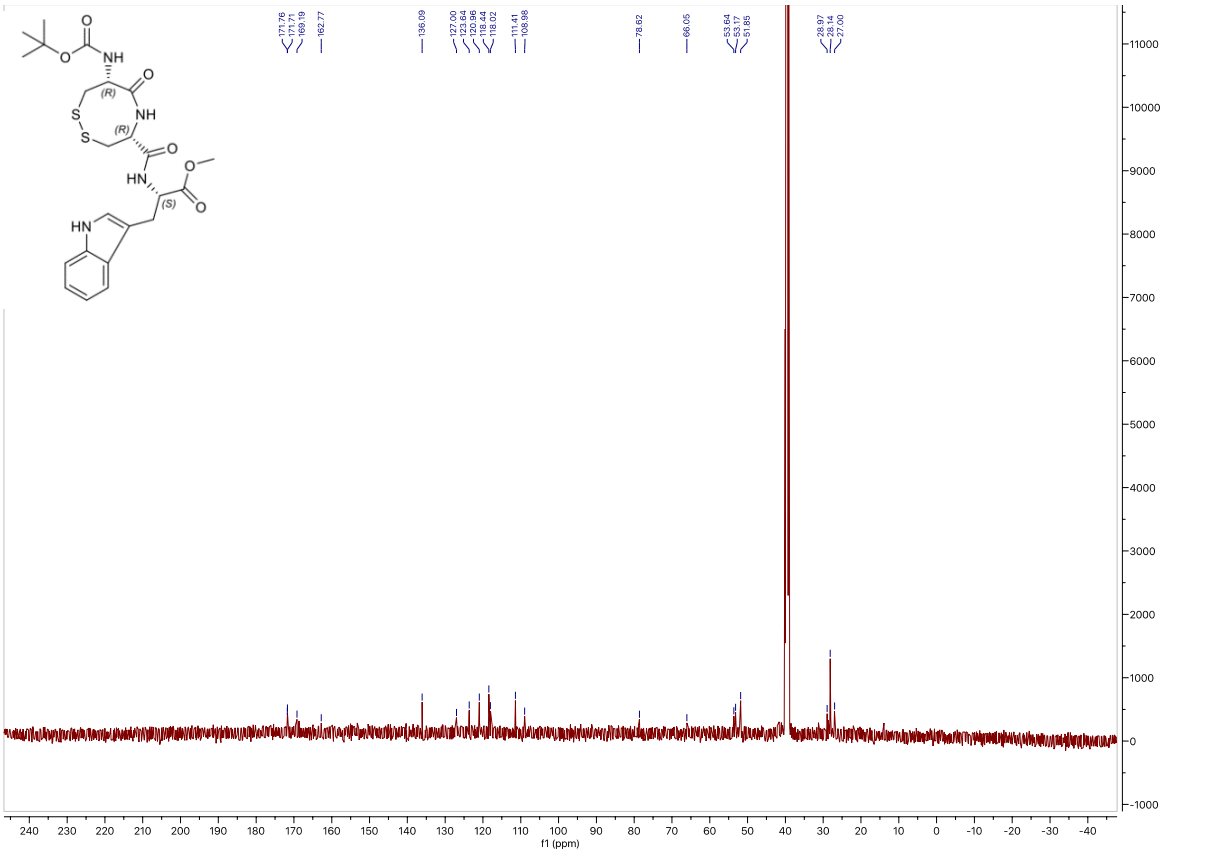
f1 (ppm)

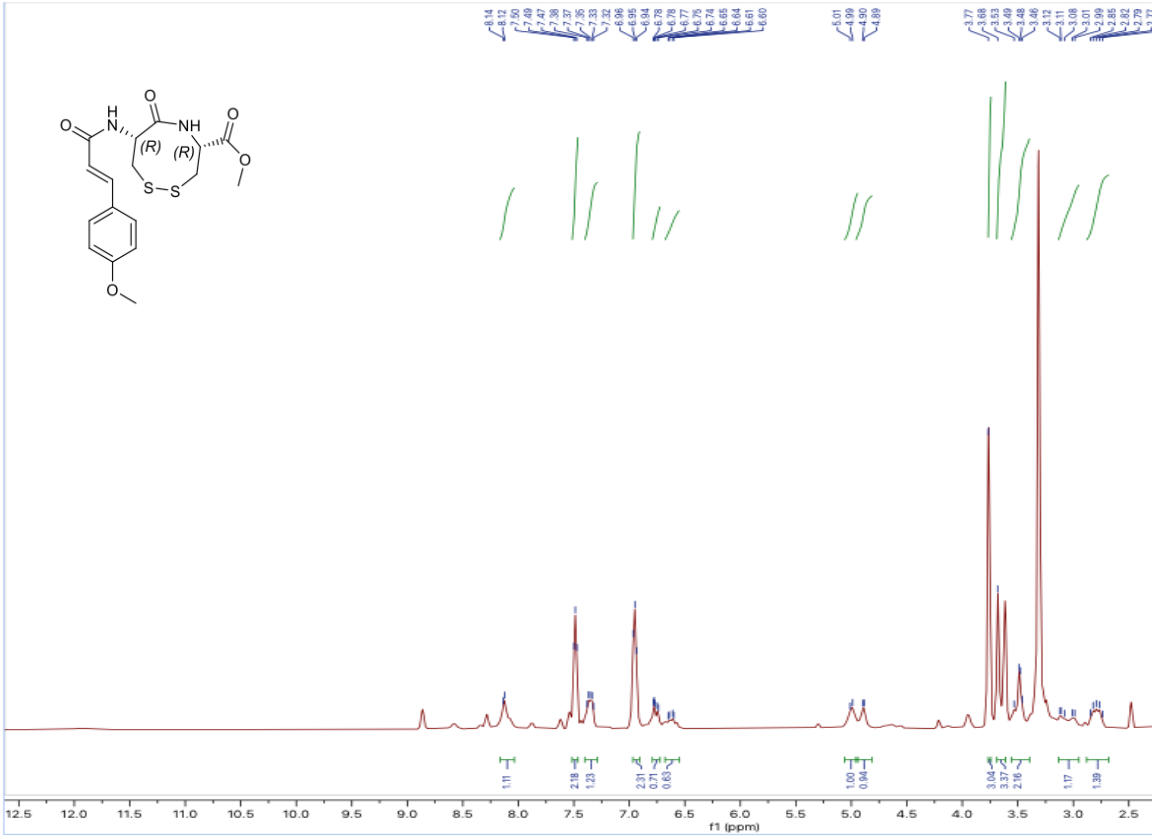
f1 (ppm)

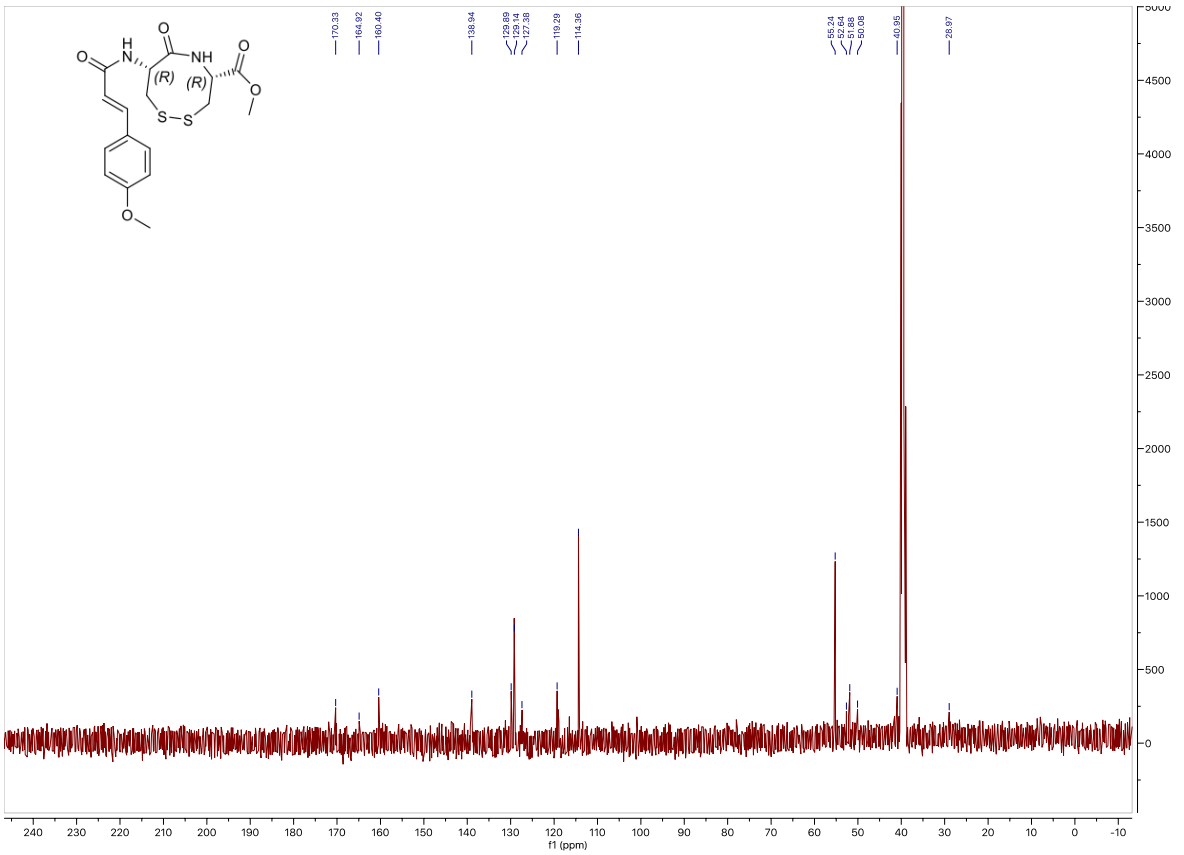
f1 (ppm)

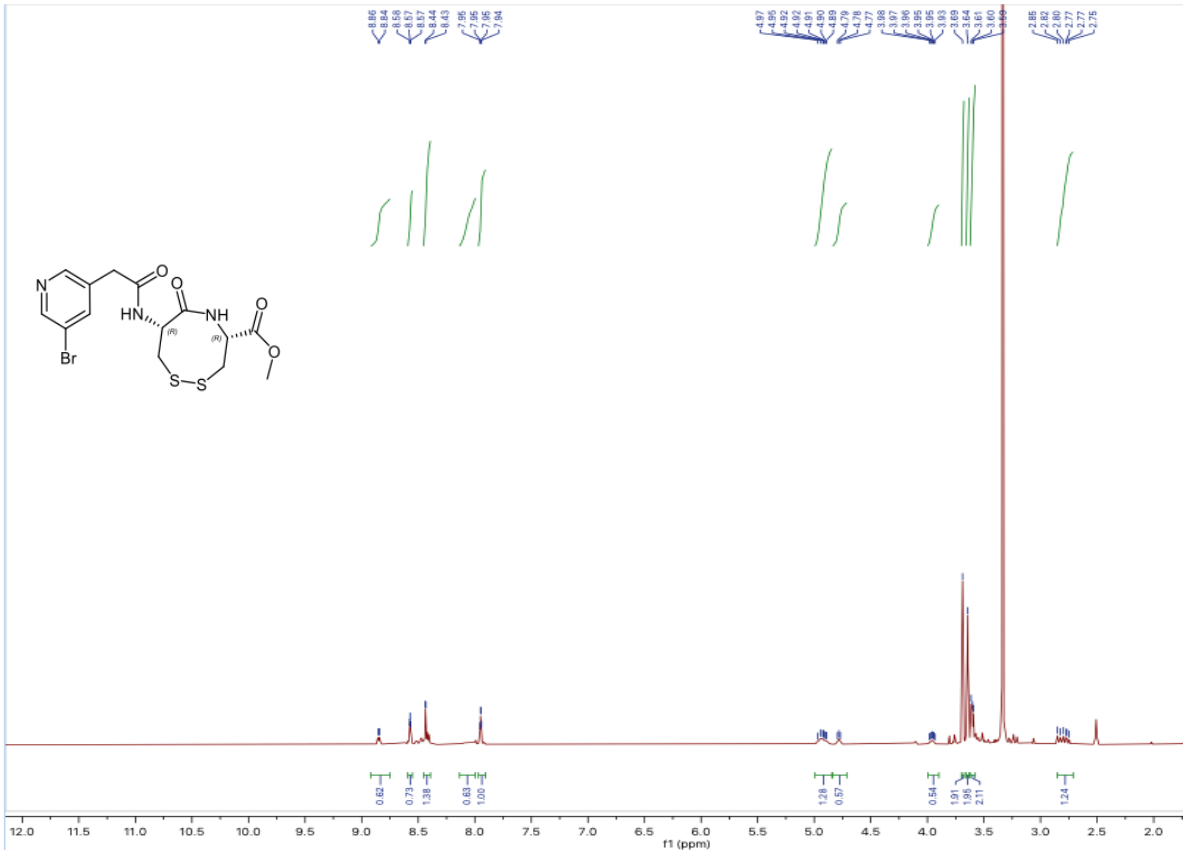
f1 (ppm)

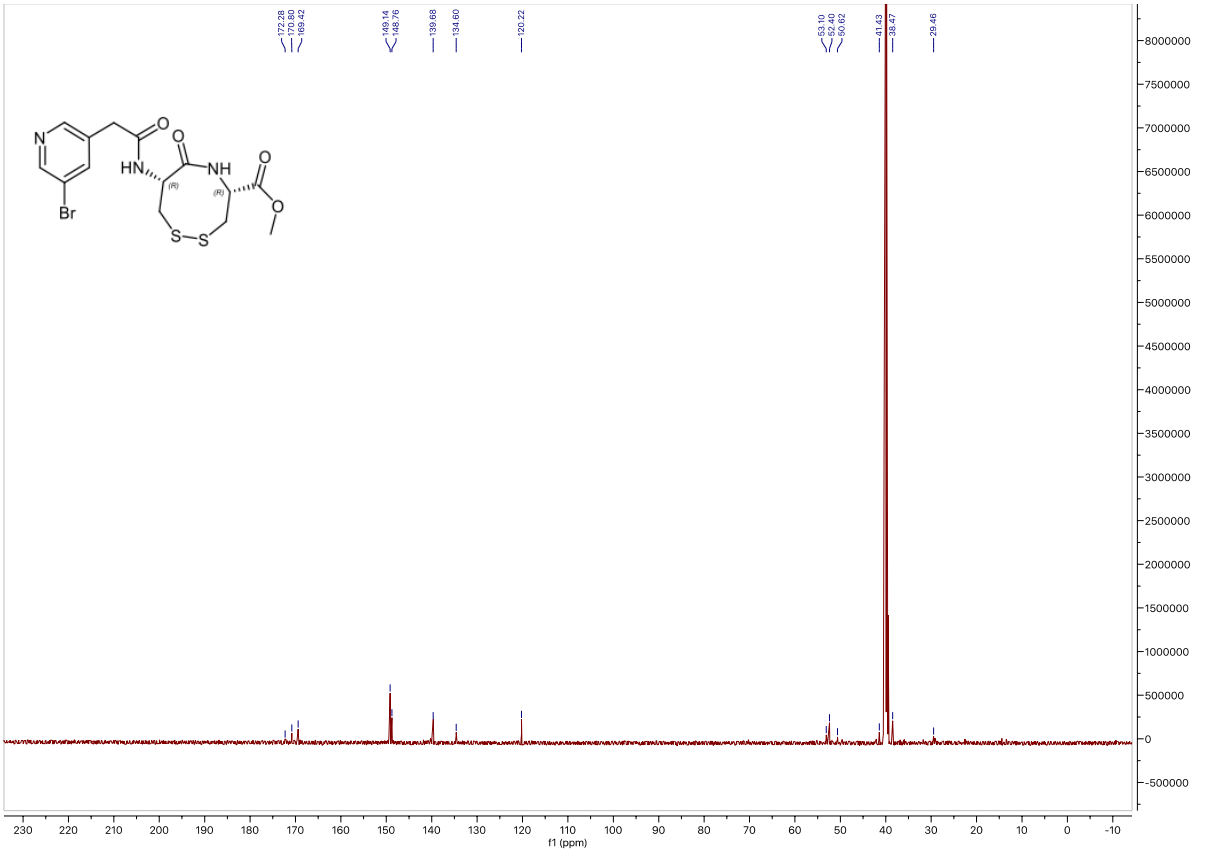
f1 (ppm)

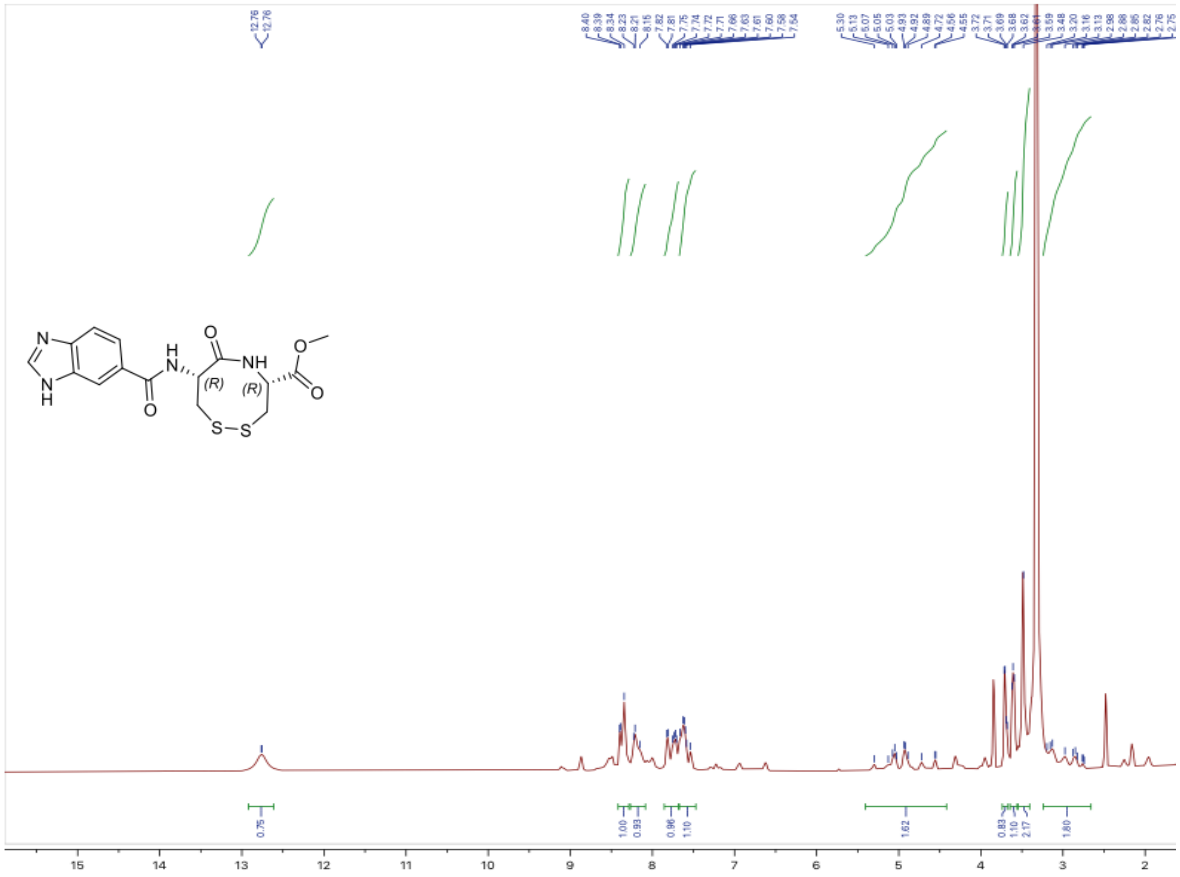

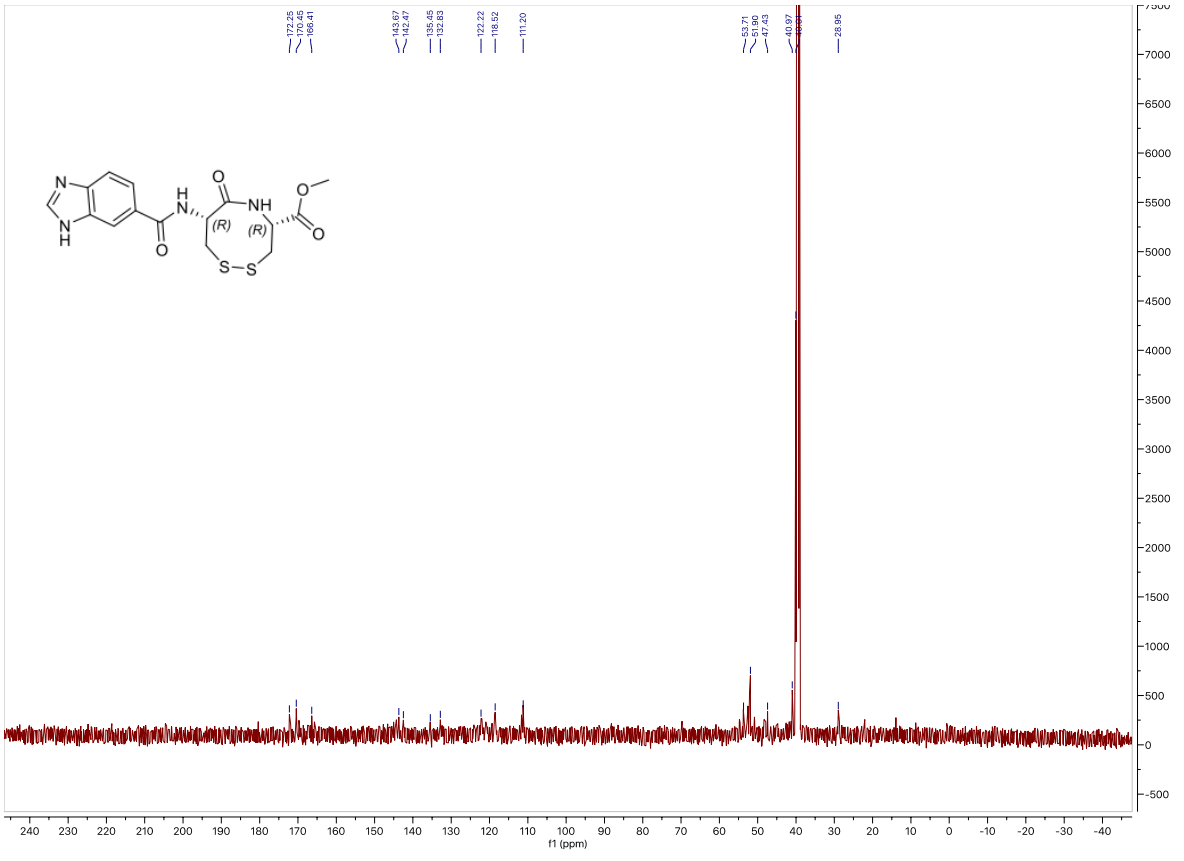

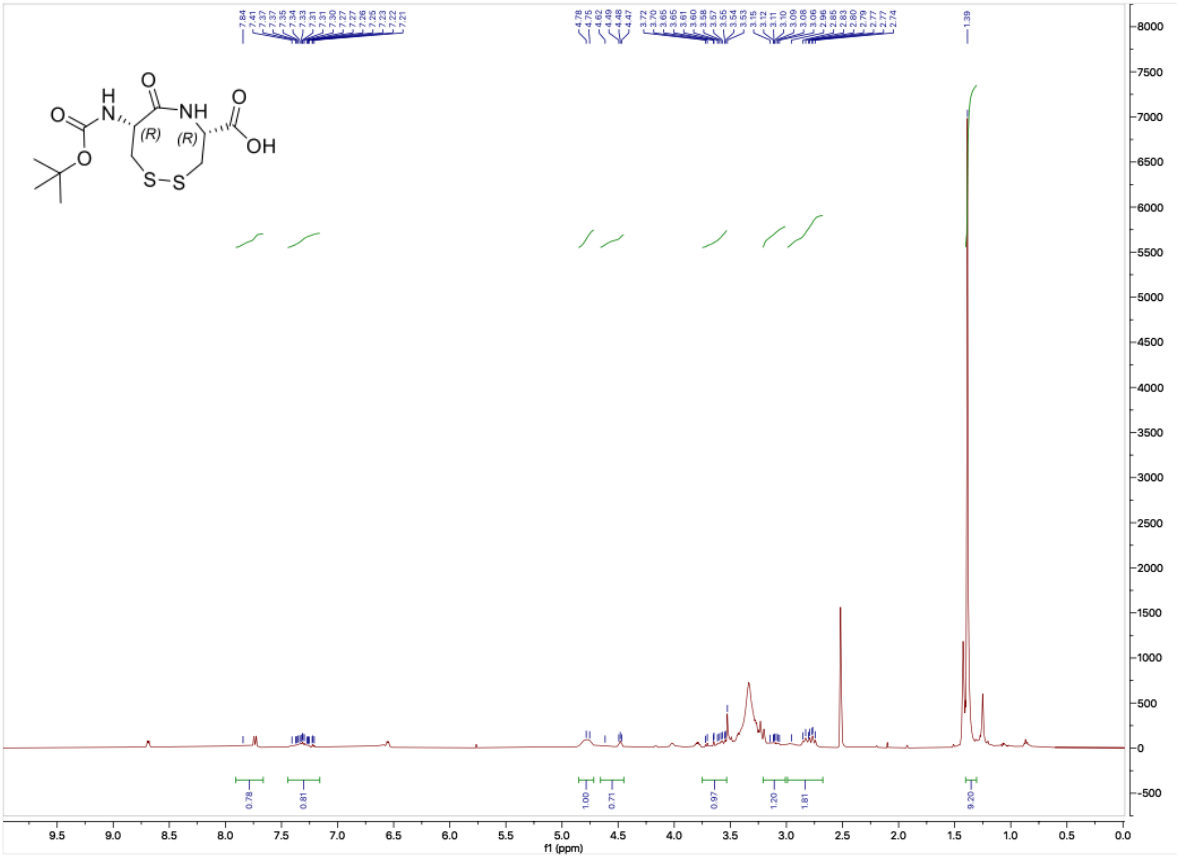
f1 (ppm)

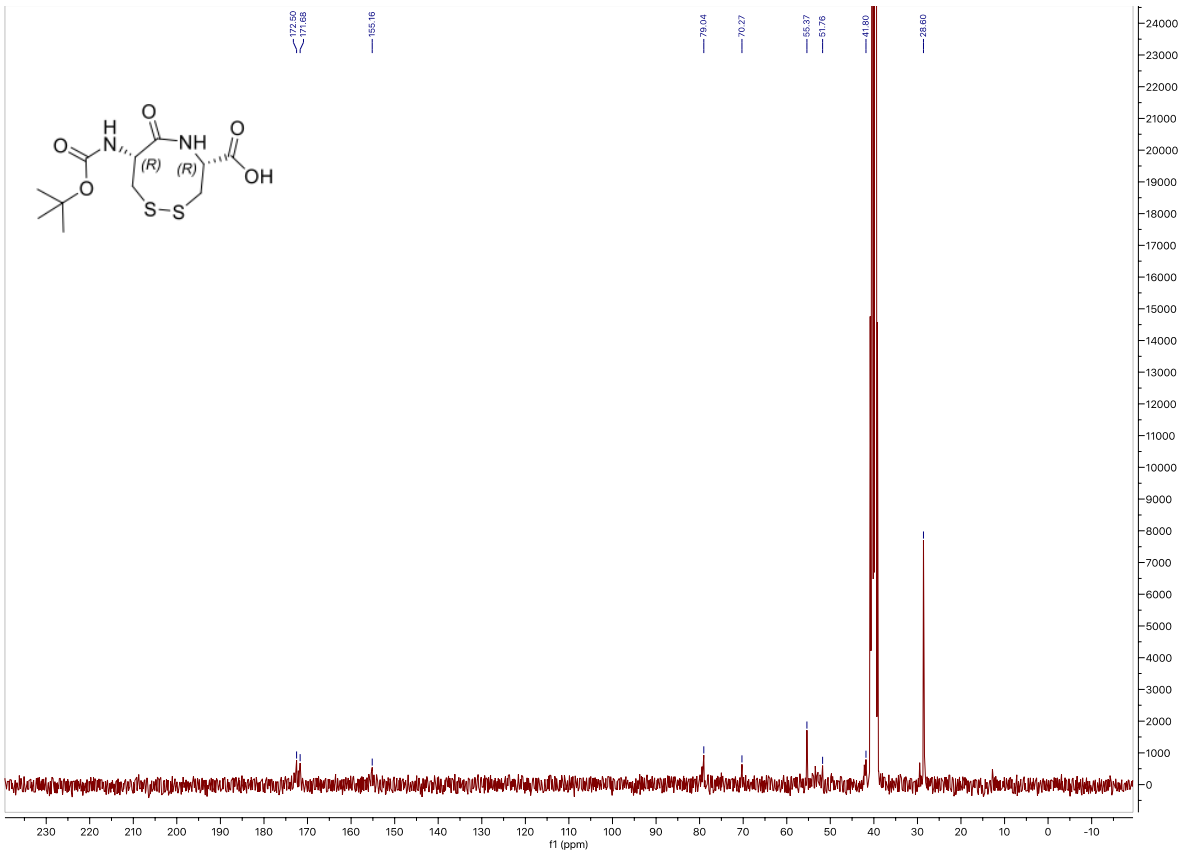
f1 (ppm)

1. **Eudistomidin C** ((*S*)-5-bromo-1-(1-(methylamino)-2-(methylthio)ethyl)-9H-pyrido[3,4-β]indol-6-ol) (**BSc5517**)

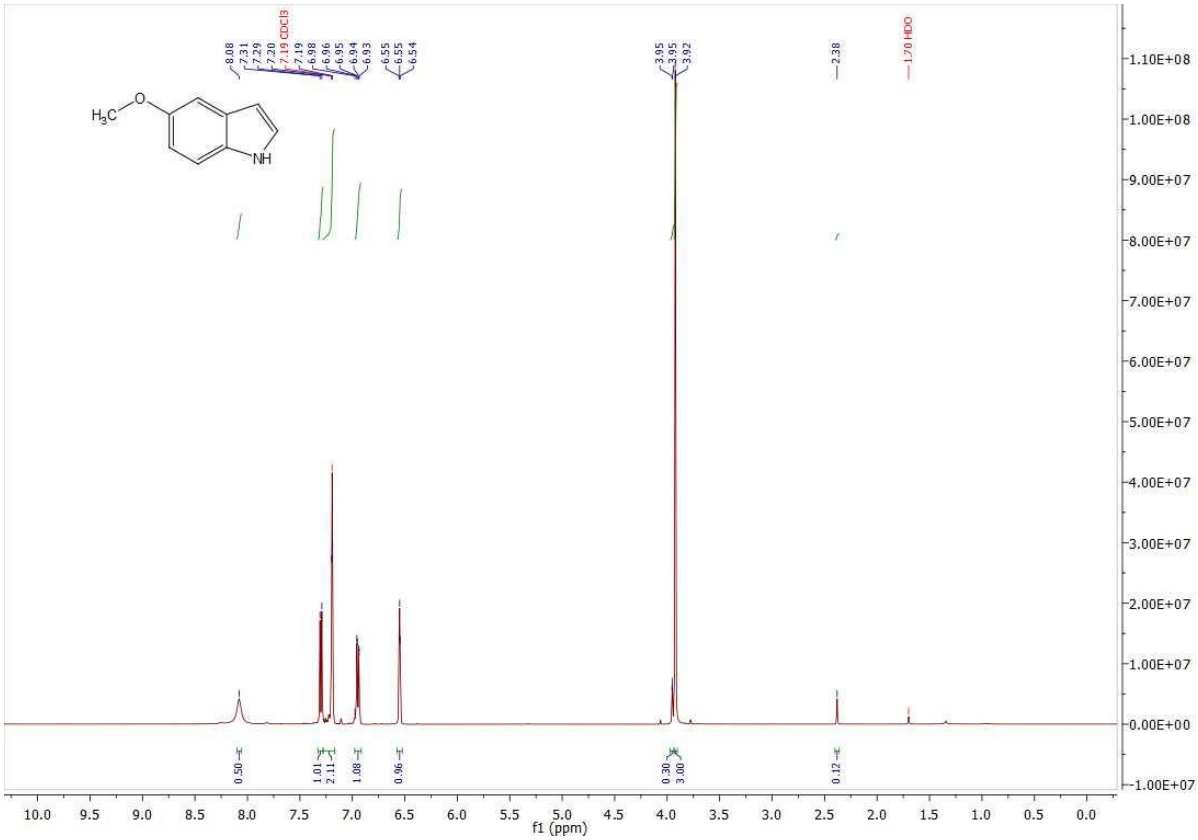
8.08
7.31
7.29
7.20
7.19 CDCl3
6.98
6.96
6.95
6.94
6.93
6.55
6.55
6.54
3.95
3.95
3.92
2.38
1.70 HDO
H3C
O
NH
0.50
1.01
2.11
1.08
0.96
0.30
3.00
0.12
f1 (ppm)

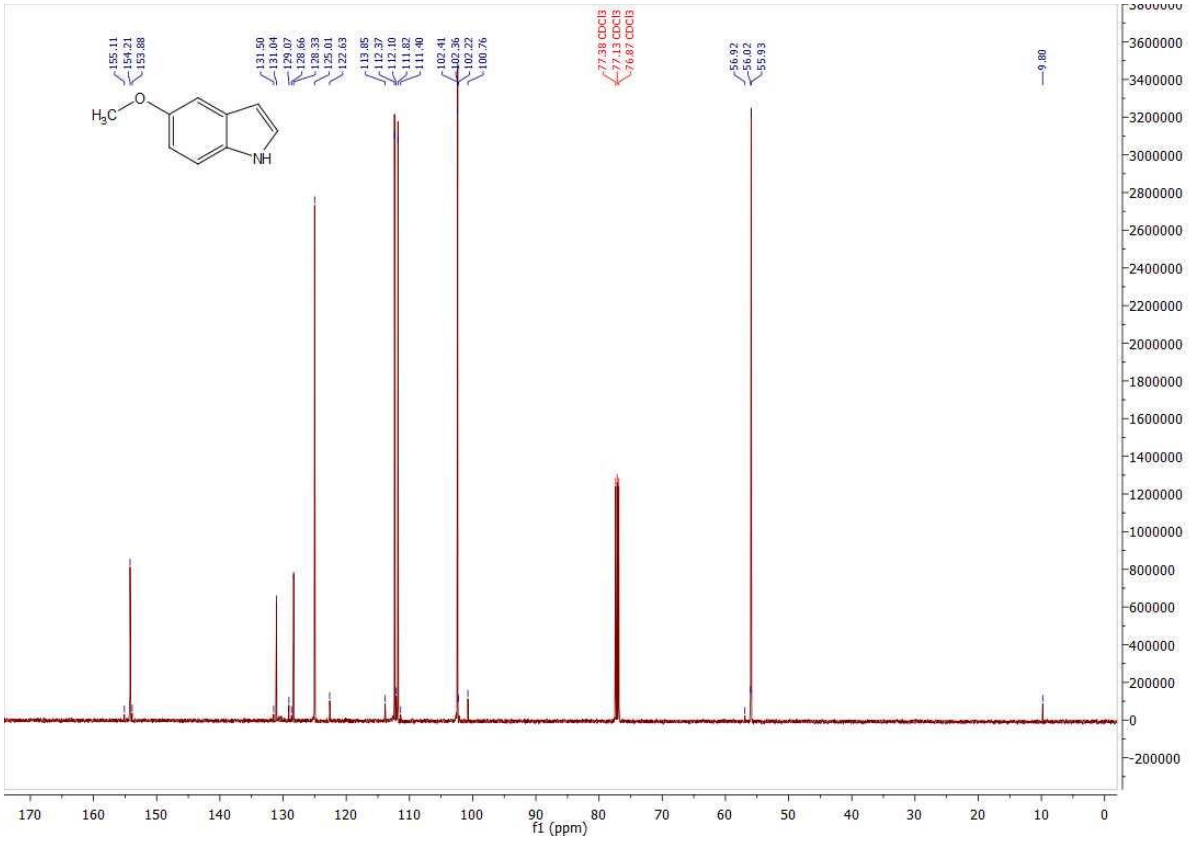
155.11
154.21
153.88
131.50
131.04
129.07
128.66
126.33
125.01
122.63
113.85
112.37
112.10
111.82
111.40
102.41
102.36
100.22
100.76
77.38 CDCl3
77.13 CDCl3
76.87 CDCl3
56.92
56.02
55.93
9.80
H3C
O
NH
f1 (ppm)

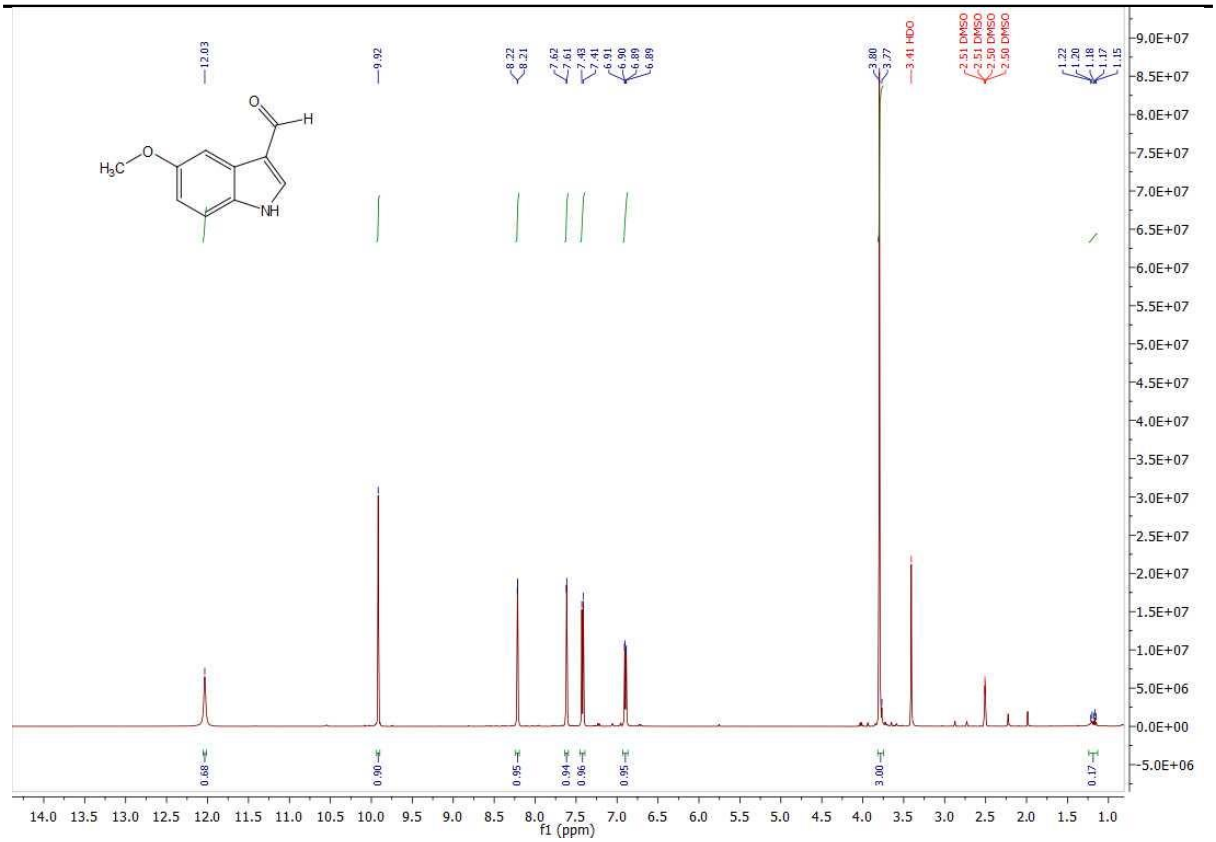
12.03
9.92
8.22
8.21
7.62
7.61
7.45
7.44
7.41
6.91
6.90
6.89
6.89
3.80
3.77
3.41 HDO
2.51 DMSO
2.51 DMSO
2.50 DMSO
2.50 DMSO
1.22
1.20
1.18
1.17
1.15
0.68
0.90
0.95
0.94
0.96
0.95
3.00
0.17
f1 (ppm)

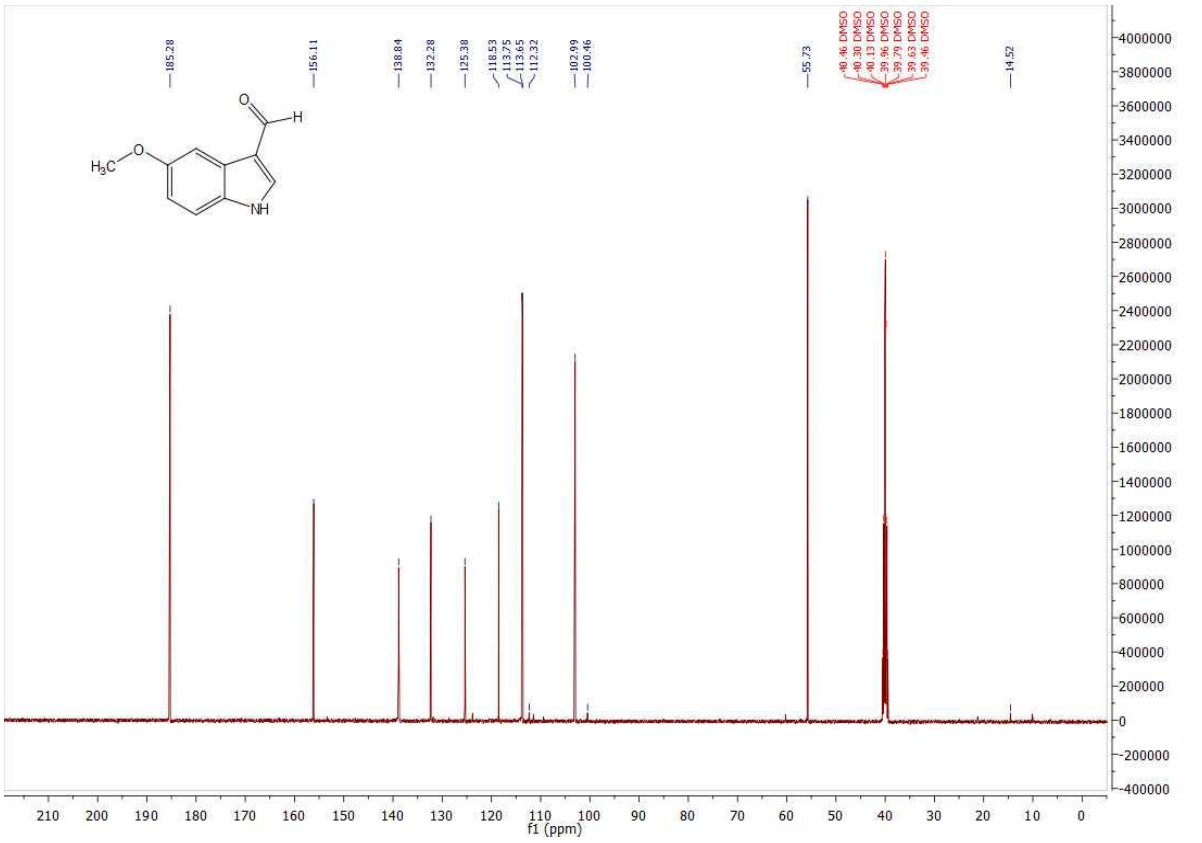
185.28
156.11
138.84
132.28
125.38
118.53
113.75
113.65
112.32
102.99
100.46
55.73
40.46 DMSO
40.30 DMSO
40.13 DMSO
39.96 DMSO
39.79 DMSO
39.63 DMSO
39.46 DMSO
14.52
f1 (ppm)

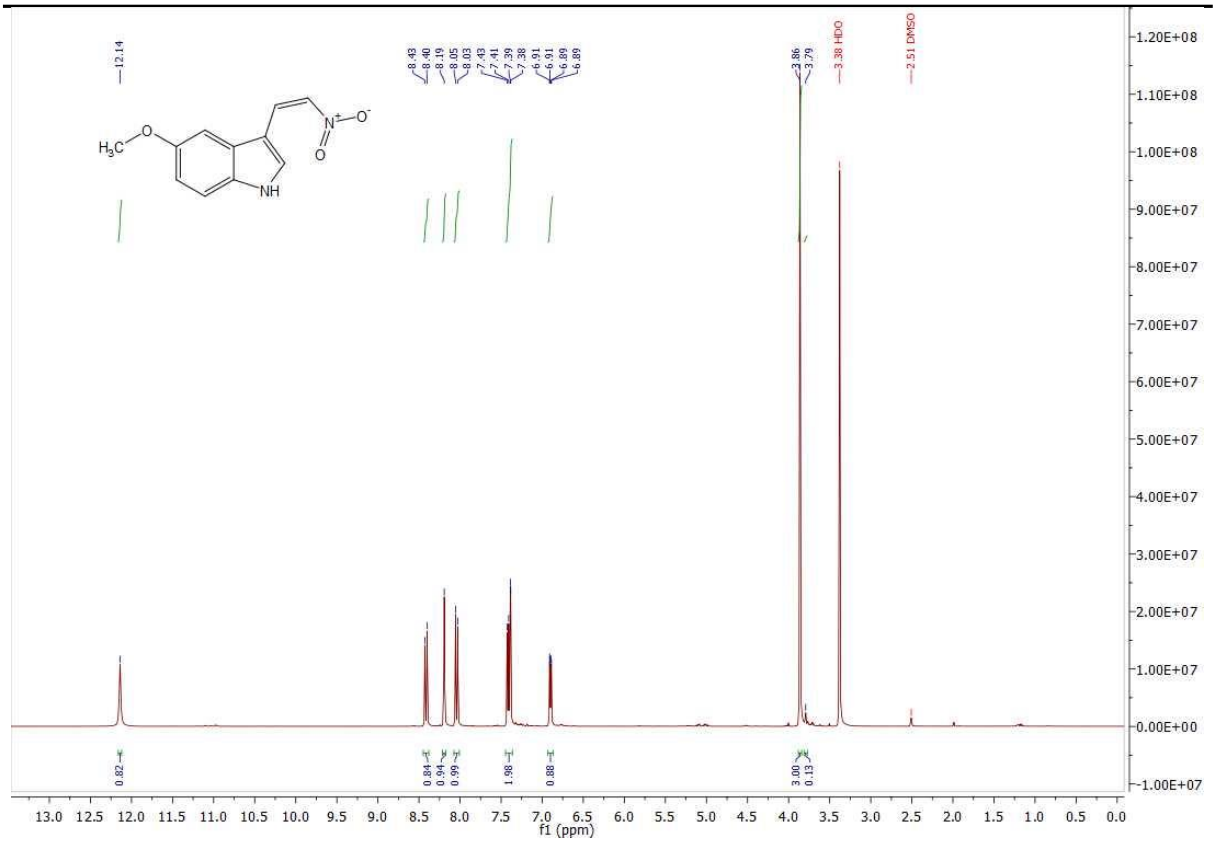
12.14
8.43
8.40
8.19
8.05
8.03
7.43
7.41
7.39
7.38
6.91
6.91
6.89
6.89
3.86
3.79
3.38 HDO
2.51 DMSO
0.82
0.84
0.94
0.99
1.98
0.88
3.00
0.13
f1 (ppm)

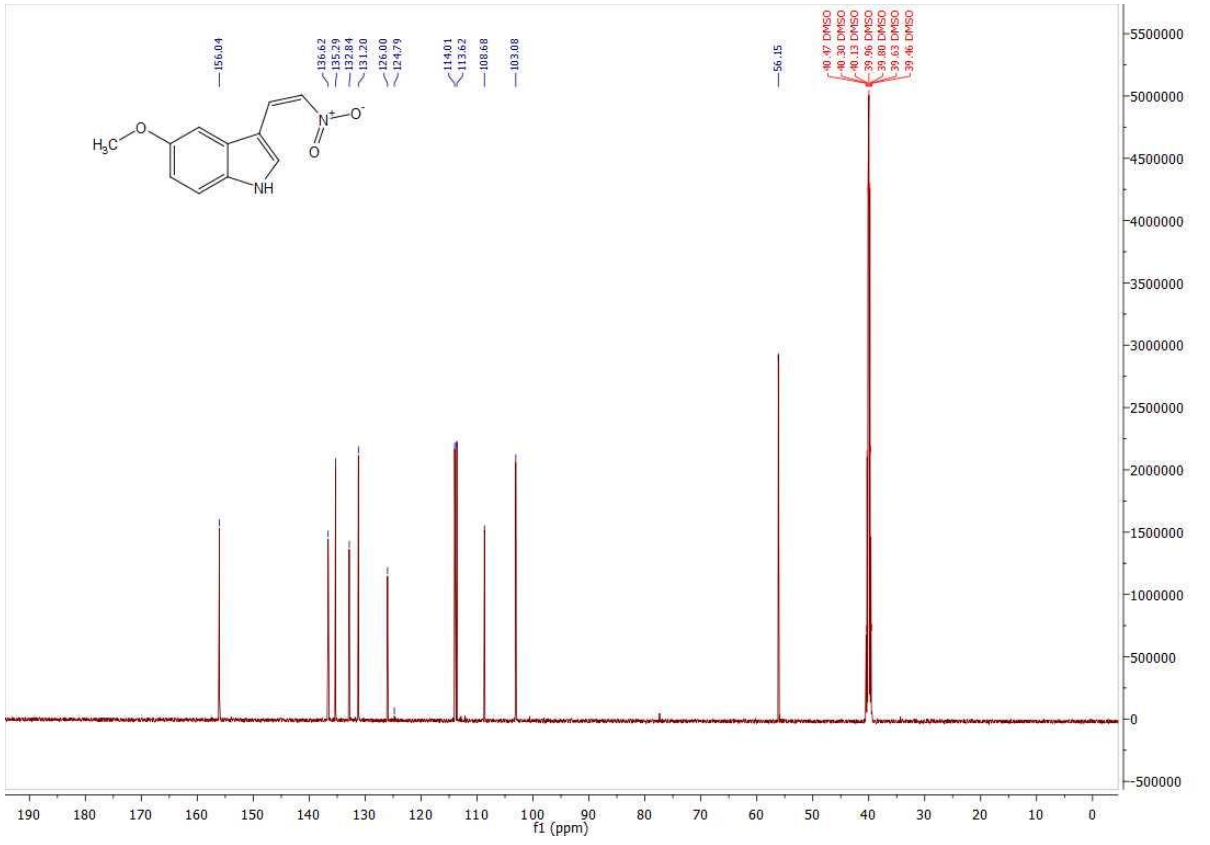
156.04
136.62
135.29
132.84
131.20
126.00
124.79
114.01
113.62
108.68
103.08
56.15
40.47 DMSO
40.30 DMSO
40.13 DMSO
39.96 DMSO
39.80 DMSO
39.63 DMSO
39.46 DMSO
f1 (ppm)

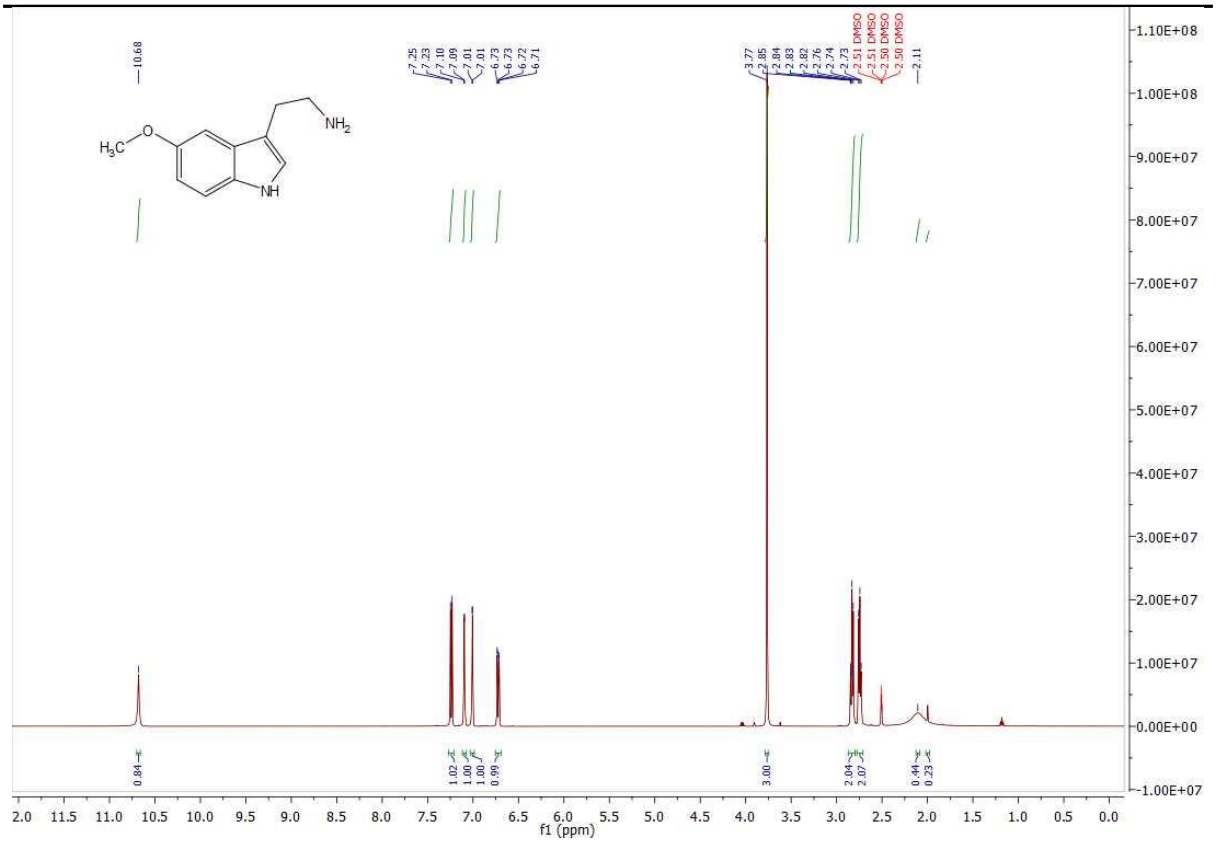
10.68
7.35
7.33
7.10
7.09
7.01
7.01
6.73
6.72
6.71
3.77
2.85
2.84
2.83
2.82
2.76
2.74
2.73
2.51 DMSO
2.51 DMSO
2.50 DMSO
2.50 DMSO
2.11
NH2
O
H3C
NH
0.84
1.02
1.00
1.00
0.99
3.00
2.04
2.07
0.44
0.23
f1 (ppm)

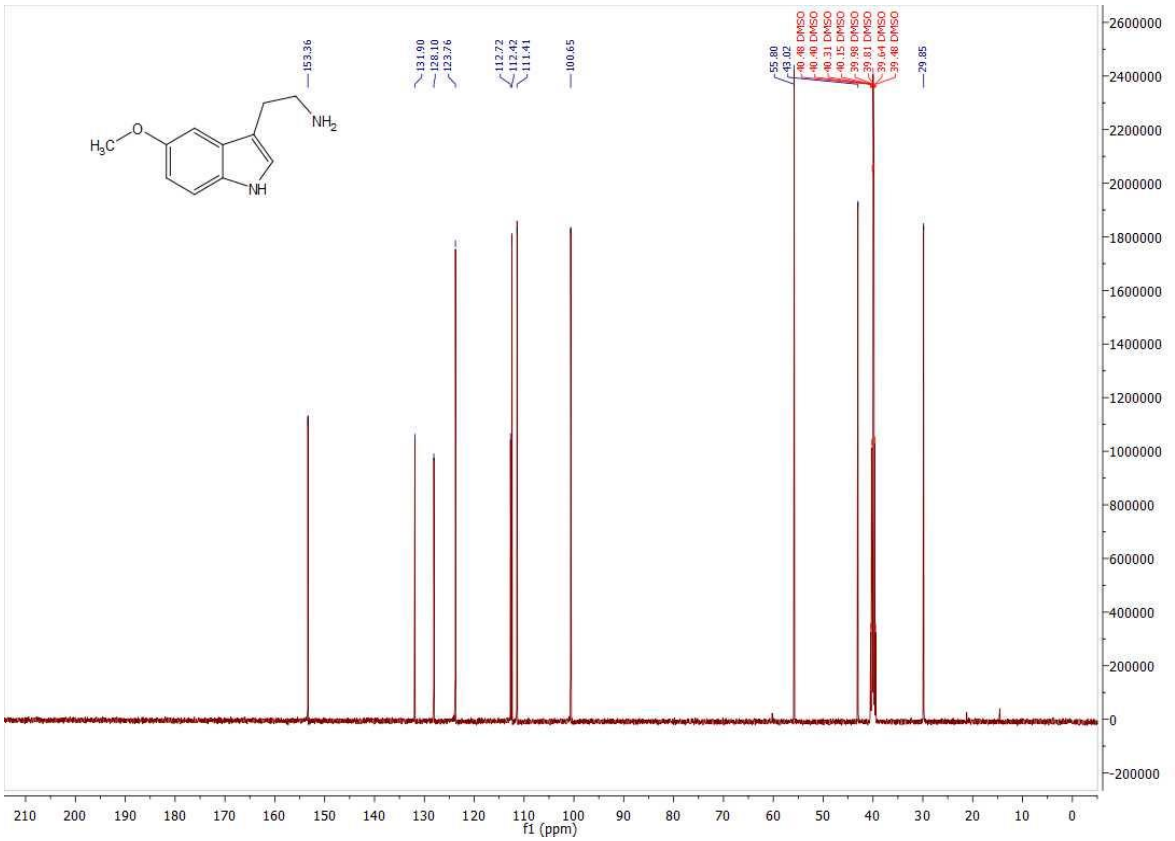
153.36
131.90
128.10
123.76
112.72
112.42
111.41
100.65
55.80
49.47
40.46 DMSO
40.40 DMSO
40.31 DMSO
40.15 DMSO
39.98 DMSO
39.81 DMSO
39.64 DMSO
39.48 DMSO
29.85
NH2
O
H3C
NH
f1 (ppm)

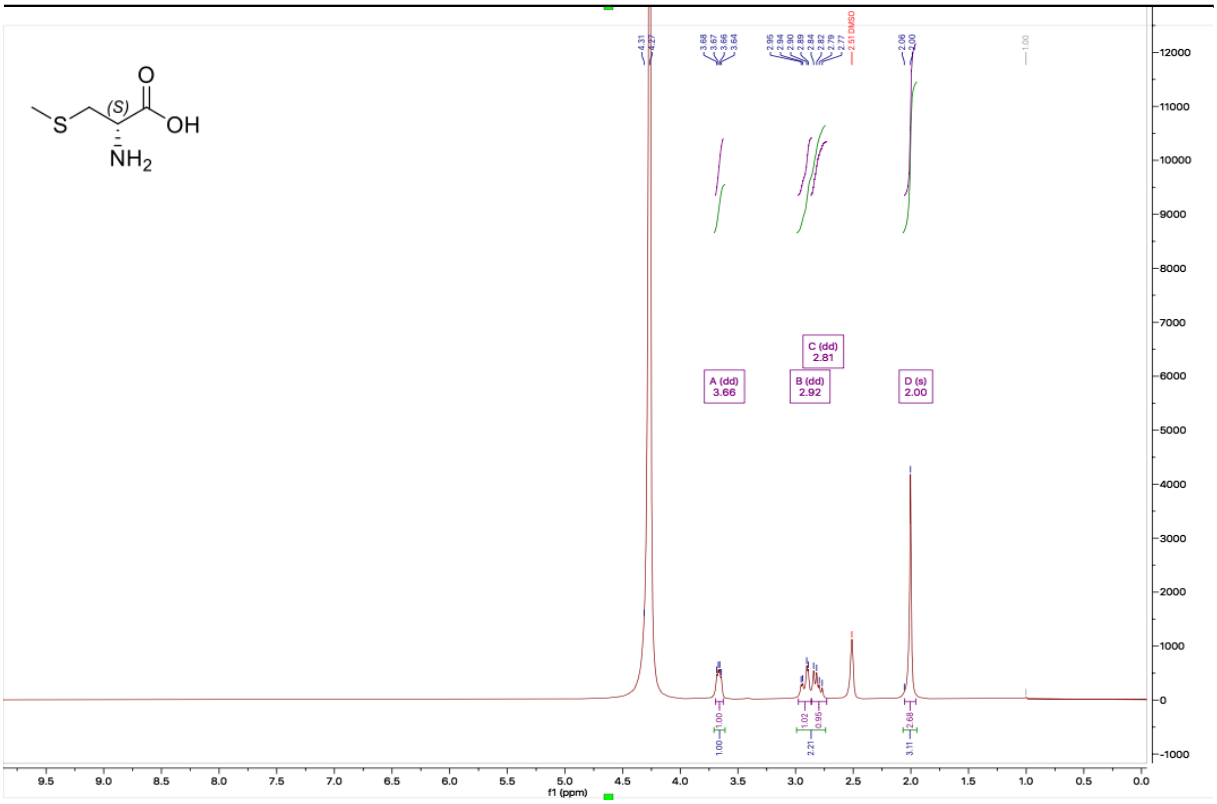
A (dd)
3.66
B (dd)
2.92
C (dd)
2.81
D (s)
2.00
f1 (ppm)

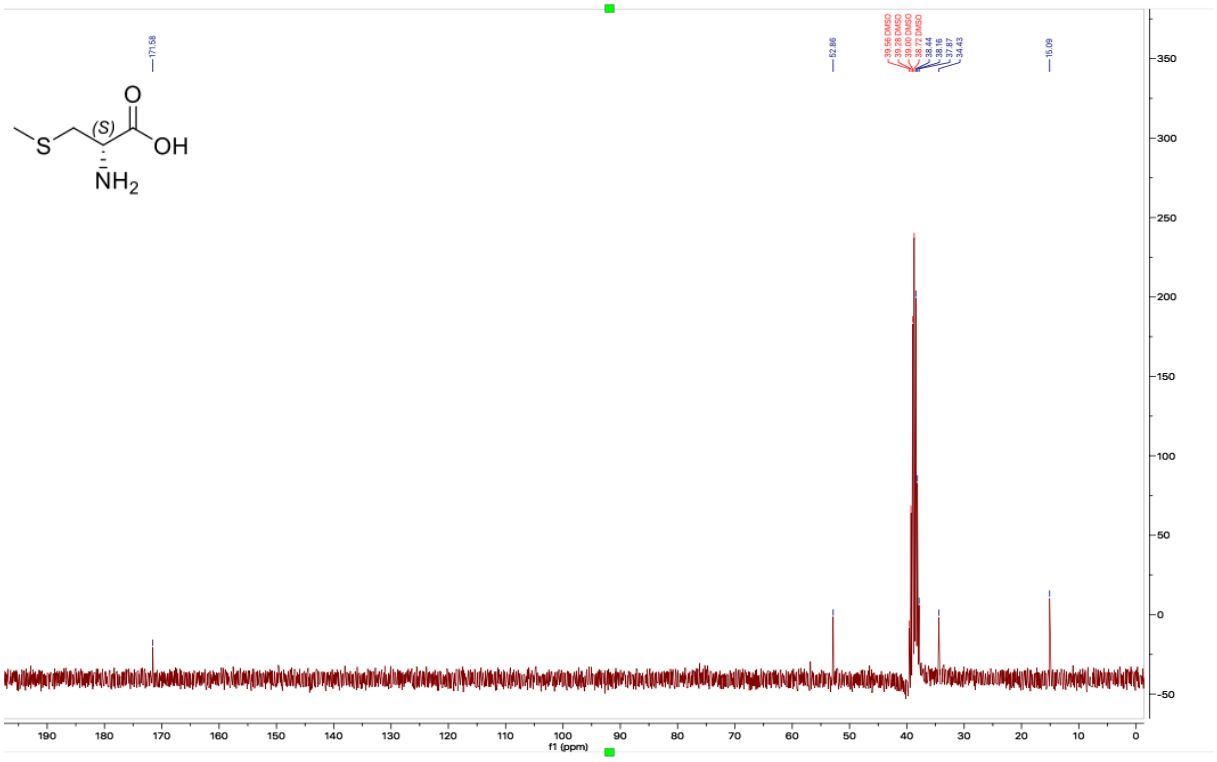
f1 (ppm)

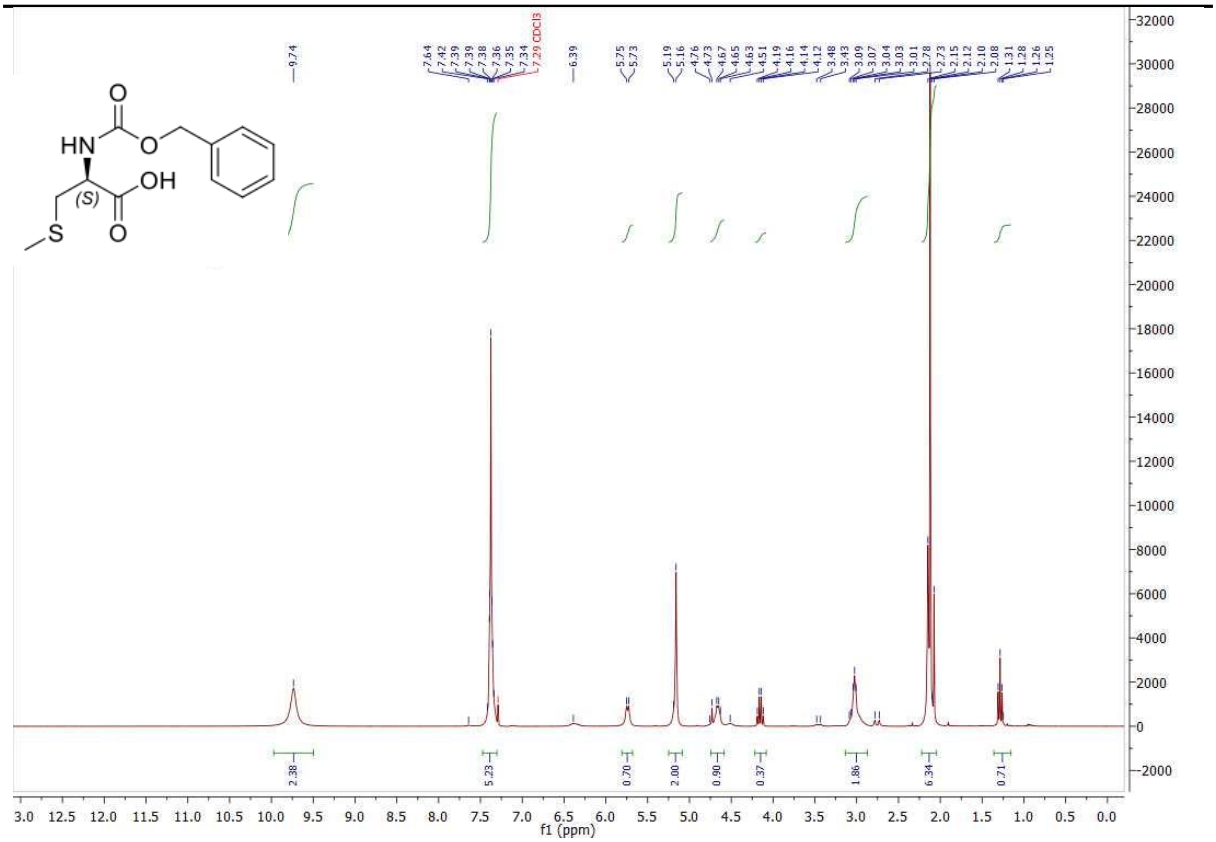
HN
O
O
OH
(S)
S
O
f1 (ppm)

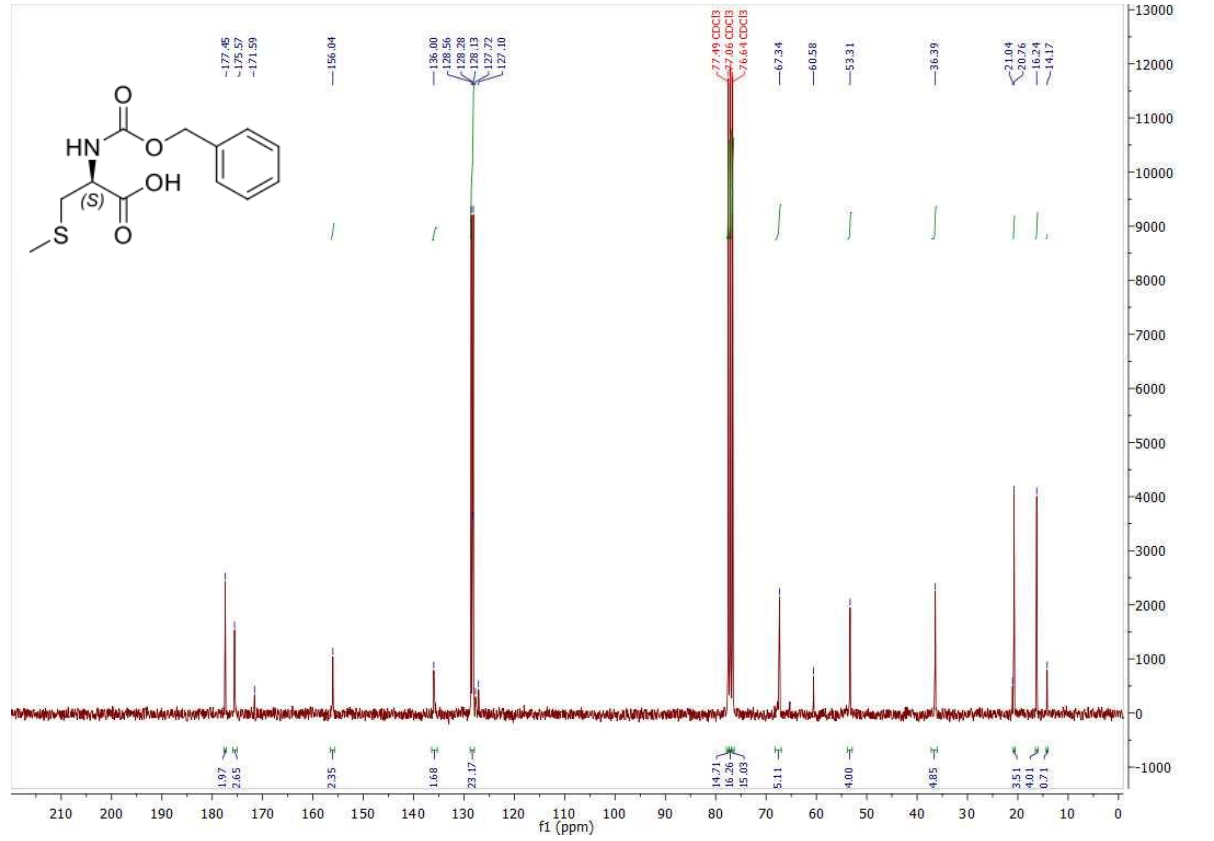
HN
O
O
OH
(S)
S
O
f1 (ppm)

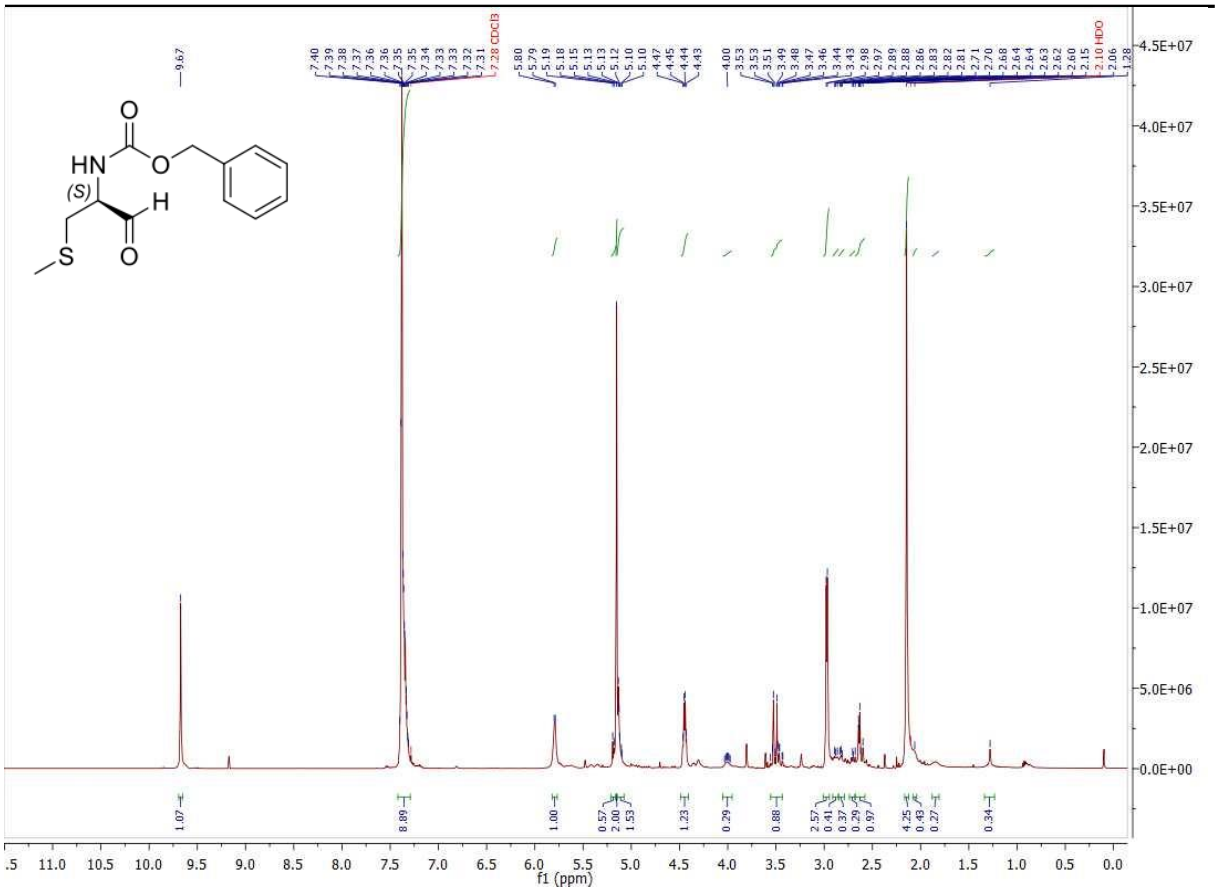
9.67
7.40
7.39
7.38
7.37
7.36
7.36
7.35
7.35
7.34
7.33
7.32
7.31
7.28 CDCl3
5.80
5.79
5.19
5.18
5.15
5.13
5.12
5.10
4.47
4.45
4.44
4.43
4.00
3.53
3.51
3.49
3.48
3.47
3.46
3.44
3.43
2.98
2.97
2.89
2.88
2.86
2.83
2.82
2.81
2.71
2.70
2.68
2.64
2.64
2.63
2.62
2.60
2.15
2.10 HDO
2.06
1.28
HN
O
O
(S)
H
S
O
4.5E+07
4.0E+07
3.5E+07
3.0E+07
2.5E+07
2.0E+07
1.5E+07
1.0E+07
5.0E+06
0.0E+00
1.07
8.89
1.00
0.57
2.00
1.53
1.23
0.29
0.88
2.57
6.41
0.37
0.29
0.97
4.25
0.43
0.27
0.34
f1 (ppm)

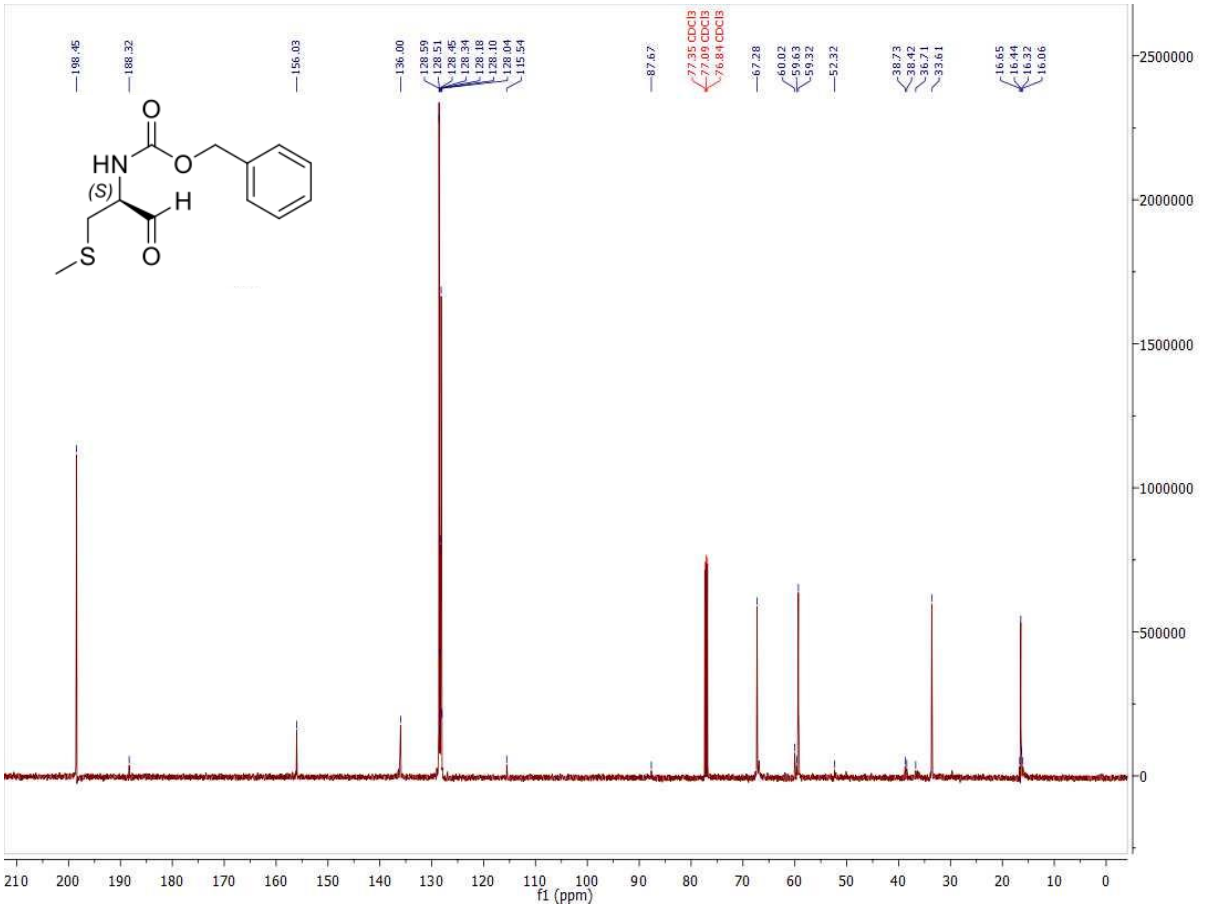
198.45
188.32
156.03
136.00
128.59
128.51
128.45
128.34
128.18
128.10
128.04
115.54
87.67
77.35 CDCl3
77.09 CDCl3
76.84 CDCl3
67.28
60.02
59.63
59.32
52.32
38.73
38.42
36.71
33.61
16.65
16.44
16.32
16.06
HN
O
O
(S)
H
S
O
2500000
2000000
1500000
1000000
500000
0
f1 (ppm)

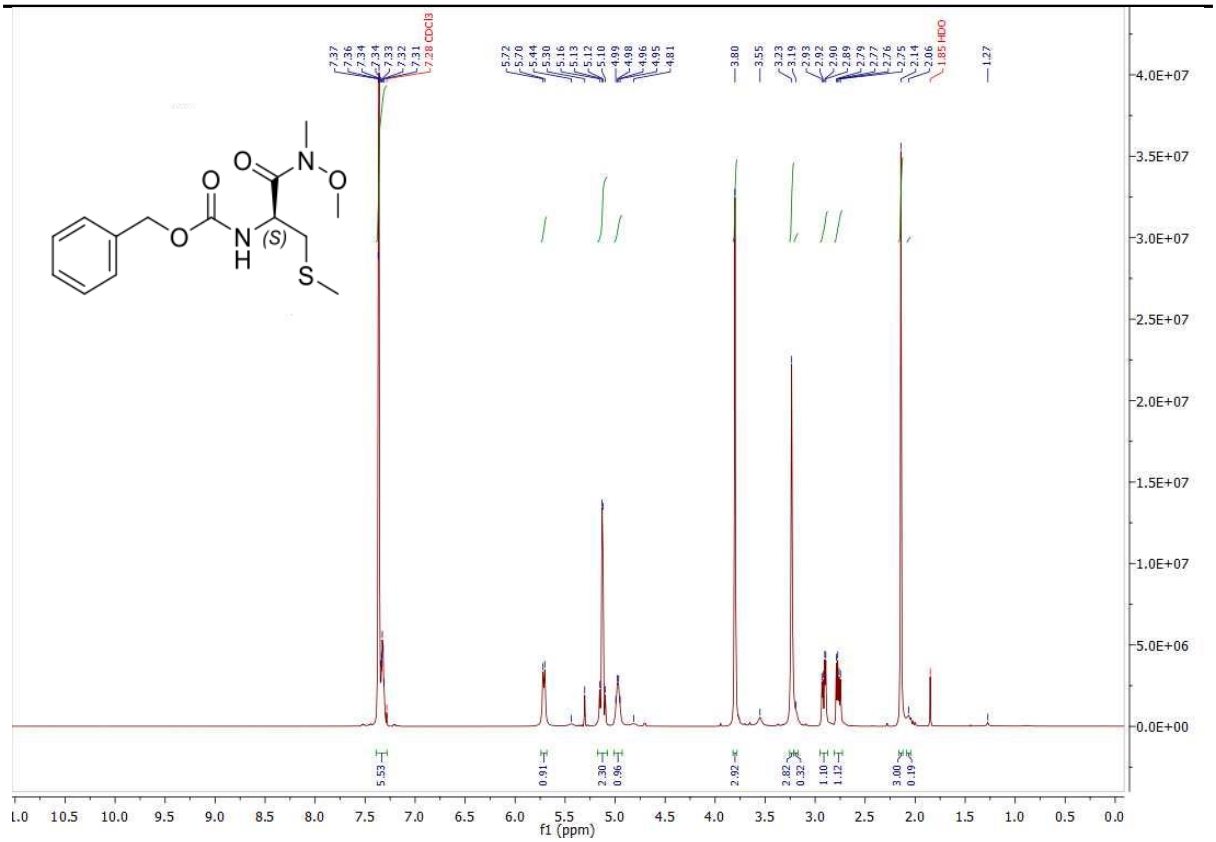
7.37
7.36
7.34
7.34
7.33
7.32
7.31
7.26 CDCl3
5.72
5.70
5.44
5.30
5.16
5.13
5.12
5.10
4.99
4.98
4.96
4.95
4.81
3.80
3.55
3.23
3.19
2.93
2.92
2.90
2.89
2.79
2.77
2.76
2.75
2.14
2.06
1.85 HDO
1.27
O
N
O
O
O
N
H
(S)
S
4.0E+07
3.5E+07
3.0E+07
2.5E+07
2.0E+07
1.5E+07
1.0E+07
5.0E+06
0.0E+00
5.53
0.91
2.30
0.96
2.92
2.82
0.32
1.10
1.12
3.00
0.19
f1 (ppm)

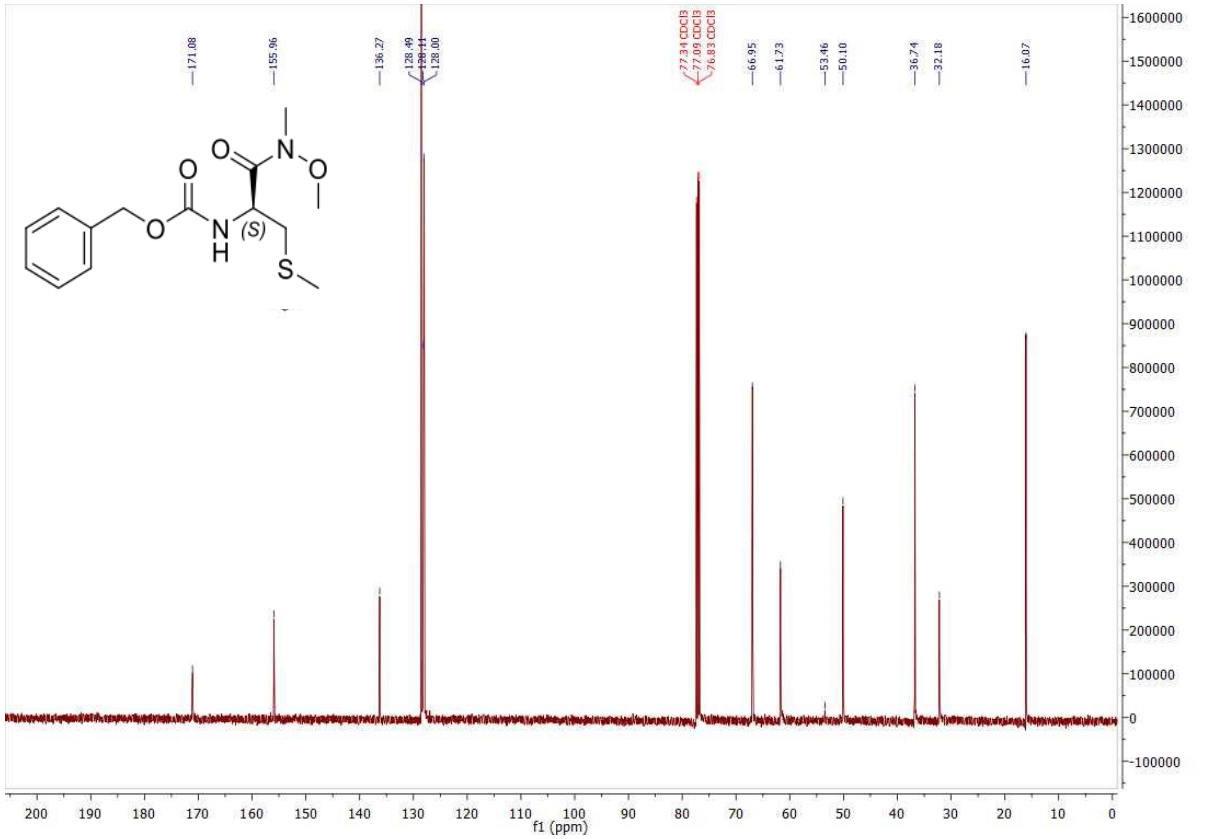
171.08
155.96
136.27
128.49
128.11
128.00
77.34 CDCl3
77.09 CDCl3
76.83 CDCl3
66.95
61.73
53.46
50.10
36.74
32.18
16.07
O
N
O
O
O
N
H
(S)
S
1600000
1500000
1400000
1300000
1200000
1100000
1000000
900000
800000
700000
600000
500000
400000
300000
200000
100000
0
-100000
f1 (ppm)

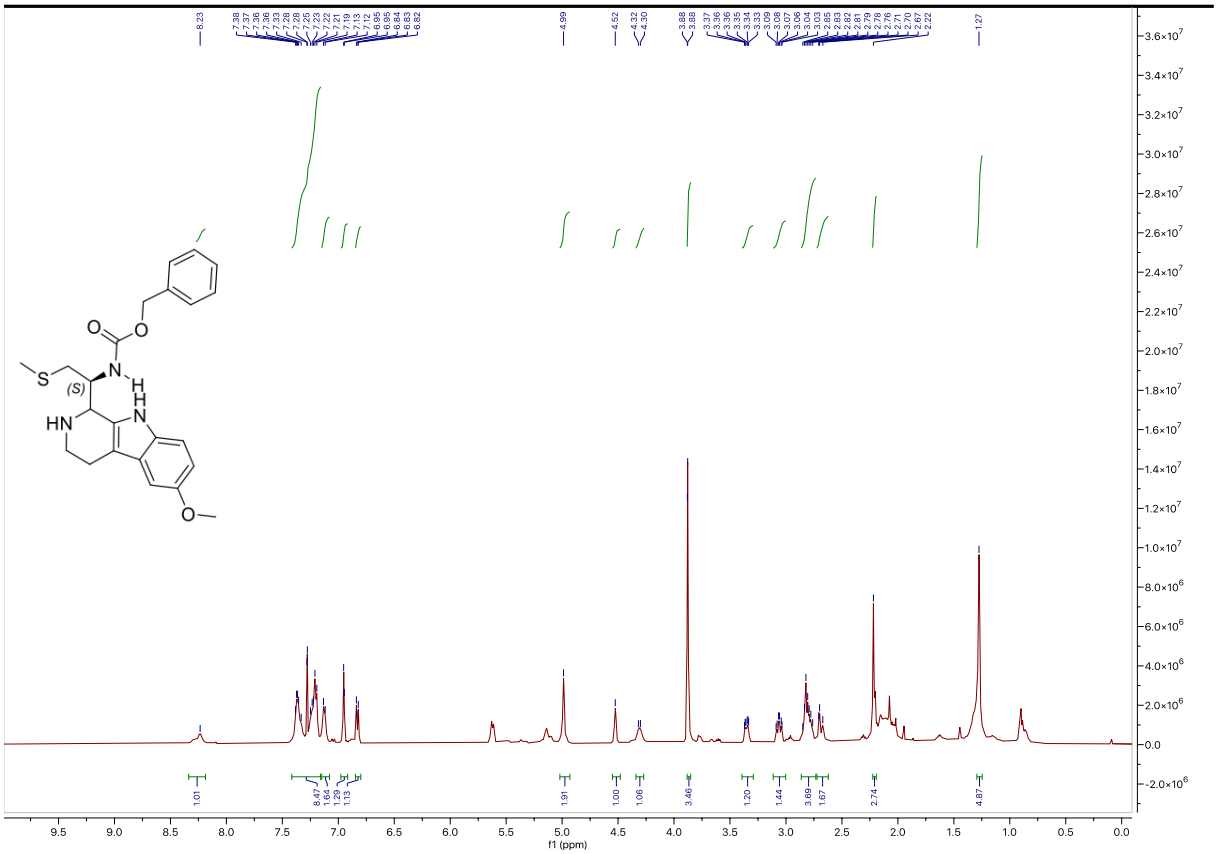
8.23
7.38
7.37
7.36
7.36
7.33
7.28
7.25
7.23
7.22
7.21
7.19
7.12
7.10
6.95
6.84
6.83
6.82
4.69
4.52
4.32
4.30
3.88
3.88
3.37
3.36
3.35
3.35
3.34
3.33
3.09
3.08
3.07
3.06
3.04
3.03
2.85
2.85
2.82
2.81
2.79
2.78
2.76
2.71
2.70
2.67
2.22
1.27
O
O
N
H
S
(S)
HN
N
O
1.01
8.47
1.64
1.70
1.13
1.91
1.00
1.06
3.46
1.20
1.44
3.69
1.67
2.74
4.87
f1 (ppm)

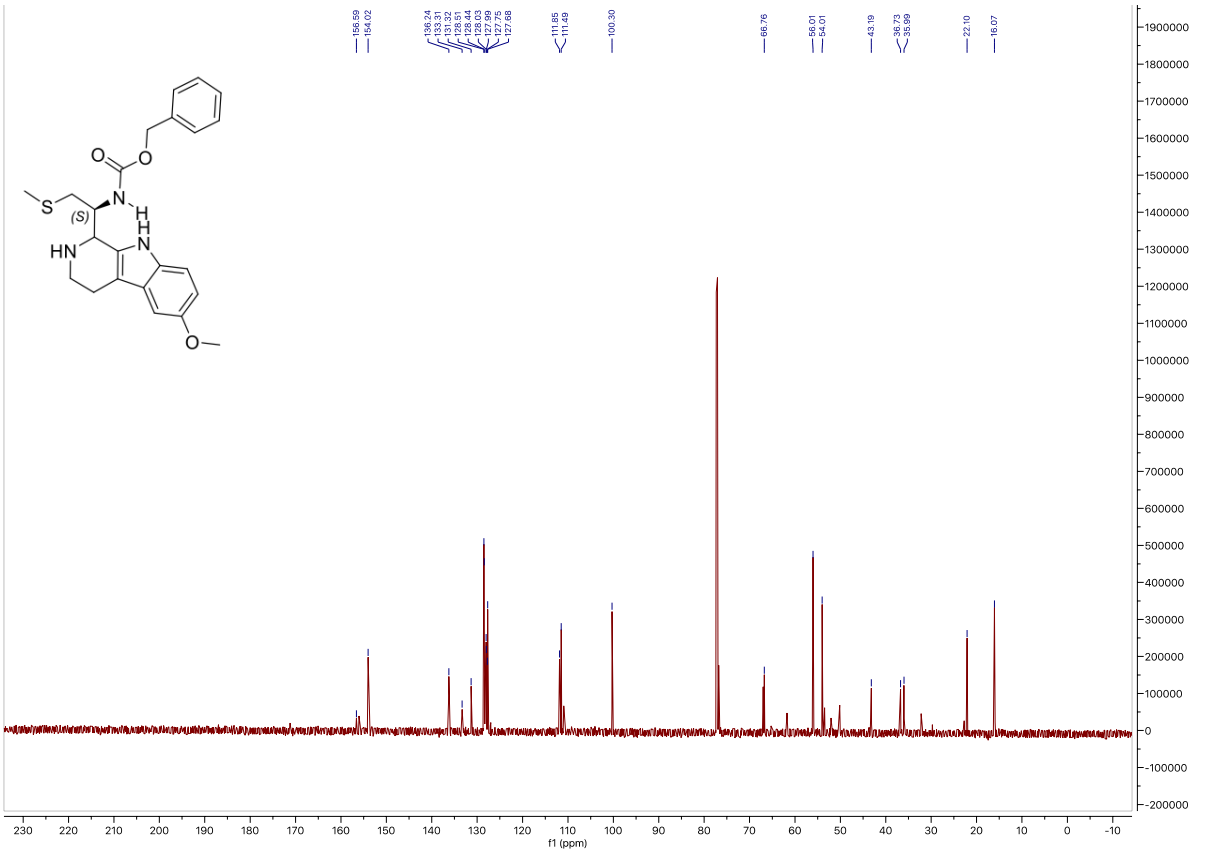
156.89
154.02
136.24
133.31
133.22
128.51
128.44
128.03
127.93
127.75
127.68
111.85
111.49
100.30
66.76
56.01
54.01
43.19
36.73
35.99
22.10
16.07
O
O
N
H
S
(S)
HN
N
O
f1 (ppm)

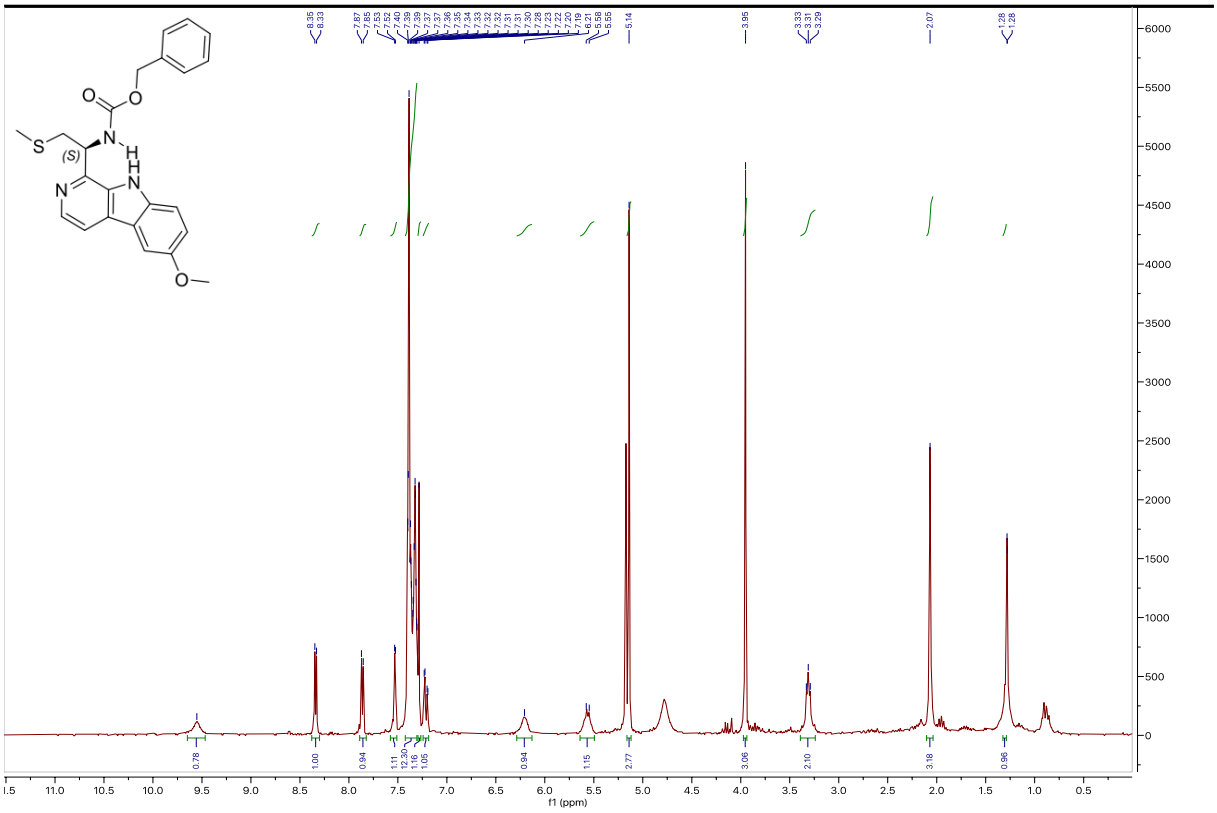
8.35
8.33
7.87
7.85
7.53
7.52
7.40
7.39
7.39
7.37
7.37
7.36
7.35
7.34
7.33
7.32
7.32
7.31
7.31
7.30
7.28
7.23
7.22
7.20
7.19
6.21
5.58
5.55
5.14
3.95
3.33
3.31
3.29
2.07
1.28
1.26
0.78
1.00
0.94
1.11
12.30
1.16
1.05
0.94
1.15
2.77
3.06
2.10
3.18
0.96
f1 (ppm)

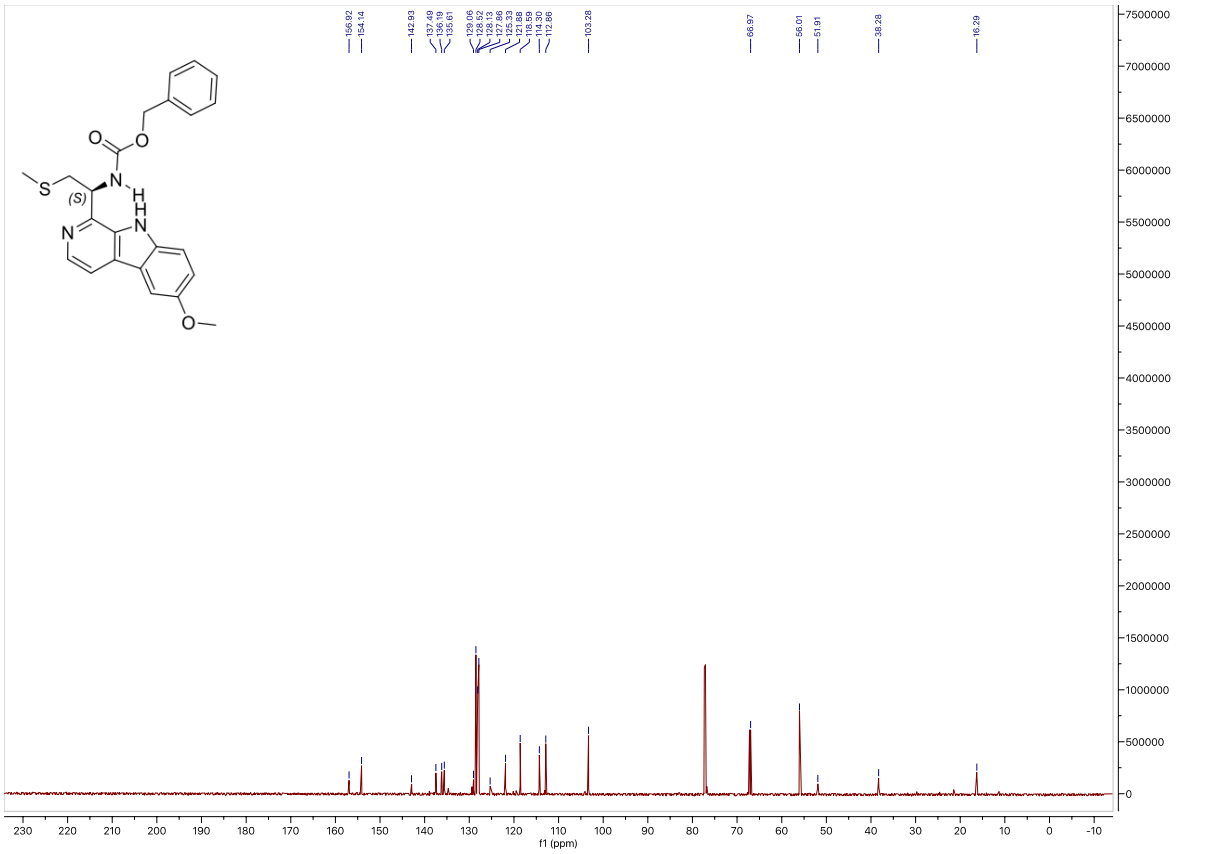
156.92
154.14
142.93
137.49
136.61
136.61
129.06
128.52
128.13
127.86
125.93
121.88
118.59
114.30
112.86
103.28
66.97
56.01
51.91
38.28
16.29
f1 (ppm)

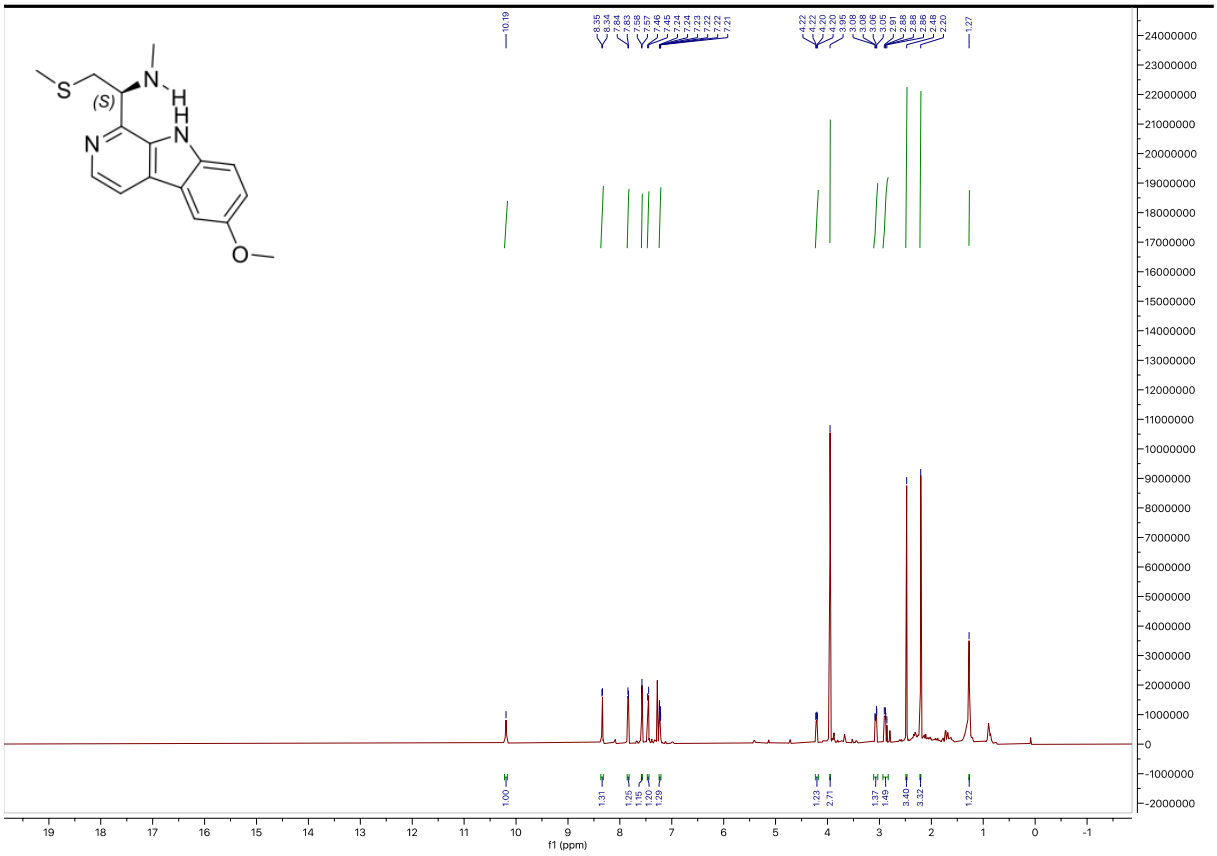
10.19
8.35
8.34
8.34
7.83
7.58
7.57
7.46
7.45
7.24
7.24
7.23
7.22
7.22
7.21
4.22
4.21
4.20
4.20
3.98
3.98
3.08
3.06
3.05
2.91
2.88
2.88
2.46
2.48
2.20
1.27
1.00
1.31
1.25
1.15
1.20
1.29
1.23
2.71
1.37
1.49
3.40
3.32
1.22
f1 (ppm)

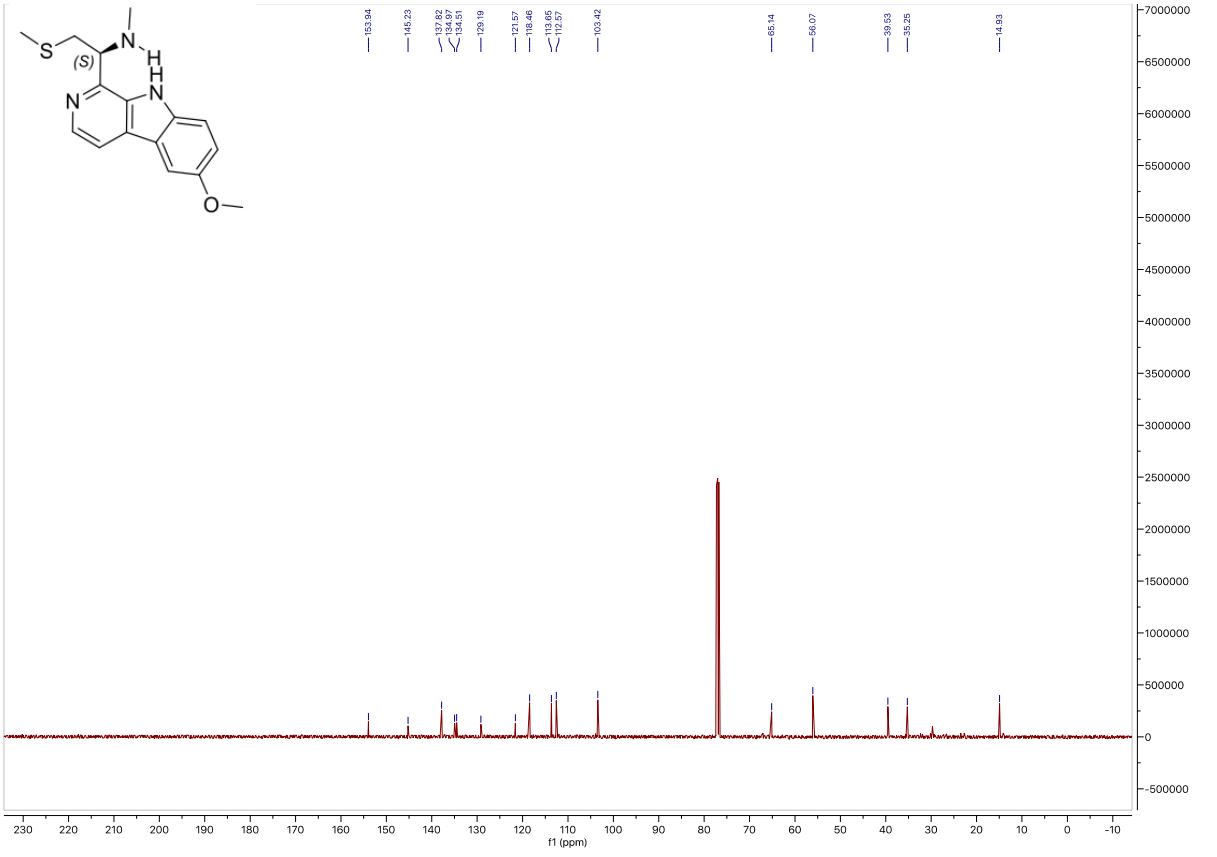
153.94
145.23
137.82
134.97
134.51
129.19
121.57
118.46
113.65
112.57
103.42
65.14
56.07
39.53
35.25
14.93
f1 (ppm)

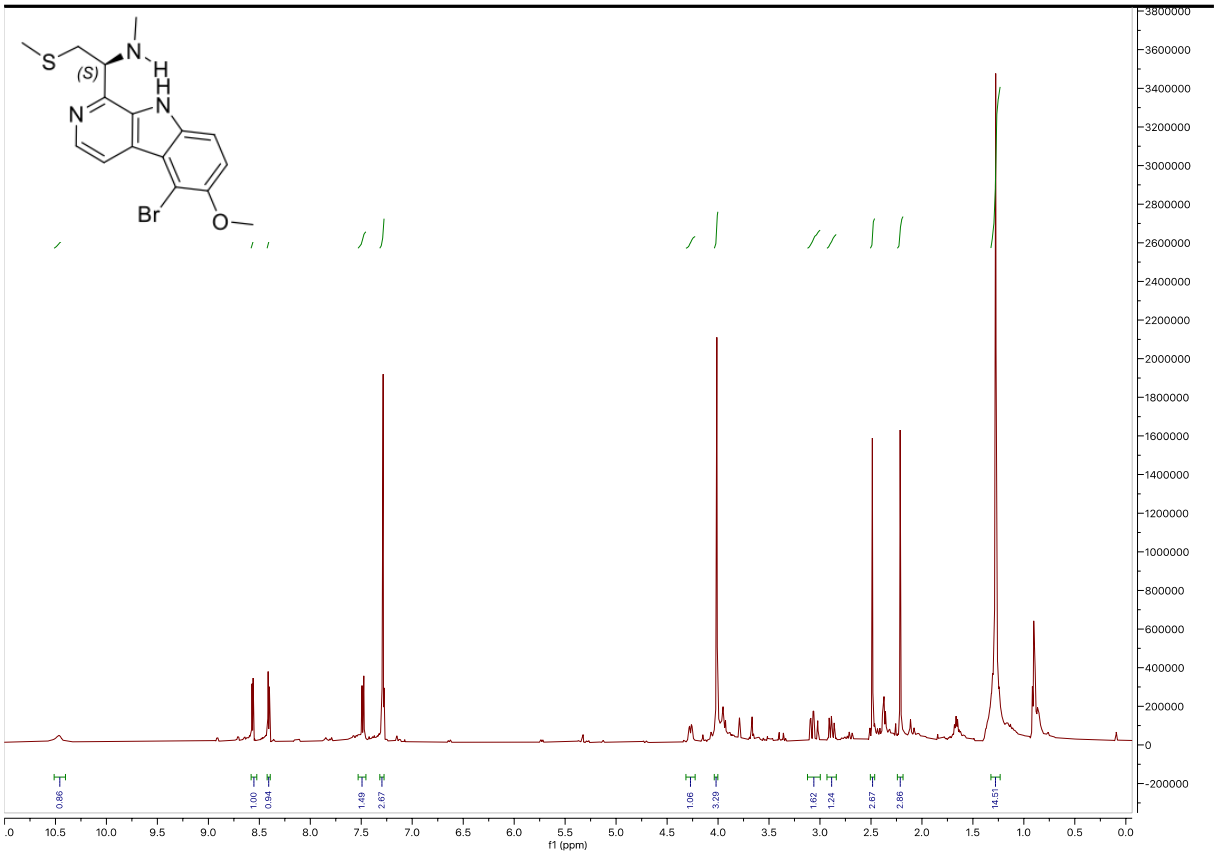
(S)
N
H
N
S
N
Br
O
0.86
1.00
0.94
1.49
2.67
1.06
3.29
1.62
1.24
2.67
2.86
14.51
f1 (ppm)

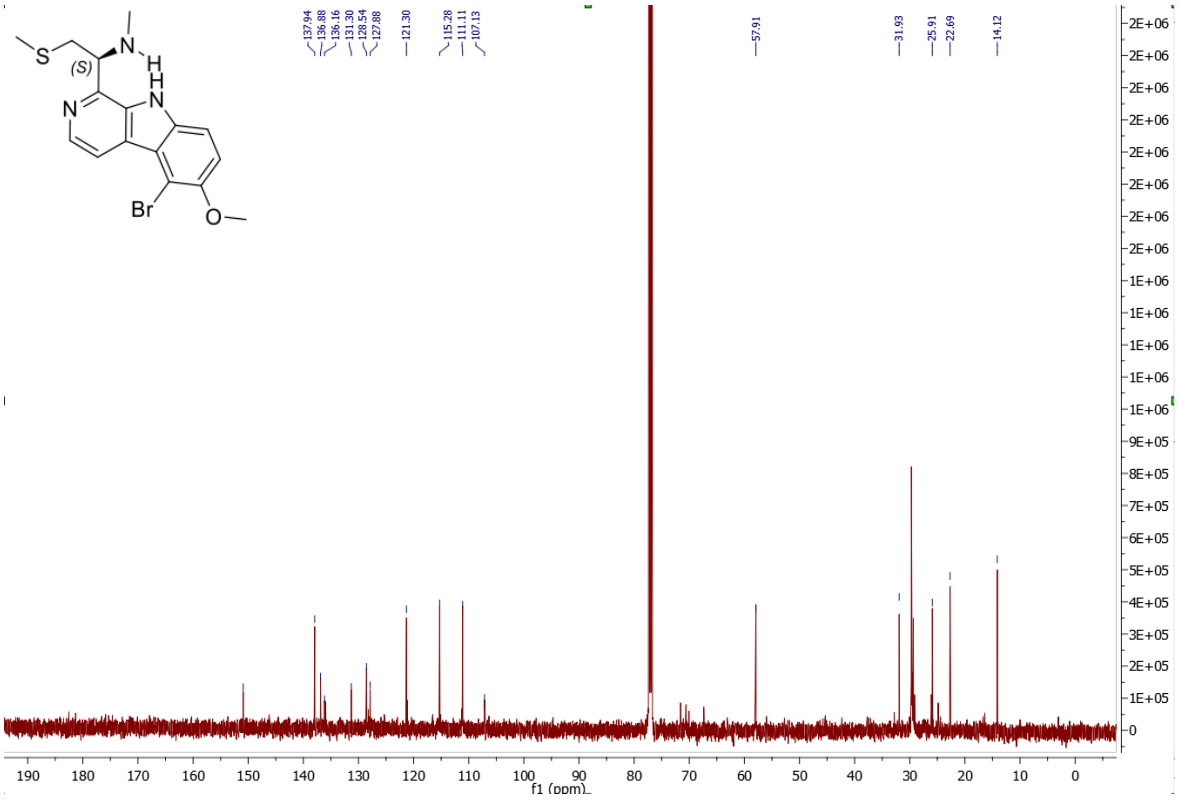
(S)
N
H
N
S
N
Br
O
137.94
136.88
136.16
131.30
128.54
127.88
121.30
115.28
111.11
107.13
57.91
31.93
25.91
22.69
14.12
f1 (ppm)

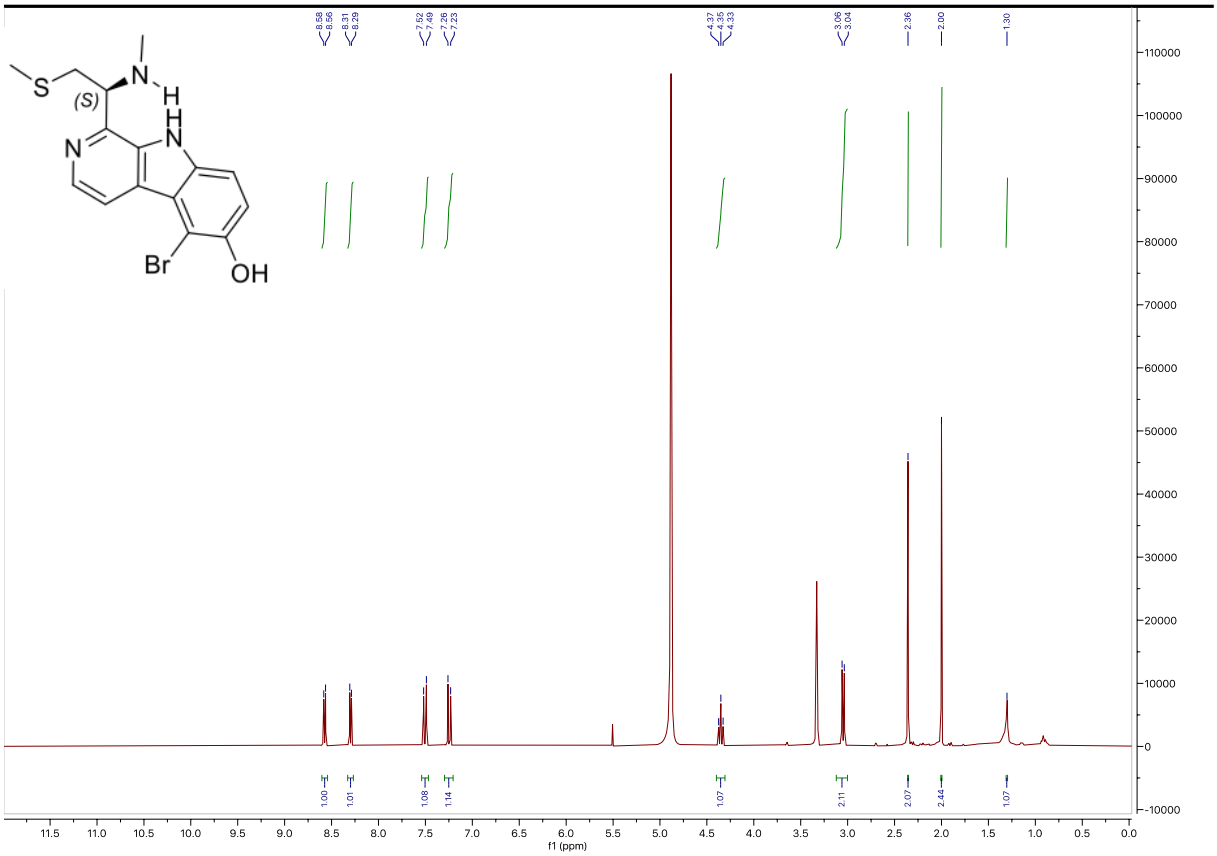
8.58
8.56
8.31
8.29
7.52
7.49
7.26
7.23
4.37
4.35
4.33
3.06
3.04
2.36
2.00
1.30
S
(S)
N
H
N
N
Br
OH
1.00
1.01
1.08
1.14
1.07
2.11
2.07
2.44
1.07
f1 (ppm)

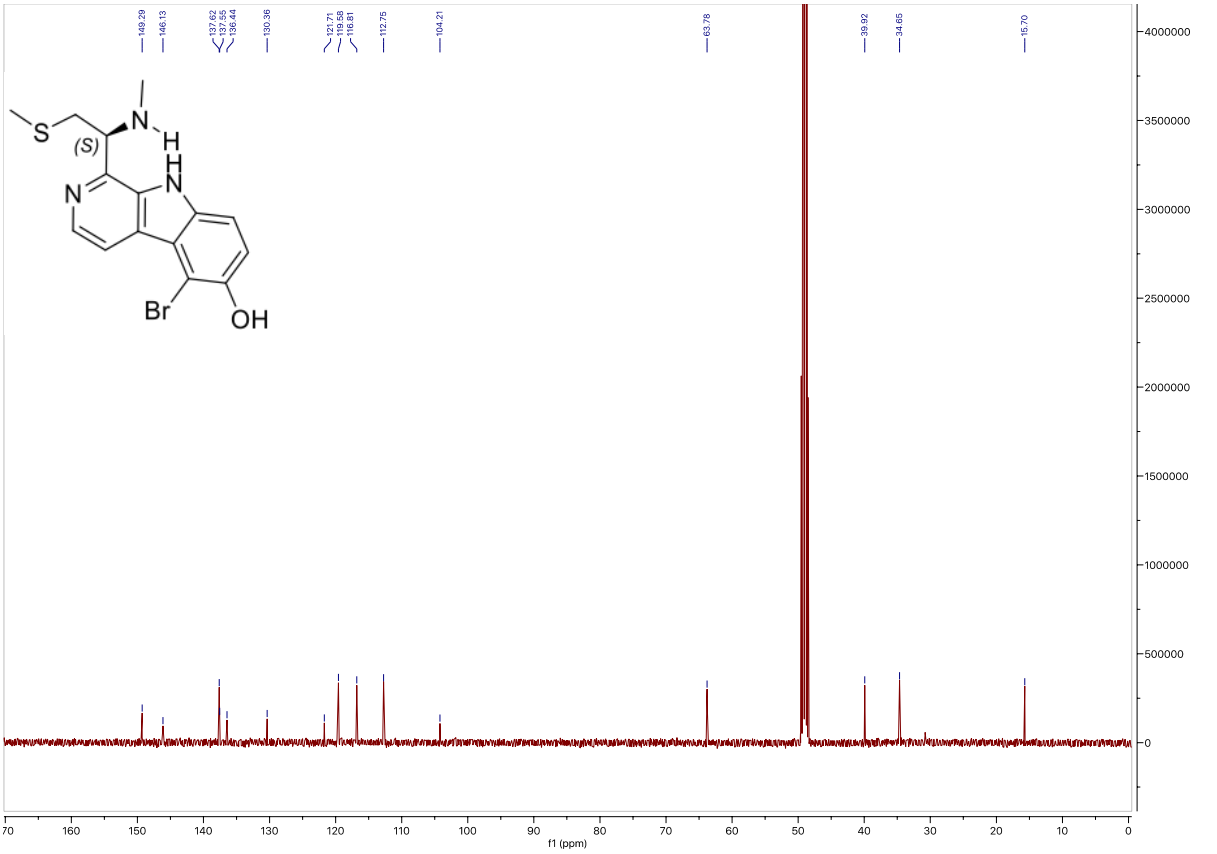
149.29
146.13
137.62
137.35
136.44
130.36
121.71
119.58
116.81
112.75
104.21
63.78
39.92
34.65
15.70
S
(S)
N
H
N
N
Br
OH
f1 (ppm)

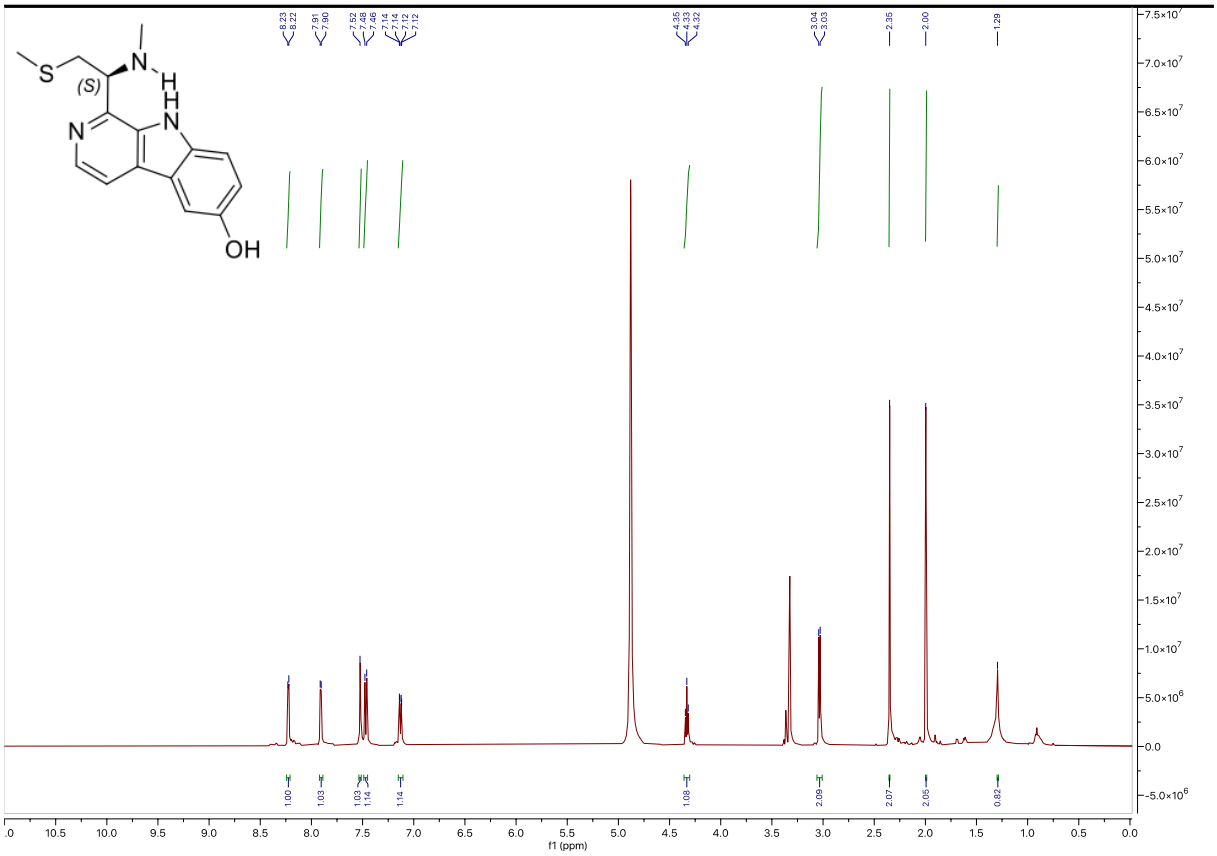
8.23
8.22
7.91
7.90
7.52
7.48
7.46
7.14
7.12
7.12
4.35
4.33
4.32
3.04
3.03
2.35
2.00
1.29
(S)
N
H
N
S
N
OH
1.00
1.03
1.03
1.14
1.14
1.08
2.09
2.07
2.05
0.82
f1 (ppm)

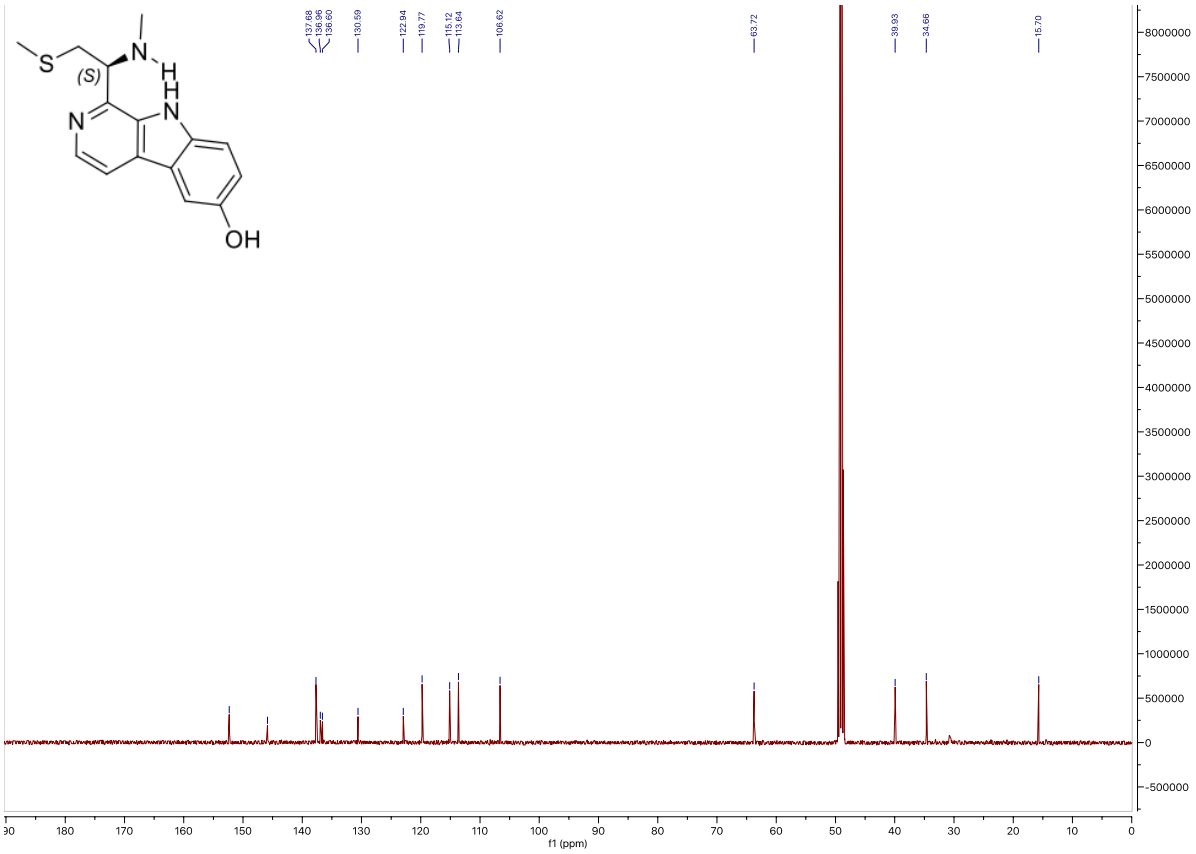
137.68
136.96
136.60
130.59
122.94
119.77
115.12
113.64
106.62
63.72
39.93
34.66
15.70
(S)
N
H
N
S
N
OH
f1 (ppm)

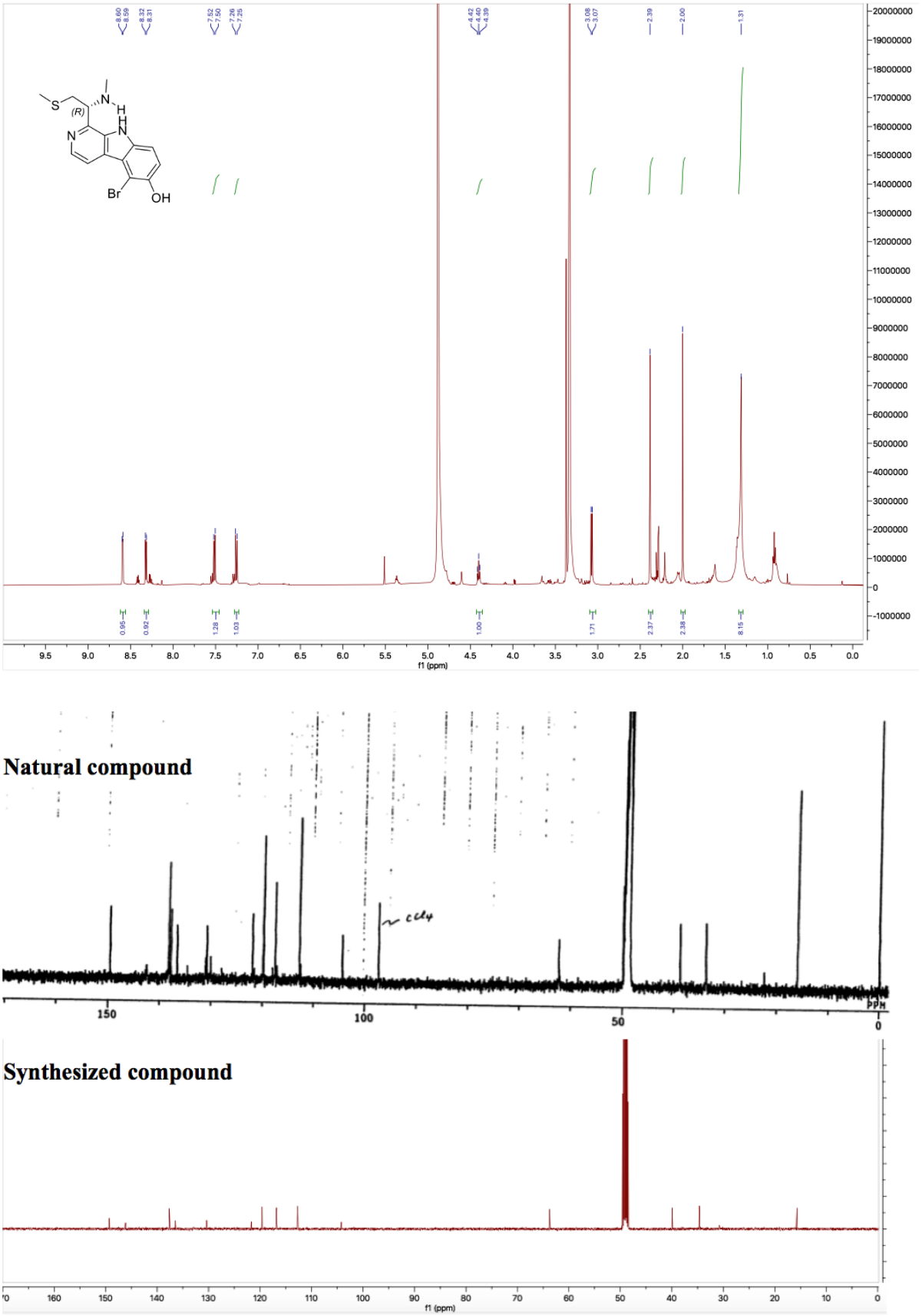

Figure A1: Comparaison of the ^{13}C NMR spectra of the natural and synthesized Eudistomidin C ((*S*)-5-bromo-1-(1-(methylamino)-2-(methylthio)ethyl)-9*H*-pyrido[3,4-β]indol-6-ol) (**BSc5517**).

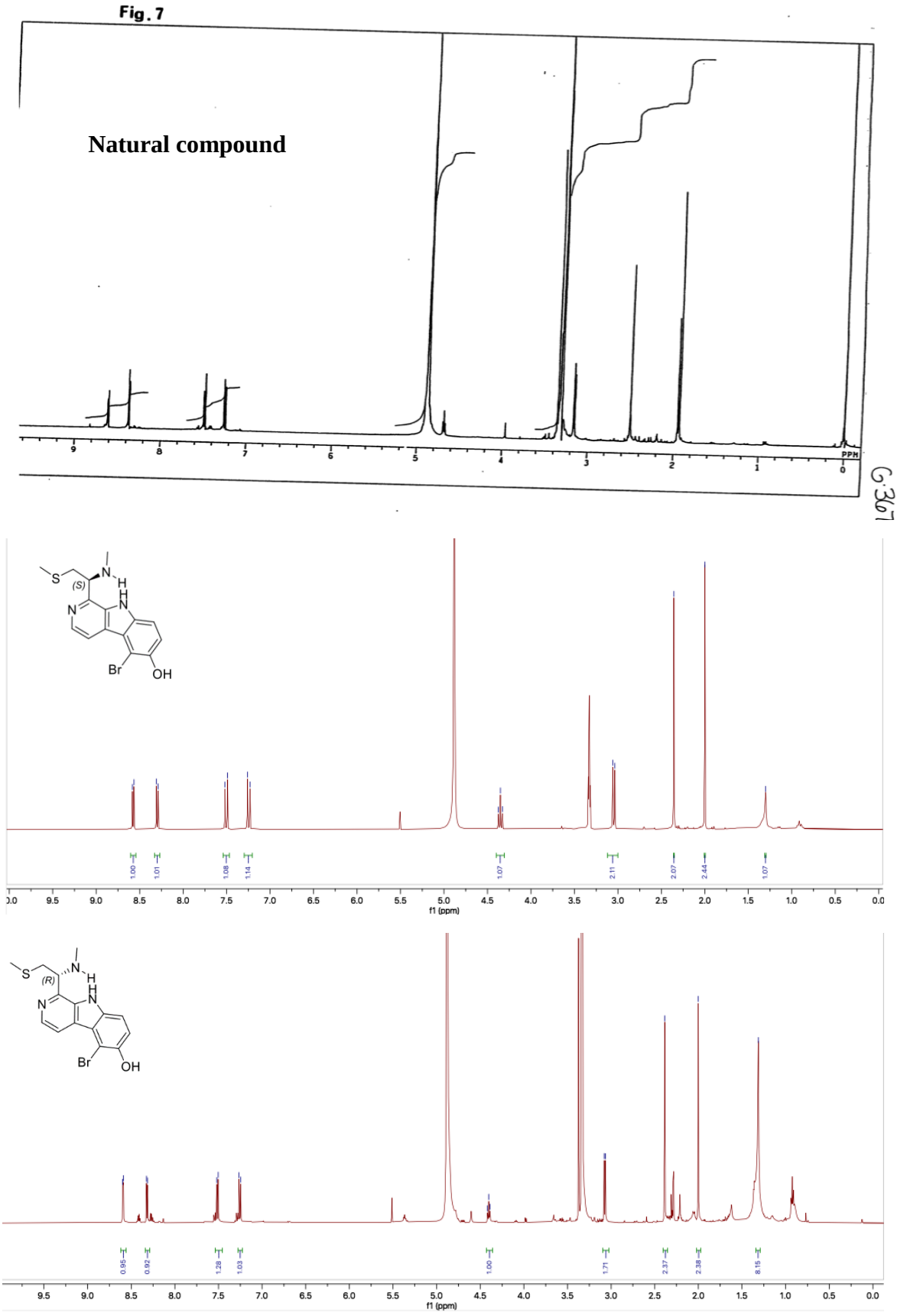

Figure A2: Comparison of the ^{1}H NMR spectra of the natural and synthesized Eudistomidin C (**BSc5517**) (enantiomers (*S*) and (*R*)) **BSc5517** and **BSc5580** respectively.

3. HPLCs analysis of the compounds utilized for biological assays

```
================================================================================
Injection Date  : 06.05.2021 14:24:41            Seq. Line :   4
Sample Name     : AK513 2nd  6f-7d               Location : Vial 42
Acq. Operator   : Dennis                            Inj :   1
                                                 Inj Volume : 10 µl
Acq. Method     : C:\HPCHEM\1\METHODS\PEPTIDE.M
Last changed    : 08.04.2021 10:33:24  by Dennis
Analysis Method : C:\HPCHEM\1\METHODS\PEPTIDE.M
Last changed    : 25.05.2021 07:48:02  by Dennis
CH3CN
```

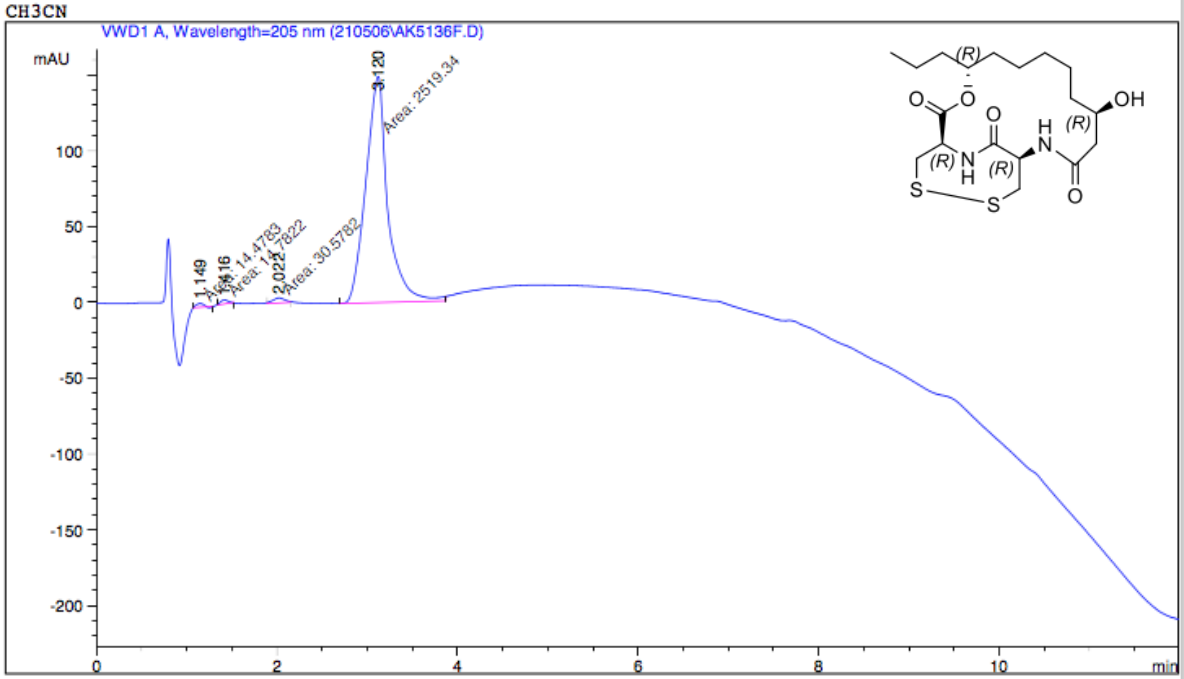


```
================================================================================
                          Area Percent Report
================================================================================

Sorted By             :      Signal
Multiplier            :      1.0000
Dilution              :      1.0000

Signal 1: VWD1 A, Wavelength=205 nm

Peak RetTime Type  Width     Area      Height     Area
  #   [min]       [min]  mAU   *s   [mAU   ]      %
----|-------|----|-------|----------|----------|--------|
   1   1.149 MM    0.1005   14.47828    2.40075   0.5614
   2   1.416 MM    0.0906   14.78217    2.71838   0.5731
   3   2.022 MM    0.1509   30.57817    3.37648   1.1856
   4   3.120 MM    0.2812 2519.33984  149.30392  97.6799

Totals :                   2579.17847  157.79953

 Results obtained with enhanced integrator!
================================================================================
                          *** End of Report ***
```

```
==========================================================================
Injection Date  : 20.09.2021 13:42:13          Seq. Line :   5
Sample Name     : AK020 1d                     Location : Vial 42
Acq. Operator   : Dennis                          Inj :   1
                                               Inj Volume : 10 µl

Acq. Method     : C:\HPCHEM\1\METHODS\PEPTIDE.M
Last changed    : 25.05.2021 07:48:02  by Dennis
Analysis Method : C:\HPCHEM\1\METHODS\PEPTIDE.M
Last changed    : 01.12.2021 11:26:15  by Dennis
CH3CN
```

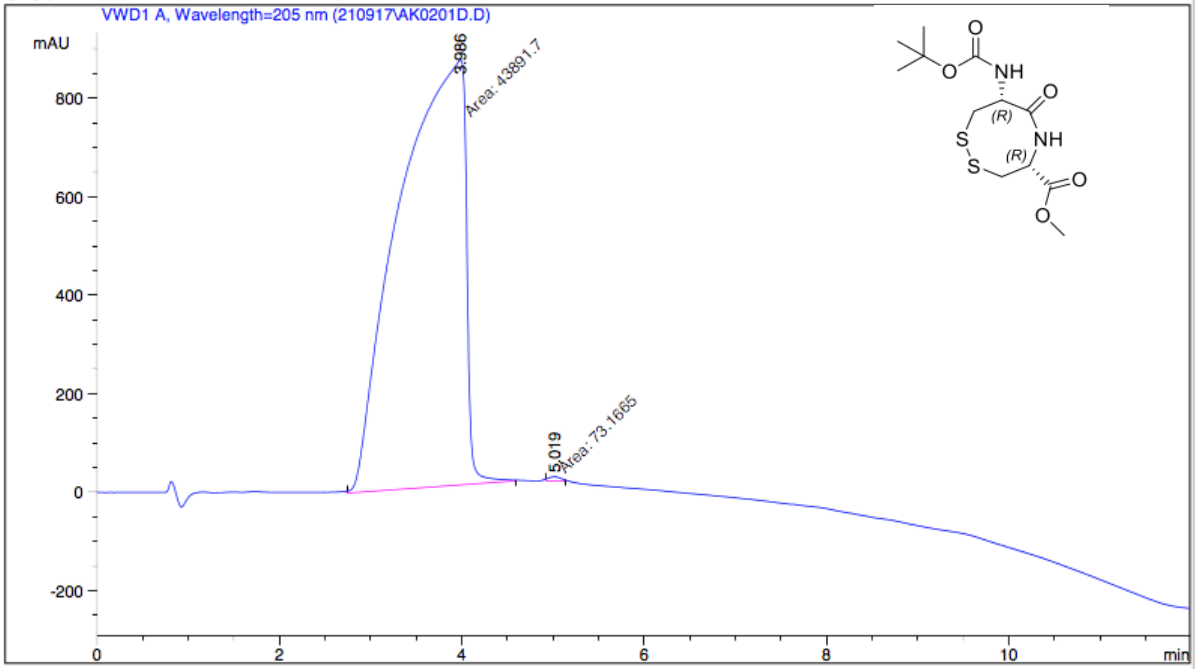


```
==========================================================================
                        Area Percent Report
==========================================================================

Sorted By             :      Signal
Multiplier            :      1.0000
Dilution              :      1.0000


Signal 1: VWD1 A, Wavelength=205 nm

Peak RetTime Type  Width     Area      Height     Area
  #   [min]       [min]  mAU   *s   [mAU   ]      %
----|-------|----|-------|----------|----------|--------|
   1   3.986 MM    0.8478 4.38917e4   862.81995  99.8336
   2   5.019 MM    0.1496   73.16650    8.15328   0.1664

Totals :                  4.39648e4   870.97322

 Results obtained with enhanced integrator!
==========================================================================
```

```
================================================================================
Injection Date  : 14.04.2021 11:27:50            Seq. Line :   1
Sample Name     : AK020´9 5b-7c                  Location : Vial 1
Acq. Operator   : Dennis                            Inj :   1
                                                 Inj Volume : 10 µl
Acq. Method     : C:\HPCHEM\1\METHODS\LARBIG.M
Last changed    : 14.04.2021 08:27:13  by Dennis
Analysis Method : C:\HPCHEM\1\METHODS\PEPTIDE.M
Last changed    : 01.12.2021 11:26:15  by Dennis
CH3CN
```

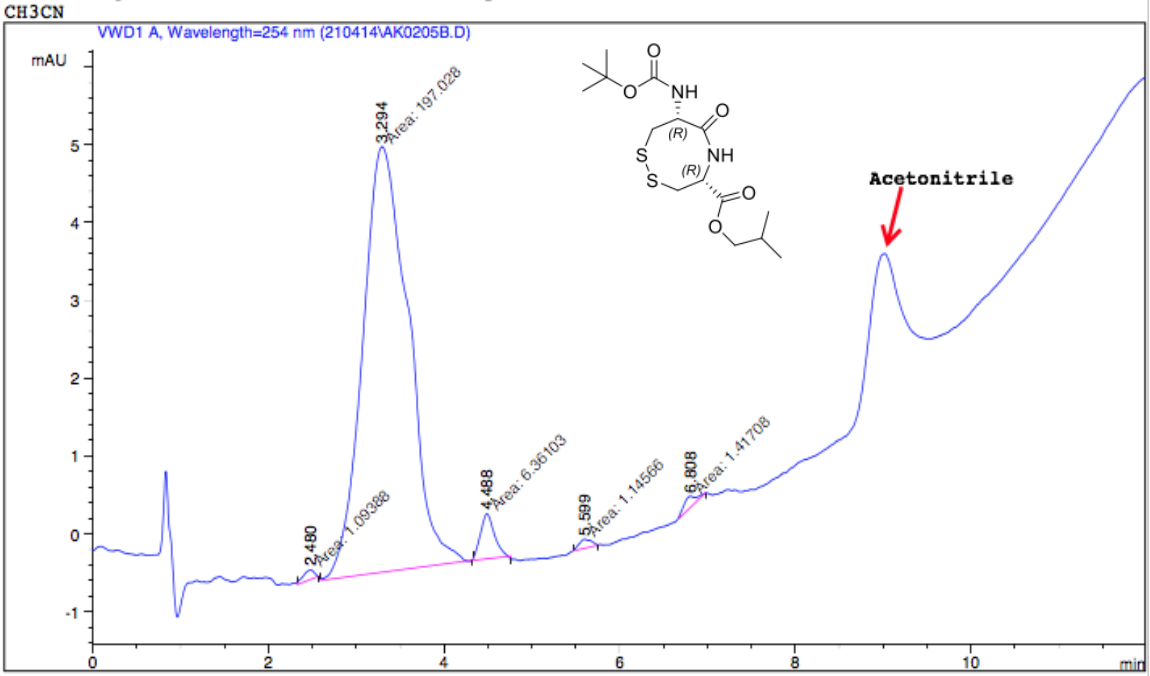


```
================================================================================
                          Area Percent Report
================================================================================

Sorted By             :      Signal
Multiplier            :      1.0000
Dilution              :      1.0000

Signal 1: VWD1 A, Wavelength=254 nm

Peak RetTime Type  Width     Area      Height     Area
  #   [min]        [min]  mAU   *s   [mAU   ]      %
----|-------|----|-------|----------|----------|--------|
   1   2.480 MM    0.1478    1.09388 1.23346e-1   0.5283
   2   3.294 MM    0.6005  197.02837    5.46818  95.1616
   3   4.488 MM    0.1836    6.36103 5.77280e-1   3.0723
   4   5.599 MM    0.1613    1.14566 1.18342e-1   0.5533
   5   6.808 MM    0.1615    1.41708 1.46263e-1   0.6844

Totals :                  207.04603    6.43341

 Results obtained with enhanced integrator!
================================================================================
                          *** End of Report ***
```

EC-012 rein Produkt nach Säule

```
======================================================================
Injection Date  : 01.12.2020 15:52:43            Seq. Line :  12
Sample Name     : EC-012 rein                     Location : Vial 92
Acq. Operator   : Dennis                             Inj :   1
                                                 Inj Volume : 10 µl
Acq. Method     : C:\HPCHEM\1\METHODS\LARBIG.M
Last changed    : 30.11.2020 15:26:03  by Dennis
Analysis Method : C:\HPCHEM\1\METHODS\LARBIG.M
Last changed    : 20.02.2022 14:51:18  by Dennis
CH3CN
```

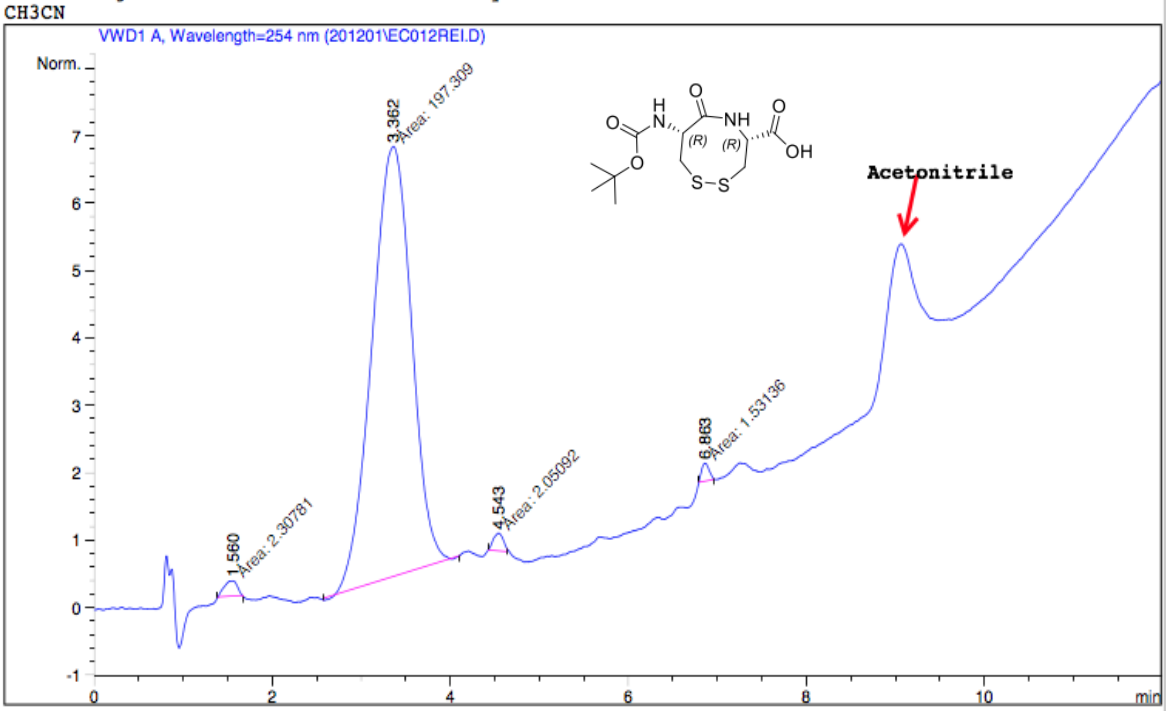


```
======================================================================
                        Area Percent Report
======================================================================

Sorted By             :      Signal
Multiplier            :      1.0000
Dilution              :      1.0000

Signal 1: VWD1 A, Wavelength=254 nm

Peak RetTime Type  Width     Area      Height     Area
  #   [min]        [min]  mAU   *s    [mAU   ]     %
----|-------|----|-------|----------|----------|--------|
   1   1.560 MM    0.1704    2.30781 2.25717e-1   1.1357
   2   3.362 MM    0.5154  197.30864    6.38038  97.1013
   3   4.543 MM    0.1298    2.05092 2.63255e-1   1.0093
   4   6.863 MM    0.0965    1.53136 2.64547e-1   0.7536

Totals :                  203.19873    7.13390

 Results obtained with enhanced integrator!
```

Data File C:\HPCHEM\1\DATA\201207\AK1504C.D Sample Name: AK150 4c-5c

AK150 4c-5c

```
==================================================================
Injection Date  : 07.12.2020 19:08:59          Seq. Line :   7
Sample Name     : AK150 4c-5c                   Location : Vial 15
Acq. Operator   : Dennis                           Inj :   1
                                               Inj Volume : 10 µl
Acq. Method     : C:\HPCHEM\1\METHODS\LARBIG.M
Last changed    : 30.11.2020 15:26:03  by Dennis
Analysis Method : C:\HPCHEM\1\METHODS\LARBIG.M
Last changed    : 29.01.2022 09:01:51  by Dennis
CH3CN
```

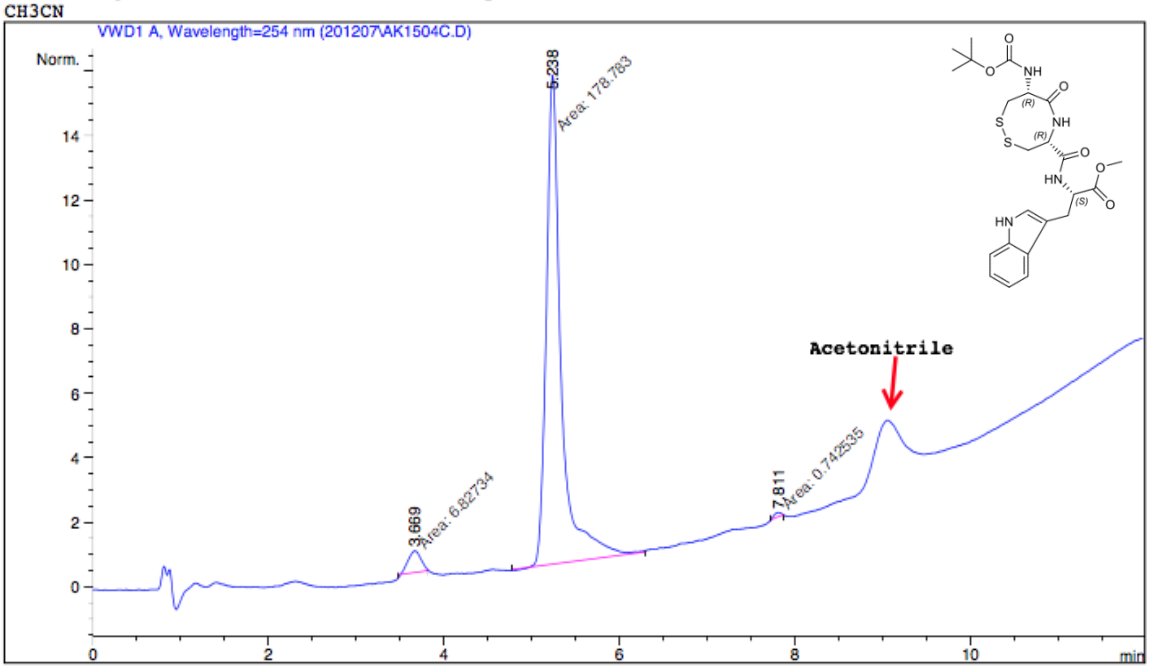


```
==================================================================
                      Area Percent Report
==================================================================

Sorted By             :      Signal
Multiplier            :      1.0000
Dilution              :      1.0000

Signal 1: VWD1 A, Wavelength=254 nm

Peak RetTime Type  Width     Area      Height     Area
  #   [min]        [min]  mAU   *s    [mAU   ]      %
----|-------|----|-------|----------|----------|--------|
   1   3.669 MM    0.1705    6.82734 6.67323e-1   3.6637
   2   5.238 MM    0.1962  178.78345   15.18335  95.9379
   3   7.811 MM    0.0921 7.42535e-1 1.34434e-1   0.3985

Totals :                   186.35332   15.98511

 Results obtained with enhanced integrator!
==================================================================
                        *** End of Report ***
```

```
================================================================================
Injection Date  : 01.09.2021 22:34:46            Seq. Line :  19
Sample Name     : AK400 8f                      Location : Vial 11
Acq. Operator   : Dennis                           Inj :   1
                                                Inj Volume : 10 µl

Acq. Method     : C:\HPCHEM\1\METHODS\PEPTIDE.M
Last changed    : 25.05.2021 07:48:02  by Dennis
Analysis Method : C:\HPCHEM\1\METHODS\LARBIG.M
Last changed    : 20.08.2021 15:46:54  by Dennis
CH3CN
```

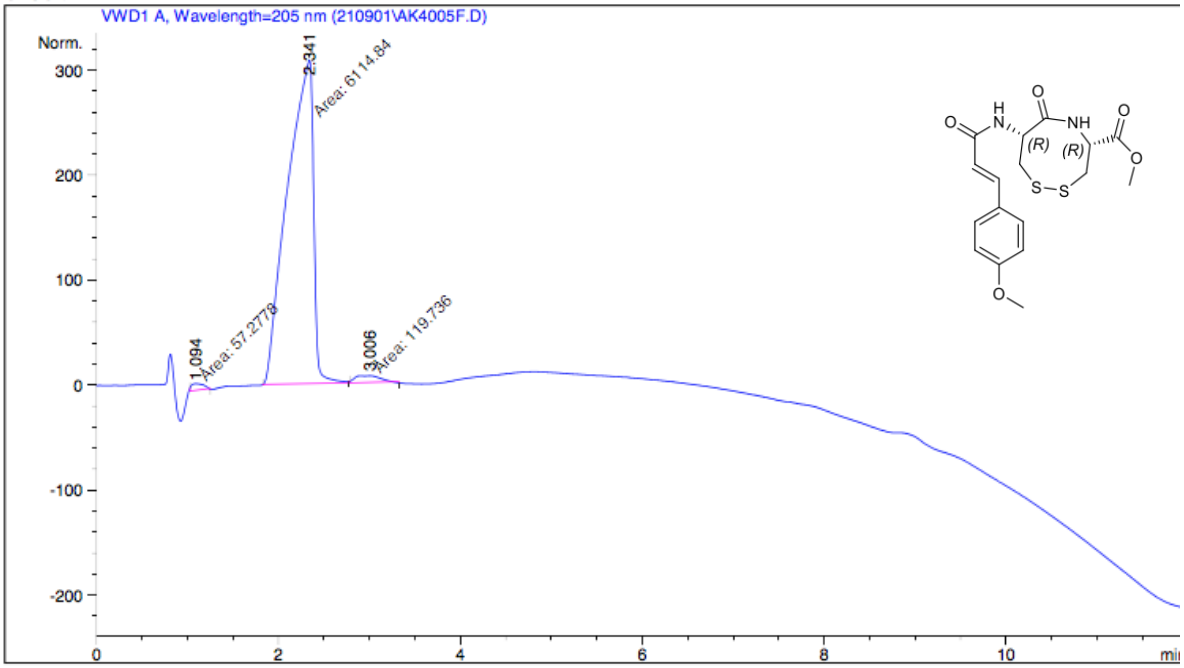


```
================================================================================
                          Area Percent Report
================================================================================

Sorted By             :      Signal
Multiplier            :      1.0000
Dilution              :      1.0000


Signal 1: VWD1 A, Wavelength=205 nm

Peak RetTime Type  Width     Area      Height     Area
  #   [min]        [min]  mAU   *s   [mAU   ]      %
----|-------|----|-------|----------|----------|--------|
   1   1.094 MM    0.1503   57.27784    6.35227   0.9103
   2   2.341 MM    0.3302 6114.83789  308.64798  97.1866
   3   3.006 MM    0.3178  119.73589    6.28025   1.9030

Totals :                  6291.85161  321.28050

 Results obtained with enhanced integrator!
================================================================================
                          *** End of Report ***
```

```
Injection Date  : 22.09.2021 19:42:27            Seq. Line :   8
Sample Name     : AK410´ 4e-5d                   Location : Vial 62
Acq. Operator   : Dennis                            Inj :   1
                                                 Inj Volume : 10 µl

Acq. Method     : C:\HPCHEM\1\METHODS\PEPTIDE.M
Last changed    : 22.09.2021 19:40:38  by Dennis
                  (modified after loading)
Analysis Method : C:\HPCHEM\1\METHODS\PEPTIDE.M
Last changed    : 01.12.2021 11:26:15  by Dennis
CH3CN
```

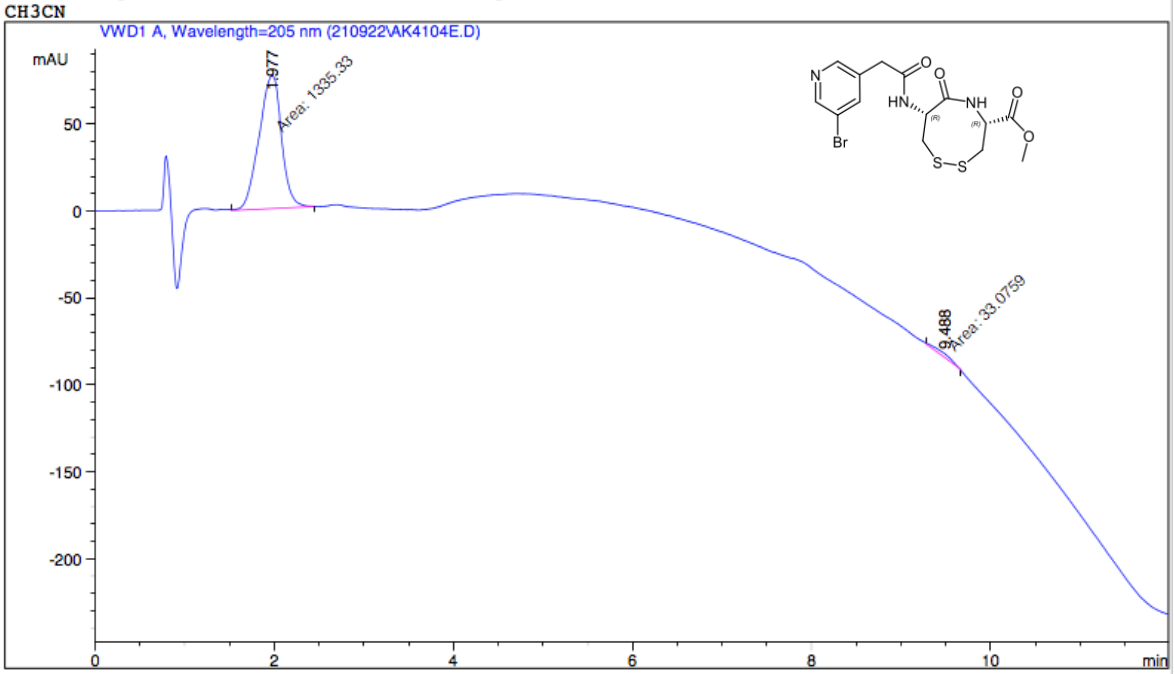


```
================================================================================
                          Area Percent Report
================================================================================

Sorted By             :      Signal
Multiplier            :      1.0000
Dilution              :      1.0000


Signal 1: VWD1 A, Wavelength=205 nm

Peak RetTime Type  Width     Area      Height     Area
  #   [min]        [min]  mAU   *s   [mAU   ]      %
----|-------|----|-------|----------|----------|--------|
   1   1.977 MM    0.2916 1335.32776   76.32817  97.5829
   2   9.488 MM    0.2458   33.07587    2.24278   2.4171

Totals :                  1368.40363   78.57095

 Results obtained with enhanced integrator!
================================================================================
```

```
==========================================================================
Injection Date  : 22.09.2021 20:16:39            Seq. Line :  10
Sample Name     : AK420´ 8c-9d                   Location : Vial 64
Acq. Operator   : Dennis                            Inj :   1
                                                 Inj Volume : 10 µl
Acq. Method     : C:\HPCHEM\1\METHODS\PEPTIDE.M
Last changed    : 22.09.2021 20:13:46  by Dennis
                  (modified after loading)
Analysis Method : C:\HPCHEM\1\METHODS\PEPTIDE.M
Last changed    : 01.12.2021 11:26:15  by Dennis
CH3CN
```

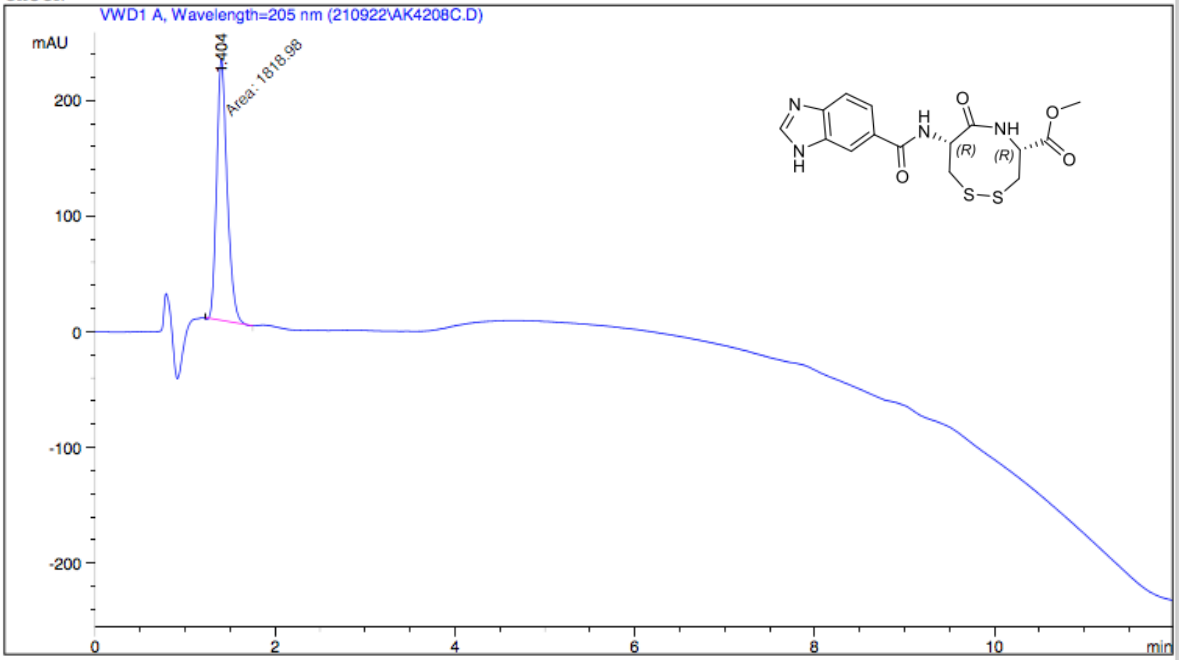


```
==========================================================================
                        Area Percent Report
==========================================================================

Sorted By             :      Signal
Multiplier            :      1.0000
Dilution              :      1.0000


Signal 1: VWD1 A, Wavelength=205 nm

Peak RetTime Type  Width     Area      Height     Area
  #   [min]       [min]  mAU   *s   [mAU   ]      %
----|-------|----|-------|----------|----------|--------|
   1   1.404 MM    0.1343 1818.98035  225.69624 100.0000

Totals :                  1818.98035  225.69624

 Results obtained with enhanced integrator!
==========================================================================
                        *** End of Report ***
```

```
==========================================================================
Injection Date  : 26.06.2022 12:42:50          Seq. Line :   1
Sample Name     : 3d                            Location : Vial 33
Acq. Operator   : Dennis                           Inj :   1
                                                Inj Volume : 10 µl
Different Inj Volume from Sequence !     Actual Inj Volume : 30 µl
Acq. Method     : C:\HPCHEM\1\METHODS\LARBIG.M
Last changed    : 15.06.2022 13:00:43  by Dennis
Analysis Method : C:\HPCHEM\1\METHODS\LARBIG.M
Last changed    : 27.07.2022 08:34:44  by Dennis
CH3CN
```

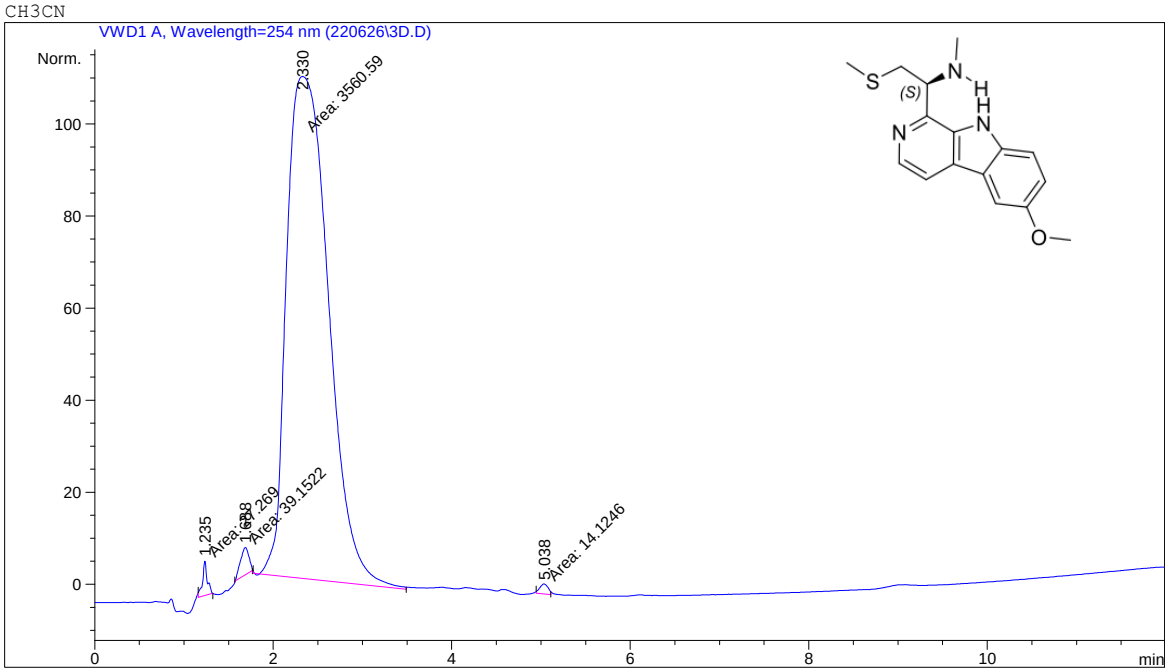


```
==========================================================================
                        Area Percent Report
==========================================================================

Sorted By             :      Signal
Multiplier            :      1.0000
Dilution              :      1.0000


Signal 1: VWD1 A, Wavelength=254 nm

Peak RetTime Type  Width     Area      Height     Area
  #   [min]        [min]  mAU   *s   [mAU   ]      %
----|-------|----|-------|----------|----------|--------|
   1   1.235 MM    0.0600   27.26902    7.57347   0.7489
   2   1.688 MM    0.1092   39.15224    5.97516   1.0753
   3   2.330 MM    0.5443 3560.58765  109.03267  97.7879
   4   5.038 MM    0.1080   14.12455    2.18030   0.3879

Totals :                  3641.13345  124.76159

 Results obtained with enhanced integrator!
==========================================================================
                        *** End of Report ***
```

```
==========================================================================
Injection Date  : 28.06.2022 13:20:44            Seq. Line :  10
Sample Name     : 7c                              Location : Vial 27
Acq. Operator   : Dennis                             Inj :   1
                                                 Inj Volume : 10 µl
Different Inj Volume from Sequence !     Actual Inj Volume : 30 µl
Acq. Method     : C:\HPCHEM\1\METHODS\LARBIG.M
Last changed    : 28.06.2022 13:17:37  by Dennis
                  (modified after loading)
Analysis Method : C:\HPCHEM\1\METHODS\LARBIG.M
Last changed    : 27.07.2022 08:34:44  by Dennis
CH3CN
```

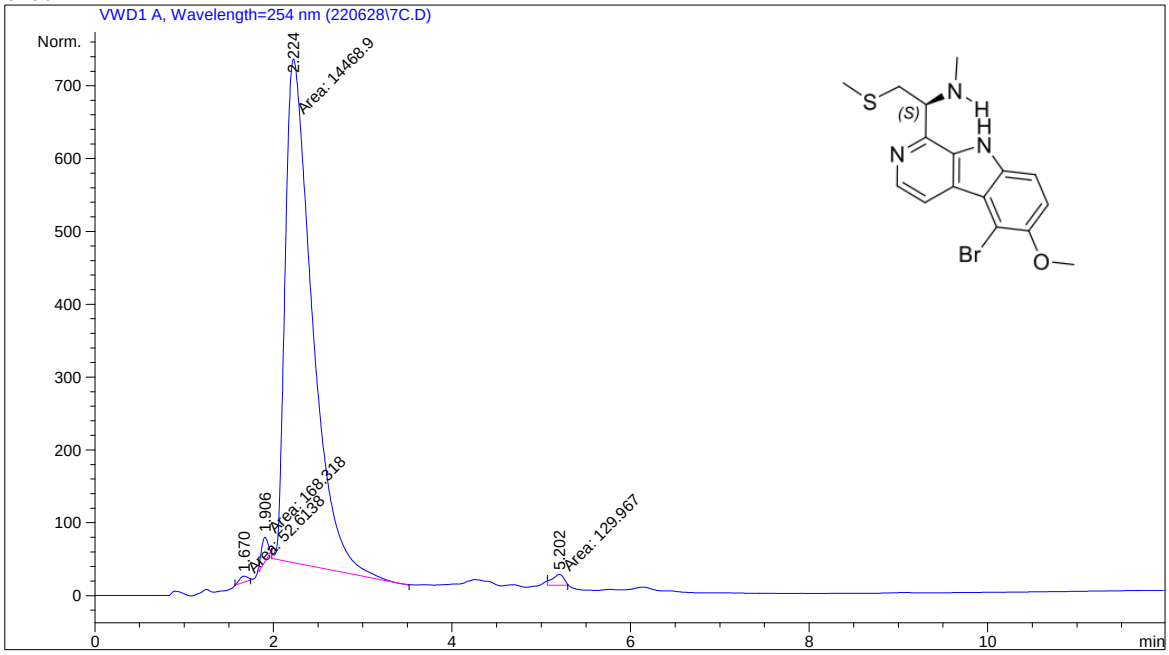


```
==========================================================================
                        Area Percent Report
==========================================================================

Sorted By             :      Signal
Multiplier            :      1.0000
Dilution              :      1.0000


Signal 1: VWD1 A, Wavelength=254 nm

Peak RetTime Type  Width     Area      Height     Area
  #   [min]        [min]  mAU   *s   [mAU   ]       %
----|-------|----|-------|----------|----------|--------|
   1   1.670 MM    0.1046   52.61385    8.38636   0.3550
   2   1.906 MM    0.0822  168.31786   34.12273   1.1358
   3   2.224 MM    0.3487 1.44689e4   691.47711  97.6322
   4   5.202 MM    0.1472  129.96696   14.71870   0.8770

Totals :                  1.48198e4   748.70490

 Results obtained with enhanced integrator!
==========================================================================
                        *** End of Report ***
```

ED27´3 1e-2b

```
==========================================================================
Injection Date  : 30.03.2022 11:50:44          Seq. Line :   1
Sample Name     : ED27´3 1e-2b                  Location : Vial 11
Acq. Operator   : Dennis                           Inj :   1
                                               Inj Volume : 10 µl
Acq. Method     : C:\HPCHEM\1\METHODS\LARBIG.M
Last changed    : 15.03.2022 18:05:40  by Dennis
Analysis Method : C:\HPCHEM\1\METHODS\LARBIG.M
Last changed    : 27.07.2022 08:34:44  by Dennis
CH3CN
```

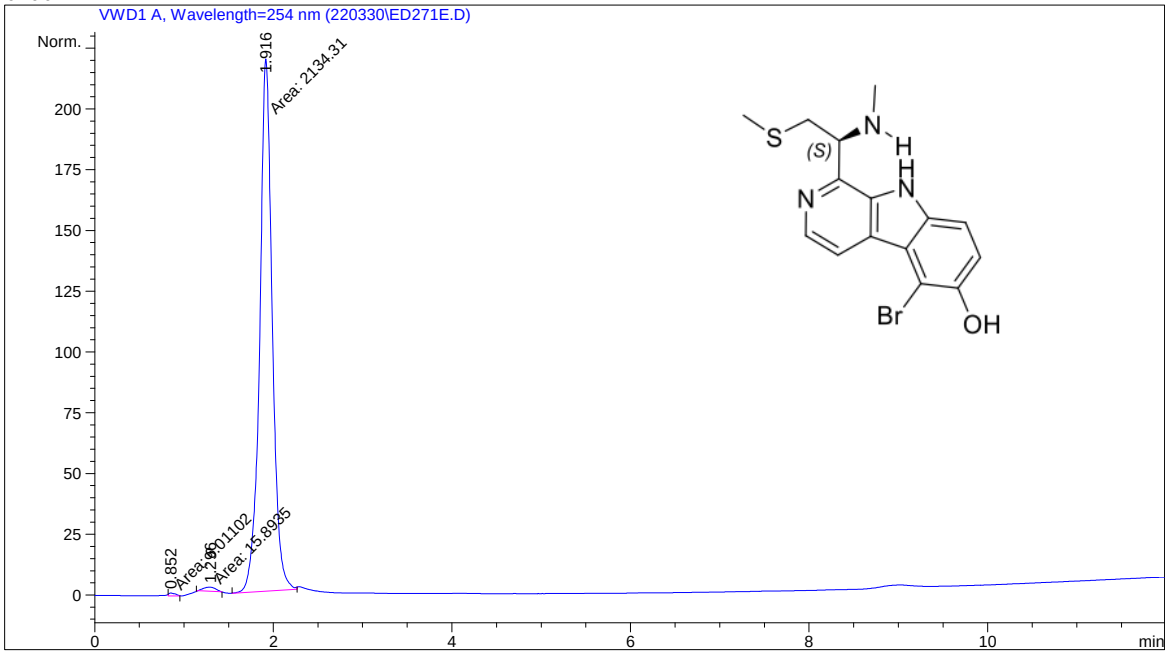


```
==========================================================================
                          Area Percent Report
==========================================================================

Sorted By             :      Signal
Multiplier            :      1.0000
Dilution              :      1.0000

Signal 1: VWD1 A, Wavelength=254 nm

Peak RetTime Type  Width     Area      Height     Area
  #   [min]        [min]  mAU   *s    [mAU   ]      %
----|-------|----|-------|----------|----------|--------|
   1   0.852 MM    0.0834    6.01102    1.20125   0.2788
   2   1.296 MM    0.1594   15.89355    1.66207   0.7371
   3   1.916 MM    0.1622 2134.30835  219.32698  98.9841

Totals :                   2156.21291  222.19030

 Results obtained with enhanced integrator!
==========================================================================
                          *** End of Report ***
```

```
==========================================================================
Injection Date  : 16.07.2022 15:03:12          Seq. Line :  11
Sample Name     : 3c                            Location : Vial 41
Acq. Operator   : Dennis                            Inj :   1
                                                Inj Volume : 10 µl
Different Inj Volume from Sequence !     Actual Inj Volume : 20 µl
Acq. Method     : C:\HPCHEM\1\METHODS\LARBIG.M
Last changed    : 16.07.2022 15:01:32  by Dennis
                  (modified after loading)
Analysis Method : C:\HPCHEM\1\METHODS\LARBIG.M
Last changed    : 27.07.2022 08:34:44  by Dennis
CH3CN
```

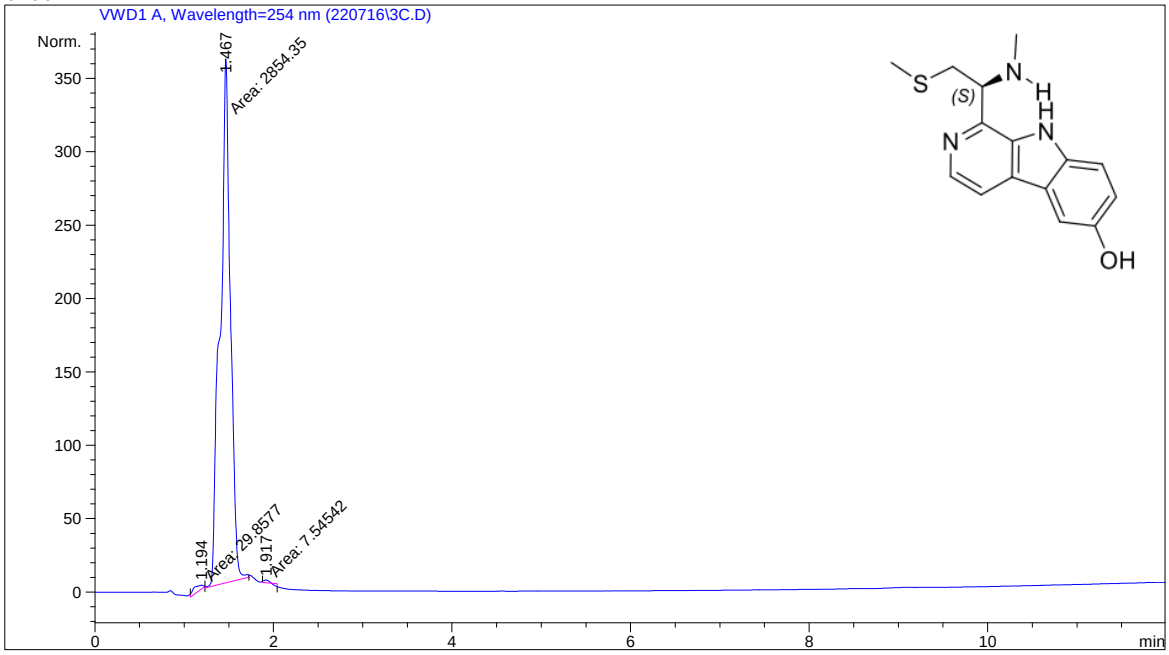


```
==========================================================================
                        Area Percent Report
==========================================================================

Sorted By             :      Signal
Multiplier            :      1.0000
Dilution              :      1.0000


Signal 1: VWD1 A, Wavelength=254 nm

Peak RetTime Type  Width     Area      Height     Area
  #   [min]        [min]  mAU   *s    [mAU   ]      %
----|-------|----|-------|----------|----------|--------|
   1   1.194 MM    0.1388   29.85772    2.78804   1.0325
   2   1.467 MM    0.1327 2854.34644  358.54672  98.7066
   3   1.917 MM    0.0661    7.54542    1.90313   0.2609

Totals :                  2891.74958  363.23789

 Results obtained with enhanced integrator!
==========================================================================
                          *** End of Report ***
```

4. Mass spectra of the synthesized compounds

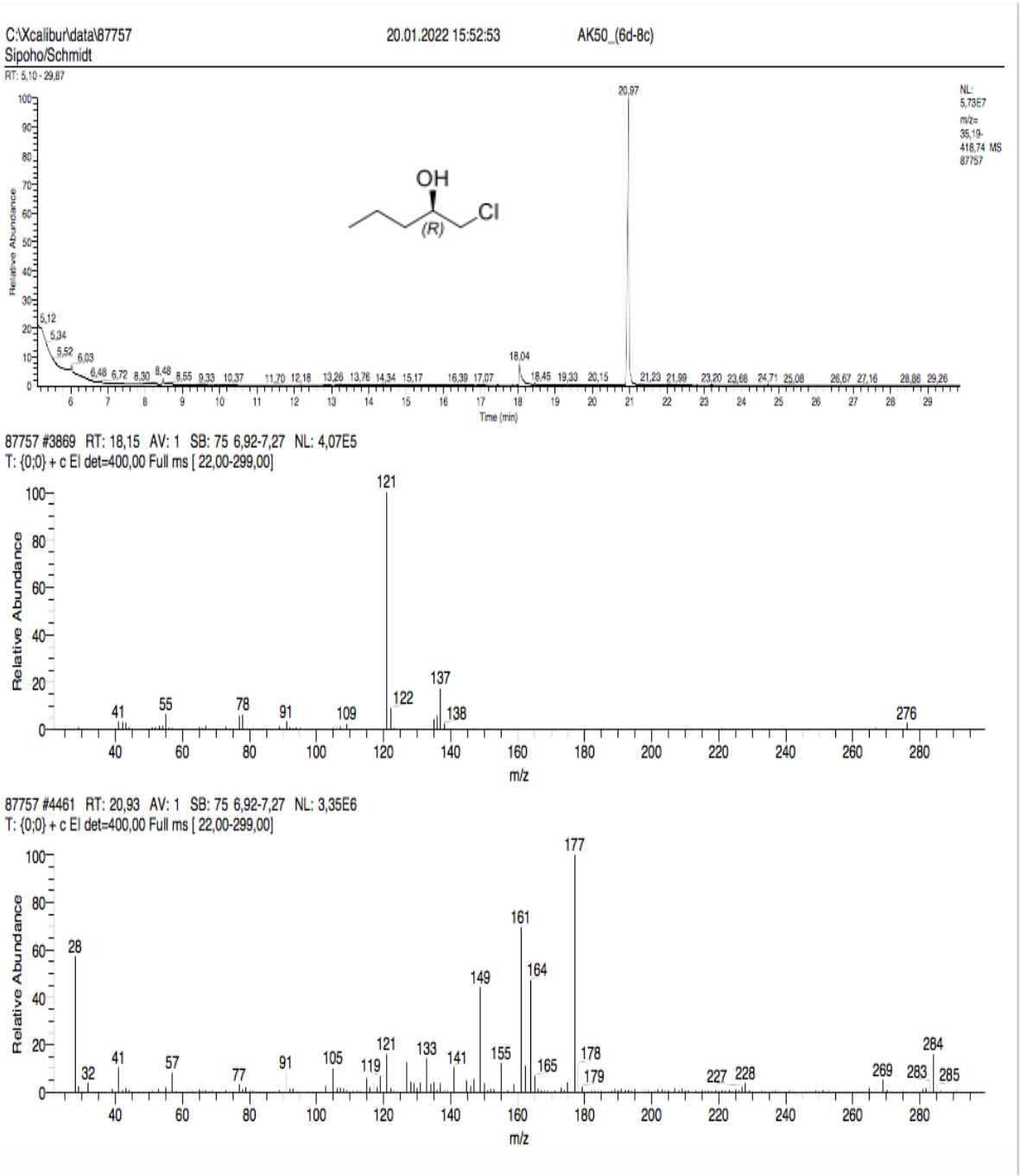
C:\Xcalibur\data\87757
Sipoho/Schmidt
20.01.2022 15:52:53
AK50_(6d-8c)
RT: 5,10 - 29,87
NL: 5,73E7 m/z= 35,19-418,74 MS 87757
OH
Cl
(R)
Relative Abundance
Time (min)
87757 #3869 RT: 18,15 AV: 1 SB: 75 6,92-7,27 NL: 4,07E5
T: {0;0} + c EI det=400,00 Full ms [22,00-299,00]
Relative Abundance
m/z
87757 #4461 RT: 20,93 AV: 1 SB: 75 6,92-7,27 NL: 3,35E6
T: {0;0} + c EI det=400,00 Full ms [22,00-299,00]
Relative Abundance
m/z

Mass spectrum

Analysis	D:\Data\Schmidt\86934_APCI_P1-D-1_01_11972.d	Acquisition Date	06.09.2021 09:28:22
Sample Name	86934_APCI	Ionisation	APCI Positive
Method	apci sehr kleine masse.m	Mass Range	50 m/z - 1000 m/z
Client	Sipoho AK 501	Operator	rudolph

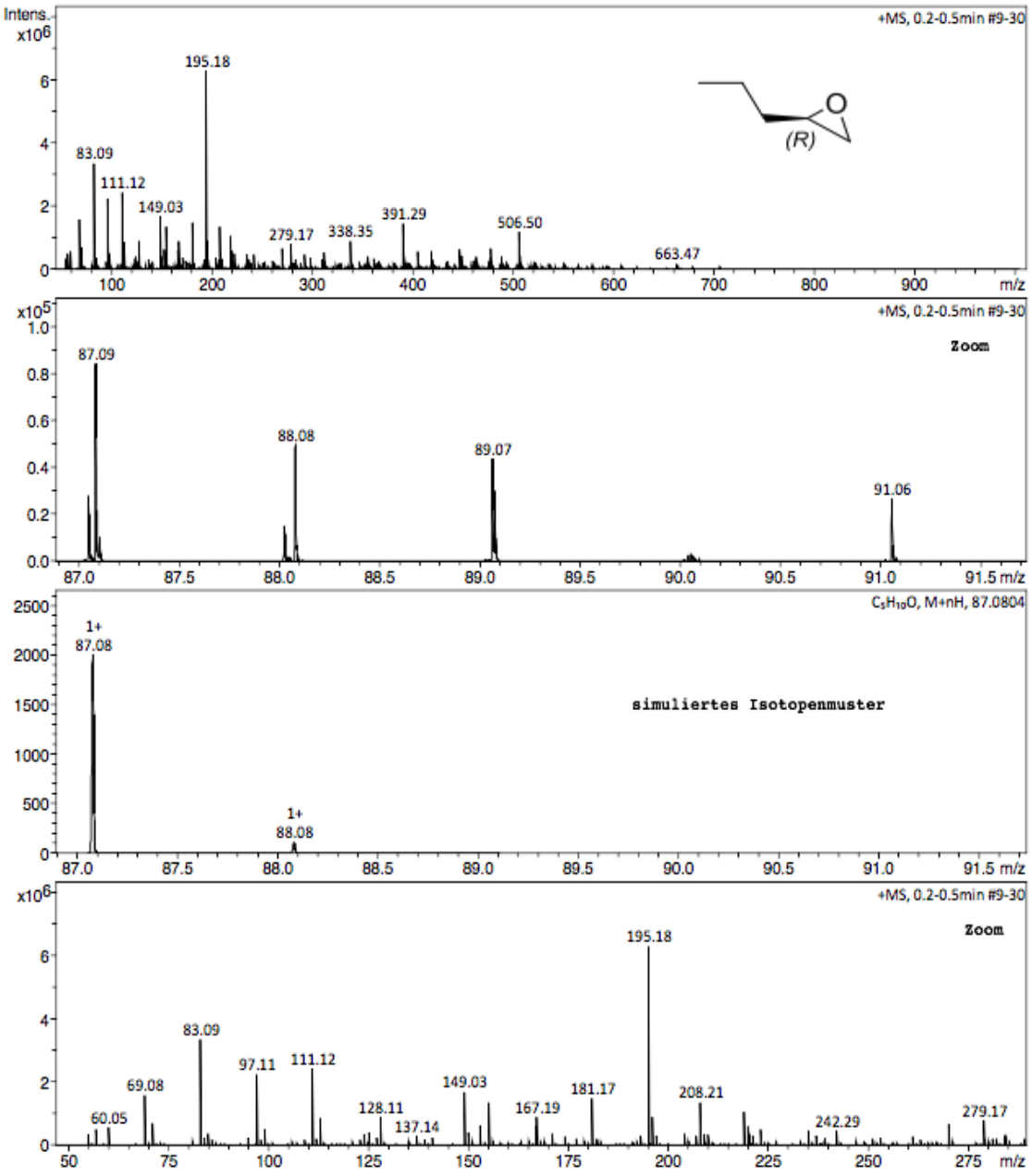

Mass Spectrometry Facility, Department of Chemistry, Technische Universität Darmstadt Instrument: Bruker Impact II

Page 1 of 1

HPLC-ESI-Messung

Mass spectrum

Analysis	D:\Data\Schmidt\86058_ESI_P1-D-1_01_8975.d	Acquisition Date	16.03.2021 19:15:43
Sample Name	86058_ESI	Ionisation	ESI Positive
Method	as 50-1500 1hz.m	Mass Range	50 m/z - 1600 m/z
Client	KenfackSipoho AK 502_ 2b-7c	Operator	Rudolph

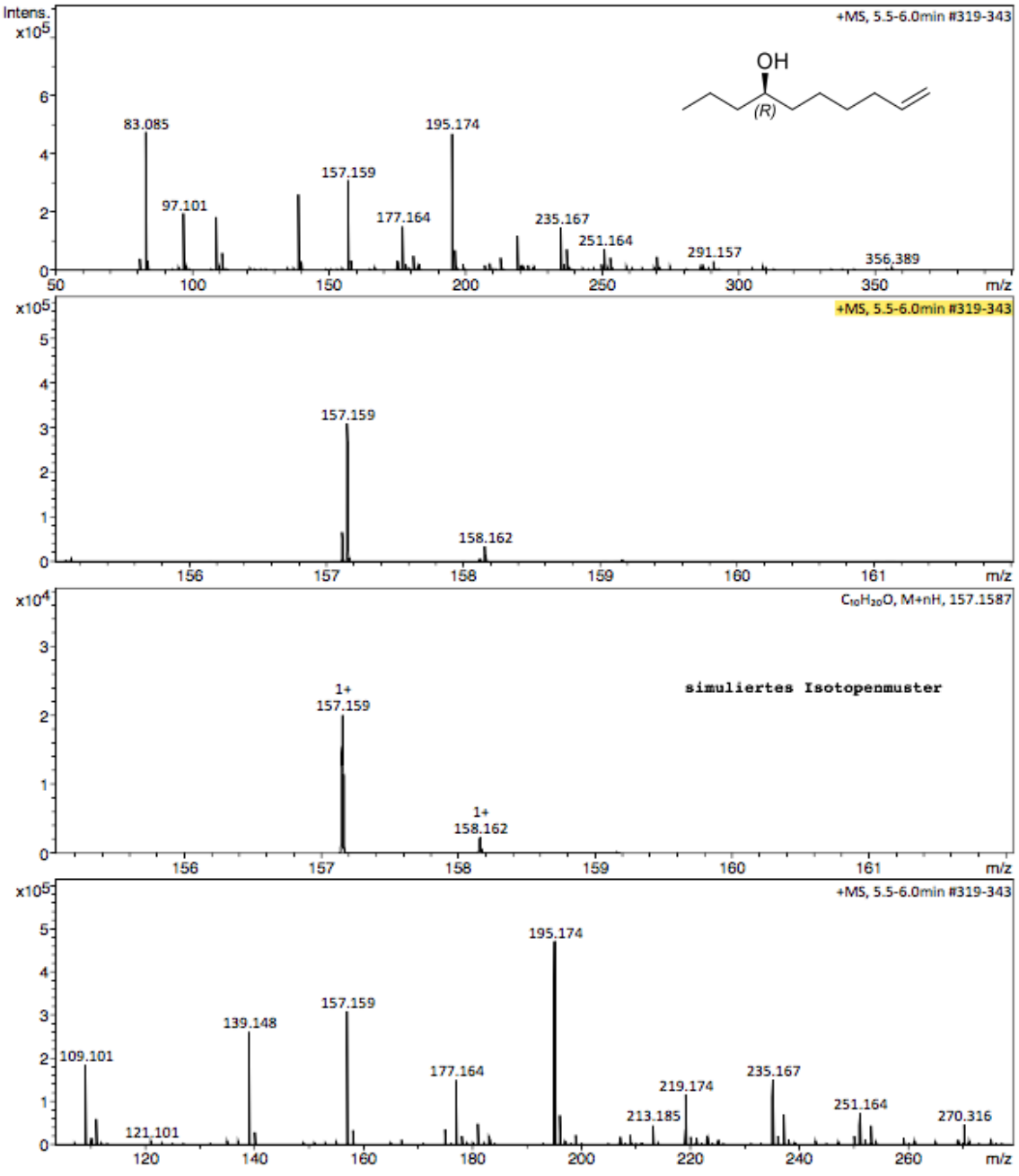

Mass Spectrometry Facility, Department of Chemistry, Technische Universität Darmstadt Instrument: Bruker Impact II

Page 1 of 1

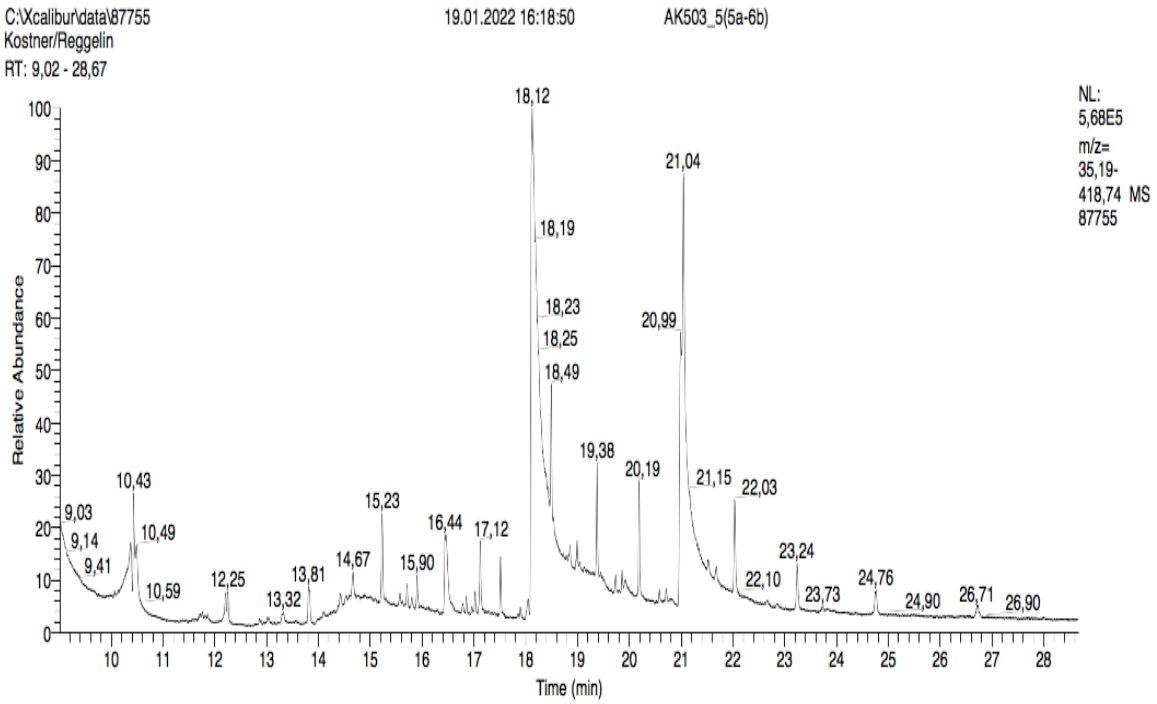
C:\Xcalibur\data\87755
Kostner/Reggelin
RT: 9,02 - 28,67
19.01.2022 16:18:50
AK503_5(5a-6b)
NL:
5,68E5
m/z=
35,19-
418,74 MS
87755
Relative Abundance
Time (min)
18,12
21,04
18,19
18,23
18,25
18,49
20,99
19,38
20,19
21,15
22,03
10,43
9,03
9,14
9,41
10,49
10,59
12,25
13,32
13,81
14,67
15,23
15,90
16,44
17,12
23,24
22,10
23,73
24,76
24,90
26,71
26,90

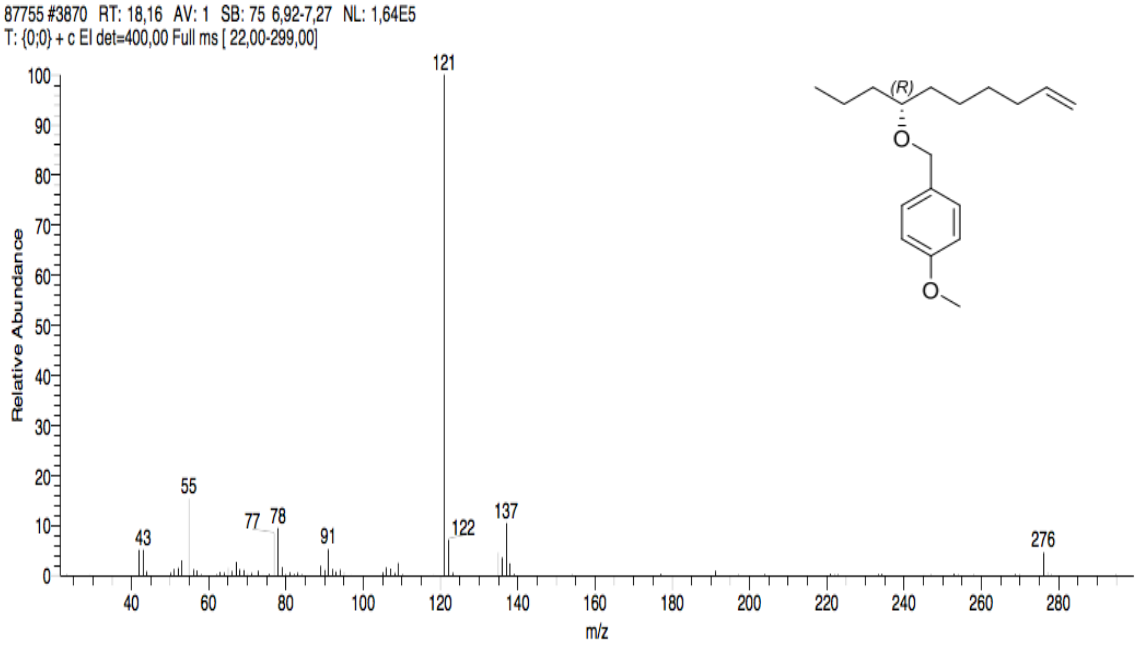
87755 #3870 RT: 18,16 AV: 1 SB: 75 6,92-7,27 NL: 1,64E5
T: {0;0} + c EI det=400,00 Full ms [22,00-299,00]
Relative Abundance
m/z
121
55
43
77
78
91
122
137
276
(R)
O
O

Mass spectrum

Analysis	D:\Data\Schmidt\86931_ESI_P1-D-5_01_11883.d	Acquisition Date	26.08.2021 15:23:46
Sample Name	86931_ESI	Ionisation	ESI Positive
Method	as 50-1000 1hz.m	Mass Range	50 m/z - 1000 m/z
Client	Sipoho AK 015_8 5e-10c	Operator	rudolph

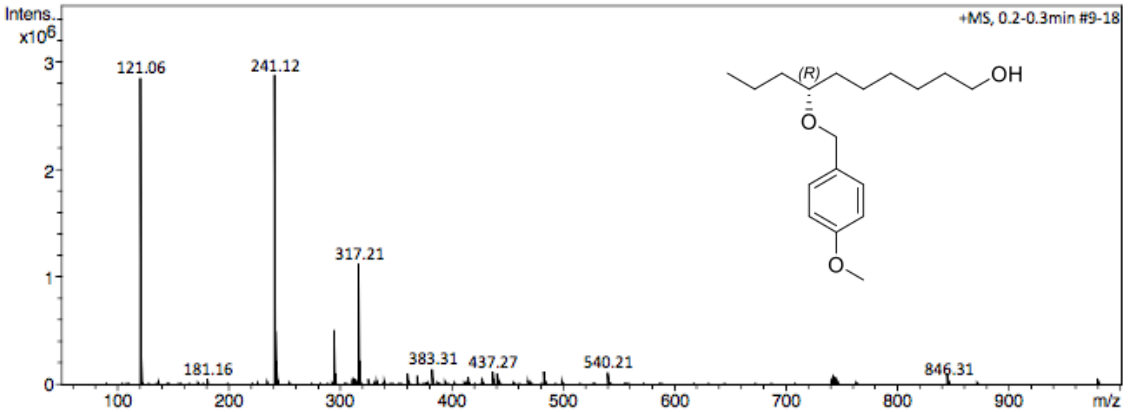

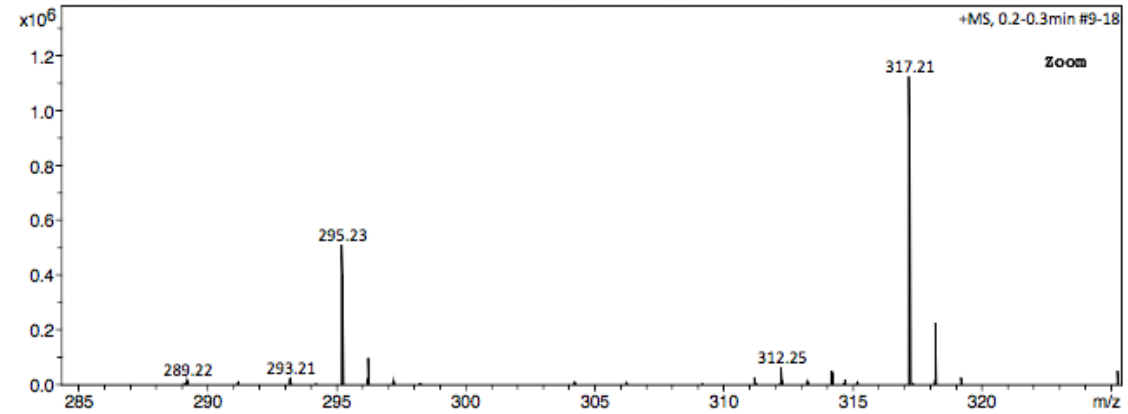

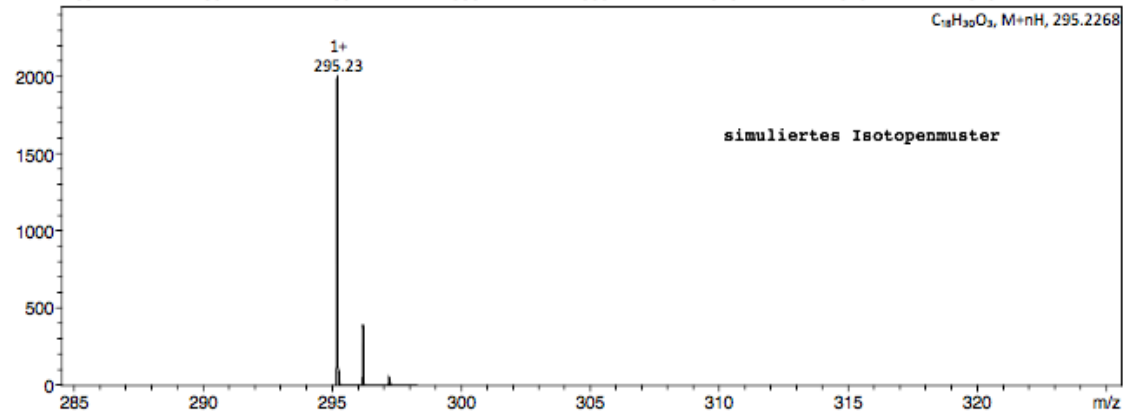

Mass Spectrometry Facility, Department of Chemistry, Technische Universität Darmstadt Instrument: Bruker Impact II

Page 1 of 1

Mass spectrum

Analysis	D:\Data\Schmidt\84625_ESI_P1-C-1_01_4883.d	Acquisition Date	20.07.2020 13:43:11
Sample Name	84625_ESI	Ionisation	ESI Positive
Method	as 50-1500-f 1hz.m	Mass Range	50 m/z - 1600 m/z
Client	Kenfack Sipoho AK 016_cp	Operator	Rudolph

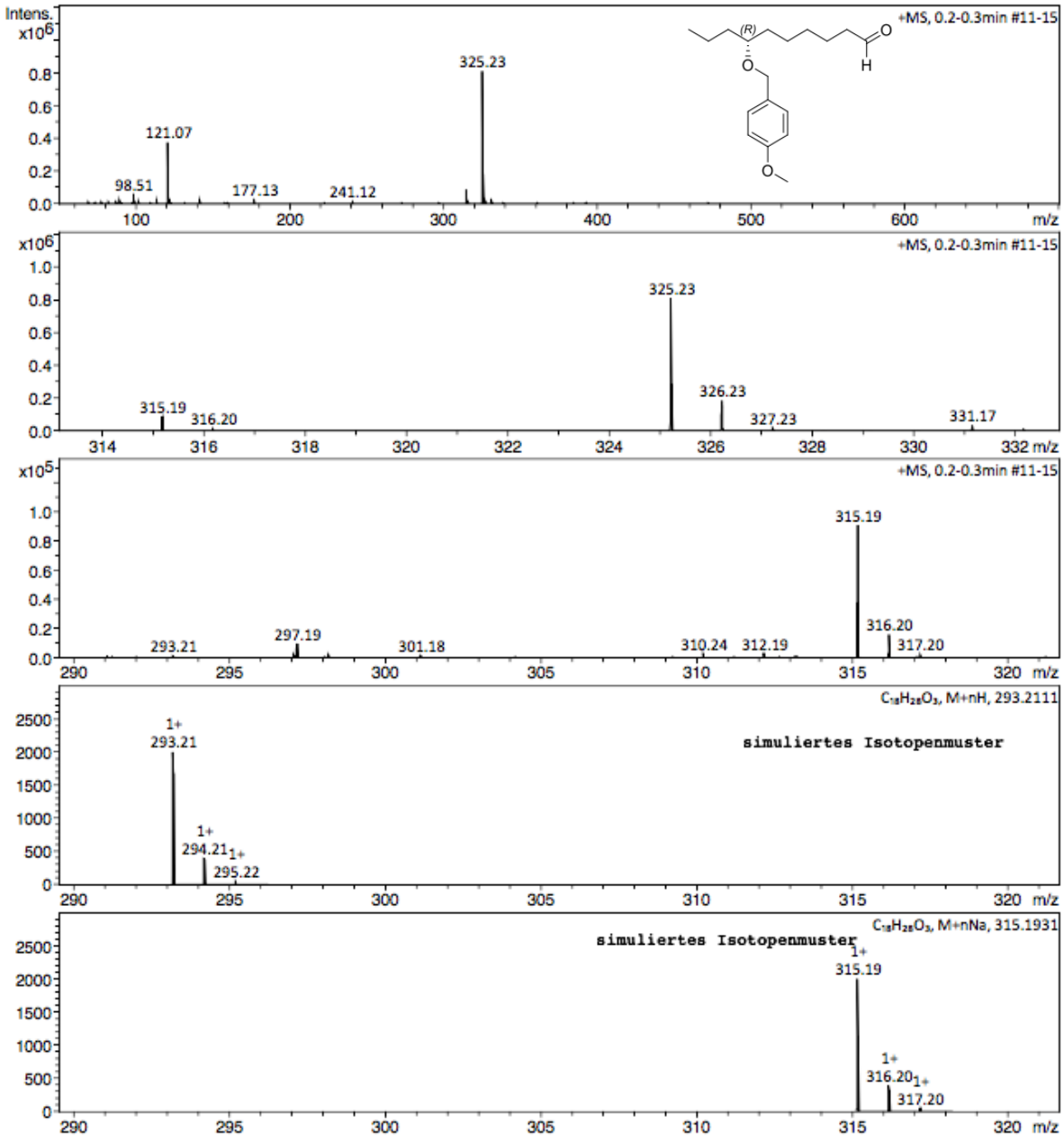

Mass Spectrometry Facility, Department of Chemistry, Technische Universität Darmstadt Instrument: Bruker Impact II

Page 1 of 1

Mass spectrum

Analysis	D:\Data\Schmidt\86925_ESI_P1-D-1_01_11874.d	Acquisition Date	26.08.2021 12:59:23
Sample Name	86925_ESI	Ionisation	ESI Positive
Method	as 50-1000 1hz.m	Mass Range	50 m/z - 1000 m/z
Client	Sipoho Thiazo	Operator	rudolph

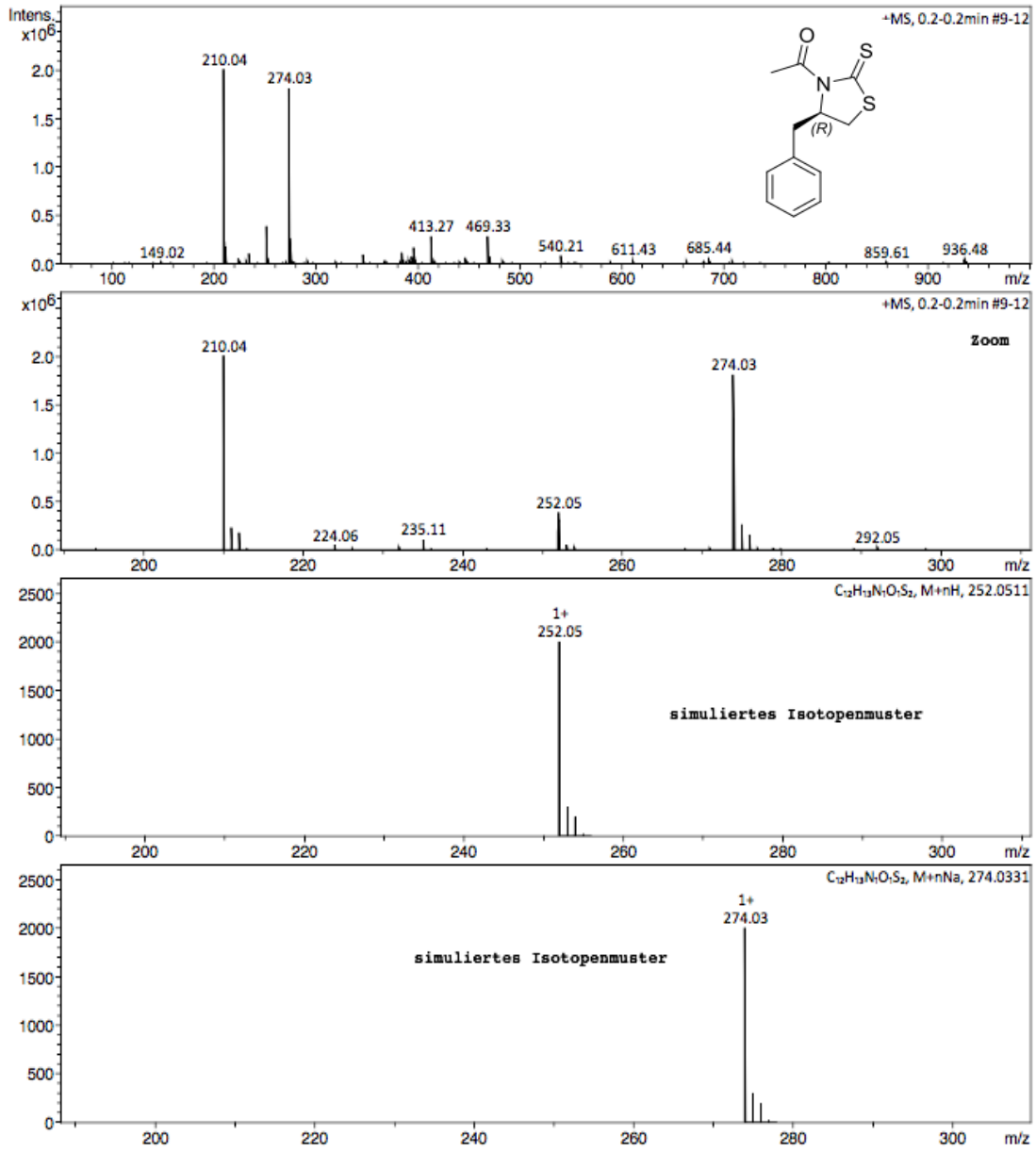

Mass Spectrometry Facility, Department of Chemistry, Technische Universität Darmstadt Instrument: Bruker Impact II

Page 1 of 1

Mass spectrum

Analysis	D:\Data\Schmidt\84626_ESI_P1-C-2_01_4884.d	Acquisition Date	20.07.2020 13:48:16
Sample Name	84626_ESI	Ionisation	ESI Positive
Method	as 50-1500-f 1hz.m	Mass Range	50 m/z - 1600 m/z
Client	Kenfack Sipoho AK 026_(14f-7c)	Operator	Rudolph

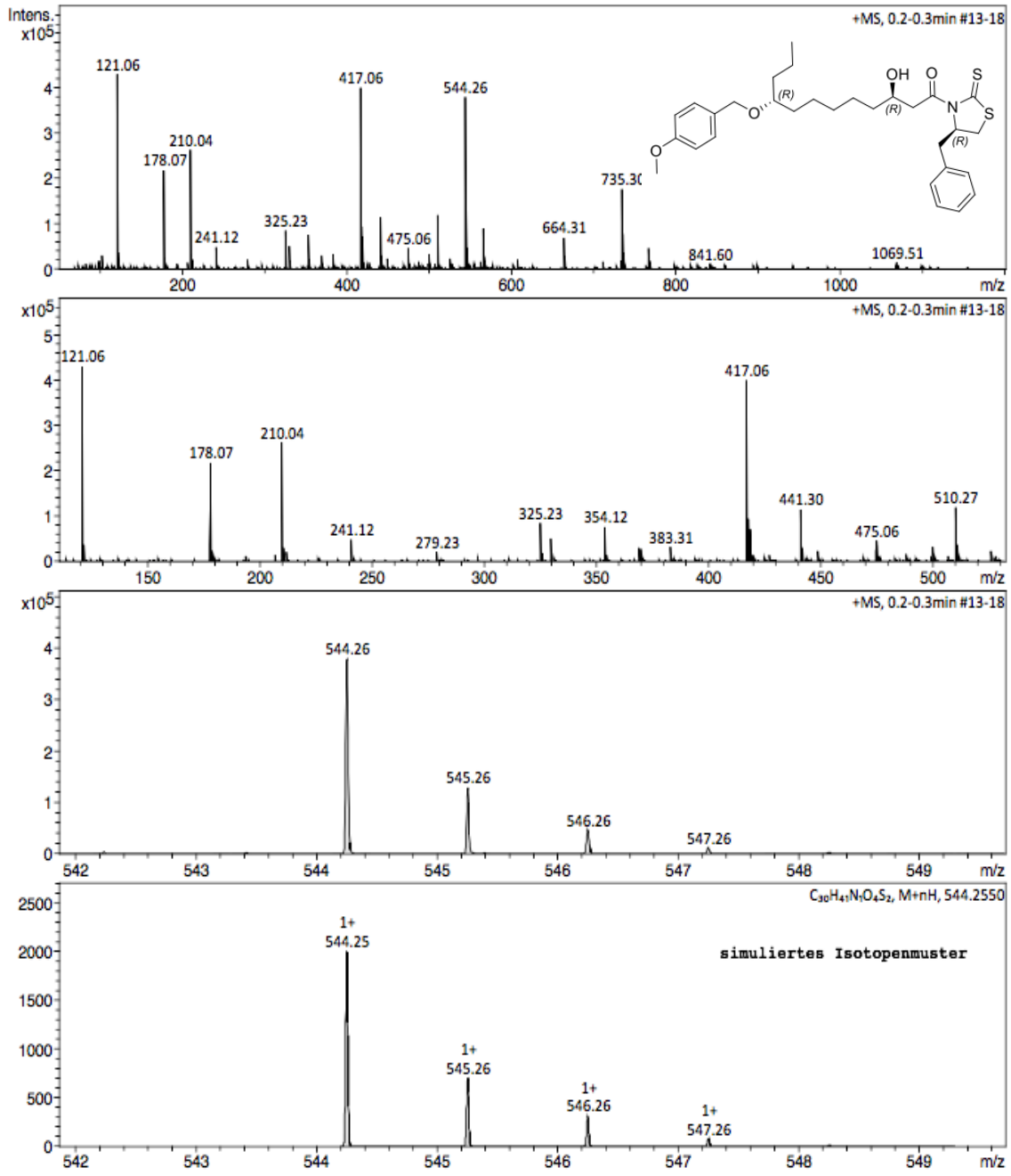

Mass Spectrometry Facility, Department of Chemistry, Technische Universität Darmstadt Instrument: Bruker Impact II

Page 1 of 1

Mass spectrum

Analysis	D:\Data\Schmidt\87903_ESI_P1-D-3_01_15462.d	Acquisition Date	07.02.2022 15:52:34
Sample Name	87903_ESI	Ionisation	ESI Positive
Method	as 50-1600 1hz.m	Mass Range	50 m/z - 1600 m/z
Client	Sipoho AK 507_3c-4c	Operator	Rudolph

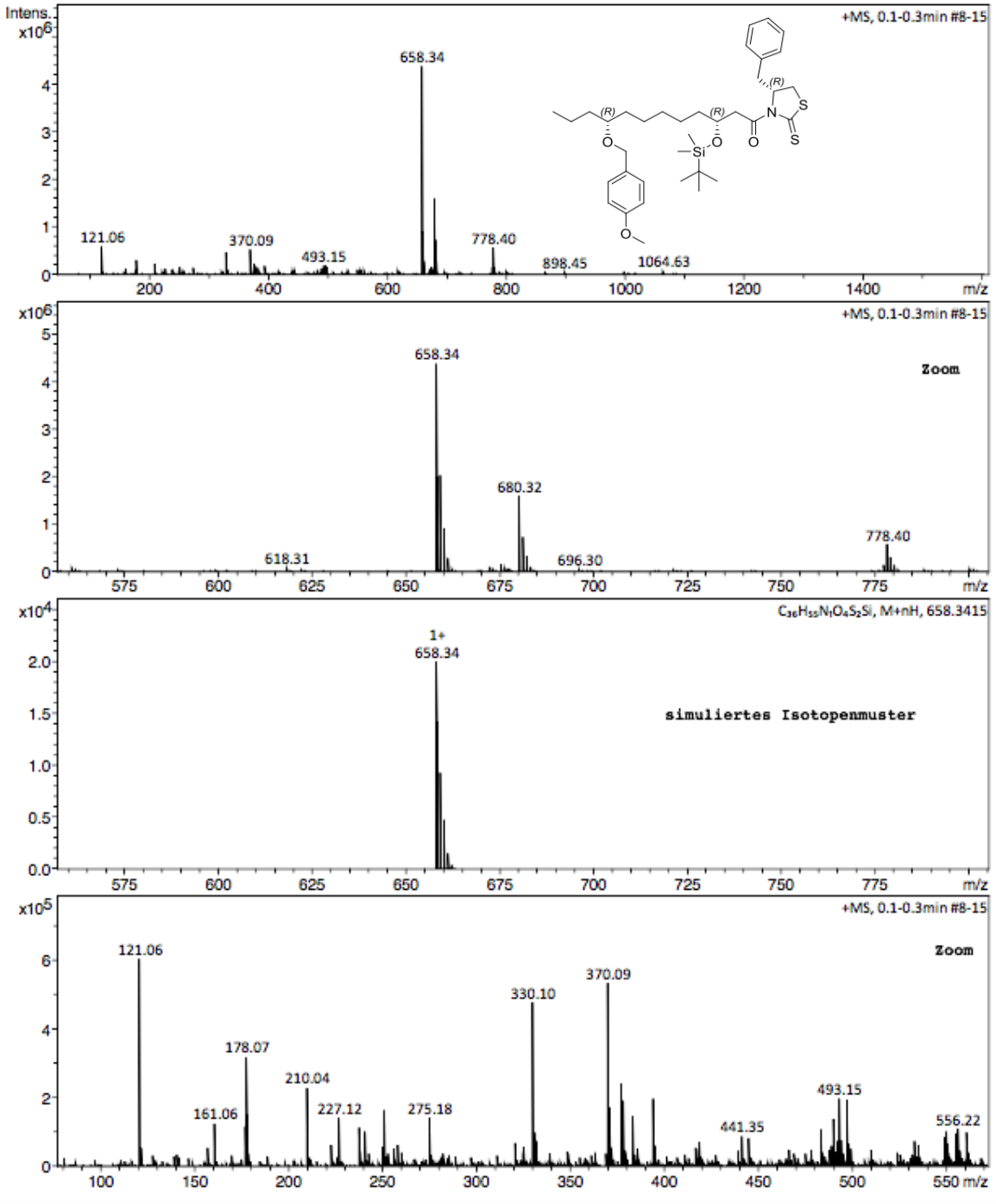

Mass Spectrometry Facility, Department of Chemistry, Technische Universität Darmstadt Instrument: Bruker Impact II

Page 1 of 1

Mass spectrum

Analysis	D:\Data\Schmidt\85511_ESI_P1-C-2_01_7010.d	Acquisition Date	27.11.2020 14:41:00
Sample Name	85511_ESI	Ionisation	ESI Positive
Method	as 50-1500-f 1hz.m	Mass Range	50 m/z - 1600 m/z
Client	Kenfack AK 028 (5a-9d)	Operator	Rudolph

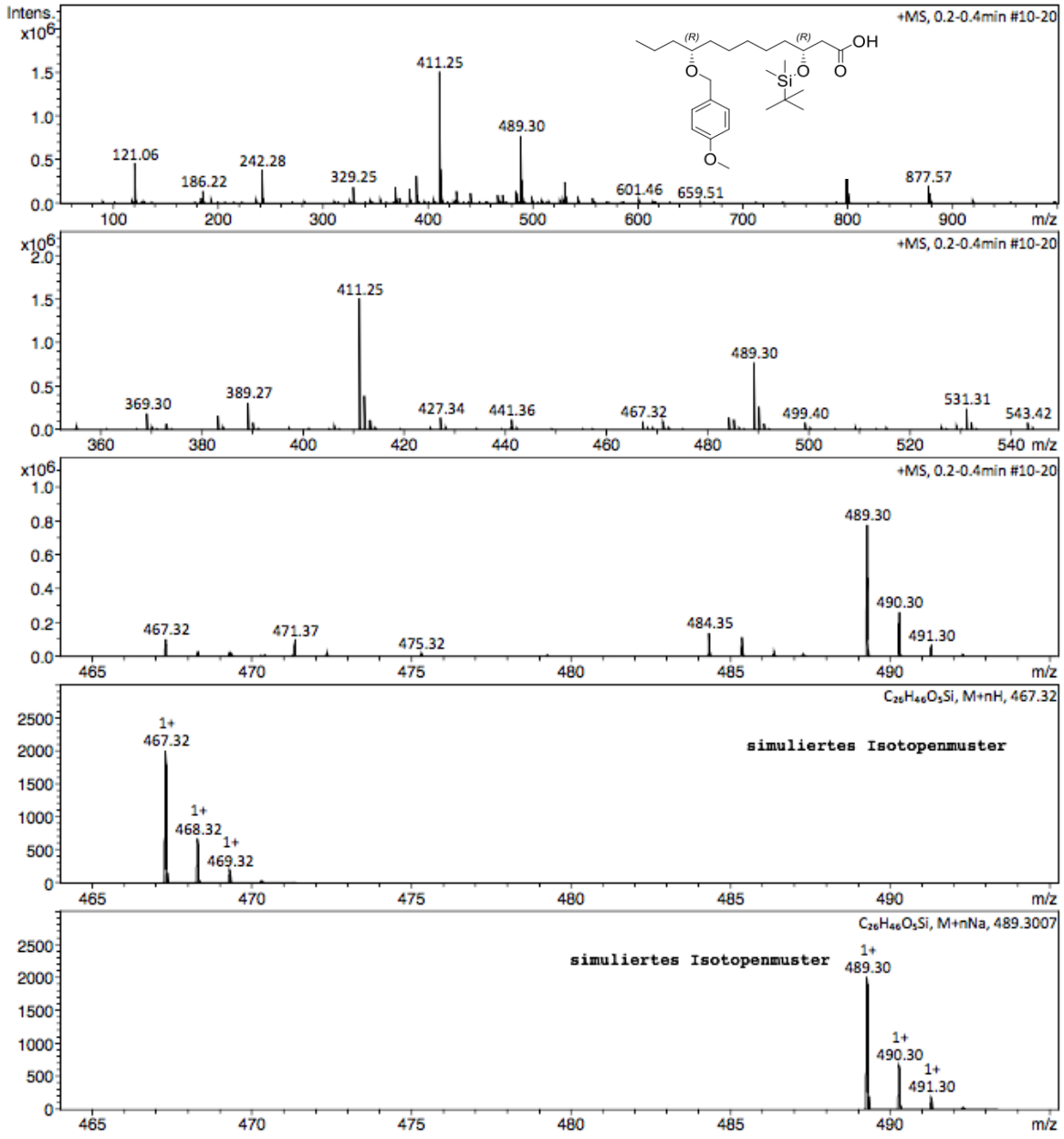

Mass Spectrometry Facility, Department of Chemistry, Technische Universität Darmstadt Instrument: Bruker Impact II

Page 1 of 1

Mass spectrum

Analysis	D:\Data\Schmidt\86933_ESI_P1-D-7_01_11881.d	Acquisition Date	26.08.2021 13:54:06
Sample Name	86933_ESI	Ionisation	ESI Positive
Method	as 50-1000 1hz.m	Mass Range	50 m/z - 1000 m/z
Client	Sipoho AK 017_cp	Operator	rudolph

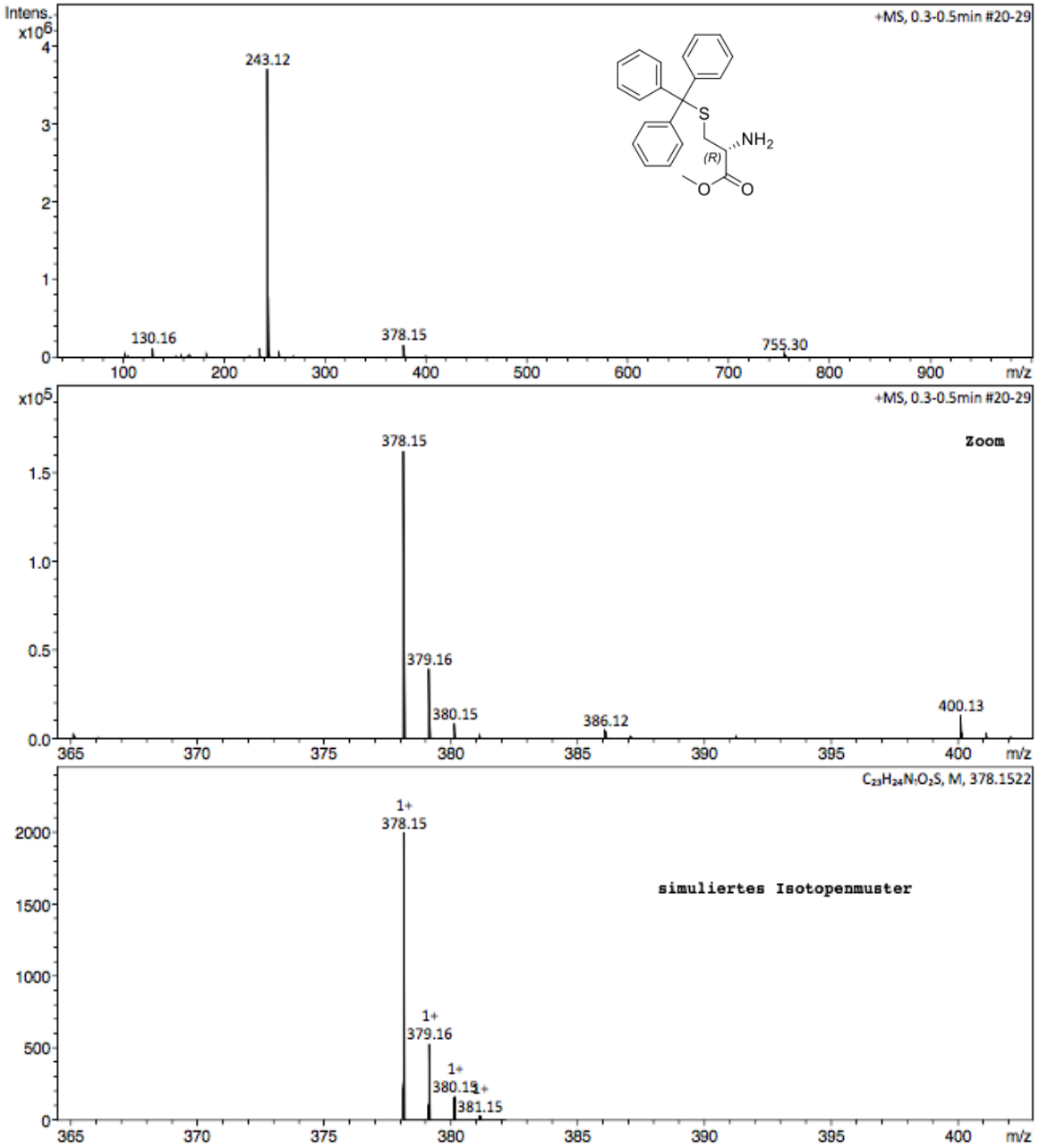

Mass spectrum

Analysis	D:\Data\Schmidt\86927_ESI_P1-D-3_01_11877.d	Acquisition Date	26.08.2021 13:15:19
Sample Name	86927_ESI	Ionisation	ESI Positive
Method	as 50-1000 1hz.m	Mass Range	50 m/z - 1000 m/z
Client	Sipoho AK 018_4 3c-6a	Operator	rudolph

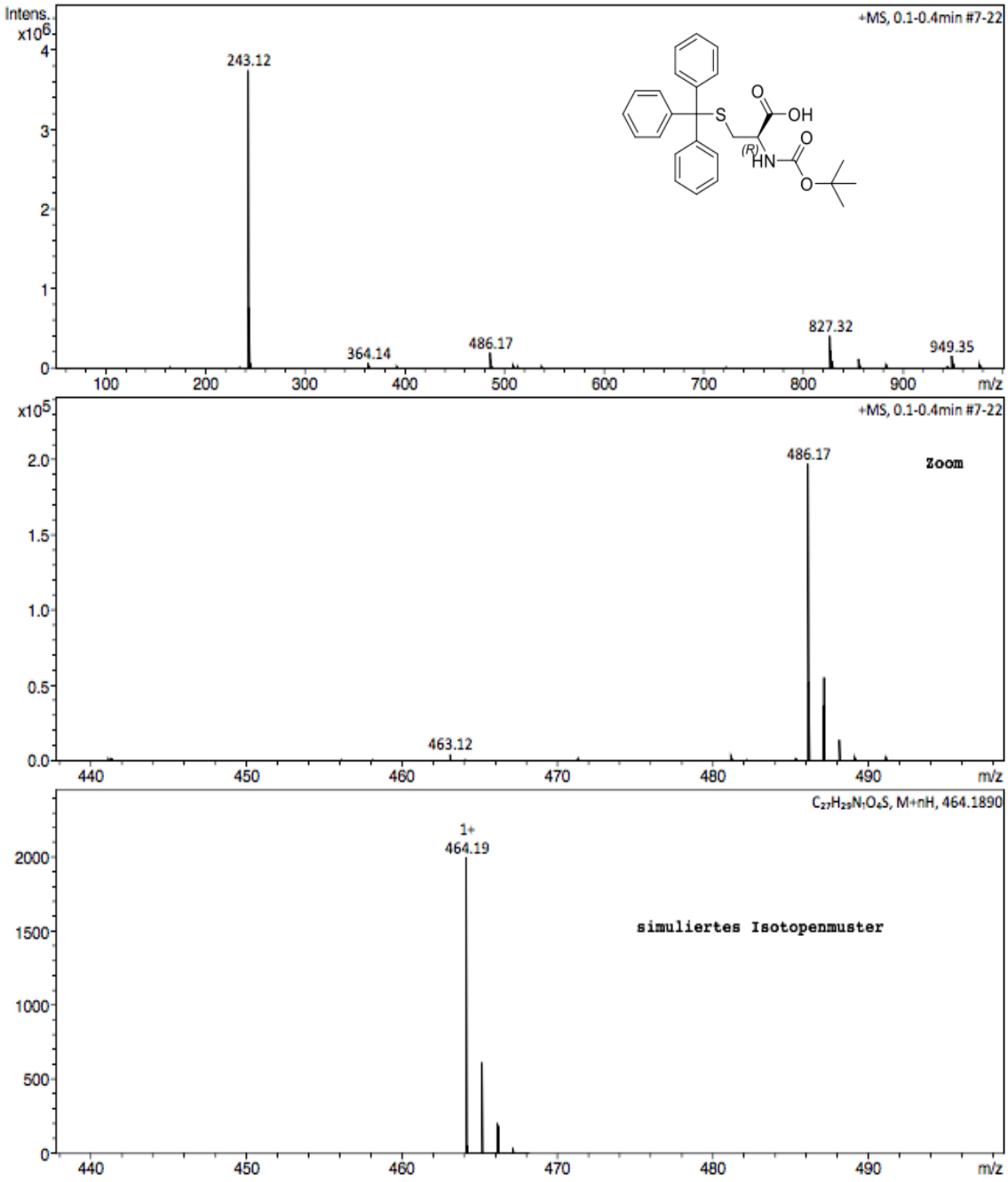

Mass Spectrometry Facility, Department of Chemistry, Technische Universität Darmstadt Instrument: Bruker Impact II

Page 1 of 1

Mass spectrum

Analysis	D:\Data\Schmidt\83965_ESI_P1-D-1_01_3671.d	Acquisition Date	22.04.2020 18:24:28
Sample Name	83965_ESI	Ionisation	ESI Positive
Method	as 50-1500-f 1hz.m	Mass Range	50 m/z - 1600 m/z
Client	Kenfack Sipoho AK 019 _12d-12a	Operator	Rudolph

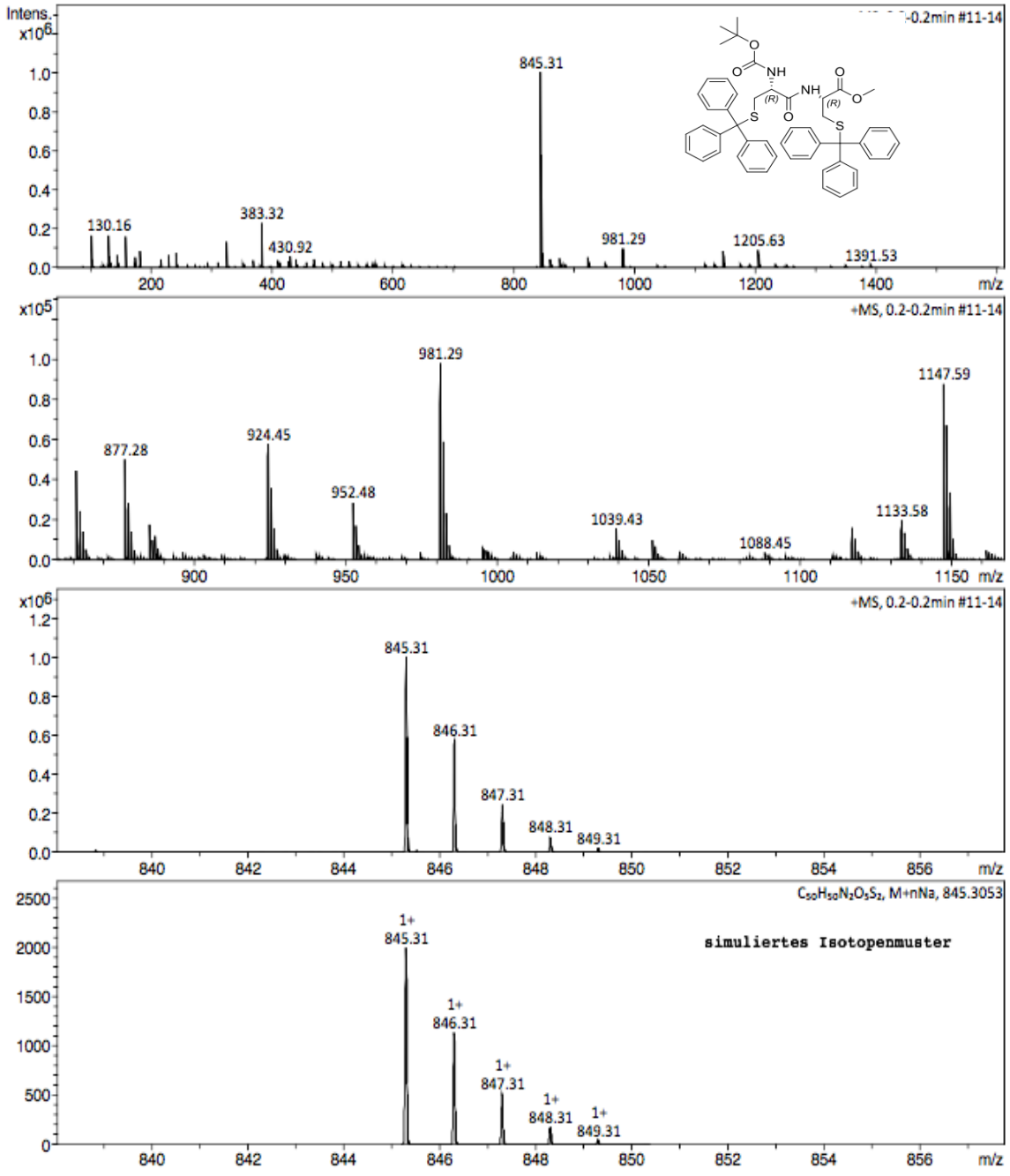

Mass Spectrometry Facility, Department of Chemistry, Technische Universität Darmstadt Instrument: Bruker Impact II

Page 1 of 1

Mass spectrum

Analysis	D:\Data\Schmidt\84386_ESI_61_01_4323.d	Acquisition Date	29.05.2020 14:57:08
Sample Name	84386_ESI	Ionisation	ESI Positive
Method	as 50-1500-f 1hz.m	Mass Range	50 m/z - 1600 m/z
Client	Kenfack Sipoho AK020_5e-7d	Operator	Rudolph

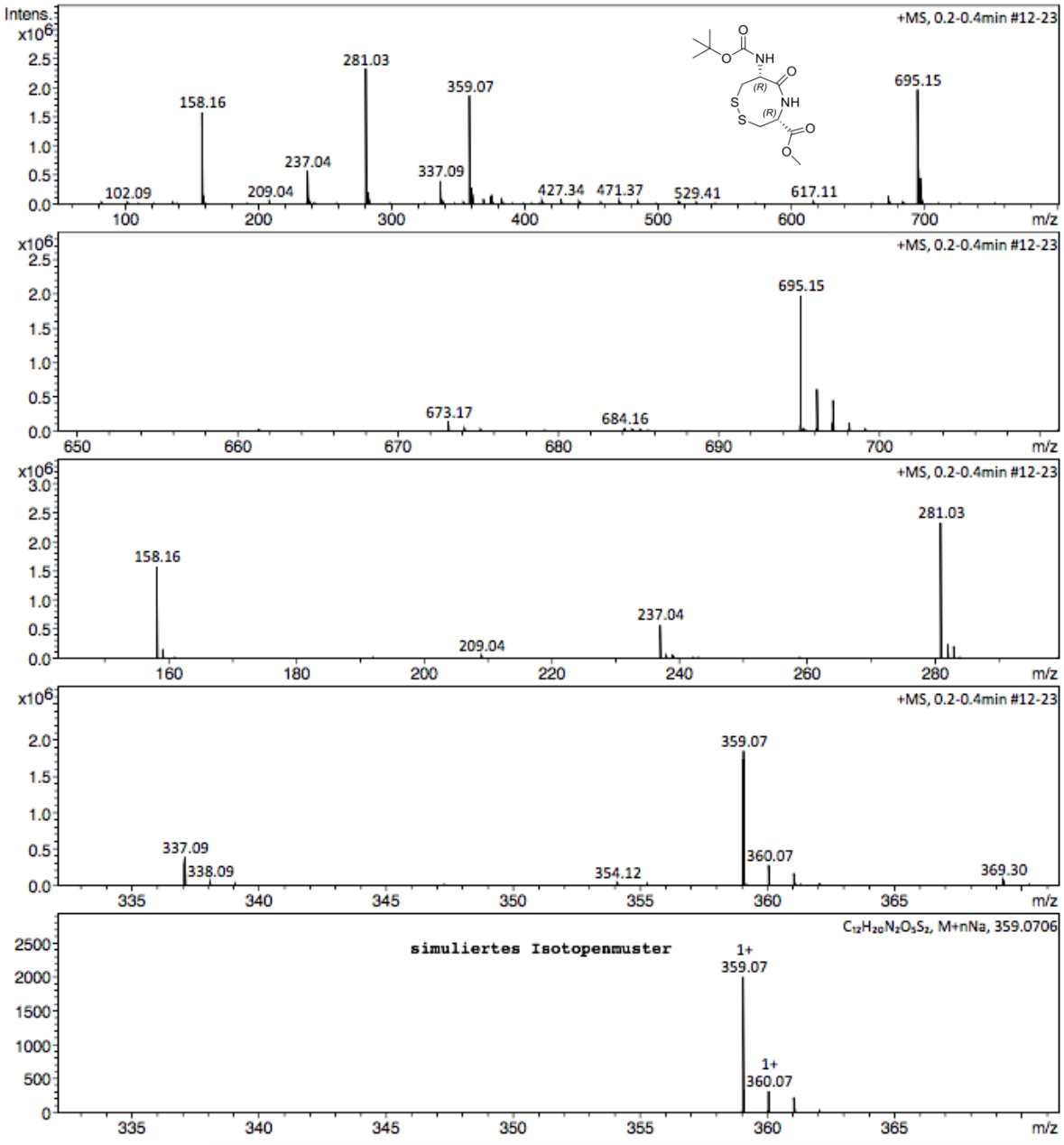

Mass spectrum

Analysis	D:\Data\Schmidt\84421_ESI_P1-D-1_01_4405.d	Acquisition Date	15.06.2020 16:12:19
Sample Name	84421_ESI	Ionisation	ESI Positive
Method	as 50-1500-f 1hz.m	Mass Range	50 m/z - 1600 m/z
Client	KenfackSipoho AK 020 a2	Operator	Rudolph

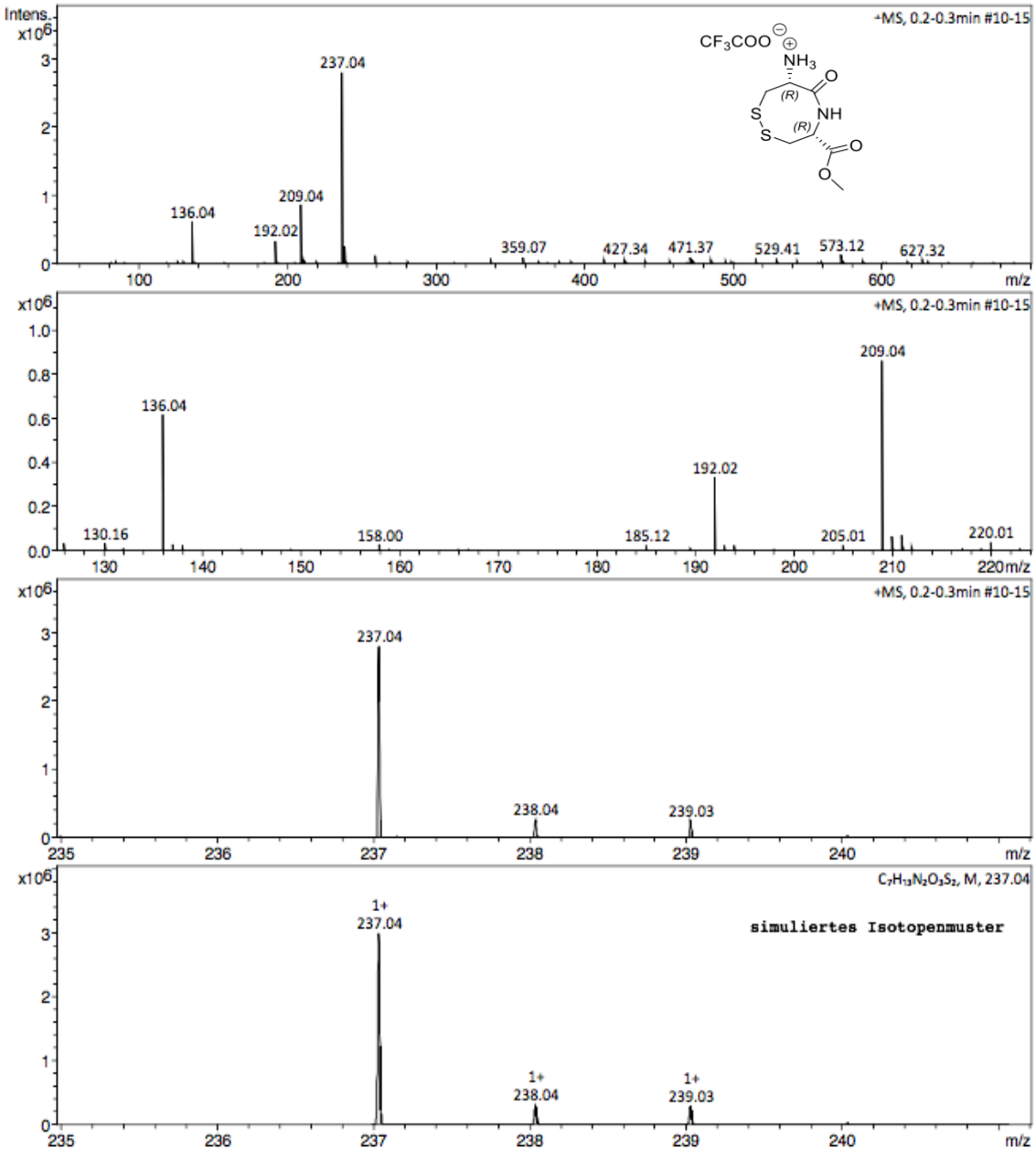

Mass Spectrometry Facility, Department of Chemistry, Technische Universität Darmstadt Instrument: Bruker Impact II

Page 1 of 1

Mass spectrum

Analysis	D:\Data\Schmidt\86928_ESI_P1-D-4_01_11878.d	Acquisition Date	26.08.2021 13:20:25
Sample Name	86928_ESI	Ionisation	ESI Positive
Method	as 50-1000 1hz.m	Mass Range	50 m/z - 1000 m/z
Client	Sipoho AK 509_ 5f-8c	Operator	rudolph

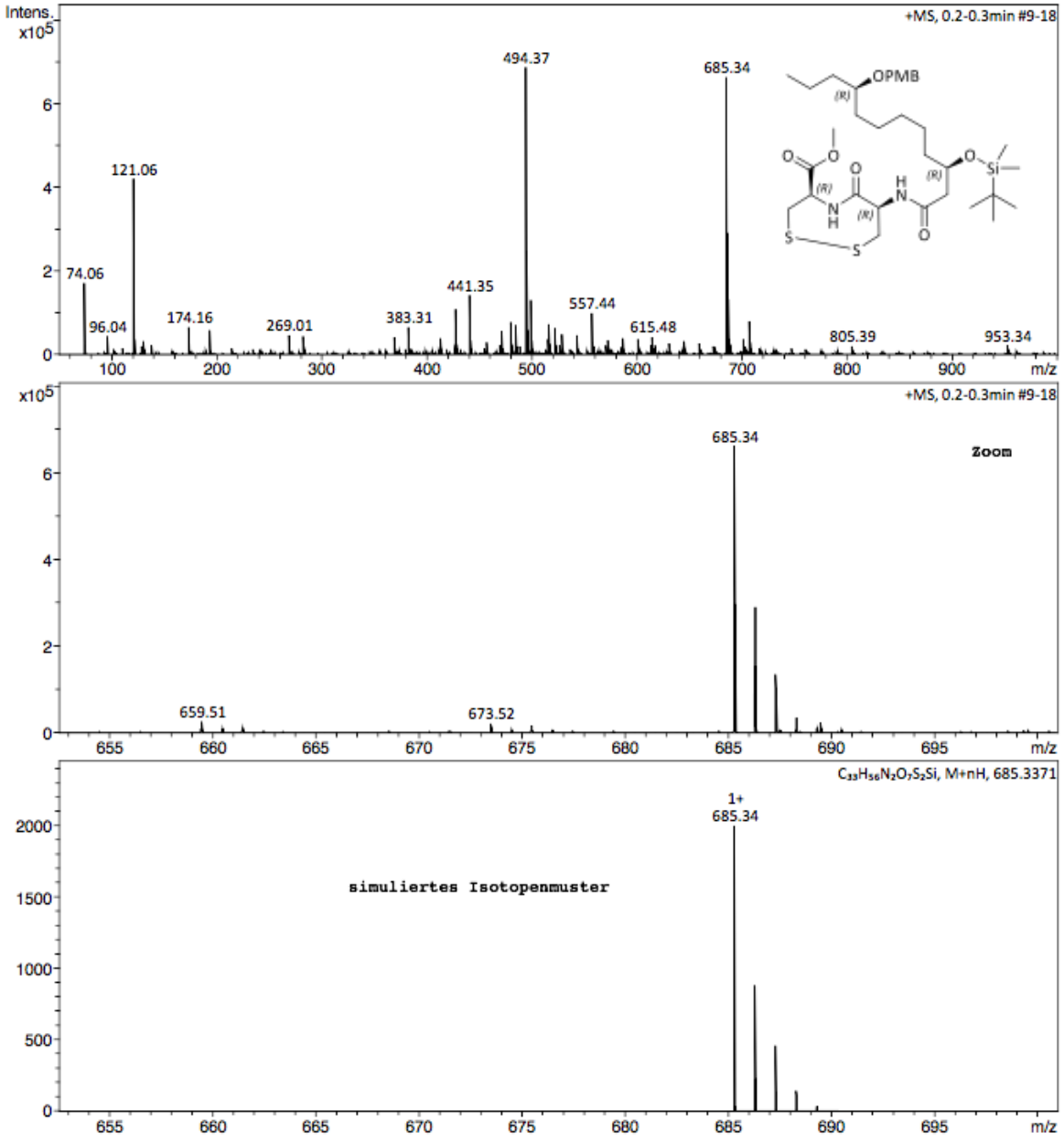

Mass Spectrometry Facility, Department of Chemistry, Technische Universität Darmstadt Instrument: Bruker Impact II

Page 1 of 1

Mass spectrum

Analysis	D:\Data\Schmidt\86987_ESI_P1-E-1_01_12096.d	Acquisition Date	14.09.2021 15:05:10
Sample Name	86987_ESI	Ionisation	ESI Positive
Method	as 50-1000 1hz.m	Mass Range	50 m/z - 1000 m/z
Client	Sipoho AK 510	Operator	rudolph

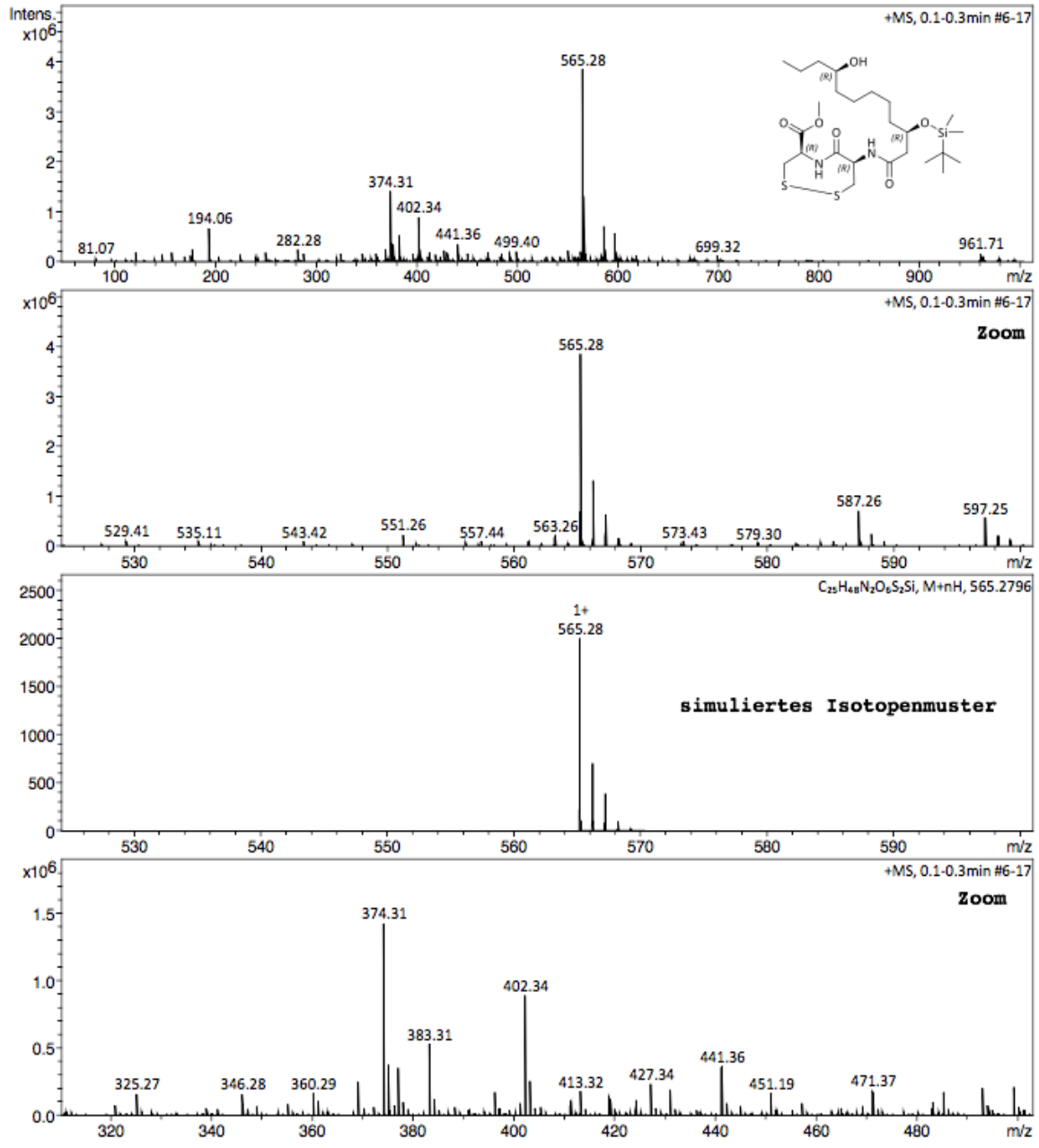

Mass Spectrometry Facility, Department of Chemistry, Technische Universität Darmstadt Instrument: Bruker Impact II

Page 1 of 1

Mass spectrum

Analysis	D:\Data\Schmidt\85942_APCI_P1-C-1_01_8627.d	Acquisition Date	02.03.2021 11:31:22
Sample Name	85942_APCI	Ionisation	APCI Positive
Method	apci_pos_1500.m	Mass Range	50 m/z - 1600 m/z
Client	KenfackSipoho AK 310 cp	Operator	Rudolph

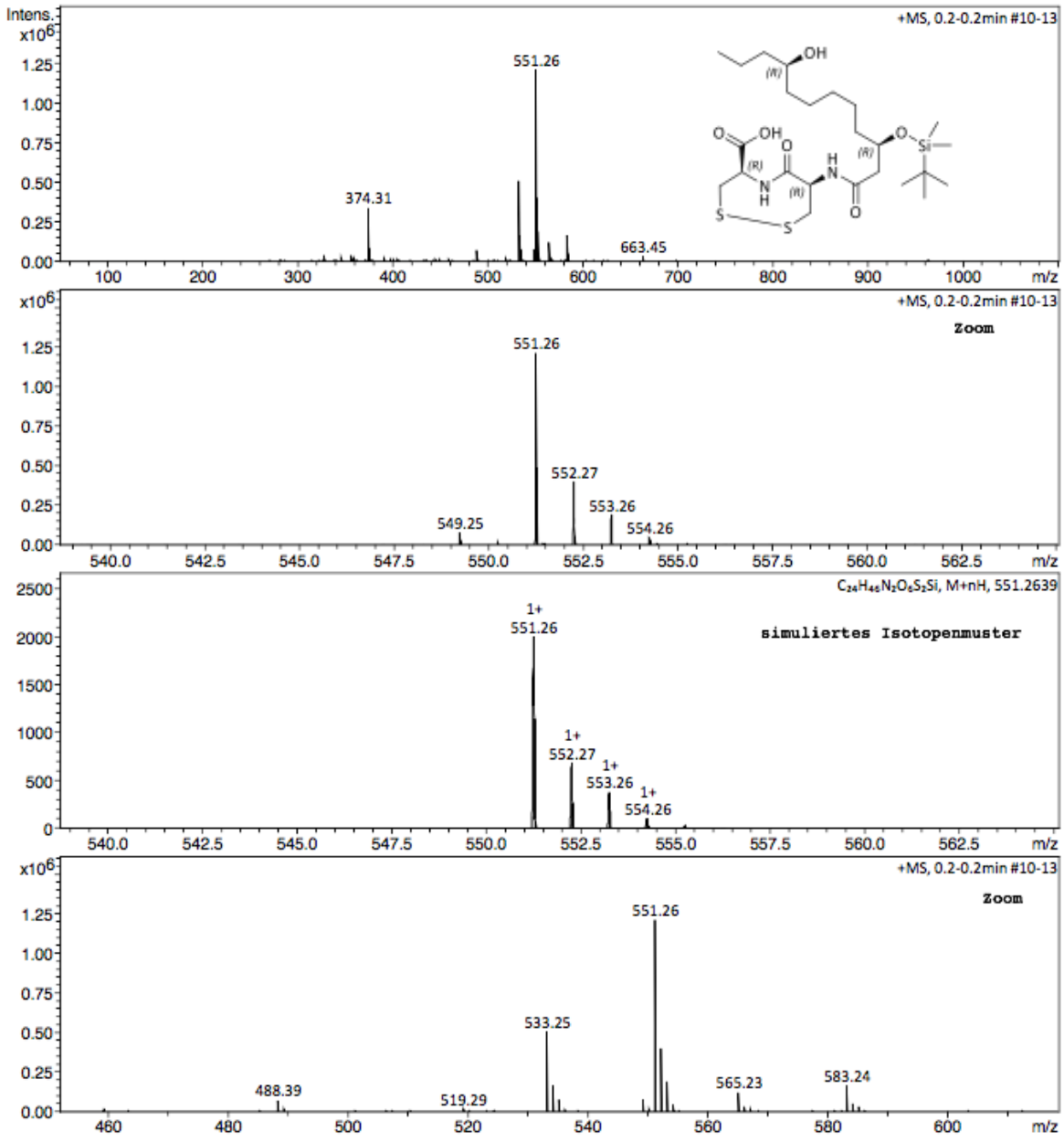

Mass spectrum

Analysis	D:\Data\Schmidt\86371_APCI_P1-D-2_01_10035.d		Acquisition Date	17.05.2021 15:53:00	
Sample Name	86371_APCI		Ionisation	APCI	Positive
Method	apci_pos_1600.m		Mass Range	50 m/z	- 1600 m/z
Client	Sipoho 512 _7a-10f		Operator	Rudolph	

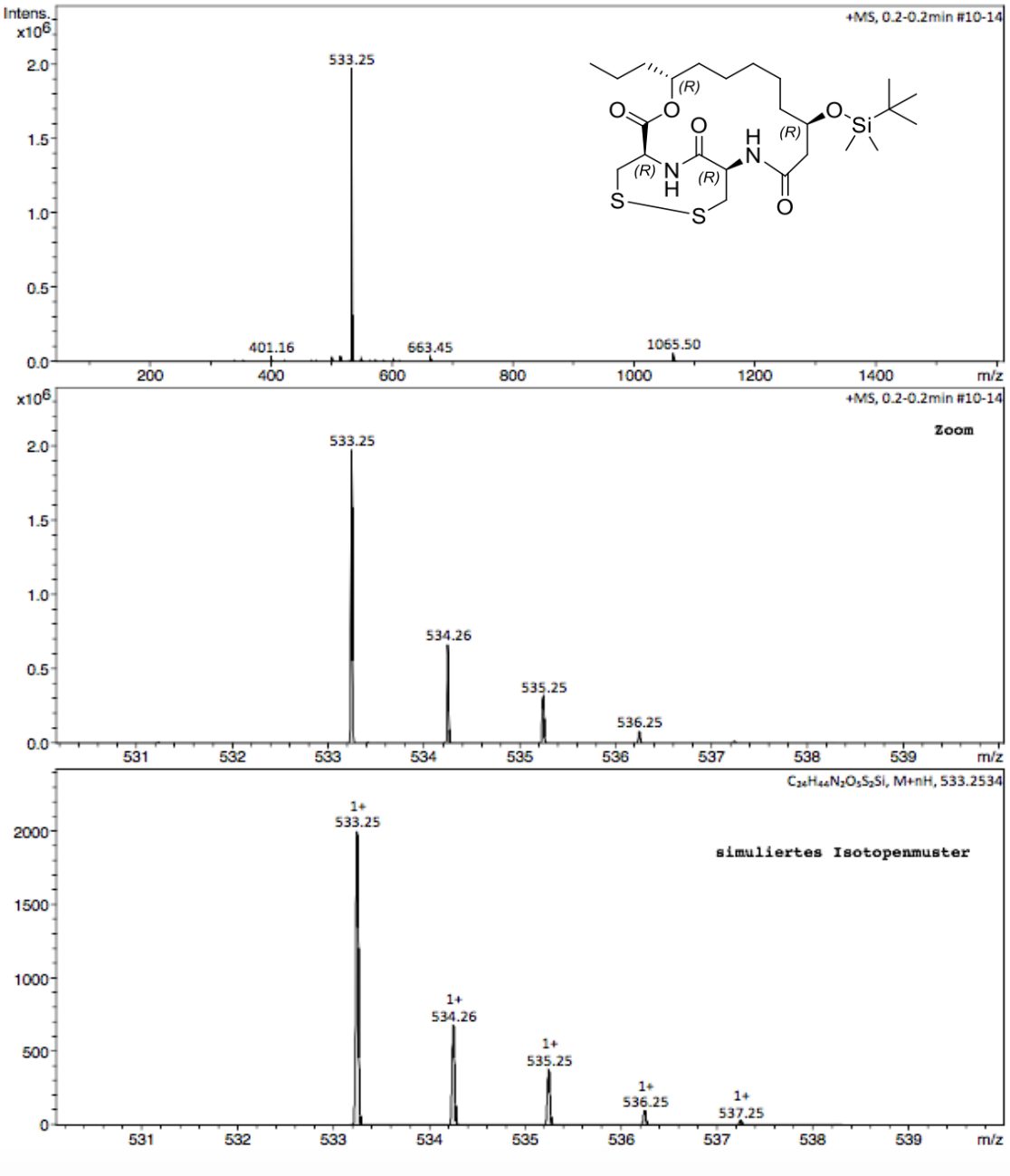

Mass spectrum

Analysis	D:\Data\Schmidt\86414_APCI_P1-D-2_01_10188.d	Acquisition Date	27.05.2021 16:11:57
Sample Name	86414_APCI	Ionisation	APCI Positive
Method	apci_pos_1600.m	Mass Range	50 m/z - 1600 m/z
Client	Sipoho AK 513_2 3f-4a	Operator	Rudolph

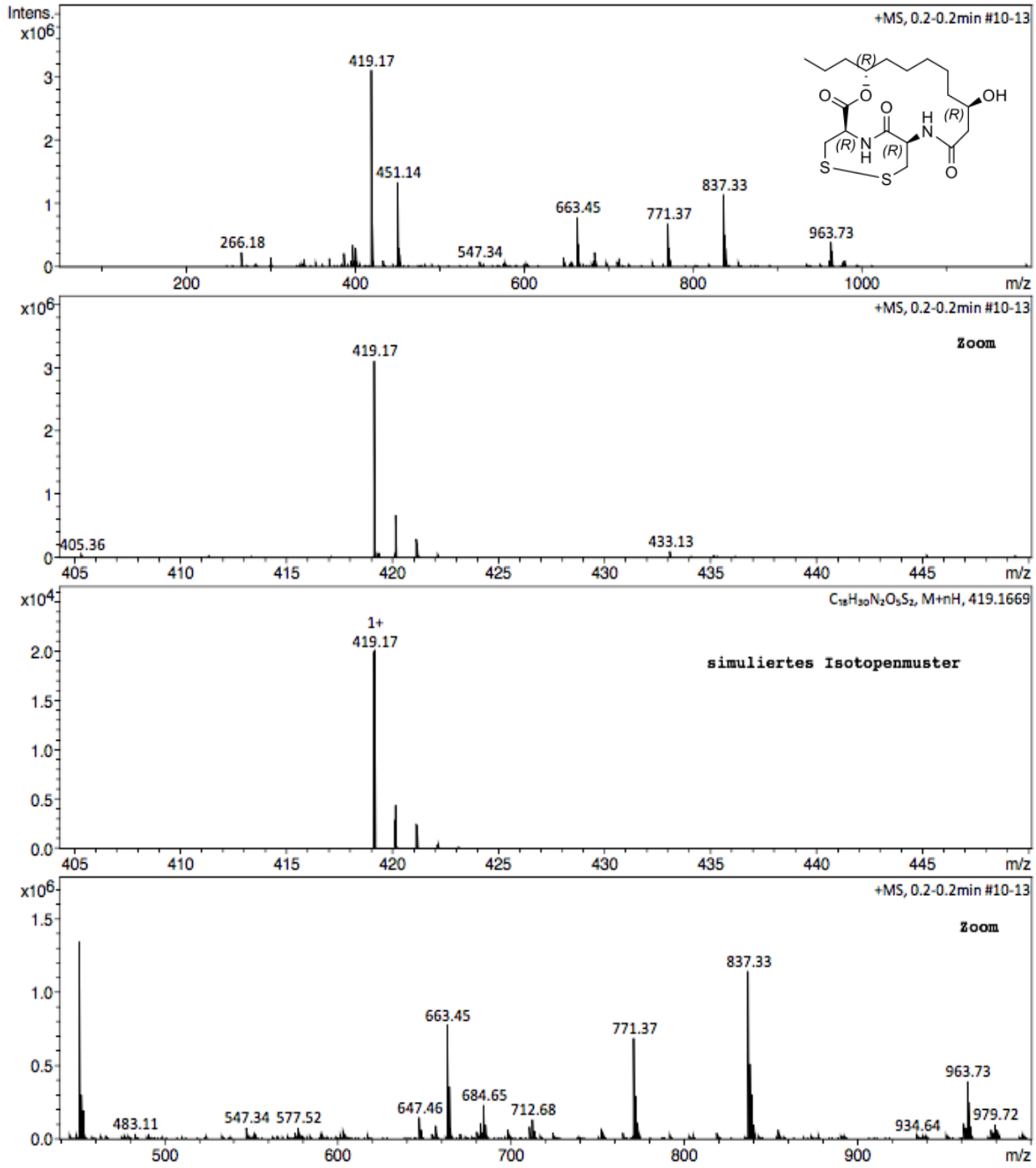

Mass spectrum

Analysis	D:\Data\Schmidt\86988_ESI_P1-E-2_01_12100.d	Acquisition Date	14.09.2021 16:05:47
Sample Name	86988_ESI	Ionisation	ESI Positive
Method	as 50-1000 1hz.m	Mass Range	50 m/z - 1000 m/z
Client	Sipoho AK 040	Operator	rudolph

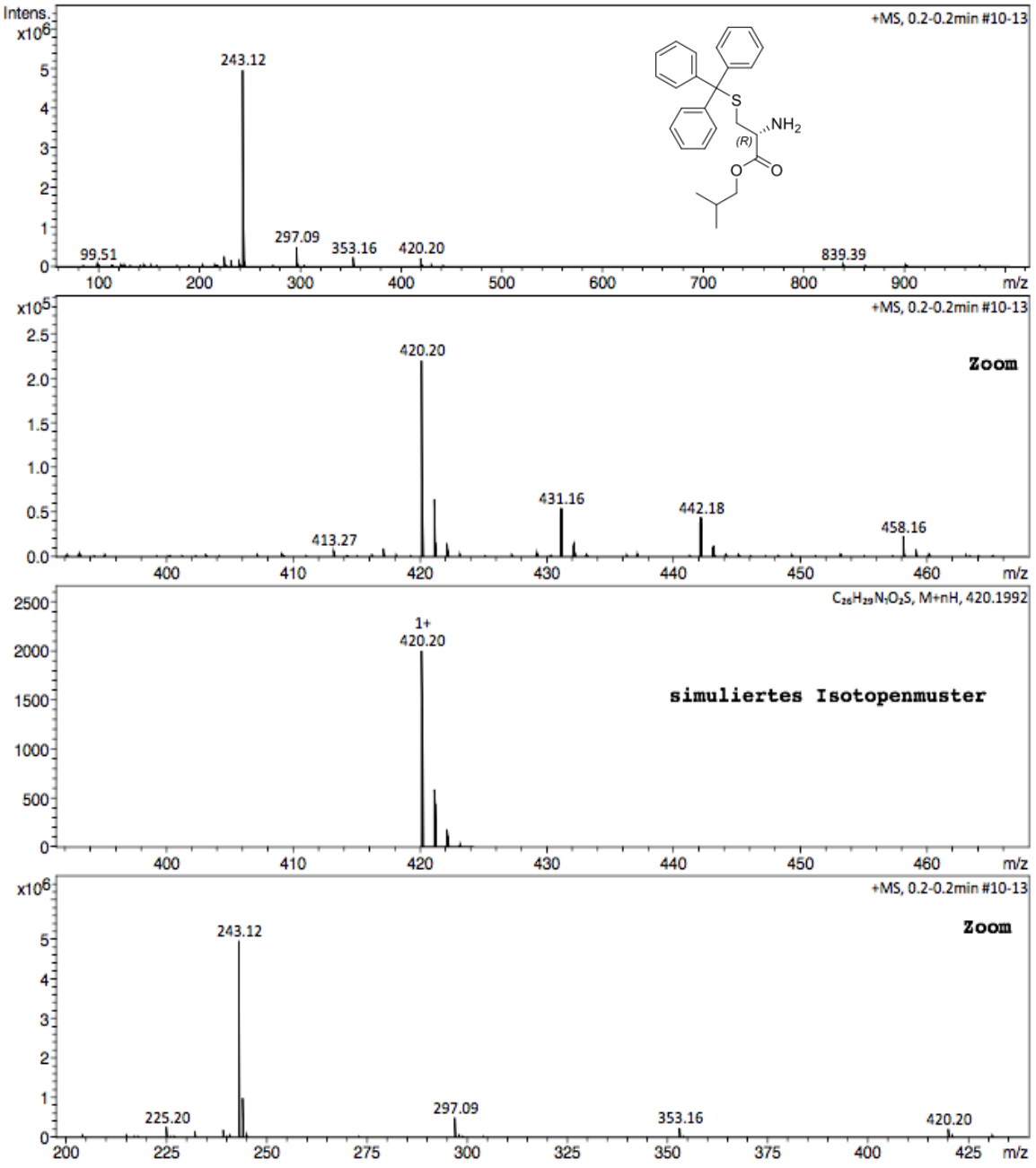

Mass spectrum

Analysis	D:\Data\Schmidt\87005_ESI_P1-E-1_01_12144.d	Acquisition Date	16.09.2021 16:10:11
Sample Name	87005_ESI	Ionisation	ESI Positive
Method	as 50-1600 1hz.m	Mass Range	50 m/z - 1600 m/z
Client	Sipoho Ze 003_ 2 f-3 d	Operator	rudolph

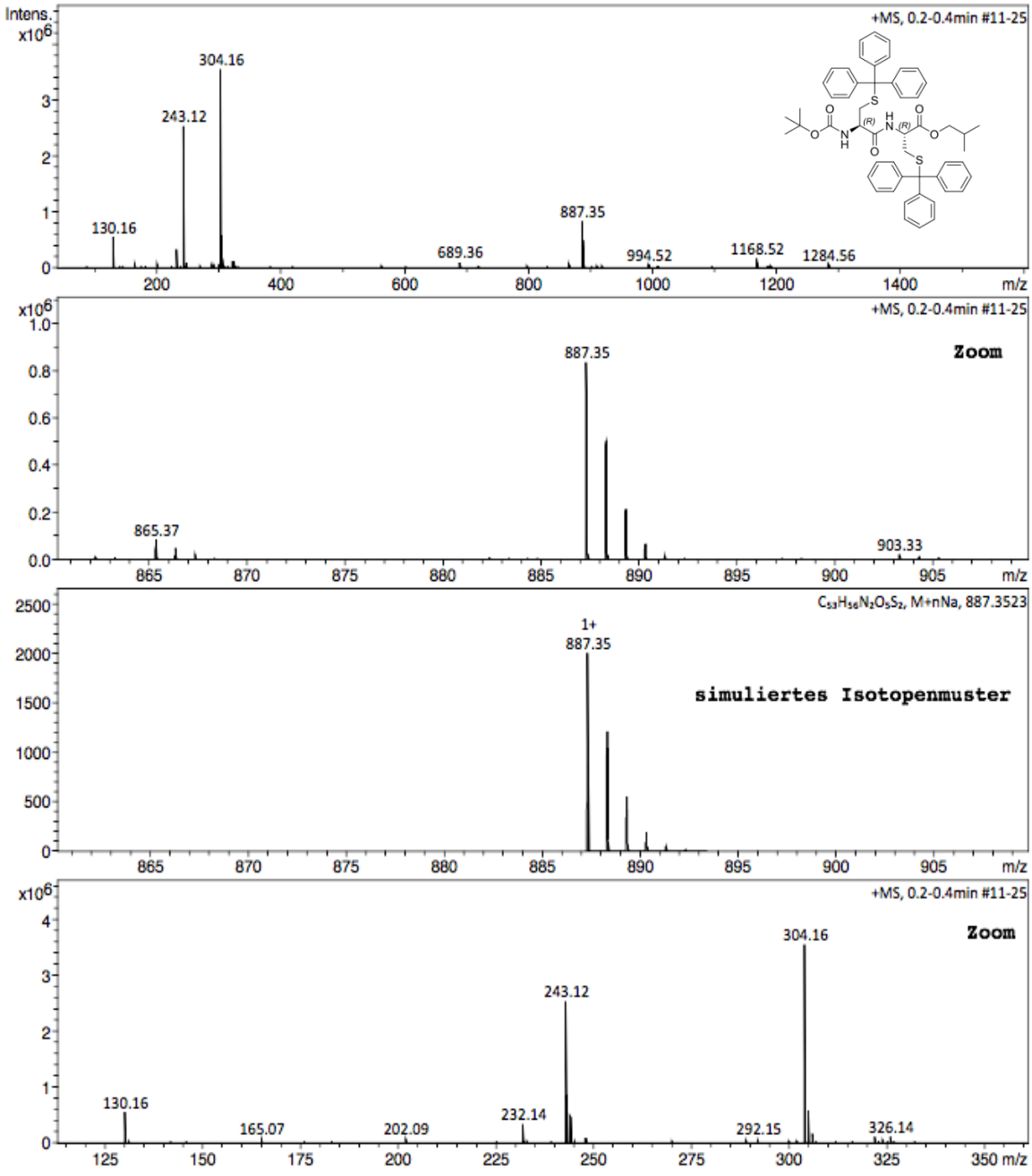

Mass Spectrometry Facility, Department of Chemistry, Technische Universität Darmstadt Instrument: Bruker Impact II

Page 1 of 1

Mass spectrum

Analysis	D:\Data\Schmidt\86771ESI_P1-D-1_01_11524.d	Acquisition Date	05.08.2021 12:19:33
Sample Name	86771ESI	Ionisation	ESI Positive
Method	as 50-1600 1hz.m	Mass Range	50 m/z - 1600 m/z
Client	Sipoho Ze 024	Operator	rudolph

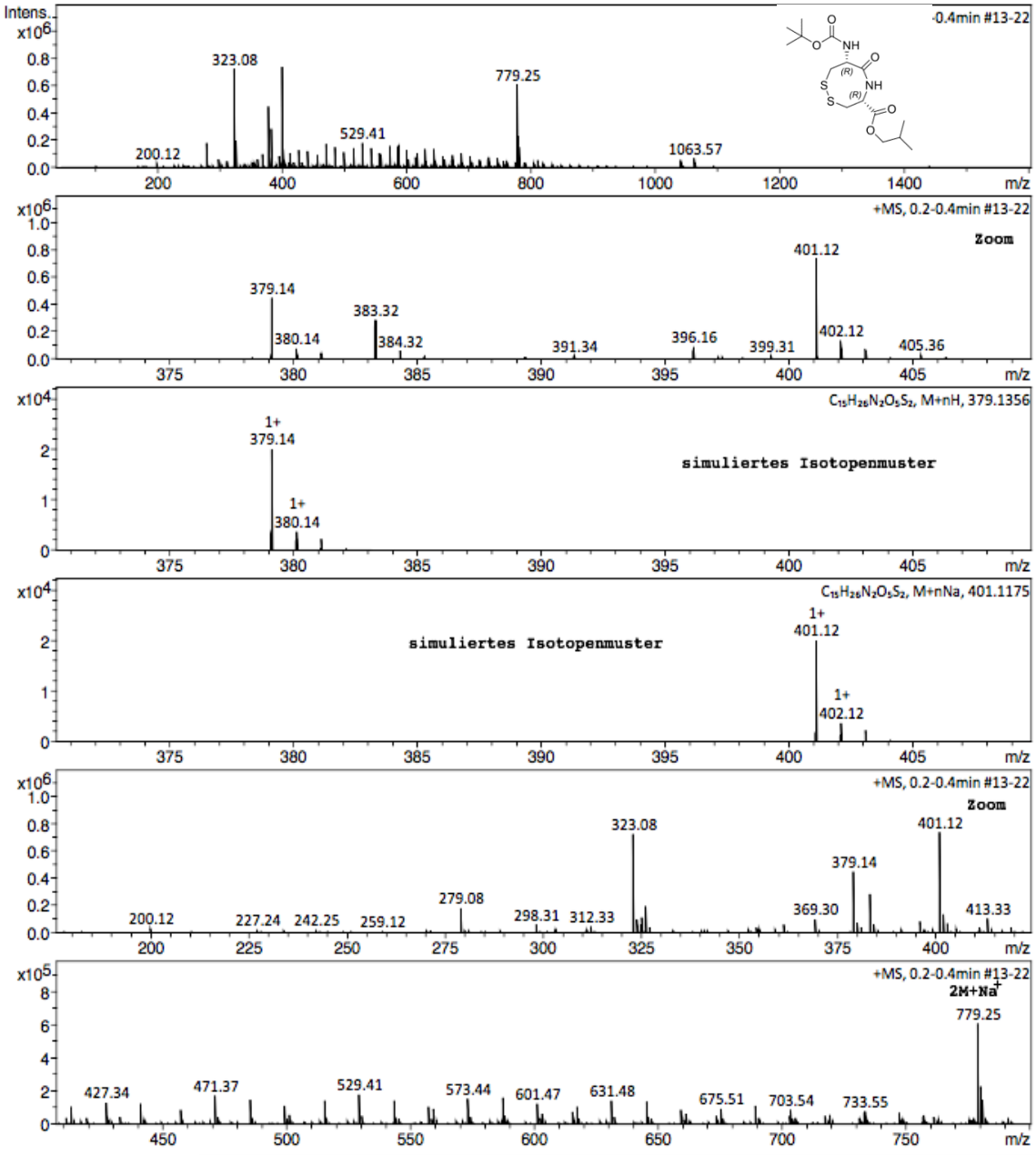

Mass Spectrometry Facility, Department of Chemistry, Technische Universität Darmstadt Instrument: Bruker Impact II

Page 1 of 1

Mass spectrum

Analysis	D:\Data\Schmidt\85569_ESI_P1-D-1_01_7121.d	Acquisition Date	09.12.2020 10:37:18
Sample Name	85569_ESI	Ionisation	ESI Positive
Method	as 50-1500-f 1hz.m	Mass Range	50 m/z - 1600 m/z
Client	Kenfack Sipoho AK 150 _5d-6a	Operator	Rudolph

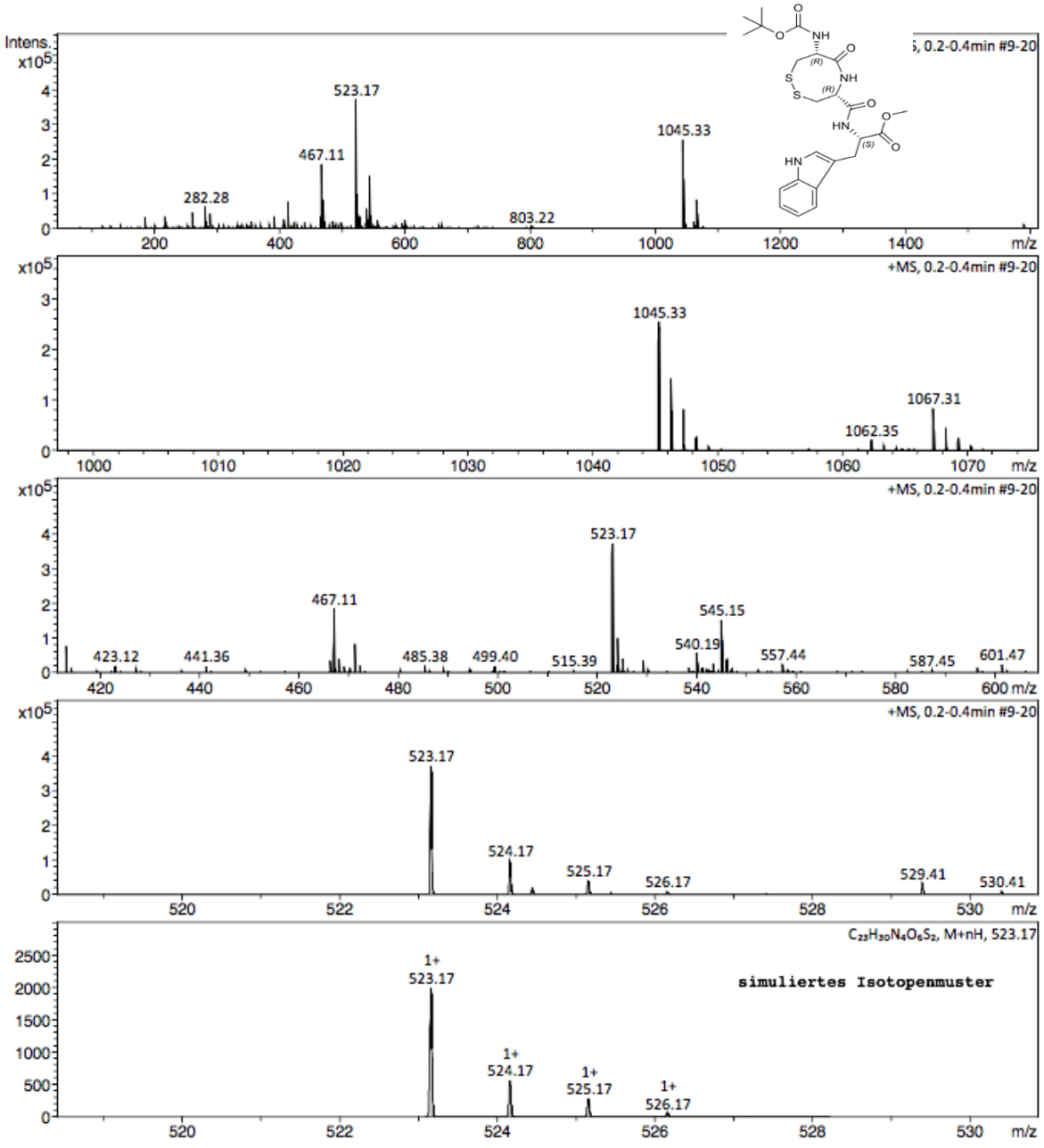

Mass spectrum

Analysis	D:\Data\Schmidt\86012_APCI_P1-C-1_01_8769.d	Acquisition Date	09.03.2021 13:25:29
Sample Name	86012_APCI	Ionisation	APCI Positive
Method	apci_pos_1500.m	Mass Range	50 m/z - 1600 m/z
Client	KenfackSipoho A400 5a_6c	Operator	Rudolph

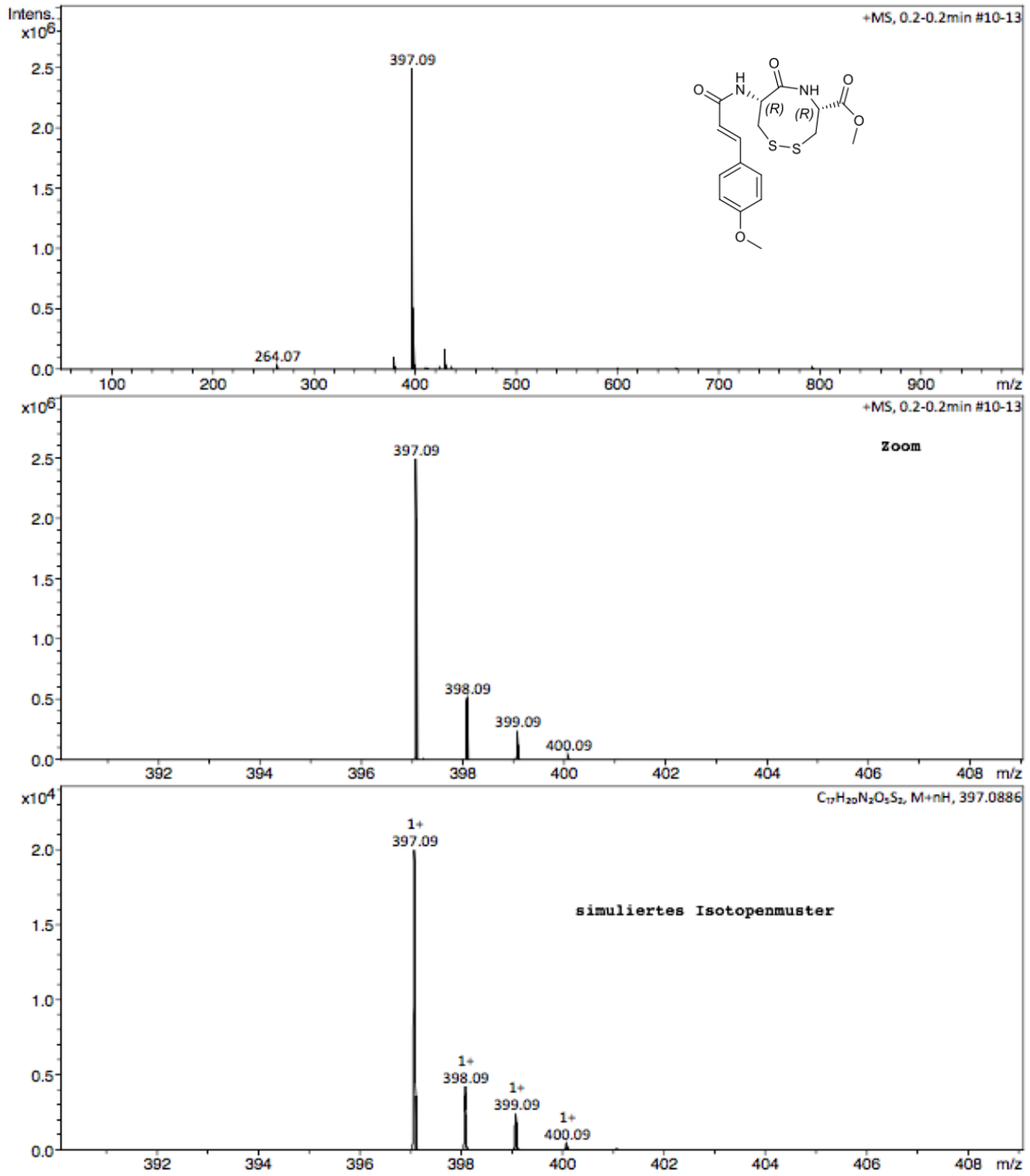

Mass Spectrometry Facility, Department of Chemistry, Technische Universität Darmstadt Instrument: Bruker Impact II

Page 1 of 1

Mass spectrum

Analysis	D:\Data\Schmidt\86026_APCI_P1-D-1_01_8945.d	Acquisition Date	16.03.2021 13:25:39
Sample Name	86026_APCI	Ionisation	APCI Positive
Method	apci_pos_1500.m	Mass Range	50 m/z - 1600 m/z
Client	KenfackSipoho AK 410_ 6b-10f	Operator	Rudolph

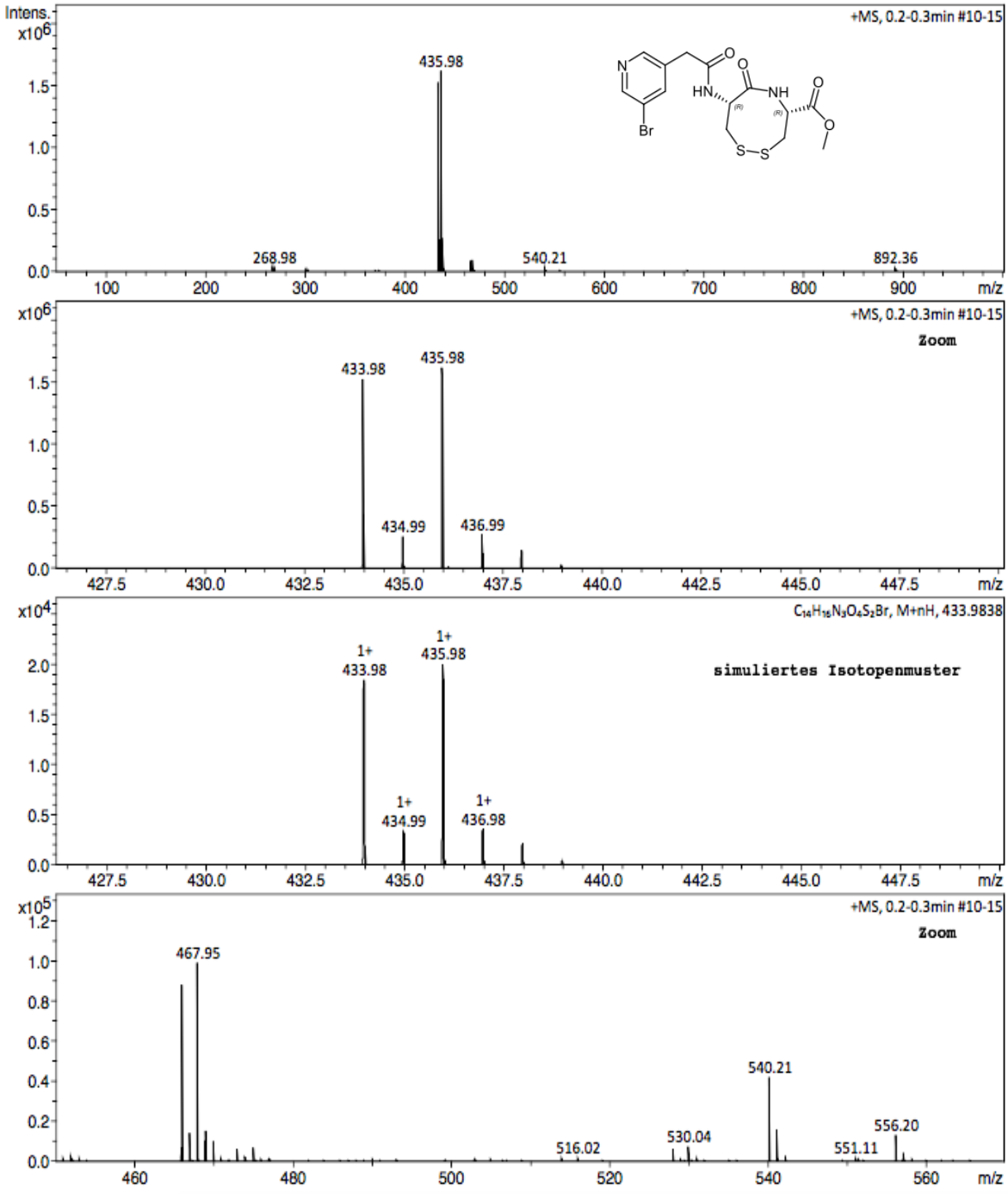

Mass spectrum

Analysis	D:\Data\Schmidt\86089_ESI_P1-D-1_01_9124.d	Acquisition Date	23.03.2021 17:41:35
Sample Name	86089_ESI	Ionisation	ESI Positive
Method	as 50-1500 1hz.m	Mass Range	50 m/z - 1600 m/z
Client	KenfackSipoho AK 420 8f-13d	Operator	Rudolph

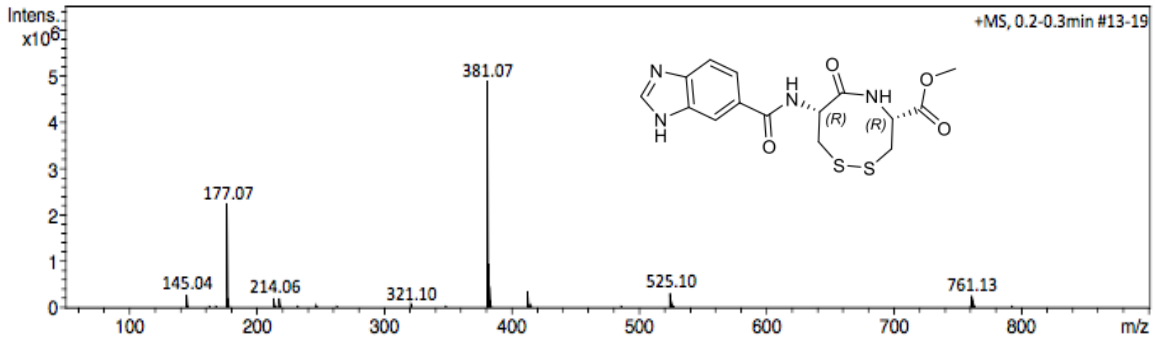

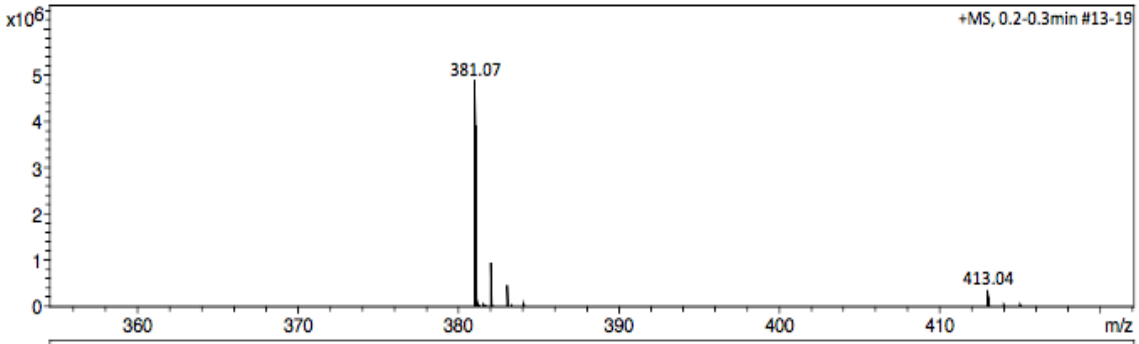

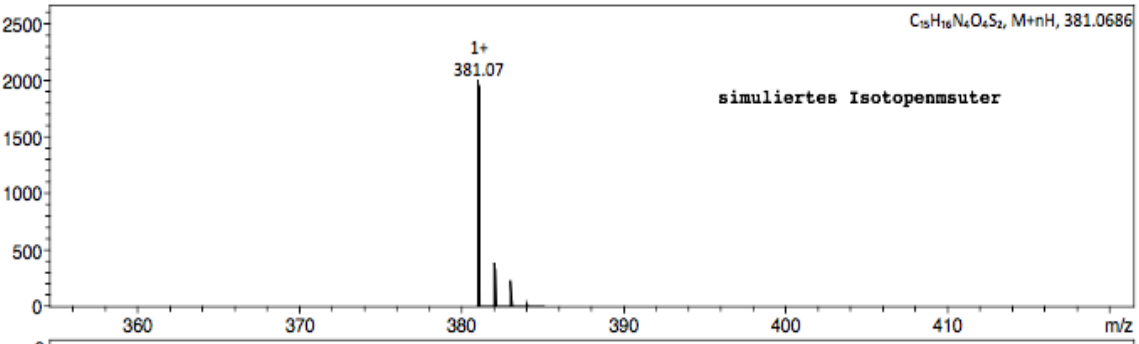

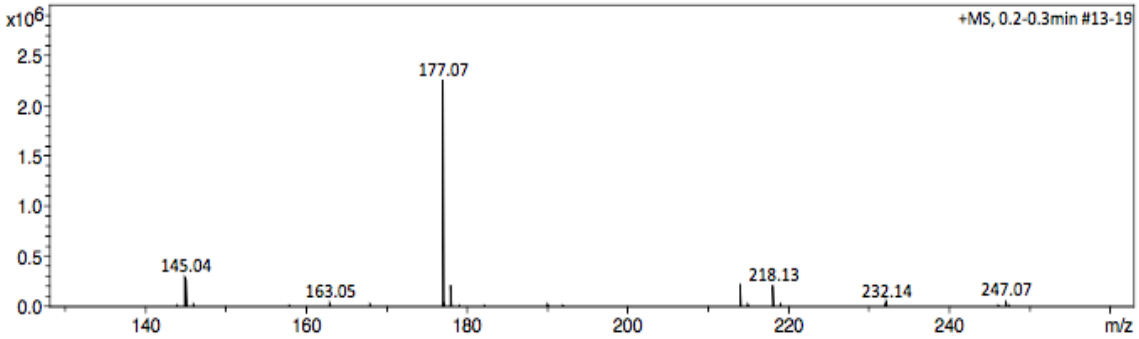

Mass Spectrometry Facility, Department of Chemistry, Technische Universität Darmstadt Instrument: Bruker Impact II

Page 1 of 1

Mass spectrum

Analysis	D:\Data\Schmidt\85510_ESI_P1-C-1_01_7007.d	Acquisition Date	27.11.2020 14:10:44
Sample Name	85510_ESI	Ionisation	ESI Positive
Method	as 50-1500-f 1hz.m	Mass Range	50 m/z - 1600 m/z
Client	Kenfack EC 006_Produkt	Operator	Rudolph

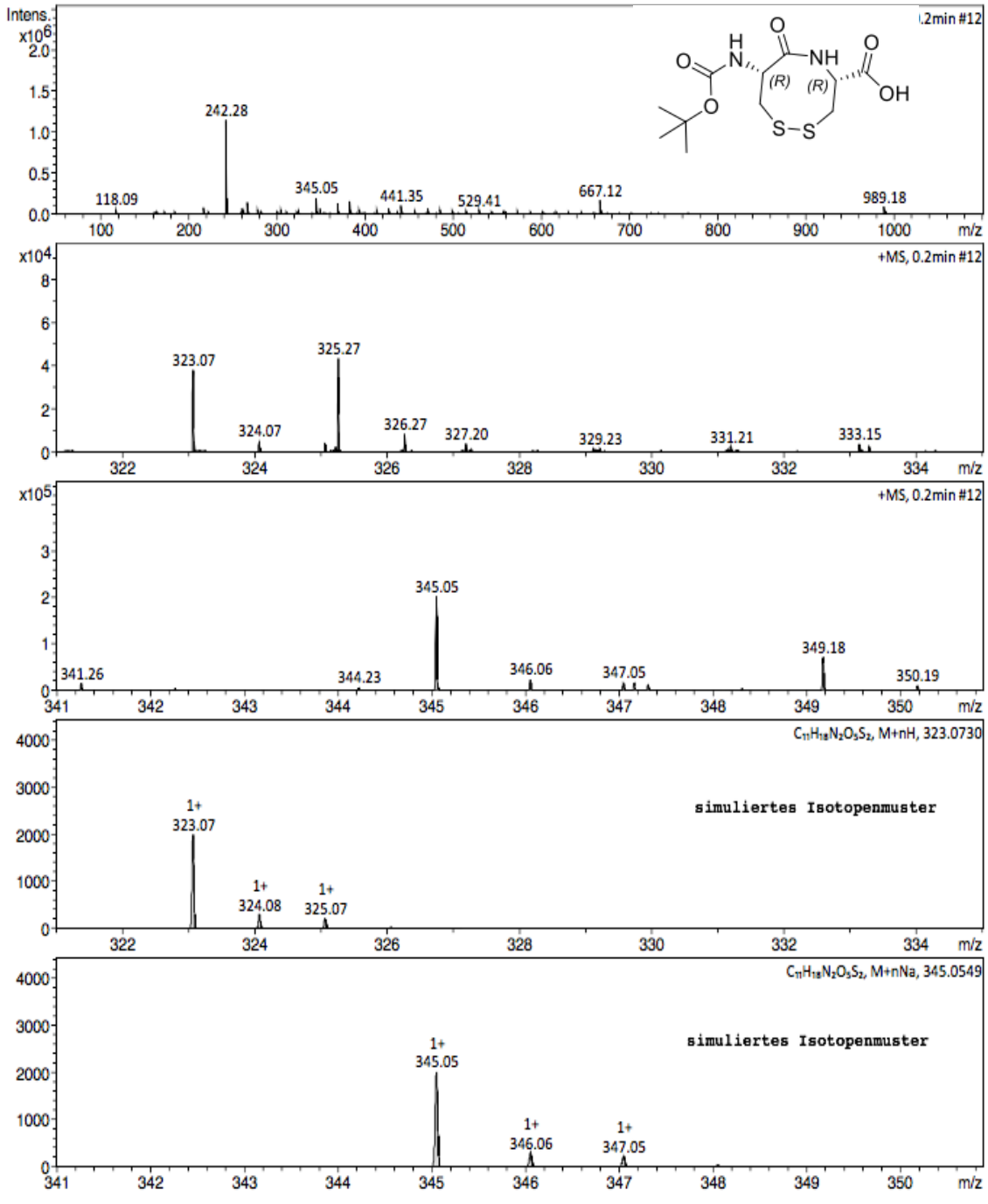

Mass Spectrometry Facility, Department of Chemistry, Technische Universität Darmstadt Instrument: Bruker Impact II

Page 1 of 1

Mass spectrum

Analysis	D:\Data\Schmidt\87055_ESI_P1-D-3_01_12261.d	Acquisition Date	27.09.2021 12:22:52
Sample Name	87055_ESI	Ionisation	ESI Positive
Method	as 30-500 1hz.m	Mass Range	30 m/z - 500 m/z
Client	Schließmann KS 20 F10	Operator	rudolph

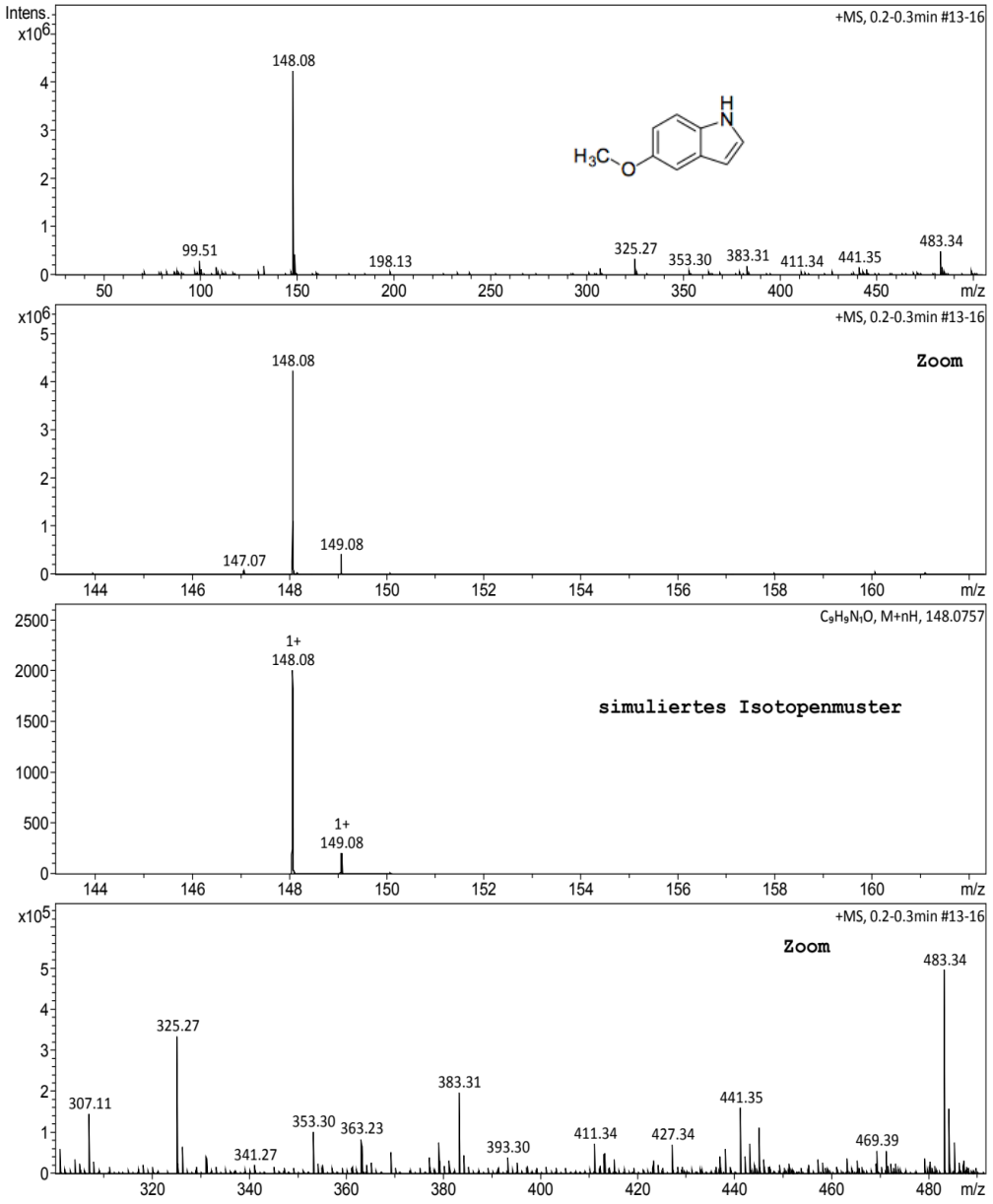

Mass spectrum

Analysis	D:\Data\Schmidt\87054_ESI_P1-D-2_01_12259.d	Acquisition Date	27.09.2021 12:04:15
Sample Name	87054_ESI	Ionisation	ESI Positive
Method	as 30-500 1hz.m	Mass Range	30 m/z - 500 m/z
Client	Schließmann KS 19	Operator	rudolph

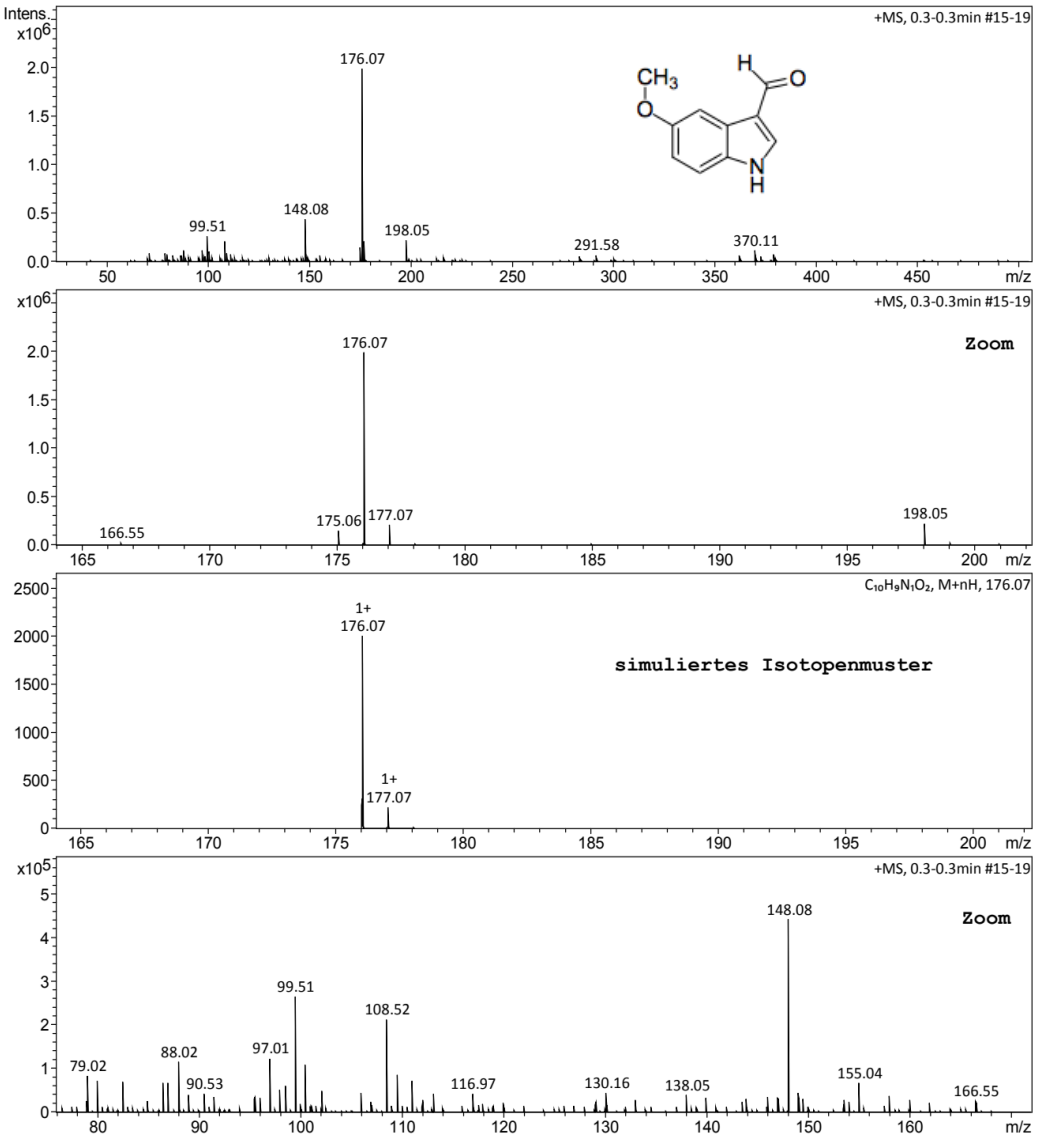

Mass Spectrometry Facility, Department of Chemistry, Technische Universität Darmstadt Instrument: Bruker Impact II

Page 1 of 1

Mass spectrum

Analysis	D:\Data\Schmidt\87057_ESI_P1-D-5_01_12264.d	Acquisition Date	27.09.2021 13:53:34
Sample Name	87057_ESI	Ionisation	ESI Positive
Method	as 30-500 1hz.m	Mass Range	30 m/z - 500 m/z
Client	Schließmann KS 25 SP	Operator	rudolph

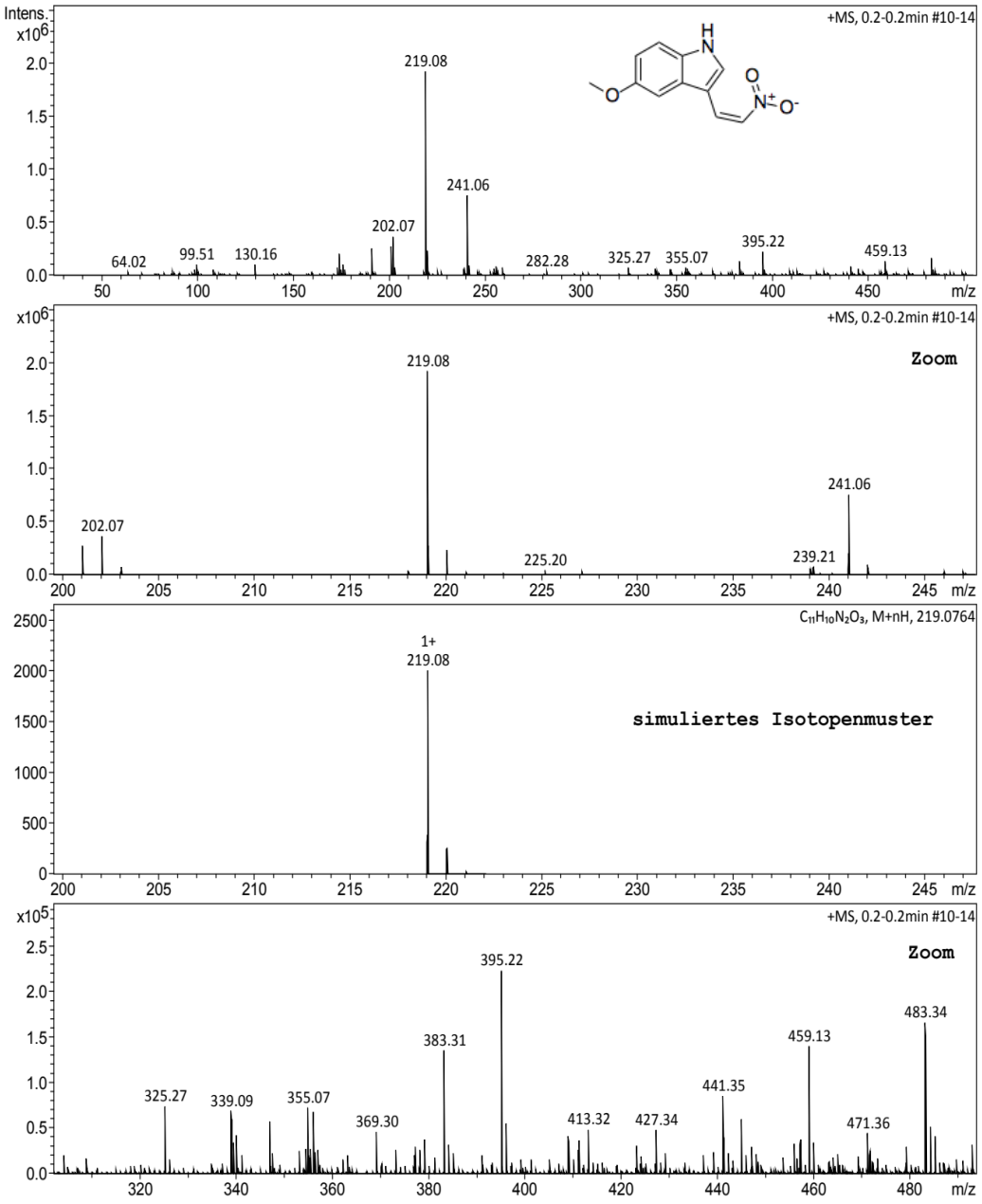

Mass spectrum

Analysis	D:\Data\Schmidt\89008_ESI_P1-E-2_01_18406.d	Acquisition Date	08.06.2022 15:29:22
Sample Name	89008_ESI	Ionisation	ESI Positive
Method	as 50-1000 1hz.m	Mass Range	50 m/z - 1000 m/z
Client	Kenfack ED 4	Operator	Rudolph

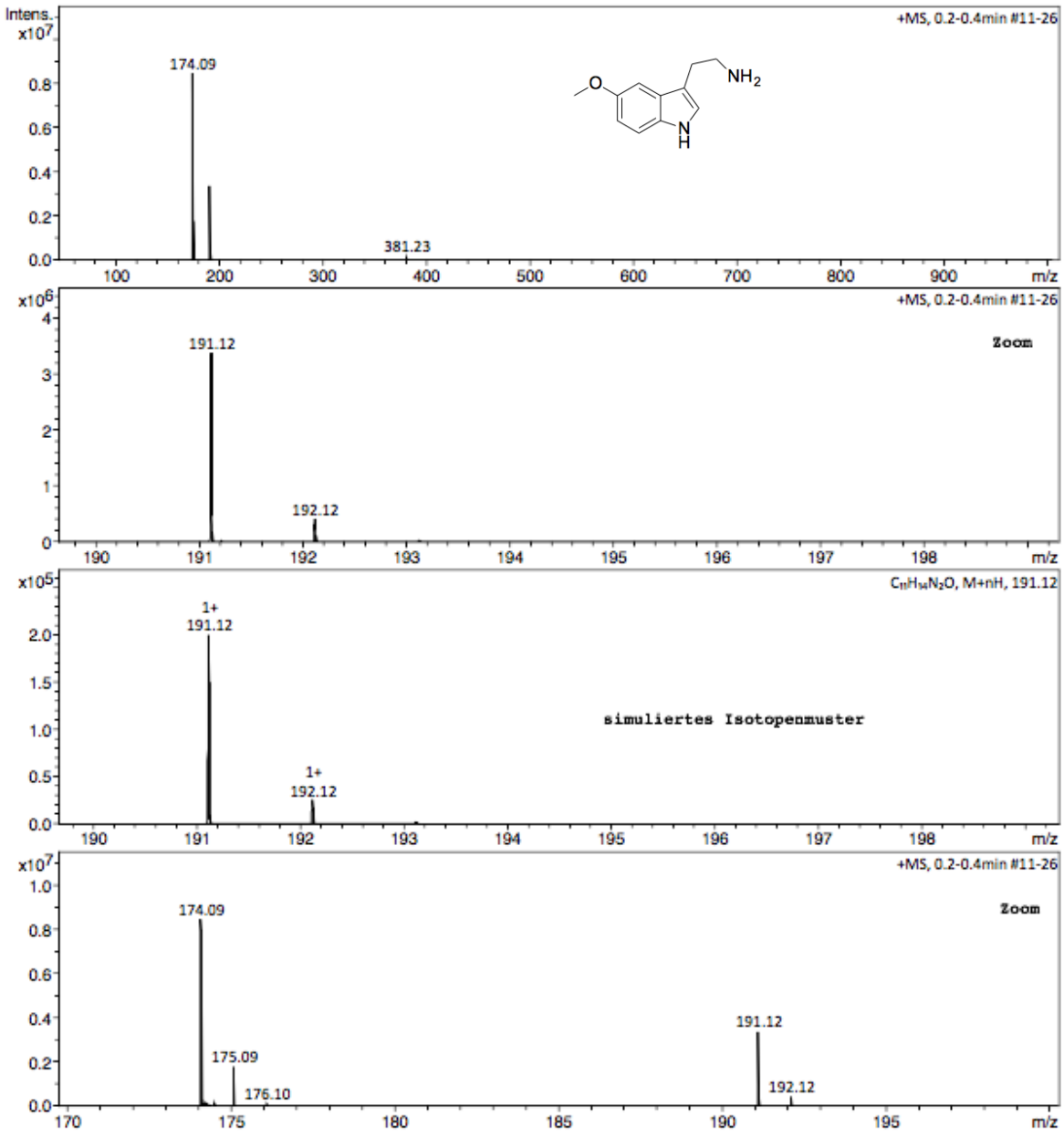

Mass spectrum

Analysis	D:\Data\Schmidt\89010_ESI_P1-E-4_01_18405.d	Acquisition Date	08.06.2022 15:24:33
Sample Name	89010_ESI	Ionisation	ESI Positive
Method	as 50-1000 1hz.m	Mass Range	50 m/z - 1000 m/z
Client	Kenfack ED 5	Operator	Rudolph

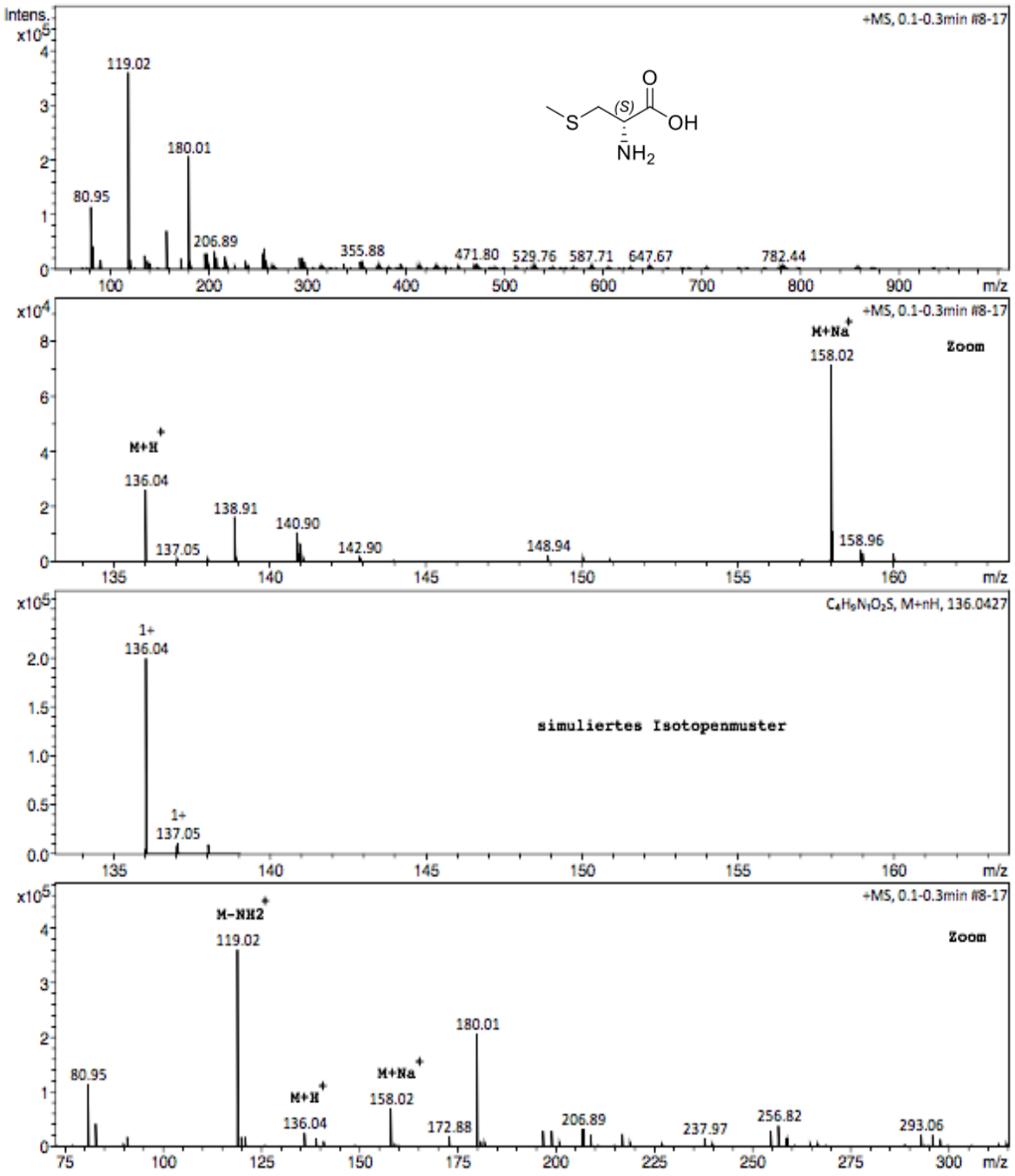

Mass Spectrometry Facility, Department of Chemistry, Technische Universität Darmstadt Instrument: Bruker Impact II

Page 1 of 1

Mass spectrum

Analysis	D:\Data\Schmidt\89012_ESI_P1-E-6_01_18408.d	Acquisition Date	08.06.2022 15:36:37
Sample Name	89012_ESI	Ionisation	ESI Positive
Method	as 50-1000 1hz.m	Mass Range	50 m/z - 1000 m/z
Client	Kenfack ED 20	Operator	Rudolph

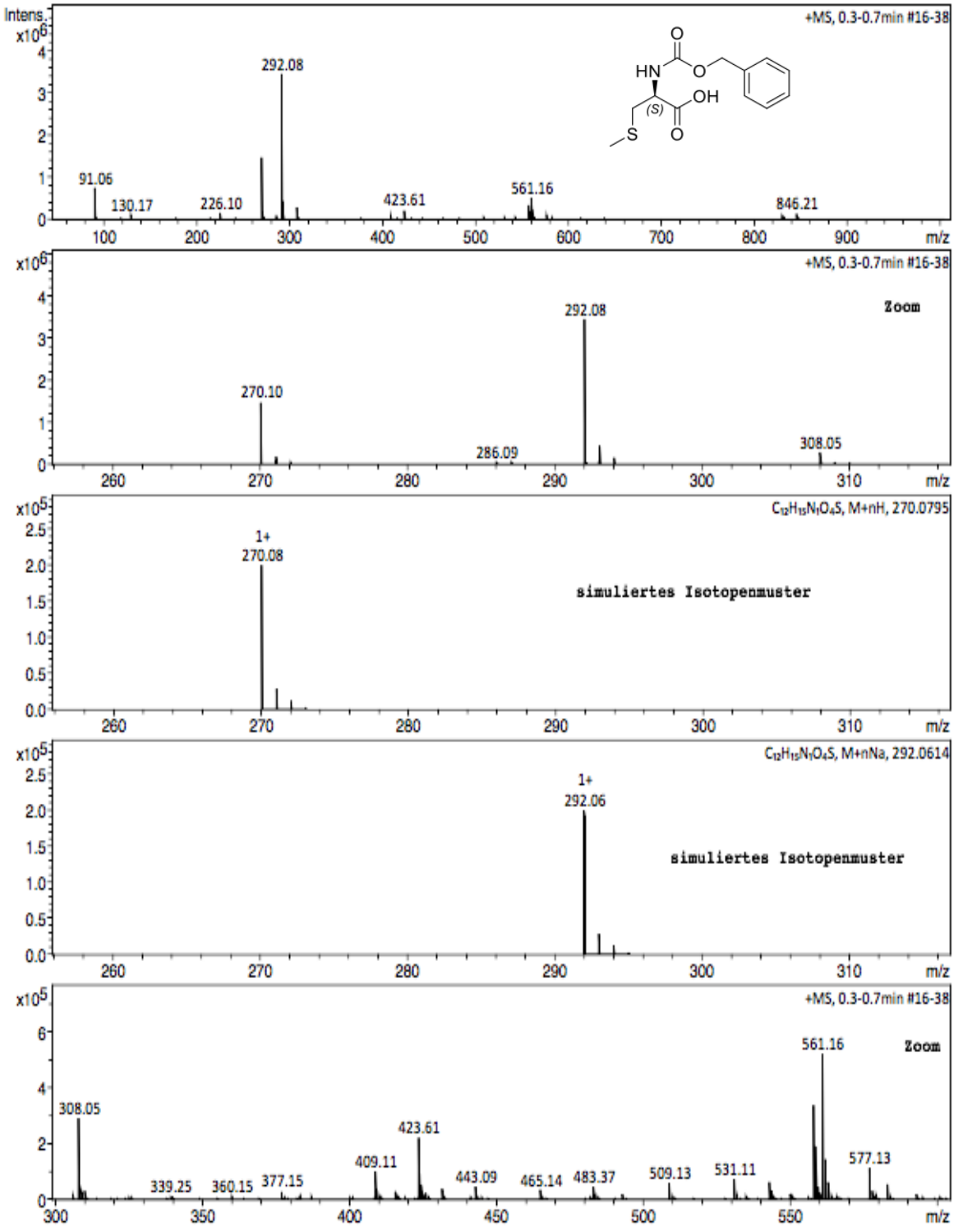

Mass Spectrometry Facility, Department of Chemistry, Technische Universität Darmstadt Instrument: Bruker Impact II

Page 1 of 1

Mass spectrum

Analysis	D:\Data\Schmidt\89006_ESI_P1-E-4_01_18398.d	Acquisition Date	08.06.2022 13:29:09
Sample Name	89006_ESI	Ionisation	ESI Positive
Method	as 50-1000 1hz.m	Mass Range	50 m/z - 1000 m/z
Client	Kenfack ED 21_2f	Operator	Rudolph

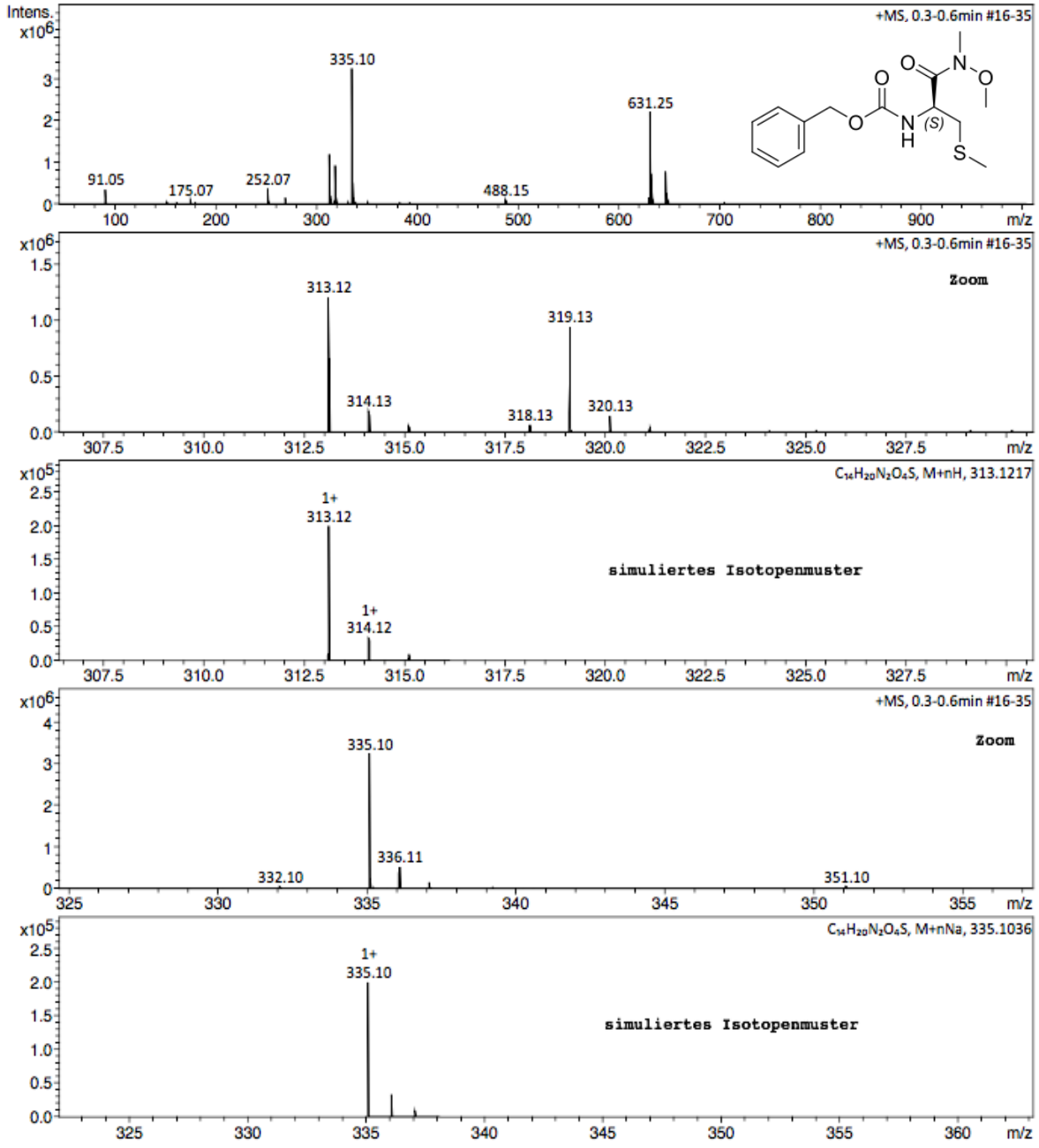

Mass Spectrometry Facility, Department of Chemistry, Technische Universität Darmstadt Instrument: Bruker Impact II

Page 1 of 1

Mass spectrum

Analysis	D:\Data\Schmidt\89007_ESI_P1-E-1_01_18401.d	Acquisition Date	08.06.2022 15:05:01
Sample Name	89007_ESI	Ionisation	ESI Positive
Method	as 50-1000 1hz.m	Mass Range	50 m/z - 1000 m/z
Client	Kenfack ED 22 cp	Operator	Rudolph

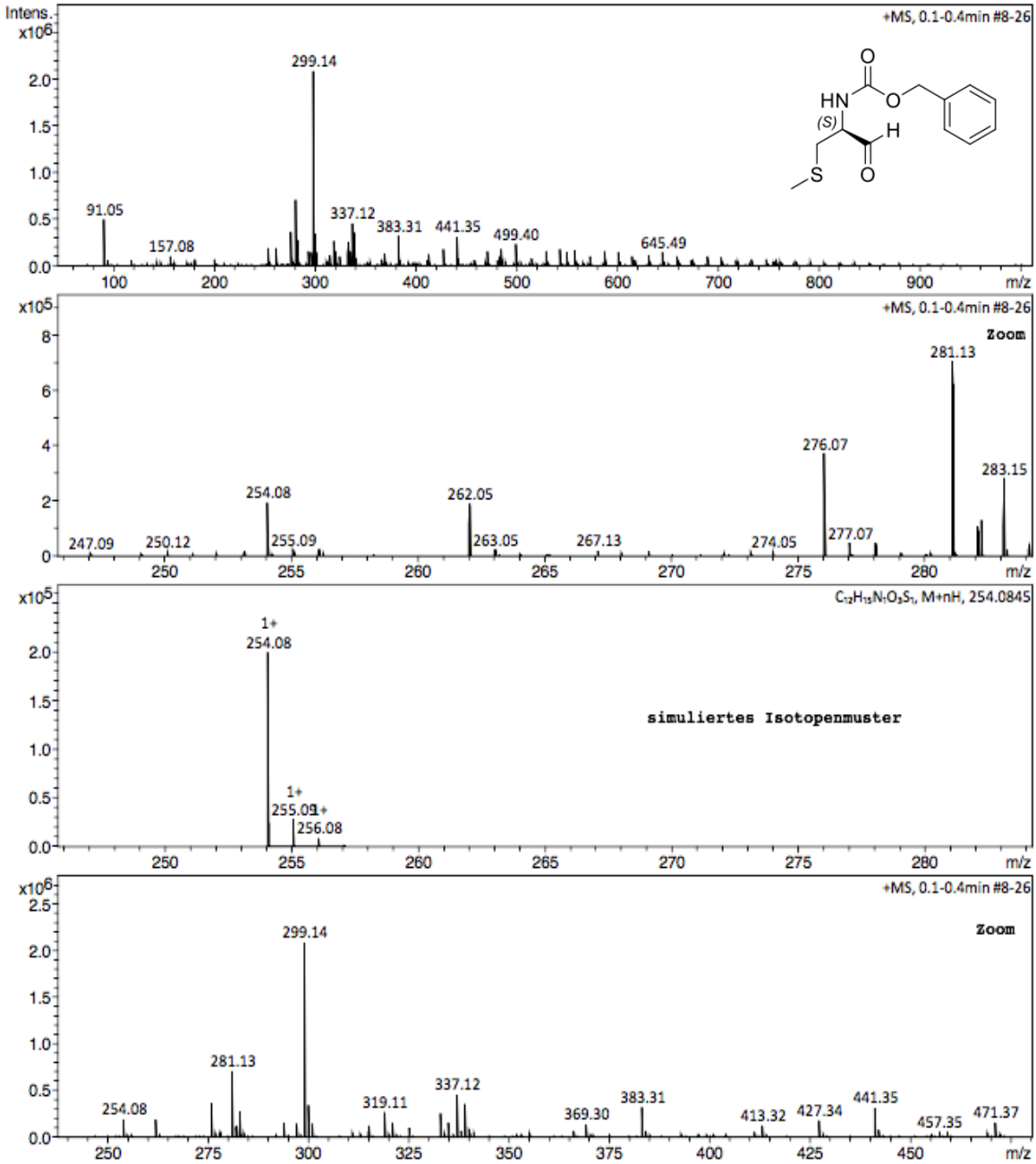

Mass Spectrometry Facility, Department of Chemistry, Technische Universität Darmstadt Instrument: Bruker Impact II

Page 1 of 1

Mass spectrum

Analysis	D:\Data\Schmidt\87243_ESI_P1-D-2_01_12879.d	Acquisition Date	03.11.2021 11:35:04
Sample Name	87243_ESI	Ionisation	ESI Positive
Method	as 50-1000 1hz.m	Mass Range	50 m/z - 1000 m/z
Client	Schliessmann KS 455P	Operator	Rudolph

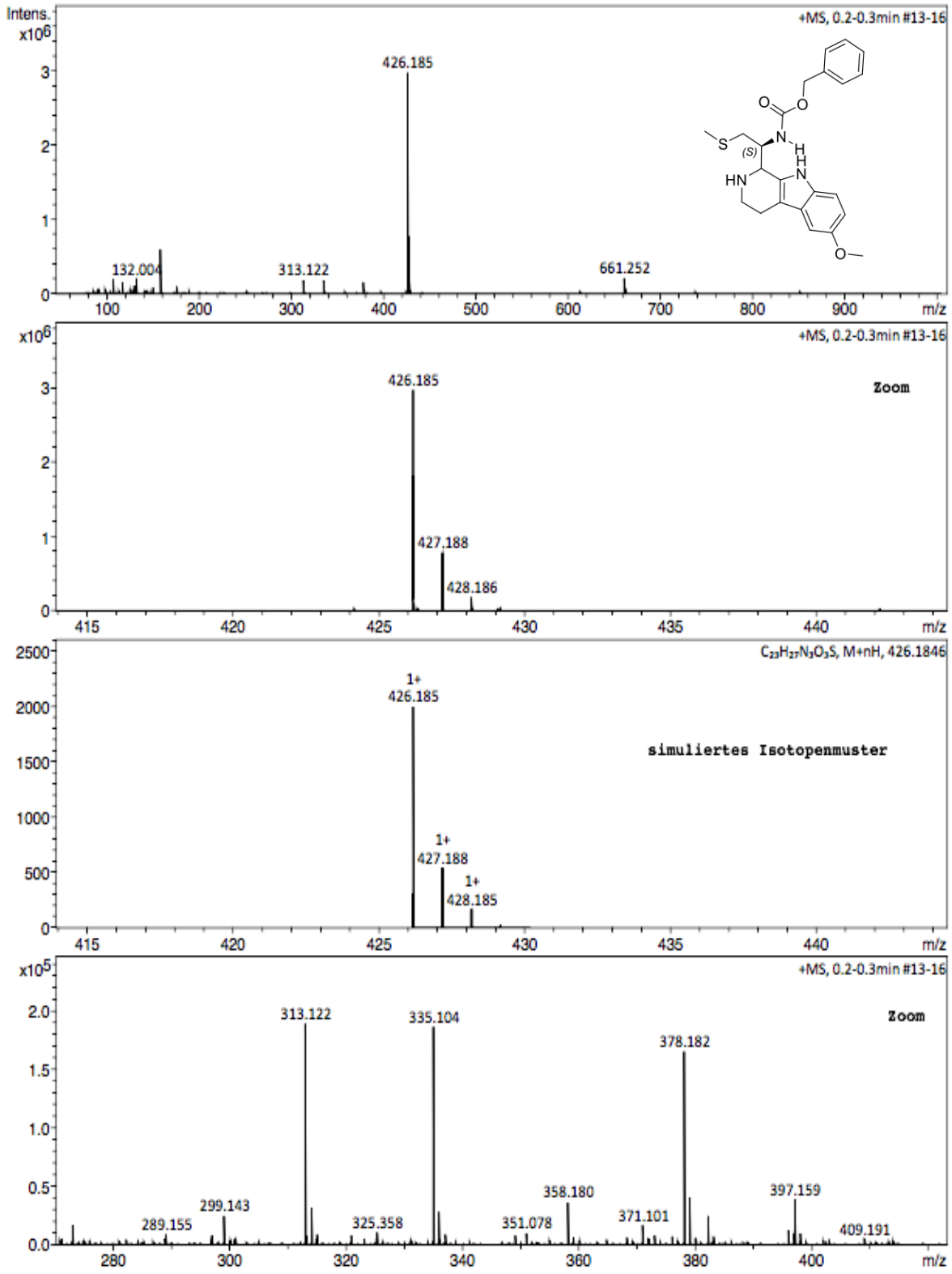

Mass Spectrometry Facility, Department of Chemistry, Technische Universität Darmstadt Instrument: Bruker Impact II

Page 1 of 1

Mass spectrum

Analysis	D:\Data\Schmidt\87338_ESI_P1-E-5_01_13112.d	Acquisition Date	10.11.2021 16:18:40
Sample Name	87338_ESI	Ionisation	ESI Positive
Method	as 50-1000 1hz.m	Mass Range	50 m/z - 1000 m/z
Client	Schliessmann KS 48 F7	Operator	Rudolph

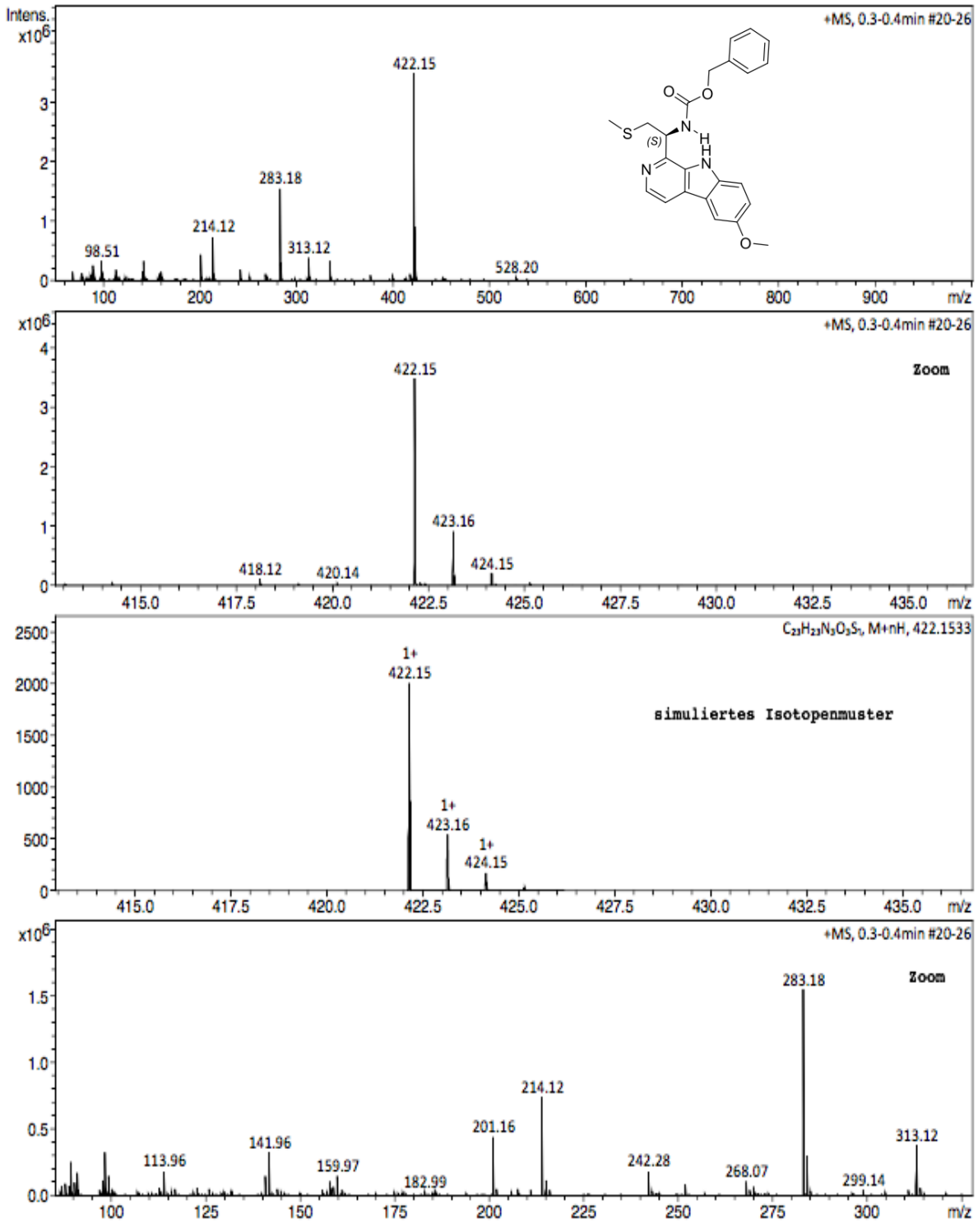

Mass Spectrometry Facility, Department of Chemistry, Technische Universität Darmstadt Instrument: Bruker Impact II

Page 1 of 1

Mass spectrum

Analysis	D:\Data\Schmidt\87979_ESI_P1-E-1_01_15612.d	Acquisition Date	10.02.2022 17:39:43
Sample Name	87979_ESI	Ionisation	ESI Positive
Method	as 50-1600 1hz.m	Mass Range	50 m/z - 1600 m/z
Client	Sipoho ED 25_8 6c-13c	Operator	Rudolph

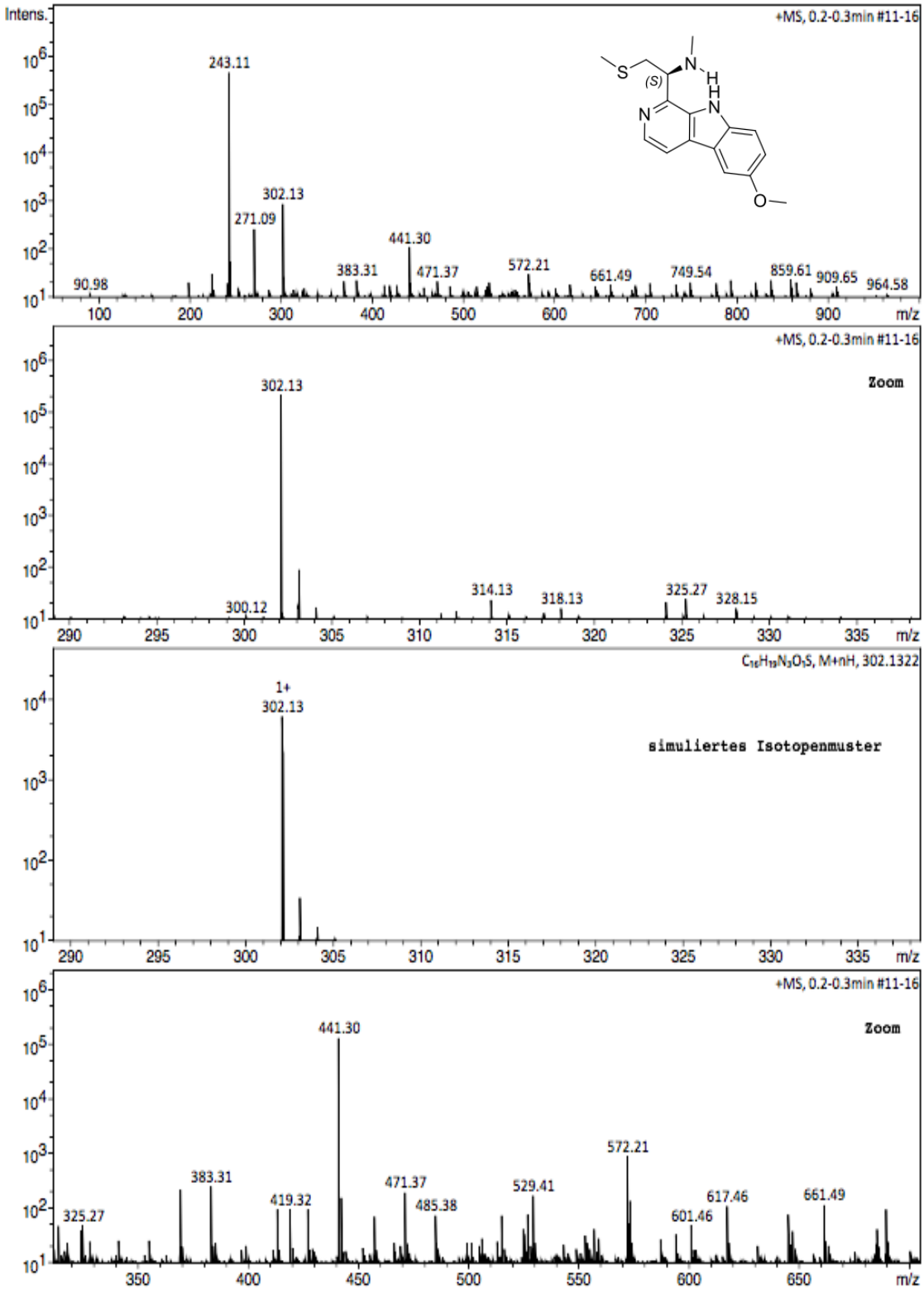

Mass spectrum

Analysis	D:\Data\Schmidt\87765_ESI_P1-E-1_01_14817.d	Acquisition Date	19.01.2022 15:30:21
Sample Name	87765_ESI	Ionisation	ESI Positive
Method	as 50-1000 1hz.m	Mass Range	50 m/z - 1000 m/z
Client	Schliessmann KS 82 RK	Operator	Rudolph

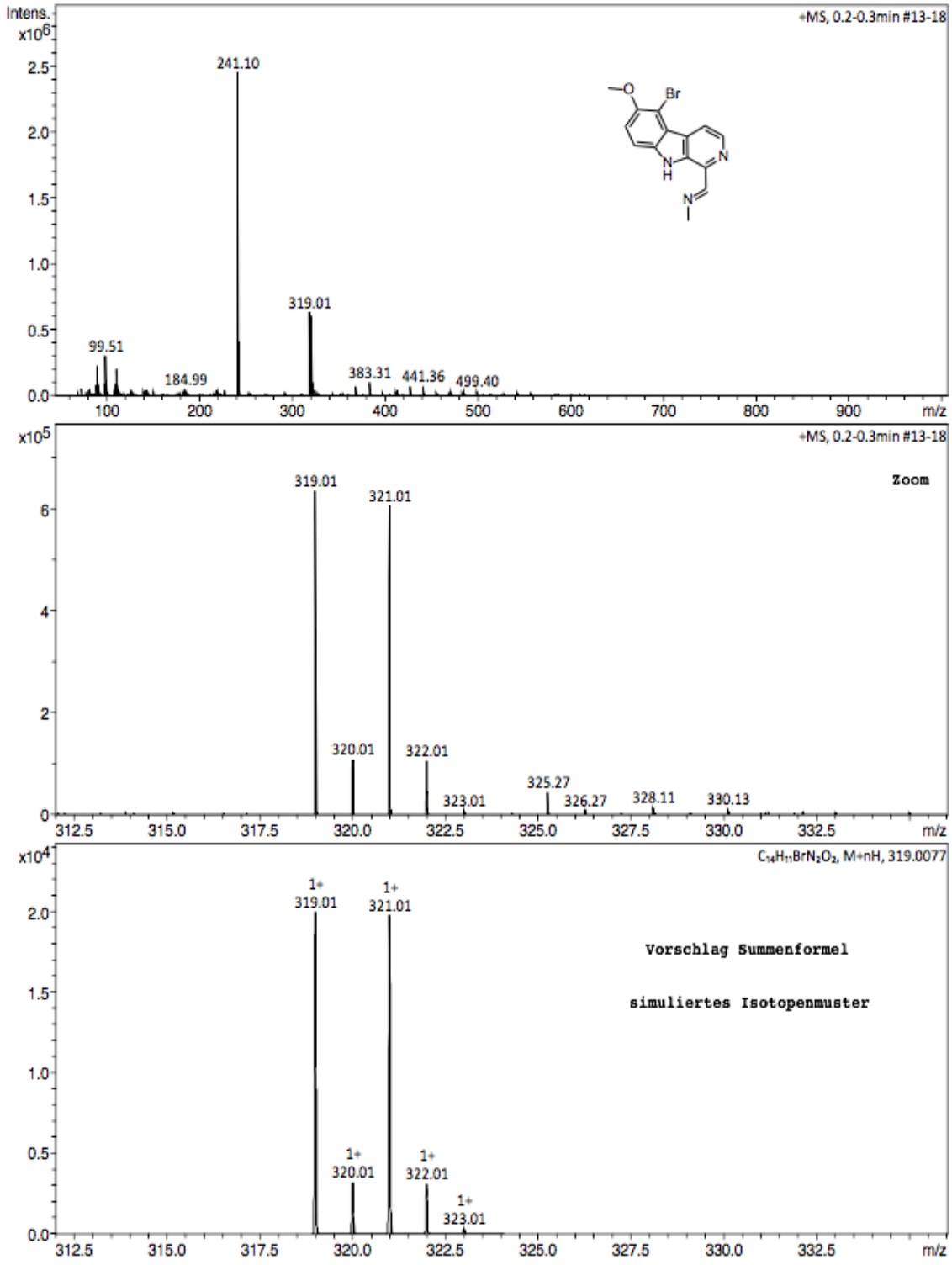

Mass spectrum

Analysis	D:\Data\Schmidt\88450_ESI_P1-B-2_01_16932.d	Acquisition Date	07.04.2022 13:28:21
Sample Name	88450_ESI	Ionisation	ESI Positive
Method	as 50-1600 1hz.m	Mass Range	50 m/z - 1600 m/z
Client	Sipoho ED27_3_1e-2b	Operator	Rudolph

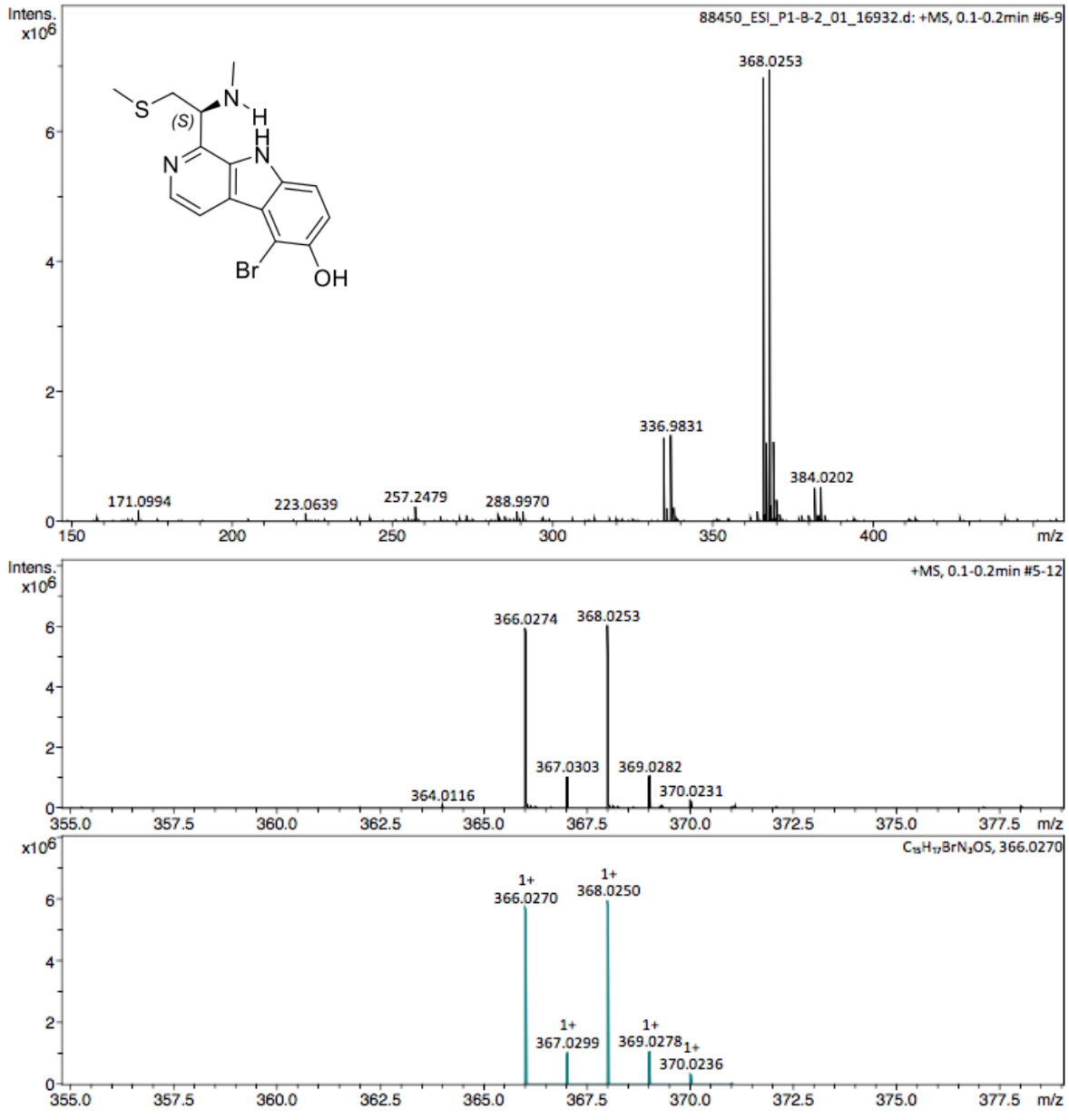

Mass spectrum

Analysis	D:\Data\Schmidt\89259_ESI_P1-E-1_01_19245.d	Acquisition Date	20.07.2022 15:58:17
Sample Name	89259_ESI	Ionisation	ESI Positive
Method	as 50-1000 1hz.m	Mass Range	50 m/z - 1000 m/z
Client	Kenfack ED 29 _2d-4b	Operator	Rudolph

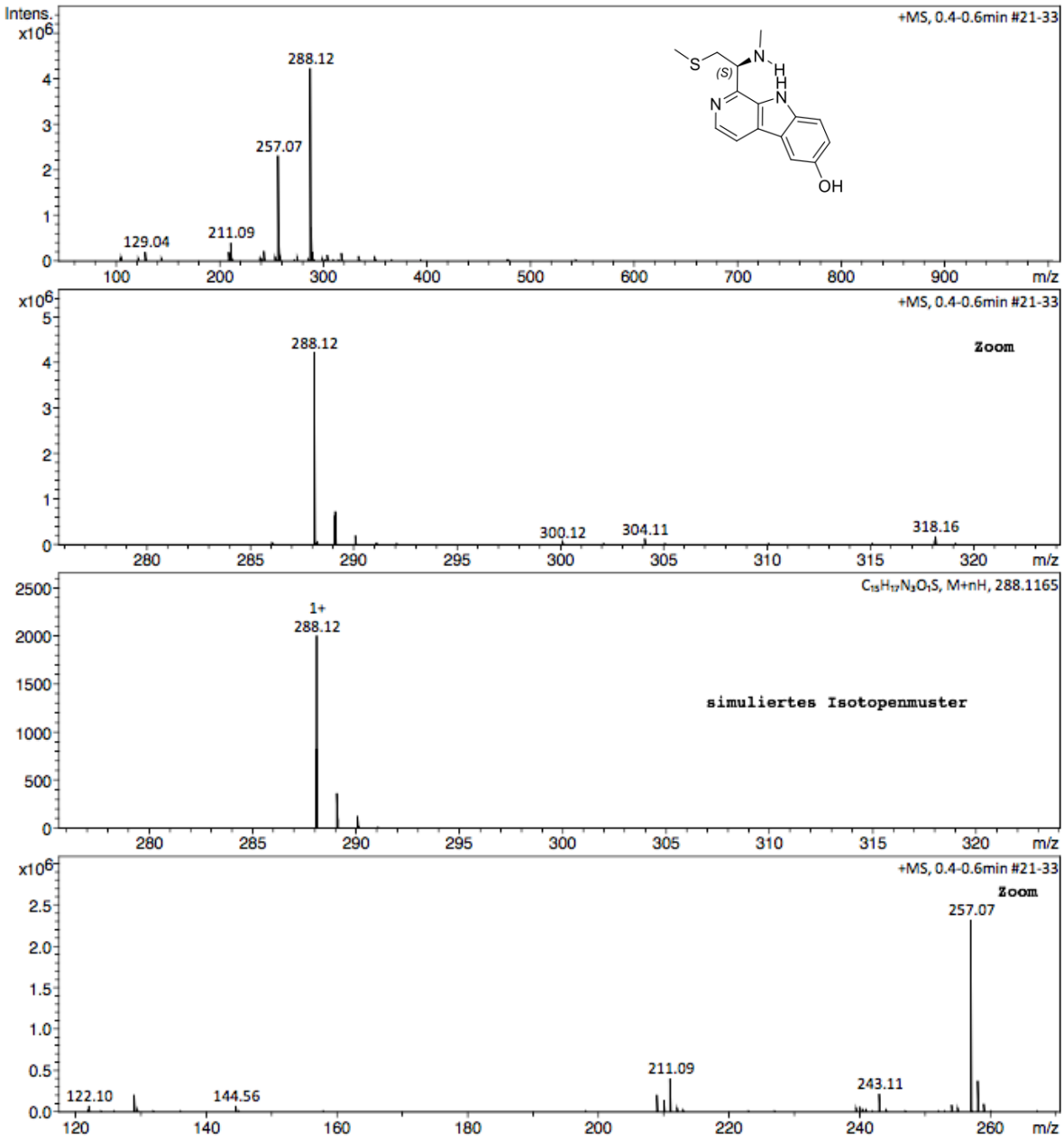

Mass Spectrometry Facility, Department of Chemistry, Technische Universität Darmstadt Instrument: Bruker Impact II

Page 1 of 1

Erklärungen

§8 Abs. 1 lit. c der Promotionsordnung der TU Darmstadt

Ich versichere hiermit, dass die elektronische Version meiner Dissertation mit der schriftlichen Version übereinstimmt und für die Durchführung des Promotionsverfahrens vorliegt.

§8 Abs. 1 lit. d der Promotionsordnung der TU Darmstadt

Ich versichere hiermit, dass zu einem vorherigen Zeitpunkt noch keine Promotion versucht wurde und zu keinem früheren Zeitpunkt an einer in- oder ausländischen Hochschule eingereicht wurde. In diesem Fall sind nähere Angaben über Zeitpunkt, Hochschule, Dissertationsthema und Ergebnis dieses Versuchs mitzuteilen.

§9 Abs. 1 der Promotionsordnung der TU Darmstadt

Ich versichere hiermit, dass die vorliegende Dissertation selbstständig und nur unter Verwendung der angegebenen Quellen verfasst wurde.

§9 Abs. 2 der Promotionsordnung der TU Darmstadt

Die Arbeit hat bisher noch nicht zu Prüfungszwecken gedient.

Darmstadt, den …September 2023

Annicet Kenfack Sipoho ----------

(name and signature)